Seismic Performance of FRP Retrofitted Exterior RC Beam-Column Joints under Varying Axial and Bidirectional Loading

A thesis submitted in partial fulfilment of the
requirements for the Degree of
Doctor of Philosophy in Civil Engineering
by

Umut Akguzel

Supervised by
Associate Professor Stefano Pampanin
Professor Athol Carr

Department of Civil and Natural Resources Engineering
University of Canterbury
Christchurch, New Zealand

January 2011

This thesis is dedicated to those
who lost their lives in earthquakes

ABSTRACT

Most of the experimental studies available in literature on the seismic assessment and retrofit of existing, poorly detailed, reinforced concrete (RC) beam-column joints typical of pre-1970s construction practice have concentrated on the two-dimensional (2D) response, using unidirectional cyclic loading testing protocols and a constant column axial load. Even more limited information is available on the performance of corner three-dimensional (3D) RC beam-column joints with substandard detailing subjected to a bidirectional-loading regime. In addition, little effort has been dedicated to the development of simple but reliable analysis and design procedure for FRP-strengthened joints.

This thesis aims to (1) investigate the effects of varying axial and bidirectional loading on the seismic performance of deficient exterior RC beam-column joints before and after retrofit and (2) develop performance-based seismic assessment and FRP-based retrofit procedures for exterior and corner beam-column joints. For this purpose, following a critical review on the seismic vulnerability of both existing and retrofitted exterior and corner beam-column joints under varying and bidirectional loading demands, a comprehensive experimental programme along with analytical and numerical studies are carried out.

A performance-based retrofit approach was adopted in order to achieve the desired ductile failure mode by modifying the hierarchy of strength within the beam-column joint system. In order to achieve this, existing retrofit design methodology available in literature was refined and a step-by-step procedure was proposed for the assessment of the as-built and proceeding retrofit design of FRP-retrofitted exterior beam-column joints. In addition, the role and importance of accounting for the correct demand conditions (e.g., the variation of axial loads) in the assessment of the existing joint and the design of the FRP retrofit scheme were discussed. In order to assist the retrofit design and assessment procedure a semi-empirical analytical model was developed to evaluate the joint shear resistance after FRP retrofit. Both the proposed assessment methodology and design procedure along with the analytical procedure were verified by experimental studies performed in this thesis and experimental tests available in the literature. Parametric analyses were also carried out to indicate the

effectiveness of strengthening with different materials, configurations and failure limit states.

The feasibility and efficiency of a retrofitting intervention using GFRP composites were investigated based on the quasi-static cyclic tests conducted on four 2D exterior (plane frame) and two 3D corner (space frame) RC joints. All specimens were of 2/3 scale, designed according to pre-1970s construction practice. The properties of the specimens are summarized briefly as follows:

(1) Specimen 2D1 was tested under varying axial load as an exterior 2D benchmark unit;
(2) Specimen 2D2 was tested under constant axial load with minimum retrofit solution designed according to the proposed methodology;
(3) Specimen 2D3 was tested under varying axial load with the same retrofit scheme adopted in 2D2;
(4) Specimen 2D4 was tested under varying axial load with improved retrofit scheme;
(5) Specimen 3D1 was tested under bidirectional loading with varying axial load as a benchmark;
(6) Specimen 3D2 was tested under bidirectional loading with varying axial load with improved retrofit scheme adopted in Specimen 2D4.

The test outcomes highlighted the potentially unconservative effects of neglecting the actual multiaxial load demand, when assessing the behaviour of existing beam-column joints and designing a proper retrofit intervention. Corner beam-column joints within a frame building were confirmed to be particularly vulnerable. However, with an adequate retrofit design accounting for the multiaxial load effects, the implemented retrofit solutions provided the necessary improvements of the behaviour of the as-built specimens. This resulted in the development of a more appropriate hierarchy of strength with the formation of plastic hinges in the beam and protection of the weaker mechanisms. The experimental findings were also used to identify the critical damage limit states and engineering parameters to be adopted within the framework of performance-based seismic retrofit design.

In addition to the experimental and analytical studies, FEM numerical studies based on microplane concrete model approach were carried out. Three-dimensional finite element (FE) models for retrofitted 2D exterior joint (Specimen 2D2) and as-built 3D corner joint (Specimen 3D1) were developed and analysed. The analysis results showed good agreement with the experimental results.

ACKNOWLEDGEMENTS

There are a large number of people who I owe thanks to. During the darkest moments, they gave me strength, courage and confidence to continue on my way during the past years.

I would like to express my profound gratitude to my primary supervisor Associate Professor Stefano Pampanin. This thesis would not have been possible without his wisdom, inspiration, never ending patience and invaluable advice. Above all, his cordiality will always remain with me.

I am also grateful to my co-supervisor Professor Athol Carr for his kind advice, technical assistance and encouragement.

The financial support provided by the University of Canterbury through a Targeted Doctoral Scholarship, the New Zealand Foundation for Research, Science and Technology (FRST) through the Research Program "Retrofit Solutions for NZ", and the Christchurch Heritage Trust Society are gratefully acknowledged. Without the financial aid from these organisations, my PhD research and experience would not have been possible. The material support and technical assistance provided by Sika and BBR-Contech are also kindly appreciated.

I would like to thank the technicians and staff of the Department of Civil and Natural Resources Engineering who helped me on this project. In particular, without the assistance of Mosese Fifita and Richard Newton the laborious experimental programme of this thesis would not have been completed. The assistance of John Maley, Michael Weavers, Tim Perigo, Russell McConchie and Stuart Toase in making the experimental research a smooth experience has also been much appreciated.

To my fellow postgraduate colleagues, I would like to acknowledge those who supported me extensively throughout my studies: Dr. Dion Marriott, Kam Weng Yuen, Dr. Alejandro Amaris, Patricio Quintana Gallo, Dr. Didier Pettinga, Masoud Moghaddasi, Michael Newcombe, Vinod Sadashiva, Ali Sahin Tasligedik and numerous others. My gratitude goes also to fellow PhD student

Tobias Smith for proof reading the thesis. Thank you all for providing insightful comments and suggestions on a range of topic.

Special thanks for the technical support on the numerical studies are given to the University of Stuttgart research group in particular Professor Rolf Eligehausen, Professor Josko Ozbolt and fellow postgraduate student Goran Periskic with special thanks to Giovacchino Genesio for his advice and support on my studies during my research period at the University of Stuttgart.

Many thanks are due to my friends and colleagues from Turkey. The fruitful discussions with my previous mentors and colleagues, in particular Associate Professor Sevket Ozden, Dr. Onur Ertas, Dr. Selcuk Altay and Dr. Osman Kaya are also gratefully appreciated. This undertaking could never have been achieved without their continuous encouragement, support and friendship.

I am particulary indebted to Elizabeth Ackermann for the immense support she provided me over the past years. Her encouragement and support has always accompanied me to face the difficulties.

Finally, I would like to express my deepest gratitude to my mother and father for their love, unwavering support and understanding during my PhD studies.

TABLE OF CONTENTS

LIST OF FIGURES

LIST OF TABLES

NOTATION

A, B, C = quadratic equation coefficients;
A_e = effective area in the joint;
A_f = FRP area;
A_s = reinforcement area;
b_c = width of column;
b_j = effective width of joint;
b_w = width of beam;
C_E = environmental reduction factor;
C_c = compressive force provided by concrete;
C_s = compressive force provided by reinforcement;
c = neutral axis depth;
c_1 = 0.64 = empirical coefficient in the calculation of FRP debonding;
c_2 = 2 = empirical coefficient in the calculation of FRP debonding;
d = effective depth;
$d_{b,b}$ = diameter of the longitudinal beam bar;
$d_{b,c}$ = diameter of the longitudinal column bar;
d_{fb} = depth of FRP sheet on beam;
d_{fc} = depth of FRP sheet on column;
E_c = modulus of elasticity of concrete;
E_D = cumulative energy dissipation;
E_f = modulus of elasticity of FRP;
$f_c(y)$ = compressive stress of concrete as a function of distance y from the centroidal axis
$f`_c$ = cylinder compressive strength of concrete;
$f`_{cc}$ = compressive strength (peak strength) of confined concrete;
f_{ct} = tensile strength of concrete;
$f`_{co}$ = compressive of strength of unconfined concrete;

f_{fl} = average normal stress in the FRP in the transverse longitudinal direction (at mid-width of the joint);

f_{ft} = average normal stress in the FRP in the transverse direction (at mid-width of the joint);

f_f = stress in FRP;

$f_{f,deb}$ = debonding stress in FRP;

$f_{f,max}$ = maximum stress in FRP;

f_{fu}* = tensile fracture stress of FRP reported by the manufacturer;

f_{fu} = design tensile strength of FRP;

f_l = average stress of longitudinal reinforcement of the column inside the joint core at the midheight of the joint;

f_t = average stress in the horizontal stirrups (at mid-width of the joint);

f_s = stress in reinforcement;

f_{sx} = steel stress coordinate on the strain hardening curve from experimental data;

f_{su} = ultimate stress in reinforcement;

f_v = compressive stress on the column at the mid-depth of the joint core;

f_y = yield stress of reinforcement;

f_{yh} = yield strength of transverse reinforcing steel;

G_f = fracture energy of the material;

h_b = height of beam;

h_c = overall depth of column in the direction of the horizontal shear to be considered;

jd = internal forces lever arm in the beam section;

l = longitudinal (column) direction;

l_b = distance from column center to contraflexure point;

l_b` = half clear span length;

l_{bt} = FRP bond length along *t* direction;

$l_{b,max}$ = the effective bond length of FRP sheet;

l_{bl} = FRP bond length along *l* direction;

l_c = height of column;

K_p = peak-to-peak stiffness;

$M_{b,Rij}$ = moment capacity of the beam with FRP retrofit scheme Rij;

$M_{bdeb,Rij}$ = debonding moment capacity of beam with FRP retrofit scheme Rij;

$M_{by,Rij}$ = yielding moment capacity of beam with FRP retrofit scheme Rij;

M_{boy} = yielding moment capacity of as-built beam;

M_{col} = column moment at the top of the joint;

$M_{c,Rij}$ = moment capacity of the column with FRP retrofit scheme Rij;

$M_{cdeb,Rij}$ = debonding moment capacity of column with FRP retrofit scheme Rij;

$M_{cy,Rij}$ = yielding moment capacity of column with FRP retrofit scheme Rij;

M_{coy} = yielding moment capacity of as-built column;

$M_{j,Rij}$ = moment capacity of joint with FRP retrofit scheme Rij;

$M_{jdeb,Rij}$ = debonding moment capacity of joint with FRP retrofit scheme Rij;

M_j = equivalent joint moment;

M_{jo} = equivalent as-built joint moment;

m = bidirection interaction exponent;

N_v = compressive axial force of the column;

N_h = compressive axial force of the beam;

N_g = gravity load value in the column;

n = bidirection interaction exponent;

n_{fb} = number of sheet on beam;

n_{fc} = number of sheet on column;

$n_{sf,b}$ = number of beam sides covered with FRP;

$n_{sf,c}$ = number of column sides covered with FRP;

P_u = ultimate FRP bond strength;

p_c = principal compression stress;

p_t = principal tensile stress;

p_{tc} = principal tension strength contribution due to plain concrete;

p_{tf} = principal tensile strength contribution due to FRP;

p_{tt} = total principal tensile strength;

R_1 = 1st generic FRP retrofit scheme;

Rij = FRP retrofit scheme;

R_n = n*th* generic FRP retrofit scheme;

s_1 = slip limit in the discrete bond model;

s_2 = slip limit in the discrete bond model;

s_3 = slip limit in the discrete bond model;

T = tensile force at the bottom beam bars;

T_f = tension force in FRP;

T_s = tension force in steel;

$\tan\theta$ = average direction of the principal stresses;

t = transverse (column) direction;

t_f = FRP thickness per layer;

t_s = strip thickness in the cross section;

V_b = beam shear force;

V_c = horizontal column shear force;

$V_{c,s}$ = supplied column shear force due to FRP retrofitted joint;

$V_{c,req}$ = required column shear force;

V_{jh} = horizontal shear force acting on the joint core;

V_{cx} = horizontal column shear force in x-direction;

V_{cy} = horizontal column shear force in y-direction;

y = distance from the centroidal axis;

α = proportionality coefficient for axial load variation;

α_x = proportionality coefficient for axial load variation (x-direction);

α_y = proportionality coefficient for axial load variation (y-direction);

γ = average angle of joint shear distortion;

γ_t = target joint shear distortion;

Δ_y = yield displacement;

Δ_u = ultimate horizontal displacement;

$\boldsymbol{\varepsilon}$ = macro-strain tensor;

ε_1 = maximum principal strain in the joint panel;

ε_2 = minimum principal strain in the joint panel;

ε_c = concrete strain;

ε_{cc} = strain at maximum concrete stress;

ε_{cu} = ultimate compression strain (crushing strain);

ε_f = FRP strain;

ε_{fdeb} = debonding FRP strain;

ε_{fu} = design FRP rupture strain;

ε_{fu}* = ultimate FRP strain reported by the manufacturer;

ε_{ij} = components of the strain tensor;

ε_l = average normal strain along normal direction *l* of joint panel;

ε_s = reinforcement strain;

ε_{sh} = strain hardening of the steel;

ε_{sp} = spalling strain of concrete;

ε_{su} = ultimate strain of the mild steel defined by the maximum obtained stress;

ε_{sx} = strain coordinate on the strain hardening curve from experimental data;

ε_{sy} = reinforcement yield strain;

ε_t = average normal strain along normal direction *t* of joint panel;

Θ = the measured angle of any points to the principal axes along the biaxial loading path (skew angle);

θ = direction of the principal compression stresses;

μ = displacement ductility;

ν = Poisson`s ratio;

v_{jh} = joint nominal shear stress;

v_f = nominal shear stress contribution due to the FRP;

ρ = top beam reinforcement ratio;

ρ' = bottom beam reinforcement ratio;

ρ_b = total main beam reinforcement ratio;

ρ_s = stirrup reinforcement ratio;

ρ_{sc} = longitudinal column steel ratio;

ρ_{sh} = stirrup reinforcement ratio;

ρ_{ft} = FRP reinforcement ratio in the transverse direction;

ρ_{fl} = FRP reinforcement ratio in the longitudinal direction;

τ_m = adhesive (plain bar only) component;

τ_f = frictional residual bond component;

τ_{max} = maximum bond strength;

$\boldsymbol{\sigma}$ = macro-stress tensor;

σ_1 = maximum principal stress in the concrete;

σ_2 = minimum principal stress in the concrete;

σ_{ij} = components of the stress tensor;

σ_l = average in concrete along direction *l*;

σ_t = average in concrete along direction *t*;

ϕ = curvature of reinforced concrete section;

ω = geometric coefficient;

ABBREVIATIONS

2D = two-dimensional (e.g., two-dimensional (2D) exterior plane frame beam-column joints)

3D = three-dimensional (e.g., three-dimensional (3D) corner space frame beam-column joints)

CFRP = carbon fibre-reinforced polymer

FEM = finite element modelling

FRP = fibre-reinforced polymer

GFRP = glass fibre-reinforced polymer

MASA = macroscopic space analysis

Chapter 1 INTRODUCTION

1.1 BACKGROUND AND RESEARCH MOTIVATION

The problem of non-seismically designed reinforced concrete (RC) frame structures before 1970s is common amongst all of the seismically active regions in the world. The inadequacy of these existing structures has been repeatedly highlighted by heavy damage or total collapse caused by recent earthquakes [1-6]. In fact, before the mid-1970s, many RC buildings were designed mainly for the actions due to static gravity loads with no consideration given to the lateral strength required to resist the inertial forces of the structure's mass stemming from strong ground motions. In addition, deficiencies in seismic performance are generally a consequence of the lack of ductility which is a consequence of two major failings in the design process: poor detailing of reinforcement, and the lack of a capacity design philosophy [7].

Exterior beam-column joints are regarded as one of the most vulnerable and critical structural elements in pre-1970s RC structures. The lack of joint reinforcement and details in the joint region, the poor bond properties due to the use of plain round bars and inefficient anchorage into the joint region, can be attributed to the poor seismic performance of these elements. As a result many poorly designed and constructed buildings in earthquake-prone areas often suffer shear and/or bond (anchorage) failures during earthquakes, leading to a partial or total collapse of the structure [8]. Experimental studies on existing beam-column joints designed according to pre-seismic code construction practices also confirmed the vulnerability of these structural elements [9-16].

From the mid-70s, as seismic hazards and their detrimental effects were recognized and understood, a considerable amount of research has been devoted to developing seismic retrofitting strategies and techniques. Nevertheless, the seismic upgrading of exterior beam-column joints in existing RC moment resisting frames designed prior to modern seismic code provisions is still imposing a serious challenge in earthquake engineering. It is of crucial importance to devise effective and economical

rehabilitation techniques to mitigate the seismic vulnerability of existing structures and to increase the safety of the occupants for future earthquake events.

During the last two decades, the studies and applications of composites in construction, more particularly in the strengthening of existing buildings, represented one of the fastest growing new areas within structural engineering. Retrofit techniques based on the use of externally bonded fibre-reinforced polymers (FRPs), are becoming an attractive and more widely accepted solution for the seismic strengthening of existing buildings. The technique of using fibre-reinforced polymer (FRP) systems for structural enhancement mitigates several disadvantages and is gaining preference over traditional strengthening methods such as concrete jacketing, steel plate bonding and sprayed concrete. FRPs offer excellent corrosion resistance to environmental agents, as well as higher strength and stiffness-to-weight ratios when compared to conventional construction materials.

In the past, the efficiency of retrofit solutions on beam-column joints using FRP materials has been investigated through experimental studies by various researchers. The tests unanimously indicated the effectiveness of the strengthening procedure achieving significant improvements in the strength, stiffness and ductility of the retrofitted joints. Nevertheless, close examination of the previous studies reveals some significant knowledge gaps and questions that need to be addressed. In this context, typical limitations and drawbacks identified from the previous research are summarised in the following:

(a) Effects of variation of axial load and bidirectional loading:

Most of the available literature, as well as design guidelines related to the seismic assessment and FRP retrofit of existing RC buildings, have concentrated on the in-plane (2D) response (e.g., [17-34]). In fact under an earthquake excitation, exterior and corner joints of a frame structure are subjected to varying axial load (associated with overturning moments developing in the structure in addition to the vertical component of ground motions) and bidirectional lateral load reversals. In general, the research in the field of retrofitted structures under multidimensional earthquake conditions is very limited. Scarce information is available in literature on the response of deficient exterior joints under varying axial load and biaxial bending effects, either before or after retrofitting (e.g., [16, 35-37]).

Bidirectional loading, more representative of the actual response of a structure under earthquake loading, can significantly affect the response of poorly detailed beam-column joints. A remarkable

reduction in the joint shear strength capacity occurs due to the simultaneous loading in the two orthogonal directions. This is further aggravated by the concurrent variation of axial load, the joint panel zone may experience excessive damage and/or premature failure, due to the increase in strength and deformation demand.

When underestimating or overlooking such effects, the incorrect and non-conservative assessment of the sequence of events could occur, leading to inadequate design of the retrofit intervention. Consequently, as a controversial outcome of an inappropriate retrofit intervention, it would be possible to activate a global failure mechanism (i.e., due to the formation of a soft storey), which would have not occurred in the as-built (pre-retrofit) configuration. Thus, careful study is required to understand the behaviour of retrofitted exterior RC beam-column joints, to assess the effects of this behaviour on structural response and to devise appropriate design methods.

(b) Performance-based seismic assessment and design procedure for the seismic retrofit of RC beam-column joints using FRP composite materials:

In spite of the number of experimental studies on the behaviour of FRP retrofitted beam-column joints, relatively limited work [38, 18, 20, 24] has been dedicated on the development of a simple, but reliable analysis and design procedure for FRP-strengthened joints. Recently refined analytical procedures [39] proposed for the evaluation of strengthened beam-column joints are still somehow too complex to be implemented and adopted by practicing engineers on a daily basis.

In addition, to implement a performance-based seismic evaluation and retrofit design of existing beam-column joints, simple methods should be devised to evaluate the expected level of damage limit states. In order to provide some aid to the engineering decisions necessary in the assessment, retrofit design criteria and FRP scheme selection, the correspondence between limit states and critical engineering parameters should be established based on various practical cases. For example, seismic performance of different types of exterior and corner beam-column joint configurations (i.e., as-built and retrofitted) under various loading conditions (i.e., uni- and bidirectional loading with varying axial load) can be examined.

(c) Numerical studies on beam-column joints:

The majority of the research effort regarding numerical studies has been focused on the FE modelling of strengthened RC beams to address the bonding issue of FRP plates and sheets (e.g., [40-55]). Studies regarding the modelling of RC joints with FRP materials are relatively limited. Furthermore, it is interesting to note that, to the best knowledge of the researcher of this study, there have been no numerical studies conducted for the biaxial and varying axial load conditions, either on as-built or retrofitted corner beam-column joints.

This research was motivated in order to fill these gaps in literature, contribute to the knowledge and highlight the effects of bidirectional loading as well as varying axial load on the seismic performance of deficient exterior RC beam-column joints before and after retrofit with FRP materials. In order to accomplish these objectives comprehensive experimental as well as analytical and numerical investigations have been carried out in this thesis. This research is part of a more extensive ongoing research project at the University of Canterbury focusing on seismic retrofit solutions for existing reinforced concrete buildings in New Zealand [56].

1.2 OBJECTIVES AND SCOPE OF THE RESEARCH

The objectives of this research project are as follows:

(1) To gather, by quasi-static tests, information on the unidirectional cyclic behaviour of as-built 2D exterior (plane frame) and the bidirectional cyclic behaviour of as-built 3D corner (space frame) beam-column joints under varying axial load.

(2) To develop and validate an analytical model to evaluate the shear resistance of a retrofitted joint.

(3) To refine the existing retrofit design methodology and propose a simplified step-by-step analytical procedure for the detailed assessment of each component in as-built and retrofitted configurations for exterior beam-column joints.

(4) To investigate the feasibility and efficiency of a retrofitting intervention using glass fibre reinforced polymer (GFRP) composites, based on the unidirectional quasi-static cyclic testing of retrofitted 2D exterior beam-column joints under constant and varying axial loads and the bidirectional

cyclic tests of retrofitted 3D corner beam-column joints under varying axial load. Attention is given to the investigation of possible negative effects of bidirectional loading and concurrent varying axial load on the performance of the retrofitted corner joints when designed according to unidirectional behaviour assumptions (i.e., retrofitted based on the design procedure proposed for 2D exterior beam-column joints under varying axial load).

(5) To review and improve the performance-based engineering assessment and retrofit design of exterior beam-column joints by proposing damage limit states based on the experimental findings.

(6) To introduce a conceptual deformation-based retrofit design procedure to identify and evaluate the FRP retrofit scheme for shear strengthened beam-column joints based on a selected target performance.

(7) To make recommendations for upgrading the FRP retrofit scheme of proposed 3D corner beam-column joints in order to enhance the seismic performance and eliminate the brittle failure modes.

(8) To carry out numerical studies to calibrate and develop versatile finite element (FE) models to simulate the response of 2D FRP retrofitted exterior and 3D as-built corner beam-column joints tested under unidirectional cyclic loading, with constant axial load and bidirectional cyclic loading with varying axial loads.

1.3 ORGANISATION OF THESIS

This thesis, which consists of 11 chapters, is divided into three main parts as follows:

Part I, which includes chapters 2, 3, 4, 5 and 6, is devoted to the investigation on 2D exterior (plane frame) RC beam-column joints. In **Chapter 2**, the seismic deficiencies of pre-1970s RC frame structures, with particular attention given to the failure mechanisms of exterior beam-column joints in light of observations from recent earthquakes and findings of previous researchers, are presented. A brief summary of the research conducted on the retrofit of existing beam-column joints using FRP materials along with an overview of FRP composites are given. In **Chapter 3,** to provide a clear understanding of mechanics and behaviour, the effects of axial load variations on the seismic behaviour of RC structures, with a particular emphasis on columns and beam-column joints designed according to modern seismic provisions, are examined.

In **Chapter 4,** a procedure is proposed and explained in detail for the assessment of as-built and the design of FRP-retrofitted exterior beam-column joints. In addition to this, an analytical model to evaluate the shear resistance of the retrofitted exterior joint is developed and validated against the experimental results available in literature.

The information on the experimental programme (i.e., test units, instrumentation, test set-up, loading sequence etc.) pertaining to the 2D exterior beam-column joints, is given in **Chapter 5**. The test results are presented and analysed in **Chapter 6**. Also, in this chapter, the proposed assessment procedure is verified by the experimental results.

Investigations on the 3D corner (space frame) beam-column joints are performed in **Part II** of the thesis. In this part, emphasis is placed on studying the effects of bidirectional with concurrent varying axial loading on the seismic performance of as-is and retrofitted reinforced concrete corner beam-column joints. This part consists of three chapters. In **Chapter 7**, a review of the RC structures, with a particular emphasis placed on RC beam-column joints under bidirectional and concurrent varying axial loading is provided. The experimental programme (i.e., test setup, fabrication, loading protocol, retrofit application etc.) used in the investigation of 3D exterior joints is described in **Chapter 8** with the experimental findings of these tests being presented in **Chapter 9**. The damage limit states based on the experimental findings of this study are also provided in this chapter. Furthermore, a deformation-based retrofit design procedure is also conceptually presented.

Finally, **Part III** of the thesis includes the chapters on the numerical studies and conclusions. In **Chapter 10** the numerical studies conducted on 2D retrofitted exterior and 3D as-built corner beam-column joints are presented. Detailed information on the finite element modelling of these joints, along with analysis of results and comparison with experimental results are provided. Finally, **Chapter 11** compiles a summary of the research outcomes. The major conclusions and contributions resulting from this research, as well as recommendations for the future research are given.

1.4 REFERENCES

1. Rosenblueth E, Meli R. The 1985 earthquake: Causes and effects in Mexico City. *Concrete International*. 1986; **8**(5):23-34.
2. Okada T. Needs to evaluate real seismic performance of buildings - Lessons from the 1995 Hyogoken-nambu earthquake. *INCEDE Report No. 15*, Shibaura Institute of Technology, Japan, 1997.

3. EERI. Kocaeli, Turkey, Earthquake of August 17, 1999 reconnaissance report. *Earthquake Spectra*. 2000; **16**(Sup. A).
4. EERI. Chi-Chi, Taiwan, Earthquake of September 21, 1999 reconnaissance report. *Earthquake Spectra*. 2001; **17**(Sup. A).
5. Bruneau M. Building damage from the Marmara, Turkey earthquake of August 17, 1999. *Journal of Seismology*. 2002; **6**:357-77.
6. Sezen H, Whittaker AS, Elwood KJ, Mosalam KM. Performance of reinforced concrete buildings during the August 17, 1999 Kocaeli, Turkey earthquake, and seismic design and construction practise in Turkey. *Engineering Structures*. 2003; **25**:103-14.
7. Priestley MJN, Seible F, Calvi GM. *Seismic Design and Retrofit of Bridges*. Wiley: New York, 1996.
8. Moehle J, Mahin SA. Observations on the behaviour of reinforced concrete buildings during earthquakes. *ACI Special Publication, SP-127*. 1991.
9. Clyde C, Pantelides CP, Reaveley LD. Performance-based evaluation of exterior reinforced concrete building joints for seismic excitation. *Report No. PEER 2000/05*, University of California, Berkeley, 2000.
10. Hakuto S, Park R, Tanaka H. Seismic load tests on interior and exterior beam-column joints with substandard reinforcing details. *ACI Structural Journal*. 2000; **97**(1):11-25.
11. Ghobarah A, Said A. Relevance of beam-column damage and collapse in RC frame assessment. *Journal of Earthquake Engineering*. 2001; **5**(1):113-29.
12. Liu A. Seismic assessment and retrofit of pre-1970's reinforced concrete frame structures. *PhD Dissertation*, University of Canterbury, Christchurch, 2001.
13. Pampanin S, Calvi GM, Moratti M. Seismic behaviour of RC beam-column joints designed for gravity loads. *12th European Conference on Eartquake Engineering*, London, Paper no. 726, 2002.
14. Pantelides CP, Hansen J, Nadauld J, Reaveley LD. Assessment of reinforced concrete building exterior joints with substandard details. *Report No. PEER 2002/18*, University of California, Berkeley, 2002.
15. Chen T. Retrofit strategy of non-seismically designed frame systems based on a metallic haunch system. *M.E. Thesis*, University of Canterbury, Christchurch, 2006.
16. Hertanto E. Seismic assessment of pre-1970s reinforced concrete beam-column joint subassemblies. *M.E. Thesis*, University of Canterbury, Christchurch, 2006.
17. Gergely J, Pantelides CP, Nuismer RJ, Reaveley LD. Bridge pier retrofit using fiber-reinforced plastic composites. *Journal of Composites for Construction, ASCE*. 1998; **2**(4):165-74.
18. Gergely J, Pantelides CP, Reaveley LD. Shear strengthening of RC T-joints using CFRP composites. *Journal of Composites for Construction, ASCE*. 2000; **4**(2):408-16.
19. fib. *Externally bonded FRP reinforcement for RC structures, fib Bulletin no. 14*. Federation International du Beton (fib): Lausanne, Switzerland, 2001.
20. Ghobarah A, Said A. Seismic rehabilitation of beam-column joints using FRP laminates. *Journal of Earthquake Engineering*. 2001; **5**(1):113-29.
21. Granata PJ, Parvin A. An experimental study on Kevlar strengthening of beam-column connections. *Composite Structures*. 2001; **53**:163-71.
22. Bakis CE, Bank LC, Brown VL, Cosenza E, Davalos JF, Lesko JJ, et al. Fiber-reinforced polymer composites for construction-state-of-the-art review. *Journal of Composites for Construction, ASCE*. 2002; **6**(2):73-87.
23. Clyde C, Pantelides CP. Seismic evaluation and rehabilitation of R/C exterior building joints. *Proceedings of the Seventh US National Conference on Earthquake Engineering*, Boston, 2002.
24. El-Amoury T, Ghobarah A. Seismic rehabilitation of beam-column joints using GFRP sheets. *Engineering Structures*. 2002; **24**:1397-407.

25. Ghobarah A, Said A. Shear strengthening of beam-column joints. *Engineering Structures*. 2002; **24**:881-8.
26. Antonopoulos CP, Triantafillou TC. Experimental investigation of FRP-Strengthened RC beam-column joints. *Journal of Composites for Construction, ASCE*. 2003; **7**(1):39-49.
27. Ghobarah A, El-Amoury T. Seismic rehabilitation of deficient exterior concrete frame joints. *Journal of Composites for Construction, ASCE*. 2005; **9**(5):408-16.
28. fib. *Retrofitting of concrete structures by externally bonded FRPs, with emphasis on seismic applications, fib Bulletin no. 35*. Federation International du Beton (fib): Lausanne, Switzerland, 2006.
29. Al-Salloum YA, Almusallam TH. Seismic response of interior RC beam-column joints upgraded with FRP sheets. I: Experimental study. *Journal of Composites for Construction*. 2007; **11**(6):575-89.
30. Pampanin S, Bolognini D, Pavese A. Performance-based seismic retrofit strategy for existing reinforced concrete frame systems using fiber-reinforced polymer composites. *Journal of Composites for Construction*. 2007; **11**(2):211-26.
31. American Concrete Institute (ACI). *Guide for the design and construction of externally bonded FRP systems for strengthening concrete structures. ACI 440 2R.* ACI Committee 440, Farmington Hills, Mich., 2008.
32. Karayannis CG, Sirkelis GM. Strengthening and rehabilitation of RC beam-column joints using carbon-FRP jacketing and epoxy resin injection. *Earthquake Engineering and Structural Dynamics*. 2008; **37**(No. 5):769-90.
33. Tsonos AG. Effectiveness of CFRP-jackets and RC-jackets in post-earthquake and pre-earthquake retrofitting of beam-column subassemblages. *Engineering Structures*. 2008; **30**(No. 3):777-93.
34. Parvin A, Altay S, Yalcin C, Kaya O. CFRP rehabilitation of concrete frame joints with inadequate shear and anchorage details. *Journal of Composites for Construction, ASCE*. 2010; **14**(1):72-82.
35. Pampanin S, Akguzel U, Attanasi G. Seismic upgrading of 3-D exterior R.C. beam column joints subjected to bi-directional cyclic loading using GFP composites. *FRPRCS-8*, Patras, Greece, 2007.
36. Di Ludovico M, Prota A, Manfredi G, Cosenza E. Seismic strengthening of an under-designed RC structure with FRP. *Earthquake Engineering and Structural Dynamics*. 2008; **37**(1):141-62.
37. Engindeniz M. Repair and strengthening of pre-1970 reinforced concrete corner beam-column joints using CFRP composites. *PhD Dissertation*, Georgia Institute of Technology, Atlanta, 2008.
38. Pantelides CP, Gergely J, Reaveley LD, Volnyy VA. Retrofit of RC bridge pier with CFRP advanced composites. *Journal of Structural Engineering*. 1999; **125**(10):1094-9.
39. Antonopoulos CP, Triantafillou TC. Analysis of FRP-Strengthened RC beam-column joints. *Journal of Composites for Construction, ASCE*. 2002; **6**(1):41-51.
40. Malek AM, Saadatmanesh H, Ehsani MR. Prediction of failure load of RC beams strengthened with FRP plate due to stress concentration at the plate end. *ACI Structural Journal*. 1989; **95**(1):142-52.
41. Arduini M, Nanni A. Parametric study of beams externally bonded FRP reinforcements. *ACI Structural Journal*. 1997; **94**(5):493-501.
42. Ravinovich O, Frostig Y. Closed-form high-order analysis of RC beams strengthened with FRP strips. *Journal of Composites for Construction, ASCE*. 2000; **4**(2):65-74.
43. Ravinovich O, Frostig Y. Nonlinear high-order analysis of cracked RC bemas strengthened with FRP strips. *Journal of Composites for Construction, ASCE*. 2001; **127**(4):381-9.
44. Teng JG, Chen JF, Smith ST, Lam L. *FRP Strengthened RC Structures*. John Wiley & Sons: New York, 2001.
45. Chansawat K. Nonlinear finite element analysis of reinforced concrete structures strengthened with FRP laminates. *Ph.D.*, Oregon State University, United States -- Oregon, 2003.

46. Pesic N, Pilakoutas K. Concrete beams with externally bonded flexural FRP-reinforcement: analytical investigation of debonding failure. *Composites Part B: Engineering*. 2003; **34**(4):327-38.
47. Yang ZJ, Chen JF, Proverbs D. Finite element modelling of concrete cover separation failure in FRP plated RC beams. *Construction and Building Materials*. 2003; **17**(1):3-13.
48. Yang QS, Peng XR, Kwan AKH. Finite element analysis of interfacial stresses in FRP-RC hybrid beams. *Mechanics Research Communications*. 2004; **31**(3):331-40.
49. Lu XZ, Ye LP, Teng JG, Jiang JJ. Meso-scale finite element model for FRP sheets/plates bonded to concrete. *Engineering Structures*. 2005; **27**(4):564-75.
50. Pham HB, Al-Mahaidi R. Finite Element Modelling of RC Beams Retrofitted with CFRP Fabrics. SP-230: 7th International Symposium on Fibre-Reinforced (FRP) Polymer Reinforcement for Concrete Structures: American Concrete Institute; 2005.
51. Ali N, Bruno M, Emre Y, Viacheslav K. Finite element modeling of concrete structures reinforced with internal and external fibre-reinforced polymers. *Canadian Journal of Civil Engineering*. 2007; **34**(3):340.
52. Lu XZ, Teng JG, Ye LP, Jiang JJ. Intermediate crack debonding in FRP-strengthened RC beams: FE analysis and strength model. *Journal of Composites for Construction*. 2007; **11**(2):161-74.
53. Tan Y, Xue W-C. FEM analysis on innovative FRP/concrete composite beams. *Harbin Gongye Daxue Xuebao/Journal of Harbin Institute of Technology*. 2007; **39**(SUPPL. 2):296-9.
54. Hedong N, Karbhari VM. FE investigation of material and preload parameters on FRP strengthening performance of RC beams, I: model development. *Journal of Reinforced Plastics and Composites*. 2008; **27**(5):507-22.
55. Barbato M. Efficient finite element modelling of reinforced concrete beams retrofitted with fibre reinforced polymers. *Computers & Structures*. 2009; **87**(3-4):167-76.
56. Pampanin S. Alternative performance-based retrofit strategies and solutions for existing R.C. buildings. In: A. Ilki FK, S. Pala and E. Yuksel, editor.: London: Springer; 2009. p. 267-95.

PART I

INVESTIGATION ON TWO-DIMENSIONAL (2D) EXTERIOR RC BEAM-COLUMN JOINTS

Chapter 2 SEISMIC PERFORMANCE AND REHABILITATION OF EXISTING 2D BEAM-COLUMN JOINTS WITH FRP MATERIALS

2.1 INTRODUCTION

This chapter consists of three parts. In the first and second part the seismic vulnerability of existing reinforced concrete (RC) buildings and plane frame exterior RC beam-column joints designed to early codes before mid-1970s is examined. The typical detailing and deficiencies in the seismic performance of these structures are identified, summarised and discussed in comparison with current code requirements and based on the observations from recent earthquakes and experimental studies. The third part starts with an introduction to fibre-reinforced polymer (FRP) products, properties and applications in structural engineering. This is followed by a comprehensive review of experimental studies on upgrading the seismic performance of existing RC exterior beam-column joints with FRPs.

2.2 VULNERABILITY OF EXISTING STRUCTURES

In recent decades, the accumulation of knowledge from the observations of earthquake damage through reconnaissance visits and the major advances gained in the seismic design of RC structures through comprehensive research have become major factors in the improvement and changing of the building codes. For example, the Uniform Building Code [1] was modified to include some ductile detailing requirements as a result of the 1964 Alaska earthquake in the United States of America. After the 1971 San Fernando earthquake, the engineering community realised that improved seismic detailing would be necessary for concrete buildings [2]. Earthquake damage after the 1968 Tokachi-Oki earthquake in Japan also demonstrated the need for designing buildings with more attention towards the effects of earthquakes. A large proportion of the structural damage, especially severe damage or collapse, was found in buildings constructed prior to 1971 [3].

Improved understanding of the nonlinear dynamic response and the post-elastic behaviour of structures led to a significant development in the methods for design and detailing of reinforcement in

RC structures in the 1970s. In New Zealand, a major step was made with the introduction of 'capacity design' principles into seismic design procedure, which was first described by Hollings [4] and further developed in 1975 in a book by Robert Park an Thomas Paulay [5].

According to capacity design principles, the earthquake resistance of the structural members at the critical regions of the primary lateral force resisting system is designed in such a way that earthquake energy is dissipated in a controlled and predictable fashion. In order to reduce the inelastic deformation demand at these regions (typically referred to as "plastic hinges") sufficient ductility, intended as the ability to deform plastically without losing significant strength, should be provided through careful detailing. All other potential brittle regions are then protected against premature failure, such as shear and anchorage failure, under severe seismic loading.

In RC frames, ductility is usually achieved through stable hysteresis loops developing at the plastic hinges which are designed to be located in the beams. In this way, stable and large hysteretic energy can be dissipated without significant loss of resistance. Yielding and thus hinging of beams is also considered as more desirable than plastic hinge development in the columns because the columns have to support upper stories and failure of these may cause the total collapse of the frame. For instance, due to inadequate hierarchy of strength considerations in pre-1970s design practice, the columns may be designed only for gravity loading without taking into account the moment capacity of the adjacent beams. As a result of weaker (than beam) columns a column sway mechanism may form, leading to a soft storey mechanism in the structure (Figure 2–1a). Therefore, modern seismic design codes adopted the capacity design principles to ensure the designer implements a *beam sidesway mechanism* (Figure 2–1b) in the design rather than a *column sidesway mechanism* (Figure 2–1a) so that energy can be dissipated uniformly throughout the structure. In order to achieve this, the beams are designed to be weaker than the column, which is generally referred to as *strong column-weak beam design*.

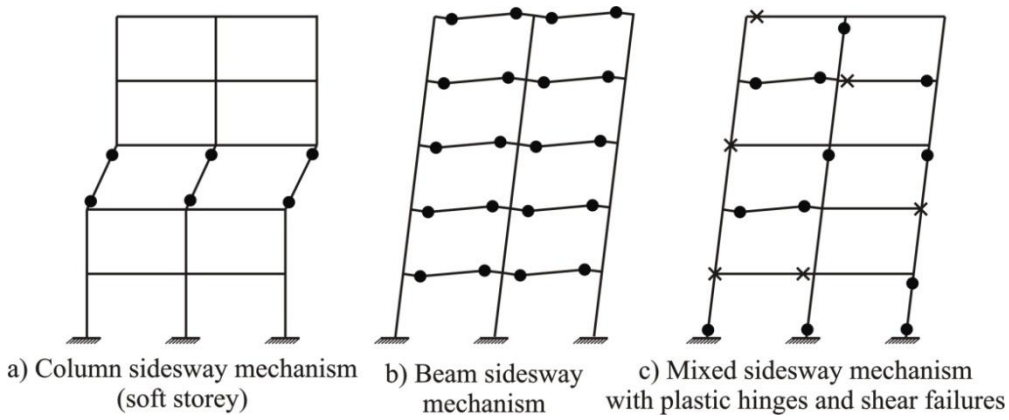

Figure 2–1 Mechanisms of post-elastic deformation of seismically loaded moment resisting frames

Before the mid-1970s, many RC building structures were designed to provide enough resistance to the code-specified lateral forces at the time of construction. For instance, wind loading was the only lateral loading considered in the design of the buildings constructed in the early 1930s [2]. In addition, allowable-stress design rather than a strength design philosophy, common before the late 1960`s, contributes greatly to uncertainty of the inelastic response [6].

As a consequence of ductility deficiency due to the poor detailing of reinforcement and the lack of a capacity design process, non-ductile modes of failure, such as shear failure of limited ductile deformation mechanisms, a mixed failure mechanism (Figure 2–1c) may result, involving different actions in different members; flexural hinges at some locations combine with shear failure of members of joints at other locations [6].

The deficiencies in the seismic performance of the existing RC frame structures have also been highlighted by the damage caused by recent earthquakes [7-15]. Inspection of collapsed and damaged buildings after these earthquakes revealed that many collapses of RC structures could be attributed to the poor quality of construction and the use of non-ductile detailing. Unfortunately, most existing structures were not built in compliance with modern seismic codes that embody much of the latest knowledge in effective earthquake-resistant building design. Apart from that, in many countries (i.e., Turkey, 1999 Kocaeli earthquake) the known seismic treat is still ignored and existing modern seismic codes are poorly implemented (i.e., [16]). Nonetheless, recent earthquakes still continue to teach important lessons with implications for practicing engineers. The most significant of these is the acknowledgement of the high vulnerability of existing structures and the need for proper assessment and retrofitting of these buildings to improve their seismic performance against future earthquakes. In Figure 2–2, examples of structural damage observed in the Marmara, Turkey earthquake of August 17, 1999 are given to illustrate a number of detailing deficiencies due to the non-ductile design.

Major problem areas and typical deficiencies of pre-1970s RC structures based on the observations after devastating earthquakes and laboratory testing of elements and subassemblages containing typical early detailing are summarized as follows:

- The column deficiencies include (a) tie configuration with 90 degree hooks; (b) tie spacing too large to provide adequate confinement; (c) lap splice located above the floor slab at regions of high moment; (d) lap splice length too short to provide force transfer; (e) tie spacing at lap splice too large, and (f) plain round type longitudinal bars with low bond capacity used.

- The beam deficiencies include (a) transverse shear ties not closed and with 90 degree hooks; (b) transverse shear tie spacing too large; (c) transverse shear ties sized for gravity loads only and are too small; (d) transverse shear ties are missing at beam mid-span; (e) top longitudinal steel reinforcement discontinuous at the beam centre so it cannot account for seismic bending or reversals; (e) bottom longitudinal steel reinforcement often discontinuous at the column faces or lapping only slightly within the beam-column joint; (f) longitudinal steel reinforcement at end frames terminating without hooks or with hooks that bend away from the joint providing inadequate development length and continuity, and (g) plain round type longitudinal bars with low bond capacity.
- The frame deficiencies include (a) weak column/strong beam characteristics making floors vulnerable to collapse from failed columns; (b) shear capacity less than that required to form plastic hinges for both columns and beam; (c) beam-column joint with inadequate shear capacity; (d) beam-column joint with inadequate confinement; (e) beams often framing eccentrically to the columns; (f) no bottom slab reinforcement passing through the column reinforcement cage in interior flat slab/column frames, and (g) gravity systems too rigid and with inadequate deformation compatibility with the lateral system [2].

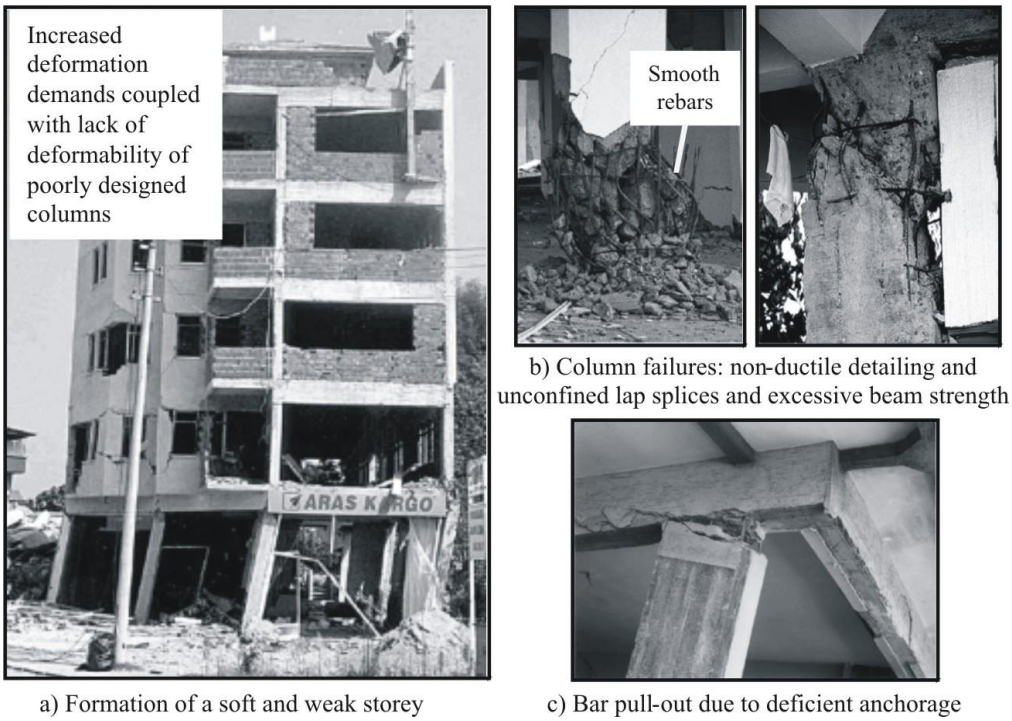

Figure 2–2 A view of collapsed RC building and close-up of the damage to moment frame elements [15]

2.3 SEISMIC PERFORMANCE OF EXISTING EXTERIOR BEAM-COLUMN JOINTS

Reinforced concrete (RC) frame structures designed before the mid-1970s are considered to have substandard detailing according to current seismic design criteria due to the structural deficiencies mentioned in the previous section. Field reports have often indicated that beam-column joints, which are one of the most vulnerable and critical structural element, often suffer shear and/or bond (anchorage) failures leading to a partial or total collapse of the structure. It is well recognized that beam-column joints play an important role in maintaining the building frame integrity under seismic action in order to preserve gravity load carrying capacity as well as lateral load strength. In this section particular attention is given in the understanding of structural characteristics of existing exterior beam-column joints based on the seismic performance information gained from the observations from recent earthquakes and experimental studies.

A joint can be defined as a column segment which also belongs to the beam at the intersection of the two members. Joints can be classified into many types depending on the kinematics constraints imposed by the surrounding members and their response to seismic actions. As an example, the joint illustrated in Figure 2–3a, part of an exterior frame, is considered a one-way interior joint for loading in the plane of the frame, however joint in Figure 2–3b is a one-way exterior joint in the orthogonal direction. In Figure 2–3c a `true` two-way interior joint can be seen which is subjected to seismic response as an interior joint in either, or both, of the two orthogonal directions [17]. Lastly, in Figure 2–3d a corner joint is shown.

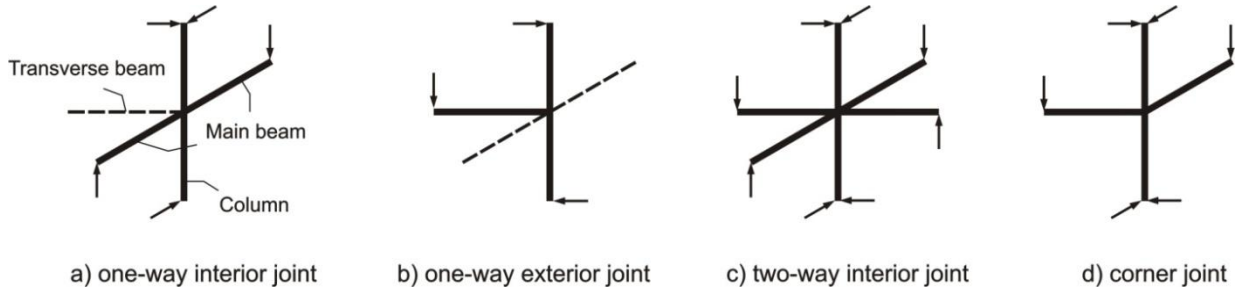

Figure 2–3 Categories of beam-column joints

The scope of this study covers two typologies: the one-way exterior joint given in Figure 2–3b and the corner joint as presented in Figure 2–3d. Throughout this thesis, the one-way exterior joint is referred to as a “2D plane frame beam-column joint”, “2D exterior beam-column joint” or “2D joint”; and the corner joint is referred to as a “3D space frame beam-column joint”, “3D corner beam-column joint” or “3D corner joint”. Other joint types such as one-way and two-way interior joints are ignored because they fall outside the scope of the present study. In addition, the terms “joint”, “connection”

and “subassemblage” are equally adopted to indicate the entire substructure extracted from a frame and given by columns, beams, and their intersection zone. The term “joint region” or “joint panel” is restricted to the portion defined by the beam-column intersection.

Observations after earthquakes have emphasised that in many cases the collapse of many residential RC frame buildings were caused by the failure of seismically inadequate building joints, especially for the exterior and corner beam-column connections without beams framing into all four sides (Figure 2–4) [18]. Although the frame of the structure remained intact, many of the beam-column joints were severely damaged due to the lack of transverse reinforcement in the joint and inadequate beam bar anchorage. It was also observed that, even when the beams and columns in RC concrete frame buildings are slightly damaged after the main shocks or aftershocks, the integrity of these buildings may be threatened due to the risk of heavy joint damage.

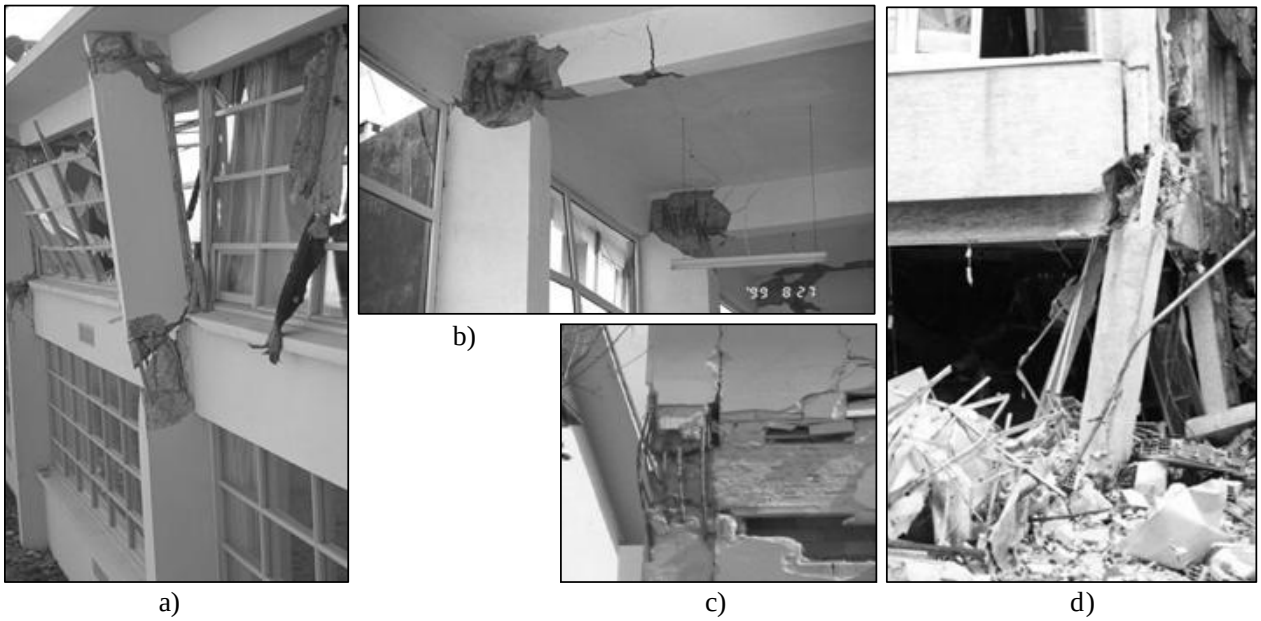

Figure 2–4 Damage to exterior beam-column joints: a) one-way exterior joint (1964 Alaska (US) earthquake) [19]; b) one-way exterior joint (1999 Kocaeli (Turkey) earthquake) [10]; c) corner joint (2009 L’Aquila (Italy) earthquake [20]; d) corner joint (1999 Kocaeli (Turkey) earthquake) [10].

A considerable amount of research has been carried out in the past on existing exterior beam-column joints with little or no transverse reinforcement in the joint region to determine seismic performance and failure mechanisms. Although there is a large database of experimental work published on substandard existing beam-column joints in literature, a review of relevant research on one-way exterior beam-column joints without any slabs and tested under cyclic lateral loading are given. Detail information on the effects of biaxial loading on RC structures with a particular emphasis given to 3D space frame corner beam-column joints is provided in Part 2 of the thesis.

Hakuto *et al.* [21] tested two full-scale one-way exterior beam-column joints with substandard reinforcing details typical of buildings constructed in New Zealand before the 1970s (Figure 2–5a). The units contained very little transverse reinforcement in the members and in the joint core. In Unit O6, the beam bar hooks were bent into the joint core whereas in unit O7 the hooks at the ends of the beam longitudinal bars were bent out of the joint core. For both units deformed longitudinal reinforcement was used. The units were tested under simulated seismic loading with no axial load applied to the columns. Test results indicated that when the ends of the hooks were bent into the joint core, seismic performance was significantly improved. The unit O6 was able to withstand a nominal joint horizontal shear stress of $0.0053f_c`$ when plastic hinging occurred in the beam (Figure 2–5b). However, Unit O7 with the hooks bent out of the joint core behaved unsatisfactorily during testing (Figure 2–5c). It failed in shear with a maximum nominal joint horizontal stress of $0.0045f_c`$.

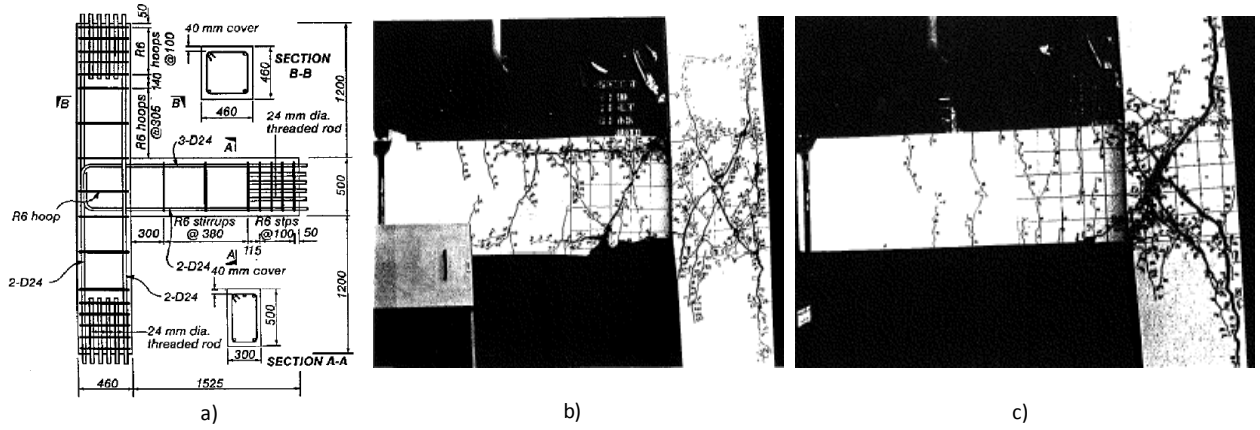

Figure 2–5 Experimental study by Hakuto *et al.* [21]: a) details of unit O6; b) observed cracking of unit O6 near end of testing; c) observed cracking of unit O7 near end of testing

Test results indicated that after diagonal tension cracking in the joint core, the beam and column forces are transferred across the joint core mainly by a diagonal compression strut. The crushing of the diagonal compression strut will occur when the compressive strength of the strut is sufficiently weakened by diagonal tension strains and by the repeated opening and closing of diagonal tension cracks in alternating directions. The stage of diagonal compression failure is best estimated by determining the value of horizontal shear stress when a limiting diagonal compressive stress is reached. Accordingly, the most simple failure criterion for a beam-column joint without shear reinforcement would appear to be the diagonal compression failure criteria. The main mechanisms of joint shear resistance in units O6 and O7 are illustrated in Figure 2–6. In Figure 2–6b, the bearing stresses at the bend act according to strut and tie model considerations, and the diagonal compression strut effectively engages the beam reinforcement. The detail of Figure 2–6c does not provide an effective node point at the top of the diagonal compression strut unless a considerable quantity of

column hoops exists above the joint core to equilibrate the horizontal component of force of the compression strut, as shown in Figure 2–6d.

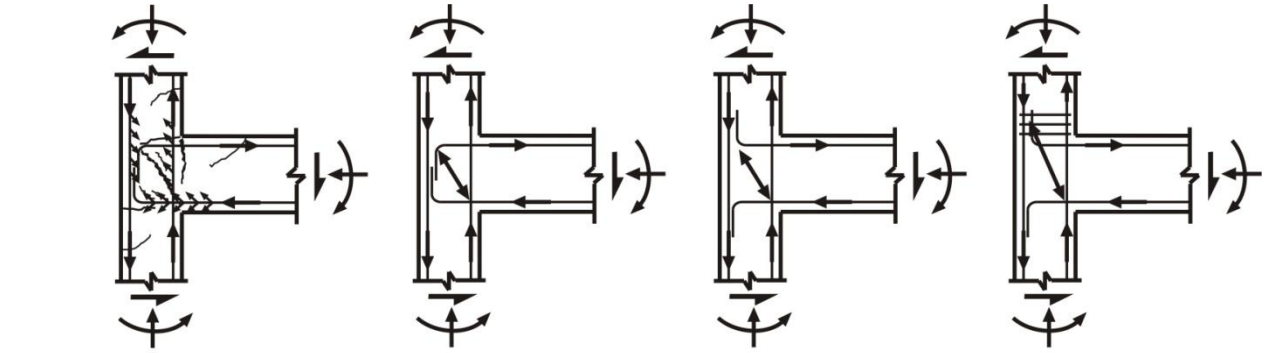

Figure 2–6 Main mechanisms of joint shear resistance of exterior beam-column joints with beam bars bent into the joint or outside the joint (modified after [21])

An assessment method based on the limiting of shear strength of a joint at the onset of initial cracking in the joint panel was also discussed by the authors. Although this approach seems to be valid for the assessment, it is noted that this criteria may be too conservative due to the fact that the joint core may be capable of transferring significantly higher shear forces after diagonal tension cracking by means of a diagonal compression strut. The joint, however, does not necessarily reach its maximum lateral load-carrying capacity when diagonal cracking first occurs. Diagonal tension is important because tension strains at right angles to the concrete diagonal compression strut will weaken the compressive strength of the strut. In this case, $k_1\sqrt{f_c`}$ can be used for a diagonal tension criterion, since the tensile strength of the concrete is a function of $\sqrt{f_c`}$ where k factor is obtained from experimental testing and $f_c`$ is the concrete compression strength. Diagonal compression failure occurs when a limiting joint shear stress $k_2 f_c`$ is reached, and would appear to be a more appropriate failure criterion than the assumed failure criteria for the joint as a certain level of nominal shear stress. The main reason is the effect of column axial load is taken into account explicitly in the stress state of the joint region.

Beres *et al.* [22] reported the results of thirty-four beam-column joint subassemblies which were constructed in full scale according to non-seismic code provisions in North America. They were tested under simulated seismic loading. Fourteen experiments were conducted on exterior beam-column joints to study the effects of column axial force, transverse confinement, and amount of reinforcement in the joint. Damage to the specimens was observed in the joint-panel and the adjacent regions leading to a critical loss of strength. In some specimens the initiation of the damage and the subsequent strength degradation was attributed to the positive beam reinforcement, buckling of the longitudinal column bars at the lightly confined splice region, and prying of the bent-down negative reinforcing at

exterior connections. The beneficial effects of a higher axial load on the column were emphasised by researchers. In all cases the specimens with higher axial load delayed the onset of critical shear cracking and also helped to provide better confining action to the embedded bars, delaying their incipient pullout. For exterior joints the peak strength values were reached at about 1.5-2.7% interstorey drift with about 40% scatter of the peak capacities. Higher column axial force or the presence of 2-#3 ties within the joint produced higher maximum strength capacities and a more gradual strength degradation. Specimen details and experimental result of an exterior specimen are given in Figure 2–7.

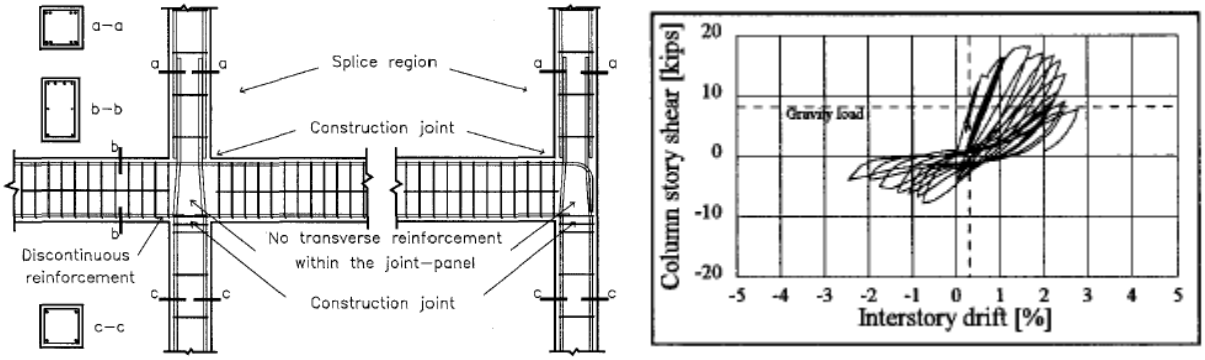

a) b)

Figure 2–7 Experimental study by Beres *et al.* [22]: a) elevation view of an interior and exterior beam-column joint region; b) typical column shear force vs. interstory drift plots

Calvi *et al.* [23] and Pampanin *et al.* [24] reported the results of experimental programme on existing (as-built) RC frame subassemblies and systems comprised of quasi-static tests carried out in the laboratory of the Department of Structural Mechanics at the University of Pavia. Six one-way beam-column joint subassemblies (including two exterior knee joints, two exterior tee joints, and two interior joints) and a three-storey three-bay frame system (referred to as the *Pavia frame*) were tested (Figure 2–8).

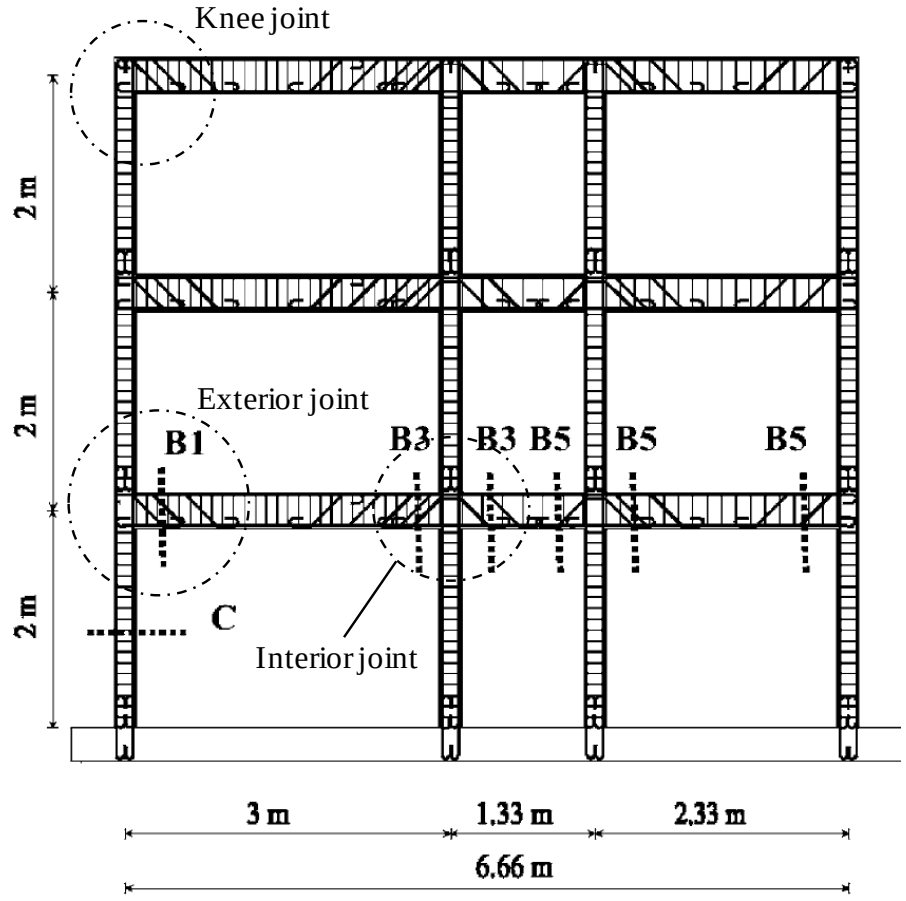

Figure 2–8 Frame tested at University of Pavia (from Calvi *et al.* [23])

The experimental tests on gravity load designed beam-column subassemblies and frame provided interesting information on local and global damage mechanisms. The observed global response of the three-storey frame system presented some peculiarities when compared with typical weak-column, weak-beam inelastic mechanisms. Severe damage was observed in the exterior tee-joints at the first storey level, as well as (more moderate), damage at the second storey level. In addition, as expected, hinging of the column base sections at the ground level occurred. However, as evident from the experimental deformed shape shown in Figure 2–9, a pure soft storey mechanism did not occur at the first floor, as would have been reasonably expected from preliminary analytical predictions if the joint damage/inelastic behaviour had not been considered.

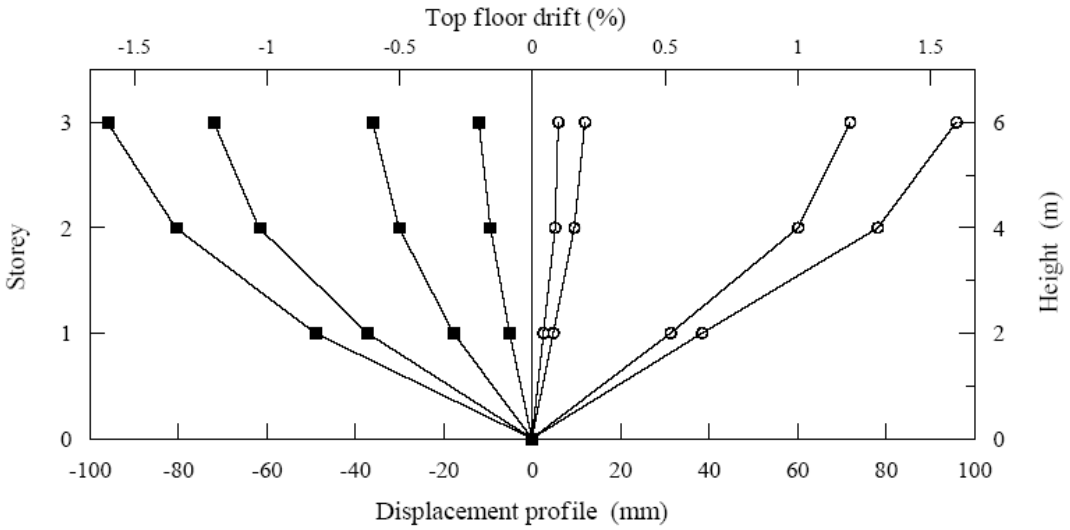

Figure 2–9 Pavia frame displacement profile at increasing level of top drift

Pampanin *et al.* [24] presented the results of a series of tests on six 2/3 scale beam-column subassemblies designed for gravity only with structural deficiencies typical of Italian construction practice between the 1950`s and 1970`s. These deficiencies are characterised by the use of smooth bars, inadequate detailing of reinforcement, poor anchorage with hooked-ended bars and absence of capacity design principles (Figure 2–10a). Among the specimens, two exterior tee joints were tested under quasi-static loading. In order to better represent the actual conditions of the stress level in the joint due to the sway of the frame building, the column axial load was varied by means of a hydraulic jack during testing. Test results indicated extensive joint shear damage in the joint panel zone observed in the concrete leading to a large shear distortion. It was observed that the combination of hook-end anchorage with plain round bars led to a peculiar brittle mechanism consisting of the expulsion of a concrete "wedge" at the outer side of the column (Figure 2–10b). This was caused by the combined shear damage in the joint region and concentrated compression force at the end of the beam longitudinal bars. Development of the concrete wedge mechanism is schematically illustrated in Figure 2–11. As a result, a brittle local failure and loss of bearing-load capacity was observed.

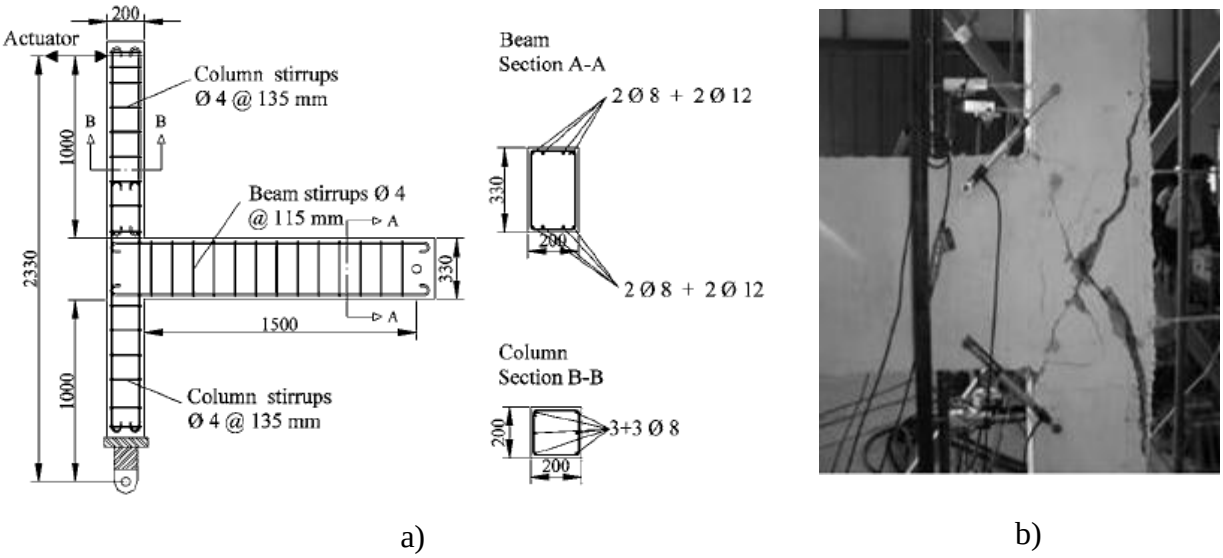

a) b)

Figure 2–10 Experimental study by Pampanin *et al.* [24]: a) dimensions and reinforcement details; b) observed concrete wedge mechanism

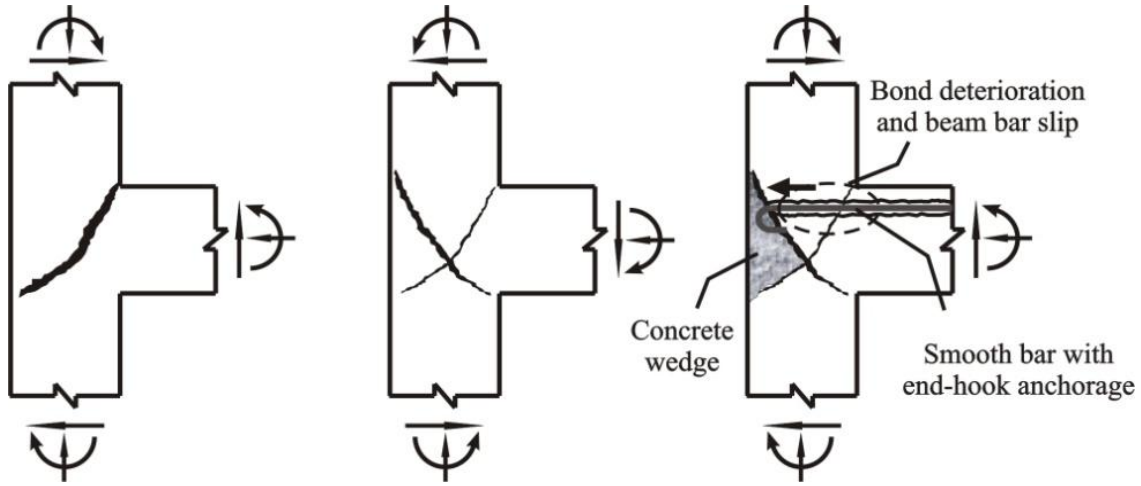

Figure 2–11 Development concrete wedge mechanism as described in [24]

In light of aforementioned experimental observations either on prototype frame or on exterior subassemblages, the term *shear hinge* was introduced [23, 25] to describe the shear failure mechanism, alternative and dual to a typical flexural plastic hinge. The shear hinge mechanism can delay the occurrence of undesirable column sway mechanism, because the concentration of shear deformation in the joint area can reduce the deformation demand on adjacent structural members, also spreading the interstorey drift demand along two storeys. However, the main shortcoming of a shear hinge mechanism is the intrinsic lack of ductility due to the rapid strength degradation in the joint after first cracking. The observed global mechanism, related to joint damage, suggests the definition of a shear hinge. Fundamental differences with the familiar concept of *flexural plastic hinge* can related to

(a) the structural behaviour activating the hinge: shear instead of flexure; (b) the post-elastic behaviour: while a plastic hinge mechanism is typically expected to provide satisfactory ductility capacity, a shear hinge might be characterised by severe strength degradation; (c) energy dissipation characteristics: the shear damage mechanism is not expected to provide a reliable source of energy dissipation under cyclic loading as is the case of a stable hysteresis under ductile flexural behaviour.

This research also indicated that alternative damage and failure modes may be encountered in older beam-column joints depending on the type (exterior or interior) of joint and the adopted structural details as shown in Figure 2–12 for exterior joints with no transverse reinforcement. The anchorage solution adopted in an exterior beam-column joint is of particular importance because it affects the efficiency of the shear transfer mechanism in the joint region, which strongly depends on a compression strut mechanism upon the onset of diagonal cracking in the joint. For example, in the case of the anchorage solution adopted in Figure 2–12a where the beam bars are bent into the joint, a limited resistance against the horizontal expansion of the joint is provided, until the hook opens under the combined action of the diagonal strut and the pulling tension force in the beam reinforcement. Another typical older construction practice, which is widely used in New Zealand and Japan, can be seen in Figure 2–12c. As expected, rapid strength degradation would occur due to the lack of an effective node point for the development of an efficient compression strut mechanism in the joint panel. In Figure 2–12d, the worst case scenario of construction practice which was used widely in the Mediterranean, is illustrated.

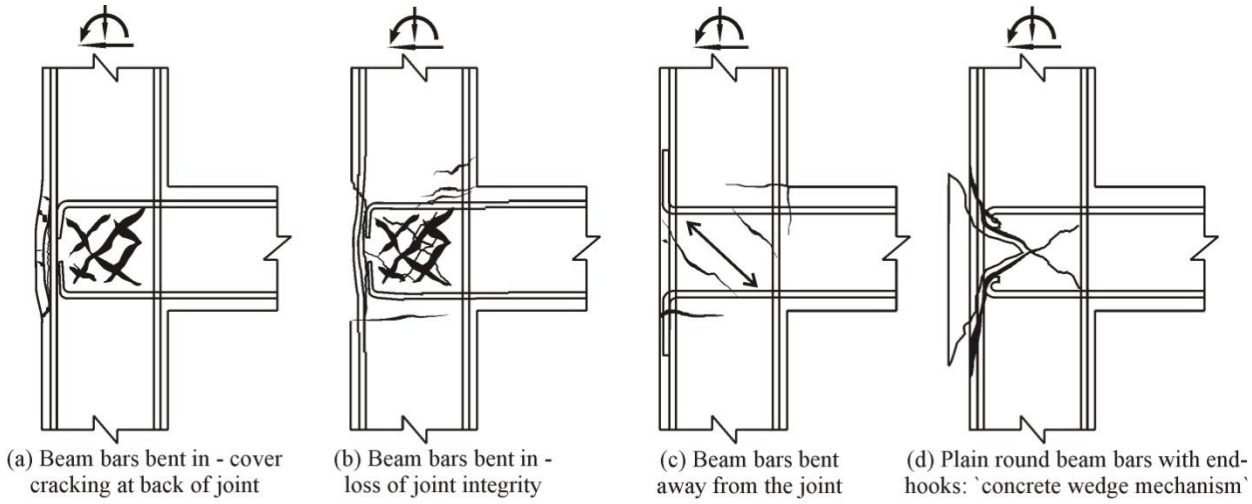

Figure 2–12 Alternative damage mechanisms expected in exterior joints depending on the structural detailing (after [23-25])

Ghobarah and Said [26] tested a full-scale RC external beam-column joint. The specimen was tested under cyclic loading applied at the beam tip. The column was subjected to a axial load level of $0.2f_c`A_g$. For the control specimen, T1, before the first yield of longitudinal beam steel, a diagonal shear crack was noted in the joint area forming an X-pattern. At failure, these cracks extended to the back of the column (Figure 2–13). A high rate of strength deterioration was observed at a ductility factor of 2.

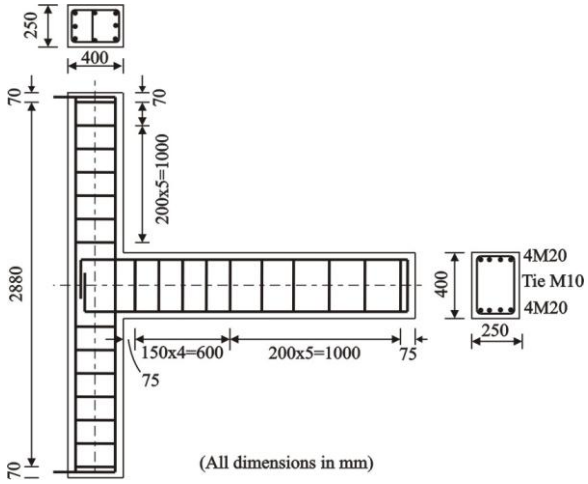

a)

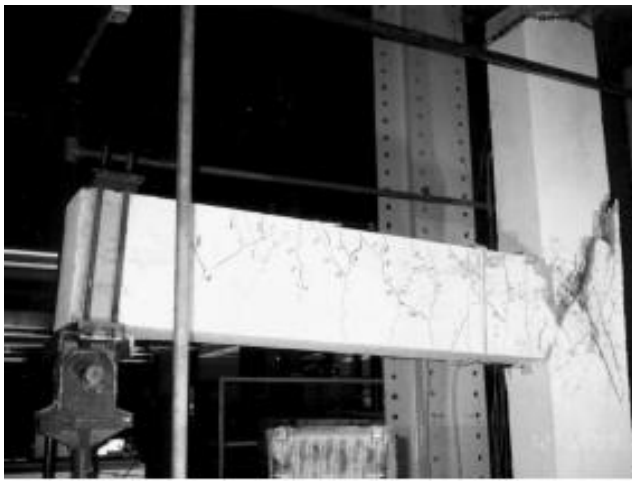

b)

Figure 2–13 Experimental study by Ghobarah and Said [26]: a) specimen details; b) joint shear failure

Kuang and Wong [27] carried out reversed cyclic-load tests on five full scale RC exterior beam-column joints to investigate the effects of different types of beam bar anchorage and location of lap splices in column reinforcement on the shear strength and hysteretic behaviour. Test specimens were detailed according to BS 8110 (1997) [28], which is the building design code of practice in regions of no or low-to- moderate seismicity. As a consequence, this building design code does not generally include any provision for seismic resistance considerations. There is no transverse reinforcement placed in the joint regions. Specimens were tested under reversed cyclic loading and columns of all the specimens were subjected to an axial load of approximately 13 to 16% of the column's compression capacity ($f_c`A_g$). The specimens performed poorly in terms of shear strength except in the case of the specimen in which U-anchorage (hooks at the ends of the beam bars were bent into the joint) was adopted, and also the laps of both tension and compression bars were located at the end of the beam region. All specimens failed in joint shear. No buckling of the longitudinal reinforcement in columns was observed. The following conclusions were drawn from the study (a) the type of beam reinforcement anchorage had a significant effect on the performance; (b) laps in column reinforcement located at the column end zones did not seem to affect the shear strength of beam-column joints; (c)

shear failure in the joint may occur before the yielding occurs in the beams; (d) the criterion of initial diagonal tension cracking provides very good correlations with the test data.

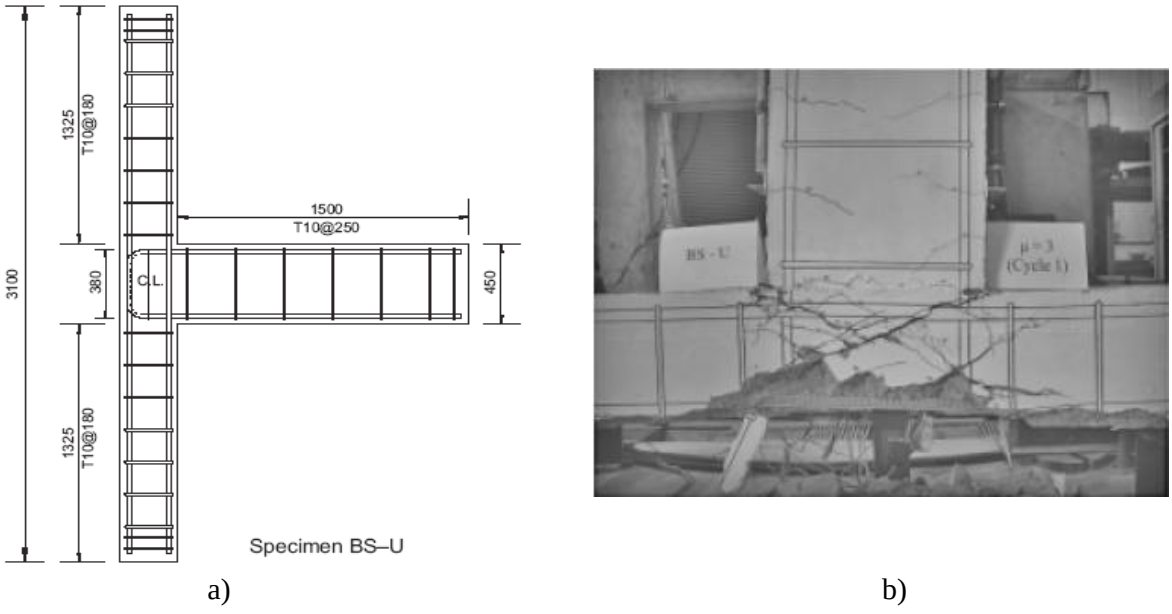

a) b)

Figure 2–14 Experimental study by Kuang and Wong [27]: a) details of unit BS-U; and b) failure mode

Four half-scale RC exterior beam-column joints of a typical RC building built in 1964, were tested by Clyde *et al.* [29] to investigate their behaviour in a shear-critical failure mode. There is no transverse reinforcement within the joint core, and the beam longitudinal bars are not adequately anchored in the connection. The joints were subjected to quasi-static cyclic loading at the end of the beam. An axial compressive load equal to $0.10f_c`A_g$ was applied to two of the specimens. The other two specimens received an axial compressive load of $0.25f_c`A_g$. Apart from a very slight variation in the peak lateral load capacity, all joints failed through the development of the limiting shear capacity. It was also observed that the specimens subjected to a lower axial load were over one and a half times as ductile as the beam-column joints with higher column compression. Furthermore, higher axial load levels improved the shear capacity of the joint. The increase was 8% in shear capacity as a result of increased confinement due to axial compressive load. Details of the specimens and some failure close-ups are given in Figure 2–15.

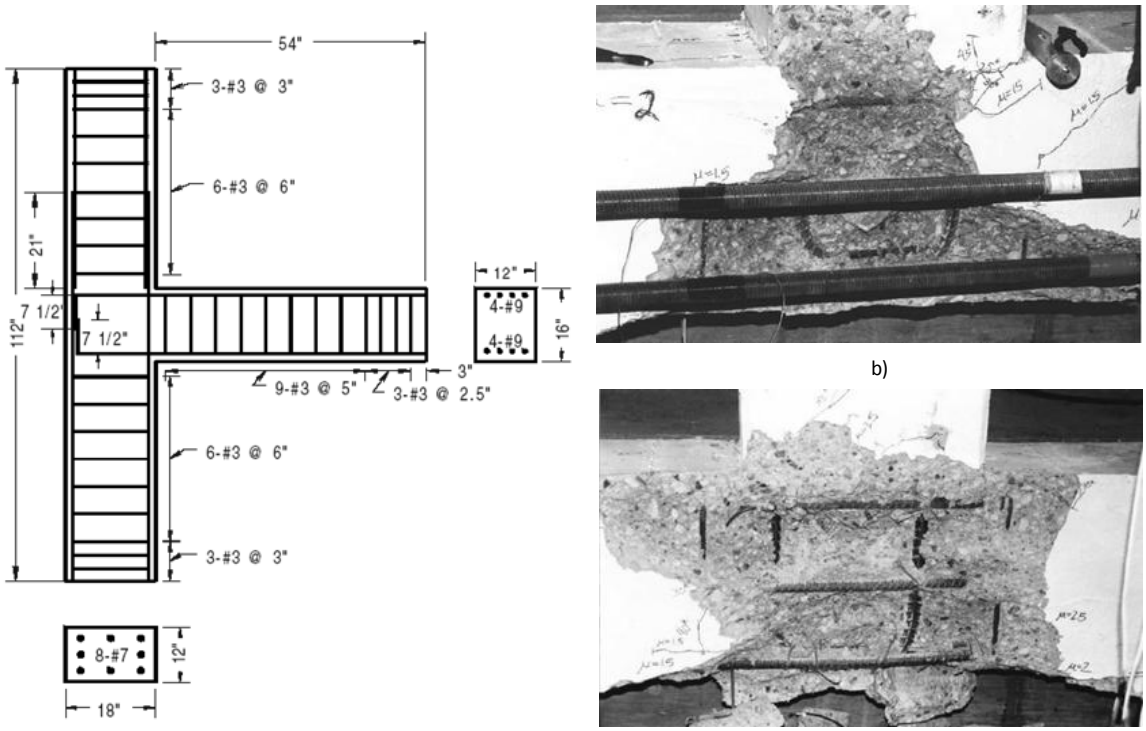

Figure 2–15 Experimental study by Clyde *et al.* [29]: a) details of units; b) damage to specimen under $0.10f_c`A_g$ axial load level; c) damage to specimen under $0.25f_c`A_g$ axial load level

A total of six full-scale RC exterior beam-column joints in RC buildings designed to the code in the U.S before 1970 were tested under quasi-static cyclic loading by Pantelides *et al.* [30]. There was no transverse reinforcement within the joint core. However, all units satisfied the requirement for column to beam flexural capacity ratio, and the top beam reinforcement into the joint satisfied bar anchorage requirements. The influence of two different levels of axial compression load, $0.10f_c`A_g$ and $0.25f_c`A_g$ in the columns was investigated. The research has shown that there are primarily two failure modes related to joints with substandard details described above; a bond-slip failure mode, and a joint shear failure mode. It was observed that the presence of the higher axial load was beneficial in terms of the joint strength coefficient and principal tensile stress, but was detrimental for displacement ductility and energy dissipation. The four units with the joint shear failure mode failed at the end of the test due to loss of the column axial compression capacity. The remaining two units with the bond-slip failure mode failed at the end of the test due to the loss of lateral load capacity. The units with a bond-slip failure mode had a lower joint strength coefficient, ultimate plastic shear angle, principal tensile stress, and energy dissipation than the units with the joint shear failure mode. Details of the specimens and some failure close-ups are given in Figure 2–16.

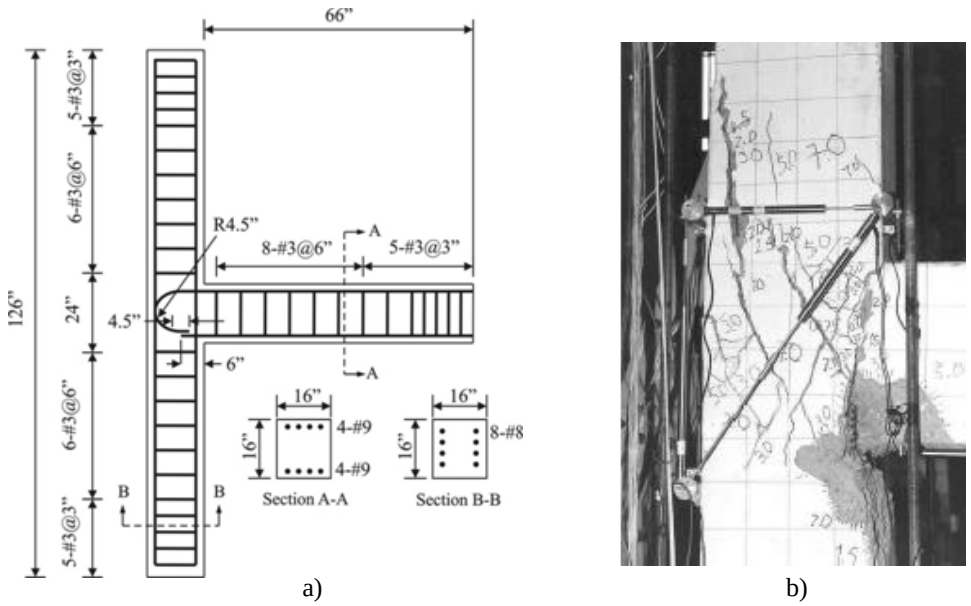

a) b)

Figure 2–16 Experimental study by Pantelides *et al.* [30]: a) units 1 and 2; b) damage to unit 1

Hertanto [31] and Chen [32] performed a series of tests on six two-third scale exterior beam-column joints with typical detailing of pre-1970s buildings under quasi-static cyclic loading in the Structural Laboratory of the University of Canterbury. The reinforcement detailing and beam dimensions were varied to investigate their effect on the seismic behaviour. Four specimens used conventional deep beam solutions, with two of them using deformed longitudinal bars and beam bars bent into the joints and the two others using plain round longitudinal bars and beam bars with end hooks. The other two specimens used a wide and shallow beam configuration, more appealing for architectural reasons and still adopted in several seismic prone countries, one with deformed longitudinal bars and beam bars bent in to the joint, the other with plain round longitudinal bars and beam bars with end hooks. The space frame units used plain round longitudinal reinforcement and the beam bars end were hooked into the joint. One stirrup was placed in all units` joints. All units were tested under varying axial load to simulate the column behaviour in the real structure under earthquake loading. Test results highlighted the significance of the type of longitudinal reinforcement in the performance. The use of plain round bars can lead to joint shear failure, which will result in severe strength degradation. It was also noted that the use of shallow beam in the exterior beam-column joint could avoid the joint cracking due to the beam size although the strength provided was lower when compared with the use of a deep beam with equal moment capacity. The variation of axial load can both strengthen and weaken the joint core. In the positive loading direction, the joint strength is slightly higher than in the negative direction, due to the different axial load applied to the column. Alternative strength degradation curves corresponding to different reinforcement detailing of beam-column joint units were

proposed based on the test results. Final appearances and crack developments of the selected specimens are given in Figure 2–17.

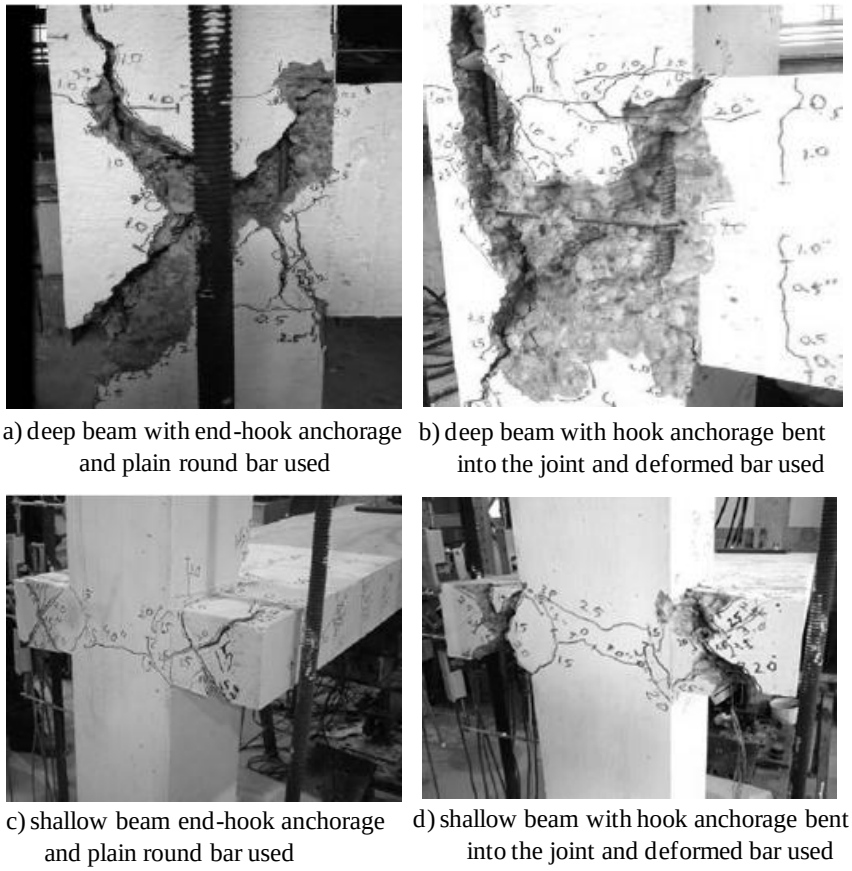

a) deep beam with end-hook anchorage and plain round bar used

b) deep beam with hook anchorage bent into the joint and deformed bar used

c) shallow beam end-hook anchorage and plain round bar used

d) shallow beam with hook anchorage bent into the joint and deformed bar used

Figure 2–17 Final appearances and crack developments of the selected specimens in experimental study by Hertanto [31] and Chen [32]

Parvin *et al.* [33] tested three as-built full scale existing beam-column joints designed for gravity load with common pre-1970s deficient reinforcement details (Figure 2–18) under cyclic loading. The first specimen U.S.2 had continuous longitudinal reinforcement and was tested under 24% of the column axial load capacity. The remaining specimens namely, U.S.3 and U.S.4, had lap splicing at the column and were tested under 24 and 12% of the column axial load capacity respectively. All specimens had no ties in the joint core and the beam bottom steel reinforcing bars were inserted in the joint with a short embedment length of 150 mm typical of pre-seismic code construction in the United States. In all three control specimens two modes of failure, namely the joint shear core and debonding of the beam bottom bar reinforcements, were observed (Figure 2–18). It was also observed that in the pull direction of loading, due to the adequate anchorage of the longitudinal reinforcement, shear forces were transferred to the joint core. Since no transverse reinforcement was present within the joint core to resist the shear stresses, the joint shear forces were resisted by only the concrete and the yielding of

the beam longitudinal reinforcements was not observed. It can be concluded that the lack of transverse reinforcements at the joint region was the main governing deficiency in the pull direction of loading.

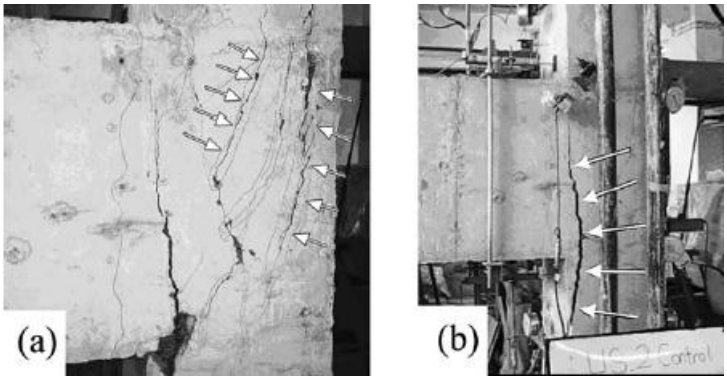

Figure 2–18 Experimental study by Parvin *et al.* [33]: Crack patterns a) due to the shear failure; b) due to the beam bottom longitudinal reinforcement

In the push direction of loading, the resulting tension at the bottom fibre of the beam cross section caused slippage of the longitudinal bars inside the joint that were shortly embedded without enough development length in the column. Thus, an abrupt reduction in the lateral load carrying capacity of all control joints was observed. In the push direction of loading, the shear deformations at the joint region were insignificant and nearly no shear damage was observed (Figure 2–19). This was due to the slippage of the bottom rebars, which in turn resulted in the separation of the beam from the column at the joint interface. Figure 2–19 also clarifies these phenomena by providing the direction of the internal forces in the longitudinal reinforcements that created shearing forces at the joint region, which then resulted in diagonal shear cracks.

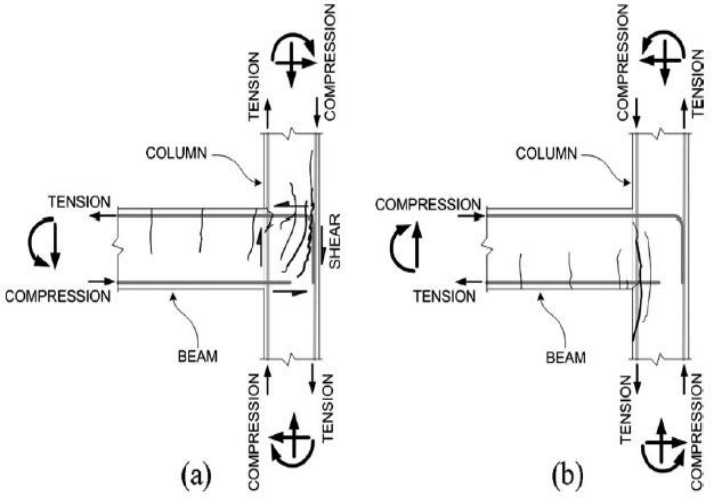

Figure 2–19 Internal forces and crack patterns: a) pull direction of loading; b) push direction of loading (after Parvin *et al.* [33])

Genesio and Sharma [34] tested five full scale beam-column connections under reversed cyclic loading without any axial load application on the columns. All the specimens were detailed according to the pre-1970s construction practice with different anchorage schemes employed in the joint regions (Figure 2–20). The specimens JT1-1, JT2-1 and JT4-1 were designed to fail in shear in the joint panel, before the yielding of the beam bars occurred. For the specimen JT3-1 an interaction between joint shear failure and pullout of the beam bottom bars was expected, due to the straight anchorage.

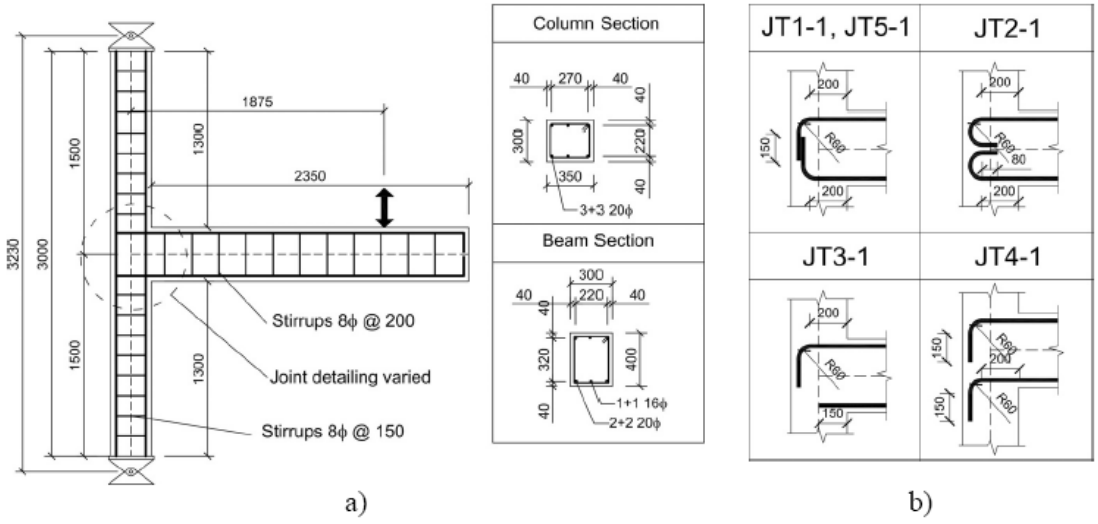

Figure 2–20 Experimental study by Genesio and Sharma [34]: Specimen details

With the tests JT1-1 to JT4-1 the influence of the anchorage of the beam bars on the shear strength of joints without transverse reinforcement in the core was shown. The anchorage of the beam bars with 90°-hooks was confirmed to be much more efficient than 90°-hooks bent out, straight anchorage and plain round bars with 180°-hook. In the joint JT5-1 the flexural failure of the beam occurred after the first diagonal cracking of the joints was shown that this failure mode does not provide any improvement in the ductility of the beam-column connection in comparison to the shear behaviour without yielding of the beam bars.

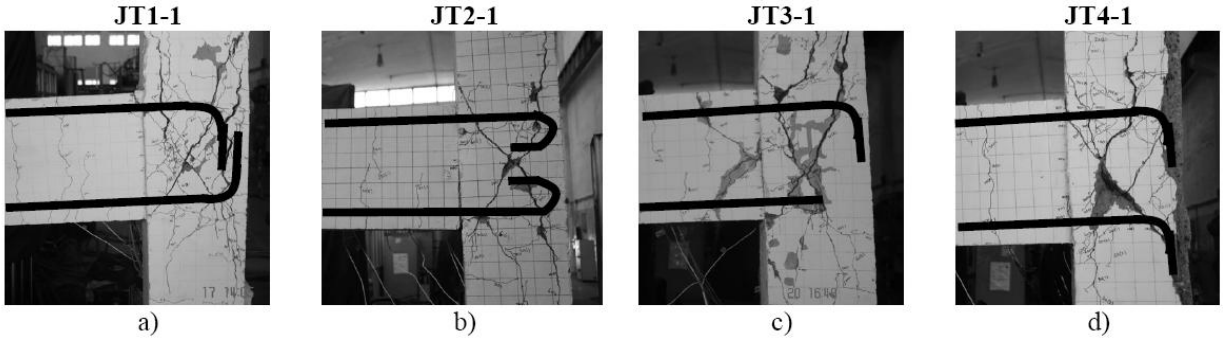

Figure 2–21 Experimental study by Genesio and Sharma [34]: Influence of anchorage of beam bars in the core on the cracking pattern

2.4 RETROFIT OF EXTERIOR RC BEAM-COLUMN JOINTS WITH FRP MATERIALS

Several rehabilitation techniques have been investigated and adopted in practical applications to enhance the seismic performance of the existing beam-column joints. These techniques are ranging from conventional techniques, such as epoxy repair [35-39], removal and replacement [40, 39, 41], reinforced or prestressed concrete jacketing [42-45, 21, 46-48], steel jacketing [42, 37, 45, 49, 50], concrete masonry unit jacketing or partial masonry infills [51, 45]. A comprehensive review of the state of the art on the use of conventional strengthening techniques can be found in Engindeniz *et al.* [52].

More recent approaches include the use of a diagonal metallic haunch system introduced at the beam-column connections to protect the joint panel zone from extensive damage and brittle shear mechanisms [53] or employing of selective-weakening and joint post-tensioning as a seismic retrofit strategy and technique for non-ductile exterior beam-column joints [54]. An overview of these more recently developed retrofit techniques can be found in Pampanin [55].

The aforementioned techniques generally referred to as conventional or traditional techniques, cause various difficulties in their practical application. To overcome the difficulties associated with these techniques recent research efforts have focused on the use of epoxy-bonded fibre-reinforced polymers (FRPs). FRP reinforcing systems have been widely used in various forms (e.g., epoxy-bonded flexible sheets, shop manufactured strips, and near-surface-mounted rods) for upgrading the existing beam-column joints since 1998. The FRP systems were shown to provide significant benefits and advantages over the conventional techniques including:

- higher strength-to-weight ratio (≈15 and 35, respectively, for glass and carbon, when compared with that of steel)
- higher stiffness-to-weight ratio (≈1 and 3, respectively, for glass and carbon, when compared with that of steel)
- high corrosion resistance
- lighter unit weight, resulting in less-expensive equipment for economical handling, shipping, and transportation as well as lighter erection equipment
- high durability, leading to lower life-cycle costs
- easier-to-control tension crack growth by the confining of the concrete
- better customization for specific needs and tailorability
- fast field installation, easy applicability and limited disruption to building occupancy

- no significant increase in member size
- simple onsite corrections in the case of installation defects of bonding of FRP with concrete substrate

However, some limitations exist to FRP composite wrap applications:

- uncertainties about the durability of FRPs, as their long-term performance data is limited
- concerns of fire resistance, adverse effects from smoke and toxicity, and poor resistance of resins to UV rays
- limited knowledge of material properties and application procedures [56]

In the following section an overview of FRP composite materials, such as clarification of some technical terms relevant to this technology, properties of basic constituent materials and manufacturing methods are given. This is followed by a concise survey of the state-of-the-art survey of published experimental studies on upgrading the seismic performance of deficient exterior plane frame beam-column joints using FRP materials. Note that, the scope of this section is limited to the rehabilitation of plane frame exterior beam column joints using FRP materials, hence other cases such as interior beam-column connections and exterior beam-column joints with slab are not included due to the irrelevancy in relation to the scope of this study. Rehabilitation of 3D corner beam-column joints using FRP materials are covered in Chapter 8. In the last subsection, design guides, codes and specifications for design with FRP materials, which are most widely referred to by the international engineering community are presented.

2.4.1 An overview of FRP Composites: Definitions, raw materials and manufacturing methods

Fibre-reinforced polymer reinforcing systems for strengthening deficient concrete structural members and for repairing damaged or deteriorated concrete structures have been used since mid-1980s [57]. Historically, composites were first applied as flexural strengthening materials for RC bridges by Meier [58] and Rostasy [59], and as confining reinforcement of RC columns by Fardis and Khaili [60] and Katsumata *et al.* [61]. Since the first research efforts, the range of applications have expanded to include the strengthening of various structural elements such as beams, slabs, columns, shear walls, chimneys, vaults, domes and trusses. A review of the state of the art on the subject can be found in literature [62-64, 57].

The term *composite material* (often referred to as *composite*) is a generic term used to describe a judicious combination of two or more materials to yield a product that is more efficient from its constituents. One constituent is called the *reinforcing* or *fibre phase* (one that provides strength); the other in which the fibres are embedded is called the *matrix phase* [56]. The matrix acts as a binder and holds the fibres in the intended position, giving the composite material its structural integrity by providing shear transfer capability. Another function of the matrix is to protect the fibre against the external environment into which the composite is placed. Fibre forms used in FRP products for structural engineering are called as *continuous fibres* because they are indefinitely long. These fibres are used at a relatively high volume percentage (from 20 to 60%) to reinforce the polymer resin: thus the term *fibre-reinforced polymer* (FRP). This combination of two dissimilar materials leads to a component that has enhanced strength, stiffness, and toughness over the properties of the individual parts. Three types of fibres are commonly used to produce strengthening sheets and fabrics: glass fibres, carbon fibres, and aramid fibres.

Glass fibres have the lowest cost compared to the other two civil engineering fibres carbon and aramid. In addition to this, their very high *specific strength* (the ratio of the tensile strength of a material to its unit weight) makes them one of the most popular structural materials in the upgrading of concrete structures. Glass is an amorphous inorganic compound of primarily metallic oxides that is produced in fibrous form. The diameter of an individual glass fibre or filament ranges from approximately 3 to 24 μm. Two hundred individual filaments are formed into one strand and, during the production stage, many strands are formed. A glass fibre has a distinctive bright colour to the naked eye and considered to be an isotropic material. Approximate properties of glass fibres are given in Table 2-1. The most important grades of glass for the rehabilitation of structural members are as follows:

- *E-glass* (electrical glass) has good heat and electrical resistance and is used for general-purpose structural applications, as well as in the retrofitting of structural components.
- *S-glass* is used to produce the high-performance fibres used primarily in the aerospace industry, due to its greater strength, corrosion and heat resistance.

Table 2-1 Approximate properties of common grades of glass fibres [57]

Grade of Glass Fibre	Density [g/cm^3]	Tensile Modulus [GPa]	Tensile Strength [MPa]	Max. Elongation (%)
E	2.57	72.5	3400	2.5
A	2.46	73	2750	2.5
C	2.46	74	2350	2.5
S	2.47	88	4600	3.0

Carbon fibre is a solid semicrystalline organic material, consisting on the atomic level of planar two-dimensional arrays of carbon atoms. Carbon fibres have diameters from 5 to 10 μm with a characteristic charcoal-black colour. They are used in structural engineering applications in FRP strengthening sheets and fabrics, strips and prestressing tendons. Carbon fibres are very durable and perform well in hot and moist environments and when subjected to fatigue loads. They do not absorb moisture. They are however, thermally and electrically conductive. It was noted in research that degradation of the polymer resin in the FRP composite may occur due to an electropotential mismatch between carbon fibre with metallic materials [65, 66]. Approximate properties of common grades of carbon fibres are given in Table 2-2.

Table 2-2 Approximate properties of common grades of carbon fibres [57]

Grade of Carbon Fibre	Density [g/cm^3]	Tensile Modulus [GPa]	Tensile Strength [MPa]	Max. Elongation (%)
Standard	1.7	250	3700	1.2
High strength	1.8	250	4800	1.4
High modulus	1.9	500	3000	0.5
Ultrahigh modulus	2.1	800	2400	0.2

Aramid fibres are occasionally used in FRP strengthening applications to wrap columns. They consist of aromatic polyamide molecular chains. They are resistant to fatigue, both static and dynamic, and have high tensile elastic characteristics. They have a distinctive yellow colour and are the lightest of the high-performance fibres, having a density of 1.4 g/cm^3. Aramid fibre sheets for retrofit and repair were developed mainly in Japan during the seismic retrofitting facilities in Japan after the Hyogoken-Nanbu (Kobe) earthquake in 1995 [57]. However, due to their relatively high price, difficulty in processing and high moisture absorption (up to 6% by weight) and low melting temperatures they are less attractive as FRP material for structural engineering applications.

The nonfibrous part of the FRP material that binds the fibres together (also known as the *matrix* or *binder*) is composed of the primary polymer ingredient and called *polymer resin* or simply *resin*.

Epoxy resins are commonly used in many FRP products, ranging from the manufacturing of carbon fibre-reinforced precured FRP strips to the application of the dry fibre sheets and fabrics in the field (in this case they are often referred to as *saturants*). In field applications, resins act as both the matrix for the FRP composite and as the adhesive to attach the FRP composite to the substrate. Typically, when they are combined with several additives or modifiers (e.g., fillers, and hardeners) the term *resin system*, rather than *resin*, is used as an all-inclusive term for a binder ready for use at the time of application. The additives are used to modify the properties of the resin to provide protection to fibres from moisture ingress and ultraviolet radiation, add colour, and modify surface tension and so on. Approximate properties of the thermosetting polymer resins for FRP products are given in Table 2-3.

Table 2-3 Approximate properties of the thermosetting polymer resins [57]

	Density [g/cm^3]	Tensile Modulus [GPa]	Tensile Strength [MPa]	Max. Elongation (%)
Polyester	1.2	4.0	65	2.5
Epoxy	1.2	3.0	90	8.0
Vinylester	1.12	3.5	82	6.0
Phenolic	1.24	2.9	40	1.8

Currently, *pre-cured* and *formed-in-place* systems are two popular FRP strengthening systems used in the rehabilitation of RC structures. In recent years, a new method of pre-manufactured strip called *near surface mounting* (NSM) has been developed. In this method, a thin, narrow FRP strip (3 by 18 mm) is inserted and then bonded adhesively into a machined groove at the surface of the concrete member.

When pre-cured FRP strips are used, the FRP composite is produced by the *pultrusion* method in which an automated and continuous process is used to produce FRP parts from raw materials. The “pultrusion process” derives its name by using the word “pul” meaning from pulling force applied to fibres passing through a heated die and combining it with the word “trusion” from extrusion process that consists of extruding (pushing) hot molten material (metal or polymer) through a die [56]. A pultrusion process is used for manufacturing composites that have uniform cross-sectional shapes – such as “I,” “L,” “T,” rectangular and circular sections and hollow rectangular and circular tubes (similar to steel shapes), as well as FRP rebars used in the construction industry Figure 2–22.

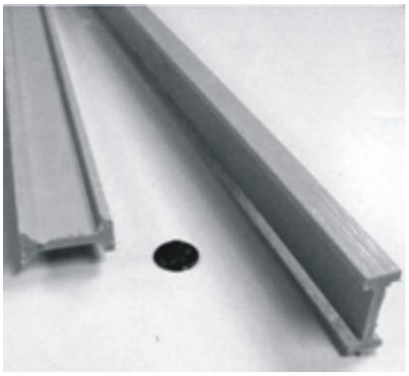

a) Leadline pultruded I-bars (Mitsubishi Chemical Corp.)

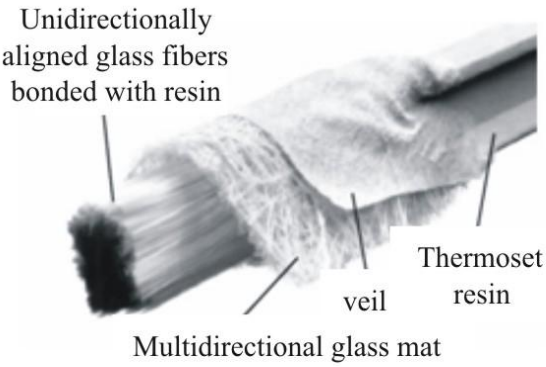

b) Primary constituent materials of a pultruded I -bar component (Courtesy of Strongwell Corporation, 2004)

Figure 2–22 Pultruded I-shaped beams

The pre-cured systems consist of factory manufactured laminates (known as *strips* and *plates* produced by the pultrusion method) of carbon or glass-reinforced thermosetting polymers (typically epoxy and vinylester) that are bonded to the surface of the concrete using an epoxy adhesive. The manufactured pre-cured laminates typically have a volume fraction of fibres in the range of 55 to 65% and are cured at high temperatures (>300°F), but are bonded in the field at ambient temperatures (Figure 2–23a).

The second, formed-in-place, system is used in structural engineering rehabilitation applications, as well as in industry (i.e., marine and aerospace industry). The method which is often referred to as *hand layup* (also known *as laminating*, *wet layup* or simply *layup)* consists of constructing an FRP composite part by laying up, or rather, putting down, manually successive layers of unidirectional sheets, woven or stitched fabrics of dry fibres (usually glass, carbon, or aramid) and impregnating them with a liquid polymer resin, which then cures at ambient temperatures in the field to produce a solid FRP composite element (Figure 2–23b). The solid part takes the form and shape of the surface to which it is applied. The formed-in-place FRP systems typically have a fibre volume fraction of between 20 and 40%. It is important to note that, although it seems to be a simple method, a significant degree of skill and good quality control are required to produce a high quality composite material (Figure 2–23b,c).

a) Column strengthening based on prefabricated (precured) FRP strengthening system (Courtesy of Takenaka corporation)

b) Column strengthening with wet lay-up method (bond critical application) (Courtesy of QuakeWrap)

c) FRP shear strengthening of a beam with wet lay-up method (contact critical application) (Courtesy of BBR-Contech)

Figure 2–23 FRP strengthening systems

Two primary types of fibre systems are used when the hand layup method is used for FRP strengthening: glass fibre reinforced polymer (GFRP) laminates (or strips) or wrap systems and carbon fibre reinforced polymer (CFRP) laminates (or strips) or wrap systems. Typically, only longitudinal properties of these strengthening systems with some data on physical properties are reported in manufacturer-published *spec sheets*. The strips and the fibres must be used with a compatible resin system applied with a controlled volume fraction in order to achieve an FRP composite with measurable properties. Typical properties of strips and commonly available unidirectional fibre sheet and fibre fabric materials are listed in Table 2-4.

Table 2-4 Properties of typical commercially produced FRP sheet and fabric strengthening materials

	Standard Modulus Carbon Fibre Tow Sheet[1,3]	High-Modulus Carbon Fibre Tow Sheet[1,2]	Glass Fibre Unidirectional Fabric[1,2]
Thickness (mm)	0.165-0.330	0.165	0.356
Typ. width (mm)	600	600	1200
Fibre architecture	Unidirectional	Unidirectional	Unidirectional
Fibre tensile strength, longitudinal (MPa)	3790	510	220-470
Fibre tensile strain (max.), longitudinal (%)	1.67-1.7	0.94	2.1-4.5
Fibre tensile modulus, longitudinal (GPa)	230	370	72

Source: [1]MBrace (Wabo); [2]Tyfo (Fyfe); [3]Replark (Mitsubishi)

In order to achieve a good strengthening performance and function, the FRP composite needs to be firmly adhered to, or be firmly in contact with, the surface of the existing structural element. This is a crucial issue because the interface or interfacial region, which is produced as a result of FRP application on the concrete, is a vital part of the FRP strengthening system. The loads from the concrete to the FRP composite are transferred through this interface between the FRP composite and the concrete substrate. As observed in the experimental studies performed on RC elements

strengthened in shear and flexural with externally bonded FRPs (also in case of axial tensile strengthening), failure of this interfacial region through debonding or delamination often controls the strength of the elements. Such applications are termed as *bond critical* (Figure 2–23c). In the case of the use of FRP confininig to increase the load-carrying and the displacement capacity (i.e., ductility) of deficient columns, the interface bond is not as critical as long as the FRP system is in close contact with the concrete. The FRP material is wrapped around the column continuously, so as to confine the lateral expansion of the cracked concrete. Such applications are called *contact critical* (Figure 2–23b).

The performance of a FRP strengthening system depends strongly on the condition of the surface to which the FRP strengthening system is applied. For this reason, the surface of the concrete substrate must be clean and sound prior to FRP application. All dust, grease, curing compounds, impregnations, waxes, foreign particles, disintegrated materials and other bond inhibiting materials should be removed from the surface. This is followed by the common steps given below for a hand layup manufacturing process:

- application of a primer sealant and filling of holes with putty,
- coating the concrete surface with a thin layer of liquid resin system (also called the *saturant*),
- predetermined appropriate length of fibre tow sheets is cut and placed on the wet resin layer,
- depression of the fibre sheets into the resin by plastic serrated rollers to make the fibres wet-out by the resin and to force excess resin and air out of the FRP composite. In case of insufficient resin to wet-out the fibres, a second overcoat layer can be applied,
- application of the additional resin to the surface of the existing layer in case of multiple layers of FRP sheets are used.

In typical applications no specific measures are taken apart from rolling and forcing out the resin and air with hand rollers to consolidate the layup. In this application method, installer needs to develop a "feel" for, and experience with, the application process so as to know how much adhesive to apply and how to squeeze out and remove the air bubbles. The steps described above are also used in this study for the application of GFRP unidirectional sheets on the beam-column joint subassemblies. More detailed information is given in Chapter 5, "Experimental Programme for 2D Beam-Column Joints".

Last but not least, during the application process the *pot life* of the resin has a crucial influence on the rate of the installation. Pot life is defined as the time that the mixed resin will stay in liquid form before beginning to gel and then cure. A typical resin used for structural hand layup will have a pot

life of 1 to 4 hours between 60 and 80°F (15 and 27°C). At higher ambient temperatures pot life will decrease, and at lower temperatures some resins will not cure.

2.4.2 Previous Research on Exterior RC Beam-Column Joints Retrofitted with FRP

Gergely *et al.* [67] tested four benchmark and eleven retrofitted 1/3 scale concrete beam-column joints under a quasi-static lateral cyclic loading to investigate the influence of the composite curing process, the CFRP layout, and the surface preparation of the concrete specimens (Figure 2–24). The observed failure mode in the strengthened specimens was the gradual delamination (measured average strains in the composite = 0.1% to 0.35%) from the face of the beam leaving the joint with no effective external reinforcement. The lateral load capacity increase for specimens with wire-brushed surfaces varied between 9 and 67 percent, while it varied between 46 and 93 percent for those with water-jetted surfaces. The following results were monitored by the researchers:

(a) water jetting the concrete surface and using a high strength adhesive resulted in very good performance; (b) an elevated temperature cure system did not have any substantial effect on the joint shear improvement; (c) the most effective fibre orientation in the joint region was found to be at 45°; (d) without proper anchorage of the sheets in the joint region, just adding more inclined layers would be less effective in the increase of joint strength.

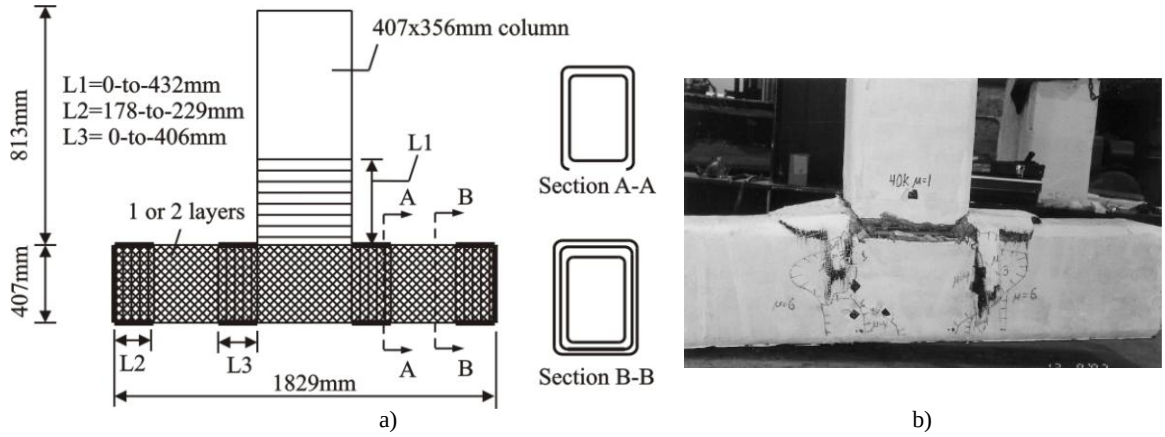

Figure 2–24 Experimental study by Gergely *et al.* [67]: a) CFRP layout on the specimen; b) final state of Specimen 14 which had a higher lateral load capacity

Granata and Parvin [68] tested six exterior beam-column connections to demonstrate the ability of FRP fabric to enhance the moment capacity of the scaled down beam-column connections. The overlay, beam and column wrap thickness were the variables for the experiment. FRP overlay configurations for the specimens B-C 4 to B-C 6 are given in Figure 2–25. Kevlar®, which is a type of aramid fibre, was selected for the FRP material. Specimens were loaded at the free end of the beam.

Test results highlighted the importance of the thickness, and hence the flexural stiffness, of the column wraps. In addition, it was seen that the thickness of the wraps affects the maximum rotation before fibre failure. Specimens using 8 or 11 layers of column wrap (B-C 1, B-C 2, and B-C 4) had fibre failure at a 0.08 radian joint rotation; whereas a 0.06 radian joint rotation was observed in the case of 14 and 16 layers of column wrap (B-C 3, B-C 5, and B-C 6).

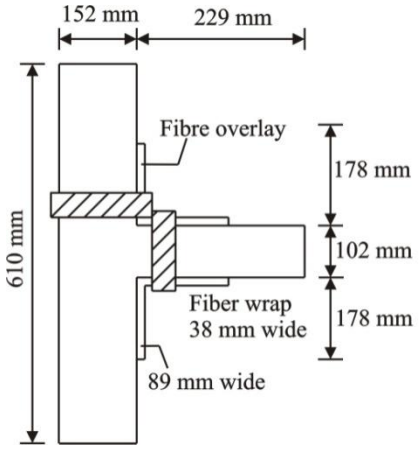

Specimen	Thickness			Shear rein.	Max shear
	Overlay	Column wrap	Beam wrap		
B-C 1	0.20 cm	0.20 cm	0.20 cm	No	6.23 kN
B-C 2	0.20 cm	0.20 cm	0.20 cm	No	6.00 kN
B-C 3	0.30 cm	0.41 cm	0.30 cm	No	10.04 kN
B-C 4	0.20 cm	0.20 cm	0.20 cm	Yes	6.53 kN
B-C 5	0.20 cm	0.20 cm	0.20 cm	Yes	8.56 kN
B-C 6	0.30 cm	0.41 cm	0.30 cm	Yes	10.62 kN

Figure 2–25 Experimental study by Granata and Parvin [68]: a) CFRP layout on the specimen; b) configuration of FRP reinforcement and results of scaled-down beam-column specimens

An experimental study was conducted by Ghobarah and Said [69] to evaluate the performance of a full-scale RC external beam-column joint repaired and retrofitted by GFRP laminates after testing the control specimen (Figure 2–13). Test results of this control specimen have been reviewed in section 2.3. The retrofit scheme consisted of wrapping the joint area with one layer of GFRP laminates in the form of a "U" and tying the free end of the "U" together using threaded steel rods driven through the joint section Figure 2–26. Due to the intentional under-design of the FRP tensile capacity, tension failure in the fibre composite material started at a ductility level of 4. Researchers then tested another beam-column joint rehabilitated with two layers of GFRP laminates. As expected, the increase in the design strength of the fibre prevented the joint shear failure, thus allowing a ductile plastic hinge to develop in the beam.

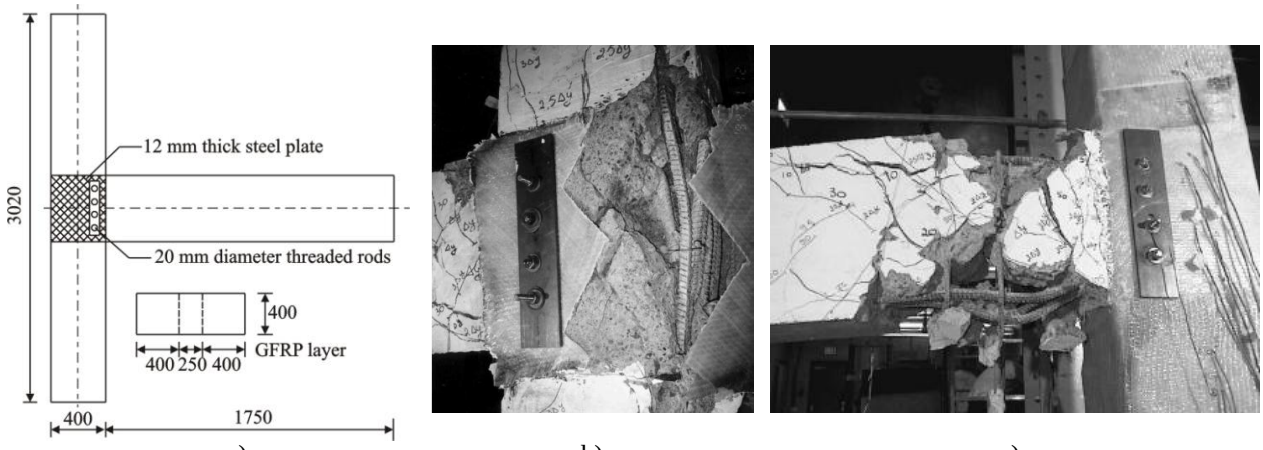

a) b) c)

Figure 2–26 Experimental study by Ghobarah and Said [69]: a) CFRP layout on the specimen; b) final state of repaired and retrofitted specimen; c) second specimen retrofitted with two layers of FRP

Liu [70] tested one retrofitted unit of the as-built specimen EJ1 (see section 2.3) with the beam bar hooks bent away from the joint core, and the retrofit was done by solution wrapping the column above and below the joint core using fibre-glass. Test results showed that fibre-glass jacketing in the column areas adjacent to the joint core restrained the opening of the beam bar hook, and actuated the postulated alternative force transfer path across the joint when the axial column load was low, leading to more improved stiffness and strength performance. The attained initial stiffness was more than twice the measured initial stiffness for the as-built unit EJ1. However, it was noted that a great deal of strength and stiffness degradation occurred, mainly due to large crack openings in column areas adjacent to the joint core and severe bond degradation along the member's longitudinal reinforcement. Test results are given in Figure 2–27.

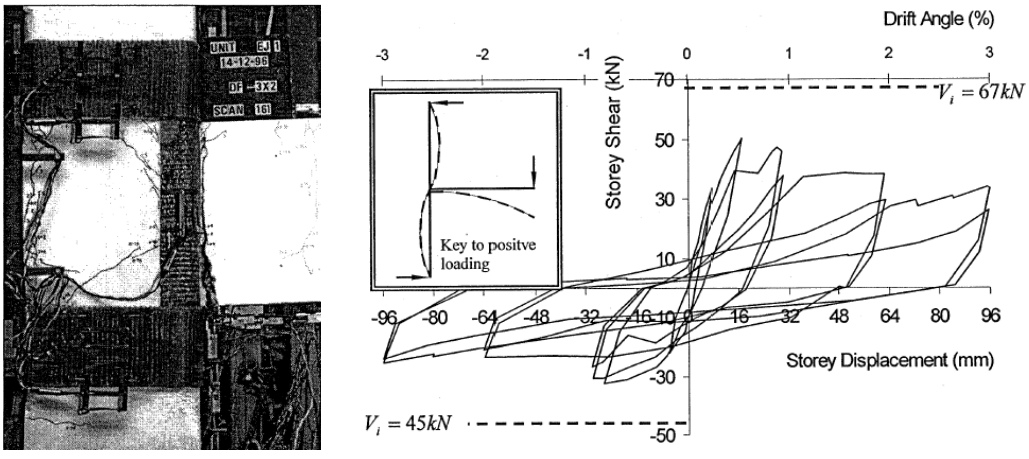

a) b)

Figure 2–27 Experimental study by Liu [70]: a) CFRP layout and state of the specimen at end of test; b) hysteresis loops

Clyde and Pantelides [71] also tested one retrofitted unit with the same specimen details described in the experimental works on as-built specimens (see section 2.3). CFRP sheets were used in the retrofit of a single, one-way exterior joint. CFRP layout and performance comparison between rehabilitated and baseline specimens are given in Figure 2-29. The joint shear type failure seen in the as-is beam-column joints was successfully prevented. The CFRP composite wrap provided a joint shear strength increase of 5%, a 44% increase in displacement ductility and an increase of 78% in drift capacity.

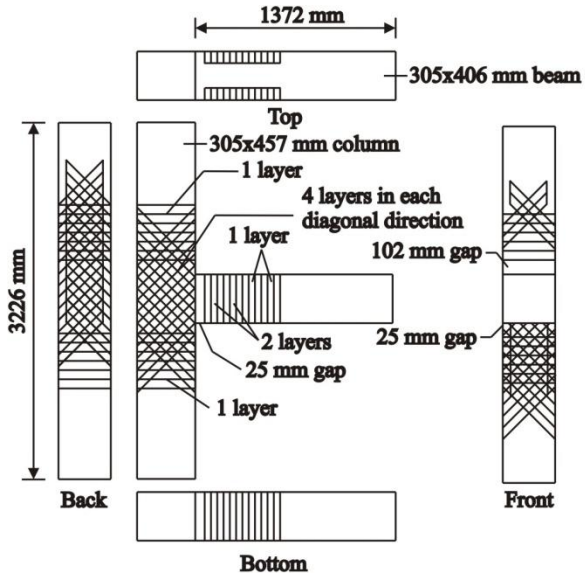

Specimen	Axial Load Level	Joint Shear Stress (psi)	Drift (%)	Disp. Ductility
As-is (1st)	$0.1f_c`Ag$	0.20 cm	2.95	2.8
As-is (2nd)	$0.1f_c`Ag$	0.20 cm	3.57	2.6
Retrofitted	$0.1f_c`Ag$	0.41 cm	5.77	3.9

Figure 2–28 Experimental study by Clyde and Pantelides [71]: a) CFRP layout of the specimen; b) comparison of results

Three beam-column joints, namely a control specimen and two rehabilitated specimens, were tested under quasi-static load by El-Amoury and Ghobarah [72]. GFRP sheets are wrapped around the joints to prevent the joint shear failure. To enhance the bond between the GFRP and the concrete, steel plates were also provided. A steel angle was installed to overcome the problem of debonding in the composite sheets at the beam-column corner (Figure 2–29). Both retrofitted specimens exhibited an increase of approximately 100% in load-carrying capacity; Specimens TR1 and TR2 respectively dissipated three and six times the energy dissipated by the reference specimen. The composite sheets were completely debonded from the beam and column faces of the specimen TR1. The specimen TR2 failed in joint shear, through the use of two U-shaped steel plates, eliminated debonding of the GFRP and reduced the strength degradation.

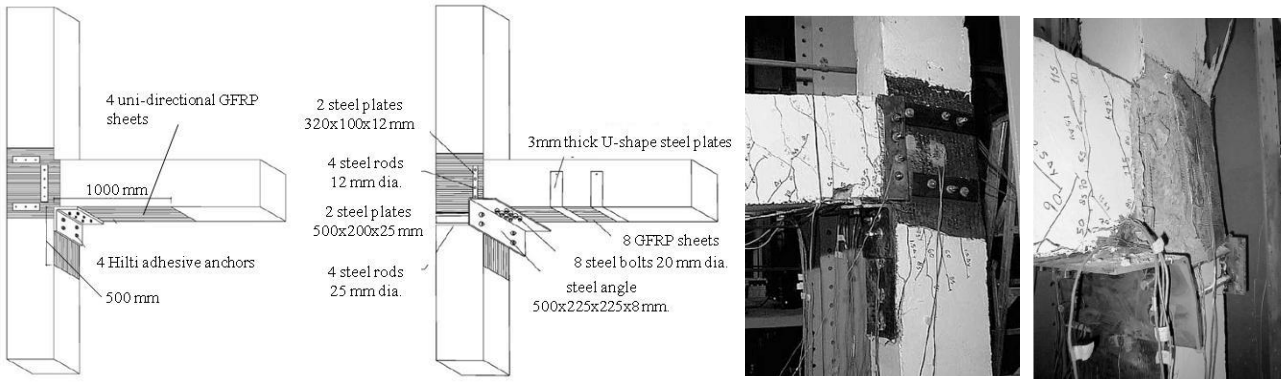

Figure 2–29 Experimental study by El-Amoury and Ghobarah [72]: a), b) retrofitting scheme of Specimen TR1 and TR2; c), d) failure pattern of TR1 and TR2, respectively

Ghobarah and Said [73] reported the results of three one-way exterior beam-column joints retrofitted with the modified schemes of the study in previously presented literature [69]. The rehabilitation schemes are given in Figure 2–30. Specimen T2R was rehabilitated with two layers of "U" shaped GFRP sheeting extending above and below the joint, with added cover plates and anchors through the joint. As expected, the proposed rehabilitation scheme was successful in providing lateral confinement and shear resistance to the joint area, hence adding strength and resistance to the joint. The presence of the bolted steel plate allowed the fibre to develop its full capacity and prevented premature delamination of the fibre wrap; the failure was due to a beam plastic hinge formation. In Specimen T4, one bidirectional "U" shaped GFRP sheet, of the same height as the joint, was applied without any cover plates or anchors through the joint. Test results of this specimen showed that the unanchored GFRP did not contribute much to the shear strengthening of the joint. During the test, the FRP delaminated as the joint shear cracking occurred under the fibre wrap. The last joint, Specimen T9, was rehabilitated with three diagonal GFRP layers, which were facilitated by the triangular steel bars fitted at the four corners of the joint panel. This scheme could not prevent the expansion of the joint core, which led to delamination and a simultaneous failure of the beam and joint. Overall, the test results highlighted the importance of anchoring the edges of the FRP in the joint area in order to develop the full strength of the fibre and confinement of the joint.

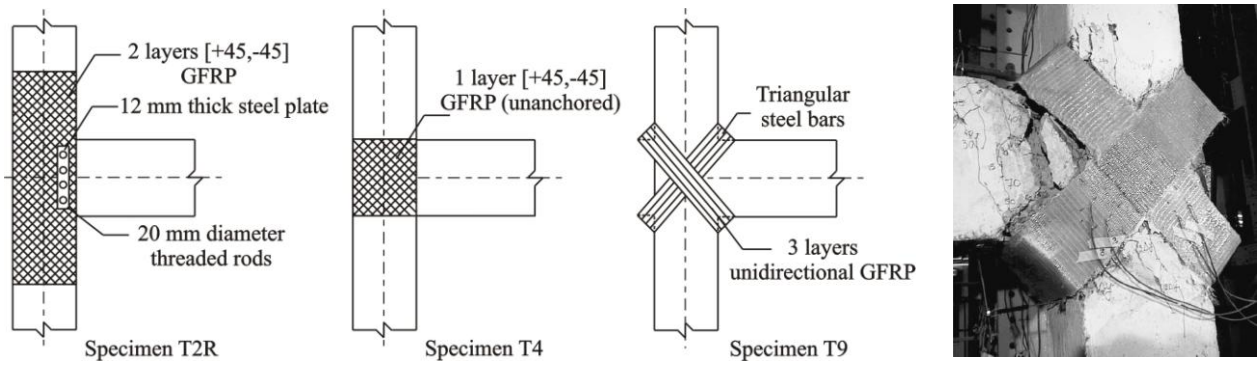

a) b)

Figure 2–30 Experimental study by Ghobarah and Said [73]: a) retrofitting scheme of specimens; b) Failure mode of rehabilitated specimen T9

Antonopoulos and Triantafillou [74] performed an experimental programme to clarify the role of the various parameters (e.g., area fraction and distribution of FRP, column axial load, internal joint reinforcement, initial damage, carbon versus glass fibres, sheets versus strips, and the effect of transverse stub beams) on the effectiveness of FRP strengthened shear-critical beam-column joints. For this purpose, eighteen 2/3-scale exterior RC joints are tested under reversed cyclic lateral loading with various configurations. All specimens were designed to fail in joint shear, both before and after strengthening, to evaluate the contribution of FRP. The details of specimens are given in Figure 2–31. The designs of all the tested joints and details of the alternative strengthening configurations examined are given in Figure 2–32.

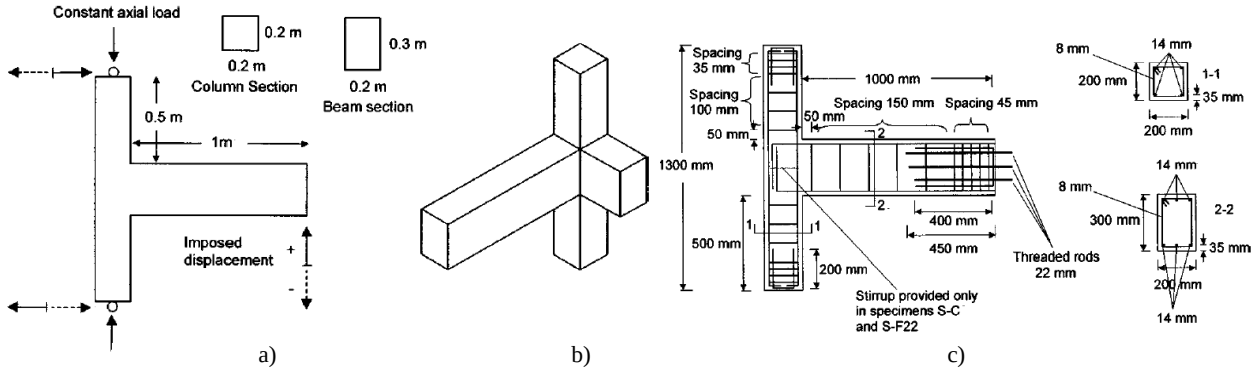

a) b) c)

Figure 2–31 Experimental study by Antonopoulos and Triantafillou [74]: Specimen details

Test results demonstrated that (a) debonding dominates the behaviour of external reinforcement unless very low area fractions are employed or proper mechanical anchorages are provided; (b) flexible sheets are more effective than strips for the same reinforcement area; (c) due to premature debonding both the strength and the dissipated energy increase considerably, but not proportionally; (d)

increasing the FRP area fraction in the beam is nearly as effective as it is for equal increase in both the beam and the column, implying that the effectiveness of column FRP is rather limited; (e) mechanical anchorages increase the effectiveness of both sheets and strips, and wrapping of longitudinal FRP sheets with transverse layers proved to be a highly effective anchorage system; (f) the effect of high axial load on the shear capacity of FRP strengthened joints are quite positive, and (g) the effectiveness of the FRP increases as the transverse steel reinforcement in the joint decreases.

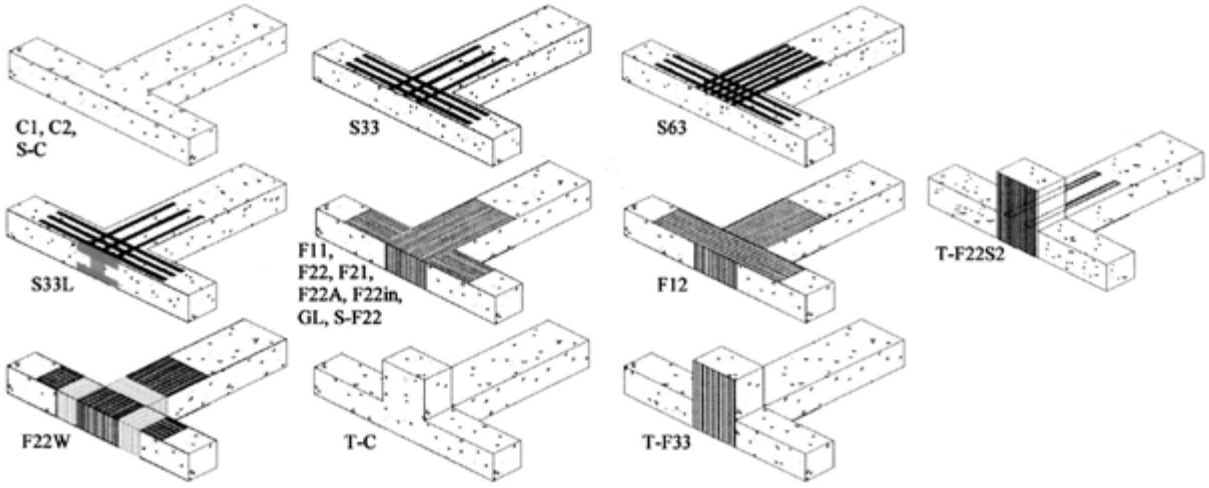

Figure 2–32 Experimental study by Antonopoulos and Triantafillou [74]: Description of specimens and strengthening alternatives

Ghobarah and El-Amoury [75] tested six beam-column subassemblies to assess the performance of proposed rehabilitation schemes using GFRP materials and steel elements. All specimens were designed to pre-seismic codes and tested under quasi-static seismic load. Two of the specimens (T-B11 and T-B12) were strengthened by using CFRP sheets attached to the bottom beam face. To overcome the potential debonding of the sheets from concrete surface, various types of steel plate and threaded rod application were employed (Figure 2–33).

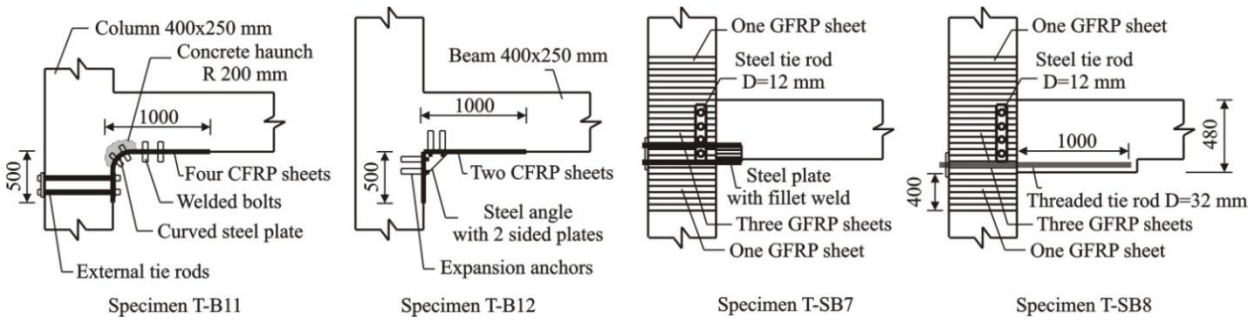

Figure 2–33 Experimental study by Ghobarah and El-Amoury [75]: Rehabilitation scheme of the specimens

The test showed that the GFRP jacket of the joint was found to be an effective system to provide confinement and shear strength. Brittle joint shear failure was avoided. CFRP sheets attached to the beam bottom face were found effective in replacing the anchorage deficient beam bars when an adequate anchorage system is provided. External steel tie-rods welded to the existing deficient beam reinforcement were found to be a simple and effective technique to improve the anchorage conditions of these bars, so that tensile strength could be fully developed. The summary of test results is given in Table 2-5.

Table 2-5 Experimental study by Ghobarah and El-Amoury [75]: Summary of test results

Specimen	Failure Mode	Ultimate tip load (kN)	Storey drift at ultimate load (%)	Maximum storey drift (%)
T-B12	FRP deboding	55 kN	1.95	0.20
T-B11	Beam hinging	86 kN	1.68	0.30
T-SB8	Shear of rehab. section	152 kN	2.43	0.20
T-SB7	Fracture of rehab. rods	127.9 kN	4.22	0.30

As part of an extensive experimental-analytical investigation on existing beam-column subassemblies and frame systems Pampanin *et al.* [76] published the results of two 2/3 scale exterior retrofitted beam-column joints. The specimens were designed and constructed according to the Italian construction practice of the 1950-1970s and retrofitted using CFRP overlays. A quasi-static cyclic loading protocol was followed along with the fluctuation in the column axial load to properly simulate the variation during the lateral cyclic sway of a frame building. Specimen details are given in Figure 2–34. A multi-level retrofit strategy, following *hierarchy of strength* considerations within the joint subassembly, was adopted to achieve the desired performance. The target performance of the retrofit solution was controlled using the proposed procedure based on the moment–axial load, *M-N*, performance domain. Detail information on the concept of *hierarchy of strength* along with *sequence of event* and construction of *M-N performance* domain regarding the assessment and retrofit design of beam-column joints is introduced in Chapter 3 and elaborated in Chapter 4. Accordingly, in order to achieve more ductile behaviour along with the protection of the joint panel from brittle failure, retrofit design parameters were established to guarantee sufficient shear strengthening in the joint without excessively increasing the joint capacity and relocating the plastic hinge region at a controlled distance from the beam-column interface. For this purpose, two layers of vertical FRP laminates were used on the external side face of the column in order to increase the column flexural capacity as well as the joint shear strength. In addition, a U-shape horizontal laminate was wrapped around the column in the joint level to increase the joint shear strength and prevent the expulsion of a concrete wedge. Also, additional smaller strips were used to wrap the main FRP laminates and provide proper anchorage.

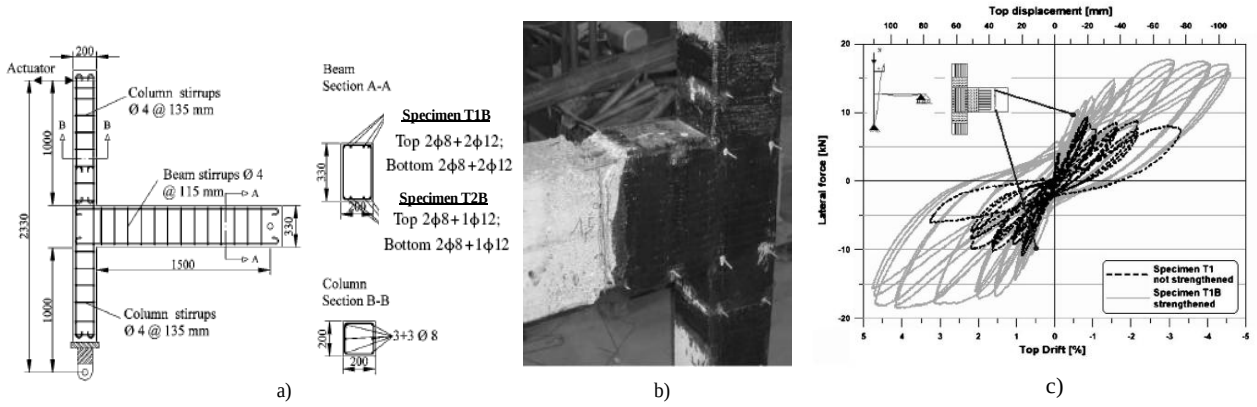

Figure 2–34 Experimental study by Pampanin *et al.* [76]: a) details of retrofitted specimens; b) failure mode of specimen T1B; c) comparison of as-built and retrofitted exterior joints

The results of the tests provided very satisfactory confirmation of the efficiency of the adopted retrofit solution. It was shown that a properly designed FRP-retrofit solution for exterior beam-column joints can protect and avoid the formation of a brittle shear hinge mechanism and re-establish a more desirable hierarchy of internal strengths and sequence of events, enforcing a beam plastic hinge mechanism. An improved and more stable hysteresis behaviour was observed with increased ductility and energy dissipation capacity.

Karayannis and Sirkelis [77] performed a series of tests under cyclic loading on twelve external beam-column joints repaired and/or strengthened with a combination of epoxy resin injection and CFRP. The specimens were tested under constant axial load with an increasing full cyclic displacement. Specimen characteristics and CFRP application sheets are given in Figure 2–35a. Two series of tests were considered depending on the presence of steel reinforcement in the joint core, i.e., with or without. With the exception of the control specimen with no steel reinforcement in the joint core, all other specimens failed by flexural beam hinging (Figure 2–35b). The specimen, with no shear reinforcement and strengthened by two layers of CFRP sheets, presented an increase of 186% of maximum observed load and an increase of 78% of energy absorption in comparison with the corresponding values of the as-built specimen.

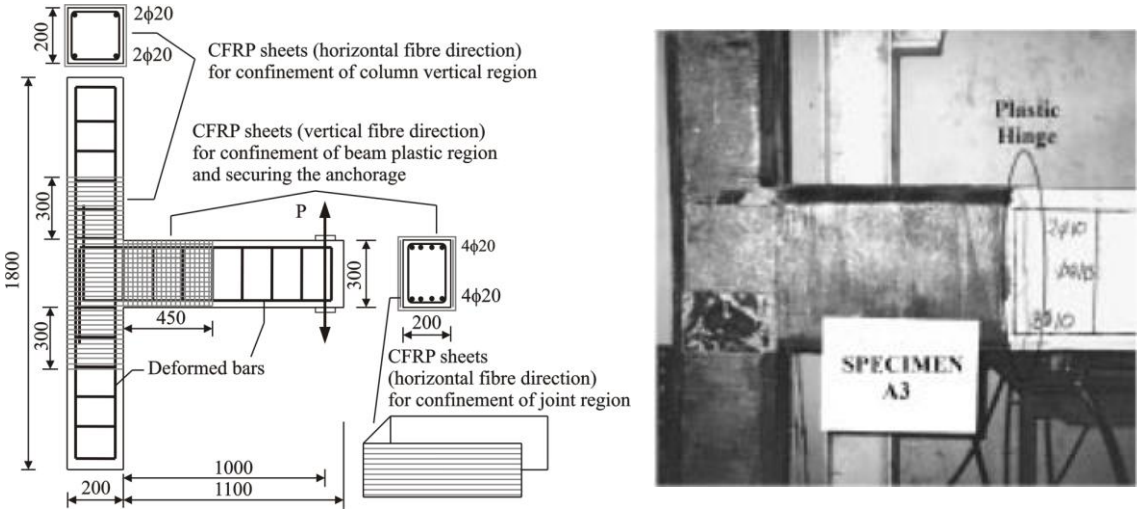

Figure 2–35 Experimental study by Karayannis and Sirkelis [77]: a) specimen details; b) damage mode of CFRP strengthened specimen

Parvin *et al.* [33] performed an experimental study under a quasi-static cyclic loading on six full scale as-built and CFRP-strengthened RC exterior beam-column joints, with the focus on delaying or avoiding the pull-out of the bottom beam reinforcements and joint shear failures. The effects of various CFRP retrofit configurations and axial load levels are also considered. The characteristics of the specimens and schematic drawings of the CFRP wrapping configurations are given in Figure 2–36. Test results exhibited debonding and rupture of the CFRP sheets at the beam faces (Figure 2–37). Examination of the performance of the two retrofit configurations revealed that in the push direction of loading, the Specimen RC3U3 outperformed the RC2U1. A maximum lateral load with a 15% increase in the strength capacity was observed due to the additional CFRP layers (Figure 2-37). However, drift capacities were comparable.

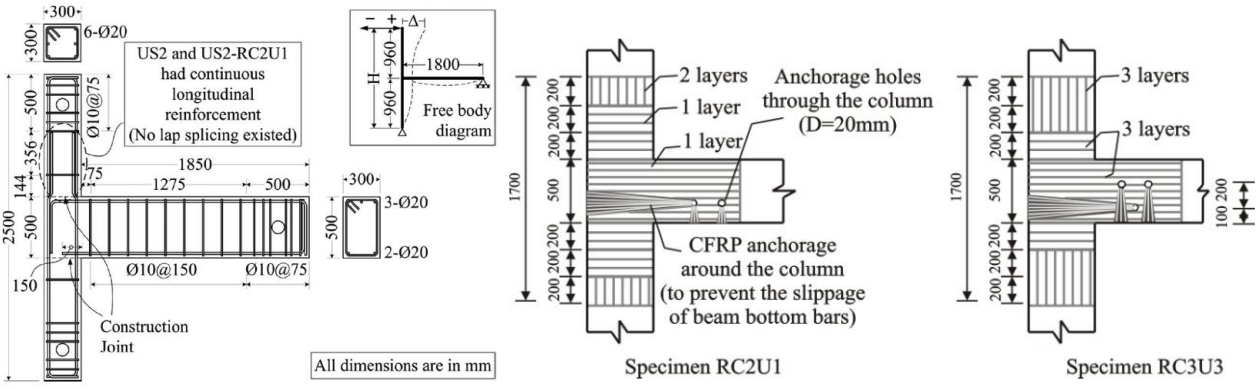

Figure 2–36 Experimental study by Parvin *et al.* [33]: a) specimen details; b) CFRP configuration

a) Specimen U.S.2-RC2U1 b) Specimen U.S.3-RC3U3 c) Specimen U.S.4-RC3U3

Figure 2–37 Experimental study by Parvin *et al.* [33]: Failure modes of the specimens

2.4.3 Existing Guidelines and Design Proposals

Due to the substantial difference in mechanical and physical properties in comparison to conventional construction materials, there is a need for developing specialised standards and codes for FRP materials. The development of standards and codes for the design of structures strengthened with externally bonded FRP materials is ongoing in both the research community and construction industry through experimental investigations, theoretical studies and field implementations. Recent publications on the design of FRP strengthening systems are AC 125 [78], AC187 [79], JSCE [80], *fib* [81], TR 57 [82], TR 55 [83], *fib* [84], ACI 440.2R [85].

It is important to note that the aforementioned guidelines do not include clauses related to beam-column joints. Furthermore, in literature, relatively limited information is available on the design of the strengthening of external joints using FRP materials. Gergely *et al.* [86] have calculated the FRP contribution in the shear strengths considering FRP as stirrups. Gergely *et al.* [67] also specified a retrofit design proposal for beam-column joints which utilized the limit states based on principal tensile stresses. Tsonos [87] followed the same approach but he considered the contribution of FRP by estimating the design value of the effective strain $\varepsilon_{f,e}$ using the expression for fully wrapped or properly anchored FRPs in *fib* (2001) [81]. Antonopoulos and Triantafillou [88] proposed a more accurate model to evaluate the shear strength contribution of FRP in the joint. However, this model is not easy to incorporate in practical design procedures due to its complexity and need for extensive computational effort. Pampanin *et al.* [76] adopted a simplified version of the previously mentioned analytical model with proper modifications to account for the variation of axial load on the joint region, referring to principle stresses instead of nominal shear stresses. However, still there is a strong need for an unified approach in the clarification of design philosophy, recommendations and steps for engineering practice.

2.5 SUMMARY

In this chapter the seismic vulnerability of existing reinforced concrete frame structures with a particular focus on the exterior beam-column joints designed to early codes before mid-1970s has been reviewed based on the observations from recent earthquakes and experimental studies. Experimental studies of existing beam-column joints designed according to pre-seismic code construction practice, have reported that collapse of complete structural components due to joint panel degradation may occur before any significant damage take place in either beams or columns. It can be concluded that there are mainly two modes of failure governing the behaviour of deficient exterior beam-column joints a) joint shear failure due to the lack of transverse reinforcement in the joint region and excessive tensile or compression stresses in the joint; b) debonding and consequent slippage of the beam reinforcements due to inadequate anchorage lengths/solutions and use of plain round bars.

In the next section, a brief review of the state of the art on the use of conventional strengthening techniques and an overview of FRP composite materials is covered. A comprehensive review of published experimental studies on the rehabilitation of 2D RC beam-column joints with FRP composite materials is also presented. The review of these studies shows that the FRP strengthening technique is a promising alternative to the traditional techniques by indicating substantial performance enhancements in terms of strength, ductility, and energy dissipation. Nevertheless, it is also revealed that there are some knowledge gaps that need to be addressed. Following are the important points:

(a) Economical considerations are generally disregarded in the design of FRP intervention. Most of the researchers employing FRP materials sometimes accompanied the intervention with steel elements in various configurations to prevent the brittle mode of failures. However, it is obvious that there is a certain cut-off value, which is referred in this study as *the minimum retrofit solution*, governing the amount of FRP used in the intervention. This point should be investigated under controlled test conditions to obtain the optimum values where satisfactory performance behaviour as well as minimum construction costs are achieved;

(b) In the next stage the so-called minimum retrofit solution should also be tested against more severe conditions such as axial load fluctuations in the column for plane frame joints and bidirectional loading in the corner joints. Up to now, all the work was conducted under the assumptions of constant axial load conditions and very few works related to bidirectional performance of rehabilitated joints are performed in literature;

(c) An urgent need exists for performance-based, easy and robust assessment and FRP retrofit design methods for beam-column joints to be devised for practicing engineers. In the following sections, investigations and discussions with a particular emphasis on these aspects will be covered.

2.6 REFERENCES

1. International Conference of Building Officials. *Uniform building code (UBC).* Whittier, Calif., 1968.
2. Faison H, Comartin CD, Elwood KJ. Reinforced concrete moment frame building without seismic details. *Housing Report No. 111,* Encyclopedia of Housing Construction in Seismically Active Areas of the World, USA, 2004.
3. Bertero VV, Borcherdt RD, Clark PW, Dreger DS, Filippou FC, Foutch DA, et al. Seismological and engineering aspects of the 1995 Hyogoken-Nanbu (Kobe) earthquake. *UCB/EERC-95/10*, University of California, Berkeley, 1995.
4. Hollings JP. Reinforced concrete sesimic design. *Bulletin of the New Zealand National Society for Earthquake Engineering*. 1969; **2**(3):217-50.
5. Park R, Paulay T. *Reinforced Concrete Structures*. Wiley: New York, 1975.
6. Priestley MNJ, Calvi GM. Towards a capacity-design assessment procedure for reinforced concrete frames. *Earthquake Spectra*. 1991; **7**(3):413-37.
7. Rosenblueth E, Meli R. The 1985 earthquake: Causes and effects in Mexico City. *Concrete International*. 1986; **8**(5):23-34.
8. California S. Loma Prieta`s call to action. *Report on the Loma Prieta earthquake of 1989*, University of California, Sacramento, California, 1991.
9. Okada T. Needs to evaluate real seismic performance of buildings - Lessons from the 1995 Hyogoken-nambu earthquake. *INCEDE Report No. 15*, Shibaura Institute of Technology, Japan, 1997.
10. Sezen H, Elwood KJ, Whittaker AS, Mosalam KM, Wallace JW, Stanton JF. Structural engineering reconnaissance of the August 17, 1999, Kocaeli (Izmit), Turkey Earthquake. *Report No. PEER 2000/09*, University of California, Berkeley, 1999.
11. EERI. Kocaeli, Turkey, Earthquake of August 17, 1999 reconnaissance report. *Earthquake Spectra*. 2000; **16**(Sup. A).
12. EERI. Chi-Chi, Taiwan, Earthquake of September 21, 1999 reconnaissance report. *Earthquake Spectra*. 2001; **17**(Sup. A).
13. Bruneau M. Building damage from the Marmara, Turkey earthquake of August 17, 1999. *Journal of Seismology*. 2002; **6**:357-77.
14. Aydan O, Ulusay R, Miyajima M. The Bingol Earthquake of May 1, 2003. Japan Society of Civil Engineers, Tokyo, 2003.
15. Sezen H, Whittaker AS, Elwood KJ, Mosalam KM. Performance of reinforced concrete buildings during the August 17, 1999 Kocaeli, Turkey earthquake, and seismic design and construction practise in Turkey. *Engineering Structures*. 2003; **25**:103-14.
16. Ministry of Public Works and Settlement. *Turkish Seismic Code, Specification for Structures to Be Built in Disaster Areas.* Ankara, Turkey, 1998.
17. Priestley MJN. Displacement-based seismic assessment of reinforced concrete buildings. *Journal of Earthquake Engineering*. 1997; **1**(1):157-92.
18. Moehle J, Mahin SA. Observations on the behaviour of reinforced concrete buildings during earthquakes. *ACI Special Publication, SP-127*. 1991.
19. NISEE. Earthquake image information system: Karl V. Steinbrugge collection. University of California, Berkeley.
20. Kaplan H, Bilgin H, Yilmaz S, Binici H, Oztas A. Structural damages of L'Aquila (Italy) earthquake. *Natural Hazards and Earth System Sciences*. 2010; **10**:499-507.

21. Hakuto S, Park R, Tanaka H. Seismic load tests on interior and exterior beam-column joints with substandard reinforcing details. *ACI Structural Journal*. 2000; **97**(1):11-25.
22. Beres A, Pessiki SP, White RN, Gergely P. Implications of experiments on the seismic behaviour of gravity load designed RC beam-to-column connections. *Earthquake Spectra*. 1996; **12**(12):185-98.
23. Calvi GM, Magenes G, Pampanin S. Relevance of beam-column damage and collapse in RC frame assessment. *Journal of Earthquake Engineering*. 2002; **6**(Special Issue No. 1):75-100.
24. Pampanin S, Calvi GM, Moratti M. Seismic behaviour of RC beam-column joints designed for gravity loads. *12th European Conference on Eartquake Engineering*, London, Paper no. 726, 2002.
25. Pampanin S, Magenes G, Carr A. Modelling of shear hinge mechanism in poorly detailed RC beam-column joints. *Proc FIB Symp Concrete Structures in Seismic Regions, Federation International bu Beton*, Athens, Paper no. 171, 2003.
26. Ghobarah A, Said A. Relevance of beam-column damage and collapse in RC frame assessment. *Journal of Earthquake Engineering*. 2001; **5**(1):113-29.
27. Kuang JS, Wong HF. Effects of beam bar anchorage on beam-column joint behaviour. *Structures & Buildings*. 2006; **SB2**(159):185-98.
28. British Standards Institution. *BS 8110 Structural use of concrete. Part 1: Code of practice for design and construction.* BSI, London, 1997.
29. Clyde C, Pantelides CP, Reaveley LD. Performance-based evaluation of exterior reinforced concrete building joints for seismic excitation. *Report No. PEER 2000/05*, University of California, Berkeley, 2000.
30. Pantelides CP, Hansen J, Nadauld J, Reaveley LD. Assessment of reinforced concrete building exterior joints with substandard details. *Report No. PEER 2002/18*, University of California, Berkeley, 2002.
31. Hertanto E. Seismic assessment of pre-1970s reinforced concrete beam-column joint subassemblies. *M.E. Thesis*, University of Canterbury, Christchurch, 2006.
32. Chen T. Retrofit strategy of non-seismically designed frame systems based on a metallic haunch system. *M.E. Thesis*, University of Canterbury, Christchurch, 2006.
33. Parvin A, Altay S, Yalcin C, Kaya O. CFRP rehabilitation of concrete frame joints with inadequate shear and anchorage details. *Journal of Composites for Construction, ASCE*. 2010; **14**(1):72-82.
34. Genesio G, Sharma A. Seismic retrofit solution for reinforced concrete exterior beam-column joints using a fully fastened haunch - Part 2-1: As-built joints. *Test report, No. WS 221/07 - 10/01*, University of Stuttgart, Stuttgart, 2010.
35. Popov E, Bertero VV. Repaired R/C members under cyclic loading. *Earthquake Engineering and Structural Dynamics*. 1975; **4**:129-44.
36. French CW, Thorp GA, Tsai WJ. Epoxy repair techniques for moderate earthquake damage. *ACI Structural Journal*. 1990; **87**(4):416-24.
37. Beres A, El-Borgi S, White RN, Gergely P. Experimental results of repaired and retrofitted beam-column joint tests in lightly reinforced concrete frame buildings. *Technical Report NCEER-92-0025*, SUNY/Buffalo, 1992.
38. Filiatrault A, Lebrun I. Seismic rehabilitation of reinforced concrete joints by epoxy pressure injection technique. *Seismic Rehabilitation of Concrete Structures, ACI SP-160*. 1996:73-92.
39. Karayannis CG, Chalioris CE, Sideris KK. Effectiveness of RC beam-column connection repair using epoxy resin injections. *Journal of Earthquake Engineering*. 1998; **2**(No. 2):217-40.
40. Lee DLN, Wight JK, Hanson RD. Repair of damaged reinforced concrete frame structures. *Proceedings of the Sixth World Conference on Earthquake Engineering*, New Delhi, India, pp. 2486-91, 1977.
41. Tsonos AG. Seismic rehabilitation of reinforced concrete joints by the removal and replacement technique. *European Earthquake Engineering*. 2001; **3**:29-43.

42. Corazao M, Durrani AJ. Repair and strengthening of beam-to-column connections subjected to earthquake loading. *Technical Report NCEER-89-0013*, SUNY/Buffalo, 1989.
43. Choudhuri D, Mander JB, Reinhorn AM. Evaluation of seismic retrofit of reinforced concrete frame structures: Part I - Experimental performance of retrofitted subassemblages. *Technical Report NCEER-92-0030*, SUNY/Buffalo, 1992.
44. Alcocer SM, Jirsa JO. Strength of reinforced concrete frame connections rehabilitated by jacketing. *ACI Structural Journal*. 1993; **90**(3):249-61.
45. Bracci JM, Reinhorn AM, Mander JB. Seismic retrofit of reinforced concrete buildings designed for gravity loads: Performance of structural model. *ACI Structural Journal*. 1995; **92**(6):711-23.
46. Tsonos AG. Seismic retrofit of R/C beam-to-column joints using local three-sided jackets. *European Earthquake Engineering*. 2001; **1**:pp. 48-64.
47. Tsonos AG. Seismic repair of exterior R/C beam-to-column joints using two-sided and three-sided jackets. *Structural Engineering and Mechanics*. 2002; **13**(1):17-34.
48. Karayannis CG, Chalioris CE, Sirkelis GM. Local retrofit of exterior RC beam–column joints using thin RC jackets—An experimental study. *Earthquake Engineering and Structural Dynamics*. 2008; **37**:727-47.
49. Biddah A, Ghobarah A, Aziz TS. Upgrading of nonductile reinforced concrete frame connections. *Journal of Structural Engineering*. 1997; **123**(8):1001-9.
50. Ghobarah A, Aziz TS, Biddah A. Rehabilitation of reinforced concrete frame connections using corrugated steel jacketing. *ACI Structural Journal*. 1997; **4**(3):283-94.
51. Aycardi LE, Reinhorn AM, Mander JB. Seismic resistance of reinforced concrete frame structures designed only for gravity loads: Experimental performance of subassemblages. *ACI Structural Journal*. 1994; **91**(5):552-63.
52. Engindeniz M, Kahn LF, Zureick A-H. Repair and strengthening of reinforced concrete beam-column joints: State of the art. *ACI Structural Journal*. 2005; **102**(2):187-97.
53. Pampanin S, Christopoulos C, Chen T-H. Development and validation of a metallic haunch seismic retrofit solution for existing under-designed RC frame buildings. *Earthquake Engineering and Structural Dynamics*. 2006; **35**(14):1739-66.
54. Kam WY, Pampanin S. Selective weakning techniques for retrofit of existing reinforced concrete structures. *Proc, 14th World Conf on Earthquake Engineering*, Beijing, 2008.
55. Pampanin S. Alternative performance-based retrofit strategies and solutions for existing R.C. buildings. In: A. Ilki FK, S. Pala and E. Yuksel, editor.: London: Springer; 2009. p. 267-95.
56. GangaRao HVS, Taly N, Vijay PV. *Reinforced Concrete Design with FRP Composites*. CRC Taylor & Francis: LA, 2006.
57. Bank LC. *Composites for Construction: Structural Design with FRP Materials*. John Wiley & Sons: NY, 2006.
58. Meier U. Bridge repair with high performance comosite materials. *Mater Tech (Duebendorf, Switz)*. 1987; **4**:125-8 (in German).
59. Rostasy FS. Bonding of steel and GFRP plates in the area of coupling joints. Talbrucke Kattenbuch. *Research Report No. 3126/1429*, Federal Institute for Materials Testing, Braunschweig, Germany (in German), 1987.
60. Fardis MN, Khalili H. Concrete encased in fiberglass reinforced plastic. *ACI Structural Journal*. 1981; **78**(6):440-6.
61. Katsumata H, Kobatake H, Takeda H. A study on the strengthening with carbon fiber for earthquake-resistant capacity of existing reinforced columns. *Proceedings of Workshop on Repair and Retrofit of Existing Structures*, U.S.-Japan Panel on Wind and Seismic Effects, U.S.-Japan Cooperative Program in Natural Resources,Tsukaba, Japan, 1987.
62. Hollaway LC, Head PR. *Advanced Polymer Composites and Polymers in the Civil Infrastructure*. Elsevier: London, 2001.
63. Teng JG, Chen JF, Smith ST, Lam L. *FRP Strengthened RC Structures*. John Wiley & Sons: New York, 2001.

64. Bakis CE, Bank LC, Brown VL, Cosenza E, Davalos JF, Lesko JJ, et al. Fiber-reinforced polymer composites for construction-state-of-the-art review. *Journal of Composites for Construction, ASCE*. 2002; **6**(2):73-87.
65. Alias MN, Brown R. Damage to composites from electrochemical processes. *Corrosion*. 1992; **48**:373-8.
66. Torres-Acosto AA. Galvanic corrosion of steel in contact with carbon-polymer composites. *Journal of Composites for Construction, ASCE*. 2002; **6**(2):116-22.
67. Gergely J, Pantelides CP, Reaveley LD. Shear strengthening of RC T-joints using CFRP composites. *Journal of Composites for Construction, ASCE*. 2000; **4**(2):408-16.
68. Granata PJ, Parvin A. An experimental study on Kevlar strengthening of beam-column connections. *Composite Structures*. 2001; **53**:163-71.
69. Ghobarah A, Said A. Seismic rehabilitation of beam-column joints using FRP laminates. *Journal of Earthquake Engineering*. 2001; **5**(1):113-29.
70. Liu A. Seismic assessment and retrofit of pre-1970's reinforced concrete frame structures. *PhD Dissertation*, University of Canterbury, Christchurch, 2001.
71. Clyde C, Pantelides CP. Seismic evaluation and rehabilitation of R/C exterior building joints. *Proceedings of the Seventh US National Conference on Earthquake Engineering*, Boston, 2002.
72. El-Amoury T, Ghobarah A. Seismic rehabilitation of beam-column joints using GFRP sheets. *Engineering Structures*. 2002; **24**:1397-407.
73. Ghobarah A, Said A. Shear strengthening of beam-column joints. *Engineering Structures*. 2002; **24**:881-8.
74. Antonopoulos CP, Triantafillou TC. Experimental investigation of FRP-Strengthened RC beam-column joints. *Journal of Composites for Construction, ASCE*. 2003; **7**(1):39-49.
75. Ghobarah A, El-Amoury T. Seismic rehabilitation of deficient exterior concrete frame joints. *Journal of Composites for Construction, ASCE*. 2005; **9**(5):408-16.
76. Pampanin S, Bolognini D, Pavese A. Performance-based seismic retrofit strategy for existing reinforced concrete frame systems using fiber-reinforced polymer composites. *Journal of Composites for Construction, ASCE*. 2007; **11**(2):211-26.
77. Karayannis CG, Sirkelis GM. Strengthening and rehabilitation of RC beam-column joints using carbon-FRP jacketing and epoxy resin injection. *Earthquake Engineering and Structural Dynamics*. 2008; **37**(No. 5):769-90.
78. AC 125. *Acceptance criteria for concrete and reinforced and unreinforced masonry strengthening using fiber-reinforced composite systems.* ICC Evaluation Service, Whittier, CA, 1997.
79. AC 187. *Acceptance criteria for inspection and verification of concrete and reinforced and unreinforced masonry strengthening using fiber-reinforced polymer (FRP) composite systems.* ICC Evaluation Service, Whittier, CA, 2001.
80. JSCE. *Recommendations for upgrading of concrete structures with use of continuous fiber sheet* Concrete Engineering Series 41, Japan Society of Civil Engineers, Tokyo, Japan, 2001.
81. fib. *Externally bonded FRP reinforcement for RC structures, fib Bulletin no. 14*. Federation International du Beton (fib): Lausanne, Switzerland, 2001.
82. TR 57. *Strengthening concrete structures with fibre composites: Acceptance, inspection and monitoring.* Concrete Society, Camberley, Surrey, England, 2003.
83. TR 55. *Design guidance for strengthening concrete structures using fibre composite materials.* Concrete Society, Camberley, Surrey, England, 2004.
84. fib. *Retrofitting of concrete structures by externally bonded FRPs, with emphasis on seismic applications, fib Bulletin no. 35*. Federation International du Beton (fib): Lausanne, Switzerland, 2006.
85. American Concrete Institute (ACI). *Guide for the design and construction of externally bonded FRP systems for strengthening concrete structures. ACI 440 2R.* ACI Committee 440, Farmington Hills, Mich., 2008.

86. Gergely J, Pantelides CP, Nuismer RJ, Reaveley LD. Bridge pier retrofit using fiber-reinforced plastic composites. *Journal of Composites for Construction, ASCE*. 1998; **2**(4):165-74.
87. Tsonos AG. Effectiveness of CFRP-jackets and RC-jackets in post-earthquake and pre-earthquake retrofitting of beam-column subassemblages. *Engineering Structures*. 2008; **30**(No. 3):777-93.
88. Antonopoulos CP, Triantafillou TC. Analysis of FRP-Strengthened RC beam-column joints. *Journal of Composites for Construction, ASCE*. 2002; **6**(1):41-51.

Chapter 3 EFFECTS OF VARIATION OF AXIAL LOAD ON THE SEISMIC BEHAVIOUR OF RC BEAM-COLUMN JOINTS

3.1 INTRODUCTION

Review of the previous research on as-built and retrofitted 2D exterior beam-column joints in Chapter 2 has revealed that in most cases the axial load, representing the gravity load, is applied to the column and kept constant throughout the tests. However, exterior and corner columns of a frame structure are subjected to varying axial load due to the earthquake overturning moment. As demonstrated in the second part of this thesis, variation of axial load on the column can alter failure mechanisms in beam-column joints which may jeopardise the integrity of the frame structure during an earthquake. Therefore, it is of great importance to take into account the interaction between the lateral loads and varying axial load fluctuations on the columns, during the assessment and retrofit design of exterior beam-column joints.

Very little experimental and analytical work has been carried out on 2D beam-column joints, accounting for the variation of the axial load during testing. Generally, the effect of axial load on columns or beam-column joints were examined by modifying the level of constant axial load on subsequently tested specimens, and then comparing the results with the performance of a benchmark specimen tested under a given value of constant axial load. It is interesting to note that, in case of experimental studies on interior beam-column or 3D corner beam-column joints in literature, tests were conducted under biaxial loading and concurrent axial load variation. Due to the complexity of the problem and sequence of the investigation in this thesis, these cases are covered in Part 2. Hence, this second part of the thesis consists of four chapters in total and is devoted to the investigation of the possible effects of axial load fluctuations on RC structures, with a particular focus on 2D exterior beam-column joints.

In this chapter in order to provide a clear understanding of mechanics and behaviour, axial load effects on columns and beam-column joints designed according to modern seismic provisions, are examined. After that the expected effects of varying axial loads on exterior 2D beam-column joints are reviewed and discussed. For this purpose, a critical compilation of available experimental studies and analytical investigations are reviewed.

3.2 EFFECTS OF AXIAL LOAD VARIATIONS ON RC STRUCTURES

Columns and beam-column joints are essential and very critical structural elements in both bridges and buildings. Columns support vertical loads from the floors and roof and transmit these loads to the foundations, while beam-column joints transfer loads, including shear and moments at the ends of the beams into the columns. As mentioned, beam-column joints can be a critical region in RC frame buildings designed for inelastic response to severe seismic actions. If not properly designed, failure of these elements has catastrophic consequences for a structure. These elements are subjected not only to vertical loading effects from gravity, but also to combined variable axial force, moments, and shears due to actions such as wind or earthquake loadings.

Columns and beam-column joints, especially the exterior ones, in multicolumn bent bridges or tall buildings, can be subject to variable axial forces, corresponding proportionally to the applied lateral forces. During an earthquake, lateral inertial forces produce overturning moments which are translated into axial forces in the column, compressive on one side of the frame and tensile on the opposite. These forces are largest in the external columns of the frames and in the bottom storey (Figure 3–1).

On the columns of high rise RC frames, their elasto-plastic properties, such as instantaneous rigidities, crack stresses, and yield stresses are varied from moment to moment by the fluctuating axial forces during earthquakes. For example, on the exterior columns, at the tension side, cracking occurs earlier and the column rigidities and strengths may decrease substantially compared to interior joints. Internal forces of a column with crack patterns under either low or tension axial forces, along with their effects are shown in Figure 3–1. Test observations indicated that when axial compression decreases, specimens exhibit much softer behaviour than those tested under constant axial load levels [1]. This may be attributed to the following three reasons (1) axial compression was reduced and the location of the neutral axis was shifted towards the extreme compressive fibre. Subsequently, the effective area of the cracked section was reduced and less material was effective in resisting flexural demand; (2) strain reversals were large because of the axial-force variation and thus reinforcement softened as a result of the Bauschinger effect; (3) previously opened flexural cracks were closed slowly, because axial compression was being relieved. In addition, cracks on the opposite face widened quickly, because of

the continuous shifting in the neutral axis location. On the other hand, when axial compression increase the reverse of these tendencies is observed. For example, typically, it is observed that the presence of the compression force in the concrete ensures that the cracks, which opened up in the previous half-cycle with the tension yield of the reinforcement, close with the load reversal. The resulting compression force in the concrete can follow an inclined trajectory, with the transverse component of this force resisting some of the shear. This action, together with the closure of the crack in the compression zone, reduces the shear pinching effects. As illustrated in Figure 3–1, the inclination of the compression force (from vertical) in columns, reduces as the magnitude of the axial load increases. It is well known that, with increasing load, initially there is an increase in the shear carried by the concrete, but at high axial load levels this value decreases.

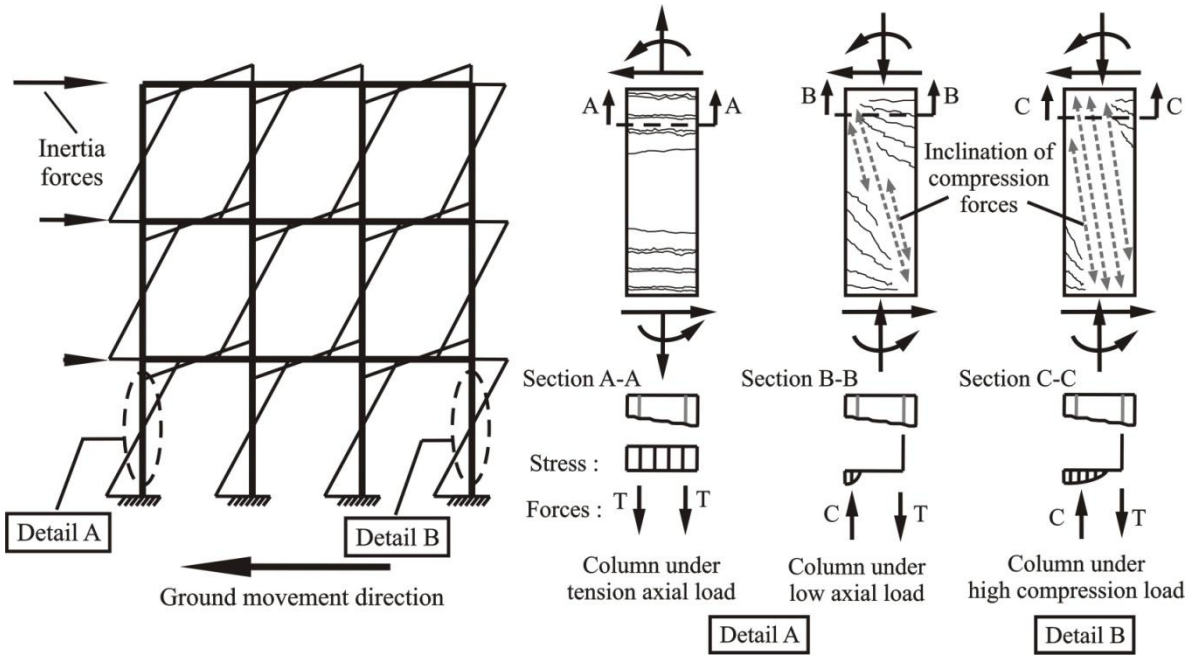

Figure 3–1 Statics of laterally loaded frame and external actions with internal forces of exterior columns under various axial load levels

Under earthquake excitation, columns in a structure are also subjected to the vertical actions of ground motions, which are nonproportional to horizontal loading. It has been shown that, in some cases, particularly for near-fault situations, the vertical ground motions cannot be ignored [2]. There is a wealth of earthquake records that exhibit a vertical component with ground acceleration well in excess of the corresponding horizontal value [3, 4]. Coupling of overturning moment forces with the forces produced by vertical ground motion may induce tension loads which are large enough to crack columns. The Petunia II apartment building's performance during the 1967 Venezuela earthquake can be given as an example of this type of failure [5]. With the columns cracked in tension, the entire axial load must be carried by the steel reinforcing bars, which can possibly be straining the column enough

to produce bond failure. Whether or not bond failure occurs in the column, tension loading on the joint core provides an adverse stress condition, which can increase the rate of deterioration [6]. Park and Paulay [7] also noted that flexural strength, stiffness, ductility and energy dissipation capacity of RC columns, are all affected by the presence of axial force.

As will be seen in the following, the effect of high dynamic axial force on the lateral hysteretic response cannot be neglected for RC structures, because of significant change in the hysteretic moment-curvature relationship, as well as the overall structural behaviour.

In light of aforementioned observations, it can be said that unsatisfactory response in terms of lateral displacement ductility of a column may emerge from a design based on constant axial load assumptions. In the case of overturning effects and/or vertical ground motion, the preliminary assumption of a relatively low axial load ratio in the column may be exceeded. As a consequence of increasing axial load, shear demand will also intensify in the columns, in which case insufficient shear strength may lead to a catastrophic failure. Further to this, significant decreases in the column shear strength may occur in the case of changes in axial load from compression to tension.

A great deal of experimental and analytical research has been conducted recently which has led to the current approach for the seismic design of RC columns and beam-column joints. Due to the complicated nature of the response of RC structures, which is affected by many phenomena (i.e., cracking and crushing of the concrete, yielding of steel and strain hardening, creep and shrinkage, degree of concrete confinement), there are still many facets of the behaviour that are not fully understood. The significance of considering non-proportional variations in axial load in the seismic design of RC structures is also emphasised by many researchers [8]. The researchers indicated that axial load non-proportional variations are not just another parameter that can be considered within the frame work of current approaches, but that its effects are so significant that new methodology and models are needed to assess the inelastic cycle response of RC columns under coupled fluctuations in axial and lateral loads.

Due to the recognition of the significant effects of large variations of axial forces, research in the early 1990s was facilitated towards the understanding of these effects on the seismic response of RC columns. However, most of the previous research conducted was limited to experimental and analytical studies of these elements, subjected to horizontal seismic loading, with axial load level held constant at a particular level. For the sake of completeness in the clarification of varying axial load effects on the RC structures and particularly on beam-column joints, a brief review of the

investigations on the RC columns, with axial load varying during cyclic lateral loading, can be found in Appendix A.

3.3 INFLUENCE OF AXIAL FORCE VARIATIONS ON BEAM-COLUMN JOINTS

Before investigating the influence of axial load on the behaviour of beam-column joints, it is deemed to be useful to provide information on the basic qualitative mechanics and inner workings of these elements. This information is of crucial importance not only for this section, but also for the remainder of the thesis. The first part of this section is devoted to the behaviour of beam-column joints which are designed to modern code provisions; afterwards, the behaviour of older type deficient 2D exterior beam-column joints, either in as-built or retrofitted condition, will be examined in detail.

To start with, simple considerations of statics can be applied to an interior beam-column joint portion of a frame structure under lateral loading (Figure 3–2) to gain some information on the basic mechanics. Shear forces are developed due to a moment gradient present along the axis of beams and columns, which in turn leads to the formation of horizontal and vertical shears. Equilibrium of the joint region suggests that the sum of beam moments must be equal to the sum of column moments. Joint shear stress can be obtained by dividing one of these moments by the joint volume. Accordingly, a unique shear stress value in the joint region is obtained although horizontal and vertical joint shears are not equal. Same considerations can be made for any type of joint in a frame structure (i.e., external, edge or top).

In the next stage, the statics of an isolated interior beam-column joint will be reviewed to illustrate the inner mechanism of a typical beam-column joint. As a result of the forces transmitted into the joint by connected frame members, concrete flexural compression from the beam and the column will develop at opposite corners of joints in laterally loaded frames, suggesting the formation of *diagonal concrete compression strut*. As seen in Figure 3–3, tension and compression forces will be acting at the boundaries on the column reinforcement, passing through the joint and beam reinforcement. Consequently, *bond forces* are generated and introduced into the joint core from bars at the outer face of the column, and the tension force developed in the top bars of the beam. In RC frame structures designed according to modern seismic codes, potential plastic hinges in beams or columns are detailed to ensure that they can provide the necessary ductility and associated energy dissipating capacity through inelastic deformation. However, due to the fact that the response of joints is governed by shear or bond mechanisms, both of which exhibit poor hysteretic properties, they are not regarded as a reliable source of energy dissipation [9].

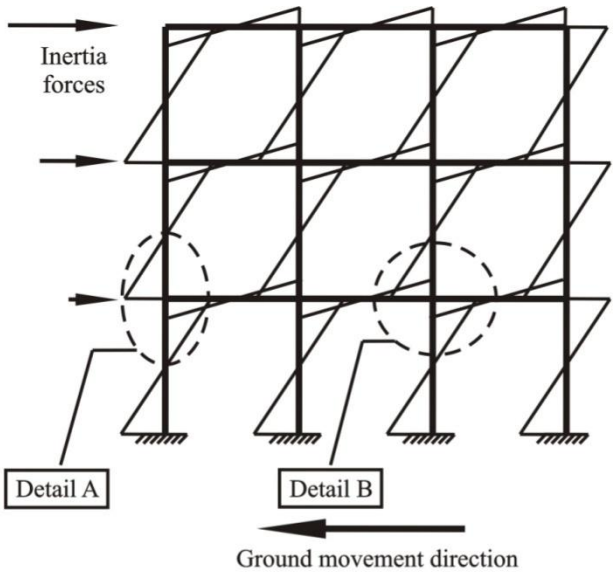

a) Statics of laterally loaded frame

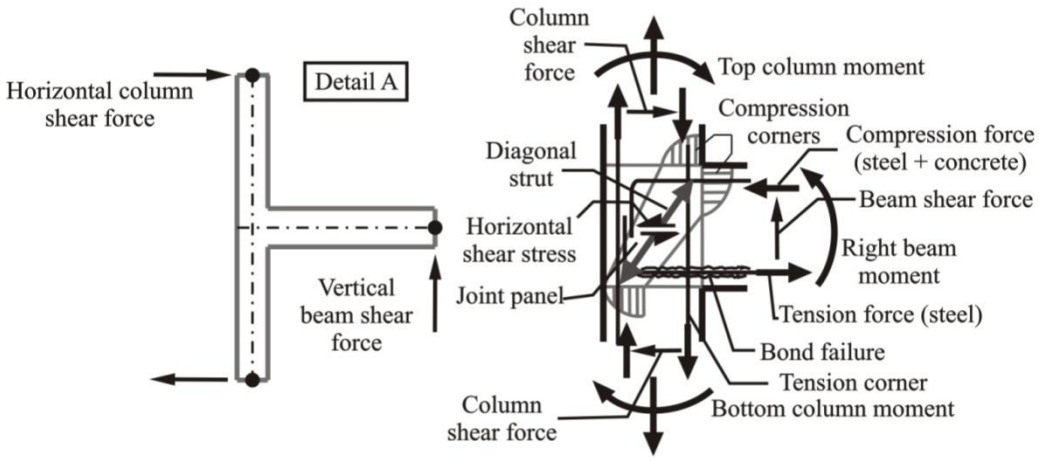

b) External forces and idealized internal actions of exterior beam-column joint

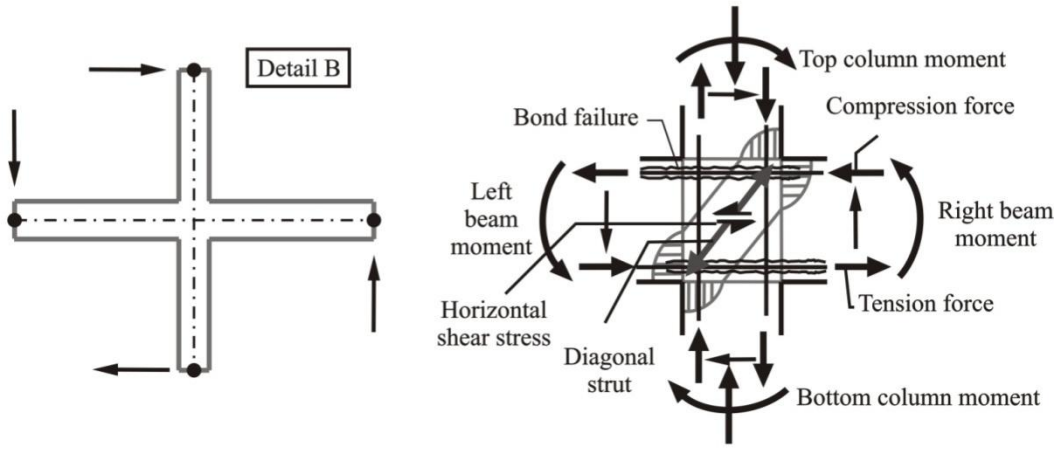

c) External forces and idealized internal actions of interior beam-column joint

Figure 3–2 External actions and internal resultants at exterior and interior joints

In general, any corresponding failure to resist the aforementioned mechanisms may be recognised as a joint shear failure. It follows then that joint failures, whether or not they arise from shear, can result from any or all three possible sources a) loss of bond resistance along the joint boundary; b) inability to resist joint internal stresses, resulting from successful development of perimeter bond forces; c) inability to sustain diagonal compression strut in joint core [10]. At this point, it is interesting to note that, although joint dimensions are not treated as an active variable in the design of joints, in practical terms, due to its beneficial effects on the performance, the dimensions of columns (e.g., depth and width) are generally modified. For instance, increasing column depth offers the dual benefit of reducing joint shear stress and lowering bond demand along beam bars passing through a joint, tending to suppress all three of the modes of failure.

Although it seems to be a straightforward and an easy task to define a joint resistance mechanism, the principles to be applied for design of RC beam-column joints, have still not reached consensus in the research community. Due to the interaction of several phenomena such as shear, bond, fatigue and confinement, the resolution of the RC connection behaviour problem still remains a great challenge for structural engineers. Furthermore, the inherent interaction of the two materials (reinforcement and concrete), and the material non-linearity, render the problem internally indeterminate, therefore most test results will accommodate more than one alternative physical interpretation [10]. Hence, recommendations for different building codes, which are often entirely empirical, conflict with each other [11].

Among the common conflicting views, the function of transverse reinforcement and whether or not column axial force is beneficial can be given as typical examples. In order to illustrate these, two models, forming the basis of design requirements of New Zealand and the United States, are reviewed in the following paragraphs.

In the New Zealand code of practice and the CEB model code [10], the design rules are based around two shear mechanisms. Accordingly, some of the internal forces, particularly those generated in the concrete, will combine to develop a *diagonal strut* (Figure 3–3b). This mechanism is very efficient if the compression stresses in the diagonal strut are not excessive. In addition, it is postulated that a fraction of the total horizontal force that is to be transmitted by the beam top flexural reinforcement to the joint by means of bond, will be transmitted to the diagonal strut. Similarly, a fraction of the total force developed in the vertical column bars may be transmitted to the same mechanism of the joint. Similar concrete compression, shear, and bond forces at the lower right-hand corner of the joint will combine into equal and opposing diagonal compression forces. When axial force is not applied to the

column, the inclination of the strut is similar to that of potential failure plane in (Figure 3–3b). With axial compression in the column, transmitted through the joint, the inclination of this strut will be steeper.

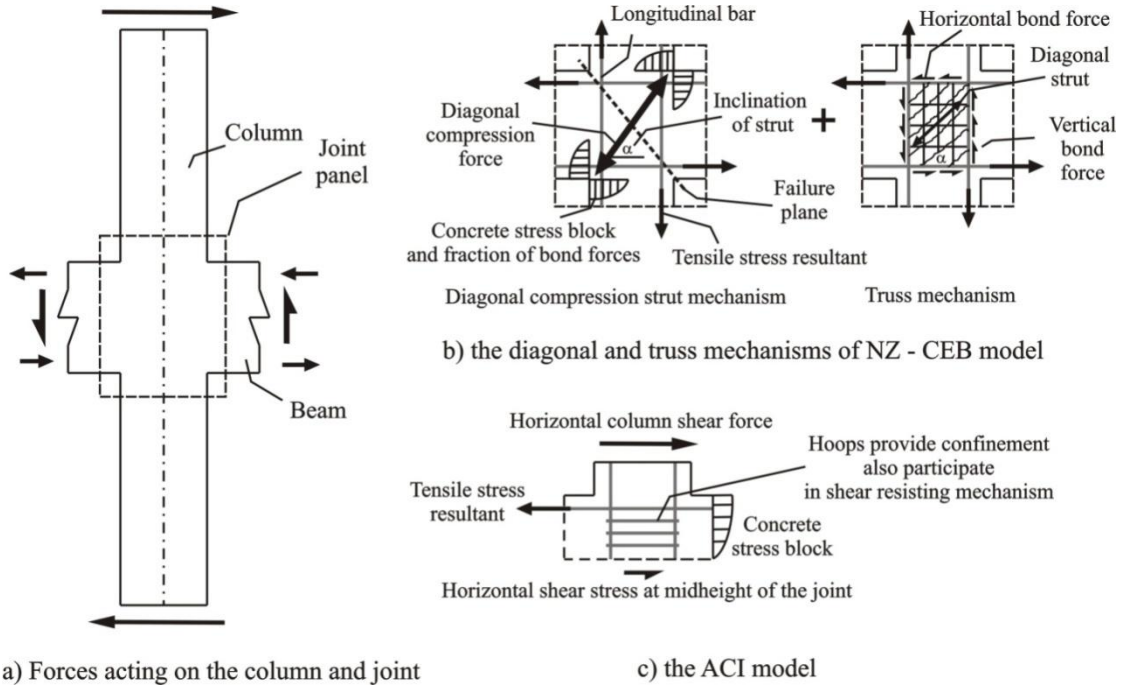

Figure 3–3 Different approaches of design model for beam-column joints

Other forces, transmitted to the joint core from beam and column bars by means of bond, necessitate a *truss mechanism*. For example in the top beam bars, the bond force is expected to be introduced to the core concrete in the form of shear flow as suggested in Figure 3–3b. Similar bond forces, introduced to the concrete at the four boundaries of the joint core model in Figure 3–3b, being in equilibrium, will generate a total diagonal compression force. Contributions of this mechanism are based on the assumption that, in a thoroughly cracked core of a joint, no (diagonal) tensile stresses can be transmitted by the concrete. To prevent shear failure by diagonal tension, usually along a potential corner to corner failure plane, both horizontal and vertical shear reinforcement will be required. Such reinforcement will enable a diagonal compression field to be mobilized which provides a feasible load path for both horizontal and vertical shearing forces. When beams with very small amounts of flexural reinforcement are used, or when column sections relative to beam sizes are large, joint shear stresses may be rather small and no or very few diagonal cracks may develop. As the concrete core in such cases will resist shear by means of diagonal tensile stresses, the truss mechanism in Figure 3–3b will hardly be mobilized. The amount of horizontal joint shear reinforcement required may be significantly more than would be provided in columns in the form of ties or hoops, particularly when axial compression on columns is small [7].

The shear mechanisms of exterior joints can be regarded as similar to that of the interior joints explained previously. The shear transfer mechanisms *concrete strut* and *truss* within the joint core are similar to that postulated for interior beam-column joints. However, the joint shear will be less than that of interior joints, because only one beam frames into the column (Figure 3–2). It is important to note that due to the earthquake, induced overturning moments and the vertical component of the earthquake motion in frame structures, the net axial compression may be reduced and may even result in net tension acting on the column and the joint. Under this condition, critical situations may arise; design objectives in providing a favourable strength hierarchy in the subassembly (i.e., strong-column/weak-beam) may be altered due to the change in the hierarchy of strength of the elements (e.g., beam, column and joint panel). This will be covered in detail in the following chapter.

Axial compression forces influence the depth of the column flexural compression zone, hence it is reasonable to expect that the column axial force will affect the mechanism of a joint. To be conservative, the concrete contribution to the joint shear resistance, resulting from strut action, is accounted for only if the axial force in the column is significant. According to Paulay and Priestley [9], axial load improves joint performance by increasing the inclination (from horizontal) at which the main strut develops. Another beneficial effect of the increase in axial load can be accounted for the improvement of the bond conditions between the reinforcing steel and concrete. On the other hand, as column compression continues to increase, the compression zone will extend further along the joint boundaries; a more pronounced diagonal compression strut also decreases in inclination, suggesting that its contribution to shear resistance will become less significant. This may also result in attracting larger shear forces in the joint region. At this point, when the joint shear force is large and extensive, diagonal cracking in both directions has occurred in the joint core and the strength of the diagonal compression field, rather than the joint reinforcement, may control the strength of the joint. However, large axial load levels may result in failure of the joint from diagonal crushing. Because of these reasons, the angle of a diagonal compression within the chosen shear mechanism, along with the axial load levels on columns, is kept within certain limits. Moreover, excessive tensile strains in the horizontal joint ties are permitted to develop as a result of the functioning of the joint shear reinforcement. The diagonal compression strength of the concrete may reduce due to the tensile strains in both the horizontal and vertical directions. Eventually, diagonal compression failure of the core concrete under repeated cycles will occur.

On the other hand, in a distinctively different approach used in North American practice [12], the joint is treated as part of the column and the integrity of the connection is secured by horizontal hoop

reinforcement, which is provided in the column within the joint region. The role of hoop bars in the diagonal compression strut model is to confine the concrete. The shear stress level is checked to ensure it does not exceed a certain level and confinement reinforcement is provided in the same way as is required for a column. A critical value of horizontal joint shear, that is assumed to be the input to the joint when adjacent beams develop their flexural resistance, can cause dilation of the joint core. Accordingly, severe bond deterioration of the reinforcing bar in the joint occurs, and the internal forces can only be transferred via a diagonal concrete strut. Due to these contrasting views of the function of transverse reinforcement, different detailing criteria are employed in the design of the connection of modern ductile RC frame structures.

The aforementioned models to describe the flow of forces for the prediction of strength in beam-column joints are postulated based on empirical interpretations of specialized experiments. As an alternative approach, Pantazopoulou and Bonacci [13] developed a formulation to evaluate the basic mechanics of a joint. The formulation allows determination of the magnitude and the direction of principal concrete stresses and strains based on the equilibrium of stress resultants, compatibility of deformations within the joint, and incorporate available models of material nonlinear behaviour. The authors also studied the sensitivity of the joint behaviour to various design parameters, using the developed model. It was shown that the shear strength of a joint depends on the usable compressive strength of concrete, which decreases with the increasing principal tensile strain at the centre of a planar joint region. Since the principal tensile strain increases with increasing column axial force, this would accelerate the strength degradation. It was also observed that axial force and average joint shear stress tend to increase shear distortion.

Bonacci and Pantazopoulou [14] reported the investigation of the influence of various design variables (i.e., axial load, amount of transverse reinforcement, concrete strength) based on the observations drawn from a database of eighty-six beam-column joint tests compiled from published literature and the model developed in the preceding paragraph. The particular aspects of the response that was considered in the parametric study were the joint shear stress and shear deformation that can be tolerated up to the point of hoop yield. In Figure 3–4, the measured maximum joint shear stress factor was plotted against the nominal column axial stress (normalized by compressive concrete strength) for the entire collection of tests that failed due to shear or beam hinging. Researchers indicated that due to the scatter of the experimental values of shear stress factor, the axial load has no discernible coherent influence on the strength of beam-column joint. Lastly, the authors commented that the deformability, rather than the strength of such members is affected by the presence of axial load; however, due to the

scarcity of available experimental information regarding deformations, no generalized conclusions can be warranted.

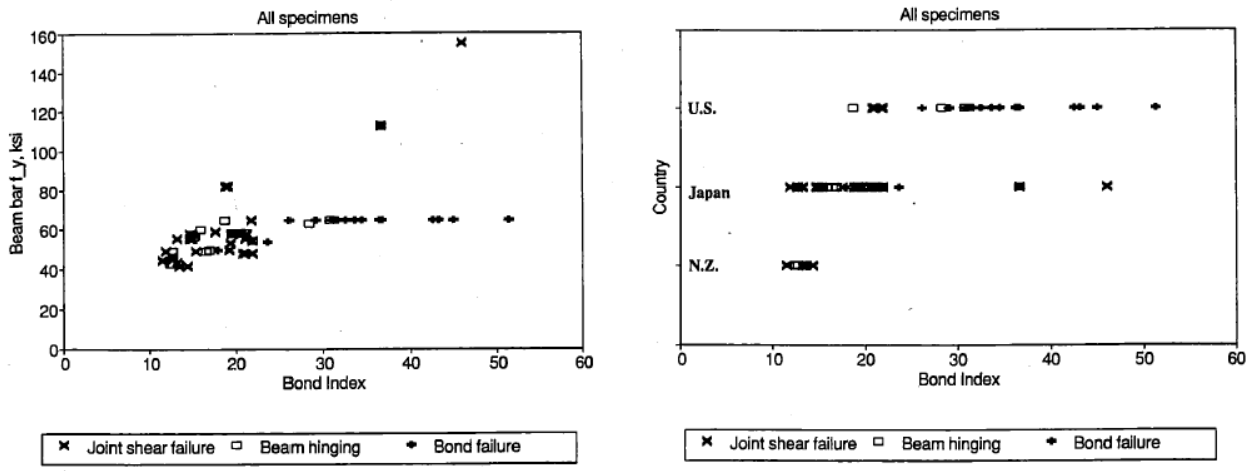

Figure 3–4 Influence of column axial stress on joint strength for interior connections: a) joint shear failures; b) beam hinging (units in psi)

Tsonos *et al.* [15] conducted an experimental investigation to compare the response of beam-column joints subjected to seismic type loading under constant and variable axial load. A total of fourteen ductile exterior beam-column connections were tested to study various parameters (i.e., varying axial load, P-Delta effect, and joint shear stress level). A comparison of the seismic performance of specimens tested under constant axial load and other specimens with variable axial load levels indicated that axial load changes during seismic loading produces significant deterioration in the beam-column joint earthquake resistance. P-Delta effects did not significantly affect the overall joint behaviour and therefore they can be ignored in detailing beam-column connections.

Of the eight specimens tested in the investigation performed by Uzumeri [16], three exterior reinforced concrete beam-column joints were tested under constant axial compressive load equal to $0.42f'_cA_g$. The three specimens were not reinforced in the joint area. Two of the specimens contained a transverse stub beam on one side of the column, whereas the third specimen had no transverse stub. Load reversals after bond loss caused large deformations in the concrete, resulting in splitting along column bars and anchorage failure of the beam steel. In all three cases, the beam remained intact, while the joint rapidly deteriorated with increasing imposed displacements. The presence of this axial load is of help at the early stages of loading. However, at the latter stages, when the concrete core acts as a series of struts, it is proposed that the large axial load may be detrimental, rather than helpful. The researchers concluded from this study that whether a large axial force continues to be of help once joint deterioration starts is debatable.

To examine this important effect an additional unit was tested at the University of Toronto by Seckin and Uzumeri [17] under low axial load. In contrast to the idea that high column compressive force improves the shear carrying capacity of the joint and delays bond failure by improving the anchorage conditions, it was found that with the exception of an early reduction of stiffness in the inelastic cycles, the level of column axial force had a negligible effect.

Townsend and Hanson [6] performed research on twenty-two reinforced concrete beam-column T shaped connections. The three test parameters examined in detail included: the magnitude of column axial load including axial tension, the magnitude of hinge rotation, and the number of cycles of inelastic loading. These specimens were tested under column axial tension ($0.25f'_cA_g$), column axial compression ($0.15f'_cA_g$), and no column load. It was shown that increased column tension causes the moment capacity to decrease more rapidly, representing a faster rate of concrete deterioration, than the specimens with no column load or column compressive load. In Figure 3–5 hysteresis data for three specimens tested under different axial load amplitudes are given. As seen in this figure, the most rapid loss in moment capacity occurred during the first several cycles, and that increased column tension causes the moment capacity to decrease more rapidly.

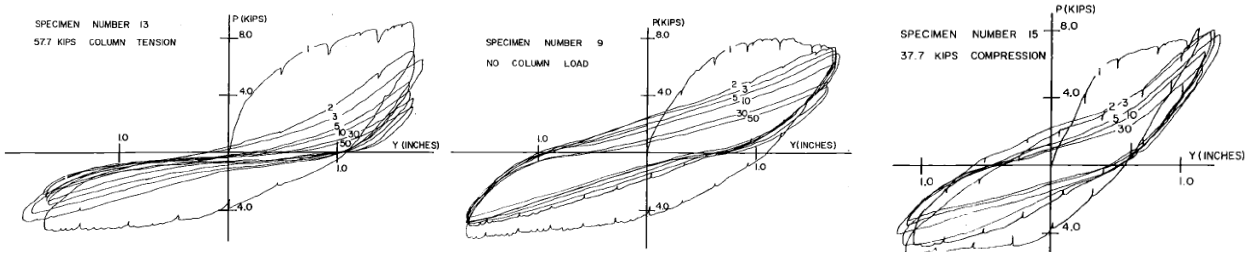

a) Column under axial tension b) No column load c) Column under compression load

Figure 3–5 Effect of tension axial load on the specimens studied by [6]

An experimental study of three exterior beam-column joints performed by Scarpas indicated that the horizontal joint shear reinforcement may be reduced considerably [18]. However, the vertical shear reinforcement (i.e., intermediate column bars) was the same in all units. The effect of the axial load was studied in one of the units when it was reduced from $0.15f'_cA_g$ to $0.075f'_cA_g$; this resulted in a dramatic reduction of the stiffness, strength, and energy dissipation of the specimen in the later loading cycle.

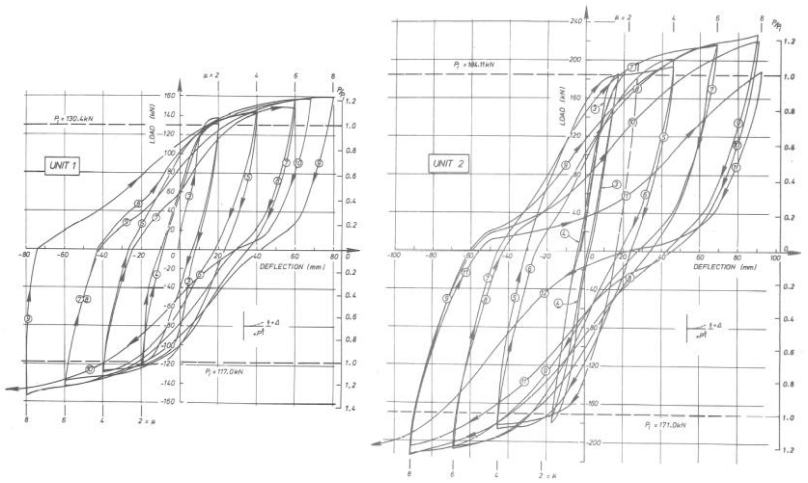

a) b)

Figure 3–6 Experimental study by Scarpas [18]: a) specimen tested under $0.075f'_cA_g$ axial load level; b) specimen tested under $0.15f'_cA_g$ axial load level

As seen in the previous chapter, a large number of tests of deficient 2D exterior beam-column joints designed before the 1970s, without modern code seismic provisions or capacity design principles (i.e., insufficient shear reinforcement, widely spaced column ties, and little or no transverse reinforcement within beam-column joint regions) have been conducted by researchers in countries located in high seismic areas, as well as in low ones. This chapter presents the findings and discussions based on the investigations of axial load effects on the test specimens, either in as-built or retrofitted configurations. It is already emphasised that similar to the existence of disparities among design models for beam-column joints, there is also dispute on the effect of axial load on beam-column joint strength, despite the availability of extensive experimental evidence. In the case of weak column–strong beam design, it is obvious that increasing the column axial load up to the balanced point, improves the joint shear strength, because the column moment capacity is positively affected by the axial load. However, in light of previous discussions on the unfavourable effects of the variation in axial load on the tested well-designed beam-column joints, it can be intuitively said that the seismic performance of older beam-column joints will be more drastically affected by the fluctuation of axial load levels. It is important to note that, due to the very few experimental studies on the performance of older type joints under varying axial load, a summary of other researchers' findings on the effects of different constant axial load levels will also be provided.

Same resistance mechanisms employed for well-designed beam-column joints can be used to qualitatively describe the behaviour of older type joints. However, due to the lack of horizontal and vertical reinforcement in the joint region and also in most cases the use of smooth reinforcement bars in older construction before 1970s, the truss mechanism due to bond transfer, will be invalid in the

shear resisting mechanism in the joint. As a consequence, the only resisting mechanism can be taken as the diagonal compression strut due to compression forces acting on the periphery of the joint panel. From this point of view, increase of the column axial load may be beneficial in the shear strength of the joint panel. The compression block depth of the column, which affects the compressive diagonal strut, will definitely increase with the increase in column axial load. Therefore, this will lead to an increase in the shear strength, because the concrete's contribution to the shear resistance will be higher. Another positive effect of increasing axial load will emerge from the fact that the improvement of the bond strength due to axial load, increases between the beam reinforcing bars and the surrounding concrete. Since the horizontal shear force is transferred into the joint by bond and anchorage of the beam reinforcement, better resistance of the bonded forces will be achieved due to higher axial loads.

From the experimental findings discussed in Chapter 2, due to the intrinsic lack of alternative and reliable sources of shear transfer mechanisms within the panel zone region, performance of old-type joints appears to be particularly sensitive to the cracking in the joint panel. Actually, it has been shown that most of the joint shear failures take place after cracking in the joint panel. It is obvious that, in the case of older type beam-column joints, the beneficial effects of high axial loads are limited by the onset of the diagonal tension cracks in the joint panel. Due to the lack of inadequate transverse reinforcement in the joint region for shear and confinement, there will be no shear carrying mechanisms in the joint panel to limit the crack widths. Moreover, the Poisson's effect will encourage the widening of the cracks and acceleration of the crack propagation along the diagonal compression strut. Consequently, a rapid deterioration in the shear strength of the joint will occur under high axial load. Ultimately, the failure of the diagonal strut will be triggered.

Hakuto *et al.* [19] reported the comparable observations as given previously in the preceding chapter. Test results indicated that a diagonal compression strut was activated following diagonal tension cracking in the joint core. The crushing of the diagonal compression strut occurred when the compressive strength of the strut is sufficiently weakened by diagonal tension strains and by the repeated opening and closing of diagonal tension cracks in alternating directions. Accordingly, the authors concluded that the most simple failure criterion for a beam-column joint without shear reinforcement would appear to be diagonal compression failure criteria. It was also deduced that the presence of axial compression in the column would delay the appearance of diagonal tension cracking. When axial compressive load is present on columns, a greater horizontal joint shear stress would be tolerable, but some joint core hoops would be necessary to prevent column bar buckling. It was also pointed out that if the axial compression stress is very high, diagonal compression failure by crushing

of the diagonal compression strut could also occur, before the horizontal shear stress level at first diagonal cracking is reached.

Thirty-four full scale bare interior and exterior beam-column joints were tested by Beres *et al.* [20] under reversed cyclic loading to identify the different damage mechanisms and to study the effect of critical details on strength and deformation. In the interior joints the higher column axial force of $0.39f'_cA_c$ resulted in higher peak strength values, with a more rapid strength degradation. Higher column axial force or the presence of 2-#3 ties within the joint produced higher maximum strength capacities and a more gradual strength degradation. The researchers also conducted an investigation on the influence of various parameters on the joint shear strength factors, which are recommended by [21] and used in the calculation of joint shear strength. Although as was expected, the actual joint shear strength factor values were 30-40% below the limiting values specified by the ACI-ASCE 352 Recommendations for "properly" detailed connection regions, a strength increase of 15-25% was detected when higher column axial load was used. The researchers stated that there was a beneficial effect of higher levels of axial load on the column. In all cases the specimens with higher axial load delayed the onset of critical shear cracking and also helped to provide better confining action to the embedded bars, delaying their incipient pullout. In a building subjected to the overturning effects during an earthquake, the columns on the compressed side of the buildings would perform better than those on the other side.

Liu [22] also stated the beneficial effects of higher axial loads on the performance of tested exterior beam-column joints designed according to pre-1970`s codes. A total of four exterior beam-column joints with the reinforcement details similar to units studied in Hakuto *et al.* [19]. Two of the units were tested under zero axial load, with the other two specimens being tested under axial load of $0.23f'_cA_g$ and $0.25f'_cA_g$. It was observed that units tested under axial load, showed a large increase in the stiffness and strength. Compressive axial column load delayed premature concrete tension cracking initiated by the beam bar hooks.

Pampanin *et al.* [23] carried a series of tests on six 2/3 scale beam-column subassemblies designed for gravity only with structural deficiencies typical of the Italian construction practice between the 1950`s and 1970`s. Among the specimens, two exterior tee-joints were tested under quasi-static loading with concurrent varying of the axial load which was varied during the tests as a function of the lateral load. The axial load vs. lateral-force relationships for exterior and interior joints was evaluated with preliminary pushover analyses on the three-storey-three-bay RC frame system. Significant variations of the axial load up to 40-50% (increase and decrease) with respect to the value due to the gravity load

only case were observed. During the tests of the beam-column joint specimens, a simplified bilinear relationship between the axial load and lateral load was adopted as shown in Figure 3–7a. Extensive joint shear damage in the joint panel zone was observed in the concrete leading to a large shear distortion. A lateral load-displacement plot of an exterior beam-column joint tested under varying axial load is given in Figure 3–7b. An increase in the lateral load capacity of the specimen in the negative direction of loading, which corresponded to increase in axial load, can be noticed in the figure.

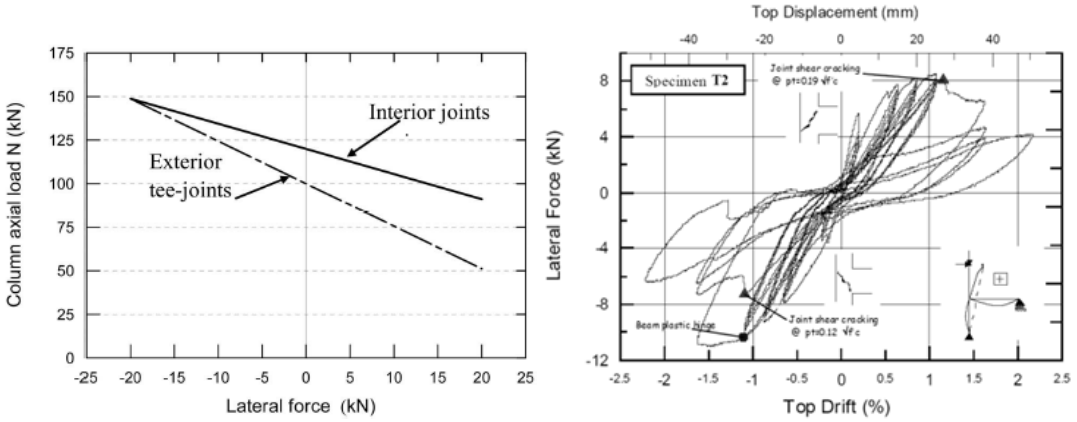

a) Axial load versus lateral load relationships for interior and exterior joints

b) Lateral load-displacement plot of an exterior beam-column joint tested under varying axial load

Figure 3–7 Experimental study by Pampanin *et al.* [23]: a) Axial load variation vs. lateral force; b) load-displacement hysteresis loop

Clyde *et al.* [24] reported the test results of four half-scale non-ductile exterior beam-column joints. The joints were subjected to quasi-static cyclic loading. Two levels of axial compression load in the columns were investigated. An axial compressive load equal to $0.1f'_cA_g$ was applied to two of the specimens. The other two specimens received an axial compressive load equal to $0.25f'_cA_g$. Although constant axial load was applied to the columns at the beginning of the tests, the testing setup caused the axial load to fluctuate during the test. Researchers noted that, although in an actual building the compressive load in a column would vary differently, the fluctuations were considered reasonable.

The load versus drift curve for a specimen tested with 10% axial load and the relationship between the column axial load and drift are given in Figure 3–8. Ultimate failure of the beam-column specimen is attributed to the development of the limiting joint shear capacity. It was observed that as a result of the stiffness loss due to progressive cracking in the joint and column at higher drift levels, the overall axial load in the column deteriorated during the test, as can be seen in this figure.

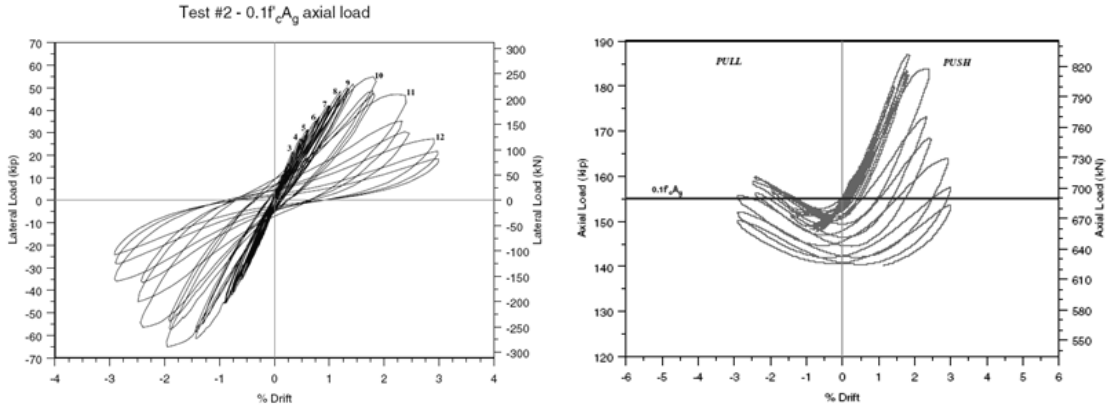

a) b)

Figure 3–8 Experimental study by Clyde *et al.* [24]: Specimen tested under $0.10f'_cA_g$ axial load level a) load-drift curves; b) axial load variation

The load versus drift curve for a specimen tested under 25% axial load of the column capacity is given in Figure 3–9. Extensive cracking in the joint and column resulted in loss of stiffness at high drift levels. The column load reduction from the $0.25f'_cA_g$ axial load is due to the closure of cracks that opened in the push cycle and closed in the pull cycle. It was observed that, by the end of the test, the compressive load had dropped 17% from the original value. Overall, it was reported that only a very slight variation in the peak lateral load was sustained by each specimen. The level of column axial load compression did not appreciably affect the strength in regards to cyclic load capacity. There was a distinct difference in ductility, however, between the specimens with 10% axial load and those with 25% axial load. The specimens with the lower axial load were over one and a half times as ductile as the beam-column joints with higher column compression. The lower drift percentage for the specimens with 25% axial load confirms their more brittle characteristics when compared to the 10% axial load specimens.

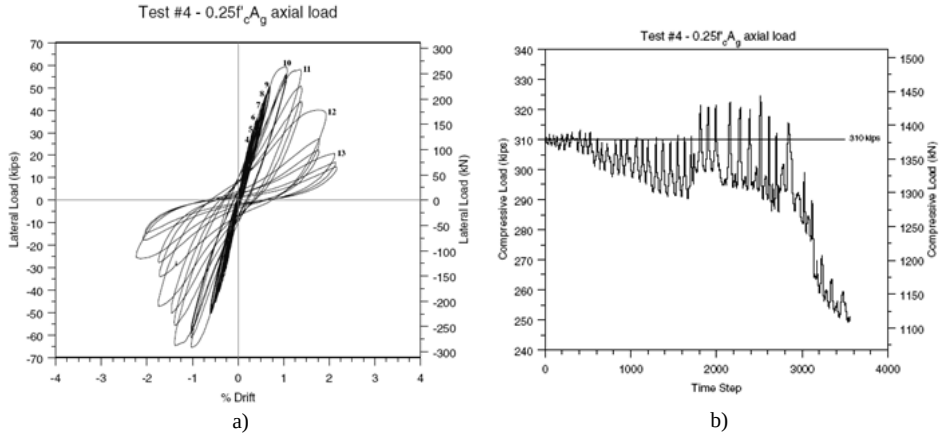

a) b)

Figure 3–9 Experimental study by Clyde *et al.* [24]: Specimen tested under $0.25f'_cA_g$ axial load level a) load-drift curves; b) axial load variation

Hertanto [25] and Chen [26] performed a series of tests on six two-third scale exterior beam-column joints with typical detailing of pre-1970s buildings under quasi-static cyclic loading. Details of this study were given in Chapter 2. A varying axial load was also applied on the top of the column, with 75 kN initial loads representing the gravity load. The axial load was then varied during the test in proportion to the lateral load, with a proportion coefficient of 1.8 (e.g., $N=N_g\pm1.8V_c$). Experimental results showed that the strength of the specimen was slightly increased with the increase in axial load level, however, the opposite trend was observed in the negative direction where the axial load is decreasing. It was also noted that the axial load applied in the positive loading direction could be double the axial load applied in the negative loading direction, although the difference in terms of joint principal tensile stress was not that high (Figure 3-10). The horizontal shear in the joint area reached 117 kN and -94 kN in the positive and negative loading directions respectively. The principal tensile stress reached $0.3\sqrt{f'_c}$ and $0.27\sqrt{f'_c}$ in the positive and negative loading directions respectively. The axial load applied to the top of column was varied from $0.17\sqrt{f'_c}$ to $0.4\sqrt{f'_c}$.

Parvin *et al.* [27] performed an experimental study under a quasi-static cyclic loading, on six full scale as-built and CFRP-strengthened RC exterior beam-column joints, with the focus on delaying or avoiding the pull-out of the bottom beam reinforcement and joint shear failures. The specimens were subjected to 24 and 12% of ultimate axial loads. Test results of as-built specimens indicated that by increasing the axial load from 12 to 24% of the column's ultimate axial load capacity, the lateral load carrying capacity of the beam-column joint specimens increased by approximately 20 and 5% for push and pull directions of loading, respectively. Furthermore, in both push and pull directions of loading, initial secant stiffness magnitudes of the specimen tested with 24% of ultimate axial load increased with the increase in the axial load. The effect of applied axial load on the lateral load versus deformation relationship of CFRP-retrofitted joints was not significant in the pull direction of loading. However, in the push direction of loading, with a decrease in axial load from 24 to 12%, a decrease of 12% in the lateral load carrying capacity was observed.

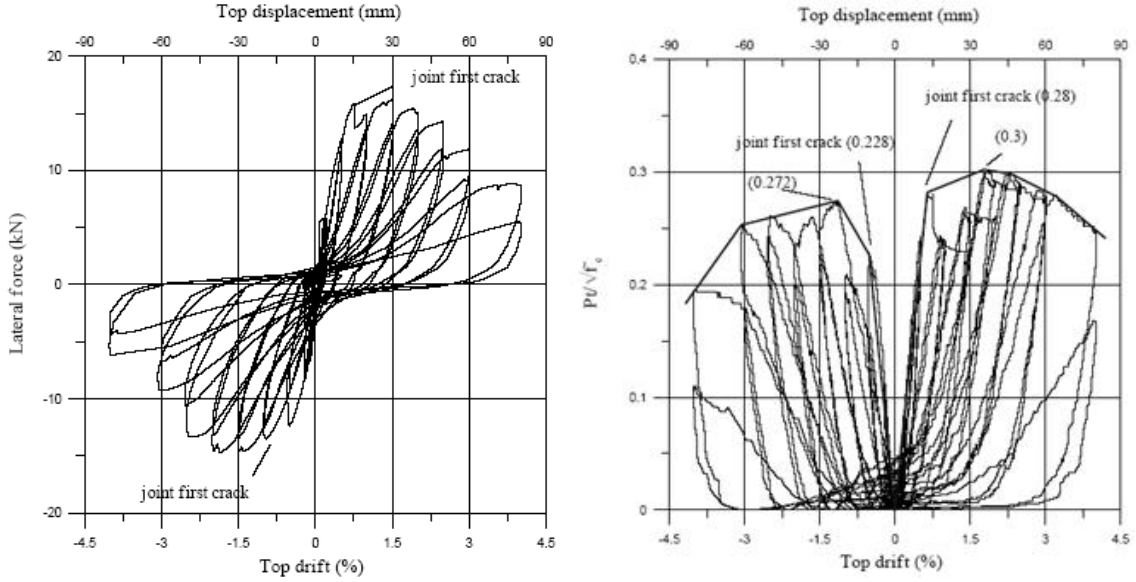

a) b)

Figure 3–10 Experimental study by Hertanto [28] and Chen [26]: a) load-drift curves; b) principal tensile stress versus top drift

Ghobarah and El-Amoury [29] tested two beam-column subassemblies as control specimens under axial column loading of 600 and 300 kN. These load levels represent 20% and 10% of the column section capacity. The objective of this research was to develop effective selective rehabilitation schemes for reinforced concrete beam-column joints using advanced composite materials. The joints were designed to simulate non-ductile detailing characteristics of pre-seismic code construction. The control specimens showed joint shear failure when subjected to cyclic loading at the beam end. No significant differences were observed between the behaviour of joints T1 and T2 subjected to different axial column loads.

The results of a comprehensive experimental programme, aimed at providing a fundamental understanding of the behaviour of shear-critical exterior RC joints strengthened with FRP under simulated seismic load, are reported by Antonopoulos and Triantafillou [30]. Amongst the role of various parameters, the effect of axial load on the effectiveness of FRP is also examined through 2/3-scale testing of 18 exterior RC joints. During testing, application of the axial load was controlled manually and kept constant at a level of 46 kN for all specimens except for specimen F22A, which received a force of 115 kN. Specimen F22 was retrofitted with two layers of FRP sheets on both the beam and the column. The results demonstrated the important role the effect of high axial load on the shear capacity of FRP strengthened joints. F22A exhibited a 2.5 times higher load capacity when compared to specimen F22. The strength increase was from 65% to about 85% and the energy increase was from 50% to 70%, respectively.

3.4 SIGNIFICANCE OF VARIATION OF AXIAL LOAD: CONCEPT OF HIERARCHY OF STRENGTH AND SEQUENCE OF EVENTS

The seismic performance of RC frame structures is strongly dependent on the *hierarchy of strength* within the lateral-load carrying system. Recent experimental and analytical investigations on the seismic performance of existing RC frame buildings designed without seismic provisions have corroborated the inherent weakness of these systems stemming from low ductility and lack of capacity design principles [31-36]. As a consequence, at the global level, a weak-column strong-beam, as typically seen in gravity only designed RC frame structures, could induce a soft-storey mechanism; at the local level, local brittle failures may occur due to inadequate protection of the joint panel, such as the shear collapse of the panel due to the lack of transverse reinforcement within the beam-column joint subassembly. In order to achieve a satisfactory seismic performance, a proper retrofit strategy should aim to convert the (often inadequate) hierarchy of strength within the existing beam-column joint subassemblies (consisting of beams-column and joint panel zone elements) so that likely brittle modes of failure (e.g., joint shear failure, column hinging and soft storey mechanism, shear failure in beams and columns) can be protected and converted into more ductile and energy-dissipating modes of failure. By boosting the strength of those members whose failure is not desirable (i.e., protection of the joint region) or, according to an alternative and counter-intuitive approach referred to as selective weakening [37, 38], by weakening those elements whose failure is desirable, it would be possible to attain a global performance characterized by the failure of more ductile and energy-dissipating components with the development of plastic hinges in the beams and a beam-sway global mechanism.

In order to achieve the desired performance within the retrofitted joint subassembly, a procedure was proposed based on moment-axial load, *M-N*, performance domain [39]. By generating a *M-N* performance domain which comprises the internal hierarchy of strengths within a beam-column joint system (represented by capacity curves of each element) and the actual demand curves for beam-column joint systems (the variation of axial load due to the effects of lateral loads on a frame system), the evaluation of the *sequence of events* (progression of the damage or failure mechanisms within the subassembly) can be easily be performed.

It is worth noting that the actual *sequence of events* shall not be confused with *the hierarchy of strength*. The proper understanding of the 'hierarchy of strength' concept is also essential to avoid major mistakes in assessing the structure and choosing the suitable retrofit strategy. This apparently subtle difference can actually lead to major consequences in the evaluation of the expected seismic performance of the structure and selection of the most appropriate retrofit/upgrading intervention. As

noted previously, the hierarchy of strength within a frame system, beam-column joint or structural element is fundamentally and, in principle, solely represented by capacity curves, thus being independent of the demand. The actual sequence of events, instead, defines the order of occurrence of damage and/or failure mechanisms (typically with reference to an increased level of deformation/displacement or stresses/forces) and shall be thus evaluated by considering the correct demand [37].

The capacities of beam, column, and joints refer to given limit state (e.g., for joints: cracking, equivalent yielding or extensive damage, and collapse) and are evaluated in terms of the equivalent moment occurring in the column at that stage, based on equilibrium considerations within the beam–column joint specimen. While capacity curves for each element can be found using conventional moment-curvature analysis for as-is beam and column elements, the strength evaluation and capacity curve generation of the joint region are based on the semi-empirical formulas provided in literature [40, 19]. It is important to note that, section analysis to be performed for retrofitted elements would be more challenging, due to the fact that implementation of the retrofitted section properties into the conventional programmes that are widely used for section analysis (i.e., [41, 42]) may not be possible. In addition to that, the assessment of the retrofitted joint panel zone would be a strenuous task, due to an existing complex model in the literature [43]. In these cases, the designer may need to create his or her own programme for the analysis and to generate an *M-N* domain for as-built, as well as retrofitted systems. In Chapter 4 these issues are covered and elaborated in detail.

In order to properly define the sequence of events, appropriate demand curves for beam-column joint systems should be represented in the *M-N* performance domain, after accounting for the variation of axial load due to the effects of lateral loads on a frame system. As seen previously, due to the complexity of implementing a varying axial load during testing, most of the experimental studies have been performed under a constant axial load. However, while strongly depending on the configuration of a frame structure, the amplitude of axial load variation in an exterior column, as well as beam-column joints, may have a significant effect on the performance, especially in case of poorly detailed deficient structural elements. Under these considerations, current assessment procedures for beam-column joints, which are basically developed following the empirical findings under constant axial load conditions, appear to be inadequate.

In order to illustrate the conceptual difference between hierarchy of strength and sequence of events and also to show the significance of accounting for variation of axial load in the determination of actual sequence of events within a joint subassembly, let us consider a set of exterior beam-column

joints located at different floor levels. Assuming that these beam-column joints have the same geometric and mechanical properties, naturally they would have the same capacity curves, hence the same inherent hierarchy of strength. On the other hand, the sequence of damage or sequence of events within the subassemblies could be totally different due to the different internal force demand (e.g., lateral force-overturning moment-varying axial load interaction) imposed on the beam, column and joint members.

The effects of varying axial load on the behaviour of exterior beam-column joints are clearly illustrated in Figure 3–11. Neglecting the actual variation of axial load during the frame sway (i.e., assuming a constant axial load demand), especially for exterior beam-column joints, could lead to non-conservative or incorrect evaluation of sequence of events. For instance, for an upper floor joint, due to the low variation of axial load demand (in percentage to the gravity load value), the expected mechanism is beam flexure for either constant axial load or varying axial load conditions. However, in case of a lower floor joint where the variation of axial load is comparatively high when compared to that of upper floor level joint, unexpected (if following a constant axial load analysis) damage in the joint or column (i.e., joint shear cracking and column hinging) may occur. It is noteworthy that, the sequence of these two events may be very close in case of low axial load conditions. Due to gravity load design, the concentration of flexural damage in the column at early stages could act as a structural fuse for the joint panel zone, showing significant resources of plastic deformation at a beam-column subassembly level [35, 23] even without specific ductile structural details. On the other hand, at a global level, this would result in a concentration of interstorey drift demand, with possible development of a soft storey mechanism. As clearly shown in the *M-N* performance domain plot for the lower floor joint, these brittle failure modes cannot be predicted under the assumption of constant axial load demand. For each case, disregarding the varying axial load demand on the different floor levels, assessment of the damage mechanisms will result in ductile beam flexural hinging, which in reality is not correct.

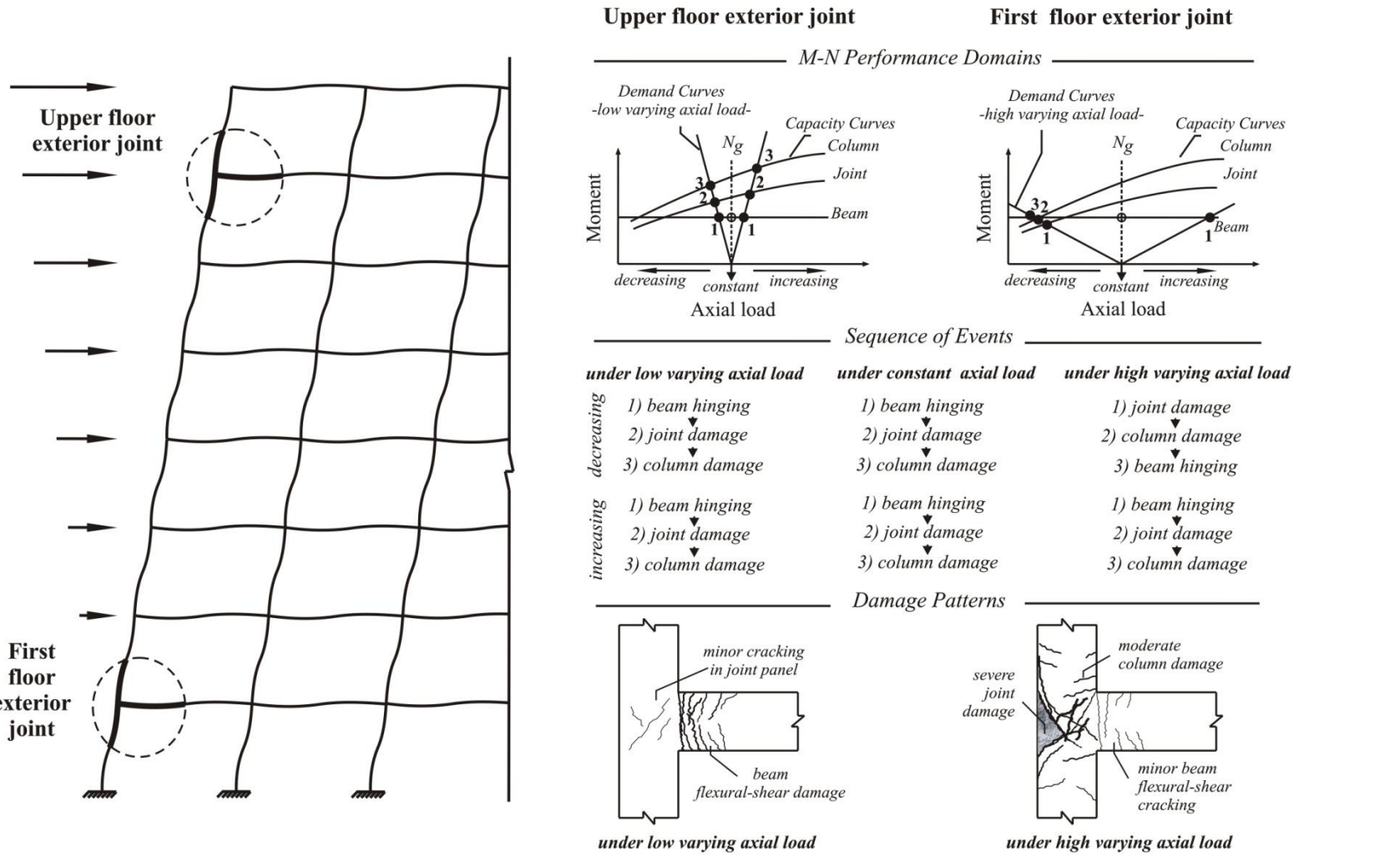

Figure 3–11 Effects of varying axial load on the behaviour of exterior beam-column joints

3.5 SUMMARY

In this chapter, a comprehensive review of the axial load effect on the seismic performance of structural elements such as columns and, in particular beam-column joints was carried out. In the course of the investigation of the axial load effects on beam-column joints, firstly, well-designed 2D exterior beam-column joints were examined with particular attention on the different shear resisting mechanism approaches. Secondly, investigation was expanded to the area of older 2D exterior beam-column joints in different configurations either in as-built or retrofitted using FRP materials.

Based on extensive experimental and analytical studies, it is demonstrated that the seismic performance of a RC structural elements are strongly influenced by the level of the axial load amplitude. Hence concurrent variation of axial load, either applied in a proportional or non-proportional fashion on an exterior column or beam-column joint can significantly affect the seismic behaviour of these elements. If not properly taken into account in the design or assessment process, the decrease in axial load level may result in the decrease of the strength of a structural element. In extreme cases, such as tension axial load generated due to vertical horizontal earthquake load and overturning moments, pure tension in the element on one side of a frame structure can occur. On the other side of the frame, excessive axial compression loading may cause failure in the compression force struts in the element.

Another interesting observation is that the variation of shear strength with changes in axial compression. Research has shown that the reduction in the axial load compression may encourage diagonal tension cracking in the joint region. On the other hand, due to the increase in axial compression, shear force demand may drastically increase in the joint region, which in turn may cause extensive cracking, joint damage and ultimately shear failure.

The literature review conducted also revealed the major drawbacks and limits on the research of retrofitted 2D exterior beam-column joints. Although favourable effects of axial load have been reported on the shear capacity of FRP strengthened joints, it should be underlined that the contribution of axial load on the behaviour of the beam-column joint response has not been typically accounted for during experimental tests. In most of the previous beam-column joint tests available in literature, the axial column load was maintained constant, without considering the real effects during the sway mechanisms.

3.6 REFERENCES

1. Abrams DP. Influence of axial force variations on flexural behavior of reinforced concrete columns. *ACI Structural Journal*. 1987; **84**(3):246-54.
2. Bozorgnia Y, Niazi M, Campbell KW. Characteristics of free-field vertical ground motion during the Northridge earthquake. *Earthquake Spectra*. 1995; **11**(4):515-25.
3. Abrahamson N, Litehiser J. Attenuation of vertical peak acceleration. *Bulletin of the Seismological Society of America*. 1989; **79**(3):549-80.
4. Ghobarah A, Elnashai AS. Contribution of vertical ground motion to the damage of RC buildings. *Proceedings of the 11th European Conference on Earthquake Engineering*, Rotterdam, Balkema, 1998.
5. Hanson RD, Degenkolb HJ. *The Venezuela Earthquake Engineering, July 29, 1967*. American Iron and Steel Institute: New York, 1969.
6. Townsend WH, Hanson RD. Reinforced concrete connection hysteresis loops. *Reinforced Concrete Structures in Seismic Zones, ACI Special Publication, SP 53-12*. 1977.
7. Park R, Paulay T. *Reinforced Concrete Structures*. Wiley: New York, 1975.
8. Saadeghvaziri MA, Foutch DA. Seismic response of reinforced concrete buildings designed for gravity loads. Part2: Experimental test on a three storey frame. *ASCE Journal of Structural Engineering*. 1990; **116**(7):1835-56.
9. Paulay T, Priestley MNJ. *Seismic design of reinforced concrete and masonry buildings*. Wiley: New York, 1992.
10. CEB. *Model code for seismic design of concrete structures*. Comite Euro-International du Beton, Bulletin d`Information: Paris, 1985.
11. Paulay T. Equilibrium criteria for reinforced concrete beam-column joints. *ACI Structural Journal*. 1989; **86**(6):635-43.
12. ACI Committee 318. *Building code requirements for structural concrete. ACI 318-02.* American Concrete Insitute, Farmington Hills, Mich., 2002.
13. Pantazopoulou S, Bonacci J. Consideration of questions about beam-column joints *ACI Structural Journal*. 1992; **89**(1):27-36.
14. Bonacci J, Pantazopoulou S. Parametric investigation of joint mechanics. *ACI Structural Journal*. 1993; **90**(1):61-71.
15. Tsonos AG, Tegos IA, Penelis GG. Influence of axial force variations on the seismic behaviour of exterior bean-column joints. *Journal of the European Association for Earthquake Engineering*. 1995; **3**:51-63.
16. Uzumeri SM. Strength and ductility of cast-in-place beam-column joints. *Reinforced Concrete Structures in Seismic Zones, ACI Special Publication, SP 53-12*. 1977.
17. Seckin M, Uzumeri SM. Examination of design criteria for beam-column joints. *European Conference on Eartquake Engineering*, Dubrovnik, 1978.
18. Scarpas A. The inelastic behaviour of earthquake resistant reinforced concrete exterior beam-column joints. *81-2*, University of Canterbury, Chrischurch, 1981.
19. Hakuto S, Park R, Tanaka H. Seismic load tests on interior and exterior beam-column joints with substandard reinforcing details. *ACI Structural Journal*. 2000; **97**(1):11-25.
20. Beres A, Pessiki SP, White RN, Gergely P. Implications of experiments on the seismic behaviour of gravity load designed RC beam-to-column connections. *Earthquake Spectra*. 1996; **12**(12):185-98.
21. ACI-ASCE 352R. *Recommendations for Design of Beam-Column Joints on Monolithic Reinforced Concrete Structures* American Concrete Insitute, Detroit, MI., 1976, 1985, 1991.
22. Liu A. Seismic assessment and retrofit of pre-1970's reinforced concrete frame structures. *PhD Dissertation*, University of Canterbury, Christchurch, 2001.
23. Pampanin S, Calvi GM, Moratti M. Seismic behaviour of RC beam-column joints designed for gravity loads. *12th European Conference on Eartquake Engineering*, London, Paper no. 726, 2002.

24. Clyde C, Pantelides CP, Reaveley LD. Performance-based evaluation of exterior reinforced concrete building joints for seismic excitation. *Report No. PEER 2000/05*, University of California, Berkeley, 2000.
25. Hertanto E. Seismic assessment of pre-1970s reinforced concrete beam-column joint subassemblies. *M.E. Thesis*, University of Canterbury, Christchurch, 2006.
26. Chen T. Retrofit strategy of non-seismically designed frame systems based on a metallic haunch system. *M.E. Thesis*, University of Canterbury, Christchurch, 2006.
27. Parvin A, Altay S, Yalcin C, Kaya O. CFRP rehabilitation of concrete frame joints with inadequate shear and anchorage details. *Journal of Composites for Construction, ASCE*. 2010; **14**(1):72-82.
28. Herhanto E. Seismic assessment of pre-1970s reinforced concrete beam-column joint subassemblies. *M.E. Thesis*, University of Canterbury, Christchurch, 2006.
29. Ghobarah A, El-Amoury T. Seismic rehabilitation of deficient exterior concrete frame joints. *Journal of Composites for Construction, ASCE*. 2005; **9**(5):408-16.
30. Antonopoulos CP, Triantafillou TC. Experimental investigation of FRP-Strengthened RC beam-column joints. *Journal of Composites for Construction, ASCE*. 2003; **7**(1):39-49.
31. Priestley MJN. Displacement-based seismic assessment of reinforced concrete buildings. *Journal of Earthquake Engineering*. 1997; **1**(1):157-92.
32. Cosenza E, Manfredi G. Some remarks on the evaluation and strengthening of underdesigned R.C. frame buildings. *Technical Report NCEER-97-0003*, SUNY/Buffalo, 1997, pp.157-175.
33. R.N. W, Mosalam K. Seismic evaluation and rehabilitation of concrete buildings. *Technical Report NCEER-97-0003*, SUNY/Buffalo, 1997, pp.177-196.
34. Prota A, Nanni A, Manfredi G, Cosenza E. Selective upgrade of beam-column joints with composites. *International Conference on FRP Composites in Civil Engineering,*, Hong Kong, 2001.
35. Calvi GM, Magenes G, Pampanin S. Experimental test on a three storey R.C. frame designed for gravity only. *12th European Conference on Eartquake Engineering*, London, Paper no. 727, 2002.
36. Pampanin S, Akguzel U, Attanasi G. Seismic upgrading of 3-D exterior R.C. beam column joints subjected to bi-directional cyclic loading using GFP composites. *FRPRCS-8*, Patras, Greece, 2007.
37. Pampanin S. Controversial aspects in seismic assessment and retrofit of structures in modern times: Understanding and implementing lessons from ancient heritage. *Bulletin of the New Zealand National Society for Earthquake Engineering*. 2006; **39**(2):120-33.
38. Kam WY, Pampanin S. Selective weakning techniques for retrofit of existing reinforced concrete structures. *Proc, 14th World Conf on Earthquake Engineering*, Beijing, 2008.
39. Pampanin S, Bolognini D, Pavese A. Performance-based seismic retrofit strategy for existing reinforced concrete frame systems using fiber-reinforced polymer composites. *Journal of Composites for Construction, ASCE*. 2007; **11**(2):211-26.
40. Priestley MJN, Seible F, Calvi GM. *Seismic Design and Retrofit of Bridges*. Wiley: New York, 1996.
41. Imbsen Software Systems. *XTRACT V3.0.8*. http://www.imbsen.com/xtract.htm, retrieved July 17, 2010.
42. Collins MP, Bentz EC. Response 2000. Reinforced Concrete Sectional Analysis using Modified Compression Field Theory. *Version 0.7.5.*, University of Toronto, Toronto, Ont., 2009.
43. Antonopoulos CP, Triantafillou TC. Analysis of FRP-Strengthened RC beam-column joints. *Journal of Composites for Construction, ASCE*. 2002; **6**(1):41-51

Chapter 4 ASSESSMENT AND DESIGN PROCEDURE FOR SEISMIC RETROFIT OF BEAM-COLUMN JOINTS USING FRP MATERIALS

4.1 INTRODUCTION

In this chapter, an analytical procedure for the evaluation of the expected performance of existing reinforced concrete (RC) beam-column joints before and after being retrofitted using FRP composite materials is presented. Focus is given to the evaluation of the shear strength vs. deformation properties of the panel zone region, either in the as-built or FRP-retrofitted configuration. Based on experimental and numerical evidences, as well as on physical models representing the mechanics of the joint region, principal tensile stresses vs. joint shear deformation relationships are adopted. They are preferred to more traditional nominal shear strength rules to evaluate, within a step-by-step iterative procedure, the combination of the joint shear contribution provided by the FRP composite material, and that provided by the concrete core alone. The hierarchy of strength and sequence of events (damage mechanisms) expected within a beam-column sub-system are visualized via moment-axial load (*M*-*N*) interaction performance domains, and used as a basis for a performance-based retrofit philosophy. Specific limit states or design objectives are targeted, with attention given to both strength and deformation limits. The proposed analytical procedure is validated using the results of a set of experimental tests available in the literature. With the intention to provide a simple design tool that can be easily implemented by practicing engineers, a worked example for the evaluation of the expected performance of a FRP retrofitted beam-column joint is provided. Furthermore, the procedure is used as a basis for a parametric study to illustrate the effects of different strengthening schemes on the behaviour of strengthened exterior joint panels under various axial load levels. Lastly, a summary of analysis results for each retrofitted 2D test unit is presented.

4.2 DESIGN METHODOLOGY: HIERARCHY OF STRENGTH AND SEQUENCE OF EVENTS

The retrofit design strategy follows in general terms capacity design principles [1]: selected components of the beam-column subassembly are upgraded to achieve ductile behaviour through the development of plastic hinge mechanisms in the beam (weak-beam strong-column mechanism), while other regions are protected from inelastic brittle mechanisms. As a critical step before any retrofit solution is designed, the assessment of the expected behaviour and performance (damage under a given intensity of loading) of an existing beam-column joint in its as-built configuration needs to be properly carried out. The internal hierarchy of strength of the system, combined with the likely demand, would provide critical information about the expected sequence of events (or damage-failure mechanism, such as beam or column flexural yielding/hinging, joint shear failure etc). In Chapter 3, the concept of hierarchy of strength and the sequence of events was introduced and discussed based on the response of a set of exterior as-built beam-column joints located at different floor levels of a regular RC frame structure (see section 3.4, Chapter 3). In this section the discussion on the effects of these phenomena will be extended to the seismic assessment and retrofit design of exterior beam-column joints.

A simple procedure to evaluate the internal hierarchy of strength has been proposed in the literature [2], based on the construction of capacity and demand curves within *M-N* (moment-axial load) performance domains. Background and further developments and details on the step-by-step procedure are provided herein along with practical design formulas, a full worked example and results of parametric investigations and experimental-analytical comparisons.

Limit-state design principles are followed in the seismic assessment and retrofit design phases. When assessing the nominal strength of a member, the possible failure mechanisms should be predicted and associated to material strains and stress levels. According to the aforementioned procedure, the capacities of the structural elements within the beam-column joint subassembly (e.g., beam, column and joint) can be evaluated by referring to specified limit states. The limit states can be listed as beam or column hinging, reinforcement yielding, concrete spalling and cracking, or extensive damage of the joint core as well as FRP debonding or failure. The corresponding limit state of the section or element in question is written in terms of the equivalent moment in the column. This can be easily achieved following equilibrium considerations within the beam-column joint system. At a later stage, in order to evaluate and control the governing mechanisms in the joint subassembly under different demand conditions of a retrofitted joint, the actual sequence of events should be determined by comparing

demand and capacities. This can be done within an *M-N* diagram (which can be referred as a performance-domain). An appropriate rehabilitation solution would aim to rearrange the existing sequence of events according to capacity design considerations.

4.3 M-N PERFORMANCE DOMAIN

The experimental results of quasi-static cyclic tests on beam-column joints before (Figure 4–1a) and after being retrofitted with FRP can be seen in Figure 4–1a and Figure 4–1b, respectively [3]. The as-built specimen (typical of pre-1970s design) failed in a brittle way, due to the formation of a joint shear mechanism. In the FRP retrofitted specimen, the joint shear damage and failure was protected, whilst a beam-plastic hinge developed and was relocated away from the beam-column-interface. Hence, brittle local mechanisms such as shear failure of the joint and column, as well as global mechanisms such as weak-column strong-beam were prevented by upgrading the internal hierarchy of strength, such that the beam plastic hinging (thus ensuring a beam-sway mechanism) became the first predicted "event". The expected hierarchy of strength and sequence of events for the as-built and retrofitted joint were evaluated using the concept of moment-axial load (*M-N*) performance domain, as shown in Figure 4–1c.

In Figure 4–1*c*, two different demand conditions corresponding to either a constant axial load or a varying axial load are illustrated in order to demonstrate the influence of the axial load variation in the sequence of events formation. As previously mentioned, most of the experimental works regarding the retrofitting of exterior beam-column joints are typically conducted under constant axial load. As comprehensively clarified in Chapter 3, due to the effects of lateral loads on a frame, as well as the vertical component of ground motions, a high level of axial load variation in the exterior beam-column joint can be generated. As shown in Figure 4–1c for the as-built condition, the sequence of events or damage (e.g., 1=joint, 2=beam, 3=column) are, in this case, the same under both demand curve conditions, thus regardless of the assumption of the axial load (see the numbers in circles). Two different retrofit schemes (in this case referred to as Scheme 1 and Scheme 2) on the same joint may produce a totally different sequence of events (see the numbers in rectangular boxes) when considering the actual variation of axial load demand.

If assuming, for the sake of simplicity, a constant axial load, the joint strengthening Scheme 1 may appear sufficient and adequate to protect the joint region, while inducing a ductile flexural hinge in the beam. However, due to the reduction of axial load during the frame sway, the actual strength of the

joint would be lower (in the direction of the reduction of axial load) than that of the beam, thus leading to a premature damage of the joint even after the retrofit intervention. Hence, an alternative retrofit Scheme 2 would be required to guarantee an appropriate ductile failure mode with the formation of flexural hinges in the beam in all realistically predicted demand conditions (see number 3 in rectangular box). The importance of accounting for the variation of axial load on the retrofit design of exterior beam-column joints is also confirmed by the experimental studies conducted in the frame of this thesis.

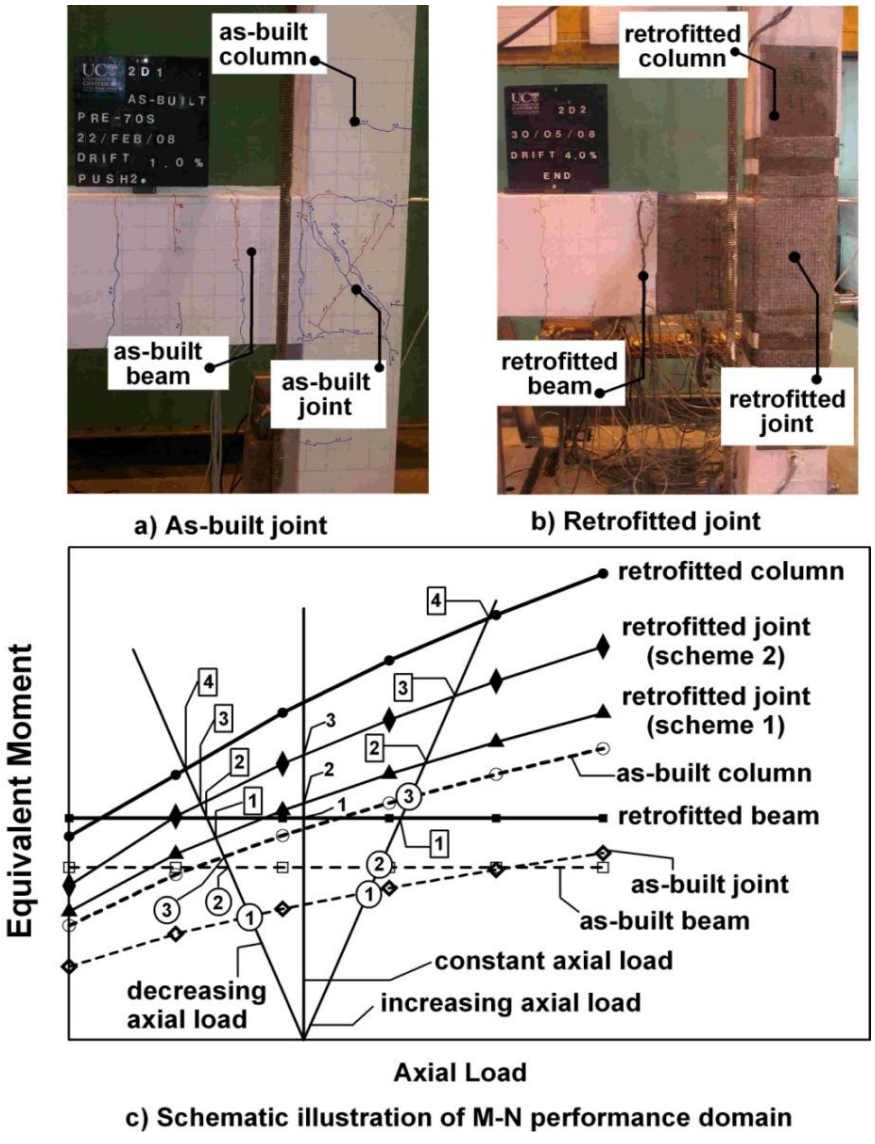

Figure 4–1 Schematic illustration of MN performance domain of as-built and retrofitted specimens with sequence of events under different demand curves

4.4 SEISMIC RETROFIT OF BEAM-COLUMN JOINT TEST UNITS

In order to develop and visualize the actual hierarchy of strength within a beam-column joint system, the capacities (flexural and shear) of beams and columns prior and after the retrofit need to be evaluated. The hierarchy of strength of a retrofitted joint would depend on the geometrical and mechanical properties of the subassemblies, as well as on the axial load ratio (demand) and upgrading scheme. It is intended that capacity design principle would be targeted in the retrofit solutions, thus providing protection of any internal (to the element) shear failure when compared to a more favourable flexural mechanism. Similarly in the assessment phase, both shear and flexural capacity of the elements need to be evaluated and compared. Before going into detail on the analytical tools to assess the capacity of each element within the joint subassembly system, some information on the FRP design process and application layouts carried out in the test specimens are discussed. Note that, detailed information on the material mechanical properties, along with the FRP application procedures, are given in Chapter 5 and 8 for 2D exterior and 3D corner beam-column joint test units, respectively.

In light of the aforementioned considerations, the main aim of the retrofit strategy adopted in this study, was to provide adequate protection to the joint region in such a way that the 'hierarchy of strength' in the as-built subassembly could be converted into a more favourable ductile failure mechanism. Accordingly, to achieve the target performance of the retrofit strategy, a simplified step-by-step design procedure following the detailed assessment of each joint component in as-built and retrofitted configuration is performed and explicitly shown within moment-axial force (*M*-*N*) performance domains. The demand curves accounting for the variation of the axial load as a function of the lateral load can also be plotted in the same domain. Hence, the performance of different retrofit techniques can easily be identified by the designer by rearranging the sequence of events to achieve capacity design provisions.

In the experimental programme of this research, a series of quasi-static cyclic tests were performed on a total of six 2/3 scale specimens, comprising four two-dimensional plane frame (2D) and two three-dimensional space frame (3D) exterior RC joints. Among the test specimens, three 2D (Specimens 2D2, 2D3 and 2D4) and one 3D exterior joint (Specimen 3D2) were retrofitted using glass fibre-reinforced polymer (GFRP) sheets with two alternative layouts. Before the tests of retrofitted specimens, one 2D as-built exterior joint (2D1) and one 3D as-built corner joint (3D1) were tested to obtain information on the unretrofitted joint behaviour. The selection of the fibre type and retrofitting

scheme were based on deficiencies underlined by tests on the as-built joints and the results provided by the post-test assessments.

The labelling used for a generic retrofit scheme Rij refers to a configuration with i number of GFRP layers in the beam and j number of GFRP layers in the column (on each side). For example, considering the R11 retrofit scheme, which is a so-called "minimum retrofit application" and adopted for specimens 2D2 and 2D3, one vertical layer of GFRP was used on two sides of the column and a U-shape horizontal sheet wrapped around the exterior face of the specimen at the joint level. Primary objectives were to increase the flexural capacity of these elements, in order to increase the joint shear strength and to prevent the expulsion of a concrete wedge which was observed in the tests of the as-built specimens.

Additional strips were wrapped around the beam elements to increase the efficiency of the U-wraps by providing a proper anchorage and to delay the debonding of the FRP from the concrete surface in which the principal fibre direction was circumferential. By this application, since flexural strengthening can cause the member to be vulnerable to shear failure, the shear strength of the flexurally strengthened region in the beam was also maintained (Figure 4–2).

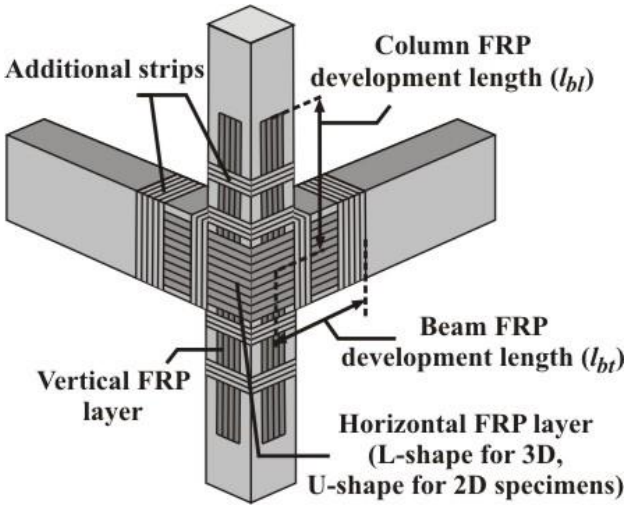

Figure 4–2 FRP application in 3D corner joint unit and FRP development bond lengths

The FRP strips were also installed around the column above and below the joint region such that its principal fibre direction was in the circumferential direction of the column perpendicular to its longitudinal axis. In this way, not only was additional shear strength provided to the member, but also axial load carrying and lateral displacement capacity of the column were increased. In general sense,

FRP confining of the deficient columns serves to prevent three important failure modes (1) internal bar rupture, (2) buckling and (3) the failure of lap splices. Note that in flexural and shear strengthening the FRP provides an additional tensile force component to carry either the bending moment or shear force. In case of FRP confining, the FRP system does not perform the role of internal steel ties or internal steel spiral reinforcement. Their main purpose is to stabilize and restrain the longitudinal steel reinforcing bars in the compression member and to provide shear reinforcement in beam-columns [4]. Based on these discussions, it can be deduced that the contribution of the confining FRP wraps to the shear capacity, the flexural hinge capacity, and the bar lap splice capacity are interrelated.

In the field applications of FRP composite materials in civil infrastructures for laid-up FRP systems instead of continuous application along the side of the member, intermittent (using finite-width segments) wrapping is generally preferred as applied in this study (although it is harder to place in the field). One of the main reasons is that this application allows moisture to migrate from concrete to air, whereas a continuous wrap will fully cover the concrete surface and could trap moisture under the wrap. As a result, the interface substrate of the FRP composite may be degraded. Furthermore, a continuous wrap causes difficulties with inspection since the surface of the concrete is not visible [4]. Another important reason is to increase the control and understanding of the designer over the anticipated behaviour of the retrofitted structural element by applying intermittent FRP strips.

In the Specimen 2D4, an upgraded R21 retrofit scheme was used where two U-shape horizontal sheets wrapped around the exterior face of the specimen at the joint level. The same R21 scheme was also adopted in the 3D corner joint, Specimen 3D2 (Figure 4–2), to highlight the possible effects of bidirectional loading on the performance of the retrofitted corner joints when designed according to uniaxial (2D) planar frame assumptions. Similar to U-shape FRP applications in 2D specimens, in the 3D specimen L-shape horizontal GFRP sheets were wrapped around the exterior face of the specimen at the joint level to ensure a proper anchorage. It is important to note that, since one of the objectives of this study is to investigate the effects of severe bidirectional loading on the behaviour of corner joints in an as-built and retrofitted configuration, the same design criteria used in 2D units was implemented on the retrofit design of the 3D specimens. The intervention was also intended to be carried out with minimum invasiveness from the outside of the building, thus allowing limited disruption of the internal activities and/or the relocation of the buildings occupants. To reduce invasiveness to the floor in the 3D configuration, in real practice, C-shape strips could be adopted and anchored on the top and bottom of the beam.

4.4.1 Design Material Properties

Environmental conditions such as alkalinity, salt water chemicals, ultraviolet light and high-humidity may cause degradation in the mechanical properties of FRP strengthening systems (e.g., tensile strength, elastic modulus) when they are exposed to certain environments. Therefore, material properties used in the design equations should be reduced due to long-term exposure of environmental affects. The material properties reported by the manufacturers typically do not consider the long-term environmental effects. In this study, design ultimate tensile strengths are determined using environmental reduction factors, C_E, recommended in the guide for the design and construction of externally bonded FRP systems for strengthening concrete structures [5]. A summary of environmental reduction factors for all types of FRP are given in Table 4-1.

Table 4-1 Environmental reduction factors [5]

Exposure Conditions	Fibre Type	Environmental reduction factors C_E
Interior exposure	Carbon	0.95
	Glass	0.75
	Aramid	0.85
Exterior exposure (bridges, piers, and unenclosed parking garages)	Carbon	0.95
	Glass	0.75
	Aramid	0.85
Exterior exposure (bridges, piers, and unenclosed parking garages)	Carbon	0.95
	Glass	0.75
	Aramid	0.85

It is stipulated in the same guideline that the material properties reported by manufacturers, such as ultimate tensile strength, f_{fu}*, and ultimate FRP strain, ε_{fu}* should be considered as initial values and reduced based on the environmental exposure condition. Design ultimate tensile strength, f_{fu}, and the design rupture strain can be determined by the equations (4-1) through (4-3). Note that, since FRP materials are linear elastic until failure, the design modulus of elasticity for unidirectional FRP can be determined from Hooke`s law as given in Eq. (4-3). The modulus, E_f, is typically unaffected by environmental conditions, so the value reported by the manufacturer can be used [5].

$$f_{fu} = C_E f_{fu}^{*} \tag{4-1}$$

$$\varepsilon_{fu} = C_E \varepsilon_{fu}^{*} \tag{4-2}$$

$$E_f = f_{fu} / \varepsilon_{fu} \quad (4\text{-}3)$$

A summary of the properties of the FRP systems used in this study are shown in Table 4-2.

Table 4-2 Summary of FRP properties

Fibre Type	Density [g/cm^3]	Effective thickness of one layer, t_f [mm]	Ultimate Tensile Strength f_{fu}* [MPa]	Modulus of Elasticity E_f [MPa]	Design Rupture Strain (%) $\varepsilon_{fu}=C_E{}^{1}\varepsilon_{fu}$*
GFRP SikaWrap - 100G High Strength E-Glass	2.56	0.36	2300	76,000	(0.65)(2.8%)=1.8%
Mbrace CFRP C5-30 High Modulus Carbon	1.9	0.165	3000	390,000	(0.85)(0.8%)=0.68%

[1] The joint specimens in this study are located in an exterior space. Therefore, per Table 4-1, environmental reductions of 0.65 and 0.85 are used for GFRP and CFRP, respectively.

In order to improve the reliability of strength prediction and account for different failure modes observed for strengthened members, as suggested in many FRP design guidelines [6, 4, 7] additional (material-based or section-related) strength reduction factors may be used in the design of an FRP strengthening system to reflect higher uncertainty with relation to the FRP material and system behaviour, when compared to more traditional reinforced and prestressed concrete solutions.

4.4.2 FRP Strengthening System Area Calculations

The type of FRP strengthening system has a crucial role in determining the tensile force resultant of an FRP layer in the section. The product data sheets of dry fibre systems report the mechanical properties of the dry fabrics and the fabric design thickness (Table 4-2). Note that, when reported in this fashion, the properties do not represent the FRP composite. In this case, the ultimate force is obtained from the strength of the fibres and the thickness of the net area of the fibres (which can be obtained by multiplying the number of FRP layers by the net thickness of the fibres in a single sheet or fabric, t_f) [4]. Also, the properties of the fibres in the direction of strengthening (e.g., on the condition that bidirectional or multidirectional fibres are used), should be used to determine the resultant forces. On the other hand, the ultimate force in bonded strip systems can be calculated by using the reported values of the strength of the FRP composite and the gross cross-sectional area of the strip. The reported properties provided by the manufacturers for the strips are typically the properties of the FRP composite, not the properties of the fibres alone.

4.5 EVALUATION OF AS-BUILT AND FRP RETROFITTED BEAM AND COLUMN CAPACITIES

4.5.1 Flexural Strength Assessment

In typical flexural strengthening applications, FRP external reinforcement is attached to the bottom tension face of a concrete flexural member, such as beam and slabs, with fibres oriented along the length of the member. In this way the effective tensile force resultant and therefore the moment capacity of the member increases in flexural strength. However, in this study a different way of flexural strengthening scheme is used for the transverse and longitudinal structural elements in exterior joints, performed to simulate the minimum invasiveness in the in-situ application of FRP. Analogous to adding steel strengthening strips or FRP sheets to the tension face of the member as seen in Figure 4–2, the FRP material on two sides of the member performs the same role of increasing the moment capacity of the section. Hence, traditional reinforced concrete design principals can be conveniently applied to analyze the nominal flexural strength of FRP-strengthened concrete members with mild steel reinforcement based on strain compatibility and force equilibrium. Two fundamental differences exist regarding the governing failure modes in FRP retrofitted RC sections: the FRP strengthening system behaves in a linear elastic fashion and it is more susceptible to detachment (debonding or delamination failures) [4].

Because of the reasons above, it is important to take into account and examine the controlling failure modes in an FRP flexural strengthened system in the design and assessment process. Failure modes include crushing of the concrete in compression, yielding of the steel in tension, shear/tension delamination of the concrete cover and debonding of the FRP from the concrete substrate [8]. The most desirable failure mode would be the yielding of internal steel, followed by concrete compression with the FRP system still attached. In the early stages of loading both the internal steel and the FRP increase their tensile stress before yielding of steel. Once the steel yields, although the internal reinforcement is not able to contribute to the tensile strength, the FRP system will continue to take load beyond the internal steel yield load. However, in the latter stages of loading the large tensile forces and the post-yield deflections developed in the FRP strengthened system, may cause the detachment (also known as *delamination* or *debonding*) of the strengthening system from the concrete surface in a number of ways.

A key difference between the behaviour of internal and adhesively applied reinforcement can be recognized: in the former case full tensile strength can be attained due to yielding of steel, whereas in

the latter case the cohesive concrete capacity cannot increase beyond a certain limit [9]. As a consequence, the full load carrying capacity of the FRP system cannot be fully exploited because of the premature detachment of the FRP from the concrete surface of the strengthened member and therefore the complete utilization of the FRP material strength is limited. Although an increase in the load capacity of the member can be obtained, maximum stress and strain in the FRP system (e.g., design rupture values) usually cannot be attained.

The problem of premature failure of FRP strengthening systems due to debonding or delamination from the concrete substrate has attracted many researchers to the investigation of this phenomenon since the 1990s. However, due to its complicated nature, a simple reliable design method is still not available. Since the scope of this study does not include the treatment of the debonding phenomena, the reader is referred to the published literature for more information [6, 10, 7, 11, 5, 12].

In the section analysis, FRP was considered to resist only tensile forces, while maintaining compatibility between the FRP and the concrete substrate and hence it was assumed that the FRP reinforcement has no contribution in resisting the compressive forces. A linear elastic stress-strain relationship (Figure 4–3) to failure was adopted in the FRP reinforcement. Hence, Hooke's law can be employed to determine the strain level in FRP from the effective stress level and vice versa.

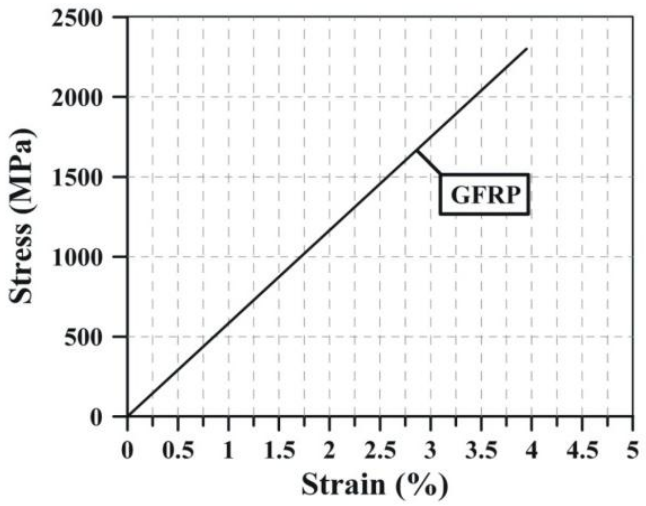

Figure 4–3 Stress-strain curve for GFRP material

Limit states for rupture and debonding were taken into account as follows: rupture of the FRP was assumed to occur if the strain in the FRP reaches its design rupture strain, ε_{fu}, (Table 4-2) whereas debonding was treated herein according to the fractural mechanics-based model of Holzenkampfer [13].

In selecting this model two considerations are taken into account. Firstly, that there is still no established consensus on the determination of debonding strain in the literature. For example, [12] performed a comparative study on the applicability of existing models for the prediction of debonding failure in RC beams externally strengthened with FRP. A total of 27 debonding models were applied to the experimental database of 163 FRP strengthened beams which were tested in three point and four point bending tests. The behaviour of each model was analysed using statistical parameters and a degree of uncertainty in the predictions. It was concluded that the existing models lack the thoroughness of bond predictability. No model predicted debonding in a comprehensive way and the results were highly conservative. As researchers indicated, there is always a balancing of the efficiency of the design to the conservativeness of the approach. Due to a very conservative model (e.g., models given in the existing design codes such as *fib* [6], concrete society TR 55 [14] and JSCE [15]), the entire capacity of the FRP strengthened member would not be utilised resulting in unused material. In this context, it should be kept in mind that in addition to safety, economy is also a crucial aspect in the design process due to the high cost of the materials.

Secondly, the model proposed by Holzenkampfer [13] was successfully implemented in previous studies [16, 2] for analytical modelling of FRP-retrofitted exterior beam-column joints. According to this model, the maximum tensile stress $f_{f,max}$ (which equals to $f_{f,deb}$) in an FRP strip of thickness, t_f, in mm when debonding occurs, (i.e., on beam side) equals to

$$f_{f,\max} = f_{f,deb} = c_1 \sqrt{(E_f f_{ct}) / (t_f n_{fb})} \quad \text{for } l_{bt} \geq l_{b,\max} \tag{4-4}$$

where c_1 an empirical coefficient taken as 0.64 for CFRP as suggested by Neubauer and Rostasy [17], l_{bt} is the *FRP development length* along the direction t (in mm) in the joint, E_f is the modulus of elasticity of FRP, f_{ct} is the tensile strength of concrete and $l_{b,max}$ the effective bond length of FRP sheet. As mentioned previously, one of the basic differences between the internal steel reinforcement and external FRP reinforcement is their bond behaviour under tensile stress. In the former case the bond length can always be designed for its full tensile strength if there is a sufficient concrete cover (e.g., reinforcing bar development lengths). However, for the latter case experimental and numerical studies have shown that there is a certain finite length that limits the maximum shear force that can be transferred between the FRP and the concrete. This leads to the concept of *effective bond length*, $l_{b,max}$, beyond which any increase in the bond length cannot increase the bond strength and hence cannot contribute in the increase of the load-carrying capacity [10]. Tensile force in the fibre-reinforced

composite and maximum anchorable force as a function of bond length is schematically shown in Figure 4–4. In this study effective bond length is calculated as follows:

$$l_{b,\max} = \sqrt{(E_f t_f)/c_2 f_{ct}} \tag{4-5}$$

where c_2 can be taken as 2 according to Holzenkampfer [13].

The effective bond length can be regarded as the minimum FRP development bond length, which is the length of FRP sheet from the centre of the column to the FRP cut-off point in the beam (l_{bt}) or the column (l_{bl}) (Figure 4–2). It is noteworthy that, apart from preventing the premature debonding failure, the effective bond length also plays another important role in achieving the aimed retrofit design objectives, such as ensuring a ductile mode of failure with plastic hinge formation in the beam. Thus the maximum value of the FRP development bond length should be determined in such a way that the desired sequence of events within the joint subassembly can be obtained. For instance, in order to achieve a plastic hinge in the beam, the equivalent moment at the FRP-ending section in the beam, $M_{by,Rij,eq}$, should be smaller than the capacity of the retrofitted section at the beam-column interface, $M_{b,Rij,eq}$ (see Figure 4–12 for the notations). This can be achieved easily by comparing the moment demands and section capacities corresponding to the applied FRP development length.

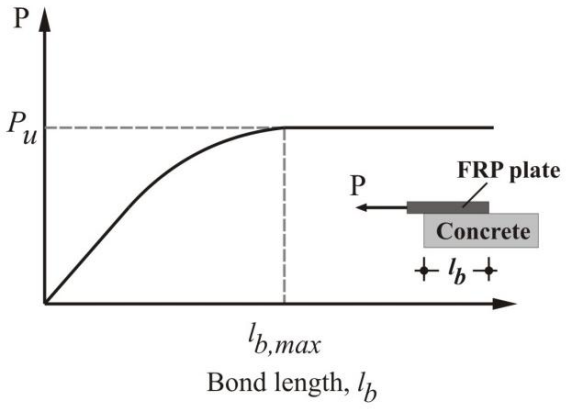

Figure 4–4 Maximum anchorable force as a function of bond length (after [7])

As mentioned in Chapter 3, conventional section analysis programmes can be used for the assessment of RC sections in as-built configurations. However, due to the application limitations in these programmes, in most situations structural engineers are generally required to carry out a section analysis calculations to obtain the strength and deformation characteristics of the retrofitted member. With the same idea, in the first stage of the analytical studies of this work, a section analysis procedure

is developed and validated with the available programmes and hand calculations. In the second stage, a set of spreadsheet programmes are developed to analyze the strains and stresses in a retrofitted section subjected to an applied bending moment and axial load in plane frame to conduct moment-curvature analyses.

The behaviour of a member subjected to bending or combined bending and axial load can be best studied by performing moment-curvature analyses. A layer-by-layer iterative procedure (sort of fibre-section analysis) can be utilised to obtain the moment-curvature response of the critical sections by idealizing the cross section as a series of rectangular layers in order to evaluate the sectional forces corresponding to a given strain distribution (Figure 4–5). The Bernoulli-Navier hypothesis of "plane sections remain plane" after bending is assumed. The position of the neutral axis is first estimated and a series of iterations are carried out until both equilibrium and compatibility conditions are satisfied. In addition, for the sake of computational ease the following assumptions are made (1) no relative slip between the external FRP reinforcement and the concrete; (2) the shear deformation within the adhesive layer is neglected due to its very thin thickness and slight variations; (3) the contribution of concrete tension strength to flexural strength is normally negligible and therefore neglected [18] and (4) FRP reinforcement has a linear elastic stress-strain relationship (Eq. (4-6)) to failure as mentioned previously.

$$f_f = E_f \varepsilon_f \tag{4-6}$$

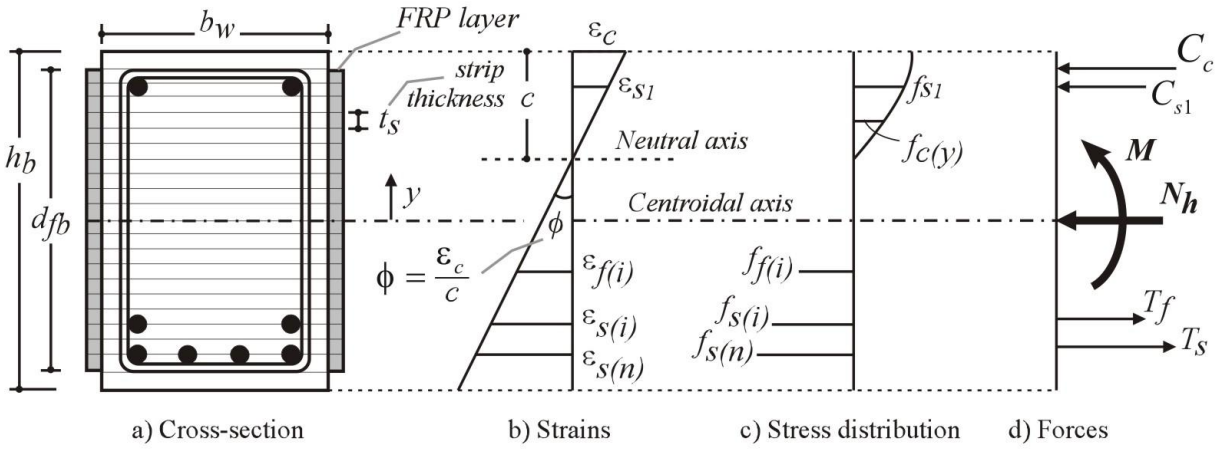

Figure 4–5 Layer-by layer sectional analysis of strengthened RC beam section with *n* layers of steel rebar

Using the nomenclature given in Figure 4–5 for axial force N_h, the force equilibrium at any level of response can be written as

$$N_h = \int f_c(y) b_w t_s dy + \sum f_{si} A_{si} + \sum f_{fi} A_{fi} \tag{4-7}$$

The moment capacity of the retrofitted section can be found by taking the moments of the stress resultants about the centroid of the section

$$M_{b,Rij} = \int f_c(y) b_w t_s y_i dy + \sum f_{si} A_{si} y_i + \sum f_{fi} A_{fi} y_i \tag{4-8}$$

The section analyses of the beam and column members of the test specimens are performed by tabulating moment and curvature of the member sections for increasing levels of concrete strain, ε_c. The damage limit states for FRP materials (e.g., FRP debonding or rupture) implemented in the analysis were explained previously. Theoretical information on the material constitutive models for the concrete and steel are provided to clarify the limit states regarding these materials.

The constitutive model originally proposed by Mander *et al.* [19] and later revisited by Dodd and Restrepo [20] was adopted for the stress-strain behaviour of reinforcing steel. In this model a generic stress-strain coordinate from the test data can be employed to better describe the non-linear strain-hardening branch of the stress-strain curve. The equations describing the monotonic stress-strain envelope used by Dodd and Restrepo [20] are summarized below. Reference to the nomenclature is also given in Figure 4–6.

For $\varepsilon_s \leq \varepsilon_{sy}$

$$f_s = E_s \varepsilon_s \tag{4-9}$$

For $\varepsilon_{sy} < \varepsilon_s \leq \varepsilon_{sh}$

$$f_s = f_y \tag{4-10}$$

For $\varepsilon_{sh} < \varepsilon_s \leq \varepsilon_{su}$

$$f_s = f_{su} + \left(f_y - f_{su}\right)\left[\frac{\varepsilon_{su} - \varepsilon_s}{\varepsilon_{su} - \varepsilon_{sh}}\right]^P \tag{4-11}$$

In Eq.(4-11) P is a parameter describing the non-linear power relationship to capture the strain-hardening curve.

$$P = \frac{\log_{10}\left(\frac{f_{su} - f_x}{f_{su} - f_y}\right)}{\log_{10}\left(\frac{\varepsilon_{su} - \varepsilon_{sx}}{\varepsilon_{su} - \varepsilon_{sh}}\right)} \tag{4-12}$$

where ε_s = reinforcement strain; ε_{sy} = reinforcement yield strain; ε_{sh} = strain hardening of the steel; ε_{sx} = strain coordinate on the strain hardening curve from experimental data; ε_{su} = ultimate strain of the mild steel defined by the maximum obtained stress; f_{sx} = steel stress coordinate on the strain hardening curve from experimental data; f_{su} = ultimate stress in reinforcement; and f_y = yield stress of reinforcement.

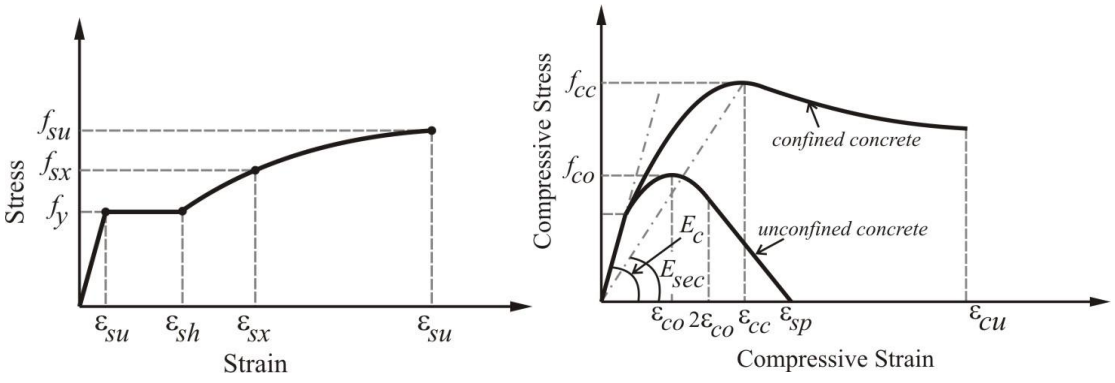

a) Model for reinforcing steel b) Confined and unconfined concrete model

Figure 4–6 Material constitutive relationships for reinforcing steel and concrete

When the member is confined the characteristics of the compression stress-strain curve change and the strength and ductility of the section are significantly improved (Figure 4–6) as a result of the action of transverse reinforcement in the form of hoops or spirals and the confining effect of the FRP which encircles and wraps the RC member.

The majority of FRP systems are used to confine columns to improve concrete compressive strength, reduce the required splice length, and increase the shear strength [21]. There are significance differences in the mechanism of FRP confining and flexural strengthening systems. In the case of flexural strengthening, the FRP is actively contributing to the flexural strength of the member. On the other hand, the FRP confining system starts to carry additional compressive stress only after the concrete in the column has begun to crack and hence dilate. The FRP serves to confine concrete by restraining the lateral expansion of the concrete and modify the compressive properties of the existing concrete similar to the action of well-detailed transverse reinforcement. As a consequence, the contribution of the concrete in the internal equilibrium is increased, rather than increasing the contribution of steel reinforcing as in the case of flexural or shear strengthening. The FRP wrapping can be referred to as a *passive strengthening system* since it plays no part in the elastic response of the axially loaded members. On the other hand, because the FRP confining is activated only after the cracking of concrete, the mechanism is somewhat similar to the shear strengthening.

To adequately describe the behaviour of a rectangular member confined by an external FRP jacket and by internal reinforcing steel hoops, the constitutive models developed by Mander *et al.* [22] and an analytical method for FRP confined concrete proposed by Wang and Restrepo [23] are adopted in this study. The concrete model proposed by Mander *et al.* [22] is widely accepted in literature and used as a benchmark stress-strain relationship for unconfined and confined concrete. This model has the advantage of describing the complete stress-strain curve as a single function and can be applied to circular and rectangular sections with different quantities of confining steel in the two perpendicular directions. In conjunction with this model, an analytical method developed by Wang and Restrepo [23] for evaluating the short-term axial load deformation behaviour of rectangular and square RC compression members confined with GFRP jackets and steel hoops is also implemented in the section analysis. In this method, the compressive load carried by a jacketed rectangular column is assumed to be comprised of three distinct components (1) the load carried by unconfined concrete area; (2) the load carried by the area of concrete confined by the FRP jacket and (3) the load carried by the area of concrete confined by the FRP jacket and the steel hoops. With the knowledge of the stress-strain relationships of each region the entire uniaxial stress-strain relationship for a column wrapped with an FRP jacket can be found.

In general, the area of concrete in the cross section of a member is usually assumed to consist of three separate regions (1) the unconfined region: the most outer region of the concrete which is defined as the cover concrete; (2) the effectively confined region: the most inner region which is subjected to the

full uniform lateral confining pressure provided by the transverse and longitudinal reinforcement and (3) the ineffectively confined region, which is between the cover concrete and the effectively confined core and subjected to a non-uniform distribution of lateral confinement [24]. The concept of effectively confined core was first introduced by Sheikh and Uzumeri [25] and defined by the smallest concrete zone within the region bounded by the peripheral hoops, because of vertical arching of the concrete between the transverse hoop sets and horizontal arching between the restrained longitudinal bars. It is interesting to note that most of the time stress-strain models spread the effectively confined area over the entire concrete core by employing a *confinement efficiency factor* in the section analysis. This factor is defined as the ratio of the effectively confined concrete core area to the concrete core area. The lateral confining pressure provided by the transverse reinforcement is reduced by this factor and smeared uniformly across the entire core area of the concrete section. Hence, the strength of the section is calculated by assuming that the confined concrete properties are uniformly distributed in the core concrete.

To achieve more accurate results and for the sake of simplicity, instead of using a smeared concrete model (e.g., [22]), a *segmented core model* [24] is adopted in this study. A cross section of RC rectangular member that is confined by an external FRP jacket and by internal reinforcing steel hoops is given in Figure 4–7. According to the segmented core model and the simplified form proposed by Manfredi and Realfanzo [26] the section is divided into two regions (confined and unconfined) and discretized. The confined region can be assumed using the given equations from 4-13 to 4-15. An equivalent cross-section was considered and parabolic areas due to the arching action were substituted by equivalent rectangular areas. Such an approach allows the simplifying of the problem from a numerical standpoint and provides important advantages for discretization of the cross section, which is divided into rectangular strips having equal height (Figure 4–5 and Figure 4–7). Depending on its position, the strip is related to different constitutive relationships for concrete.

$$d_s = \left(\frac{{w_x}^2}{6} \beta \right) \frac{1}{w_x} + \left(\frac{h_b - w_y}{2} \right) \tag{4-13}$$

$$d_l = \left(\frac{{w_y}^2}{6} \beta \right) \frac{1}{w_y} + \left(\frac{b_w - w_x}{2} \right) \tag{4-14}$$

$$\beta = \left(1 - s`/2w_x\right)\left(1 - s`/2w_y\right) \tag{4-15}$$

where β is the vertical arching coefficient and $s`$ is the clear vertical spacing between the hoop bars.

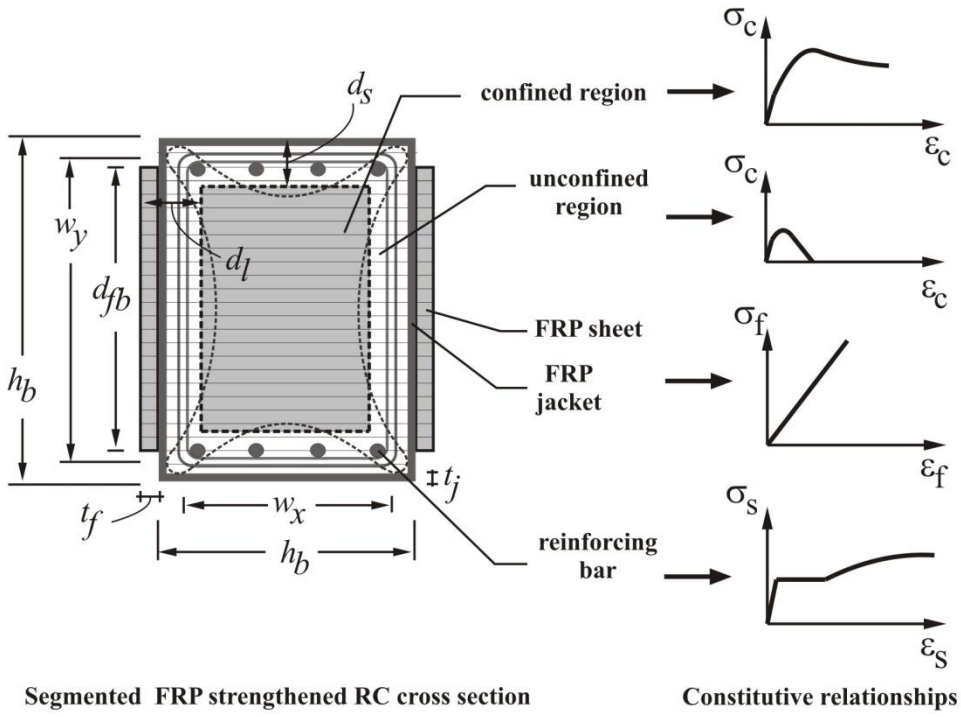

Figure 4–7 Layer-by-layer section idealization with `segmented core model`

The compressive strength of unconfined and confined concrete is denoted by f_{co} and f_{cc}, respectively. The unconfined concrete strength, f_{co}, is usually assumed to be 0.85 times the concrete cylinder strength $f`_c$ due to size effects between concrete control cylinders. The compressive strength of confined concrete f_{cc} is given by

$$f_{cc} = \alpha_1 \alpha_2 f_{co} \tag{4-16}$$

where α_1 is a strength enhancement factor that considers the concrete to be subjected to a triaxial stress state with bi-equal confining stresses, and α_2 is a reduction factor that considers the effect on the compressive strength of concrete which is confined with unequal effective lateral confining pressures, in two perpendicular directions. Mander *et al.* [22] proposed for α_1*:*

$$\alpha_1 = \left(2.254 \sqrt{1 + \frac{7.94\, F_l}{f_{co}}} - 2\frac{F_l}{f_{co}} - 1.254 \right) \tag{4-17}$$

where F_l is the maximum effective lateral confining pressure. Wang and Restrepo [23] proposed an approximate closed form solution for α_2 to evaluate the confined concrete strength

$$\alpha_2 = \left(1.4\frac{f_l}{F_l} - 0.6\left(\frac{f_l}{F_l}\right)^2 - 0.8 \right) \sqrt{\frac{F_l}{f_{co}}} + 1 \tag{4-18}$$

where f_l is the minimum effective lateral confining pressure. For rectangular sections lateral confining stresses induced by steel hoops in each *x* and *y* directions can be calculated as follows:

$$f_{l,sx} = \rho_{sx}\, f_{sh} \tag{4-19}$$

$$f_{l,sy} = \rho_{sy}\, f_{sh} \tag{4-20}$$

where ρ_{sx} and ρ_{sy} are the confinement reinforcement ratios and defined as

$$\rho_{sx} = A_{t,x} \big/ s`w_y \tag{4-21}$$

$$\rho_{sy} = A_{t,y} \big/ s`w_x \tag{4-22}$$

in which $A_{t,x}$ and $A_{t,y}$ are areas of transverse steel reinforcement parallel to the *x*- and *y-axis*, respectively; w_x and w_y are the distances between the centrelines of the perimeter hoop in the *x* and *y* directions, respectively.

The lateral confining stresses induced by FRP jacket in the *x* and *y* directions can be computed as follows

$$f_{l,jx} = \rho_{jx}\, f_j \tag{4-23}$$

$$f_{l,jy} = \rho_{jy} f_j \tag{4-24}$$

where f_j is the stress in the jacket. The reinforcement ratios ρ_{jx} and ρ_{jy} are defined as

$$\rho_{jx} = 2\frac{t_j}{h_b} \tag{4-25}$$

$$\rho_{jy} = 2\frac{t_j}{b_w} \tag{4-26}$$

where t_j is the nominal jacket thickness, and h_b and b_w are the overall column cross-section dimensions. The stresses in the jacket and in the hoops given in Eqs. (4-19), (4-20), (4-23) and (4-24) can be calculated from the constitutive material properties as

$$f_j = E_f \varepsilon_{tr} \text{ if } 0 \le \varepsilon_{tr} \le \varepsilon_{fu} \text{ or } f_j = 0 \text{ if } \varepsilon_{tr} > \varepsilon_{fu} \tag{4-27}$$

and

$$f_{sh} = E_s \varepsilon_{tr} \text{ or } f_{sh} = f_{yh} \text{ ,whichever is less} \tag{4-28}$$

where ε_{tr} is the transverse strain and f_{yh} is yield strength of hoops. According to experimental results, Wang and Restrepo [23] indicated that the relationship between axial and transverse strains ε_c and ε_{tr} can be determined by assuming the Poisson`s ratio, ν, of 0.5 as given by

$$\varepsilon_t = 0.5\varepsilon_a \tag{4-29}$$

The lateral confining stress of combined confinement due to both FRP jacket and steel hoops is equal to

$$f_l = f_{l,s} + f_{l,j} \tag{4-30}$$

Hence, the confined concrete compressive strength of the area of the column confined by jacket and the transverse steel reinforcement is found by substituting Eq. (4-30) into Eqs. (4-17) and (4-18). Once the compressive strength of the confined concrete, f_{cc}, is determined, the other parameters to generate the stress-strain relationship as depicted in Figure 4–6b may be determined from Mander *et al.* [22]. The relevant expressions are given below

$$\varepsilon_{cc} = \varepsilon_{co}\left(1 + R\left(\frac{f_{cc}}{f_{co}} - 1\right)\right) \tag{4-31}$$

$$E_c = 5700\sqrt{f_{co}} \tag{4-32}$$

$$E_{\sec} = \frac{f_{cc}}{\varepsilon_{cc}} \tag{4-33}$$

$$r = \frac{E_c}{E_c - E_{\sec}} \tag{4-34}$$

$$x = \frac{\varepsilon_c}{\varepsilon_{cc}} \tag{4-35}$$

where ε_c is variable concrete strain; ε_{cc} is the concrete strain at confined concrete strength, f_{cc}; ε_{co} is the concrete strain at unconfined concrete stress, f_{co}, which equals to 0.002; E_{sec} is the secant modulus and E_c is the elastic modulus of the confined and unconfined concrete (units in MPa). The parameter R in Eq. (4-28) is used to determine the strain at which the peak confined concrete stress is reached. This was calibrated using experimental results and was assumed by Mander *et al.* [22] to be R=5. The complete stress-strain curve, shown in Figure 4–6 is then given by Popovic`s equation,

$$f_c = \frac{f_{cc}\, xr}{r - 1 + x^r} \tag{4-36}$$

The stress-strain relationship for unconfined concrete can be obtained from the same set of equations using a lateral confining pressure, f_l=0. To define the stress-strain behaviour of the unconfined concrete region in the cross-section strip, the descending portion of the unconfined concrete stress-

strain relationship is assumed to decrease linearly from a strain of $2\varepsilon_{co}$ to reach zero stress at the spalling strain, ε_{sp}. Finally, the ultimate strain ε_{cu} attained by confined concrete is given by the following

$$\varepsilon_{cu} = 0.004 + \frac{1.4\rho_v f_{yh} \varepsilon_{su}}{f_{cc}} \tag{4-37}$$

where ρ_v is the volumetric confinement ratio and defined as

$$\rho_v = \rho_{sx} + \rho_{sy} \tag{4-38}$$

By using the aforementioned relationships parametric studies have been conducted to investigate the effect of different FRP sheet applications on a strengthened beam. The results are given in Figure 4–8 and Figure 4–9. All analysed sections are representative of the test specimens of this study. Two types of FRP sheets were used in the parametric study: glass fibre and carbon fibre reinforced polymers. The properties of FRP materials are given in Table 4-2. The average values of the yield stress, f_y, and ultimate stress, f_{su}, of the longitudinal bars were 340 and 440 MPa with concrete compressive strength, f_c`, of 18 MPa are chosen in the analysis. The environmental reduction factor of 0.75 was used as recommended in ACI-440.2R-08 [5] because exterior exposure conditions were assumed.

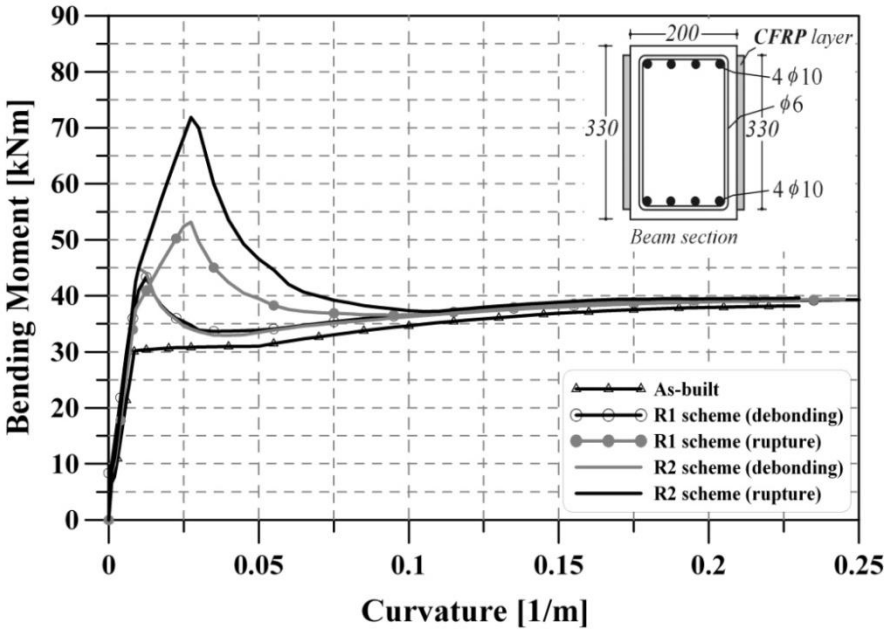

Figure 4–8 Effects of GFRP on the flexural behaviour of a beam section

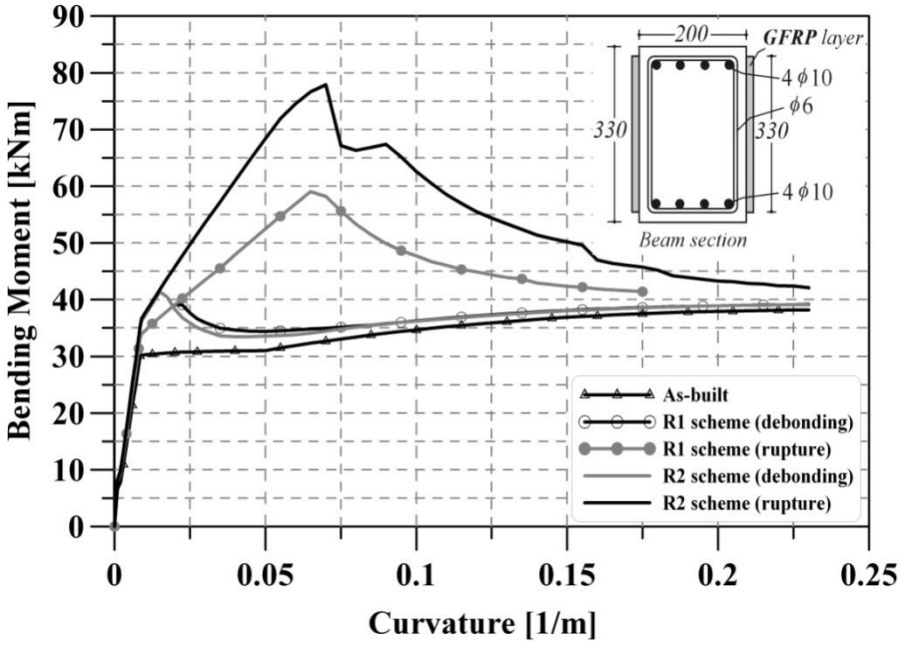

Figure 4–9 Effects of CFRP on the flexural behaviour of a beam section

The enhanced flexural behaviour of the beam section retrofitted with GFRP or CFRP (1 or 2 layers) can be seen in Figures 4-8 and 4-9, respectively. Furthermore, the effects of premature debonding are shown and compared with the behaviour of the element when assuming that no debonding would occur prior to rupture of the material. It was observed that the specimens retrofitted with GFRP material show a less abrupt softening after reaching the peak strength compared to their counterparts retrofitted with CFRP. However, it is also seen that maximum attained moment capacities either in debonding or rupture limit states are quite similar.

4.5.2 Shear Strength Assessment

In general, all members of a structure should be assessed to ensure that each member has sufficient capacity to resist the increased shear demand after retrofitting. Increasing the flexural strength may result in shear failures, which are brittle and undesirable failure modes [27-30]. Specifically in the joint subassembly, the flexurally strengthened beam and column elements should be capable of withstanding the anticipated increase in loads associated with the flexurally strengthened members. This is of crucial importance to guarantee the occurrence of anticipated ductile flexural failure before any brittle shear failure in these elements. In case of different demand conditions, further external FRP reinforcement by wrapping or partially wrapping the members needs to be applied accounting for additional shear strength requirements. Accordingly, shear strength assessment has been performed for

the retrofitted and unretrofitted members following ACI-440.2R-08 [5] and New Zealand concrete structures standard, NZS 3101 [31] recommendations. Detailed calculations are provided in Appendix B.

4.6 EVALUATION OF JOINT SHEAR CAPACITY IN THE AS-BUILT CONFIGURATION

Experimental studies on old-type beam-column joints have reported that the shear strength degradation of the joint panel zone can cause the collapse of complete structural components before any significant damage takes place in either beams or columns. Based on a series of experimental investigations on an exterior beam-column joints with plain round bars having end hooks [32], a peculiar damage mechanism, referred to as "concrete wedge" has been identified. Due to the combination of (a) slippage of the beam reinforcement, due to the use of smooth bars and inadequate anchorage in the joint area, (b) punching effects at the level of the hook anchorage on the exterior face of the joint subassembly when the beam bars are in compression and (c) cyclic shear diagonal cracking in the joint panel zone, a "concrete wedge" mechanism develops. As a consequence a sudden and severe joint shear strength reduction after first diagonal cracking (at a relatively low level of interstorey drift, 0.6-0.8%) occurs, because of the inefficiency of the diagonal strut mechanism within the joint region and the stress concentration at the beam bar end-hooks.

Obviously, this behaviour is significantly different from what is expected in joints designed with modern detailing. In addition, it cannot be properly predicted nor quantified by using traditional models reported in the literature for beam-column joints.

An alternative approach in the assessment of beam-column joints has been proposed [21, 2] based on the use of limit states which are associated to critical level of principal tensile or compression stresses. It is arguably more consistent than the use of nominal shear strength considerations in the capacity assessment. By taking into account the stress conditions in the joint panel, not only are the underlying mechanics of the problem considered, but also the influence on the joint cracking and ultimate strength of the axial load acting on the beams or columns is recognized. Furthermore, it is deemed to be more appropriate to employ a simple `diagonal strut mechanism` to account for the concrete contribution to joint shear and qualitatively describe such observed behaviour. As stated previously, this mechanism develops without any bond stress transfer from the beam and column reinforcing bars within the joint instead of a `truss mechanism`. A truss mechanism relies upon the presence of stirrups and can be developed only when good bond stress transfer is maintained along the beam and column reinforcing

bars, thus mainly for new or well-designed beam-column joints [1]. Note also that since both mechanisms depend on the strength of the core concrete, the ultimate shear capacity of the joint is governed by the failure of the concrete which in itself is limited by the gradual crushing along the cross-diagonal cracks along the potential failure planes.

Research on poorly designed joints [21, 33, 32] have provided suggestions for such limit states based on principal stresses and referring to a shear strength degradation curve e.g., shear strength envelops, expressed in terms of average value of principal tensile or compression stresses, as a function of the shear distortion in the joint, depending on different structural detailing or joint type. Based on experimental evidence [32, 34] for tee-joints with plain round bars and end hooks, the first crack in the joint core can be assumed to occur at a principal tensile stress level $p_t=0.19\sqrt{f`_c}$ which should be considered an upper limit for first diagonal cracking, with significant reduction for the second cracking as a consequence of reverse cyclic deterioration. For the assessment of as-built exterior joints with plain round bars and end hooks, the proposed strength degradation curve is given in Figure 4–11 obtained from the experimental findings conducted by the researcher.

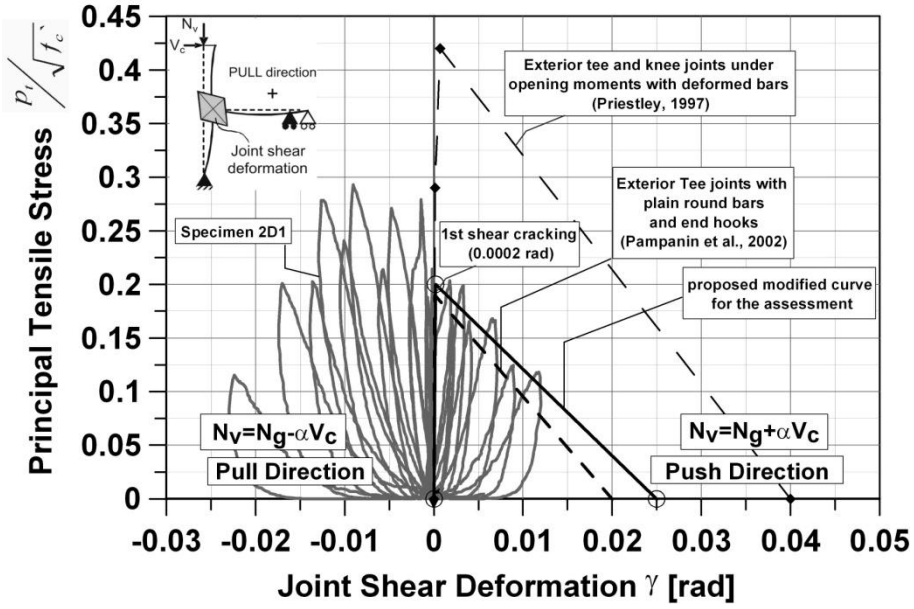

Figure 4–10 Strength degradation curves for 2D exterior joints

In order to generate the M-N performance domains and evaluate the internal hierarchy of strength and sequence of events the equivalent joint moment M_{jo} for the as-built configuration corresponding to different limit states (damage level) in the joint needs to be evaluated, and compared with the yielding

moment in the beam and columns. The external and internal actions considered for an as-built exterior beam-column joint are illustrated in Figure 4–11.

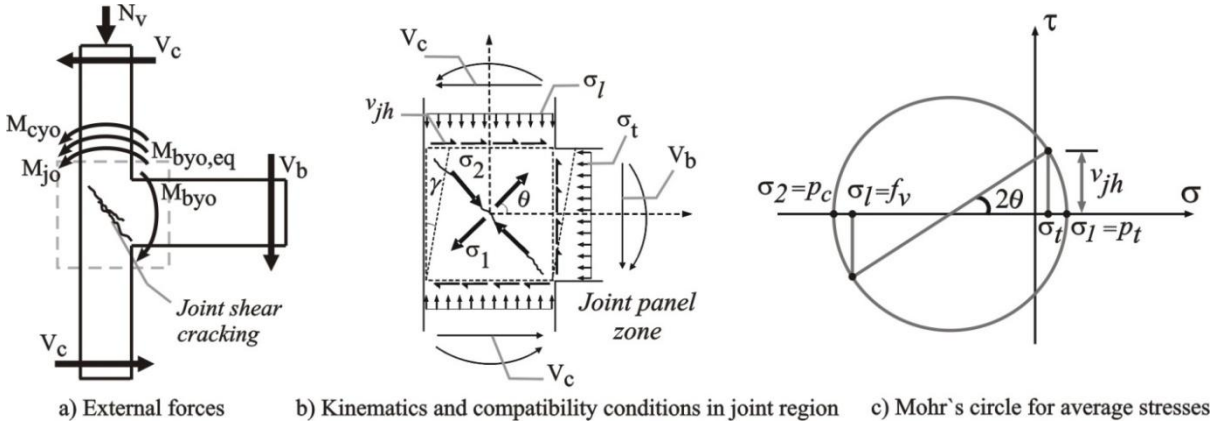

Figure 4–11 External and internal actions on as-built 2D plane frame joint and associated stresses

Using the nomenclature given in Figure 4–11 and Figure 4–12a the horizontal shear force acting on the joint core is

$$V_{jh} = T - V_c \tag{4-39}$$

where T=tensile force at the bottom beam bars and V_c=horizontal column shear force. Due to the necessary equilibrium of the subassembly external actions $V_c l_c = V_b l_b$ where V_b= beam shear force; l_c= height of column; and l_b= distance from column centre to contraflexure point. The beam yielding moment, M_{byo}, acting at the face of the joint core can be evaluated as:

$$M_{byo} = V_b (l_b - \frac{h_c}{2}) = Tjd \tag{4-40}$$

in which jd= internal forces lever arm in the beam section; and h_c=overall depth of column in the direction of the horizontal shear to be considered. For the sake of simplicity jd can be taken herein as $0.9d$, where d= effective depth. This moment capacity is not affected by any variation of axial load, thus is constant with varying axial load. After rearranging T in Eq. (4-40), replacing V_b by $V_c l_c / l_b$ it substituting into the joint horizontal shear force equation, leads to

$$V_{jh} = V_c \left(\frac{l_c}{l_b jd} \left(l_b - \frac{h_c}{2} \right) - 1 \right) \tag{4-41}$$

Since the column moment at the top of the joint, $M_{col}=V_c(l_c-h_b)/2$, where h_b= height of beam, after rearranging Eq. (4-39), the moment in the column M_{col} can be written in terms of the horizontal joint shear force, V_{jh}, as follows

$$M_{col} = \frac{V_{jh}}{\left(\frac{l_c}{l_b jd}\left(l_b - \frac{h_c}{2}\right) - 1\right)}\left(\frac{l_c - h_b}{2}\right) \tag{4-42}$$

It should be noted that the nominal horizontal shear stress, v_{jh}, at the mid-depth of the joint core is $V_{jh}/(b_j h_c)$. The effective width of the joint, b_j, is given by:

$$b_j = \min(b_c;\ b_c + 0.5\ h_c) \text{ if } b_c \geq b_w \tag{4-43}$$

$$b_j = \min(b_w;\ b_c + 0.5\ h_c) \text{ if } b_c \leq b_w \tag{4-44}$$

where b_c, b_w are the width of the column and beam respectively, and h_c is the depth of the column.

As mentioned, since the principal stresses have been shown to be a more appropriate damage indicator for beam-column joints, the Mohr`s circle can be employed along with the kinematics of the as-built joint (Figure 4–11b and Figure 4–11c) to evaluate the corresponding principal tensile, p_t, and compression, p_c, stresses in the joint panel

$$p_t = -f_v/2 \pm \sqrt{(f_v/2)^2 + v_{jh}^2} \tag{4-45}$$

where f_v = nominal compressive stress on the column at the mid-depth of the joint core is given by

$$f_v = N_v/(h_c b_c) \tag{4-46}$$

where compressive stress, N_v, is taken as positive.

A general formulation for the equivalent joint moment, M_j, thus corresponding to indentified levels of damage-limit states expressed in terms of principal stresses, in case it is found after substituting Eq.(4-46) into Eq.(4-42) as follows

$$M_j = \frac{\left(\sqrt{p_t^2 + p_t \frac{N_v}{h_c b_c}}\right) b_j h_c}{\left(l_c \left(l_b - h_c/2\right) \Big/ 0.9 d l_b - 1\right)} \frac{\left(l_c - h_b\right)}{2} \tag{4-47}$$

A more condensed expression of above equation can be written as

$$M_j = \frac{\sqrt{p_t^2 + p_t f_v}}{\omega} \left(10^3\right) \ [kNm] \tag{4-48}$$

where ω is regarded as a geometric coefficient, related to the nomenclature given in Figure 4–12.

$$\omega = \frac{2 l_b^{`} l_c - 1.8 d l_b}{0.9 d l_b A_e \left(l_c - h_b\right)} \tag{4-49}$$

where $l_b^{`}$ = half clear span length; A_e = effective area in the joint. Note that in both the as-built and retrofitted condition the equivalent joint moment, M_j would be referred to as M_{jo} and $M_{j,Rij}$, respectively. Rij which stands for the retrofitting scheme is explained in the design example section.

4.7 EVALUATION OF JOINT SHEAR CAPACITY AFTER FRP STRENGTHENING

Pantazopoulou and Bonacci [35] proposed a formulation for the assessment of joint design parameters based on the mechanics of interior beam-column joints in laterally loaded frames. Their formulation established the compatibility of the strain and stress equilibrium states at the centre of a planar joint region throughout the range of response up to failure, and assumes good bond conditions of the beam and column reinforcement. It was shown that the joint capacity could be limited by the crushing of the principal diagonal strut or by the yielding of the vertical reinforcement after hoop reinforcement yielding in the joint panel.

Antonopoulos and Triantafillou [16] proposed an extended version of the aforementioned model to evaluate the shear strength of beam-column joints of known geometry, reinforcement quantities, and retrofitted with externally bonded FRP. A comprehensive computer programme was developed to trace several possible stages of the response such as (a) yielding of the transverse or longitudinal reinforcement; (b) crushing of the concrete along the diagonal, or in the case of retrofitted specimens; (c) debonding or failure of FRP sheets.

Based on these two previous works, a new analytical model is presented to evaluate the shear resistance of a retrofitted joint, based on a combination of a mechanically-based model and empirical observations. According to the proposed model, the total shear strength of the retrofitted joint can be regarded as the parallel combination, for the same joint shear distortion, of the effects/strength of the intrinsic as-built (unretrofitted) condition and the contribution from the composite materials attached to the specimen. The evaluation of the as-built shear capacity of the joint has already been discussed in the previous section. A mechanically-based model is utilised in order to determine the joint shear resistance due to the composite material, following the basic considerations employed by the aforementioned researchers, and extending them to account for limit states based on principal tensile and compression stresses versus joint shear deformation.

In Figure 4–12a schematic illustration of the average stresses, the external and internal actions, with the nomenclature used in the design and assessment of an exterior RC joint strengthened with FRP, are shown with the idealization of the joint as a three-dimensional element. Note that the nomenclature given in this figure for column and joint moments namely $M_{cy,Rij}$, $M_{c,Rij}$ and $M_{j,Rij}$ correspond to the equivalent joint moments of these sections; whereas, although they are not shown in the figure, the equivalent beam moments in the FRP beam cut-off section and beam-column interface are represented as $M_{by,Rij,eq}$ and $M_{b,Rij,eq}$, respectively. In a similar fashion, the equivalent beam yielding moment for as-built specimen is denoted as $M_{byo,eq}$ as shown in Figure 4–11a. The joint shear stresses, assumed to be uniformly distributed over the boundaries of the joint, are introduced by direct member action, as well as by the bond that develops between the composite material and the joint core concrete.

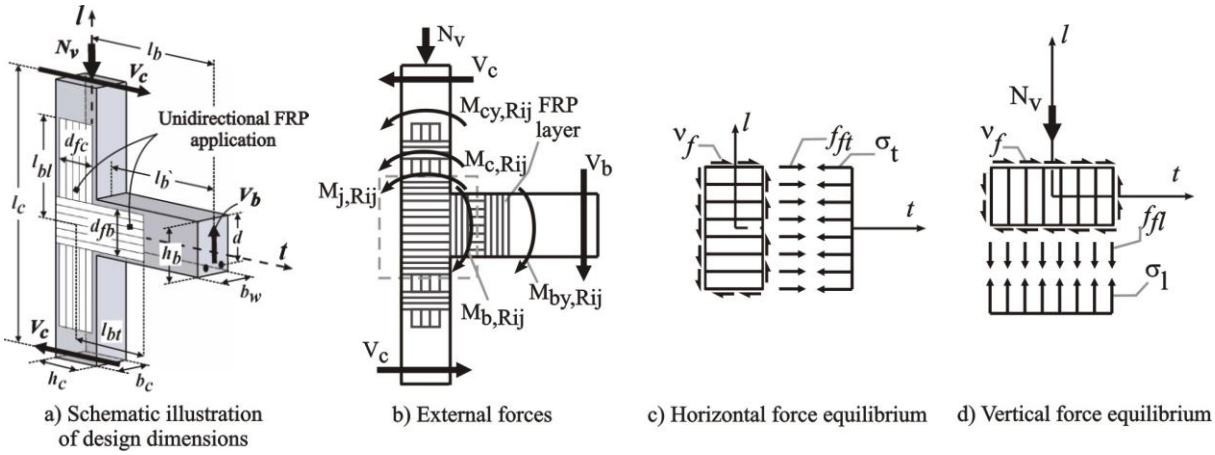

Figure 4–12 Schematic illustration of design dimensions and actions in retrofitted 2D joint

Under the equilibrium and compatibility conditions the average compressive transverse and longitudinal stresses in the concrete, σ_t and σ_l, are expressed as:

$$\sigma_t = -\rho_{ft} E_f \varepsilon_t \tag{4-50}$$

$$\sigma_l = -\rho_{fl} E_f \varepsilon_l - \frac{N_v}{h_c b_c} \tag{4-51}$$

where ρ_{ft} and ρ_{fl} are the FRP reinforcement ratio in the transverse and longitudinal direction, respectively; E_f is the elastic modulus of fibre and ε_l and ε_t are the average normal strain along normal directions *l* and *t*.

Plane stress and strain components can be written in terms of nominal shear stress in the joint, $v_{jh,}$ and direction of the principal stresses, $\tan\theta$, using the in-plane shear and normal stress expressions given in Eqs. (4-52)-(4-56). It is assumed that 1) the maximum principal stress in the concrete, σ_1, is always less than the tensile capacity (for the sake of simplicity taken as zero); and 2) the directions of principal strains and stresses coincide (nearly correct if the reinforcement has not yielded).

$$\sigma_2 = \sigma_t + \sigma_l \tag{4-52}$$

$$\sigma_t = -v_{jh} \cdot \tan\theta \tag{4-53}$$

$$\sigma_l = -\frac{v_{jh}}{\tan\theta} \tag{4-54}$$

$$\tan^2\theta = \frac{\varepsilon_1 - \varepsilon_t}{\varepsilon_1 - \varepsilon_l} \tag{4-55}$$

$$\gamma = \frac{2(\varepsilon_1 - \varepsilon_t)}{\tan\theta} \tag{4-56}$$

where σ_2 =minimum principal stress in the concrete, ε_1 = maximum principal strain in the joint panel, and γ=average angle of shear distortion. The nominal shear stress contribution due to the FRP, v_f, can be easily calculated by rearranging Eq. (4-53)

$$v_f = \frac{\rho_{ft} E_f \varepsilon_t}{\tan\theta} \tag{4-57}$$

A closed form of quadratic polynomial equation of $tan^2\theta$ can be obtained by substituting Eq. (4-53) and Eq. (4-54) into Eq. (4-52) after rearranging and replacing ε_l and ε_t (as per Eqs. (4-50) and (4-51)) into the obtained equation along with the Eq. (4-57). The procedure described above leads to

$$\left(\frac{1}{E_c} + \frac{1}{\rho_{ft} E_f}\right)\tan^4\theta + \left(\frac{N_v}{h_c b_c \rho_{fl} \rho_{ft} E_f^2 \varepsilon_t}\right)\tan^2\theta - \left(\frac{1}{E_c} + \frac{1}{\rho_{fl} E_f}\right) = 0 \tag{4-58}$$

The full step-by-step derivation of the above equation is given in Appendix C.

4.8 ITERATIVE PROCEDURE TO EVALUATE THE FRP RETROFITTED JOINT SHEAR CAPACITY

The shear capacity of the strengthened exterior RC joint, including the current state of stress and strain in the joint, can be determined by a simple iterative procedure. The input consists of:

1) *geometric data:* h_b, b_w, h_c, b_c

2) *material properties*: compressive strength of concrete, f_c`; elastic modulus of concrete, E_c; tensile strength of concrete, f_{ct}; FRP thickness per layer, t_f; design rupture strain in the FRP, ε_{fu}; and elastic modulus of the fibres, E_f

3) *FRP application scheme details*: depth of FRP sheet on beam surface, d_{fb}; depth of FRP sheet on column surface, d_{fc}; number of sheet on beam, n_{fb}; number of sheets on column, n_{fc}; number of beam sides covered with FRP, $n_{sf,b}$; number of column sides covered with FRP, $n_{sf,c}$. FRP reinforcement ratio in the transverse or longitudinal direction can be found as follows:

$$\rho_{ft} = (n_{fb} n_{sf,b} t_f d_{fb}) / (h_b b_w) \tag{4-59}$$

$$\rho_{fl} = (n_{fc} n_{sf,c} t_f d_{fc}) / (h_c b_c) \tag{4-60}$$

As an initial step, the transverse strain, ε_t, is incremented. For each value of ε_t Eq. (4-58) is solved for $\tan\theta$ so that the shear stress due to FRP, v_f, can be calculated by Eq. (4-57). Next, the normal stress in the FRP, $f_{ft}=E_f\varepsilon_t$, along the direction t (at the mid-height of the joint) is evaluated. It is important to note that as shown in Figure 4–12b, external moment actions in the beams would be twice the value of that in the columns based on the equilibrium conditions. Hence, this condition implies that strain demand in the beams will be higher than those of the columns. Based on these observations, it is deemed to be sufficient to check the FRP debonding limit states in the beam element. In other words, due to the higher strain demand in the beam compared to columns, it is expected that FRP debonding would initiate in the beam elements before the column elements, which in turn governs the response of the joint subassembly. At the end of each iteration step, two failure conditions should be checked:

- *Debonding or failure of FRP*:

The FRP will fail by tensile fracture when the tensile stress reaches the tensile strength, f_{fu} or corresponding ultimate FRP strain, ε_{fu}. As explained in section 4.5.1, debonding is treated here according to the fractural mechanics-based model of Holzenkampfer [13] and Eqs. (4-4) and (4-5) can be employed to calculate the maximum tensile stress in an FRP sheet when debonding occurs and development length along the direction t (mm).

- *Diagonal compression failure of the concrete in the joint panel zone*:

Experimental studies have shown that, for interior joints, the use of diagonal tension failure criteria in the joint core (assuming that the shear strength is reached at the stage of initial diagonal tension cracking of the joint core) may be too conservative [36]. Of note is that both previous and current experimental findings in this research have shown that FRP externally bonded exterior beam-columns joints are capable of developing sufficient compressive strut mechanism in the joint panel zone similar to interior joints [2]. By means of such diagonal compression strut mechanism the joint core maybe capable of transferring significantly higher shear forces after the first diagonal tension cracking occurred under the composite layer. When the compressive strength of the strut is sufficiently weakened by the diagonal tension cracks due to repeated opening and closing, crushing of the diagonal compression strut will finally occur. In order to satisfy capacity design considerations, the diagonal compression stress in the joint panel zone should be limited to prevent premature brittle failure of the compression strut, especially after the development of multiple diagonal cracks as shown in Figure 4–1a, which would reduce the width of the compression strut. The confinement of the joint panel zone via a U-shape FRP layer anchored back in the beam would not only increase the strength and efficiency of the diagonal compression strut, but would also help in controlling the lateral expansion of the joint core. In general principal compression stressed in the joint has been suggested to be limited by Priestley *et al.* [21]:

$$p_c \leq 0.3 f_c` \tag{4-61}$$

Prota *et al.* [37] also confirmed that the limit of $0.3f'_c$ for the principal compression stress at failure of the joint could be a reasonable design criterion, even though it could be conservative for high axial load ratios. By employing the aforementioned relationships, the FRP contribution to the increase in the joint shear capacity of poorly detailed beam-column joints can be adequately estimated in terms of principal tensile stress, p_{tf}, as a function of the amount and layout of the externally bonded reinforcement.

The whole procedure without iteration (as a valid alternative option to the iterative approach) to assess the capacity of FRP retrofitted exterior beam-column joints with plain round bars and end hooks, is summarized as a flowchart in Figure 4–13.

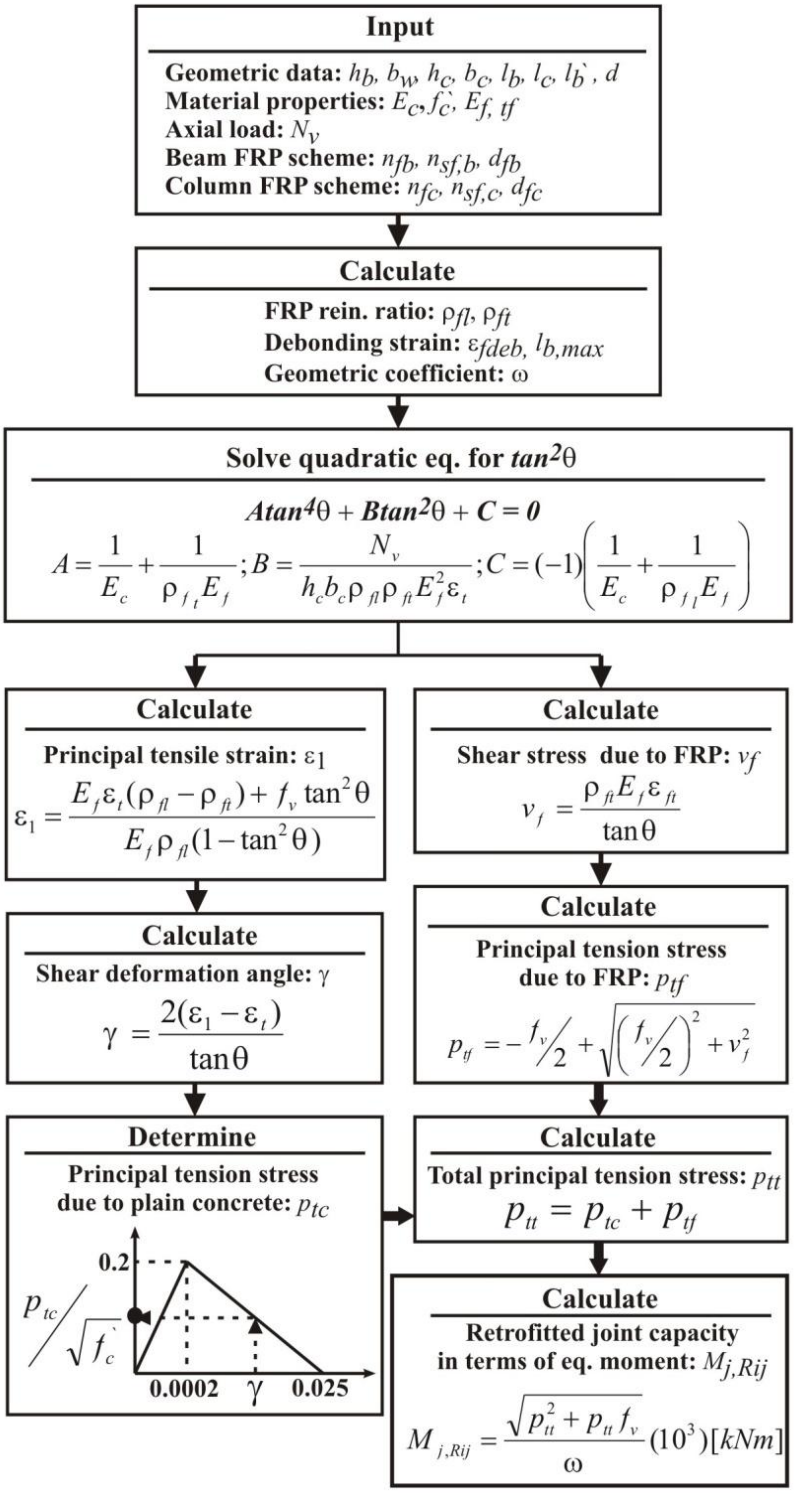

Figure 4–13 Flowchart for determining the joint shear capacity of the retrofitted specimen

4.8.1 Validation of the Analytical Model

In order to validate the proposed analytical model for the evaluation of the joint shear capacity of a FRP strengthened beam-column joints, four sets of test results available in literature are used. These tests were performed on T-joints strengthened with FRP materials under the simulated seismic testing of scaled specimens [38-41]. Detailed information on these studies can be found in Chapter 2.

The methodology for the evaluation and analytical-experimental comparison is briefly described below. Firstly, the as-built test results were re-processed in order to obtain the principal tensile strength of the unretrofitted joints. For this purpose, the load versus displacement curves were used to determine the shear force at the column face V_c and the tensile force in the main beam reinforcement T_b. Hence, the nominal shear strength of the joint, v_{jh}, and the corresponding principal tensile strength, $p_{t,}$ was calculated according to Eqs. (4-42) and (4-43), using the actual axial load used in the tests.

At a second stage, following the flowchart given in Figure 4-13 the contribution of the FRP retrofit was calculated referring to the material properties and retrofitting scheme used by the researchers. As given in the post-test evaluation of the shear-strength, a remarkably good agreement with 22 experimental results in abovementioned literature was found (Table 4-3).

It is important to note that while calculating the principal stress contribution of the as-built concrete core, the slope of the strength degradation curve proposed by Priestley [42] (Figure 4–10) is used. Once the strength of the as-built joint is determined (e.g., load at 1st shear cracking in the joint), it is relatively simple to construct the degradation curve and find the principal tensile strength corresponding to the joint shear deformation at the defined limit state of FRP. Note that, the proposed curve obtained from the test results conducted in this study, exhibits a similar trend and can thus be recommended to be used for the assessment of exterior T-joints with plain round bars and end hooks. A template of *Matlab*® code used in the retrofit design and analytical model validations is given in Appendix D. This code can be easily adopted inside spreadsheet programmes to perform the capacity assessment of exterior 2D beam-column joint strengthened with FRP following the procedure herein proposed.

Table 4-3 Comparison of analytical model predictions with experimental test results

Title	Specimen Details			FRP Retrofit Properties					Result Comparison		
	f_c` (MPa)	f_v (MPa)	Maximum Load (kN)	(L/θ)[b]	ρ_{fb} (%)	ρ_{fc} (%)	E_{II} (GPa)	Type	$p_u/\sqrt{f_c}$ – Exp	$p_u/\sqrt{f_c}$ – Anal	Anal/Exp
AT(F11)[a]	22.8	1.15	42.8	2/0°, 2/90°	0.13	0.13	230	Carbon sheet	0.86	0.83	0.97
AT(F12)	29.5	1.15	44.4	2/0°, 4/90°	0.13	0.26	230	Carbon sheet	0.78	0.87	1.11
AT(F21)	27	1.15	50.7	4/0°, 2/90°	0.26	0.13	230	Carbon sheet	0.95	0.91	0.96
AT(F22)	27.2	1.15	50.0	4/0°, 4/90°	0.26	0.26	230	Carbon sheet	0.93	0.99	1.06
AT(F22A)	27.8	2.88	57.4	4/0°, 4/90°	0.26	0.26	230	Carbon sheet	0.94	0.97	1.04
AT(F22W)	29.2	1.15	55.8	4/0°, 4/90°	0.26	0.26	230	Carbon sheet	1.02	0.99	0.98
AT(F22in)	21	1.15	41.9	4/0°, 4/90°	0.26	0.26	230	Carbon sheet	0.87	0.99	1.14
AT(S33)	26	1.15	35.3	3/0°, 3/90°	0.26	0.39	150	Carbon strip	0.64	0.77	1.19
AT(S33L)	26.3	1.15	42.5	3/0°, 3/90°	0.26	0.39	150	Carbon strip	0.79	0.77	0.97
AT(S63)	24.2	1.15	39.8	3/0°, 3/90°	0.52	0.39	150	Carbon strip	0.77	0.91	1.19
AT(GL)	19.5	1.15	43.6	2.5/0°, 2.5/90°	0.42	0.42	70	Glass sheet	0.95	0.79	0.84
GPR(4)	20	0	187	2/45°, 2/-45°	0.74	0.74	64.7	Carbon sheet	0.53	0.59	1.12
GPR(8)	20	0	187	2/45°, 2/-45°	0.74	0.74	64.7	Carbon sheet	0.53	0.59	1.12
GPR(9)	20	0	216	2/45°, 2/-45°	0.74	0.74	64.7	Carbon sheet	0.57	0.59	1.03
GPR(12)	34	0	184	2/45°, 2/-45°	0.74	0.74	64.7	Carbon sheet	0.44	0.56	1.26
GPR(13)	34	0	204	2/45°, 2/-45°	0.74	0.74	64.7	Carbon sheet	0.44	0.56	1.27
GPR(14)	34	0	229	2/45°, 2/-45°	0.74	0.74	64.7	Carbon sheet	0.51	0.56	1.10
PGR(5R)	21	0	1606	2/45°, 2/-45°	0.58	0.58	64.7	Carbon sheet	0.58	0.58	1.00
PGR(6)	21	0	1619	2/45°, 2/-45°	0.58	0.58	64.7	Carbon sheet	0.60	0.58	0.97
GS(T1R)	38	6	130	1/45°, 1/-45°	0.69	0.69	19	Glass sheet	0.50	0.51	1.02
GS(T2R)	25	6	132	4/0°	0.56	0	71	Glass sheet	0.64	0.61	0.95
GS(T4)	25	6	118	1/45°, 1/-45°	0.69	0.69	19	Glass sheet	0.54	0.53	0.98

Note: AT=Antanopolous and Triantafillou (2001); GPR=Gergely et al. (2000); PGR=Pantelides et al. (2001); GS=Ghobarah et al. (2001)

[a]Notation on brackets denotes specimens as defined by those who conducted tests;

[b]L denotes total number of layers on both sides of joint at angle θ from horizontal.

4.8.2 Design Example

A full design example of the FRP retrofit intervention, following the presented analytical procedure, is given in this section with reference to the specimen 2D4 tested in this study, whose properties and experimental response will be described in later chapters. For simplicity, one single level of axial load N_v=50 kN is considered for this design example. By varying the level of N_v, a *M-N* interaction diagram could be established for the as-built and retrofitted configuration. Thereupon, the evaluation of the hierarchy of strength and sequence of events are carried out to support the definition of the most appropriate retrofit solution to adopt.

The specimen 2D4 was retrofitted according to the R21 scheme. Recall that, a retrofitting scheme is expressed as Rij where i indicates the number of sheets applied on the beam surface whereas j indicates the number of sheets on the column (e.g., R12 suggests 1 FRP horizontal layer on the beam and 2 vertical layers on the column). SikaWrap®-100G type high strength E-glass unidirectional fibre polymers were used for the retrofitting. A summary of the geometric and material properties as well as FRP retrofit layout is given as follows

- Geometric data: h_b = 330 mm, b_w = 230 mm, h_c = 230 mm, b_c = 230 mm, l_b = 1524 mm, l_c = 2000 mm, l_b` = 1409 mm, d = 305 mm
- Material properties: f_c`= 18.4 MPa, $E_c = 5700\sqrt{f_c`} = 24450$ MPa, E_f = 76000 MPa, t_f = 0.36 mm, ε_{fu}= 2.8%
- Beam and column FRP scheme: n_{fb} = 2, $n_{sf,b}$ = 2, d_{fb} = 300 mm, n_{fc} = 1, $n_{sf,c}$ = 2, d_{fc} = 200 mm

Step 1. Calculate FRP reinforcement ratio:

$\rho_{fl} = (n_{fc}\, n_{sf,c}\, t_f\, d_{fc}) / (h_c\, b_c) = [(1)\ (2)\ (0.36)\ (200)] / [(230)\ (230)] = 0.00272$

$\rho_{ft} = (n_{fb}\, n_{sf,b}\, t_f\, d_{fb}) / (h_b\, b_w) = [(2)\ (2)\ (0.36)\ (300)] / [(330)\ (230)] = 0.00569$

Calculate debonding strain and optimum anchorage length:

$$f_{f,deb} = f_{f,\max} = c_1\sqrt{(E_f\, f_{ct})/(t_f\, n_{fb})} = (0.64)\sqrt{[(76000)((0.3)(18.4)^{(2/3)})]/[(0.36)(2)]} = 300.1 \text{ kN}$$

$$\varepsilon_{fdeb} = f_{f,deb}/E_f = (300.1)/(76000) = 0.40\ \%$$

$$l_{b,\max} = \sqrt{(E_f t_f)/c_2 f_{ct})} = \sqrt{[(76000)(0.36)]/[(2)(2.1)]} = 81 \text{ mm}$$

Note that, according to Eq. (4-5) l_{bt} should be larger than $l_{b,max}$. On the other hand, recall that an optimal anchorage length should be chosen in order to achieve the desired sequence of events as discussed in section 4.5.1. The development length, l_{bt}, is chosen as 365mm which equals to the sum of 250mm the FRP sheet length from the face of the column and half of the column length. More detailed information is provided in the following section.

Calculate geometric coefficient:

$$\omega = \frac{2l_b^{`}l_c - 1.8dl_b}{0.9dl_b A_e(l_c - h_b)} = \frac{2(1.409)(2) - 1.8(0.305)(1.524)}{0.9(0.305)(1.524)(0.0529)(2 - 0.33)} = 129.86$$

Step 2. Solve quadratic equation for $tan^2\theta$:

$$A = \left(1/E_c + 1/\rho_{ft} E_f \right) = \left(1/24{,}450 + 1/(0.00569)(76000) \right) = 0.0024$$

$$B = \left(N_v / h_c b_c \rho_{fl} \rho_{ft} E_f^2 \varepsilon_{fdeb} \right) = \left((50{,}000) / (230)(230)(0.00272)(0.00569)(76000)^2 (0.004) \right) = 0.0027$$

$$C = (-1)\left(1/E_c + 1/\rho_{ft} E_f \right) = (-1)\left(1/24{,}450 + 1/(0.00569)(76000) \right) = -0.0049$$

$$\Delta = \frac{-B + \sqrt{B^2 - 4AC}}{2A} = \frac{-(0.00266) + \sqrt{(0.0027)^2 - 4(0.0024)(-0.0049)}}{2(0.0024)} = 0.98 \Rightarrow$$

$tan\theta = \sqrt{0.98} = 0.99$

Step 3. Calculate principal tensile strain:

$$\varepsilon_1 = \frac{E_f \varepsilon_t (\rho_{fl} - \rho_{ft}) + f_v \tan^2\theta}{E_f \rho_{fl} (1 - \tan^2\theta)}$$

$$= \frac{(76{,}000)(0.004)(0.00272 - 0.00569) + ((50{,}000)/((230)(230)))(0.98)}{(76{,}000)(0.00272)(1 - 0.98)} = 0.007$$

Step 4. Shear deformation angle:

$$\gamma = \frac{2(\varepsilon_1 - \varepsilon_t)}{\tan\theta} = \frac{2(0.007 - 0.004)}{0.99} = 0.006$$

Step 5. Determine the principal tension strength contribution due to the plain concrete:

By using the strength degradation curve in Fig. 3 for the given shear deformation the principal tension stress is found as $0.15\sqrt{f_c`} = 0.15\sqrt{18.4} = 0.64$ MPa.

Step 6. Calculate nominal shear strength contribution due to FRP:

$$v_f = \frac{\rho_{ft} E_f \varepsilon_t}{\tan\theta} = \frac{(0.00569)(76{,}000)(0.004)}{(0.99)} = 1.75 \text{ MPa}$$

Step 7. Calculate principal tensile strength contribution due to FRP:

$$p_{tf} = -f_v/2 + \sqrt{\left(f_v/2\right)^2 + v_f^2} = -(0.95)/2 + \sqrt{\left((0.95)/2\right)^2 + (1.75)^2} = 1.3 \text{ MPa}$$

Step 8. Calculate total principal tensile strength:

$$p_{tt} = p_{tc} + p_{tf} = 0.64 + 1.3 = 1.94 \text{MPa}$$

Step 9. Calculate the capacity of the FRP retrofitted joint in terms of equivalent moment:

$$M_{j,Rij} = \frac{\sqrt{p_{tt}^2 + p_{tt} f_v}}{\omega}(10^3) = \frac{\sqrt{(1.94)^2 + (1.94)(0.95)}}{129.86}(10^3) = 18.2 \text{ kNm}$$

As evident in this numerical example, the proposed assessment procedure can be easily implemented into a worksheet/spreadsheet and used to choose the desired FRP material properties and retrofit layout on a case-by-case basis.

Figure 4-14 and 4-15 show, as an example, a parametric investigation on the effects of the R11, R12 and R22 retrofit schemes. The shear strength of the joint is significantly enhanced due to the GFRP even with the minimum retrofit scheme, R11. The column axial load increases, as expected, the joint overall strength; with more pronounced effects with an increased number of GFRP layers placed on the beam (e.g., R21 and R22). However, this results in a 20% reduction in ductility capacity.

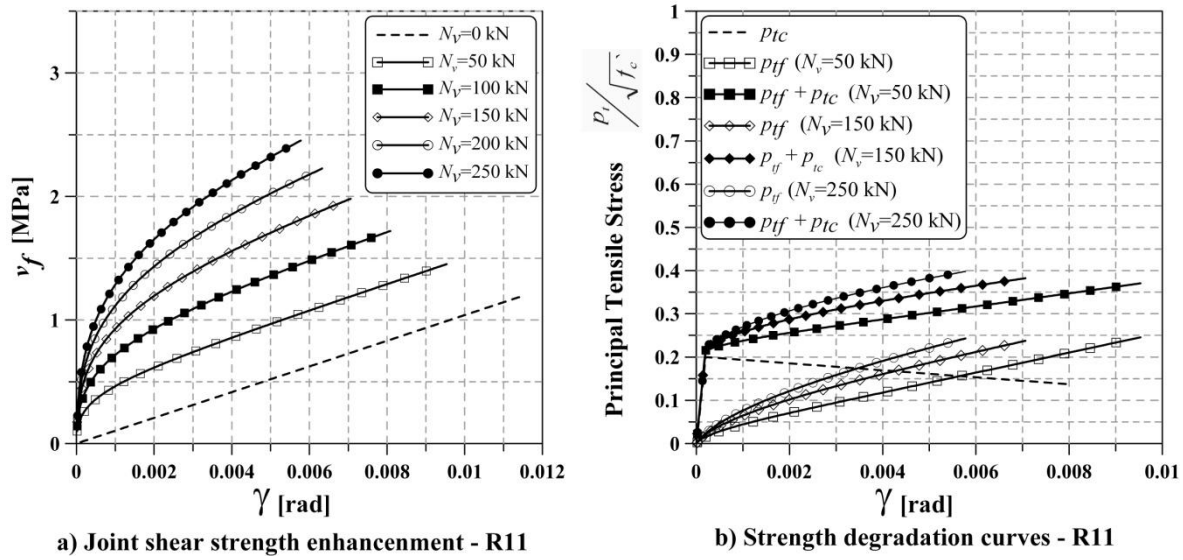

Figure 4–14 Effects of GFRP strengthening on behaviour of the joint under varying axial load

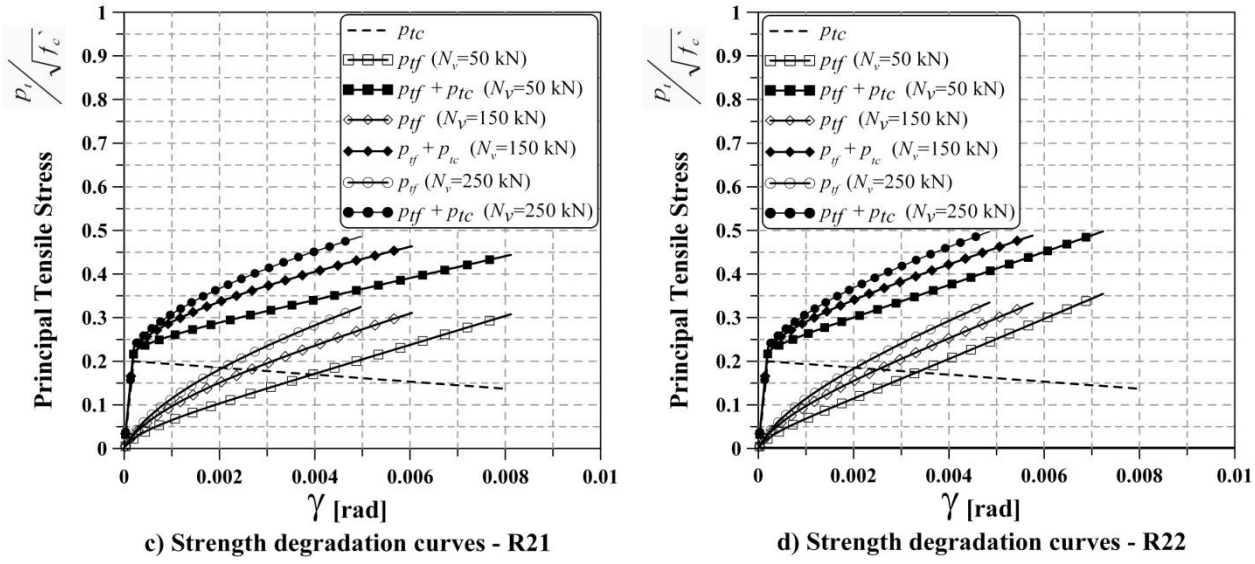

Figure 4–15 Effects of GFRP strengthening on behaviour of the joint under varying axial load (cont`d)

4.9 M-N PERFORMANCE DOMAIN AND SEQUENCE OF EVENTS OF TEST UNITS

In this section, a summary of the detailed assessment of each joint component in both the as-is and retrofitted configuration is presented in Table 4-4. The equivalent beam yield moments in the joint column interface are indicated with a subscript *eq*. These values can be calculated using Eq. (4-62). The nomenclature for the calculation of equivalent beam moments in the column is presented in Figure 4-16.

The analyses are conducted according to the previously mentioned material constitutive relationships along with empirical and semi-empirical models presented previously. Section limit states such as the first-yield limit state for reinforcing bars, spalling limit state for confined and unconfined concrete and debonding limit state for GFRP materials are defined based on the tested material properties in the structural laboratory (see Chapter 5 for more information). Note that for FRP retrofitted sections the debonding limit state is defined instead of the FRP rupture strain limit due to the fact that in most cases the debonding phenomena governs the behaviour of the retrofitted section.

$$M_{b,eq} \leq M_b \frac{l_b (l_c - h_b)}{2 l_c (l_b - l_{bt})} \tag{4-62}$$

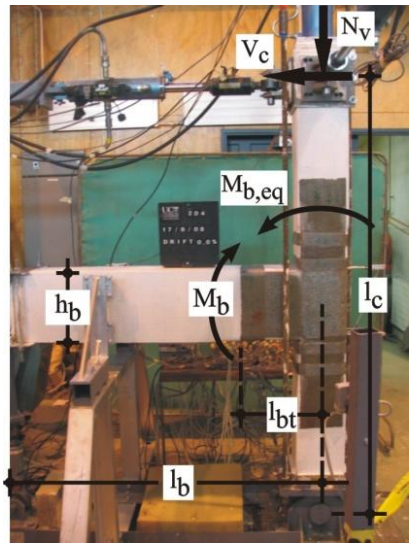

Figure 4–16 Nomenclature for the calculation of equivalent beam moments in the column

Figure 4-17 and 4-18 show the *M-N* performance domains of the 2D test units which are plotted based on the values shown in Table 4-4. Furthermore, the expected sequence of events under the varying axial load demands are also presented in Table 4-5. The variation of axial load is estimated according

to a selected prototype structure which is a typical residential medium-rise RC frame structure. Detailed information on the prototype structure and determination of the demand stemming from axial load variation is given in Appendix E. Comparisons with experimental results covered in detail in Chapter 6, not only confirm the validity of the assessment methodology and of the analytical model, but also clearly emphasise the unconservative assumptions of retrofit design if a constant axial load is assumed. As clearly shown in Figure 4-18 an inadequate consideration of the actual demand may result in unforeseen damage in the retrofitted joint panel which in turn may affect the global behaviour of the structure.

Table 4-4 Summary of capacity assessment results for 2D test units

Specimen: 2D1	**As-built Specimen**		
Beam moments	**Column and joint moments**		
M_{byo} [kNm]	N_v [kN]	M_{cyo} [kNm]	M_{jo} [kNm]
36.8	0	18.9	6.6
$M_{byo,eq}$	50	23.1	9.6
16.6	100	27.2	11.8
	150	30.9	13.7
	200	33.9	15.4
	250	35.7	16.9

Specimen: 2D2 and 2D3	**Retrofit scheme: R11**			
Beam moments	**Column and joint moments**			
$M_{by,R11}$ [kNm]	N_v [kN]	$M_{cy,R11}$ [kNm]	$M_{c,R11}$ [kNm]	$M_{j,R11}$ [kNm]
28.5	0	16.6	18.7	12.8
$M_{by,R11,eq}$ [kNm]	50	20.7	23.1	15.5
15.6	100	24.9	27.4	18.2
$M_{b,R11}$ [kNm]	150	28.3	30.9	20.9
39.1	200	31.3	34.5	23.3
$M_{b,R11,eq}$ [kNm]	250	34.7	37.3	25.5
17.7				

Specimen: 2D4	**Retrofit scheme: R21**			
Beam moments	**Column and joint moments**			
$M_{by,R21}$ [kNm]	N_v [kN]	$M_{cy,R21}$ [kNm]	$M_{c,R21}$ [kNm]	$M_{j,R21}$ [kNm]
28.5	0	16.6	18.7	15.0
$M_{by,R21,eq}$ [kNm]	50	20.7	23.1	17.9
15.6	100	24.9	27.4	21.0
$M_{b,R21}$[kNm]	150	28.3	30.9	23.9
41.36	200	31.3	34.5	26.5
$M_{b,R21,eq}$ [kNm]	250	34.7	37.3	29.0
18.7				

Table 4-5 Predicted sequence of events for as-built and retrofitted 2D Specimens

Specimen	Loading		Critical Events		Analytical Results	
	Axial Load	Direction	No	Failure Type	V_c [kN]	N_v [kN]
2D1	Varying	Pull	1	Joint shear failure	11.9	55
			2	Beam yielding	19.9	-
		Push	1	Joint shear failure	18.2	195
			2	Beam yielding	19.5	-
2D2	Constant	Pull - Push	1	Beam yielding	18.7	-
			2	Beam FRP debonding	21.2	-
			3	Joint failure	22.4	110
2D3	Varying	Pull	1	Joint FRP debonding	17.2	30
			2	Beam yielding	18.7	-
			3	Beam FRP debonding	21.2	-
		Push	1	Beam yielding	18.7	-
			2	Beam FRP debonding	21.2	-
2D4	Varying	Pull	1	Beam yielding	18.7	-
			2	Joint FRP debonding	20.12	-
			3	Column FRP debonding	23	5
		Push	1	Beam yielding	18.7	-
			2	Beam FRP debonding	22.4	-

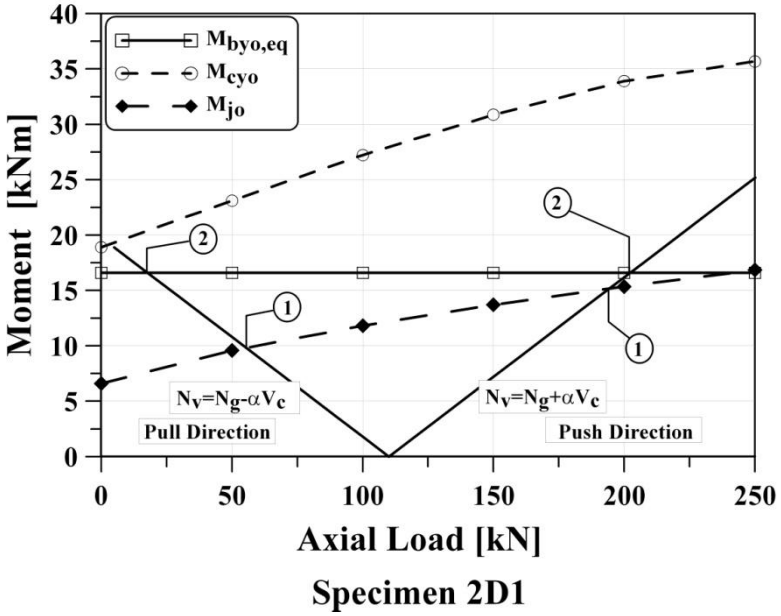

Figure 4–17 Evaluation of hierarchy of strengths and sequence of events of test units

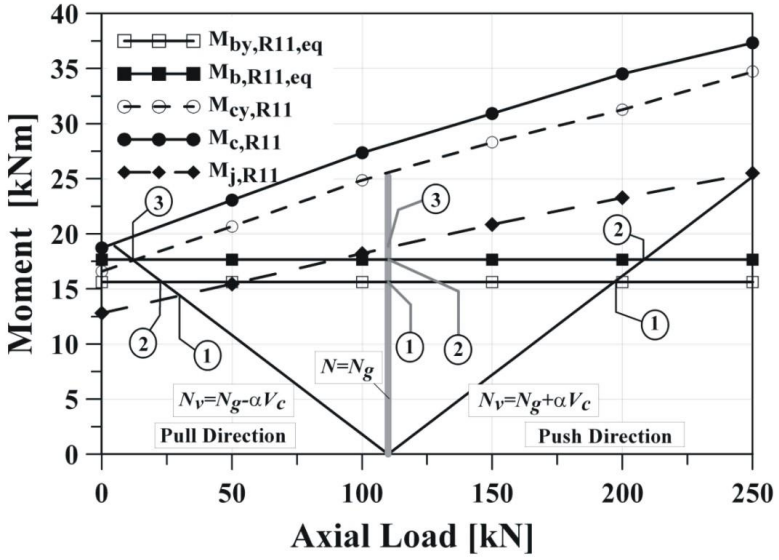

a) Specimens 2D2 and 2D3

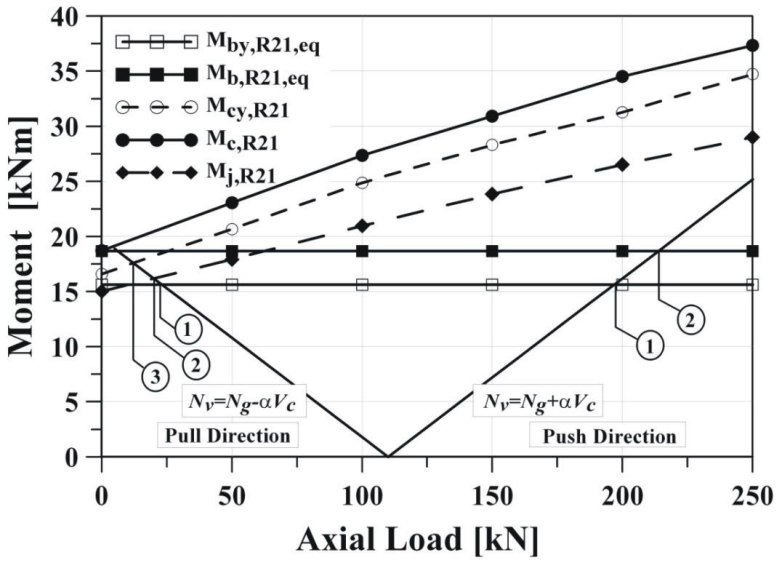

b) Specimen 2D4

Figure 4–18 Evaluation of hierarchy of strengths and sequence of events of test units (cont`d)

4.10 SUMMARY

A simple procedure is proposed for the assessment of the as-built and the design of FRP-retrofitted exterior beam-column joints. Firstly, detailed assessment of each joint component in the as-built beam column-joint is performed to obtain the hierarchy of strength and sequence of events before the retrofit intervention. The component capacities are then compared within a *M-N* performance domain in order to establish the internal hierarchy of strength and sequence of events. In addition, the role and

importance of accounting for the correct demand conditions (e.g., the variation of axial loads) in the assessment of the existing joint and the design of the FRP retrofit scheme are discussed. A semi-empirical analytical procedure is developed to evaluate the shear strength of FRP retrofitted joints. The total shear strength of the retrofitted joint considers the summation of strength contribution of the as-built plain concrete and the composite material attached to the plain concrete. The analytical model is compared and validated with experimental results available in existing literature. Results of parametric analyses are presented to indicate the effectiveness of strengthening with different materials, configurations and failure limit states (i.e., debonding or rupture of composite materials, failure of concrete).

Conclusions can be summarized as follows (1) mode of joint failure can be considered by establishing a relationship between loads applied to the joint and resulting deformations; (2) from the analysis it is shown that external bonded reinforcement has significant effect on the enhancement of the joint shear capacity even in the application of minimum retrofit strategy; (3) shear strength of the joint, either as-built or retrofitted, depends on the usable compressive strength of concrete and debonding characteristics of the composite material; (4) proposed simplified approach and step-by-step procedure can easily be adopted by designers as a powerful tool for assessment and retrofit interventions. In this way, solutions can be adopted to bring the proper sequence of events and hierarchy of strength to meet the capacity design principles leading to a more ductile and dissipating hysteresis behaviour; (5) as a final step, deformation-based retrofit strategy can be adopted in such a way that the global displacement response of the structure obtained through the assessment of demand can be linked to the demand level of joint shear deformations. Thus, joint retrofit design can be performed according to displacement-based design considerations, based on the overall lateral drift of the structure for specified performance limit. This final point is elaborated upon during the discussion of experimental results in Chapter 9.

4.11 REFERENCES

1. Paulay T, Priestley MNJ. *Seismic design of reinforced concrete and masonry buildings*. Wiley: New York, 1992.
2. Pampanin S, Bolognini D, Pavese A. Performance-based seismic retrofit strategy for existing reinforced concrete frame systems using fiber-reinforced polymer composites. *Journal of Composites for Construction*. 2007; **11**(2):211-26.
3. Akguzel U, Pampanin S. Experimental behaviour of exterior beam-column joint subassemblies retrofitted using GFRP composites. *NZSEE Conference*, Palmerston, New Zealand, 2007.
4. Bank LC. *Composites for Construction: Structural Design with FRP Materials*. John Wiley & Sons: NY, 2006.

5. ACI-440.2R-08. Guide for Design and Construction of Externally Bonded FRP Systems for Strengthening Concrete Structures. 2008.
6. fib. *Externally bonded FRP reinforcement for RC structures, fib Bulletin no. 14*. Federation International du Beton (fib): Lausanne, Switzerland, 2001.
7. fib. *Retrofitting of concrete structures by externally bonded FRPs, with emphasis on seismic applications, fib Bulletin no. 35*. Federation International du Beton (fib): Lausanne, Switzerland, 2006.
8. GangaRao HVS, Vijay PV. Bending behaviour of concrete beams wrapped with carbon fabric. *Journal of Structural Engineering*. 1998; **124**(1):3-10.
9. Saenz N, Pantelides CP. Shear friction capacity of concrete with external carbon FRP strips. *Journal of Structural Engineering*. 2005; **131**(12):1911-9.
10. Teng JG, Chen JF, Smith ST, Lam L. *FRP Strengthened RC Structures*. John Wiley & Sons: New York, 2001.
11. Pham HB, Al-Mahaidi R. Prediction models for debonding failure loads of carbon fiber reinforced concrete beams. *Journal of Composites for Construction, ASCE*. 2006; **10**(1):48-59.
12. Saxena P, Toutanji H, Noumowe A. Failure analysis of FRP-Strengthened RC beams. *Journal of Composites for Construction, ASCE*. 2008; **12**(1):2-14.
13. Holzenkampfer E. Ingenieur des verbundes geklebter bewehrung fur betonbautelie. *Ph.D. Dissertation*, TU Braunshwieg (*in German*), 1994.
14. TR 55. *Design guidance for strengthening concrete structures using fibre composite materials.* Concrete Society, Camberley, Surrey, England, 2004.
15. JSCE. *Recommendations for upgrading of concrete structures with use of continuous fiber sheet* Concrete Engineering Series 41, Japan Society of Civil Engineers, Tokyo, Japan, 2001.
16. Antonopoulos CP, Triantafillou TC. Analysis of FRP-Strengthened RC beam-column joints. *Journal of Composites for Construction, ASCE*. 2002; **6**(1):41-51.
17. Neubauer U, Rostasy FS. Design aspects of concrete structures strengthened with externally bonded CFRP-plates. *Concrete&Composites, Proceedings of the 7th International Conference on Structural Faults and Repair*, London, 109-18, 1997.
18. Priestley MNJ, Calvi GM, Kowalsky MJ. *Displacement–Based Seismic Design of Structures*. IUSS Press Pavia, 2007.
19. Mander JB, Priestley MJN, Park R. Seismic design of bridge piers. *Report 84-02*, University of Canterbury, Chrischurch, 1984.
20. Dodd LL, Restrepo JI. Model for predicting cyclic behavior of reinforcing steel. *Journal of Structural Engineering, ASCE*. 1995; **121**(3):433-45.
21. Priestley MJN, Seible F, Calvi GM. *Seismic Design and Retrofit of Bridges*. Wiley: New York, 1996.
22. Mander JB, Priestley MJN, Park R. Theoretical stress-strain model for confined concrete. *Journal of structural engineering*. 1988; **114**(8):1804-26.
23. Wang YC, Restrepo JI. Investigation of concentrically loaded reinforced concrete columns confined with glass fiber-reinforced polymer jackets. *ACI Structural Journal*. 2001; **98**(3):377-85.
24. Allington CJ. Seismic performance of moment resisting frame members produced from lightweight aggregate concrete. *PhD Dissertation*, University of Canterbury, Christchurch, 2003.
25. Sheikh SA, Uzumeri SM. Analytical model for concrete confinement in tied columns. *Journal of Structural Division, ASCE*. 1982; (ST12).
26. Manfredi G, Realfonzo R. Modellazione del comportamento di elementi presso-inflessi in c.a. confinati con tessuti in materiale composito. *X Congresso Nazionale "L'ingegneria Sismica in Italia"*, Potenza-Matera, 2001.

27. Kachlakev D, McCurry D. Testing of Full-Size Reinforced Concrete Beams Strengthened with FRP Composites: Experimental Results and Design Methods Verification. *Report No. FHWA-OR-00-19*, U.S. Department of Transportation Federal Highway Administration, 2000.
28. Chajes M, Januska T, Mertz D, Thomson T, Finch W. Shear strengthening of reinforced concrete beams using externally applied composite fabrics. *ACI Structural Journal*. 1995; **92**(3):295-303.
29. Norris T, Saadatmanesh H, Ehsani M. Shear and flexural strengthening of R/C beams with carbon fiber sheets. *Journal of Structural Engineering*. 1997; **123**(7):903-11.
30. Malvar L. Durability of composites in reinforced concrete. *Proceedings of the First International Conference on Durability of Composites for Construction*, Sherbrooke, QC, Canada, pp. 361-72, 1998.
31. NZS 3101:2006. *Concrete structures standard NZS 3101*. Standards association of New Zealand, Wellington, 2006.
32. Pampanin S, Calvi GM, Moratti M. Seismic behaviour of RC beam-column joints designed for gravity loads. *12th European Conference on Eartquake Engineering*, London, Paper no. 726, 2002.
33. Calvi GM, Magenes G, Pampanin S. Relevance of beam-column damage and collapse in RC frame assessment. *Journal of Earthquake Engineering*. 2002; **6**(Special Issue No. 1):75-100.
34. Hertanto E. Seismic assessment of pre-1970s reinforced concrete beam-column joint subassemblies. *M.E. Thesis*, University of Canterbury, Christchurch, 2006.
35. Pantazopoulou S, Bonacci J. Consideration of questions about beam-column joints *ACI Structural Journal*. 1992; **89**(1):27-36.
36. Hakuto S, Park R, Tanaka H. Seismic load tests on interior and exterior beam-column joints with substandard reinforcing details. *ACI Structural Journal*. 2000; **97**(1):11-25.
37. Prota A, Nanni A, Manfredi G, Cosenza E. Selective upgrade of beam-column joints with composites. *International Conference on FRP Composites in Civil Engineering,*, Hong Kong, 2001.
38. Gergely J, Pantelides CP, Reaveley LD. Shear strengthening of RC T-joints using CFRP composites. *Journal of Composites for Construction, ASCE*. 2000; **4**(2):408-16.
39. Ghobarah A, Said A. Seismic rehabilitation of beam-column joints using FRP laminates. 2001.
40. Pantelides CP, Gergely J, Reaveley LD. In-situ verification of rehabilitation and repair of reinforced concrete bridge bents under simulated seismic loads. *Earthquake Spectra*. 2001; **17**(3):507-30.
41. Antonopoulos CP, Triantafillou TC. Experimental investigation of FRP-Strengthened RC beam-column joints. *Journal of Composites for Construction, ASCE*. 2003; **7**(1):39-49.
42. Priestley MJN. Displacement-based seismic assessment of reinforced concrete buildings. *Journal of Earthquake Engineering*. 1997; **1**(1):157-92.

Chapter 5 EXPERIMENTAL PROGRAMME FOR 2D BEAM-COLUMN JOINTS

5.1 INTRODUCTION

In this chapter, the experimental programme performed on the tests of four 2/3 scale 2D exterior nonseismically detailed RC beam-column joints is described. One as-built and three retrofitted units were tested under unidirectional quasi-static lateral loading. In order to investigate the effect of axial load variation on the retrofitted 2D specimens, one specimen (2D2) was tested under constant axial load while the others (2D1, 2D3 and 2D4) were tested under varying axial load. Another important parameter, the retrofit scheme, was also studied in the course of the testing programme.

Detailed information on the design and fabrication of test units, material properties used in the construction and retrofitting process, the test setup and loading procedures are provided. Test units were extensively instrumented to acquire the data for the performance analysis of each unit. The evaluation of the damage modes, strength hierarchy, joint shear strength and hysteretic behaviour, including the strength, stiffness and energy dissipation characteristics were performed in detail. These engineering parameters are discussed in the next chapter following the test results section. The instrumentation used in the measurement of loads, global and local deformations with the equations used in analysing the experimental data is also described.

5.2 DESCRIPTION OF TEST UNITS

A series of experimental quasi-static cyclic tests were carried out on a total of four 2/3 scale specimens comprising of one as-built and three retrofitted exterior joint subassemblies in the first experimental campaign of this study. Test specimens represented the exterior joints of the first storey of a prototype frame, representing a middle-rise (6-9 storeys) residential building. Points of contraflexure were

assumed to occur at midheight and midspan of columns and beams, respectively. More information on the prototype frame can be found in Appendix E.

All specimens (including 3D corner joints covered in Part 3) were detailed and built according to older (pre-1970s) construction practice in New Zealand [1] as well as in Italy [2]. Numerous alternative structural detailing can be adopted which typically depends on the national code provisions, as well as on the local construction and design practice. As a typical example, although the use of no shear reinforcement in the joint is arguably the most common (or at least the worst practice case), detail in several countries (Figure 5-1), alternative structural detailing has been adopted in older (pre-1970s) construction practice.

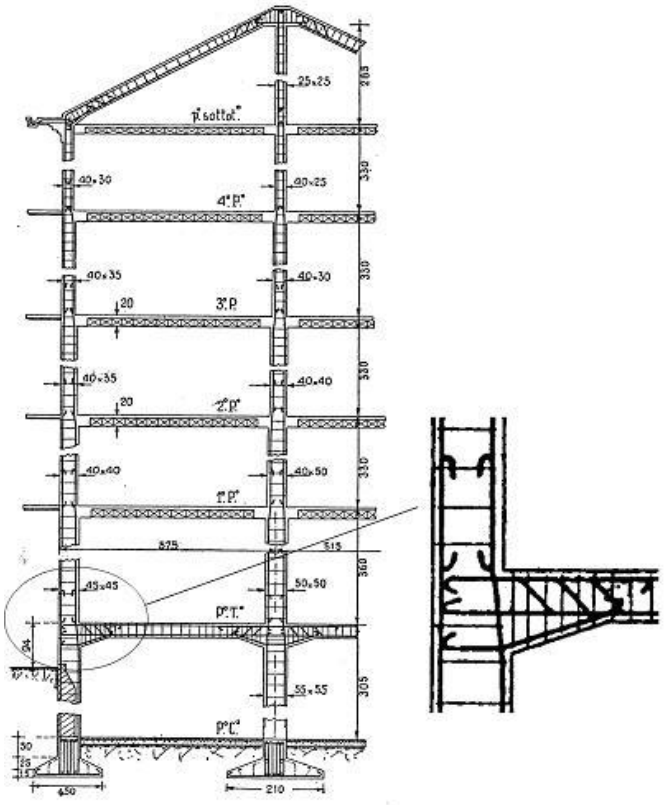

Figure 5–1 Detailing of pre-1970s RC structures in the Mediterranean countries (Italy) [3]

In Figure 5–2, a blueprint of a typical building constructed before the 1970s in New Zealand (Figure 5–2a) and the exterior beam-column joint reinforcement detailing (Figure 5–2b) are given to emphasise the point presented in the previous paragraph. The use of one or two stirrups in the joint was a common detail. At first sight these stirrups can be regarded as intended shear reinforcement provided in the joint regions. However, examination of older building codes and existing literature revealed that these stirrups were actually placed in the joints as a continuation of the column stirrups

along the elevation from above column to the upper column of the storeys. In spite of the different original intention, they still served the purpose.

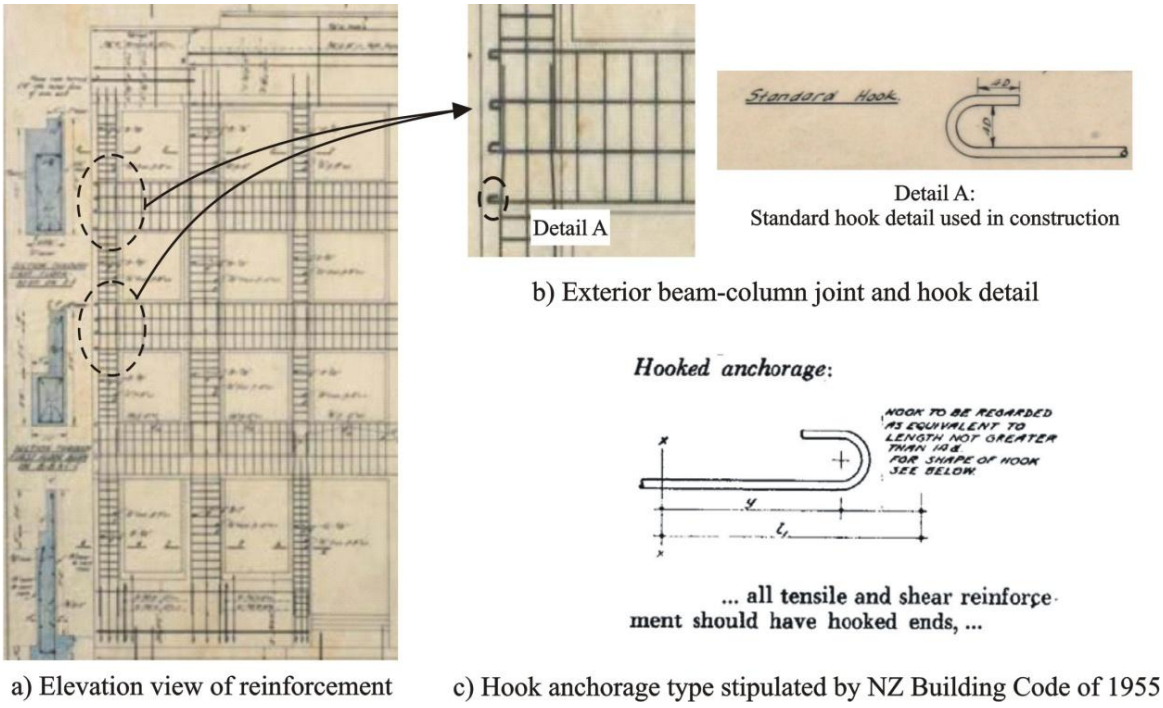

Figure 5–2 Reinforcement detail of a typical pre-1970s residential building (South British Building, Hereford Street, Christchurch, New Zealand; Courtesy of Christchurch City Council)

The use of plain round bars with a hook-end for the anchorage of longitudinal reinforcement was another commonly used reinforcing detailing in the construction practice before the 1970s. Taken from the same blueprint given in Figure 5–2a, the adopted standard hook detailing (Figure 5–2b) to meet the requirements of older building codes (Figure 5–2c) can be seen.

In this study, the aim was to adopt a worst case scenario typical of gravity load-only design of pre-1970s construction practice in the design of the specimen. For this purpose, an extracted exterior 2D beam-column joint portion of the mentioned prototype structure (described in more details in Appendix E) was chosen to replicate the actual deficient detailing and load conditions in the production of the specimens. All specimens had the same steel reinforcement detailing. As a typical application in gravity-only designed columns, inadequate anti-buckling and confinement reinforcement were employed. The column and beam both had cross sectional dimensions of 230x230. The properties of the specimen geometry and reinforcement details are summarised below and shown in Figure 5-3 and Table 5-1.

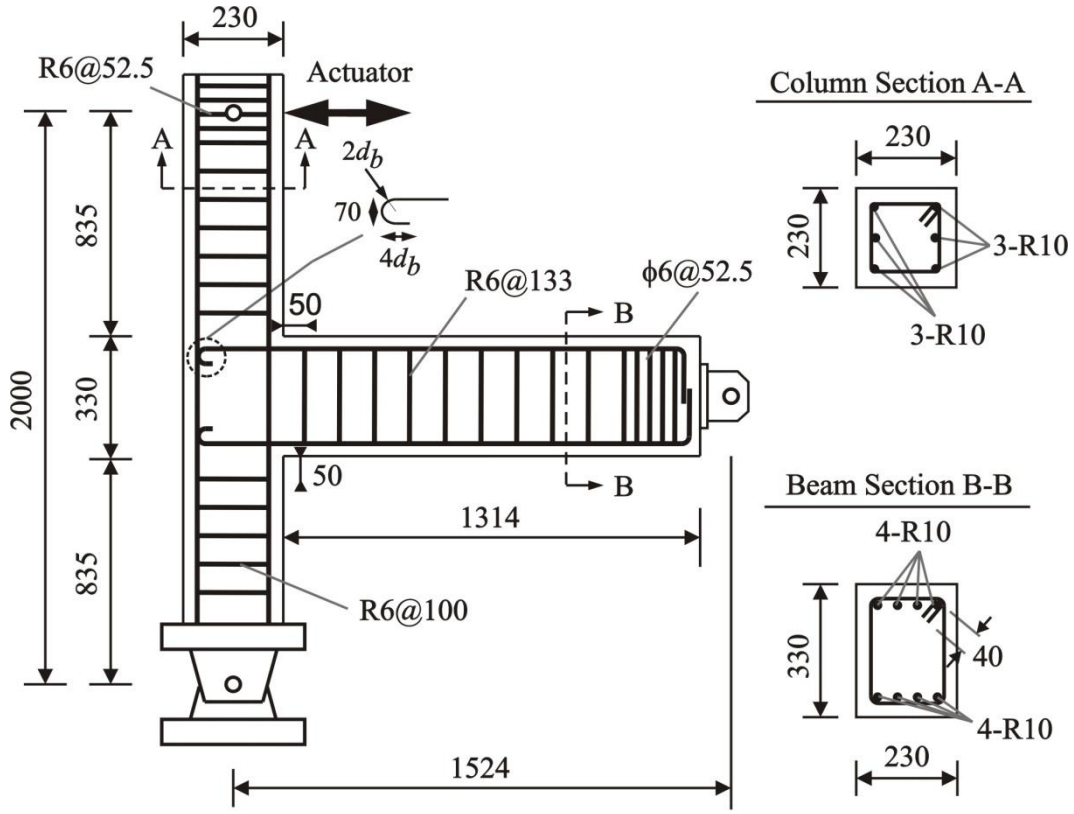

Figure 5–3 Geometry and reinforcement details of 2D test units

Table 5-1 Summary of specimen properties for unidirectional experimental programme

Specimen	f_c [a] (MPa)	Axial load range		Retrofit scheme[d]			
		N_g [b] (kN)	α[c]	Type	Beam horizontal layer #	Column vertical layer #	Joint U-shape horizontal sheet #
2D1	17.9	115	4.63	-	-	-	-
2D2	18.9	115	0	R11	1	1	1
2D3	18.0	115	4.63	R11	1	1	1
2D4	18.7	115	4.63	R21	2	1	2

Note:
[a] Compressive strength of 100mm dia. x 200mm concrete cylinder
[b] Constant axial load produced by the tributary gravity load for each prototype
[c] Proportionality coefficient
[d] Installed on each side

The columns for all units were symmetrically reinforced on the strong axis containing three 10 mm diameter Grade 300 plain round bars on both sides. The reinforcement ratio ρ_{sc} equals to 0.89% and it was comparable to the older code recommendations of the NZS95:1955 code [1] for the minimum longitudinal column steel ratio, ρ_{sc} of 0.8%. The column transverse reinforcement consisted of 6 mm diameter Grade 300 plain round bars placed at 100 mm centres. The NZS95:1955 code [1] stipulated a

maximum spacing for column stirrups of 120 mm (the least of $2/3h_c$, 12 $d_{b,c}$ or 12 inches). The first tie was 50 mm from the beam face.

Beams were symmetrically reinforced with four 10 mm diameter Grade 300 plain round bars in the top and four 10 mm diameter Grade 300 plain round bars in the bottom with both top and bottom longitudinal reinforcements ratios being ρ/ρ' =0.233%. Beam longitudinal bars anchored into the joint with a standard 180 degree hook which met the requirements of the NZS95:1955 code [1] for (a) bent radius (>2$d_{b,b}$), (b) straight length beyond the bent >4$d_{b,b}$ and clear concrete cover to the hook tip >3$d_{b,b}$. The beam transverse reinforcement for all units used 6 mm diameter Grade 300 plain round bars placed at 133mm centres with the ratio of ρ_{sh} = 0.042%. The first stirrup was 50 mm from the column face. All specimens had no transverse reinforcements installed in the joint core as typical of preseismic code construction.

The sequence of tests was formed to (1) illustrate how axial load variation affects retrofit design performed using traditional constant axial load assumptions; (2) investigate the inelastic response behaviour of retrofitted 2D plane frame beam-column joints under the constant and fluctuating axial forces; and lastly (3) verify the proposed assessment and retrofit design methodology in Chapter 4.

According to the aforementioned objectives, firstly a benchmark test was conducted on an un-retrofitted specimen (as-built configuration), Unit 2D1, under varying axial load. The next specimen was retrofitted based on the assumptions that constant axial load was acting on the columns. Hence, a minimum retrofit scheme (R11) was applied and the axial force kept constant for this control specimen during the entire test. Behaviour of this specimen was what would be expected if axial-force variations are neglected. In order to illustrate the possible effects of axial load fluctuation demands on a specimen which was designed according to constant axial load assumptions, Specimen 2D3 was tested with the same retrofit scheme, R11, but under varying axial load conditions. In the last specimen, Specimen 2D4, to improve the performance of the retrofitted joints under varying axial load conditions, a modified retrofit scheme, R21, was employed and tested under varying axial load. All tests were conducted under displacement controlled quasi-static reversed cyclic loading. Table 5-2 provides a summary of the test specimens` concrete compressive strength on the day of testing, axial load levels and wrapping configurations.

5.3 MATERIAL PROPERTIES

5.3.1 Reinforcing Steel

The longitudinal and transverse reinforcement used for all test specimens was plain round bars of mild steel Grade 300. Through the monotonic loading tests by an Avery Universal Testing Machine, the measured tensile properties of the reinforcing steel used in the specimens are given in Figure 5–44 were conducted in accordance to the NZS3112:1986 standard [4] with an average loading rate of 600 MPa/min. In Table 5-2 the average values obtained from three samples are tabulated.

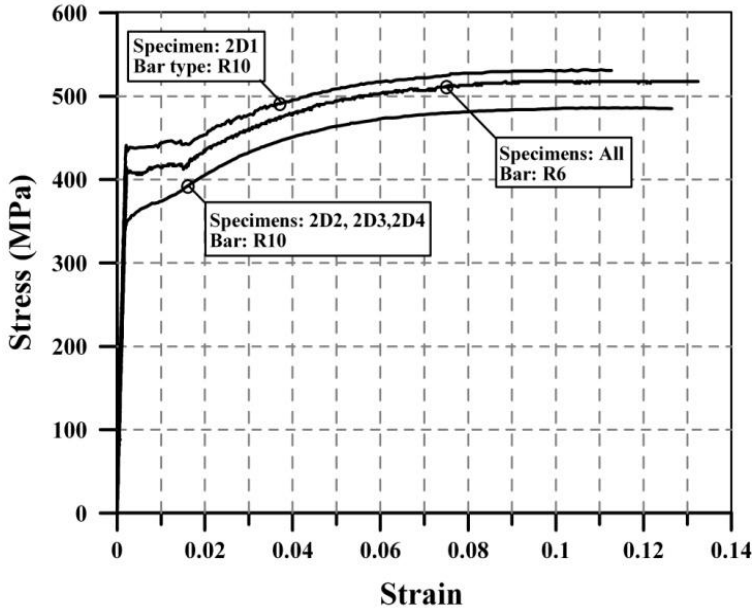

Figure 5–4 Stress – strain curves for the reinforcing steel used in 2D plane frame joint specimens

Table 5-2 Measured reinforcing steel properties for 2D plane frame joint specimens

Specimen	2D1, 2D2, 2D3, 2D4	2D1	2D2, 2D3, 2D4
Bar Type	R6	R10	R10
Yield Strength, f_y (MPa)	408	430	340
Yield Strain, ε_y	0.0024	0.0025	0.0019
Strain at commencing strain hardening, ε_{sh}	0.016	0.017	0.079
Ultimate Strength, f_u (MPa)	515	530	440

Note: R6=6mm plain round bar of 6mm diameter
R10=10mm plain round bar of 10mm diameter
Each value was obtained from the average of three coupons

5.3.2 Concrete

The concrete for the test units was a standard mix type supplied by a local commercial ready-mix concrete company. The concrete used had a maximum aggregate size of 13mm with coarse aggregate/fine aggregate/cement mix proportions of 4.3:3.9:1. The water-cement ratio was 0.695.

Several 100 mm diameter x 200 mm concrete cylinders were prepared for compressive testing and were cured in a fog room. They were tested at twenty eight days to obtain the compressive strength of the concrete. Higher slump concrete was used aimed at improving the workability in casting. The concrete cylinders were tested using the Avery Universal Testing Machine according to NZS 4671:2001 [5]. The average values obtained from three samples of concrete cylinder samples are listed in Table 5-3. In the same table the direct tensile strength of concrete obtained from Brazilian tests as given in NZS 4671:2001 [5] Part 2 are given.

Table 5-3 Measured concrete properties of 2D plane frame specimens

Specimen	At 28 days	At day of testing		
	f'_c (MPa)	*Slump* (mm)	f'_c (MPa)	f_t (MPa)
2D1	16.88	180	17.9	2.04
2D2	16.88	180	18.9	2.29
2D3	16.88	180	18.0	2.26
2D4	16.88	180	18.7	2.29

Note: f'_c = compressive strength of 100mm dia. x 200mm concrete cylinder
f_t = split cylinder tensile strength

5.3.3 Composite Material

SikaWrap®-100G type high strength E-glass unidirectional fibre polymers were used for the retrofitting. A summary of the mechanical properties of fibres as provided by the manufacturer, Sika (NZ) Ltd., is as follows: tensile E-modulus E_f = 76,000N/mm2, failure strain ε_{fu}* = 2.8% (nominal) and fibre thickness, t_f= 0.36mm. Detailed information on the properties of glass fibre fabric and epoxy impregnation resin can be found in Appendix F.

5.4 SPECIMEN FABRICATION

2D test units were cast together in T-shaped plywood formwork lying on the ground (Figure 5–6a). To prevent any buckling and deformation of the formworks, they were attached to the strong floor by

means of timber blocks and steel angles. The moulds were sealed along the edge to prevent leaking of the mix water. The inside surface of the plywood formwork was cleaned and oiled so that the specimens could be easily demolded. The internal edges were also sealed with silicone sealants to avoid bleeding of water.

All the longitudinal reinforcement and the stirrups were cut to length and bent in the factory. The stirrups were tied to the longitudinal bars with steel wires in the proper position (Figure 5–6b). The electrical strain gauges (see Section 5.8.3.1) were firmly attached on the side of the bar in the critical regions to measure the strain in the reinforcement. After the waterproof glue covering the strain gauges dried, the constructed cages were carefully placed in the moulds and fixed in the correct position before casting of the concrete (Figure 5–6b).

The designed 28-day compressive strength was 18 MPa and the specified maximum aggregate size was 13mm for all test specimens. The specified concrete type was mixed and provided by the commercial plant as prescribed (see Section 5.3.2). A high-frequency vibrator was used to consolidate the concrete and reduce honeycombing, especially in the joint region. During concrete casting, the high frequency electrical vibrators were utilised to distribute the concrete in the moulds (Figure 5–6c). Before placing the cover for curing, the concrete surface was smoothed by timber strips.

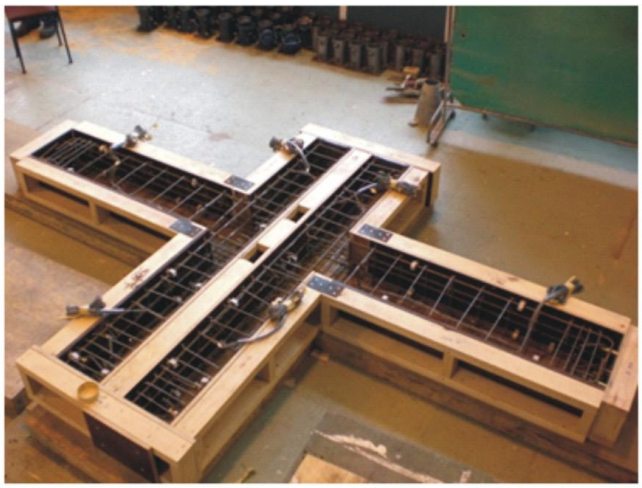

a) 2D plane frame specimens before casting

b) Close-up view of beam-column joint reinforcement of 2D specimen

c) Casting of 2D plane frame specimens

Figure 5–5 Formwork, reinforcing detail and casting of 2D plane frame specimens

5.5 RETROFIT APPLICATION

5.5.1 Design of Retrofit Intervention

The retrofit design methodology and analytical model previously presented and proposed in Chapter 4 were employed in the preliminary retrofit design of the specimens. Two alternative layouts of Glass Fibre Reinforced Polymers (GFRP) were adopted. A so-called "minimum retrofit application", R11, was applied to both Specimens 2D2 and 2D3. In the Specimen 2D4, an upgraded R21 retrofit scheme was used. Figure 5–6 presents the schematic layout of the wrapping scheme along with the mechanical properties of the GFRP material. The letters in the parentheses reflect the application sequence and the cut dimensions of the FRP sheets.

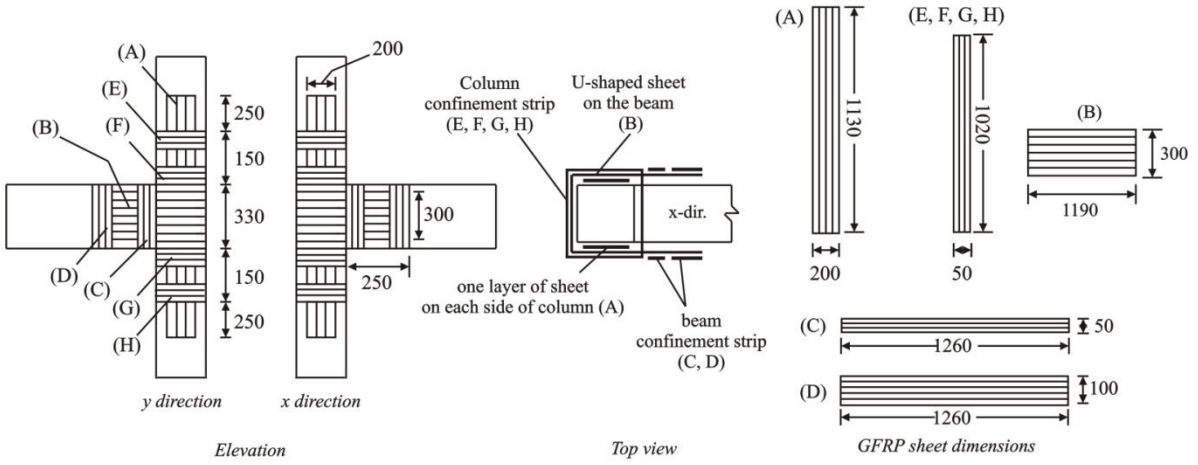

Notes:

FRP properties: Type=Uni-directional glass fibers (GFRP SikaWrap-100G); Elastic modulus=76,000 MPa; Failure strain=2.8%; Fiber thickness=0.36 mm

FRP application scheme: Specimen 2D2=R11*; Specimen 2D3=R11; Specimen 2D4=R21

*Rij refers to a configuration with i number of GFRP layers in the beam and j number of GFRP layers in the column (on each side)

Figure 5–6 Schematic illustration of GFRP retrofit configuration for 2D joint specimens

5.5.2 GFRP Application

FRP retrofitting of all specimens was undertaken by a specialist contracting service, Construction Techniques Group Ltd (BBR Contech). The whole process was completed in three days. Before the external application, the surface of the specimens was cleaned and sharp corners to be wrapped were rounded to a radius of 20 mm by grinding and sanding in order to avoid stress concentrations in these regions (Figure 5–7a). The GFRP installation locations on the specimens were marked (Figure 5–7b) and sheets were tailored to the predetermined dimensions (Figure 5–7c) according to the design drawings (Figure 5–6). The saturant for impregnation was applied in order to ease the application in

the laboratory (Figure 5–7d). In the next stage, primer and putty were applied with a trowel to level the concrete surface after patching small holes to provide improved substrate for the saturant (Figure 5–8a). The first layers of GFRP sheet were cut to the required length and bonded to the surface after the application of saturant (Sikadur®-300) to impregnate the dry fibres (*hand layup method*, see section 2.4.1 of Chapter 2 for more information). The application sequence is given in Figure 5–8: (1) vertical laminate on both sides of the column (Figure 5–8b); (2) U-shape horizontal laminate wrapped around joint (Figure 5–8c); (3) anchorage strips wrapped around the column (Figure 5–8d); (4) and lastly anchorage strips wrapped around the beam (Figure 5–8e). In each application sequence the applied sheet was smoothed by hand in the direction of fibres in order to remove any air that might have been trapped during application. The fabric was laminated using a plastic impregnating roller to achieve proper bonding and remove excessive impregnation resin. The next layer of GFRP, if needed (i.e., in case of Specimen 2D4 where a second layer of GFRP was applied in the joint region), was applied to the surface following the same procedure.

Figure 5–7 GFRP application steps: preparation of specimens and material

a) Primer and putty application

b) vertical laminate application on column

c) U-shape horizontal laminate wrapped around joint

d) GFRP strips wrapped around column

e) GFRP strips wrapped around beam

Figure 5–8 GFRP application steps: application of the material

5.6 TEST SETUP

The test rig was designed to enable unidirectional and bidirectional simulated seismic forces to be applied without any alterations to the rig. It was built on the strong floor of the Main Structures Laboratory in the Civil Engineering and Natural Resources Engineering Department at the University of Canterbury. For each direction, two C channels were welded to a steel plate and attached to the concrete strong floor by means of strong bolts. To increase the lateral stiffness, hence to minimize the deflection of the reaction frame under lateral loading, an inclined rectangular hollow section was also braced to each of these sections.

Beam and column elements were extended between points of contra-flexure, assumed to be at the mid-span in the beams and at the mid-height in the columns, where pin connections were introduced. Simple supports at the beam ends were provided by connecting pin-end steel members to the strong floor. In this way, horizontal displacement was allowed, while vertical displacement of the beam-end

was held. A universal hinge connection at the bottom of the column was used in 2D unidirectional and 3D bidirectional tests. Depending on the type of testing, the restraint conditions were modified in the universal hinge. For instance, in the case of 2D unidirectional testing, rotation of the universal hinge was restrained in other directions, but not in the x-direction. Furthermore, the out-of-plane restrainer installed on the sides of the beam element was used to prevent out-of-plane rotation and displacement.

Lateral load application was applied to the tip of the column by means of a servo-controlled 50 kN hydraulic jack connected to an automatic hydraulic pump, operated at 3000 psi pressure and a maximum flow rate of 130 litre/min. It was attached to the reaction frame using high strength bolts and connected to the column using a pin connection. For the axial load application and measurement, a 300 kN capacity vertical servo-valve hydraulic actuator and a 150 kN capacity load cell were placed between two stiff 40 mm steel plates and connected to the column base plate by two 24 mm diameter fully threaded high strength Macalloy bars. By means of 16 mm bolts and steel plates welded to the pin base, the column base was prevented from slipping. Figure 5–9 and Figure 5–10 show the front and dimetric view of the test rig used in the 2D unidirectional tests.

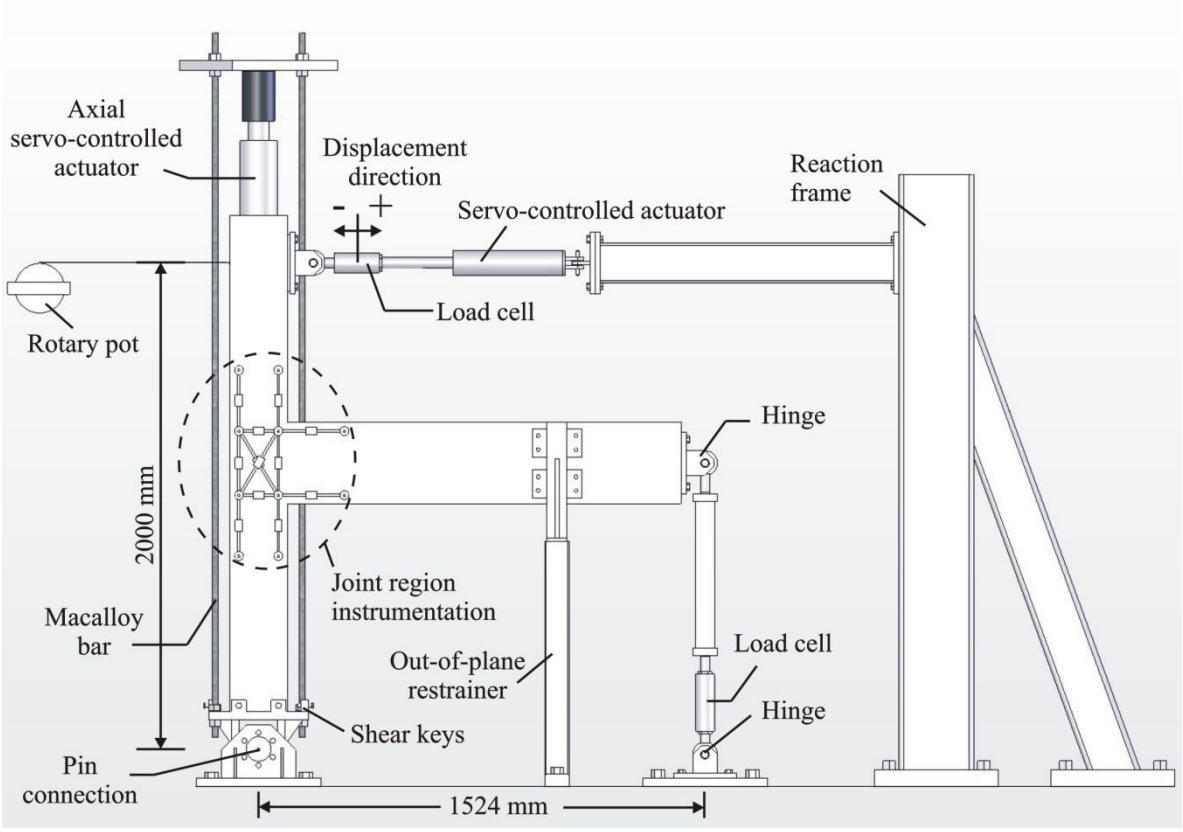

Figure 5–9 Test setup for 2D specimens: front view

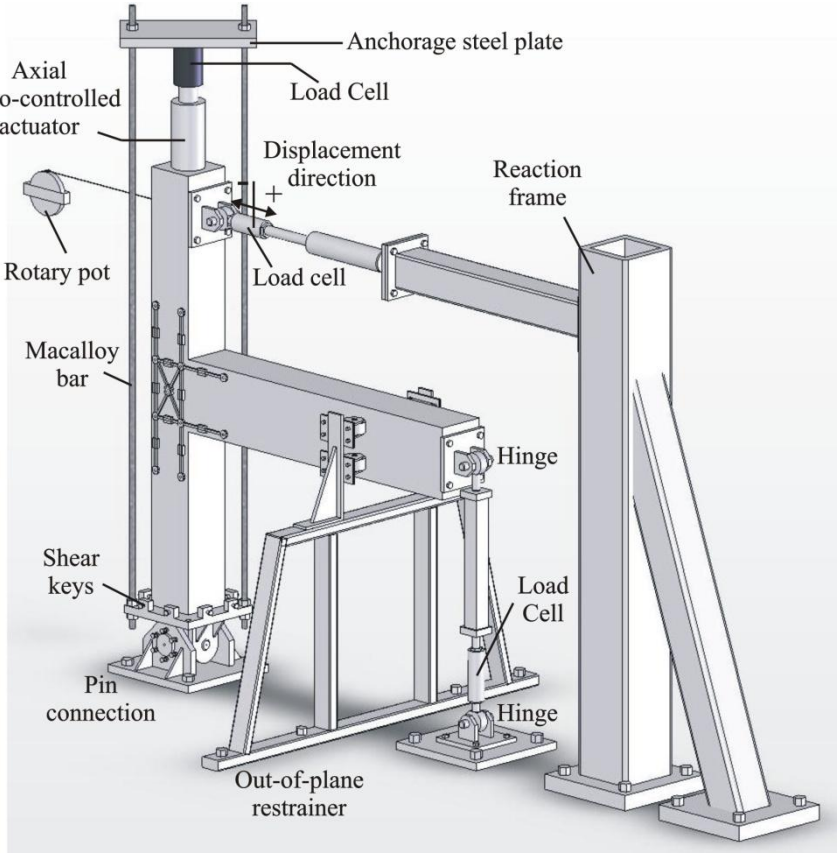

Figure 5–10 Test setup for 2D specimens: dimetric view

5.7 LOADING PROCEDURE

Cyclic horizontal lateral loading was applied to the top of the columns using a servo-valve hydraulic actuator in displacement control, until the lateral drift of the top of the column reached the targeted drift level. In the 2D tests the lateral displacement history consisted of two cycles at increasing target drift levels: 0.1, 0.2, 0.5, 1.0, 1.5, 2.0, 2.5, 3.0 and 4.0%. Note that, drift is defined as the ratio between lateral displacement and column height. In this way, during the testing it was possible to capture different performance limit states which can be used in generating mechanical and phenomenological (macro) models [6]. Unidirectional load pattern is given in Figure 5–11.

Following the testing procedure recommended by Pampanin *et al.* [7] for poorly detailed exterior beam-column joints, the axial load was varied around the gravity load value (i.e., based on tributary area) in proportion to the lateral force acting on the column as it would occur due to the frames' lateral sway. The relationship between the lateral force V_c and the variation of axial load N is given as

$$N = N_g \pm \alpha V_c \quad (5\text{-}1)$$

where N_g is gravity load and α is the proportionality coefficient. The axial load variation, N, is a function of the geometry of the building (i.e., number of bays and storeys).

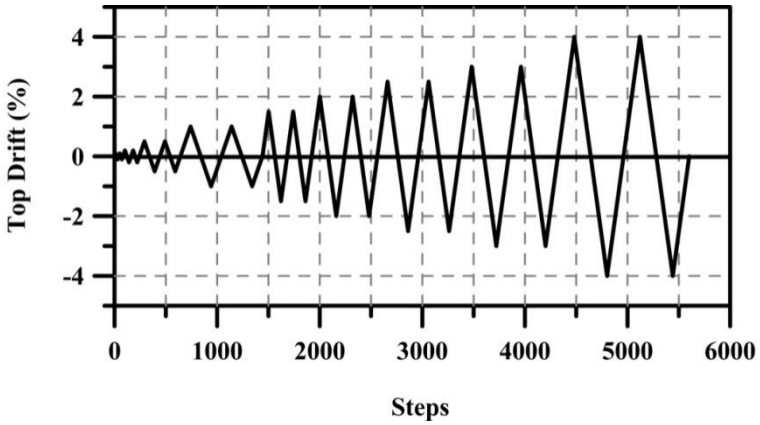

Figure 5–11 Unidirectional load pattern

The proportionality coefficient, α, can be derived by simple hand calculations or pushover analyses of the prototype frame. The identification of the proportionality coefficient, along with the gravity load calculations for the selected prototype RC frame, is presented in Appendix E. Test specimens were subjected to firstly the gravity load of 115 kN and then according to testing scheme variation of axial load corresponding with the α coefficient of 4.63 which was applied on the columns. Note that, Specimen 2D2, was tested under constant axial load. The relationship between the column axial load and column horizontal force is given Figure 5–12.

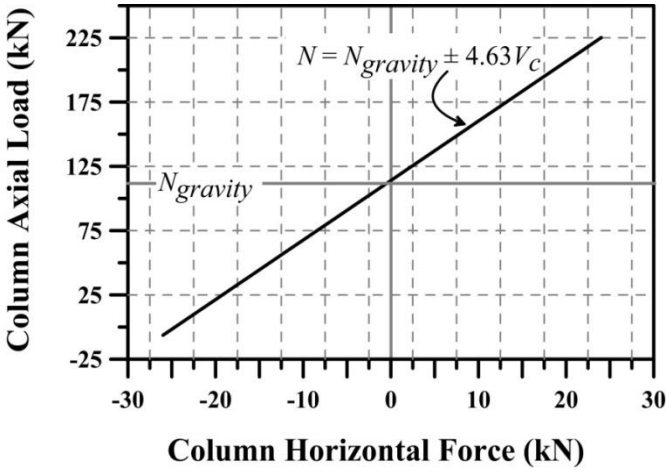

Figure 5–12 Axial load variation in 2D unidirectional specimens

5.8 INSTRUMENTATION

5.8.1 Measurement of Loads

The column axial, lateral, and beam shear forces were measured by load cells attached to each hydraulic actuator as seen in Figure 5–13 (see also Section 5.6). All load cells were calibrated in compression up to 125% of the expected load range using the Avery Universal Testing Machine. The obtained calibration factor was also assumed to be effective for the particular load cell in tension. The lateral force in the column and beam end shear were measured using 150 kN capacity load cells, while 300 kN capacity load cell was used to measure varying vertical axial force in the column.

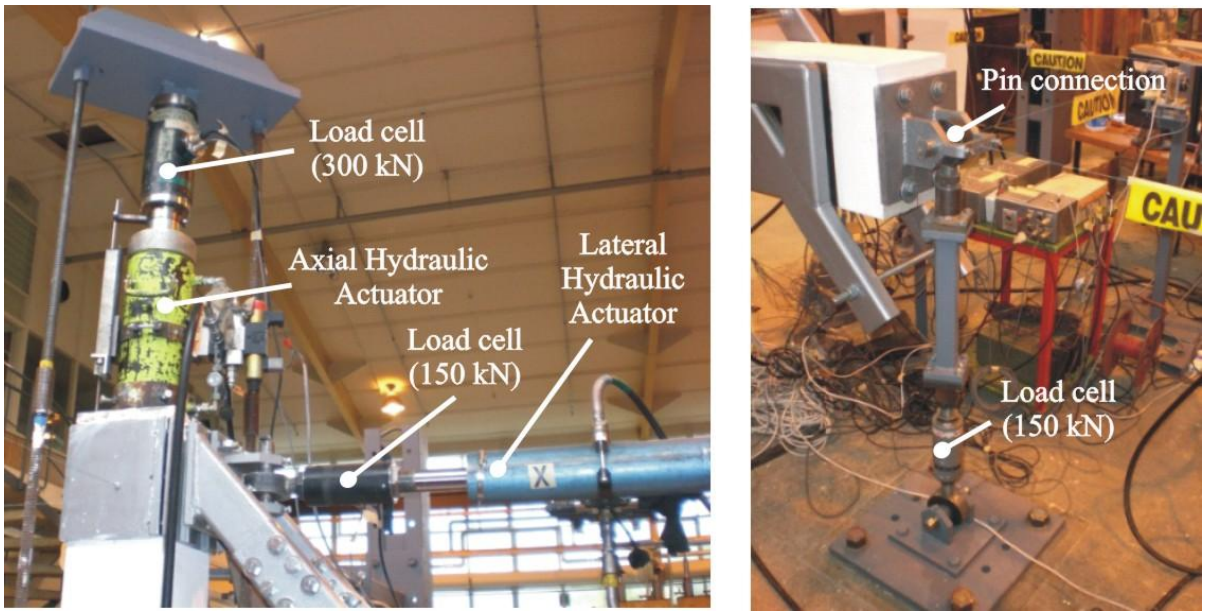

Figure 5–13 Close-up views of the load actuators and load cells

5.8.2 Measurement of Displacement and Deformations

The global horizontal displacement was measured by a loaded-spring rotary potentiometer with approximately 150mm travel length and a 5kΩ resistance. It was attached to a rigid frame some distance from the column and connected to the column using a thin string (Figure 5–9). In this way, the top column displacement measured and interstorey drift ratio was obtained.

In order to capture the local displacements and section deformations in the column, beam and joint panel critical sections, two different instrumentation layouts were employed. The as-built benchmark specimen, 2D1, was instrumented using eighteen linear potentiometers (Linear Variable Displacement

Transducers, LVDTs). In the retrofitted specimens the number of potentiometers were increased to capture the plastic hinge and possible shear deformation in the FRP cut-off region in the beam. A total of twenty-two linear potentiometers were used in the retrofitted units.

Calibrated 30 mm and 50 mm travel length potentiometers were mounted on 6 mm steel rods, which were epoxied into pre-drilled 20 mm deep holes on the specimen's concrete surface. Either 30 mm or 50 mm travel potentiometers were adjusted according the distance between the reading points. For instance, for beam-column interface deformation measurement 30 mm travel potentiometers were used, whereas 50 mm travel potentiometers were placed diagonally to capture the shear deformations within the joint panel region and FRP-beam interface. The local instrumentation arrangement for all 2D specimens is provided in Figure 5–14.

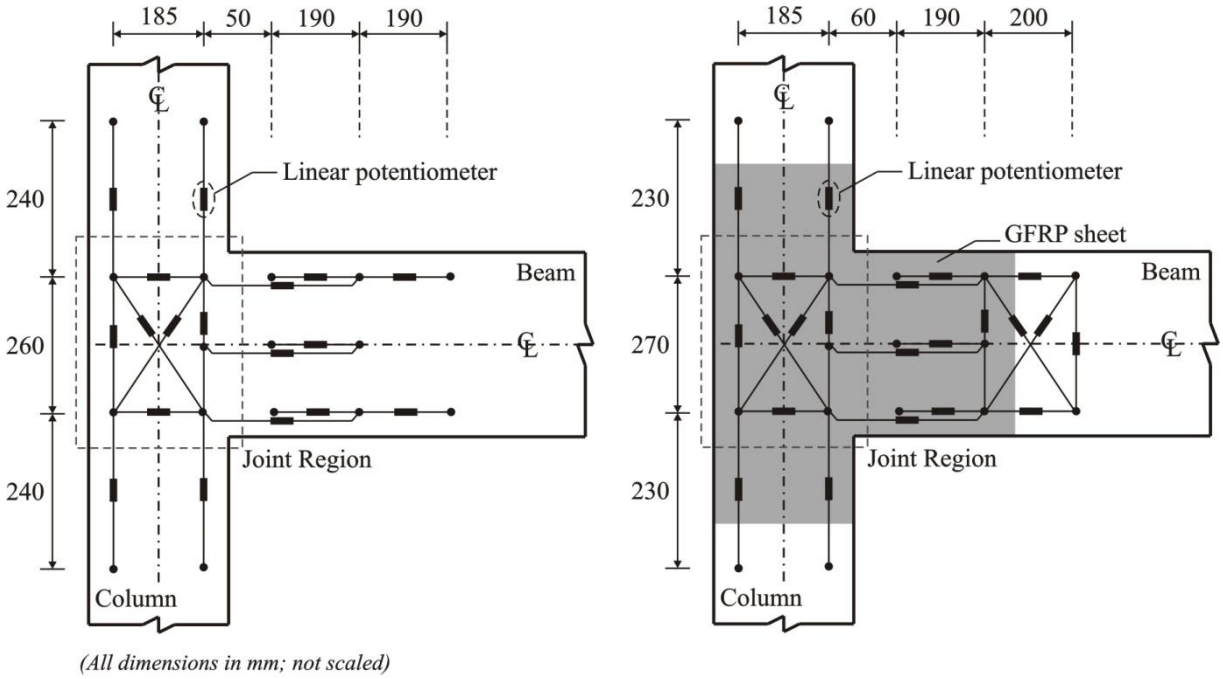

Figure 5–14 Local instrumentation for 2D as-built and retrofitted beam-column joints

The readings obtained from the potentiometers were converted into engineering parameters, such as the rotations and curvatures in the critical beam and column regions that they were attached to. The formulas are given in the following. The nomenclature used in these formulas are given in Figure 5–15. The deformed potentiometers in the beam element under external forces such as column shear force V_c and beam shear force V_b are schematically presented in the same figure.

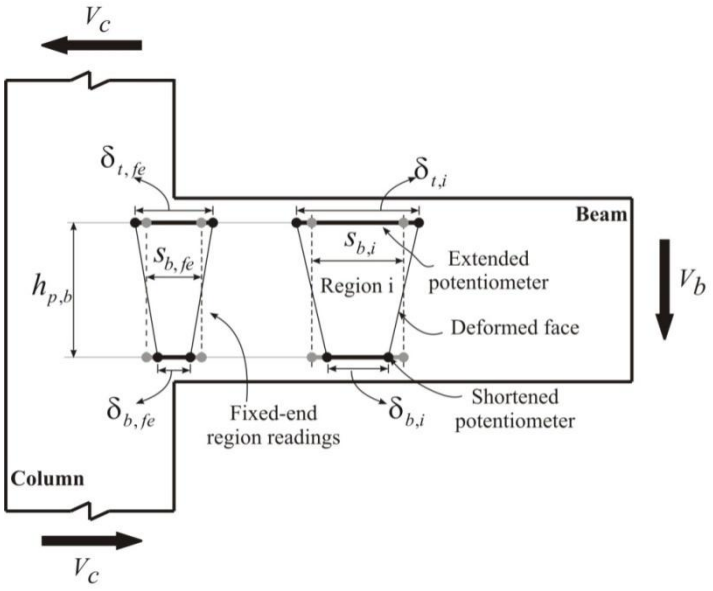

Figure 5–15 Estimation of fixed-end rotation and curvature in beam section

Fixed-end rotation θ_{fe} of the column-beam section is given by the following expression

$$\theta_{fe} = \frac{\delta_{t,fe} - \delta_{b,fe}}{h_{p,b}} \tag{5-2}$$

where

$\delta_{t,fe}$ = measured top deformation of linear potentiometer placed at column-beam interface for fixed-end rotation,

$\delta_{b,fe}$ = measured bottom deformation of linear potentiometer placed at column-beam interface for fixed-end rotation,

$h_{p,b}$ = parallel distance between two linear potentiometers attached in beam section.

The average fixed-end curvature ϕ_{fe} of column-beam section can be calculated as

$$\phi_{fe} = \frac{\theta_{fe}}{s_{b,fe}} \tag{5-2}$$

where

$s_{b,fe}$ = gauge length of the fixed end region

The rotation over the region i in the beam $\theta_{b,i}$ is given by the following expression

$$\theta_{b,i} = \frac{\delta_{t,i} - \delta_{b,i}}{h_{p,b}} \tag{5-3}$$

where

$\delta_{t,i}$ = measured top deformation of linear potentiometer placed at the i^{th} beam region,

$\delta_{b,i}$ = measured bottom deformation of linear potentiometer placed at the i^{th} beam region.

The average curvature over the region i in the beam $\phi_{b,i}$ is given by

$$\phi_{b,i} = \frac{\theta_{b,i}}{s_{b,i}} \tag{5-4}$$

where

$s_{b,i}$ = gauge length of the fixed end region i the beam

A similar approach has been followed to estimate the rotation and curvature values from the readings of potentiometers located in the column element. The deformed shape of potentiometers and the nomenclature for the formulas used for the calculations are given in Figure 5–16.

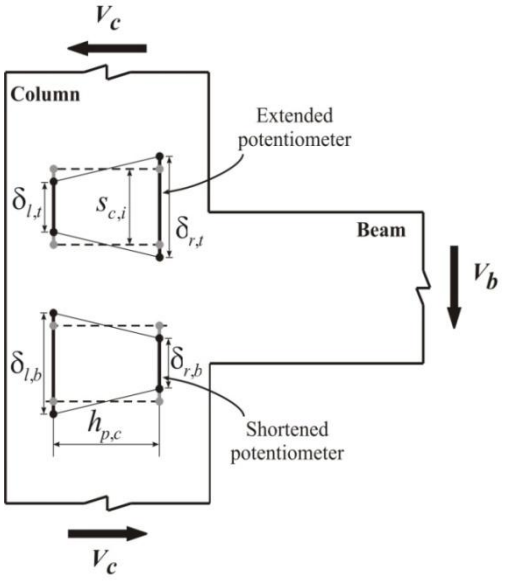

Figure 5–16 Estimation of rotation and curvature in column section

The rotation over the region i in the column in above the joint panel $\theta_{c,t}$ is given by the following expression

$$\theta_{c,t} = \frac{\delta_{l,t} - \delta_{r,t}}{h_{p,c}} \tag{5-5}$$

where

$\delta_{l,t}$ = measured deformation of left potentiometer placed above the joint panel at the i^{th} column region,

$\delta_{r,t}$ = measured deformation of right potentiometer placed above the joint panel at the i^{th} column region,

$h_{p,c}$ = parallel distance between two linear potentiometers attached in column section.

The average curvature over the region i in the column above the joint panel $\phi_{c,t}$ can be calculated as

$$\phi_{c,t} = \frac{\theta_{c,t}}{s_{c,i}} \tag{5-6}$$

where

$s_{c,i}$ = gauge length of the fixed end region i of the column

In a similar fashion the rotation over the region i in the column below the joint panel $\theta_{c,b}$ is

$$\theta_{c,b} = \frac{\delta_{l,b} - \delta_{r,b}}{h_{p,c}} \tag{5-7}$$

where

$\delta_{l,b}$ = measured deformation of left potentiometer placed below the joint panel at the i^{th} column region

$\delta_{r,b}$ = measured deformation of right potentiometer placed below the joint panel at the i^{th} column region

The average curvature over the region i in the column below the joint panel $\phi_{c,b}$ can be obtained as follows

$$\phi_{c,b} = \frac{\theta_{c,b}}{s_{c,i}} \tag{5-8}$$

In order to estimate the joint shear deformation, six potentiometers were placed in the joint region. The readings of the diagonal potentiometers were used to calculate the shear deformation. Other remaining potentiometers were used as dummy reading for the reservation purpose to calculate the shear deformation in the joint. In Figure 5–17 an assumption of the deformed shape of the joint core concrete is shown. The shear deformation in the joint region can be determined using Eq. (5-9) suggested by [8] along with the nomenclature provided in Figure 5–17.

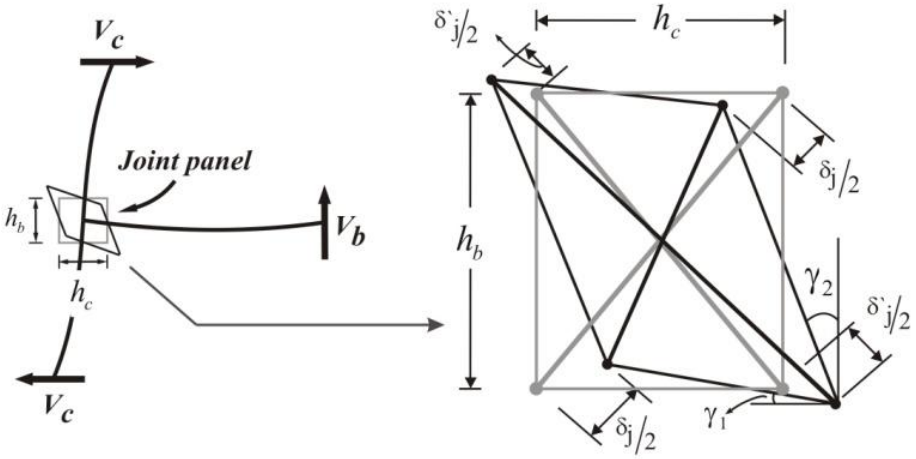

Figure 5–17 Joint shear distortion estimation

$$\gamma_j = \gamma_1 + \gamma_2 = (\delta_j - \delta_j^{`}) \frac{\sqrt{h_b^2 + h_c^2}}{2 h_b h_c} \tag{5-9}$$

where

γ_j = average joint shear distortion,

γ_1, γ_2 = deformation angles,

δj , $\delta`_j$ = the changes in the lengths of the diagonals,

h_b = height of beam,

h_c = overall depth of column in the direction of the horizontal shear to be considered.

5.8.3 Measurement of Strains

5.8.3.1 Measurement of Strains in Reinforcing Bars

TML 120-ohm electrical resistance strain gauges (Type: Tokyo Sokki FLA-3-11-3L) were used to monitor the steel strain variation along the longitudinal and transverse reinforcement in the critical regions of beams and columns. Following the surface preparation, the electrical strain gauges were attached to the sides of the bars as recommended by the strain gauge manufacturer. The locations of the strain gauges were determined based on the expected locations of yielding and hinging to occur in the specimen during testing. Two longitudinal top and bottom beam bars, all column bars and two first beam stirrup and one stirrup above and below the joint region were instrumented with strain gauges. The strain gauge arrangement is given in Figure 5–18.

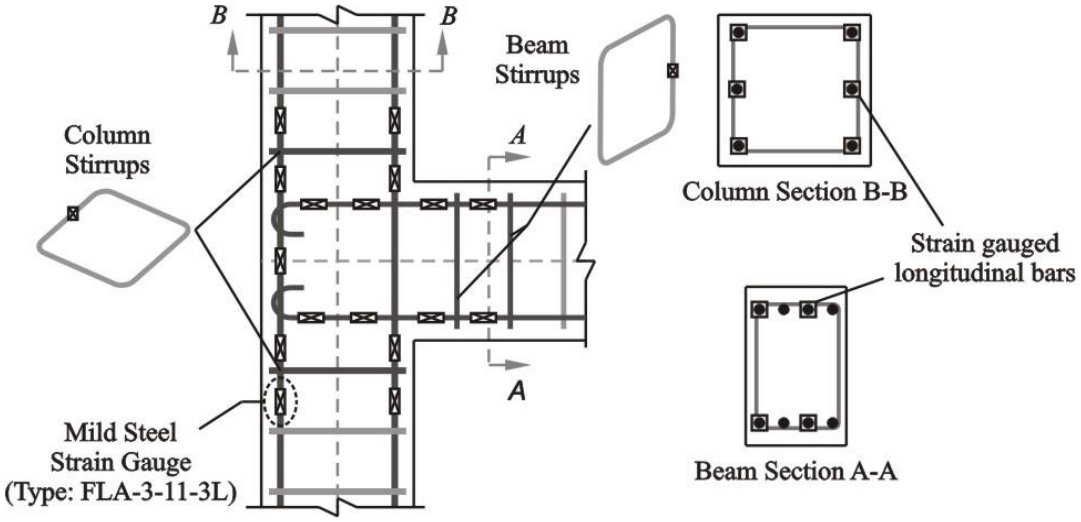

Figure 5–18 Layout of reinforcement strain gauges in 2D specimens

5.8.3.2 Measurement of Strains in FRP

The FRP sheets on one face of the 2D retrofitted specimens were extensively instrumented with special strain gauges. A total of twenty-one Tokyo Sokki BFLA-5-8-3 type composite material strain gauges were mounted in both the longitudinal and transverse fibre directions of the beam, column and joint panel regions. It was aimed to monitor the variation of the strain demand in the FRP sheets under different loading conditions and retrofitting schemes (including 3D corner specimens) and to compare the analytical predictions based on the assumed strain limits (i.e., debonding strain). It is important to note that the data gained from these measurements was also used in the numerical studies in Chapter

10 to assess and validate the models. The layout of strain gauges was kept constant in all retrofitted specimens. The location and orientation of all strain gauges is shown in Figure 5–19.

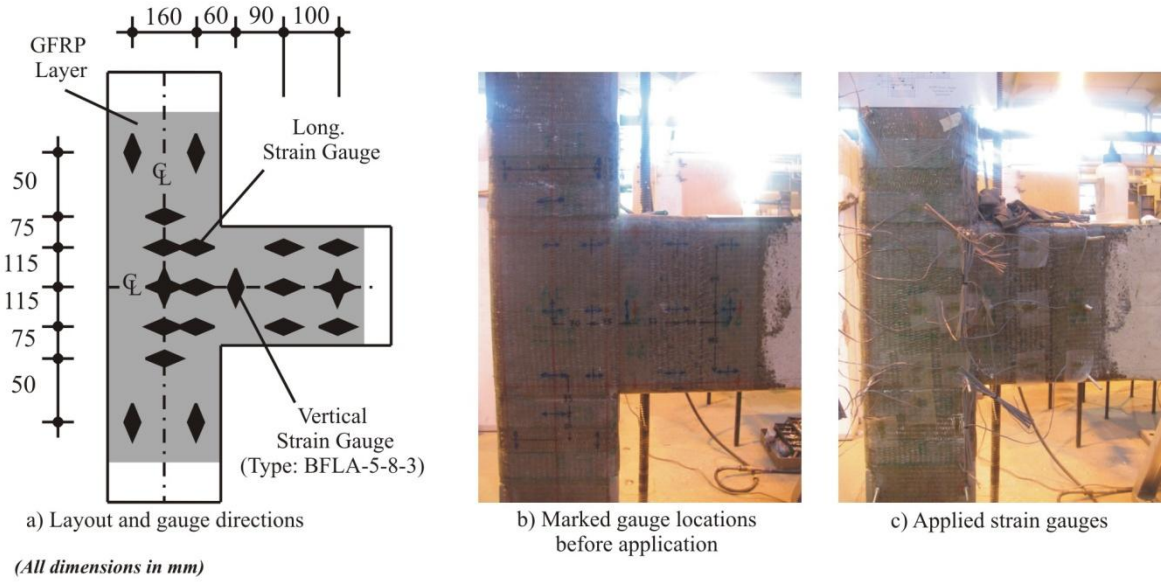

Figure 5–19 Composite material strain gauge application for 2D joint specimens

5.9 TEST CONTROL AND DATA COLLECTION

In order to increase the accuracy of the tests an automatic controller programme written in a graphical programming environment, LabView®, was employed. In each step of loading, the current state of the column top displacement was fed back to the controller programme to check whether the target displacement was reached or not. The rotary potentiometer attached to the top of the column provided this information to the controller box via a series of RS-422 cables, and the data was converted into a RS-232 fed into the controller computer. Depending on the situation, the controller programme gave the command to the servo-valve on the hydraulic actuators for the movement in the specified direction according to the imposed loading pattern.

For the axial loading control, the same procedure was followed. However, in this case, the information from the axial load cells was transferred to the controller computer. By using the Eq. 5-1, which was implemented into the controller programme, the axial load level for the next step was determined and applied following the command from the controller to the valve on the vertical hydraulic actuator.

The damage propagation and the behaviour of the specimens were carefully observed and recorded during testing. All instrumentations were connected through a series of four-pin serial cables and an

analogue-to-digital protocol converter to a data logging computer with the Universal Data Logging programme. To obtain a good definition of the crack formation, all specimens were whitewashed and a grid size of 50x50 mm was drawn on the locations of expected damage before the tests. The crack patterns were marked with different colours, designated with the corresponding point in the loading sequence and photographed. The crack width in the joint and critical regions of the test specimens was also measured and recorded.

5.10 SUMMARY

The information on the experimental programme pertaining to 2D exterior plane frame beam-column joints is given in this chapter. In the first part of the experimental campaign the main objective was to investigate the behaviour and efficiency of the retrofitted 2D exterior beam-column joint units under axial loading and retrofitting schemes. All specimens were designed and produced based on the codes before seismic considerations. In addition, the acquired experimental data from these tests has been used in the validation of the proposed retrofit design methodology, the basis for the design of the 3D corner joint units in the second experimental campaign and in the numerical studies.

The design of the specimens and test set-up, loading protocol, selection of the material types and properties were all performed based on the aforementioned objectives. All units were heavily instrumented to capture the global, as well as local behaviour during testing. The lateral test control as well as global behaviour observation were performed by utilizing a rotary potentiometer attached to the top of the column. The vertical axial load variation control was conducted by means of a hydraulic servo-valve actuator controlled by a controller programme. The local deformations such as curvatures in the beam and column fixed-end and plastic hinge sections, along with shear deformations in the joint panel were measured. Strain measurements were conducted in detail for reinforcing bars and GFRP composite sheets attached on the specimens. Important milestones in the damage propagation were observed, recorded and evaluated meticulously.

5.11 REFERENCES

1. NZS95:1955. *New Zealand Standard - Model Building By-Laws: Part IV and V.* New Zealand Standard Inst., Wellington, NZ, 1953.
2. *Regio Decreto.* November-XVIII(228) (in Italian), 1939.
3. Pampanin S, Christopoulous C. Non-invasive retrofit of existing RC frames designed for gravity loads only. *Proc FIB Symp Concrete Structures in Seismic Regions, Federation International bu Beton*, Athens, 2003.

4. NZS 4671:2001. *Steel bars for the reinforcement of concrete.* Standards association of New Zealand, Wellington, 1989.
5. NZS 3112:1986. *Methods of test for concrete.* Standards association of New Zealand, Wellington, 1986.
6. Leon R, Deierlein GG. Considerations for the use of quasi-static testing. *Earthquake Spectra*. 1996; **12**(1):87-109.
7. Pampanin S, Bolognini D, Pavese A. Performance-based seismic retrofit strategy for existing reinforced concrete frame systems using fiber-reinforced polymer composites. *Journal of Composites for Construction, ASCE*. 2007; **11**(2):211-26.
8. Hakuto S. Retrofitting of reinforced concrete moment resisting frames. *Ph.D. Dissertation*, University of Canterbury, Christchurch, 1995.

Chapter 6 TEST RESULTS OF 2D EXTERIOR BEAM-COLUMN JOINTS

6.1 INTRODUCTION

In the first part of this chapter the experimental findings of quasi-static cyclic tests on 2D plane frame beam-column joints in as-built and retrofitted configurations are presented. In order to provide useful information on the failure mechanisms, behaviour and damage propagation each specimen are examined in detail. In the second part, the effects of axial loading type on the proposed retrofit schemes and design procedure are investigated. For this purpose, global as well as local failure modes, strength, stiffness and energy dissipation characteristics, strain demands in the steel reinforcement and FRP sheets are observed and evaluated to compare the performance of the specimens. Lastly, the retrofit design methodology proposed in Chapter 4 is verified through the experimental results.

6.2 EXPERIMENTAL RESULTS

6.2.1 As-built Specimen 2D1

Specimen 2D1 can be referred to as the benchmark of all test series comprising 2D plane frame and 3D space frame joints. During the test, the axial load level was varied around the gravity load value of 114 kN, in proportion to the lateral force acting in the column with a proportionality coefficient α= 4.63. The findings are used in clarifying the effect of important aspects as the response of 2D as-built versus 2D retrofitted joints and the difference between unidirectional as-built and bidirectional as-built configurations. In addition, the test results were used for the basis of the formation of the limit states and semi-empirical analytical model to predict the shear capacity of retrofitted joint as described in Chapter 4. Following the test of this specimen and development of the analytical model, a series of retrofit solutions for this 2D specimen were designed and validated through experimental tests on other specimens.

As expected and shown by the similar studies reviewed in Chapter 2, the test results confirmed the inherent structural inadequacies of poorly detailed beam-column joints designed adhering to non-seismic pre-1970s codes. A particular brittle mixed failure mechanism typically referred to in literature as the "concrete wedge mechanism" was observed to initiate after 1.5% drift level. The lateral force-displacement response, along with crack patterns at final stage of the Specimen 2D1 is given in Figure 6-1 and Figure 6–2, respectively. The summary of the test results in terms of the maximum recorded values are tabulated for each loading direction in Table 6-1. The observed damage and crack formation during the test are presented in the following.

The first hairline cracking appeared at the bottom beam-column interface at 0.2% drift level. At this level some flexural cracking was also formed under the beam (Figure 6–3b). Joint diagonal cracks started to form at approximately 1% drift, along with some flexural cracks already formed and the beam surrounded by them in the previous drift levels (Figure 6–3d). A diagonal shear crack appeared in the joint at a stress level of $0.48\sqrt{f`_c}$ under 18.92 kN column shear force. At this point, the normalized principal tensile stress level, $p_t/\sqrt{f`_c}$, was approximately 0.21. After 1% drift level, beam cracks were stabilized with the crack widths ranging from 0.2 to 0.5 mm and no new cracks appeared in the beam till the end of the test. In the pull cycle of 1% drift, some vertical hairline cracks also formed in the column (Figure 6–3e). During the 1.5% drift joint diagonal cracks continued to develop within the joint area in an X-pattern form and spreading in the perimeter of the joint (Figure 6–3f). At 2% drift, main diagonal cracks exceeding a width of 2mm, started to propagate toward the back column faces, around 200 mm high from the joint-column level, indicating the bond-splitting failure at this region (Figure 6–4g). The cycles performed after 2.5% drift led to severe damage and spalling of the joint core concrete (Figure 6–4h) that resulted in a shear hinge mechanism. A hybrid brittle failure in the form of a concrete wedge mechanism was observed after 3% drift level (Figure 6–4j). In the pull cycle of 3% drift corresponding to an increase in the axial load, sudden buckling of column bars occurred at the upper column bond-splitting region, which can be attributed to the inadequate amount of stirrups in the column and joint region. The test was halted due to the excessive loss of load bearing capacity (Figure 6–4k).

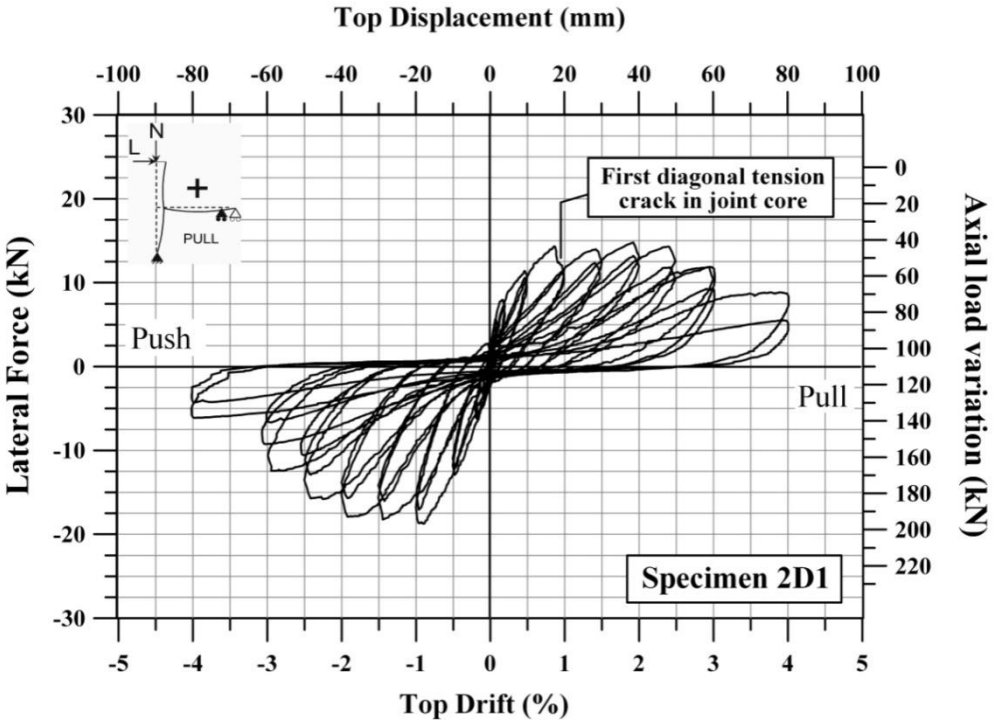

Figure 6–1 Load versus displacement response of Specimen 2D1

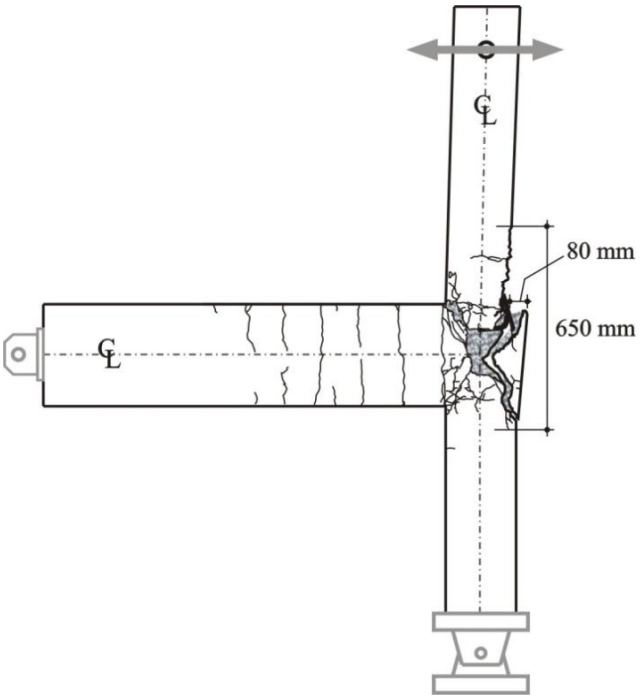

Figure 6–2 Final damage state of Specimen 2D1

Table 6-1 Summary of test results for Specimen 2D1

Drift Level	Loading		Axial Load		Strength		Joint Panel Results		
	Cycle	Direction	N^a (kN)	$N/(A_g f_c')^b$	$V_c{}^c$ (kN)	$v_{jh}{}^d$ (MPa)	$p_c{}^e$ (MPa)	$p_t{}^f$ (MPa)	γ^g (%)
0.1%	1st	Pull	85.97	0.09	4.55	1.63	-1.81	0.19	-0.0091
		Push	125.60	0.13	-3.93	2.37	-2.45	0.07	-0.0011
	2nd	Pull	83.44	0.09	5.69	1.58	-1.81	0.23	-0.0103
		Push	119.60	0.13	-3.80	2.26	-2.32	0.06	-0.0034
0.2%	1st	Pull	75.30	0.08	7.96	1.42	-1.84	0.42	-0.0149
		Push	137.70	0.15	-6.28	2.60	-2.77	0.17	-0.0046
	2nd	Pull	77.29	0.08	7.16	1.46	-1.81	0.35	-0.0126
		Push	135.80	0.14	-6.20	2.57	-2.73	0.17	-0.0034
0.5%	1st	Pull	59.73	0.06	11.40	1.13	-1.91	0.78	-0.0793
		Push	168.10	0.18	-12.93	3.18	-3.71	0.53	-0.0011
	2nd	Pull	64.25	0.07	10.57	1.21	-1.90	0.69	-0.0862
		Push	162.50	0.17	-11.87	3.07	-3.53	0.46	0.0012
1%	1st	Pull	44.89	0.05	14.30	0.85	-2.03	1.18	-0.1506
		Push	192.40	0.20	-18.74	3.64	-4.54	0.91	-0.0162
	2nd	Pull	59.91	0.06	11.27	1.13	-1.91	0.78	-0.2657
		Push	188.10	0.20	-17.09	3.56	-4.35	0.80	-0.0197
1.5%	1st	Pull	43.80	0.05	13.94	0.83	-1.98	1.16	-0.5006
		Push	194.90	0.21	-18.25	3.68	-4.54	0.86	0.1851
	2nd	Pull	55.39	0.06	12.36	1.05	-2.00	0.95	-0.6174
		Push	183.70	0.19	-16.06	3.47	-4.20	0.73	0.2204
2%	1st	Pull	43.62	0.05	14.89	0.82	-2.08	1.25	-0.9423
		Push	194.14	0.21	-18.92	2.05	-4.59	0.91	0.3400
	2nd	Pull	53.21	0.06	13.08	1.01	-2.02	1.02	-1.0260
		Push	183.70	0.19	-15.70	3.47	-4.17	0.70	0.4107
2.5%	1st	Pull	46.88	0.05	14.25	0.89	-2.05	1.17	-1.2917
		Push	180.30	0.19	-15.72	3.41	-4.11	0.71	0.6407
	2nd	Pull	61.36	0.06	11.82	1.16	-2.00	0.84	-1.3395
		Push	165.80	0.18	-12.85	3.13	-3.67	0.54	0.8699
3%	1st	Pull	57.56	0.06	11.87	1.09	-1.91	0.82	-1.6998
		Push	166.90	0.18	-12.44	3.16	-3.66	0.50	1.1517

[a] Axial load: $N=N_g \pm \alpha V_c$; [b] Axial load ratio; [c] Story column shear; [d] Horizontal joint shear stress in the joint
[e] Principal compression stress in the joint; [f] Principal tension stress in the joint; [g] Joint shear deformation

a) 0.1% drift, 1st cycle - push dir.

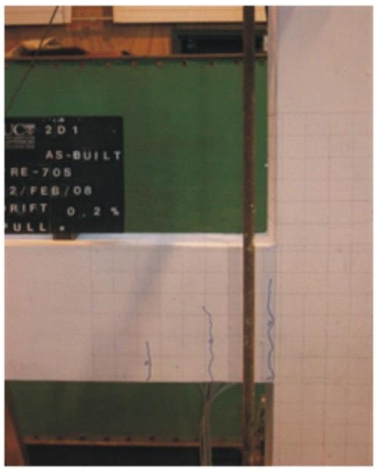

b) 0.2% drift, 2nd cycle - push dir.

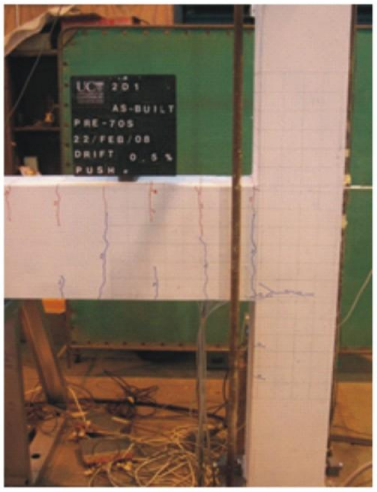

c) 0.5% drift, 2nd cycle - pull dir.

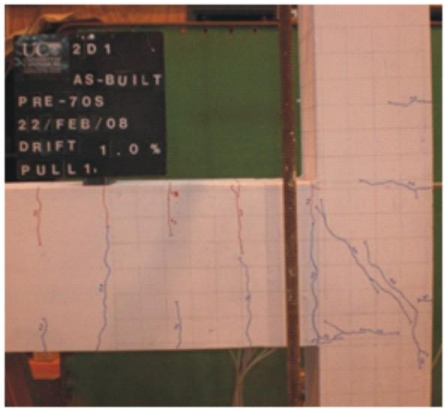

d) 1% drift, 1st cycle - pull dir.

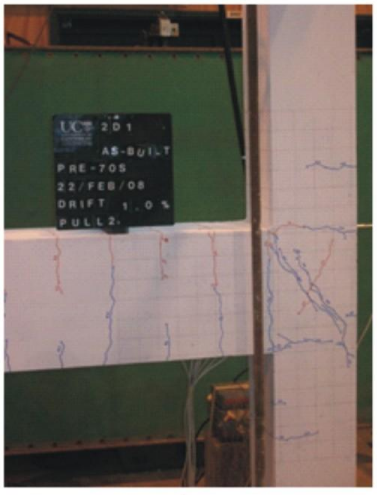

e) 1% drift, 2nd cycle - pull dir.

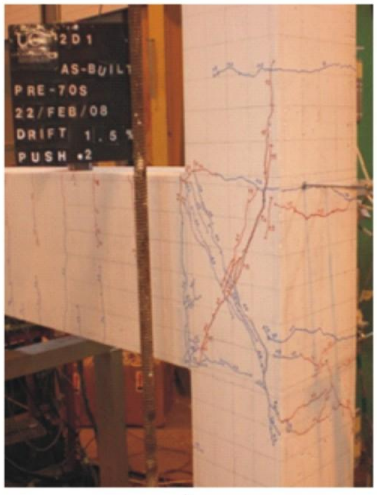

f) 1.5% drift, 2nd cycle - push dir.

Figure 6–3 Damage propagation - Specimen 2D1

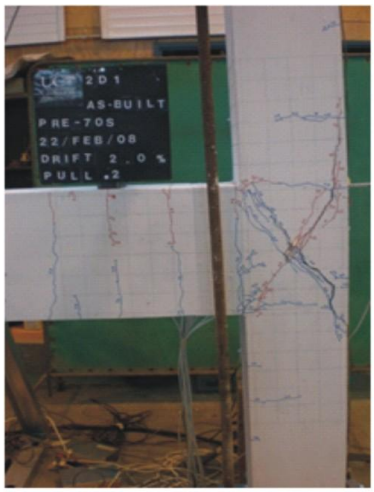

g) 2% drift, 2nd cycle - pull dir.

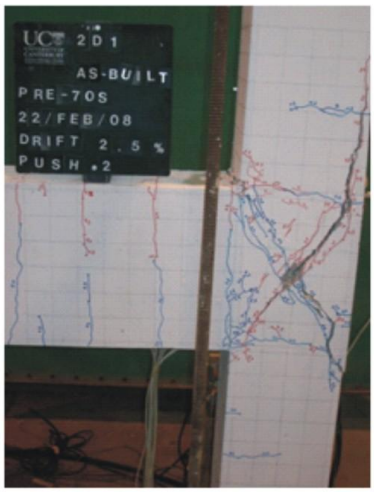

h) 2.5% drift, 2nd cycle - push dir.

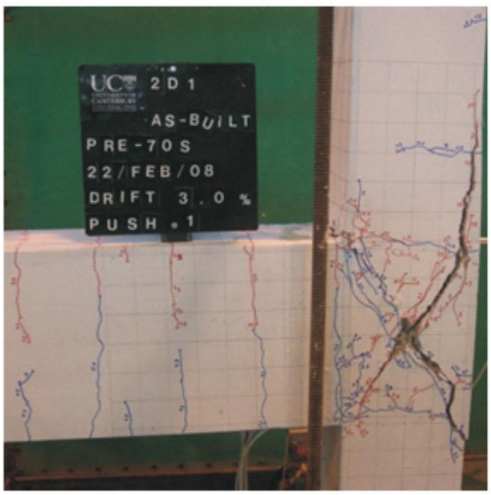

i) 3% drift, 1st cycle - push dir.

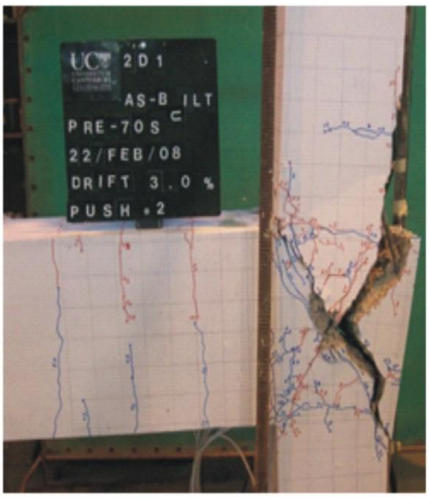

j) 3% drift, 2nd cycle - push dir.

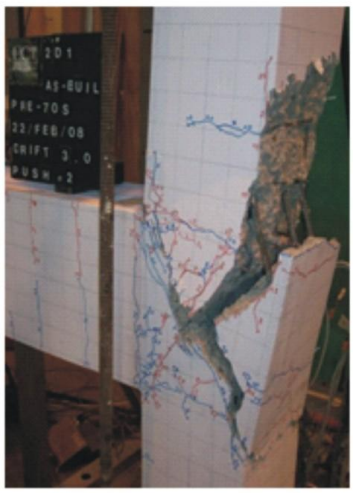

k) Final damage state, 3% drift

Figure 6–4 Damage propagation - Specimen 2D1 (cont`d)

6.2.2 Retrofitted Specimen 2D2

Specimen 2D2, strengthened with one layer of glass fibre composite sheet in the beam and column (i.e., minimum retrofit scheme, R11) was tested under a constant axial load of 110kN as a reference test for the retrofitted specimens. As mentioned previously in Chapter 2 and 3, the majority of the experimental studies were conducted similar to the test of Specimen 2D2 under constant axial load conditions. The retrofit design of the specimen as explained in Chapter 4 was performed to obtain the desired ductile failure mechanism. As expected, test results indicated that the behaviour of the specimen was very satisfactory in terms of seismic performance. Overall, no debonding was observed in the GFRP sheets and the specimen yielded under the plastic hinge formation in the beam-end FRP interface. The lateral force-displacement response, along with crack patterns at the final stage of the Specimen 2D2 are given in Figure 6–5 and Figure 6–6, respectively. The summary of the test results in terms of maximum recorded values are tabulated for each loading direction in Table 6-2. The damage propagation of the Specimen 2D2 is summarized in the following.

The first flexural cracks appeared at 0.2% drift 30 mm and 300 mm far from the FRP sheet interface in the beam (Figure 6–7b). Between 0.5 and 1.5% drift levels, new flexural cracks developed in the beam and in the column face, with widths ranging from 0.3 to 1.5mm (Figure 6–7c, d, e). The opening of the beam-column interface due to high moment demand started in the top and bottom of the sides. At 1.5% drift, the specimen reached its maximum lateral strength, 23.89 kN, in push direction loading and exhibited stable hysteresis loops throughout the test. In the following cycles, 2 and 2.5% drift, flexural cracks stabilized in the beam and damage was concentrated on the beam sheet interface crack (Figure 6–7f and Figure 6–8g). Diagonal grids of hairline cracks in the joint panel under the FRP sheets started to develop, indicating a high level of strain demand in this region. During the 3% drift, crushing and minor spalling started in the beam sheet interface. In addition to that, due to excessive compressive pressure induced by hooked beam bars at the back of the column, bulging and horizontal tearing in the joint FRP sheet was initiated. At 4% drift, finger tapping on the joint region revealed a hollow sound under some regions indicating some FRP debonding. However, overall, no major damage effecting the ductile behaviour of the specimen was observed (Figure 6–8i, Figure 6–9). The seismic performance of the retrofitted specimen was very satisfactory under constant axial load conditions.

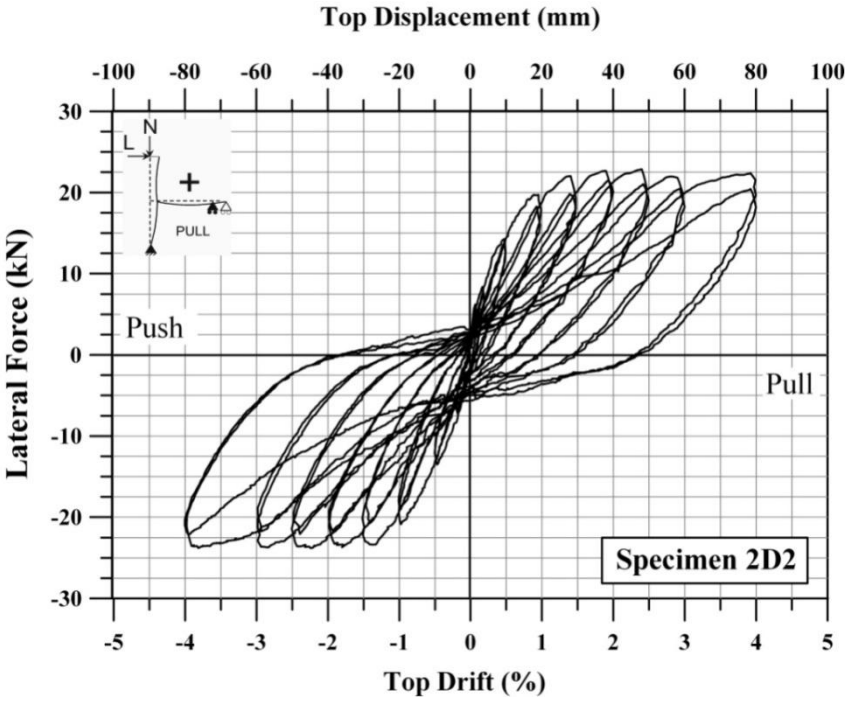

Figure 6–5 Load versus displacement response of Specimen 2D2

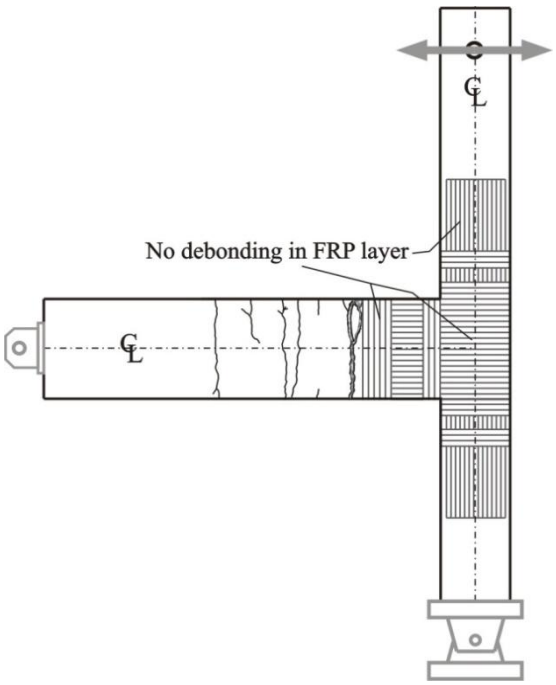

Figure 6–6 Final damage state of Specimen 2D2

Table 6-2 Summary of test results for Specimen 2D2

Drift Level	Loading		Axial Load		Strength		Joint Panel Results		
	Cycle	Direction	N^a (kN)	$N/(A_g f_c`)^b$	$V_c{}^c$ (kN)	$v_{jh}{}^d$ (MPa)	$p_c{}^e$ (MPa)	$p_t{}^f$ (MPa)	γ^g (%)
0.1%	1st	Pull	109.90	0.11	6.23	0.67	-2.28	0.20	-0.0135
		Push	110.40	0.11	-3.52	-0.37	-2.15	0.06	0.0023
	2nd	Pull	110.80	0.11	5.17	0.63	-2.27	0.17	-0.0123
		Push	110.20	0.11	-3.21	-0.36	-2.14	0.06	0.0034
0.2%	1st	Pull	110.80	0.11	8.38	0.94	-2.46	0.36	-0.0180
		Push	110.00	0.11	-7.37	-0.84	-2.38	0.30	0.0090
	2nd	Pull	110.60	0.11	7.58	0.84	-2.39	0.30	-0.0202
		Push	110.00	0.11	-6.67	-0.74	-2.32	0.24	0.0079
0.5%	1st	Pull	110.80	0.11	14.27	1.56	-2.92	0.83	-0.0641
		Push	110.40	0.11	-13.50	-1.47	-2.85	0.76	0.0460
	2nd	Pull	111.30	0.11	13.70	1.49	-2.88	0.77	-0.0709
		Push	110.40	0.11	-12.75	-1.39	-2.78	0.69	0.0460
1%	1st	Pull	109.30	0.11	19.70	2.14	-3.41	1.34	-0.2545
		Push	110.80	0.11	-20.86	-2.28	-3.55	1.46	0.0852
	2nd	Pull	108.20	0.11	18.25	1.98	-3.26	1.21	-0.3052
		Push	109.50	0.11	-18.97	-2.09	-3.36	1.29	0.0761
1.5%	1st	Pull	109.90	0.11	22.00	2.40	-3.65	1.58	-0.4673
		Push	108.45	0.11	-23.89	-2.59	-3.81	1.76	0.4000
	2nd	Pull	110.80	0.11	19.80	2.16	-3.45	1.36	-0.4451
		Push	109.70	0.11	-20.73	-2.22	-3.49	1.41	0.2621
2%	1st	Pull	110.60	0.11	22.65	2.46	-3.71	1.62	-0.5407
		Push	110.20	0.11	-20.86	-2.52	-3.77	1.69	0.3955
	2nd	Pull	110.80	0.11	21.44	2.33	-3.60	1.51	-0.5388
		Push	110.60	0.11	-21.82	-2.29	-3.56	1.47	0.3796
2.5%	1st	Pull	111.09	0.11	22.85	2.48	-3.74	1.63	0.5400
		Push	111.00	0.11	-23.76	-2.54	-3.80	1.70	0.4885
	2nd	Pull	111.70	0.11	20.87	2.23	-3.52	1.41	-0.5221
		Push	111.00	0.11	-22.05	-2.39	-3.66	1.56	0.4467
3%	1st	Pull	111.10	0.11	21.98	2.37	-3.64	1.54	-0.4598
		Push	110.60	0.11	-23.71	-2.50	-3.76	1.66	0.6706
	2nd	Pull	113.80	0.11	20.48	2.23	-3.55	1.40	-0.4075
		Push	109.70	0.11	-21.74	-2.36	-3.61	1.54	0.7487
4%	1st	Pull	111.50	0.11	22.29	2.43	-3.71	1.60	-0.3891
		Push	111.50	0.11	-23.63	-2.57	-3.83	1.72	0.9900
	2nd	Pull	111.00	0.11	20.29	2.24	-3.52	1.43	-0.4819
		Push	110.40	0.11	-22.08	-2.46	-3.71	1.63	0.9685

[a] Axial load: $N=N_g \pm \alpha V_c$; [b] Axial load ratio; [c] Story column shear; [d] Horizontal joint shear stress in the joint
[e] Principal compression stress in the joint; [f] Principal tension stress in the joint; [g] Joint shear deformation

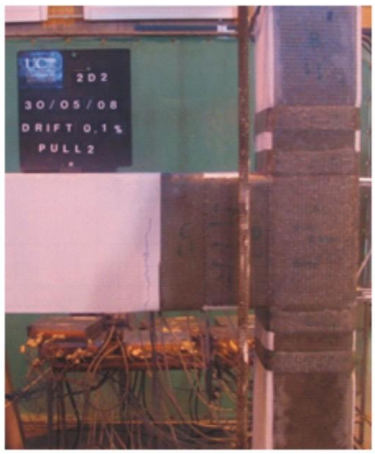

a) 0.1% drift, 2nd cycle - push dir.

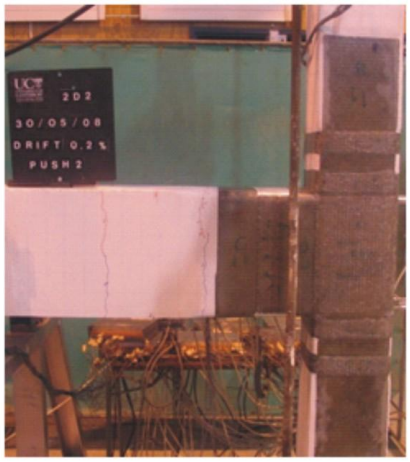

b) 0.2% drift, 2nd cycle - push dir.

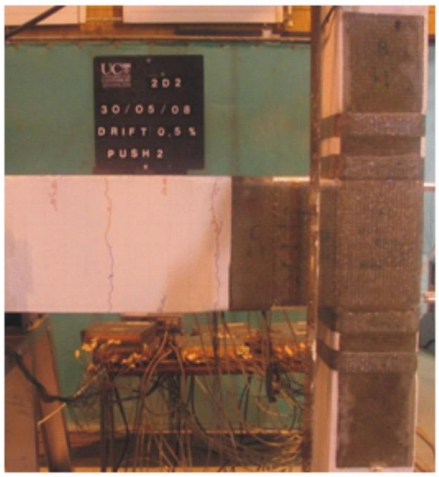

c) 0.5% drift, 2nd cycle - pull dir.

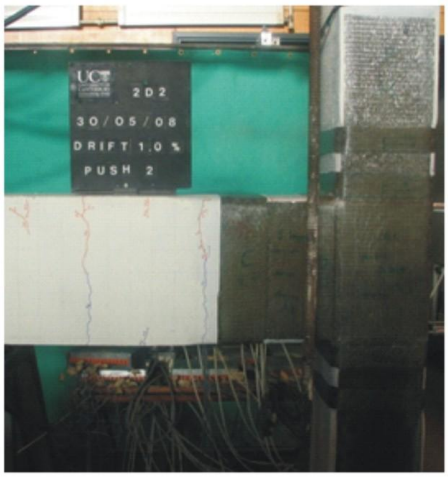

d) 1% drift, 2nd cycle - pull dir.

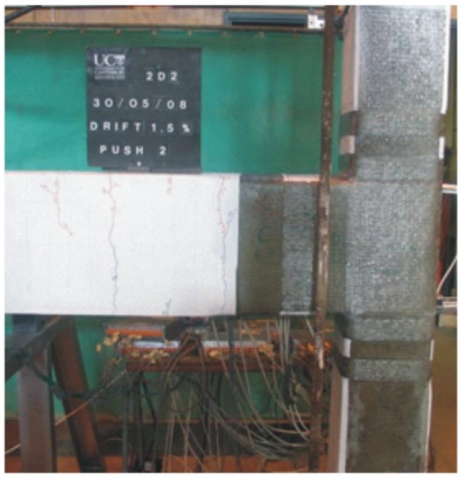

e) 1.5% drift, 2nd cycle - push dir.

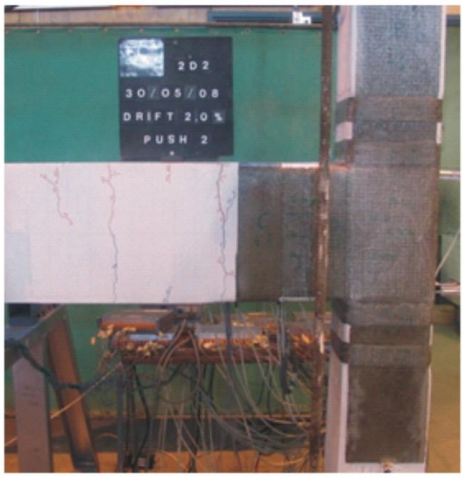

f) 2% drift, 2nd cycle - push dir.

Figure 6–7 Damage propagation - Specimen 2D2

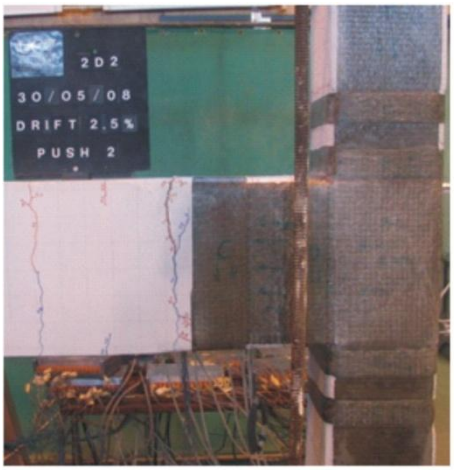

g) 2.5% drift, 2nd cycle - push dir.

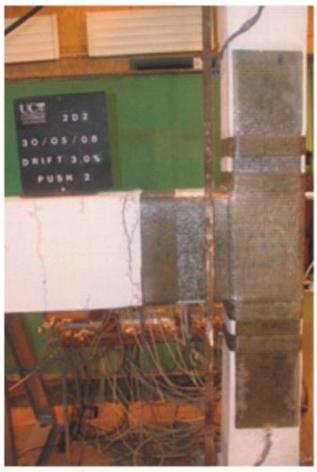

h) 3% drift, 2nd cycle - push dir.

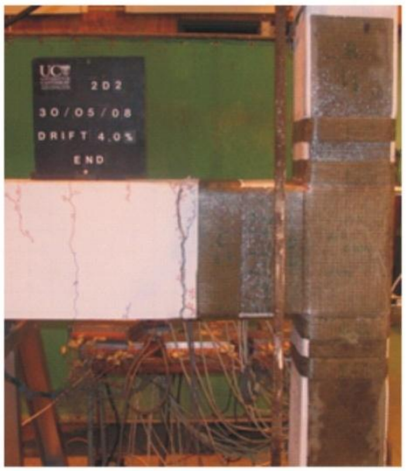

i) Final damage state, 4% drift

Figure 6–8 Damage propagation - Specimen 2D2 (cont`d)

a)

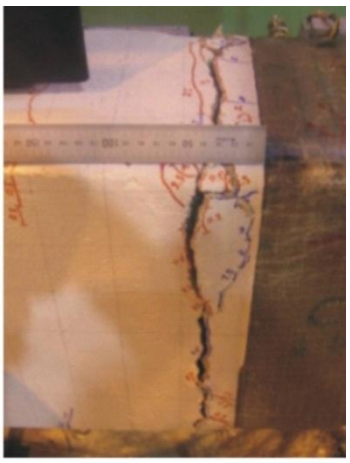

b)

Figure 6–9 Close-up views of concentrated damage in the beam-end FRP interface - Specimen 2D2

6.2.3 Retrofitted Specimen 2D3

Specimen 2D3 was retrofitted with a minimum retrofit solution (R11) similar to Specimen 2D2, but tested under varying axial load. The main purpose of this test was to investigate the possible effects of axial load fluctuation demands on a specimen retrofitted according to constant axial load assumptions. As the as-built benchmark specimen 2D1, during the test the axial load level was varied around the gravity load value, 115 kN, in proportion to the lateral force acting in the column with a proportionality coefficient α=4.63. Experimental results revealed that the same scheme (R11) was proven to be an inadequate retrofit solution in the case of 2D beam-column joints subjected to high fluctuation of the axial load. Due to the high shear demand accompanied by reduced joint strength as the axial load decreased in pull direction, a hybrid failure mechanism, consisting of gradual debonding of the GFRP sheet in the vicinity of the joint, bond deterioration and damage to the joint concrete core occurred. The mechanisms of damage propagation are studied in detail based on global as well as local test observations in the following section. The lateral force-displacement response along with the crack patterns at the final stage of the Specimen 2D3 are given in Figure 6–10 and Figure 6–11, respectively. The summary of the test results in terms of maximum recorded values are tabulated for each loading direction in Table 6-2. The damage propagation of the Specimen 2D3 is summarized in the following.

The first flexural crack appeared 150 mm away from the beam FRP sheet at 0.2% drift, which could be considered as the major flexural crack in the beam (Figure 6–12b). The maximum width of this crack was noted as 1mm in the top and 0.25mm in the bottom of the beam. Up to 1% drift level, flexural hairline cracks continued to develop along the beam approximately 120mm from each other (Figure 6–12c, d). During 1 and 1.5% drift, several hairline cracks formed at the back of column and sheet detachment started in the beam-joint interface. It was also observed that due to high strain demand in the joint region, hairline cracks started to develop in the form of diagonal grids under the laminates (Figure 6–12e, f). Finger tapping on the joint region revealed a hollow sound under the joint panel and beam-joint interface corners after 2.5% drift. It was observed that towards the end of 2% drift in the beam-column interface the FRP sheet started to debond and propagate under the joint panel FRP sheet at 2.5 and 3% drift levels. Also, after 2.5% drift the GFRP sheet and anchorage strips started to detach (Figure 6–13g) and buckle in the beam face due to compression forces in the push direction loading. During 3 and 4% drift, the beam sheets between the anchorages totally debonded leading to buckling and crushing of the concrete underneath. Minor crushing of the concrete due to the compressive pressure induced by the pull-push movement of hooked beam bars, occurred at the back

of the column face under and below the joint sheet interface (Figure 6–13h). Gradual FRP debonding in the beam and joint sheets (Figure 6–14) along with some delamination and horizontal fracture in the column anchorages governed the failure until the end of the test.

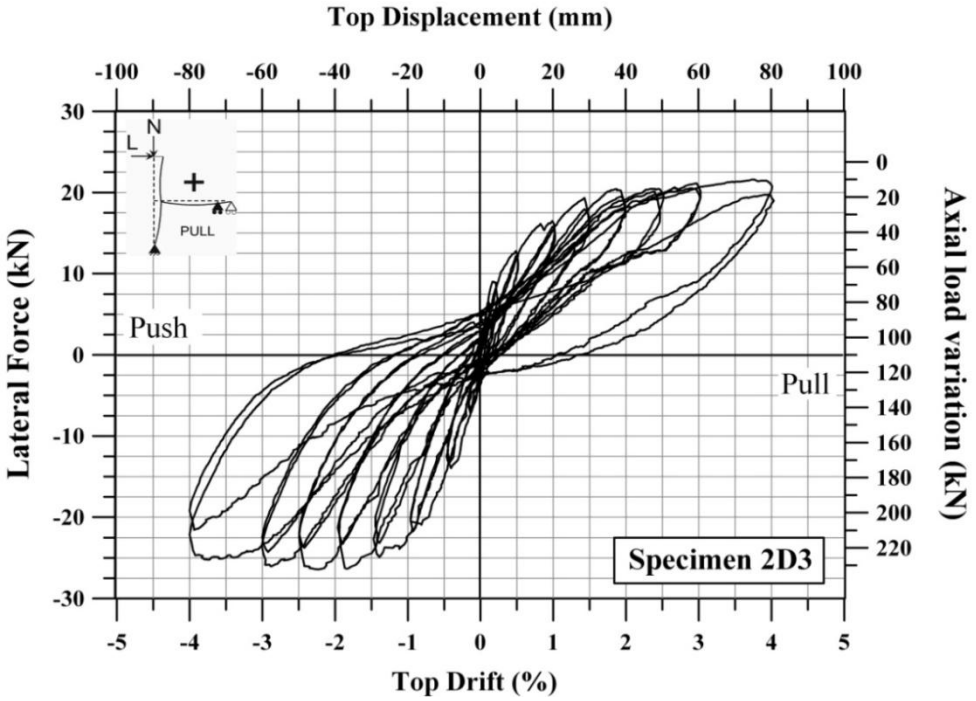

Figure 6–10 Load versus displacement response of Specimen 2D3

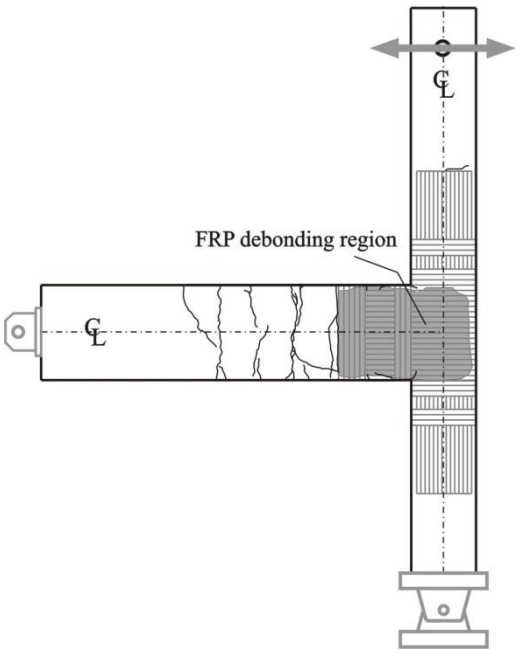

Figure 6–11 Final damage state of Specimen 2D3

Table 6-3 Summary of test results for Specimen 2D3

Drift Level	Loading		Axial Load		Strength		Joint Panel Results		
	Cycle	Direction	N^a (kN)	$N/(A_g f_c`)^b$	$V_c{}^c$ (kN)	$v_{jh}{}^d$ (MPa)	$p_c{}^e$ (MPa)	$p_t{}^f$ (MPa)	γ^g (%)
0.1%	1st	Pull	79.46	0.08	6.54	0.67	-1.76	0.26	0.0101
		Push	124.20	0.13	-2.61	-0.30	-2.39	0.04	0.0246
	2nd	Pull	83.08	0.09	6.20	0.70	-1.83	0.26	0.0101
		Push	126.30	0.13	-3.18	-0.37	-2.44	0.06	0.0235
0.2%	1st	Pull	69.87	0.07	8.92	0.99	-1.85	0.53	-0.0146
		Push	146.10	0.15	-7.19	-0.82	-2.99	0.22	0.0324
	2nd	Pull	72.76	0.08	8.14	0.90	-1.82	0.44	-0.0191
		Push	143.00	0.15	-6.70	-0.73	-2.89	0.18	0.0291
0.5%	1st	Pull	52.13	0.06	12.77	1.41	-1.99	1.00	-0.1189
		Push	177.60	0.19	-13.96	-1.55	-3.96	0.60	0.0580
	2nd	Pull	57.20	0.06	12.18	1.35	-1.99	0.91	-0.1245
		Push	174.70	0.18	-13.42	-1.50	-3.88	0.58	0.0647
1%	1st	Pull	37.83	0.04	16.39	1.78	-2.18	1.46	-0.2031
		Push	178.50	0.19	-20.92	-2.31	-4.55	1.17	0.1939
	2nd	Pull	41.63	0.04	15.64	1.73	-2.17	1.38	-0.3355
		Push	209.20	0.22	-21.82	-2.38	-5.07	1.11	0.2006
1.5%	1st	Pull	20.45	0.02	19.34	2.13	-2.33	1.95	-0.4771
		Push	211.40	0.22	-24.90	-2.70	-5.36	1.36	0.4404
	2nd	Pull	29.32	0.03	17.94	1.98	-2.28	1.73	-0.4625
		Push	219.20	0.23	-23.19	-2.51	-5.33	1.18	0.4369
2%	1st	Pull	21.72	0.02	20.22	2.19	-2.40	1.99	-0.5537
		Push	221.40	0.23	-26.24	-2.85	-5.63	1.44	0.6477
	2nd	Pull	22.62	0.02	19.49	2.11	-2.33	1.90	-0.5595
		Push	224.80	0.24	-23.24	-2.59	-5.48	1.23	0.6477
2.5%	1st	Pull	16.14	0.02	20.45	2.22	-2.38	2.07	-0.5862
		Push	229.59	0.24	-26.78	-2.90	-5.79	1.45	0.7290
	2nd	Pull	16.88	0.02	20.09	2.18	-2.34	2.02	-0.6627
		Push	221.20	0.23	-23.76	-2.59	-5.42	1.24	0.6933
3%	1st	Pull	13.73	0.01	21.10	2.30	-2.43	2.17	-0.6819
		Push	229.90	0.24	-25.88	-2.78	-5.70	1.36	0.8386
	2nd	Pull	16.70	0.02	20.48	2.22	-2.38	2.07	-0.6972
		Push	224.50	0.24	-24.07	-2.66	-5.52	1.28	0.7750
4%	1st	Pull	4.76	0.01	21.82	2.37	-2.41	2.51	0.7100
		Push	229.20	0.24	-25.18	-2.69	-5.62	1.29	0.7186
	2nd	Pull	16.51	0.02	19.70	2.24	-2.40	2.09	-1.6392
		Push	214.20	0.23	-21.54	-2.33	-5.11	1.06	0.7238

[a] Axial load: $N=N_g \pm \alpha V_c$; [b] Axial load ratio; [c] Story column shear; [d] Horizontal joint shear stress in the joint
[e] Principal compression stress in the joint; [f] Principal tension stress in the joint; [g] Joint shear deformation

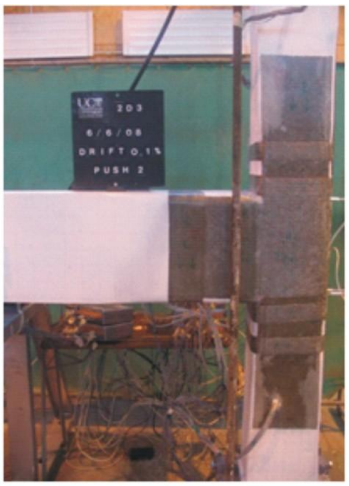

a) 0.1% drift, 2nd cycle - push dir.

b) 0.2% drift, 2nd cycle - pull dir.

c) 0.5% drift, 2nd cycle - push dir.

d) 1% drift, 2nd cycle - push dir.

e) 1.5% drift, 2nd cycle - pull dir.

f) 2% drift, 2nd cycle - push dir.

Figure 6–12 Damage propagation - Specimen 2D3

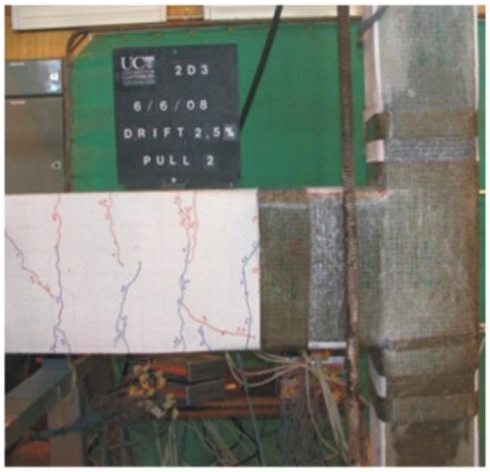

g) 2.5% drift, 2nd cycle - pull dir.

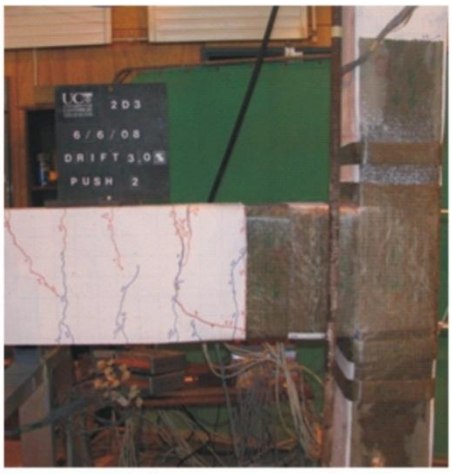

h) 3% drift, 2nd cycle - push dir.

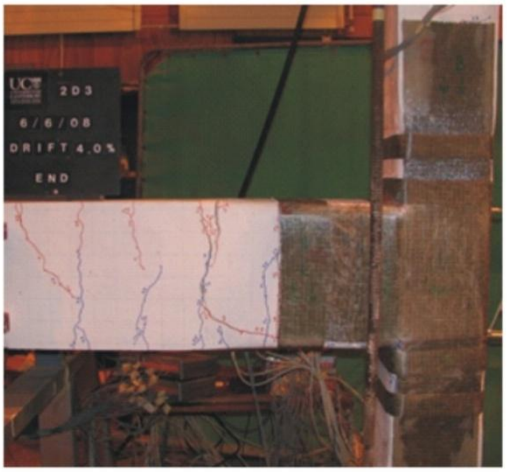

i) Final damage state, 4% drift

Figure 6–13 Damage propagation - Specimen 2D3 (cont`d)

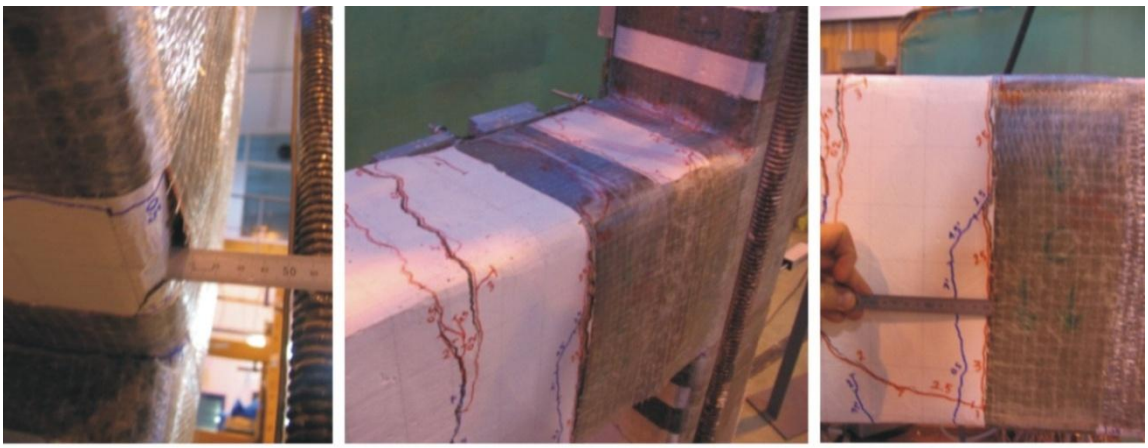

a) b) c)

Figure 6–14 Debonding in the beam horizontal and anchorage FRP sheets - Specimen 2D3

6.2.4 Retrofitted Specimen 2D4

Based on the experimental findings of Specimen 2D3, in the last 2D retrofitted specimen, Specimen 2D4, an upgraded retrofit scheme, R21, was employed. Accordingly, instead of one FRP layer application in the beam and joint level, two horizontal layers were installed. The column's FRP scheme remained the same: one vertical layer on each side. In this way, the shear strength of the joint is increased considerably to eliminate the undesired failure modes encountered in the testing of the previous specimen, 2D3. During the test the axial load level was varied around the gravity load value, 115 kN, in proportion to the lateral force acting in the column with a proportionality coefficient of 4.63. As anticipated and predicted before the test, Specimen 2D4 developed similar failure mechanism to that of Specimen 2D2, which is characterised by the plastic hinge formation in the beam GFRP interface with good energy dissipation capacity and high ductility. The lateral force-displacement response along with crack patterns at the final stage of the Specimen 2D4 are given in Figure 6–15 and Figure 6–16, respectively. The summary of the test results in terms of maximum recorded values are tabulated for each loading direction in Table 6-2. The damage propagation of the Specimen 2D4 is summarized in the following.

Following an elastic drift of 0.1% (Figure 6–17a), hairline flexural cracks started to form under the beam face at 0.2% drift (Figure 6–17b). During the cycles performed at 0.5% and 1%, new flexural cracks appeared and surrounded the beam faces with crack widths ranging from 0.2 to 0.75 mm (Figure 6–17c, d). During the subsequent drift levels, several hairline cracks formed in the column face. The width of the minor crack in the beam sheet and the opening in the beam-column joint interface reached 4 mm and 3 mm at 2.5% drift (Figure 6–17g), respectively. The specimen reached its maximum lateral strength of around 24 kN in push direction after 1% drift. In the following cycles in this direction of loading with an increase in the axial load, stable hysteresis loops were recorded throughout the test. On the other hand, as clearly seen in the hysteresis loops of pull direction with decreasing axial load (Figure 6–15), the specimen reached its yielding capacity of around 24 kN after 2.5% drift level. Up to this drift level, due to the low axial load levels, the attained maximum strength remained low in comparison to the values attained in the push direction. However, stable hysteresis loops were observed in the subsequent drift levels of 2.5%. After this level of loading, the damage was mainly concentrated in a single and wide crack at the critical section of the beam. After a storey drift of 2.5% additional cracks barely developed in the beams and the damage was basically concentrated in the flexural crack at the interface of beam FRP end and concrete. A rigid body rotation in the form of flexural plastic hinge became apparent after this drift level till the end of the test (Figure 6–17h, i). At

4% drift level, apart from minor horizontal sheet fracture at the back of the joint, no damage was observed in the beam and column sheets (Figure 6–17j).

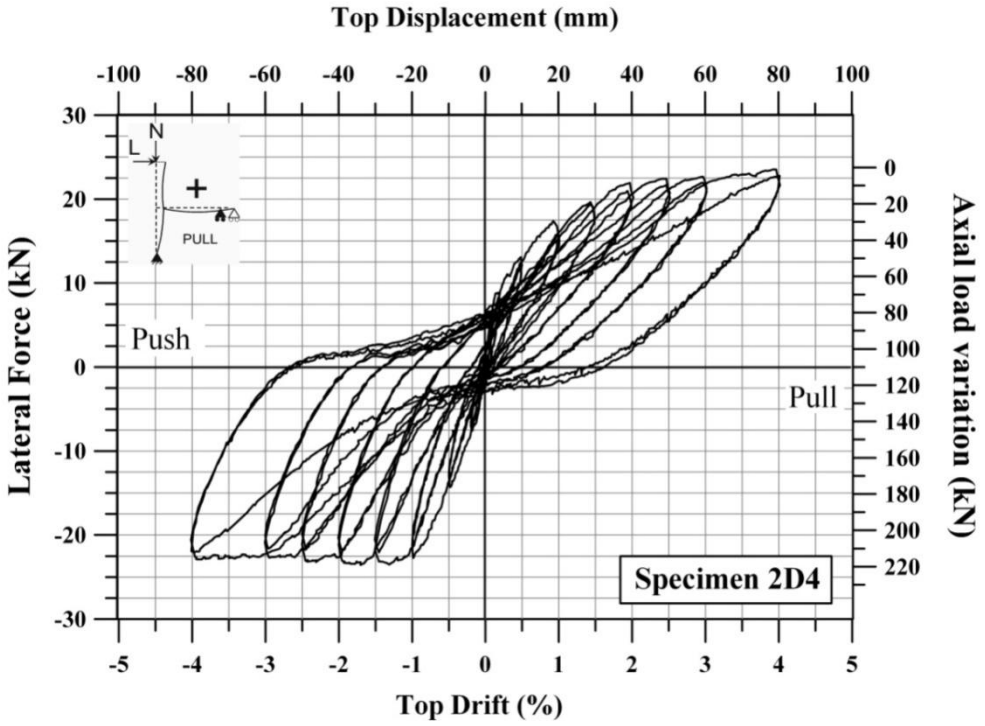

Figure 6–15 Load versus displacement response of Specimen 2D4

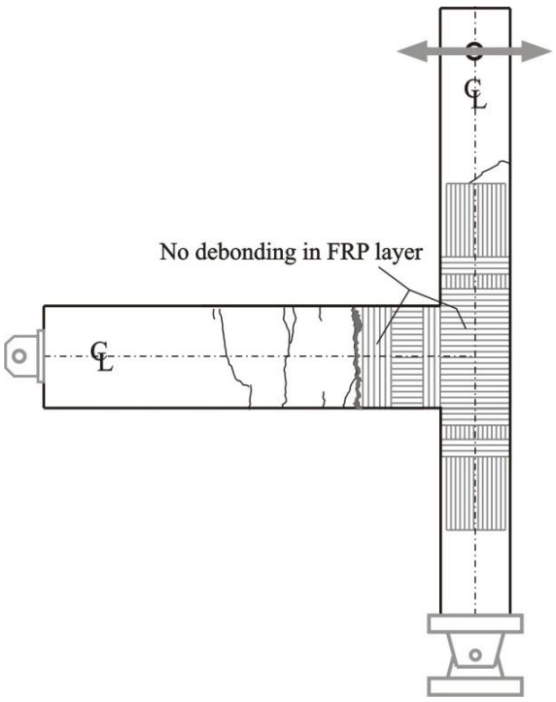

Figure 6–16 Final damage state of Specimen 2D4

Table 6-4 Summary of test results for Specimen 2D4

Drift Level	Loading		Axial Load		Strength		Joint Panel Results		
	Cycle	Direction	N^a (kN)	$N/(A_g f_c`)^b$	$V_c{}^c$ (kN)	$v_{jh}{}^d$ (MPa)	$p_c{}^e$ (MPa)	$p_t{}^f$ (MPa)	γ^g (%)
0.1%	1st	Pull	74.91	0.08	6.41	0.76	-1.75	0.33	0.2536
		Push	74.91	0.08	-4.07	0.76	-1.75	0.33	0.2536
	2nd	Pull	124.60	0.14	6.62	-0.45	-2.44	0.08	0.2760
		Push	133.50	0.15	-4.14	-0.50	-2.62	0.10	0.2771
0.2%	1st	Pull	68.05	0.08	8.86	0.96	-1.80	0.52	0.2434
		Push	148.10	0.17	-7.58	-0.83	-3.03	0.23	0.2839
	2nd	Pull	67.49	0.08	8.27	0.94	-1.78	0.50	0.2423
		Push	143.70	0.16	-7.17	-0.77	-2.92	0.20	0.2805
0.5%	1st	Pull	49.69	0.06	13.10	1.44	-1.98	1.04	0.2153
		Push	178.60	0.20	-14.30	-1.56	-3.99	0.61	0.3075
	2nd	Pull	54.70	0.06	12.34	1.35	-1.96	0.92	0.2175
		Push	175.00	0.20	-13.35	-1.47	-3.87	0.56	0.3108
1%	1st	Pull	55.62	0.06	17.38	1.23	-1.87	0.82	0.1974
		Push	216.00	0.24	-22.73	-2.48	-5.25	1.17	0.3736
	2nd	Pull	38.57	0.04	15.79	1.72	-2.12	1.39	0.1783
		Push	206.90	0.23	-20.99	-2.29	-4.97	1.05	0.3713
1.5%	1st	Pull	17.61	0.02	19.65	2.13	-2.30	1.97	0.1254
		Push	216.40	0.24	-23.44	-2.57	-5.33	1.24	0.3815
	2nd	Pull	22.06	0.02	19.41	2.06	-2.28	1.87	0.1130
		Push	216.40	0.24	-22.06	-2.43	-5.22	1.13	0.3736
2%	1st	Pull	7.05	0.01	21.92	2.39	-2.46	2.32	0.1187
		Push	108.45	0.12	-23.89	-2.59	-3.81	1.76	0.4060
	2nd	Pull	12.24	0.01	20.96	2.27	-2.38	2.15	0.0555
		Push	211.70	0.24	-21.85	-2.37	-5.10	1.10	0.3916
2.5%	1st	Pull	4.64	0.01	22.41	2.43	-2.48	2.39	0.0396
		Push	221.00	0.25	-23.16	-2.51	-5.36	1.18	0.3937
	2nd	Pull	7.42	0.01	21.65	2.37	-2.44	2.30	0.0835
		Push	215.80	0.24	-21.75	-2.38	-5.17	1.09	0.3880
3%	1st	Pull	4.26	0.00	22.65	2.47	-2.51	2.43	0.0924
		Push	217.50	0.24	-22.65	-2.46	-5.26	1.15	0.3990
	2nd	Pull	6.68	0.01	21.96	2.39	-2.45	2.33	0.0856
		Push	206.20	0.23	-21.48	-2.32	-4.98	1.08	0.3956
4%	1st	Pull	0.53	0.00	23.58	2.56	-2.60	2.51	0.3900
		Push	216.00	0.24	-22.89	-2.50	-5.27	1.19	0.4670
	2nd	Pull	5.01	0.01	22.65	2.46	-2.50	2.41	0.0266
		Push	209.50	0.23	-22.02	-2.40	-5.09	1.13	0.4903

[a] Axial load: $N=N_g \pm \alpha V_c$; [b] Axial load ratio; [c] Story column shear; [d] Horizontal joint shear stress in the joint
[e] Principal compression stress in the joint; [f] Principal tension stress in the joint; [g] Joint shear deformation

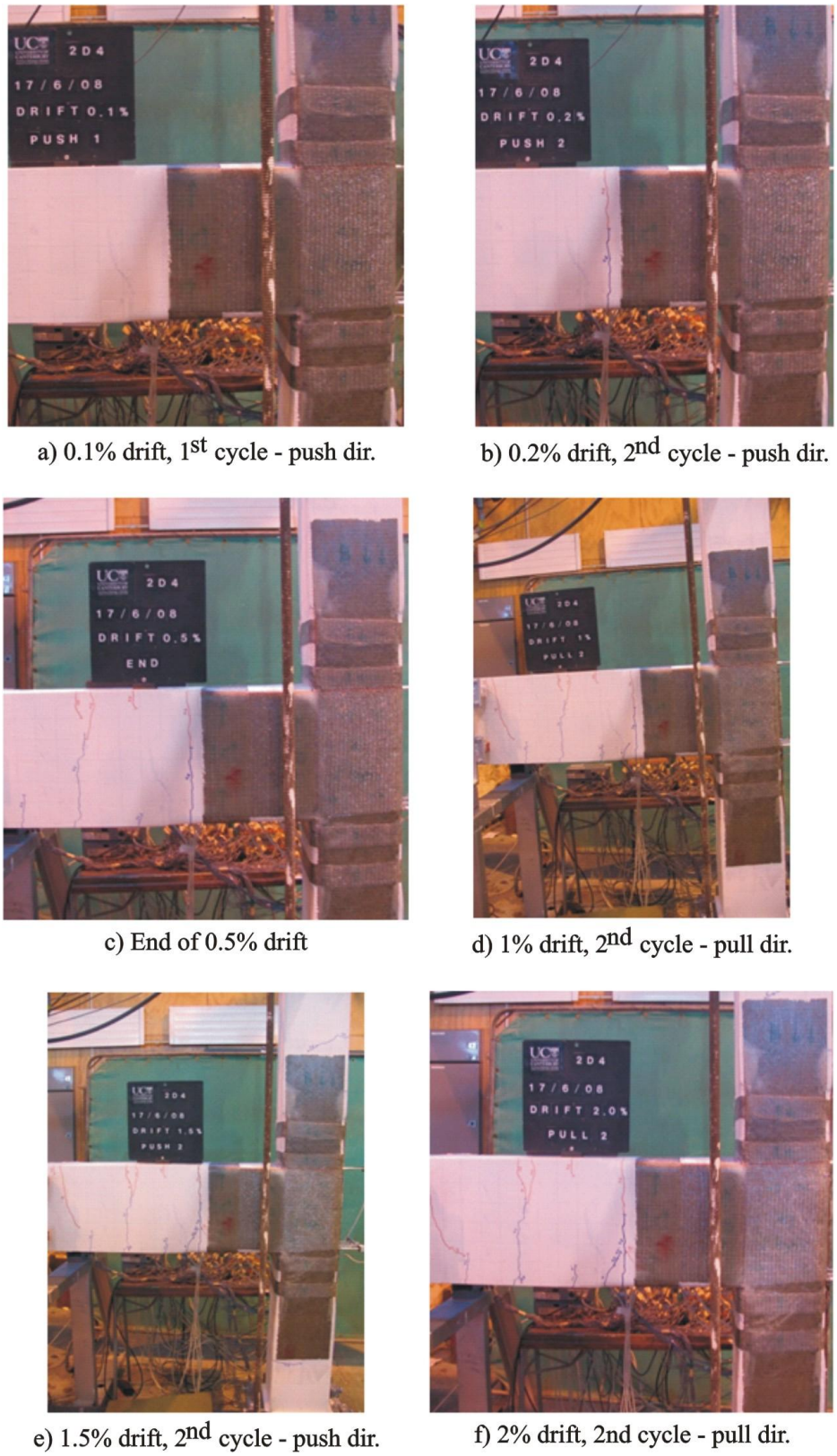

a) 0.1% drift, 1st cycle - push dir.

b) 0.2% drift, 2nd cycle - push dir.

c) End of 0.5% drift

d) 1% drift, 2nd cycle - pull dir.

e) 1.5% drift, 2nd cycle - push dir.

f) 2% drift, 2nd cycle - pull dir.

Figure 6–17 Damage propagation - Specimen 2D4

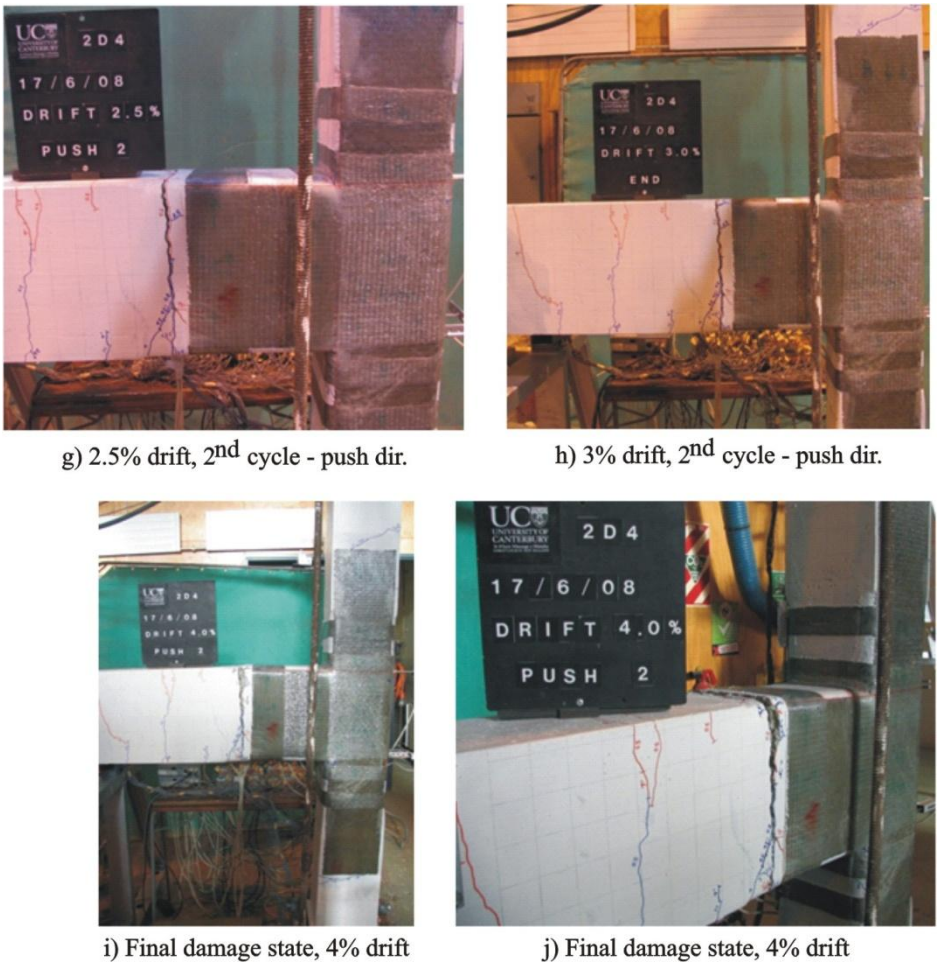

g) 2.5% drift, 2nd cycle - push dir.

h) 3% drift, 2nd cycle - push dir.

i) Final damage state, 4% drift

j) Final damage state, 4% drift

Figure 6–18 Damage propagation - Specimen 2D4 (cont`d)

6.3 ANALYSIS OF TEST RESULTS

In this section the test results are analysed and discussed based on the observed damage and recorded instrumentation readings of all the specimens. In the comparison and discussion of the findings, a particular focus is given to the effect of axial load variation to the performance of the 2D beam-column joint units retrofitted using the different schemes. With this purpose in mind, results have been carefully selected in order to analyse this specific point.

6.3.1 Strength and Failure Modes

In this subsection, the behaviour and load-displacement characteristics are summarized and compared to clarify the effects of different retrofit schemes under constant and varying axial loads on the

column. For this purpose, the final damage states and lateral load vs. displacement responses of the specimens are compared in Figure 6–19 and Figure 6–20, respectively.

Figure 6–19 Final damage states of 2D joints

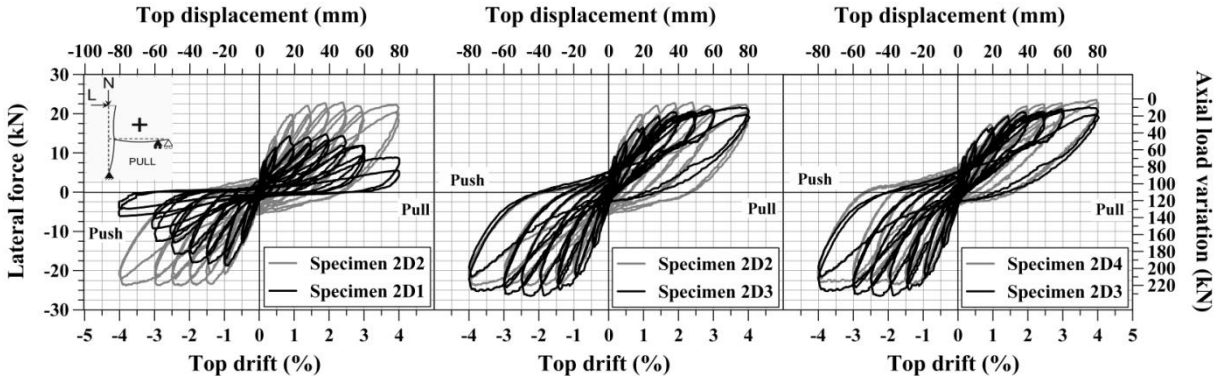

Figure 6–20 Comparison of force-drift response of 2D specimens

The as-built Specimen 2D1, tested under varying axial load, exhibited a hybrid local damage and failure mechanism. This mechanism was characterised by the combination of two separate mechanisms in the joint region (1) shear damage in the form of cross diagonal cracking due to the inadequate confinement and (2) slippage of the beam longitudinal plain round bars leading to a concentrated compressive force at the end-hook anchorages. As a result, a wide concrete wedge developed leading to the expulsion of the outer face of the column after 3% drift level (Figure 6-19a). The hysteresis loops obtained are characterised by substantial pinching (Figure 6-20), which is typical of joint shear failure. This can be attributed to the inadequate amount of stirrups in the column and joint region.

Table 6-5 presents the summary of the test results at both global and local level (joint panel zone behaviour), as measured and/or calculated at peak drift values. The displacement ductility μ is defined, as typical, as Δ_u/Δ_y, where Δ_u is the horizontal displacement corresponding to the displacement when

the load carrying capacity undergoes a 20% reduction in load or significant failure of the specimen occurs. The yield displacement Δ_y is defined as the displacement of the equivalent elasto-plastic system with the same energy absorption as the real system ([1]).

Table 6-5 Summary of test results of 2D joints

Specimen	Direction	Strength		Axial Load		Ductility	Joint Panel Results					Dissipated Energy	Failure Mode
		V_c [a] (kN)	v_{jh} [b] (MPa)	f_v [c] (MPa)	Δ_y [d] (mm)	$\mu = \Delta u^e / \Delta y$	p_c [f] (MPa)	p_t [g] (MPa)	γ_1 [h] (%)	γ_2 [i] (%)	γ_3 [j] (%)	E_{df} [k] (kNmm)	
2D1	Pull	14.89	0.82	1.61	11.04	1	-2.08	1.25	0.260	0.942	1.739	3319	Joint Shear
	Push	-18.92	2.05	3.67	-14.02	4	-4.59	0.91	0.014	0.342	1.200		
2D2	Pull	22.85	2.48	2.10	16.80	5	-3.74	1.63	0.273	0.535	0.460	9075	Ductile beam hinging
	Push	-23.89	-2.59	2.05	-18.60	4	-3.81	1.76	0.085	0.404	0.693		
2D3	Pull	21.82	2.37	0.09	23.81	3	-2.41	2.51	0.312	0.549	0.678	7526.9	GFRP debonding
	Push	-26.78	-2.90	4.34	-18.80	4	-5.79	1.45	0.193	0.641	0.834		
2D4	Pull	23.58	2.56	0.01	26.80	3	-2.60	2.51	0.374	0.390	0.410	9277	Ductile beam hinging
	Push	-23.89	-2.59	2.05	-16.48	5	-3.81	1.76	0.187	0.119	0.092		

[a] Story column shear; [b] Horizontal joint shear stress in the joint; [c] Nominal axial stress;
[d] Yield displacement defined as the displacement of the equivalent elasto-plastic system with the same energy absorption as the real system;
[e] Ultimate displacement corresponds to the displacement at a 20% reduction in load; [f] Principal compression stress in the joint; [g] Principal tension stress in the joint;
[h, i, j] Joint shear deformation at 1, 2 and 3 percent drift levels, respectively; [k] Cumulative dissipated energy for all cycles up to failure.

Specimen 2D2 (minimum retrofit scheme, R11, tested under constant axial load assumptions) exhibited the most enhanced behaviour among all the specimens. Throughout the test, the damage was concentrated at the beam region with some spalling of the cover concrete where the GFRP layer ended (Figure 6-19b). Apart from hairline cracks appearing in the column, no debonding of the GFRP sheets occurred. The behaviour was very satisfactory. Stable hysteresis behaviour was maintained until the end of the test, with a ductile yielding mechanism (Figure 6-20) and high energy dissipation. A rapid strength deterioration and early failure of the Specimen 2D1 led to a reduction of about 36% of the energy dissipation capacity when compared to the Specimen 2D2 (Table 6-5).

The pronounced effect of the FRP intervention can be seen in Table 6-5. At first sight, a considerable improvement in the global performance of the joint can be recognized in terms of strength, horizontal joint shear carrying capacity and ductility improvement, as well as shifting of the failure mode from a brittle to a ductile one through plastic hinging at the end of the beam FRP sheet.

At the local level, an important engineering parameter, shear deformation in the joint panel, is examined to evaluate the behaviour and the amount of damage sustained. The joint shear deformation of the Specimen 2D1 reached around 1% (0.942 rad) at 1% drift indicating excessive distress in the

unconfined joint panel. On the other hand, in the push direction loading and increasing axial load, the joint shear deformation demand was greatly reduced because of the stiffening of the joint. However, in the following cycles the favourable role of the axial load increase, initially improving the joint performance, drastically changed. The high level of axial loads caused a compression strut failure accompanied by the buckling of column longitudinal bars in the joint level. This was mainly attributed to the inadequate confinement of the as-built joint. The test results also indicated that the shear deformation demand in the joint panel was reduced to about 50% upon the FRP strengthening after 1% drift level. On the other hand, as aimed in the retrofit design (see Chapter 4), FRP confinement around the joint prevented this type of failure by providing confinement. In this way, parallel to supplying additional shear strength to the joint, compressive strength of the joint core concrete was also increased, allowing much higher stress levels to be carried in this region.

The test results of Specimen 2D3 revealed the deficiency of the retrofit design performed under constant axial load assumptions. As proven by the experimental results, the minimum retrofit scheme was unable to fulfil the desired performance under varying axial load conditions. Although similar performances was observed to that of Specimen 2D2 in the push direction (increasing axial load), in the pull direction (decreasing axial load) a peculiar hybrid failure mechanism occurred. This mechanism was mainly governed by the gradual debonding of the FRP sheet initiated at the last cycle of 2% drift in the beam-column interface. In the subsequent drift levels, detachment from the concrete face continued into the joint panel and beam anchorages towards the end of the FRP laminate (Figure 6-19c). This phenomenon can be attributed to the high shear demand, accompanied by reduced joint strength provided by the minimum retrofit scheme as the axial load decreased in one loading direction. In the following sections, further investigation into this mechanism is carried out by examining the strain demand experienced in the longitudinal direction of GFRP sheets during the tests.

In Figure 6-10 and Figure 6-20, the reflection of the damage propagation of the Specimen 2D3 on the hysteresis loops can be clearly seen. Basically, due to the lower axial load in the loading cycles the Specimen 2D3 achieved lower load capacities at peak drift levels. In the reloading cycles of pull direction, softening and pinching were recorded, which led to a reduction of approximately 20% when compared to the Specimen 2D4. It is anticipated that if the axial load on the columns becomes very low or the column is subjected to tension (which depends on the geometry of the building: i.e., the number of storeys, and the number and length of bays) and in the presence of typically inadequate column lap-splices, the performance of the Specimen 2D3 would be drastically affected.

At the local level, a 50% increase in principal compression stress demand in the joint panel of Specimen 2D3 was recorded, when compared to that of Specimen 2D2, from higher compression loads sustained by the GFRP confinement in the joint (Table 6-5). In the same table and also in Figure 6-21, where the normalized principal tensile stresses versus shear deformations of 2D joints are given, the increased shear distortion in the joint panel of Specimen 2D3 can be clearly seen. After 2% drift, due to the sudden loss of joint shear stiffness, the specimen behaved almost in the same manner as the as-built Specimen 2D1. Post-test examinations also supported these observations. The FRP sheet detachment from the concrete surface, the crushing of the concrete in the joint panel and the lack of a definite formation of the plastic hinge region in the Specimen 2D3, can be seen in Figure 6-22. In Figure 6-23, close-up views of the slightly damaged joint panel region under the FRP sheet of the Specimen 2D2 are given for comparison. It is clear that, although minor cracking occurred in the joint region of the Specimen 2D2, the damage was accumulated in the end region of the FRP zone of the beam.

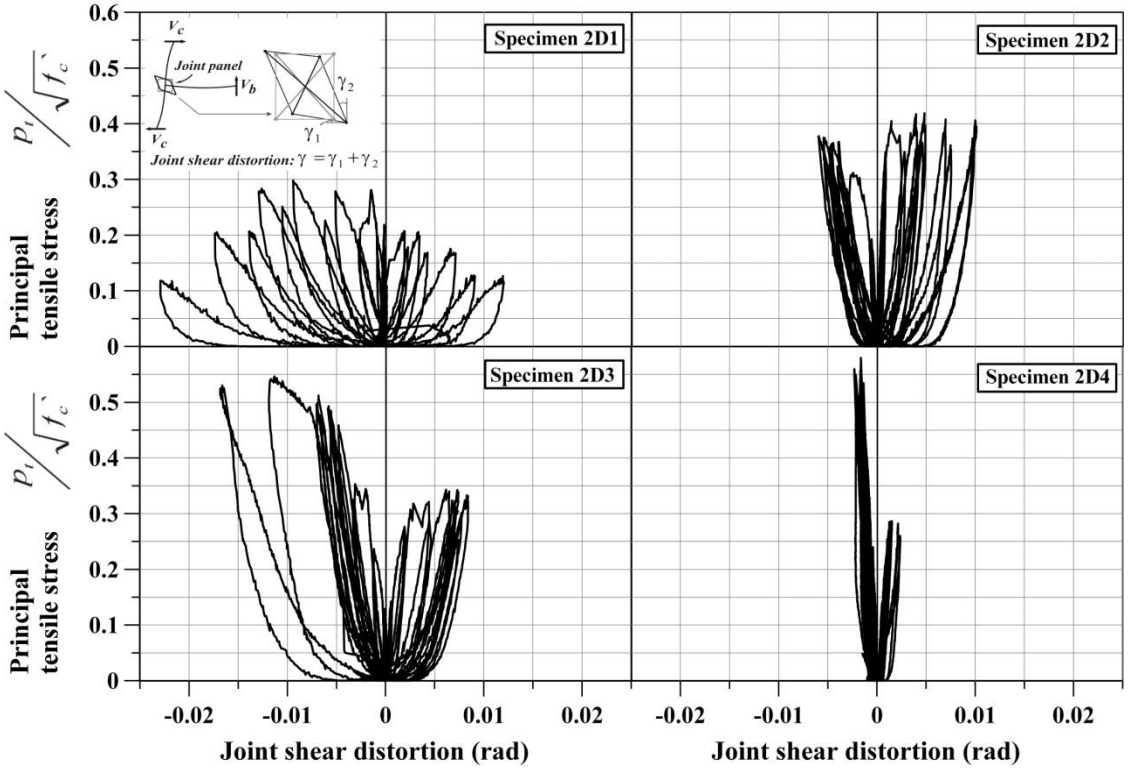

Figure 6–21 Comparison of principal tensile stress versus joint distortion of 2D joints

Similar to the Specimen 2D2, the Specimen 2D4 (implementing a modified retrofit scheme, R21, and tested under varying axial load) showed significant improvements resulting in the development of a more appropriate hierarchy of strength. Hence, the sequence of events in the subassembly was

modified, as targeted, in a way that the brittle joint shear damage mechanism was shifted to a more ductile beam hinging failure mechanism, as observed in the Specimen 2D2 (Figure 6-19). However, two major differences were noted between Specimen 2D3 and Specimen 2D4 (1) lower strength values were attained at the peak drifts in the pull direction due to the low axial load values, similar to Specimen 2D3 (Figure 6-20); (2) no debonding of the FRP was encountered till the end of the test. The joint region and column remained intact for the duration of (the end of) the test. The joint shear distortion decreased substantially indicating a lesser distress in the joint panel among the 2D specimens (Figure 6-21). Due to the stiffer joint region provided by the two layers of GFRP, the joint shear deformations in Specimen 2D4 were effectively limited to a maximum of 0.41% (0.0041 rad). The post-test examinations of the joint panel region under the FRP layer supported these observations.

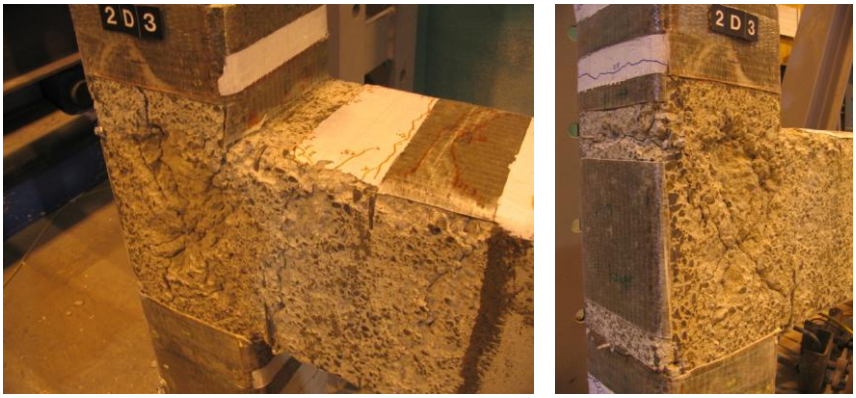

Figure 6–22 Damage state of the joint region after test under FRP sheet - Specimen 2D3

Figure 6–23 Damage state of the joint region after test under FRP sheet - Specimen 2D2

6.3.2 Stiffness and Energy Dissipation Characteristics

To further assist the evaluation and quantify the hysteretic performance of the specimens, the peak-to-peak stiffness K_p as well as the cumulative energy dissipation E_D for each drift values are evaluated

and presented in the following. It is well known that the displacement of short period systems is increased by the stiffness degradation even under uniaxial ground motion, because the displacement increases rapidly with the degradation of the period. In addition, the capacity of a structure to dissipate energy has a strong influence on its response to earthquake loading. Therefore, the findings presented here are also used to study the degree of bidirectional loading effects on the seismic performance of 3D as-built and retrofitted corner beam-column joints in Chapter 10.

The peak-to-peak stiffness is defined as the slope of the line, joining the highest load points in the load-displacement curve attained at each displacement level (positive and negative). The degradation of peak-to-peak stiffness of the 2D joint units, along with the differences in terms of percentage with benchmark specimens and retrofitted specimens are plotted and tabulated in Figure 6-24 and Table 6-6. The cumulative energy dissipated is computed by summing up the area enclosed within the load versus displacement curves; the values are given and tabulated in Figure 6-25 and Table 6-7, respectively.

Table 6-6 Degradation of peak-to-peak lateral stiffness of 2D joints

		Specimen 2D1	Specimen 2D2		Specimen 2D3		Specimen 2D4	
Drift	Cycle	K_p (kN/mm)	K_p (kN/mm)	difference with as-built (%)	K_p (kN/mm)	difference with as-built (%)	K_p (kN/mm)	difference with as-built (%)
0.1%	1st	2.77	3.02	8.9	3.08	11.0	2.95	6.4
	2nd	2.77	2.48	-10.3	3.08	11.2	2.97	7.3
0.2%	1st	1.93	2.08	7.5	2.46	27.1	2.19	13.3
	2nd	1.77	1.97	10.9	2.01	13.2	2.08	17.6
0.5%	1st	1.26	1.48	17.6	1.43	14.1	1.40	11.7
	2nd	1.16	1.38	18.9	1.34	15.7	1.33	14.8
1%	1st	0.94	1.05	11.4	0.96	1.8	1.04	10.7
	2nd	0.73	0.97	32.0	0.96	31.3	0.93	26.6
1.5%	1st	0.54	0.82	51.7	0.77	41.3	0.81	49.6
	2nd	0.49	0.70	43.0	0.71	45.1	0.70	42.9
2%	1st	0.43	0.63	47.3	0.63	47.0	0.62	44.3
	2nd	0.37	0.55	50.2	0.56	51.2	0.54	47.1
2.5%	1st	0.33	0.50	52.5	0.51	55.3	0.48	46.4
	2nd	0.26	0.45	71.8	0.45	73.4	0.44	67.4
3%	1st	0.21	0.40	89.3	0.40	91.1	0.41	91.9
	2nd		0.36		0.38		0.37	
4%	1st		0.30		0.31		0.31	
	2nd		0.27		0.26		0.28	

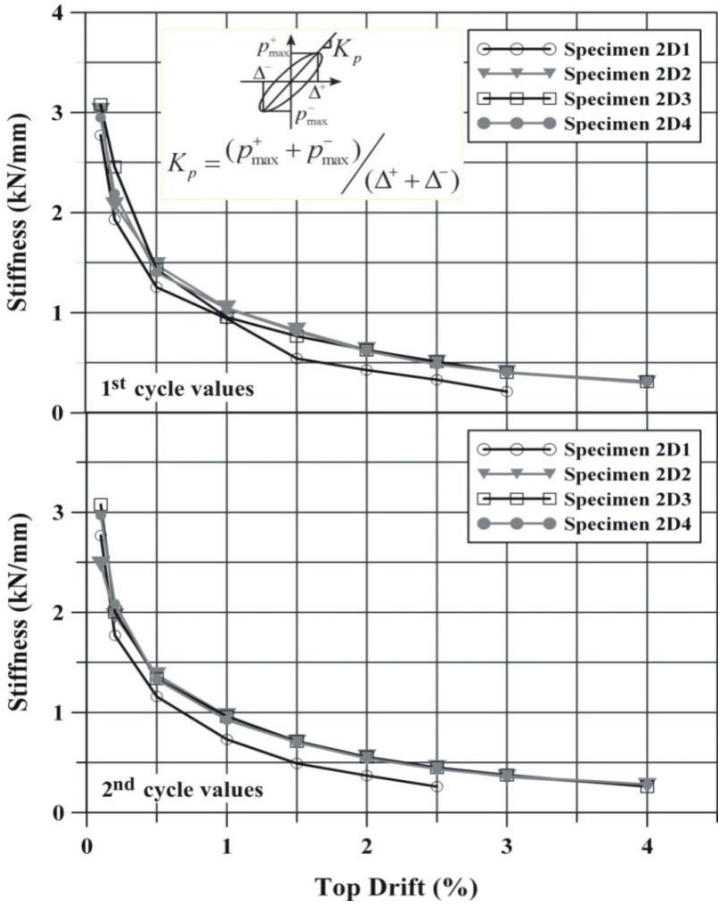

Figure 6–24 Comparison of peak-to-peak lateral stiffness degradation of 2D joints

A close examination of the stiffness degradation characteristics of the 2D joints reveals the following observations (1) the initial stiffness of the retrofitted joints is slightly higher, with around a 10% increase, than the as-built joint; (2) following the shear cracking in the joint of the as-built specimen at 1% drift, the stiffness of the specimen was reduced drastically, especially in the second loading cycles; (3) the axial load variation and FRP scheme have no significant influence on the rate of the stiffness degradation, since for the 1st as well as for the 2nd loading cycles the findings are quite comparable.

As mentioned previously, the as-built specimen experienced more stiffness reduction due to nonductile shear cracking in the joint panel. In addition, the slip due to the loss of bond in the longitudinal beam bars also made a contribution in the stiffness reduction for both as-built and retrofitted joints.

A close examination of the hysteresis loops for the pull direction loading cycles display the positive effect of high axial loads. Acting as a passive confinement, the GFRP sheet installed around the joint as a U-shape sheet and wrapped around the column as anchorage strips, played the role of increasing

the confined concrete properties and maintaining the integrity in the joint concrete region. As a result, higher stiffness values were obtained in the push direction and the bond resistance increased considerably, providing higher stiffness. On the other hand, decreasing the axial load resulted in a lower confining pressure on the bond between the steel and the concrete, which led to lesser stiffness in the pull direction loadings. These effects can be seen in Figure 6-20.

The amount of dissipated energy by the retrofitted specimens is considerably increased after 1.5 % drift compared to the as-built specimen. In all tested 2D retrofitted specimens, a small amount of pinching of the load displacement hysteresis loops can be noticed, due to plain bar slippage in the beams. However, because of the plastic hinging dominating the Specimens 2D2 and 2D4 for larger amplitude cycles, excellent dissipation capacity were obtained at large drift levels, except for the Specimen 2D3. It can be attributed to the gradual debonding in the beam sheets and loss of bond in the beam bars in the pull direction loadings. The Specimen 2D4 had the ability to dissipate almost three times the energy dissipated by the benchmark Specimen, 2D1.

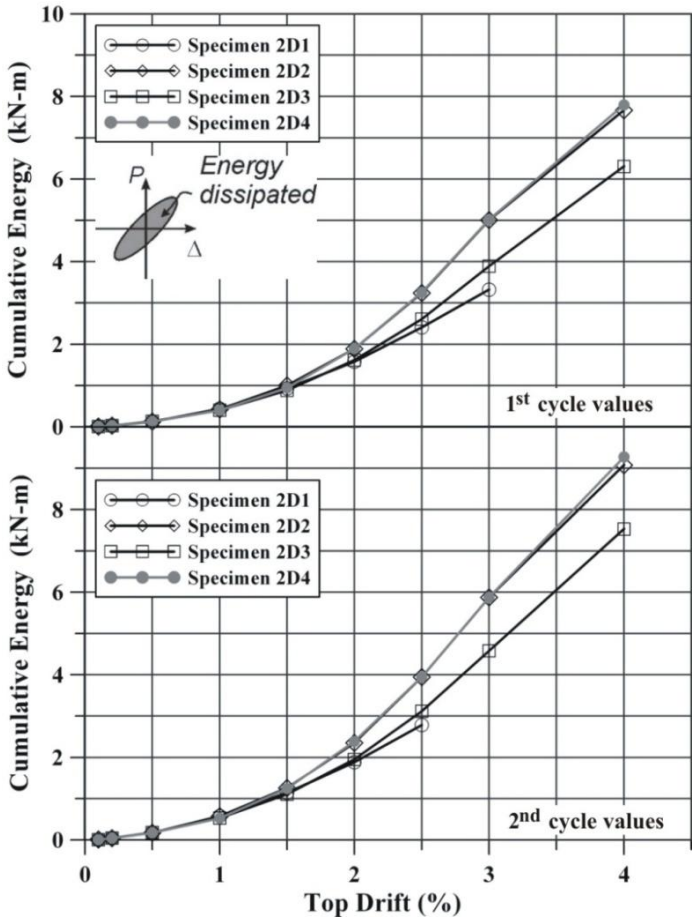

Figure 6–25 Comparison of cumulative energy dissipation of 2D joints

Table 6-7 Comparison of cumulative energy dissipation of 2D joints

Drift	Cycle	Specimen 2D1		Specimen 2D2		Specimen 2D3		Specimen 2D4	
		$ED_{per\ cycle}$ (kNmm)	$ED_{cumulative}$ (kNmm)	$ED_{per\ cycle}$ (kNmm)	$ED_{cumulative}$ (kNmm)	$ED_{per\ cycle}$ (kNmm)	$ED_{cumulative}$ (kNmm)	$ED_{per\ cycle}$ (kNmm)	$ED_{cumulative}$ (kNmm)
0.1%	1st	3.5	3.5	5.9	5.9	3.7	3.7	3.1	3.1
	2nd	3.7	7.2	3.7	9.6	3.1	6.8	3.2	6.3
0.2%	1st	20.3	27.5	20.1	29.8	24.1	31.0	20.4	26.8
	2nd	12.9	40.5	12.1	41.8	12.9	43.8	12.4	39.2
0.5%	1st	80.6	121.1	85.6	127.5	88.0	131.8	86.3	125.4
	2nd	50.4	171.5	47.7	175.2	44.4	176.3	45.3	170.7
1%	1st	264.7	436.1	248.6	423.8	226.1	402.4	229.8	400.5
	2nd	140.2	576.3	146.1	569.9	131.4	533.8	124.8	525.3
1.5%	1st	355.5	931.8	426.6	996.5	350.6	884.3	418.3	943.6
	2nd	210.6	1142.4	260.7	1257.2	221.4	1105.7	300.1	1243.7
2%	1st	432.6	1575.0	631.5	1888.8	509.5	1615.2	652.9	1896.6
	2nd	304.7	1879.7	463.2	2352.0	335.6	1950.8	487.5	2384.1
2.5%	1st	528.3	2408.0	888.9	3241.0	658.6	2609.4	874.3	3258.4
	2nd	373.2	2781.2	700.2	3941.1	508.7	3118.1	690.7	3949.1
3%	1st	538.1	3319.3	1064.0	5005.1	773.1	3891.2	1067.1	5016.2
	2nd			865.0	5870.2	689.3	4580.6	863.5	5879.8
4%	1st			1795.1	7665.3	1722.1	6302.7	1914.8	7794.6
	2nd			1409.5	9074.8	1224.2	7526.9	1482.4	9277.0

6.3.3 Strain Demand in the Steel Reinforcement

The inspection of the beam and column longitudinal bar strain readings of the Specimen 2D3 and Specimen 2D4, provides useful information on the effects of axial load variation and retrofit scheme. For this purpose, the beam and column bar strains were measured using electrical resistance strain gauges attached to the reinforcing bars at selected locations, as described in Chapter 5.

The beam longitudinal bar strain profiles of Specimen 2D3 at peak drift values in both the pull and push direction for the top and bottom beam bars, are given in Figure 6-26. In the pull direction (decreasing axial load) steel strain gauge readings at the end of the beam FRP sheet and beam-column interface, indicated that the strain readings remained elastic, which denotes that some bond still existed along the steel. On the other hand, in the push direction (increasing axial load), there is a significant increase in the steel strain values after 1% drift level at the locations of the beam FRP sheet end and the beam-column interface. It was also noticed that after the 2% drift level strain demand was more uniformly distributed and exceed the yielding value, which is around 2400 microstrain. These observations revealed that after 2% drift in the push direction steel yielding started at the end of the

beam FRP interface, which resulted in stable hysteresis loops with less pinching compared to loading in the pull directions.

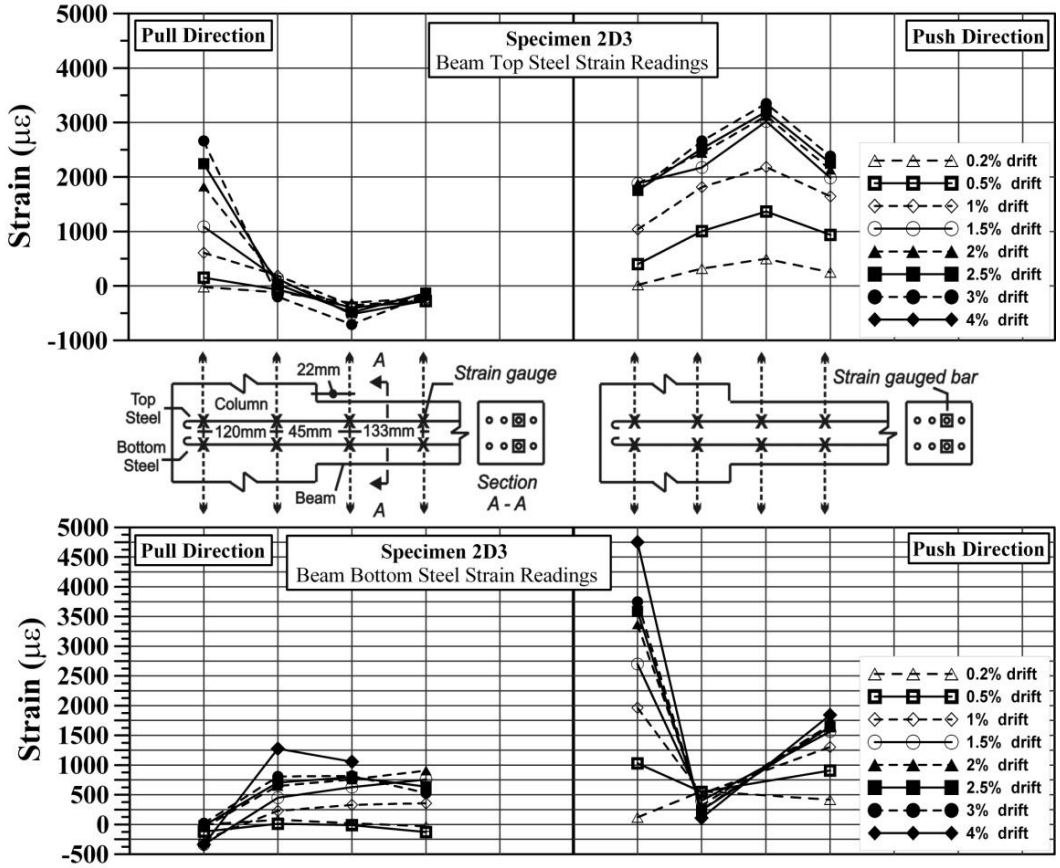

Figure 6–26 Beam longitudinal bars strain profiles of Specimen 2D3 – pull/push directions

The steel strain readings close to the joint exterior face of the Specimen 2D3 also show that in the pull direction, top steel bars yielded after 2% drift and in the push direction, bottom steel bars yielded after 1.5% drifts, respectively. These observations indicate that a degradation of bond due to the yielding occurred in this region. However, yielding of steel close to the end-hooks remained localized in this region as seen in Figure 6-26.

Figure 6-27 shows the strain distributions along the beam bars at peak drift values for Specimens 2D4 for each direction of loading. As opposed to the Specimen 2D3, the strain readings in the pull direction for bottom steel and in the push direction for top steel bars were uniformly distributed and mostly concentrated at the beam FRP end section. The uniform distribution and spread of the steel yielding along the reinforcement, clearly indicates the gradual bond deterioration that caused the softening and pinching in the hysteresis loops. This phenomenon was experienced by all the specimens, because

after the adjacent section flexural load reversals, it was difficult to maintain the bond resistance along the beam reinforcement. Hence the additional demand was resisted by the FRP sheet in the section.

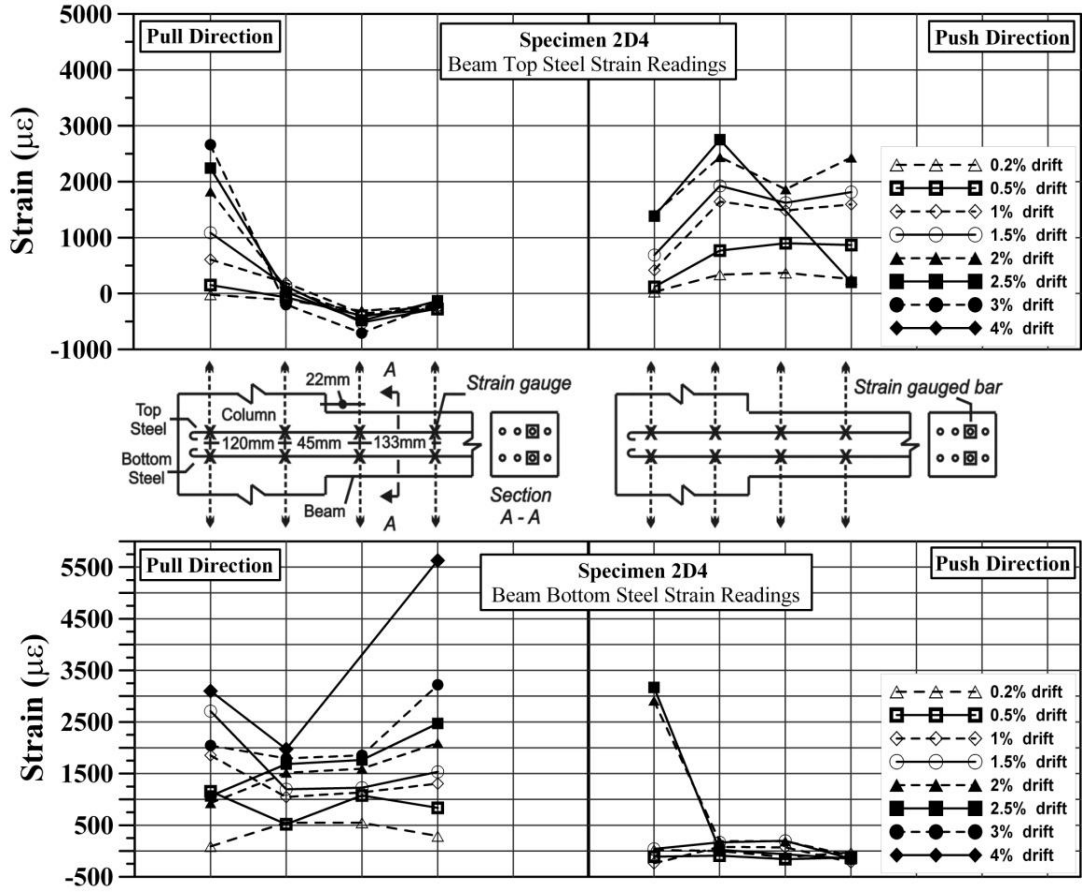

Figure 6–27 Beam longitudinal bars strain profiles of Specimen 2D4 – pull/push directions

Test results showed that the failure mechanism of the Specimen 2D4, as well as the Specimen 2D2, was governed by a single concentrated crack accompanied by minor flexural cracks at the end of the beam FRP sheet region. This observation was also made in the analysis of strain readings at the end of the beam FRP sheet critical region: very large local strains occurred in the vicinity of the beam wide flexural crack of the Specimen 2D4 (Figure 6-27).

In case of Specimen 2D2 which was tested under constant axial load, the shear capacity of the joint provided by the minimum retrofit scheme was found to be an adequate solution to carry the imposed shear forces into the joint. However, an improved retrofit scheme was required for the Specimen 2D4, to accommodate the increased shear demand in the joint stemming from the varying axial loading. In the end, two of these specimens produced similar types of desirable failure modes characterised by beam yielding at the end of beam FRP sheet, which led to increase in the energy dissipating capacity.

For both specimens after the 2% drift level, the concentration of damage in the beam FRP concrete interface was observed to be more pronounced. This failure mode, in turn, limited the amount of shear force transferred into the connection by providing a pivot point in the beam FRP sheet interface and resulted in lower strain demands in the FRP sheets. This topic is elaborated on in the following subsection.

In general, the analysis of the column longitudinal bar strain readings of both Specimens, 2D3 and 2D4, indicated that the strain demand in the bars remained in the elastic region during the tests (Figure 6-28 and Figure 6-31). Nevertheless, Specimen 2D3 experienced steel yielding in the top and bottom column regions after 3% drift as seen in Figure 6-28.

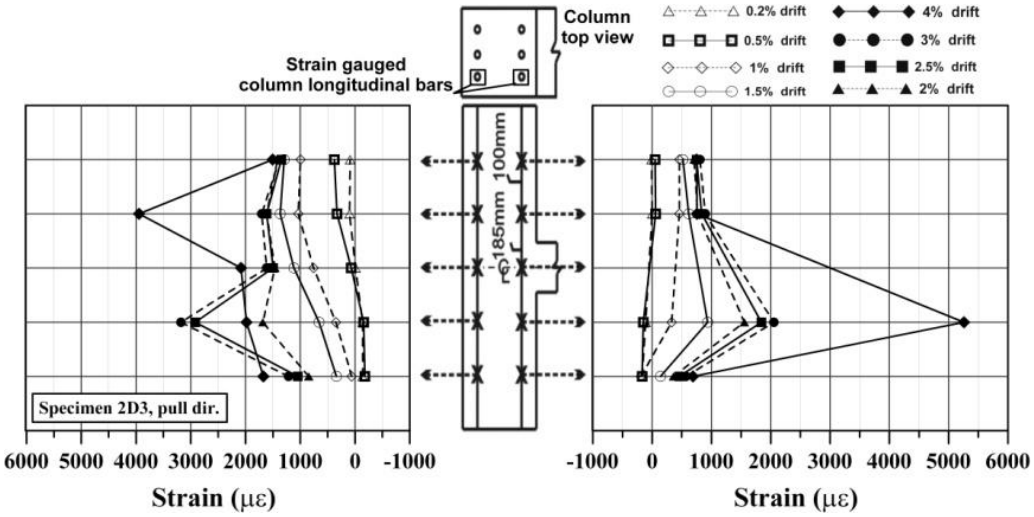

Figure 6–28 Column longitudinal bars strain profiles of Specimen 2D3 – pull direction

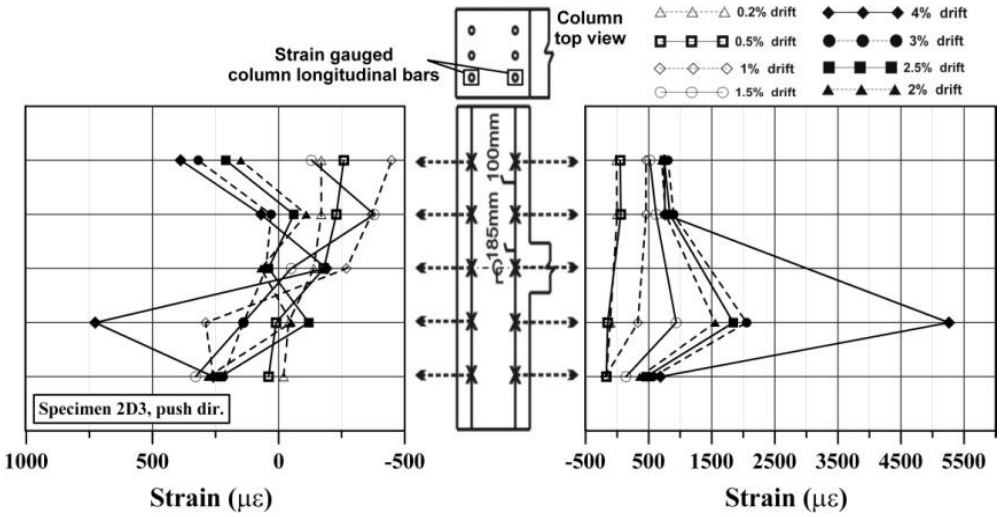

Figure 6–29 Column longitudinal bars strain profiles of Specimen 2D3 – push direction

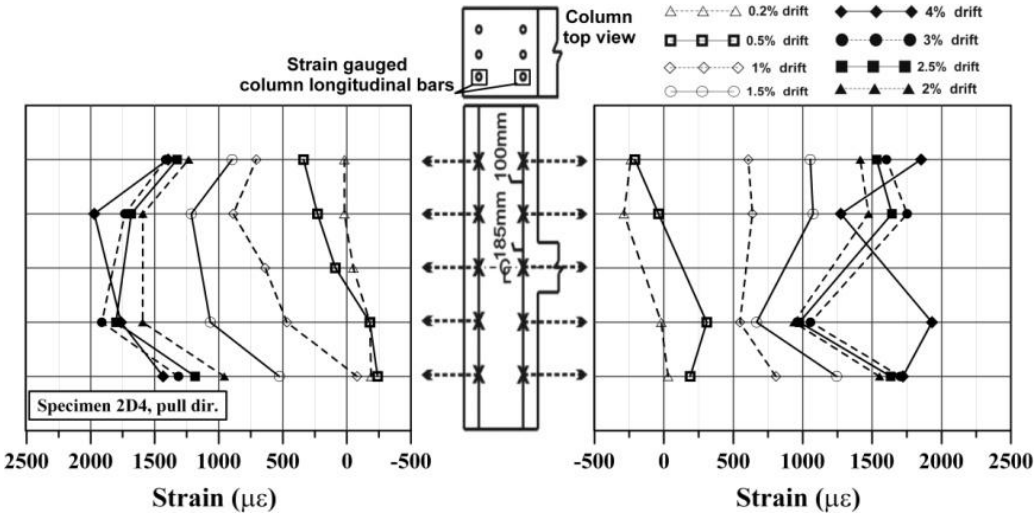

Figure 6–30 Column longitudinal bars strain profiles of Specimen 2D4 – pull direction

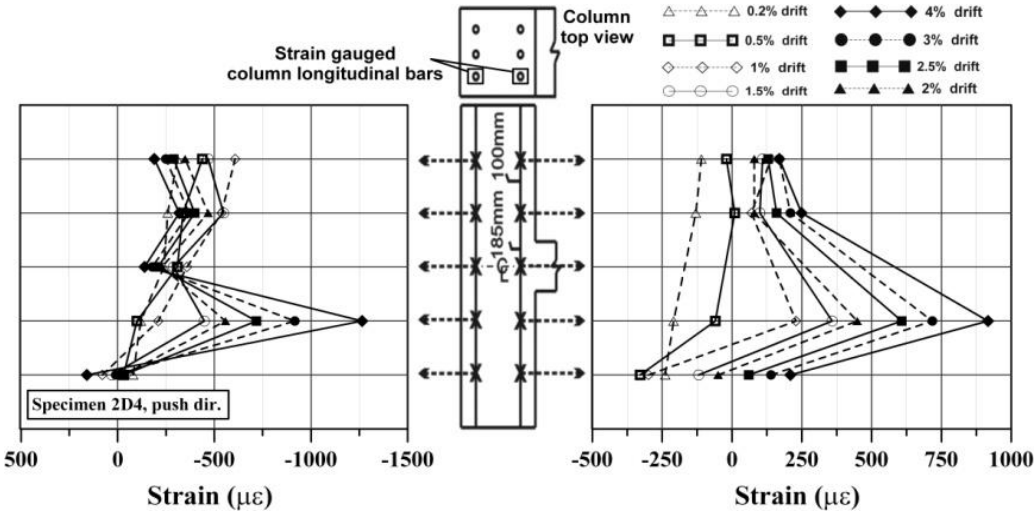

Figure 6–31 Column longitudinal bars strain profiles of Specimen 2D4 – push direction

6.3.4 Strain Demand in the GFRP Sheets

In this section, the strain demand in the GFRP sheets of the retrofitted 2D joints is examined. In Figure 6-32, the strain distribution in the horizontal GFRP sheets at peak drift values in pull direction (decreasing axial load) is presented. The reason for selecting this loading direction is that the debonding of the GFRP in 2D specimens occurred in this loading sequence during the testing of the Specimen 2D3. Following this, the strain history in the critical locations such as in the centre of the joint panel and the beam-column interface, are also given to examine the behaviour more closely.

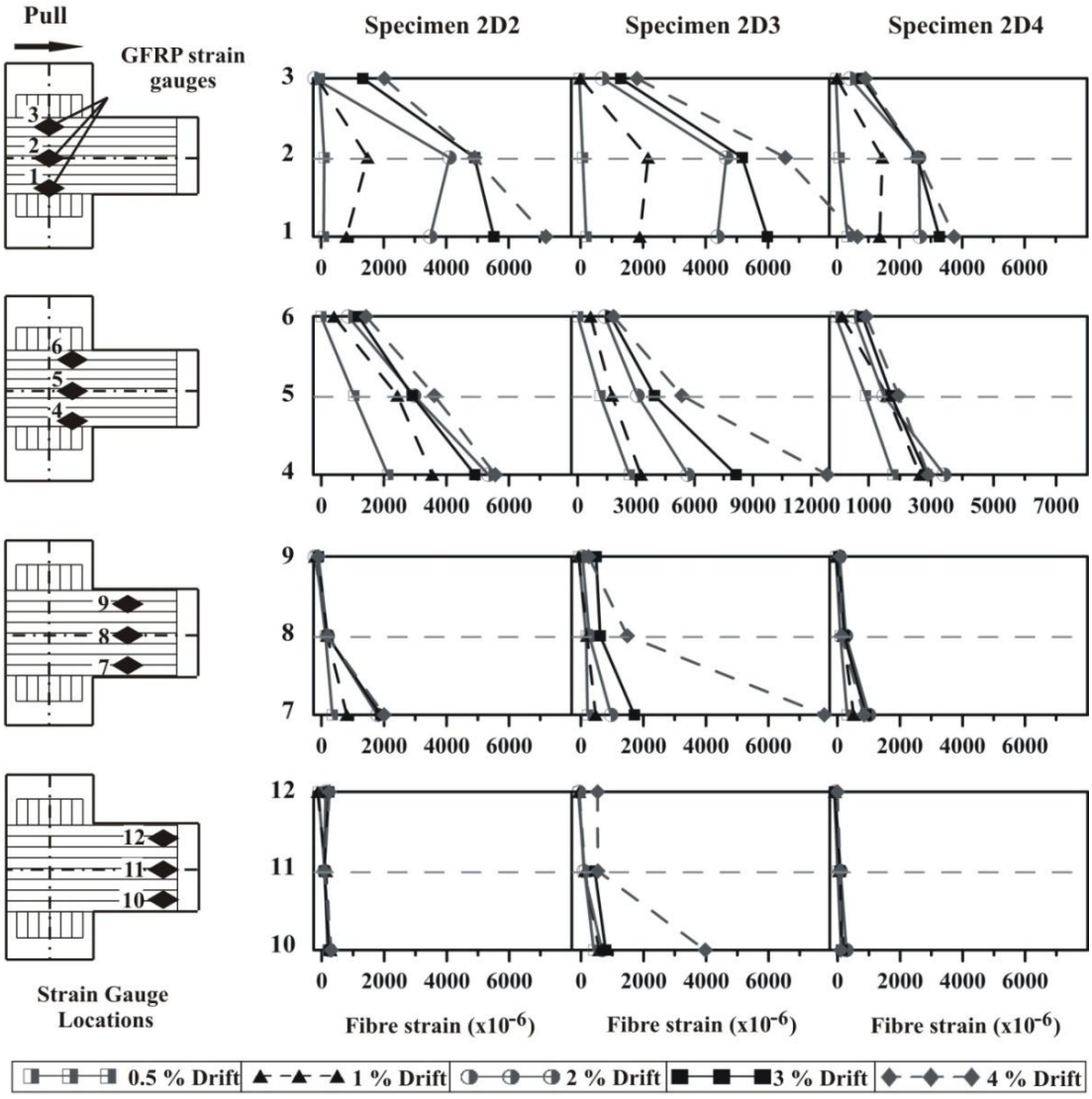

Figure 6–32 Strain distribution in the horizontal GFRP sheet of 2D exterior joints

The horizontal GFRP tensile strain profiles given for the 2D retrofitted joints show that the highest tensile strain develops in the beam-column interface. This is followed by the middle of the joint and beam sections. The strain demand in the Specimen 2D3 was the highest among the three retrofitted 2D joints. It is well recognized that debonding of the FRP from the concrete substrate depends on numerous parameters, such as material properties (both concrete and FRP) as well as geometric dimensions. The test results also showed that the retrofit scheme and the axial load variation strongly influence the debonding phenomena. For instance, in the Specimen 2D2, minor debonding initiated after 3% drift and at a strain level in the FRP of around 5000 microstrains. On the other hand, in the Specimen 2D3 gradual debonding of the FRP sheets initiated at a lower level drift (2%) with the FRP debonding strain values between 5000 to 6500 microstrains. The strain demand in the beam sheets

close to the end of the FRP laminate was observed to experience the minimum strain demand throughout the tests.

In order to track and clarify the damage propagation, the strain history of the critical regions in the joint panel is given for the Specimen 2D3 in Figure 6-33 and Figure 6-34. In the following the milestone events of the behaviour in terms of the GFRP strain history is explained briefly. Evidence through visual inspection and strain gauge readings, showed that gradual debonding of the sheets in the Specimen 2D3 started to develop at the second cycle of 2% drift and at the first cycle of 2.5% drift at the beam-column interface. Afterwards, the debonding spread under the joint panel GFRP sheet at 3% drift level. The interaction of the decrease in the joint confinement due to the low axial load levels and flexural cycles along with the increased shear force demand accelerated the deterioration of the bond between the glass fibre and the concrete. As seen in the previous section, unloading and loading after yielding of longitudinal beam reinforcement, led to a gradual build-up of permanent tensile strains. Consequently, the contribution of the steel in the flexural load carrying capacity was diminished and GFRP sheets in the joint region, as well as in the beam faces continued to carry the tension forces until debonding occurred. As soon as the debonding strain limit of 5600 microstrains for one layer of GFRP application (see Chapter 4) was exceeded in the fibre sheets, debonding occurred and the tension demand was shifted to the adjacent section. At this point, it is important to note that, the analytical bond model predictions for debonding strain value agree very well with the recorded values in the test (Figure 6-33 and Figure 6-34). In addition, this implies that the GFRP layers lose their effectiveness by early delamination from the concrete surface, rather than by reaching the tensile capacity as reported by the FRP manufacturer. For more detailed information on these issues refer to Chapter 2 and Chapter 4.

In light of these discussion and based on the experimental evidence, it was concluded that the critical section location was changing in the vicinity of the joint region depending on the damage conditions of the GFRP layers, concrete and steel reinforcement. As a result of this complex hybrid damage mechanism, in the pull direction reloading cycles of hysteresis loops, Specimen 2D3 exhibited softening which led to a typical poor energy dissipation capacity. During reloading, poor bond resistance along the longitudinal reinforcement exhibited a `pinching effect` with lower initial stiffness and significant decay in the second loading cycles.

The GFRP strain history of the Specimen 2D4 recorded and analysed at the same critical locations as in Specimen 2D3, give a similar trend of strain demand in the sheets. The highest strain values were

obtained in the beam-column interface followed by the joint centre strains. Nevertheless, no debonding was observed in these critical regions, because the strain demand remained under the debonding strain value which is predicted as 4000 microstrains for two layers of GFRP sheet application (see Chapter 4). The measured strains in the composite during the course of the testing of the specimen 2D4 were relatively small compared to that of Specimen 2D3, as shown in Figure 6-32 and in the strain history plots, Figure 6-35 and 6-36. As a consequence of enhanced joint shear strength, the weak link was shifted from the joint to the beam (change in the *sequence of events*), which resulted in the formation of a plastic hinge in the beam FRP sheet end instead of debonding in the joint.

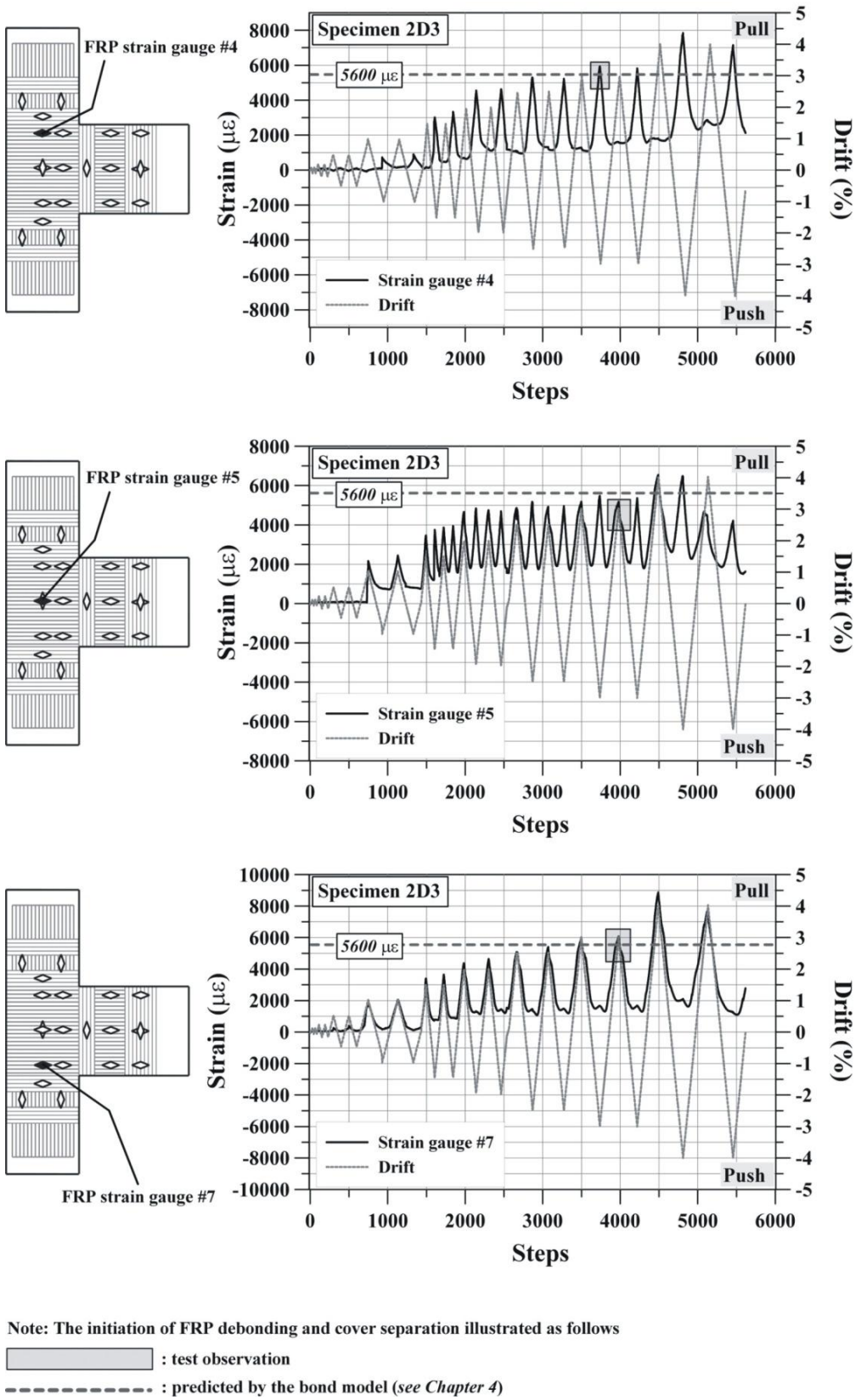

Figure 6–33 Horizontal GFRP strain profiles, Specimen 2D3, strain gauges: #4, #5 and #7

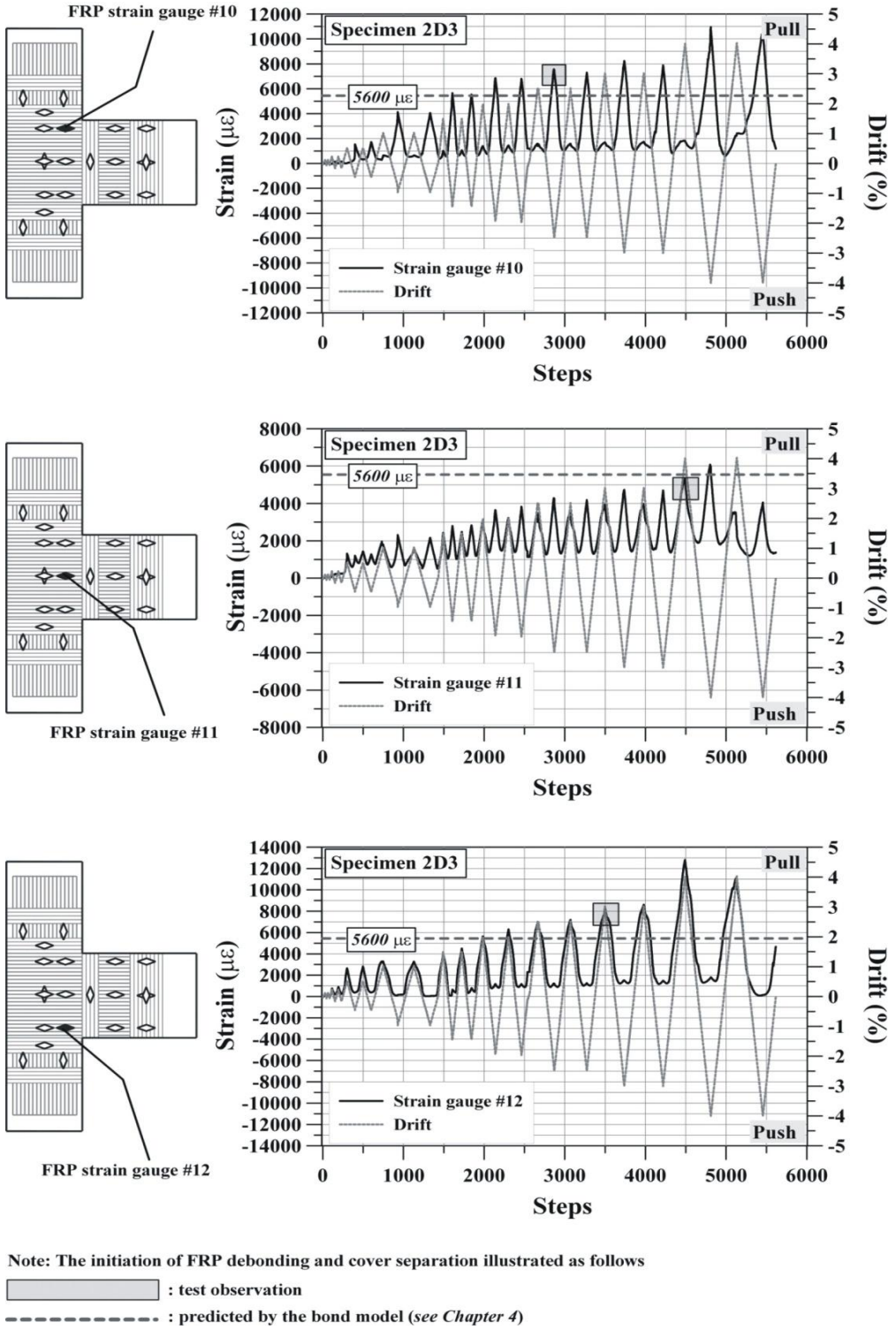

Figure 6–34 Horizontal GFRP strain profiles, Specimen 2D3, strain gauges: #10, #11 and #12

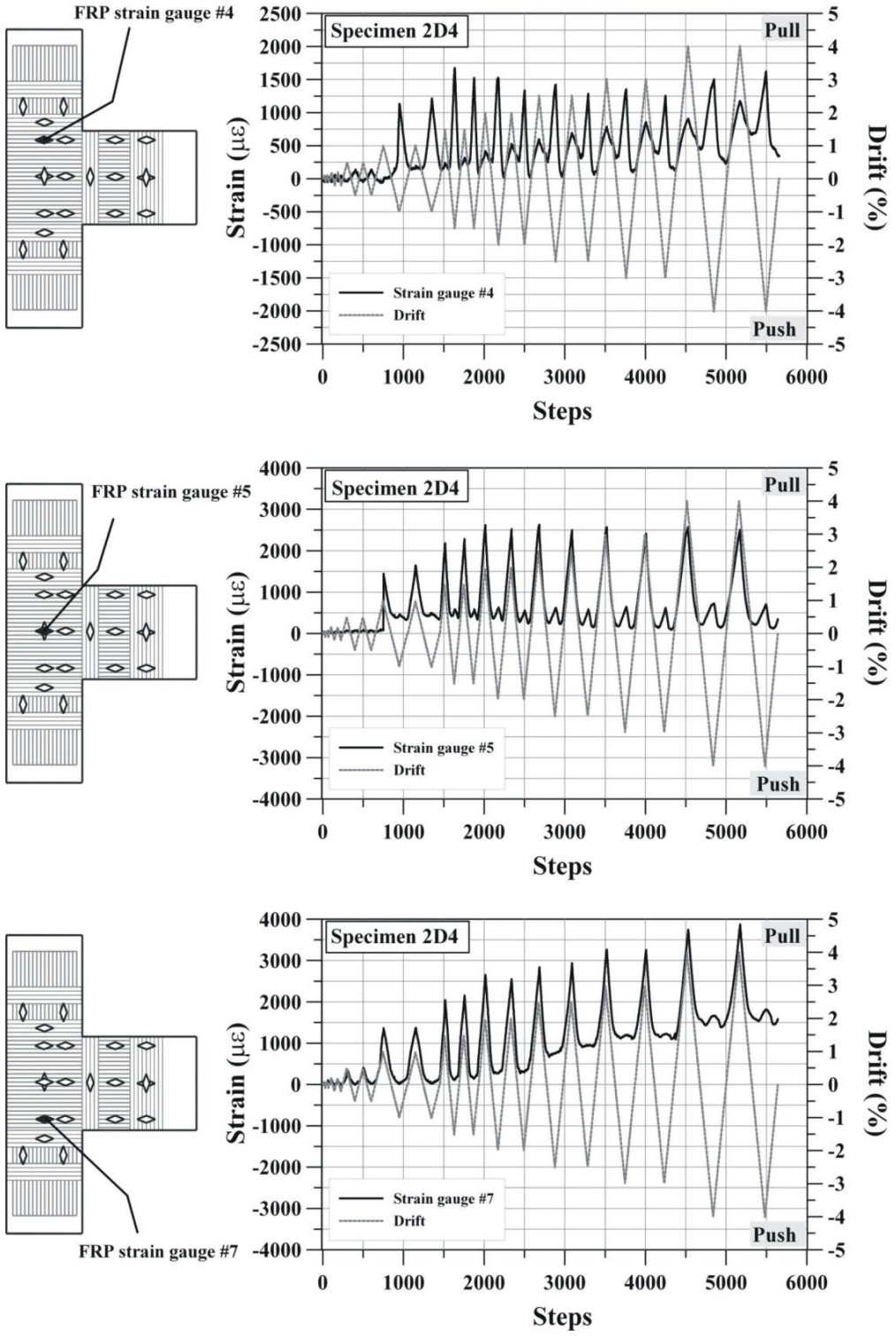

Figure 6–35 Horizontal GFRP strain profiles, Specimen 2D4, strain gauges: #4, #5 and #7

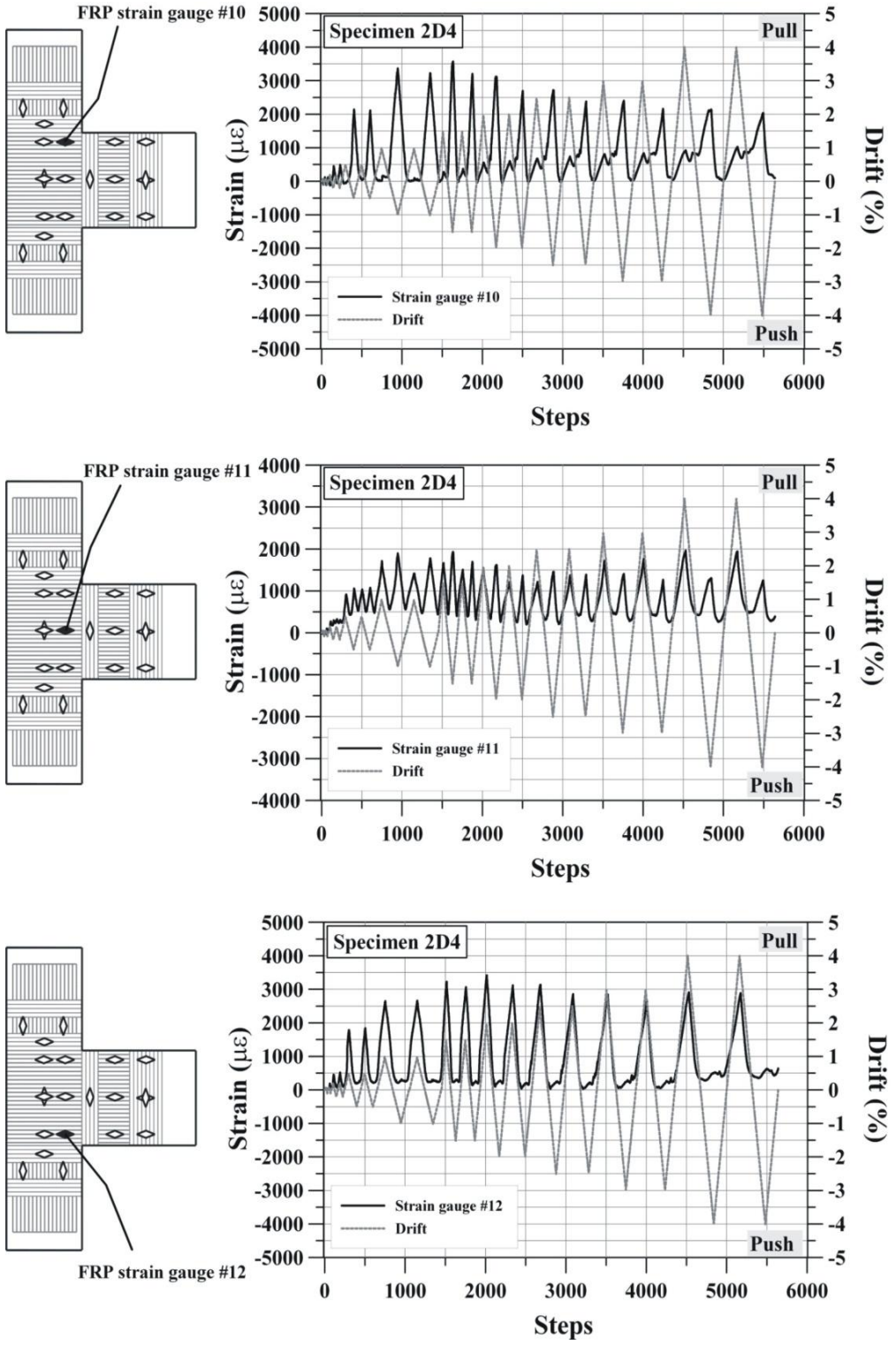

Figure 6–36 Horizontal GFRP strain profiles, Specimen 2D4, strain gauges: #10, #11 and #12

6.4 VERIFICATION OF THE PROPOSED DESIGN PROCEDURE

In Chapter 4 an analytical model and retrofit design procedure have been proposed to perform the assessment of the as-built and retrofitted section capacities and to design the appropriate retrofit intervention, which takes into account the actual demand conditions. For this purpose, the *M-N* performance domain of each specimen has been analytically evaluated (Chapter 4, Figure 4-17) and the sequence of events within the beam-column joints determined taking into account the variation in axial loads. The verification of the proposed methodology through the comparison of the experimental findings with analytical predictions is shown in Table 6-8. The comparison with experimental results not only confirms the validity of the assessment methodology and of the analytical model, but also clearly emphasises the non-conservative assumptions of retrofit design if a constant axial load was assumed.

Table 6-8 Comparison of analytical model predictions with experimental test results

Specimen	Loading		Critical Events		Analytical Results		Test Results	
	Axial Load	Direction	No	Failure Type	V_c [kN]	N_v [kN]	V_c [kN]	N_v [kN]
2D1	Varying	Pull	1	Joint shear failure	11.9	55	14.3	47
			2	Beam yielding	19.9	-	N/A*	-
		Push	1	Joint shear failure	18.2	195	19.2	194
			2	Beam yielding	19.5	-	N/A	-
2D2	Constant	Pull - Push	1	Beam yielding	18.7	-	20.2	-
			2	Beam FRP debonding	21.2	-	N/A	-
			3	Joint failure	22.4	110	N/A	-
			1	Joint FRP debonding**	17.2	30	from 20.3 to 12.8	15 50
2D3	Varying	Pull	2	Beam yielding	18.7	-	20.2	-
			3	Beam FRP debonding	21.2	-	21.0	-
		Push	1	Beam yielding	18.7	-	23.1	-
			2	Beam FRP debonding	21.2	-	22.4	-
2D4	Varying	Pull	1	Beam yielding	18.7	-	21.3	-
			2	Joint FRP debonding	20.12	-	N/A	-
			3	Column FRP debonding	23	5	N/A	5
		Push	1	Beam yielding	18.7	-	20.4	-
			2	Beam FRP debonding	22.4	-	N/A	-

* Not observed, hence the failure was governed by the previous event.
** Test values are taken at the initiation and propagation in the joint panel zone.

6.5 SUMMARY

In this chapter the experimental findings of 2D plane frame beam-column joints in as-built and retrofitted configurations are presented through the detailed examination of their failure mechanisms and behaviour. Afterwards, the effects of axial loading type on the proposed retrofit schemes and design procedure were investigated by means of global, as well as local failure modes, strength, stiffness and energy dissipation characteristics. The strain readings in the steel reinforcement and FRP sheets were also analysed and discussed to clarify the damage mechanisms and compare the performance of the specimens. Lastly, the retrofit design methodology proposed in Chapter 4 was verified through the experimental findings.

The test results of the benchmark specimen 2D1, confirmed the inherent structural inadequacies of the poorly detailed beam-column joints designed according to the non-seismic pre-1970s codes. A particular brittle mixed failure mechanism, typically referred to in the literature as the "concrete wedge mechanism" governed the overall behaviour. On the other hand, as demonstrated by the experimental evidence, a minimum retrofit scheme designed under constant load assumptions can provide satisfactory results in terms of seismic performance. However, the same scheme was proved to be an inadequate retrofit solution in the case of corner joints subjected to high fluctuation of the axial load. This was due to the high shear demand accompanied by reduced joint strength as the axial load decreased in one loading direction. As a consequence, a hybrid failure mechanism occurred consisting of gradual debonding of the GFRP sheet in the vicinity of the joint, bond deterioration and damage to the joint concrete core. Although similar ductility levels were achieved in these tests, the shift of the failure mode from ductile mode (Specimen 2D2) to a potentially more brittle mode of failure (Specimen 2D3), should not be underestimated. The lack of consideration of such a variation of axial load due to the seismic effects has to be considered a major limitation and drawback of current assessment procedures for beam-column joints.

Lastly, the proposed simplified approach and step-by-step procedure proposed in Chapter 4 was successfully verified by the experimental results. The proposed procedure can be easily adopted by designers as a powerful tool for assessment and retrofit interventions. When the designer explicitly considers the effects of the variation of axial load on the joint capacity, as illustrated in the R12 retrofit scheme (Specimen 2D4), the targeted hierarchy of strength and sequence of events can be achieved, leading to a more desirable ductile flexural mechanism.

6.6 REFERENCES

1. Park R. Evaluation of ductility of structures and structural assemblages from laboratory testing. *Bulletin of the New Zealand National Society for Earthquake Engineering*. 1989; **22**(3):155-66.

PART II

INVESTIGATION ON THREE-DIMENSIONAL (3D) CORNER RC BEAM-COLUMN JOINTS

Chapter 7 EFFECTS OF BIDIRECTIONAL LOADING ON RC BEAM-COLUMN JOINTS

7.1 INTRODUCTION

Exterior and corner columns of a frame structure are subjected to bidirectional lateral load reversals in addition to varying axial load during an earthquake. In the previous section it has been clearly seen that the interaction between the lateral loads and varying axial load should be taken into account. The problem is more serious if biaxial effects are accounted for, because significant decrease in the biaxial strength and rapid stiffness degradation may occur in the structural elements (i.e., corner columns and beam-column joints). Therefore, the inelastic biaxial interaction causes yielding and/or crushing at a load component lower than the uniaxial yield capacity. As will be demonstrated in this chapter under bidirectional excitation, in most situations the favourable effect of the lateral confinement (provided by the orthogonal and/or transverse beams) diminishes and the subsequent enhancement of joint shear capacity is no longer available. As a consequence, either for well-designed or older designed structures, the problem of designing or assessing these structural components which are subjected to bidirectional loading, imposes a great challenge to structural engineers. If these effects are not taken into account properly, disastrous results for the overall stability of the system may occur.

The intent of this chapter is to provide a general basis in understanding the behaviour of RC structures under bidirectional flexure with or without varying axial loads. Emphasis is placed on RC beam-column joint behaviour. Nevertheless, for the sake of completeness and due to the complex nature of the response and the lack of research in the area of retrofitted beam-column joints under bidirectional loading, experimental findings based on the tests conducted on RC columns along with theoretical discussions are also provided. Overall, the factors influencing the failure modes and behavioural characteristics of RC structural elements (e.g., columns and beam-column joints) under different multiaxial displacement patterns are reviewed in detail.

7.2 BIDIRECTIONAL EFFECTS ON RC STRUCTURAL ELEMENTS

Many examples of damage are found in recent earthquakes (Japan, 1978; Algeria, 1980; Italy, 1980; Greece, 1981; Mexico, 1985; Taiwan, 1999; Turkey, 1999 and 2002; and Italy, 2009) which can only be interpreted by the complex 3D behaviour of frames subjected to multi-dimensional earthquake excitations. The partial or complete collapse of RC buildings have demonstrated the vulnerability and need for retrofitting of RC corner columns and beam-column joints built without seismic considerations in order to withstand the multidirectional nature of seismic excitations and response [1-4].

In the case of 3D frames under two components of horizontal earthquake motion, corner structural elements sustain the direct sum of large axial forces from two perpendicular frames and bidirectional horizontal earthquake forces. The cyclic biaxial moment loading works in the direction of reducing the capacity of columns and joints, while increasing the deterioration of their stiffness and strength with cyclic loading. At the same time the three-dimensional character of the response of frame structures to actual earthquake motions does not introduce similar detrimental effects in the beams. It is also acknowledged that the biaxility of column moments and the three-dimensionality of the response work against fulfilling the requirement of present-day design codes to avoid collapse of RC frame structures under reversed lateral actions [5]. Due to these effects in seismic-resistant design and analysis being ignored, the performance of many RC buildings during earthquakes may differ significantly from the intended behaviour following either the current codes or adopting a given retrofit solution.

Another important point is the analyzing of the complicated inelastic behaviour of such elements under multiaxial loading effects due to the wide variety of physical phenomena involved. At the section level, such phenomenon include yielding, Bauschinger effects and buckling of the reinforcement, cracking and constitutive nonlinearity in the concrete, shear bond deterioration, and spalling of the concrete cover. Moreover in the case of beam-column joints, the presence of axial load influences the closing of cracks, the location of the neutral axis along and across the member and the plastic hinge length [6, 7]. These factors and their interaction complicate the structural response and its prediction. Clarifying the effects of biaxial bending interaction, varying axial force-bending interaction, and deterioration of beam-column joints on 3D inelastic frame response under strong earthquake excitations, is among the major concerns in the earthquake resistant design of RC frames.

The damage observed in the corner columns of Hachinohe Library in the 1968 Tokachi-oki earthquake, Oliva View Hospital in the 1971 San Fernando Earthquake, and Imperial County Services building (Figure 7–1) in the 1979 Imperial Valley earthquake, are good examples for detrimental effects of bidirectional and concurrent axial load variation. As seen in Figure 7–1a, as a consequence of significant inertia forces simultaneously developed in the two main directions (illustrated with arrows), the corner columns experienced extensive bidirectional and axial load demand. The inevitable failure occurred in the zone of the corner column where there was no adequate confinement of the concrete and no shear reinforcing steel (Figure 7–1b).

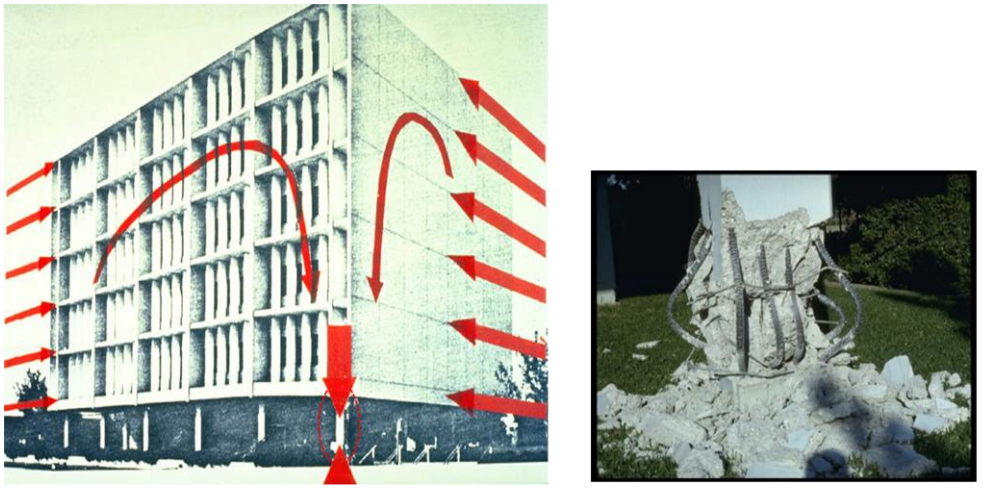

a) Imperial County Services Building – before earthquake

b) Close-up of the failure at the bottom of a corner column

Figure 7–1 Photograph of Imperial County Services building and failed corner column (Earthquake Image Information System: Karl V. Steinbrugge Collection NISEE, University of California, Berkeley)

These observations gave the impetus for many researchers to investigate the biaxial bending behaviour of RC columns [8-10]. Apart from the fact that these columns were designed to support gravity only, as these `gravity` columns did not have the detailing requirements associated with lateral force resisting system; it is noteworthy that as a general practice in the analytical or laboratory representation of space frames under earthquake excitation, a planar model of the structure was often selected and subjected to only one component of horizontal base motion. It was reported in literature that planar analyses of the Olive View Medical Centre were not successful in explaining the extent of the damage [11, 12]. Studies utilizing elastoplastic force-displacement models and hypothetical yield surfaces have indicated that inelastic interactions affected the response of these systems significantly [13]. Therefore, a detailed study was made by Aktan *et al.* [8] to investigate the response of a reinforced column to two-dimensional ground motion. For this purpose, a discrete model for the

multidimensional inelastic response analysis of reinforced concrete subjected to seismic effects was made. Case studies were conducted to compare the bidirectional and unidirectional responses of a test column, which was selected as a typical interior column of the main building of the Olive View Medical Centre. The column unit was subjected to scaled horizontal components of the 1940 El Centro, 1952 Taft, and 1971 Pacoima Dam ground acceleration records. A significant increase in the ductility requirements due to inelastic multidimensional interaction was noticed. Analysis results revealed that calculations based on one horizontal component of the ground motion in a given direction, resulting in significantly unconservative estimates of the displacement in that direction compared with that from an analysis which considers both horizontal components of the ground motion. It was also found that in the inelastic range, the calculated energy dissipation capacity and effective stiffness in a given direction were reduced significantly by the interaction with phenomena in the orthogonal direction.

In order to mitigate such problems, model building codes stipulate a strong column-weak beam design philosophy, along with the implementation of over-design factors taking into account biaxial loading in order to give appropriate redundant strength in columns. In designing ductile beam-yielding frames, special care has to be taken to avoid the excessive damage in columns caused by biaxial bending moments. Even if a beam yielding mechanism is guaranteed for one component of earthquake motion, column failure may arise under the simultaneous action of two earthquake components. Higher mode effects cause an increase in the dynamic moments and shears in columns compared to static cases, thus affecting the column over-design factor [14]. In order to prevent a plastic hinge forming in the columns, the New Zealand concrete structures standard [15] (section C2.6.5.8) stipulates these elements to be designed to sustain the maximum likely biaxial actions that can be transmitted to it by the beams from the two frames. In the same code, it is considered unlikely that the dynamic amplification of actions will occur simultaneously along both axes of a column. For this reason it is considered sufficient to design the column to sustain the overstrength actions along one axis amplified by the dynamic magnification factor (or equivalent) together with the overstrength actions from the second axis. The latter values are not amplified by a dynamic magnification factor. However, it may not be possible to achieve this ideal situation in practice due to special conditions existing at the base of a structure, the contribution of a slab to the strength of the beams, variations in axial loads, the structural system used, the presence of nonstructural elements, and of course, biaxial bending effects [16]. Therefore, careful study is required to understand the behaviour of individual columns and beam-column joints, to assess the effects this behaviour has on the structural response and to devise appropriate design and retrofit methods.

Available test results for biaxial bending under constant axial load are limited, but span over a period of almost three decades [17, 18, 6, 19-23]. Takiguchi *et al.* [18] and Kobayashi *et al.* [19] used column specimens fixed against rotation at both ends (Figure 7–2a), whereas all others used cantilever-type specimens fixed at a concrete base (Figure 7–2b). These tests have been used to verify analytical modelling of the member behaviour. Tests have generally been conducted by forcing a member to undergo controlled lateral deformations. As a matter of fact, the aforementioned tests had little in common with random deformation history of a column responding to bidirectional earthquake excitations. They were generally aimed at investigating whether the amount and detailing of confining steel required by the code for uniaxial response resulted in sufficient strength and ductility when lateral load acts at a skew angle in respect to the section principal axes.

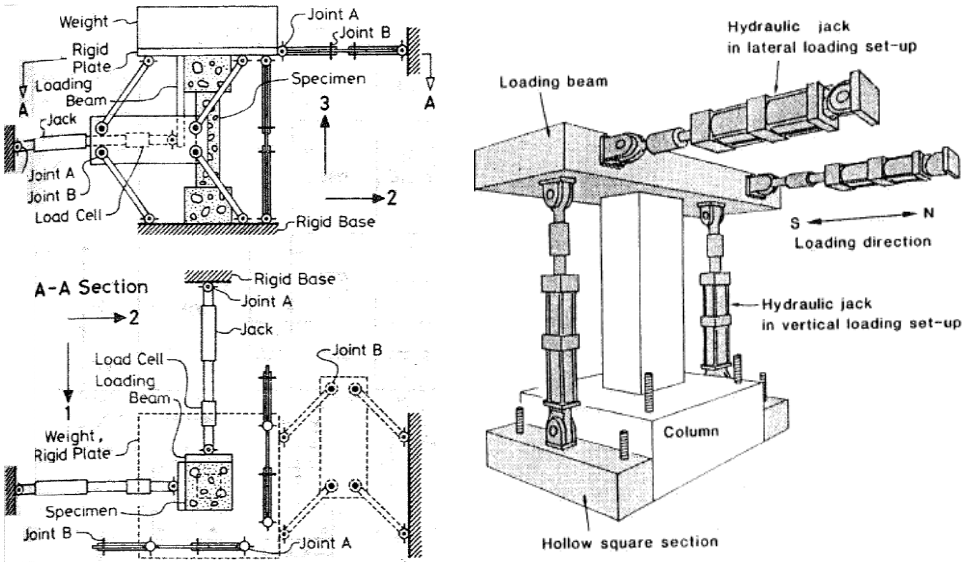

a) Test setup with column rotation at both ends are fixed (Takiguchi et al., 1980)

b) Test setup with specimen fixed at a concrete base (Saatcioglu and Ozcebe, 1989)

Figure 7–2 Typical test setups used for testing of column elements under bidirectional loading

In order to illustrate various biaxial displacement patterns employed in these tests, selected experimental works with applied biaxial displacement histories and their effects on the test results are reviewed in Appendix G.1. Furthermore, theoretical discussions are also provided regarding the calculation of flexure strength of rectangular RC columns subjected to biaxial bending in the same Appendix.

A summary of conclusions from these encompasses the following characteristics:

(1) The presence of simultaneous biaxial moments reduces the apparent yield strength along each of the principal axes of the member. Biaxial flexural loading above the yield level causes increased lateral deformation in comparison to similar members loaded uniaxially and results in permanent drifts developing at a lower amplitude,

(2) A column displaced biaxially beyond the linear response level, exhibits unstable and unusual path-dependent restoring force characteristics indicating a strong interaction between the simultaneous principal bending stiffnesses. The responses are very sensitive to the history and pattern of loading applied,

(3) In comparing the uniaxial and bidirectional response, it appears that while greater deformation demand is created in biaxial flexure, the plastic deformation capacity or ductility is reduced and may be accompanied by a reduction in hysteretic energy dissipation capacity. The increased deformation appears to be a result of accumulated damage. As a consequence, stiffness under loading in one direction decreases significantly as a result of previous or concurrent loading in the transverse direction,

(4) Locally, as a result of biaxial loading high strains may be induced at the critical section level, particularly in the corner reinforcement: such strains are greater than those obtained under strictly uniaxial loading even under similar imposed drifts at the ends. Consequently, local concentrations of damage at the critical regions will in general be higher in biaxial excitations, even under comparable global deformation demands. Conventional measures of damage developed for uniaxial cyclic loading are generally unable to quantify this type of cumulative damage [24],

(5) Individual member response to biaxial bending was shown to affect the entire structural response. As a result of biaxial effects, columns designed according to code specifications for ductile moment-resisting frames may produce structures that demand substantially more ductility than predicted by uniaxial analysis, while having less than the predicted deformability. Under biaxial loading columns may yield before beams (even in strong column-weak beam design) and the columns may be susceptible to damage [25]. Analytical studies have suggested that biaxial loading may result in increased column and decreased beam ductility demand in the frames [26],

(6) The reduction in stiffness of yielding columns may affect the overall response of a frame system because of changes to the overall stiffness and period of vibration [13]. In addition to these, initially perfectly plan symmetric structures may exhibit a torsional response as a result of bidirectional input. These asymmetric changes in lateral stiffness and resistance are accentuated by axial load fluctuations on the columns, associated with lateral response. Such fluctuations influence bidirectional strength, stiffness, cyclic hysteretic and the postultimate softening response of the members.

(7) When axial load (compression) is present with biaxial flexure, it may produce slightly higher stiffness [27], but it can overly reduce the available deformation capacity, create further magnified ductility demand and permanent drift, thus possibly resulting in collapse [26, 28, 29]. Analyses have predicted that biaxial flexure reduces the size of the axial load necessary to initiate an instability failure, particularly when deterioration of stiffness exists, and may result in a smaller margin of safety against collapse [18, 19].

(8) The actual response demand (resulting stiffness and required deformability for a given capacity) that will be developed in a three-dimensional system cannot be reliably predicted by uniaxial analysis. Since uniaxial analysis cannot simulate the column yield at a lowered moment (due to biaxial flexure and lack of beam yield), the effects of axial loads from biaxial overturning, or the induced torsion, the uniaxial analysis produces response estimates that are seriously in error [30].

(9) Some researchers also indicated that although it was shown that biaxial, rather than uniaxial, testing is important for a column suffering shear failures, the form of the biaxial displacement patterns is not significant, provided the same peak displacements were achieved [31]. It was concluded that simple orthogonal displacement patterns were found to be sufficient to represent horizontal two dimensional seismic effects.

7.3 RESPONSE OF RC BEAM-COLUMN JOINTS SUBJECTED TO BIDIRECTIONAL LOADING

Exterior three-dimensional (corner) beam-column joints were found to likely be inadequate in meeting seismic demands under bidirectional cyclic loading, because of their intrinsic higher vulnerability due to the lack of reliable joint shear transfer mechanisms. This reality has been confirmed repeatedly in past and recent earthquake events (Figure 7–3).

a) b)

Figure 7–3 Corner joint failure examples from recent earthquakes: a) 1999, Izmit/Turkey earthquake ([32]); b) 2009 L'Aquila, Italy Earthquake (courtesy of Anna Brignola)

In Figure 7–4, a typical frame structure is illustrated with two orthogonal sets of plane frames. As seen in this figure the intersecting orthogonal frames comprise of the same elements along both axes and thus are subjected to bending moments and shear forces along these two axes. The structural elements that are highlighted in the figure are subjected to multidirectional loads. During an earthquake, due to the three dimensional response of the structure, corner beam-column joints in particular experience biaxial loads with concurrent varying axial load. As a consequence of shear forces acting in more than one direction, the joint capacity would inevitably be affected and reduced due to the resultant shear stresses at any angle by simultaneous or consecutive displacements from each direction. If this occurs, corner concrete spalling and bond deterioration may occur even in well-designed joints. On the other hand, the reinforcement pull-out accompanied by more complex three-dimensional concrete wedge due to inadequate protection of the joint region may be encountered in structural elements designed without any capacity-design principles.

For the latter case, it can be argued that transverse beams provide (1) contribution to lateral confinement of joint core and enhanced bond capacity by means of longitudinal reinforcement

anchored inside the joint; (2) additional shear resistance area. It may also be presumed that for interior space frame joints biaxial loading could be less important, because of the confinement of the joint concrete on all sides by the beams framing into the column. However, as discussed later in this chapter, some researchers claim opposite views on these issues based on the experimental findings. Nevertheless, it is well recognized that in corner joints of frame, if not adequately designed against these seismic actions, unfavourable consequences may arise jeopardizing the integrity of the structure as seen in Figure 7–3. In this case the worst case scenario may be the formation of a brittle shear hinges mechanism in the corner joints.

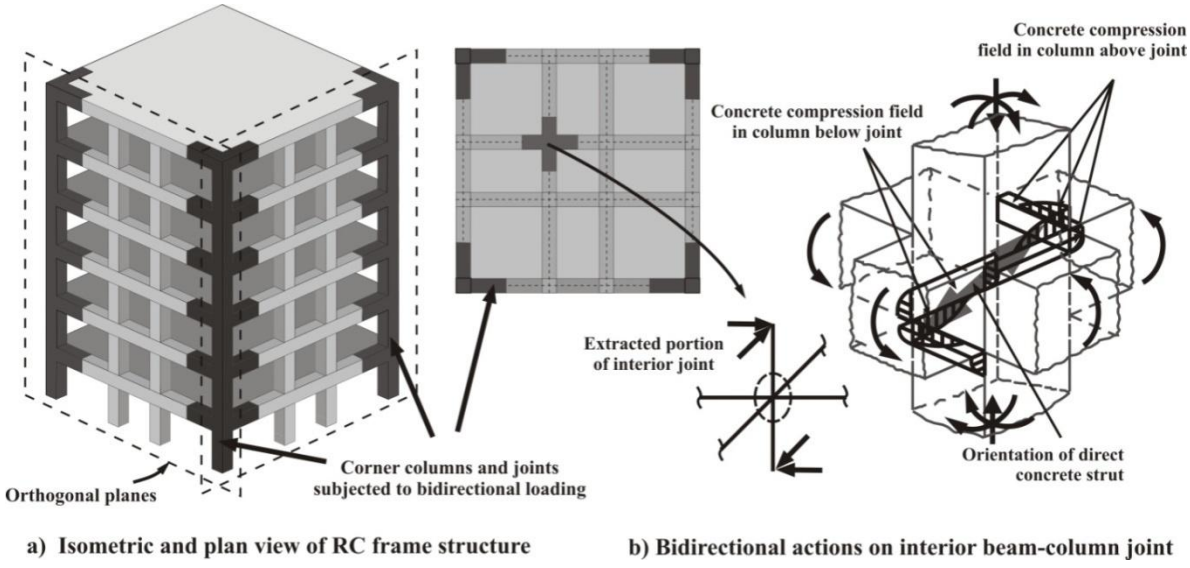

Figure 7–4 Schematic view of RC frame structure and components under bidirectional loading

When skew loading is applied to a space frame joint, the horizontal shears on the joint in each principal direction may be derived on the same basis as the horizontal shear for a plane frame joint. The vertical shear may be calculated by assessing the forces to one side of a vertical plane through the plan diagonal of the joint. If the beams in the two directions form plastic hinges adjacent to the joint core simultaneously due to skew loading, and if the beams are similar, it is evident that the applied horizontal shear force along the diagonal is $\sqrt{2}$ times that which is applied along a principal axis of the section if only plane frame action occurs [33].

In order to illustrate the resistance mechanisms of space frame joints in general, an extracted portion of an interior joint without the floor slab from a frame structure is schematically presented in Figure 7–4b. The mechanisms of resistance in a space frame joint under bidirectional loading is likely to be similar to that described for plane frames in Section 3.3 of Chapter 3. However in this case, the

orientation of the critical planes is different [34]. The complex nature of compression struts can be seen in the figure. Stress concentrations at each end of the diagonal struts could develop at six faces of joint core approximately across diagonally opposite corners.

A truss mechanism was also postulated by Beckingsale [33] by means of which horizontal and vertical reinforcement may be utilised to combine with concrete struts, to resist joint shear introduced around the exterior surface of a space frame joint. However it was noted that due to the orientation of critical planes between opposite corners of the joint cuboid, conventional joint ties will not be as effective in resisting a component of skew joint shear as they are for uniaxial shear. In this case, it was suggested that ties placed diagonally (that is with a diamond—shaped orientation relative to the joint cross section) will tend to carry skew shear more efficiently. When shear reinforcement in the joint is insufficient, a diagonal failure plane could develop. Based on these considerations, it can be deduced that more joint reinforcement might be required than for unidirectional loading for well-designed joints. With the same line of thought, in the case of retrofitted corner joints a modified or upgraded version of FRP retrofit design may be necessary. This issue is one of the topics investigated in this thesis and discussions regarding this issue are provided in Chapter 9.

For the design of corner joints, Paulay and Priestley [34] suggested to consider two truss mechanisms acting simultaneously at right angles to each other, which enable the joint shear to be considered separately in each of the two principal directions. In this way, all tie legs in the joint may be utilised. However, it was noted that it would be inappropriate to assume that full contribution of the axial compression to joint shear strength would exist simultaneously in both diagonal compression fields in perpendicular planes. In order to take into account the beneficial effects of axial compression an approximation was made by replacing the actual compression load with a factored one. With this reduced effective axial load, the required joint shear reinforcement in two principal directions may be independently calculated as for one way frames. Joints so designed performed very satisfactorily when subjected to testing simulating bidirectional earthquake attack [35].

Bresler [36] and Furlong [37] analysed square columns loaded in two principal axes by moments in the x and y direction and axial compression. Bresler proposed a simplified equation for the interaction of principal axis moment capacity on a plane of constant axial load. Using these equations Furlong generated the surface failure under different axial load levels for square columns. Based on analytical and experimental studies it was shown that the moment capacity in square columns is lower about the non-principal axis (see Appendix G.2. for more information). In a similar fashion, in order to

investigate the interaction between the strength of the joint in each direction Trowland [38] performed an analytical study to constitute a failure surface for beam-column joints. However, it is important to note that the interaction relationships derived by Furlong [37] are for flexural strength and not shear strength. Significant joint shear interaction effects will arise due to the acting of joint shears in more than one direction which in turn lead to a reduction in shear strength in one direction. The mechanisms involved in column and joint elements are quite different and the analogy is only useful for making a rough guess of the possible interaction relationship. In this preliminary work Trowland first studied the relationship between the moment and rotation of joint in plane frames to simulate the joint behaviour. In the next stage he attempted to propose a theoretical model for the behaviour of a joint subjected to biaxial loading. For this purpose several uniaxial tests of space frame interior joints were collated to find the strength along the principal axis. Afterwards, several biaxial tests were collated to find the strength along an axis 45 degrees from the principal axis. Based on the experiments done by Lean and Jirsa [39] on a series of reinforced beam-column joints, Trowland [38] proposed values of the power factor (see Appendix G, eq. G-2) m = 1.3-1.4 to be used for interaction exponents.

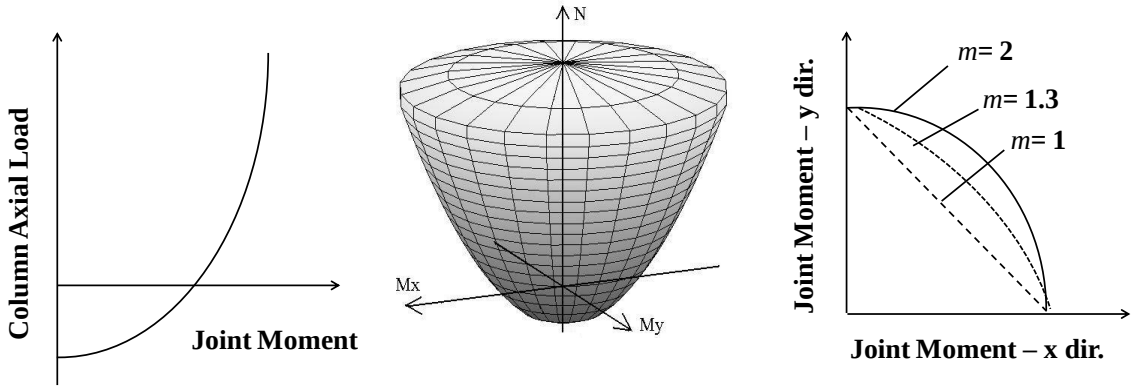

Figure 7–5 Axial force and biaxial moment interaction surface for beam-column joints proposed by Trowland [38]

When dealing with under-designed columns or beam-column joints more rapid reduction of flexural or shear strength may occur. As a consequence, the hierarchy of strength and sequence of events in corner beam-column joint subassemblies would be more drastically affected by biaxial and concurrent varying axial loadings. As noted previously, when underestimating or overlooking such effects, significant modification to the response could be derived, with the likely undesirable effects of impairing the efficiency of an expensive retrofit intervention. For this reason it is of great importance to acquire information on the possible effects of multiaxial loading conditions through testing of space frames. The behaviour of beam column joints in plane frames under seismic loading has been extensively investigated by experimental testing since the 1960's. Most of these studies were

undertaken with the aim of verifying the design of space frame joints, there has been far less experimental investigation into the behaviour of under-designed beam column joints in space frames either in as-built or retrofitted configurations. A summary of significant experimental studies on the behaviour of well-designed beam-column joints subjected to bidirectional loading is reported in Appendix G.3.

7.4 RESEARCH ON PRE-1970S 3D BEAM-COLUMN JOINTS TESTED UNDER BIDIRECTIONAL LOADING

Three two-third scale space frame corner beam-column joint subassemblies were constructed and tested under cloverleaf biaxial loading protocol by Hertanto [40] and Chen [41] to investigate the biaxial loading effect in the Structural Laboratory of the University of Canterbury. All of the units have identical dimensions between the mid-span of the beams and the mid-height of the columns of a common four-storey existing reinforced concrete frame structure constructed before the 1970s. The two specimens were deep-deep beam-column corner joint (DD1 and DD2) and the other one was deep-shallow beam-column column corner joint specimen (DS1). Plain round longitudinal bars were used for all units with hook anchorages. Specimens DD1 and DS1 had no transverse reinforcement in the joint region whereas one single joint transverse reinforcement placed in specimen DD2. Specimens DD1 and DD2 had identical beams in both x and y directions. The beams were 330 mm in depth and 200 mm in width and the column was 230 mm square with a total height of 2000 mm. The beams were symmetrically reinforced, contained four 10 mm diameter Grade 300 plain round bars in the top and in the bottom, respectively. Unit DS had a deep beam in x-direction and shallow beam in y-direction. The surface of the shallow beam was at the same level as the deep beam, which means that the centreline of the shallow beam was above the centreline of the deep beam. Columns of all specimens were the same. They were symmetrically reinforced on the y-direction, containing three 10 mm diameter Grade 300 plain round bars on both sides. Results from the tests confirmed the evidences from earthquake damage observations that the exterior 3D (corner) beam-column joint subjected to biaxial loading would have less strength and suffer higher damage in the joint area under earthquake. All units were tested under varying axial load to simulate the column behaviour in the real structure under earthquake loading.

Specimens DD-1 and DD-2, with deep beams in both the x- and y-directions, exhibited poor performance compared to their plane frame counterparts. For both units strength degradation was observed after joint cracking at 1% drift due to a loss in bond strength and bar slipping, which can be

seen in the hysteresis loops of the units given in Figure 7–6. As observed in the plane frame specimens (see section 2.3, chapter 2), the concrete wedge formed in the joint region, because the tension forces from the beam longitudinal reinforcement were not transferred properly to the joint core, but concentrated in the hook anchorages. It was noted that the single transverse reinforcement in the joint region provided in Specimen DD1 was insufficient in preventing joint diagonal crack formation. However, it was observed that in Specimen DD-2 the joints' first cracking occurred when the principal tensile stress in the joint reached $0.2\sqrt{f_c'}$ up to $0.3\sqrt{f_c'}$, higher than $0.18\sqrt{f_c'}$ observed in Unit DD-1. Final crack patterns and force-displacement curves for these specimens are given in Figure 7–6. Poor overall performance of the unit DS with shallow beam was also reported. The shallow beam could only resist about 50% of the lateral load from the deep beam. As observed in the previous units, the use of plain round longitudinal reinforcement caused loss in bond strength and the bar slipping, which can be seen in the pinching of the hysteresis loop. Researchers observed that in the direction of the joint which was very congested due to the amount of beam longitudinal reinforcement anchored in the column, cracks formed in the joint, but there was no severe spalling of concrete due to confinement provided by the shallow beam in the transverse direction. Based on the test results, researchers proposed a certain amount of strength reduction has to be considered when assessing space frame beam-column joints. In terms of global lateral strength, a 25% reduction was proposed as a reasonable value from the experimental results, while a 40% reduction was proposed for joint principal tensile stress.

At this point, it is interesting to note that, other than the authors' work [3], only two other published research papers were found on the response of FRP retrofitted corner beam-column joints under bidirectional loading. One of these two experimental research was conducted to examine the behaviour of CFRP retrofitted full-scale corner beam-column joint units with slabs [4]. Bidirectional loading was simulated by vertical loading in the beam tips. Axial load was kept constant. The second research programme was performed on a full-scale three-story framed structure in as-is and retrofitted conditions by Di Ludovico *et al.* [42] under bidirectional pseudo-dynamic (PsD) loading. The behaviour of the retrofitted corner beam-column joints was indirectly deduced from these tests. An extra research performed by Balsamo *et al.* [43] is also presented for the sake of completeness. However, note that in this experimental study uniaxial earthquake excitation was implemented. In the following sections these studies are examined in detail.

a) Damage after test – Spc. DD-1

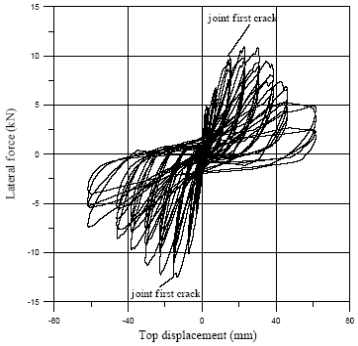

b) Force-displacement loops (*x-dir.*) – Spc. DD-1

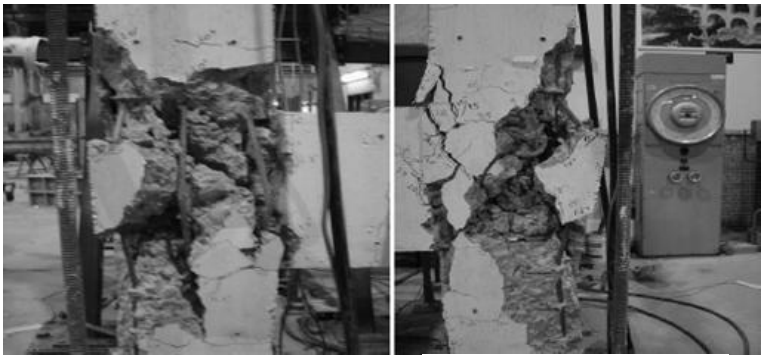

c) Damage after test x-dir. – Spc. DD-2

d) Damage after test y-dir. – Spc. DD-2

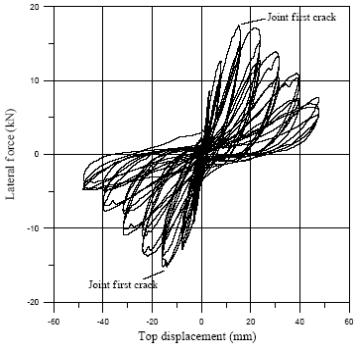

e) Force-displacement loops (*x-dir.*) – Spc. DD-2

Figure 7–6 Experimental study on 3D exterior (corner) beam-column joints subjected bidirectional loading (by Hertanto [40] and Chen [41]): Crack patterns after tests and force-displacement loops

Engindeniz [4] investigated the seismic response of pre-1970 RC corner beam-column joints and the efficacy of carbon fibre-reinforced polymer (CFRP) composites for both pre- and post-earthquake retrofit of such joints. A total of six tests were conducted on four specimens that were built to represent pre-1970 design and construction practices. All specimens were identical in member sizes and steel reinforcement detailing. Prior to the cyclic loading of the beams, a column axial load of 10% of the column's compressive load capacity was applied. The beams were then cycled around this deformed position at displacement levels corresponding to ±0.93%, ±1.40%, and ±1.87% interstorey drift ratios. Specimen details, loading regime and test setup are given in Figure 7–7.

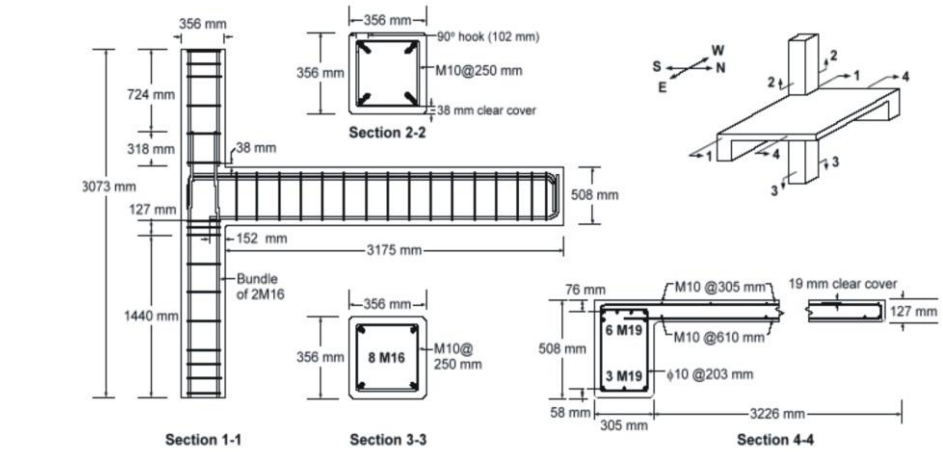

a) Specimen details

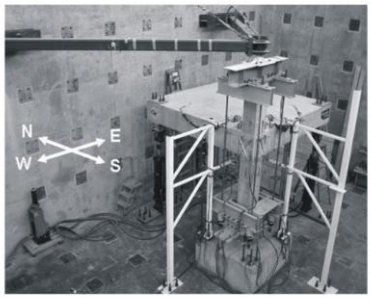

b) Test setup

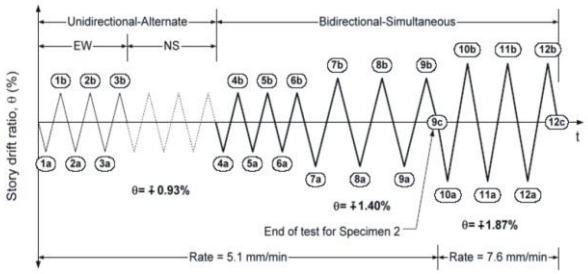

c) Loading protocol

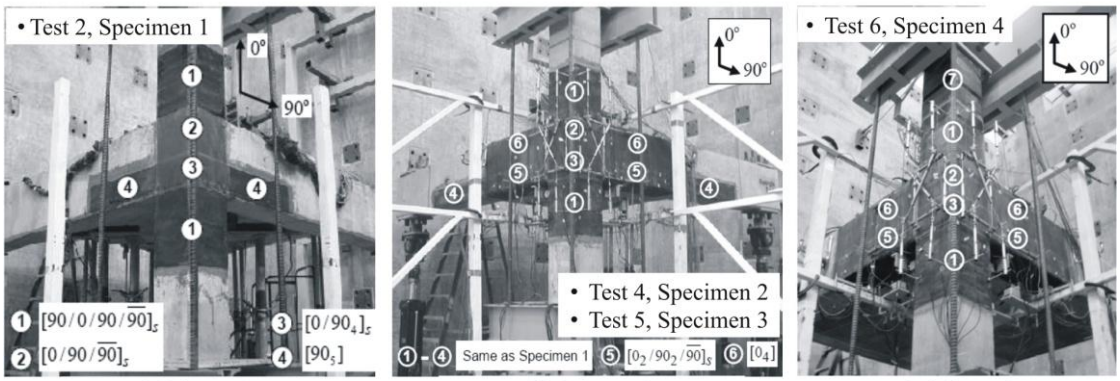

a) Scheme 1 b) Scheme 2 c) Scheme 3

d) Three different retrofit schemes with layup sequence

Figure 7–7 Experimental study by Engindeniz [4]

Two of the specimens, Specimen 1 and 2, were first subjected to severe and moderate levels of damage respectively, then repaired by epoxy injection, and strengthened by adding a #7 (22 mm diameter) reinforcing bar within the clear cover at the column inside corner and by externally bonding multiple layers of carbon fabric to form a carbon-epoxy retrofit system. Two other specimens, Specimen 3 and 4, one of which had a significantly lower concrete compressive strength, were

strengthened in their as-built condition. The CFRP scheme (Figure 7–7) was improved in light of the findings as the experimental programme progressed.

Test results (Figure 9-8) indicated that pre-1970 RC corner beam-column joints were found to be severely inadequate and susceptible to severe damage even at drift levels lower than those envisioned to occur during typical design earthquakes (i.e., ~2%). No effective energy dissipation mechanisms could be developed. Bidirectional loading played a significant role in the poor response which lead to the loss of stiffness and strength that dominate the behaviour even at relatively low interstorey drift levels. It was suggested that for the future design and analysis of corner joints the following points should be taken into account (1) the reduction in the biaxial capacity of the column due to anchorage and section losses; (2) the increased and non-uniform distributed strains in the beam bars due to forces created by the slab; and (3) the increase in the horizontal joint shear force. It was shown that such joints can be strengthened both before and after earthquake damage by using CFRP composite schemes. Regardless of the level of existing damage and concrete strength, a “rigid” joint behaviour up to interstorey drift ratios of at least 2.4% and joint shear strength factors ranging from 1.06 to 1.41 MPa were achieved. A ductile beam hinging mechanism was achieved and energy dissipation capacity was improved efficiently for joints with concrete strengths ranging from 26 to 34 MPa. However, a significant reduction was observed in the performance of Specimen 4, where concrete had a low strength (15 MPa). The formation of beam hinging did not occur due to low overall stiffness and reduced reinforcement anchorages.

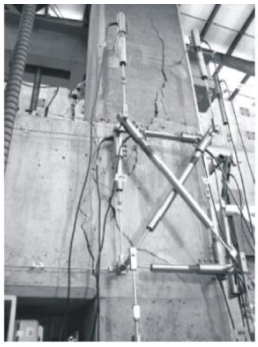

a) Test 1

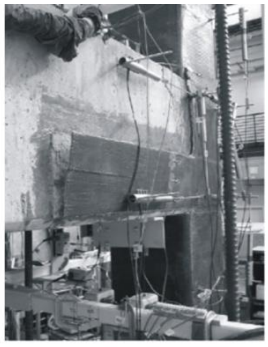

b) Test 2

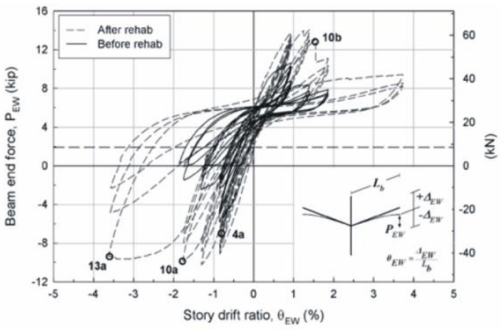

c) Force-drift hysteresis loops (Test 1 & test 2)

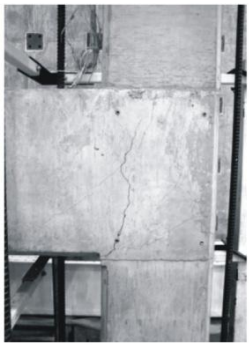

d) Test 3

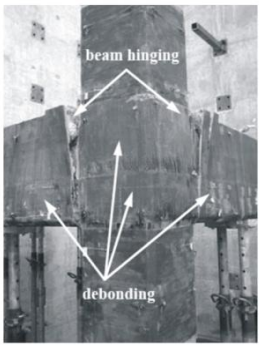

e) Test 4

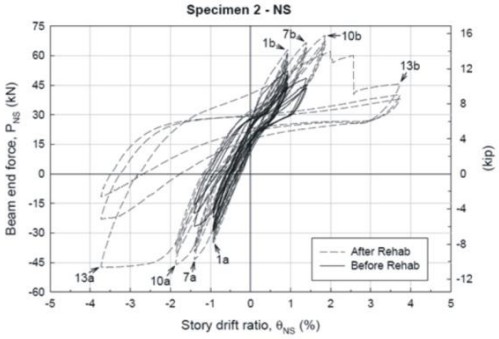

f) Force-drift hysteresis loops (Test 3 & test 4)

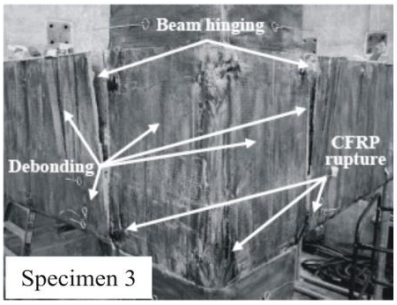

g) Test 5

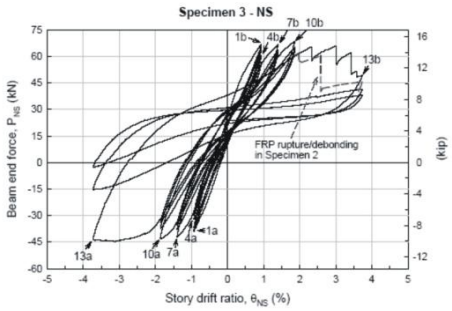

h) Force-drift hysteresis loops (Test 5)

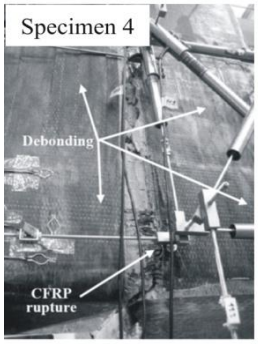

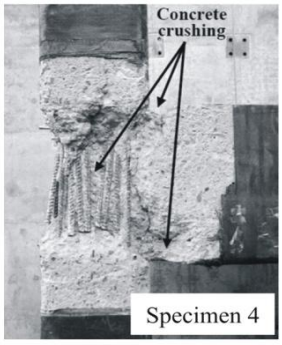

i) Test 6

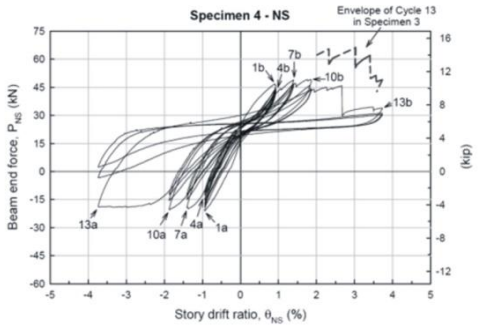

j) Force-drift hysteresis loops (Test 6)

Figure 7–8 Test results of experimental study by Engindeniz [4]

In order to evaluate the opportunity of using composite materials as an effective technique for the seismic retrofit of RC frames Di Ludovico *et al.* [42] performed experimental and analytical studies on a full-scale three-story RC frame structure. The full-scale RC structure was subjected to a bi-directional pseudo-dynamic (PsD) test in the ELSA laboratory of the Joint Research Centre (JRC) in Ispra (Italy) under the Montenegro Herceg Novi record scaled to peak ground acceleration (PGA) of 0.20g. The plan layout and the 3D view of the structure after the construction are shown in Figure 7–9.

The seismic deficiencies exhibited by the structure after the test were confirmed by post-test assessment of the structural seismic capacity performed by nonlinear static pushover analysis implemented on a lumped plasticity model of the structure. In order to allow the structure to withstand 0.30*g* PGA seismic actions, a retrofit using glass fibre-reinforced polymer (GFRP) laminates was designed. The retrofit design was targeted to achieve a more ductile and energy dissipating global performance of the structure by increasing the ductility of columns and preventing brittle failure modes. More detailed information on design assumptions and criteria along with nonlinear static pushover analysis to assess the overall capacity of the FRP-retrofitted structure can be found in Di Ludovico *et al.* [42].

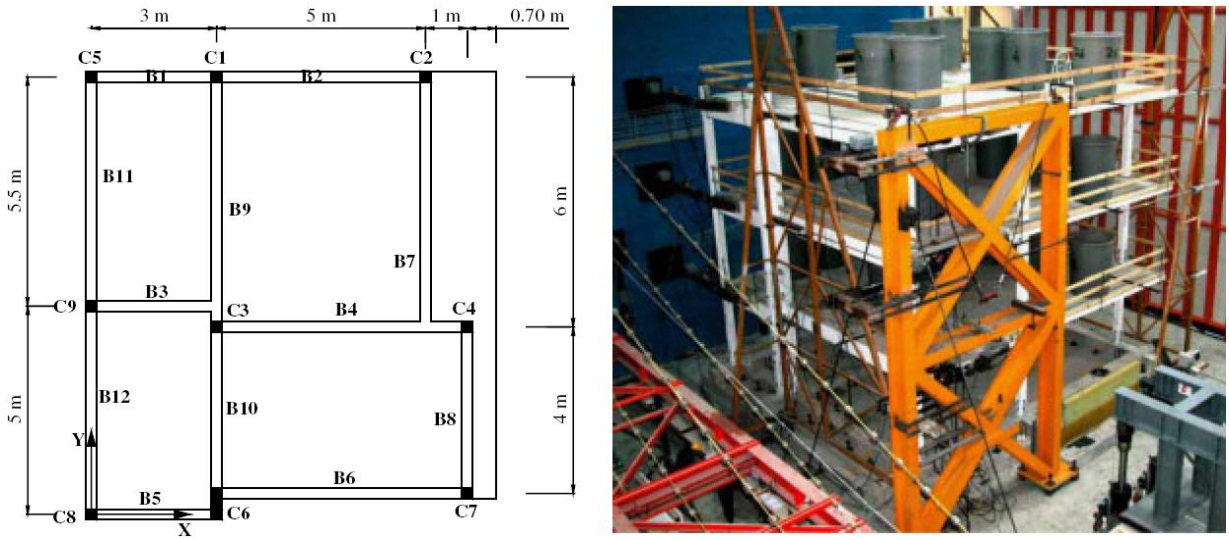

Figure 7–9 Experimental study by Di Ludovico *et al.* [42]: Plan layout and 3D view of the structure

The results of the first test, which was conducted under a PGA value of 0.20*g*, showed that the major damage concerned the ends of the square columns with crushing of concrete at all storeys. The level of damage was more significant at the second story. For each floor, the most damaged members were the columns, where torsional effects produced inclined cracks on the compressive sides. During tests, significant cracks opened on the tensile side of the columns at the beam–column interface.

A brief description of the retrofit sequence is given. Prior to laminates installation, unsound concrete was removed and restored using non-shrinking mortar. In addition, all cracks caused by the first round of testing were epoxy injected. Then, according to the design of the retrofit, the eight square columns were all confined at the ends by using two plies of GFRP uniaxial laminates, each with a unit weight of 900 g⁄m^2. At each storey, GFRP confinement was extended for 800mm from the beam–column interface. In some cases, this length was increased up to 1000mm to account for more extended concrete damage. Beam–column joints corresponding to the corner square columns were strengthened using two plies of quadriaxial GFRP laminates each having a unit weight of 1140 g/m2. This joint reinforcement was extended on the beams by 200mm on each side in order to U-wrap it and to ensure a proper bond. The joint strengthening intervention scheme along with the joint internal and external view after the retrofit is presented in Figure 7–10.

Figure 7–10 Experimental study by Di Ludovico *et al.* [42]: Column confinement and shear strengthening of exterior joints

Once FRP retrofitted, the structure was first tested with a PGA level of 0.20*g*, to have a direct comparison with the previously executed experiment, then with a PGA level of 0.30*g*. The experimental activity showed that the retrofitting intervention provided the structure with a very significant enhanced deformation capacity with respect to the ‘as-built’ configuration, which almost totally lacked the appropriate capacity to resist even the 0.20*g* PGA level of excitation. After the vertical elements and the joints were wrapped with glass fibres, the retrofitted structure was able to withstand the higher (0.30*g* PGA) level of excitation without exhibiting significant damage. After

tests, the FRP was removed and it was shown that the RC core was neither cracked nor damaged (Figure 7–11).

In summary, the experimental results highlighted the effectiveness of the FRP technique, which was designed according to the Italian guideline CNR-DT 200/2004, in improving the global performance of under-designed RC structures in terms of ductility and energy dissipation. The main goal of confining the column ends and preventing brittle mechanisms (i.e., exterior joints and rectangular column shear failure) was successfully achieved.

Figure 7–11 Experimental study by Di Ludovico *et al.* [42]: Column damages

Balsamo *et al.* [43] assessed the efficiency of the use of CFRP composites for the seismic repair of RC concrete structures on a full-scale dual system subjected to pseudo-dynamic tests. The structure consisted of two frames; one designed according the Eurocode 8 and the other according to deformation-based design method proposed by Fardis and Panagiotakos (Fardis and Panagiotakos, 1997). The dimensions of the structure are given in Figure 9-12. Two tests were performed on the original structure: the first under the design earthquake and the second under the design earthquake times 1.5. The failure of the original specimen was due to shear collapse of some shear walls, due to insufficient anchor length in the horizontal bars. After the damage, the structure was repaired using CFRP laminates and then subjected to a new series of two tests with the same input accelerogram used for the original. The main aim of the CFRP repair was to recover the structural properties that the frame had before the seismic actions by providing both columns and joints with more deformation capacity. More detail on the basis of the CFRP repair regarding the joints, columns, walls and beams can be found in Balsamo *et al.* [43]. The final appearance of CFRP wrapping of the structure is given in Figure 7–12.

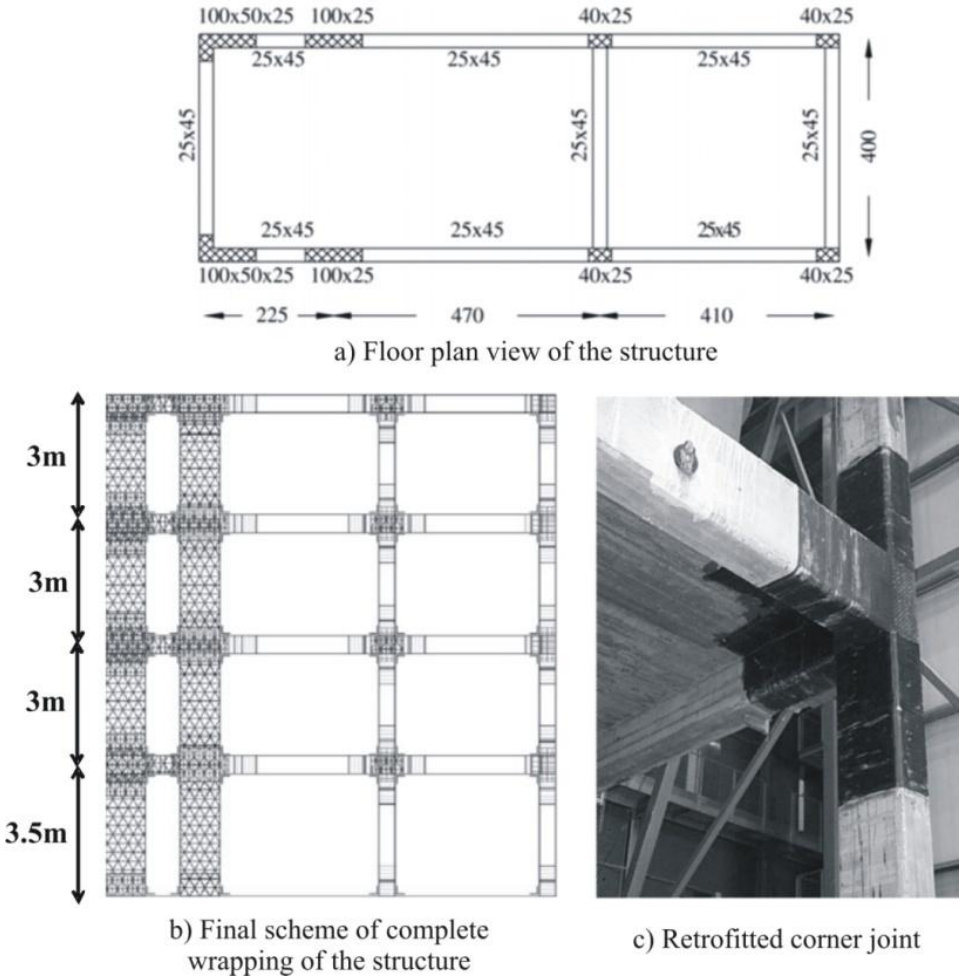

a) Floor plan view of the structure

b) Final scheme of complete wrapping of the structure

c) Retrofitted corner joint

Figure 7–12 Experimental study by Balsamo *et al.* [43]

7.5 SUMMARY

Results from all these studies clearly show that simultaneous multiaxial loading can significantly change the nature of the seismic response of structures from what would be predicted using a uniaxial view. Simultaneous biaxial ground motion combined with axial load variation has a considerable effect on the behaviour.

In a global sense, these effects govern the location and the manner of inelasticity developed in a structure that can result in a change in mode of response of the building system. In the case of multiaxial earthquake excitations the corner columns and also joints are induced by high response demands, while the capacities of members are decreased, relative to their uniaxial values, by the simultaneous loads. In light of these reflections and gained information, the current code-based practice of estimating seismic response demands for design, employing independent planar frame

analyses along a building`s principal axes is deemed to be an inadequate method because it ignores all the demand increases that occur in the three dimensional response.

Almost all the works cited previously were basically focused on the need either to produce design guidelines for, or to check the performance of beam-column joints designed according to modern building codes. As a consequence, a significant amount of information has been gathered to improve the seismic behaviour of interior as well as exterior beam-column joints with or without slabs. On the other hand, it is also recognized that there is a substantial lack of information and experimental investigation on the seismic behaviour of substandard beam-column joints. For a clear understanding of these effects and for the establishment of rational design provisions, it seems essential to add test data on the behaviour of beam-column joints in two-way framed structures subjected to bidirectional loading reversals. In addition, there is a strong need for research to resolve the question of the efficiency of the FRP retrofitting technique used to strengthen the under-design corner beam-column joints subjected to multiaxial loading conditions.

7.6 REFERENCES

1. Okada T, Murakami KU, K., Nishikawa T, Tanaka H. Analysis of the Hachione library damaged by '68 Tokachi-oki earthquake. *Transactions of the Japan Concrete Institute*. 1970; **167**:47-58.
2. Zeris CA. Three dimensional nonlinear response fo reinforced concrete buildings. *PhD Dissertation*, University of California California, 1986.
3. Pampanin S, Akguzel U, Attanasi G. Seismic upgrading of 3-D exterior R.C. beam column joints subjected to bi-directional cyclic loading using GFP composites. *FRPRCS-8*, Patras, Greece, 2007.
4. Engindeniz M. Repair and strengthening of pre-1970 reinforced concrete corner beam-column joints using CFRP composites. *PhD Dissertation*, Georgia Institute of Technology, Atlanta, 2008.
5. CEB. *RC frames under earthquake loading*. Comite Euro-International du Beton, Bulletin d`Information: Paris, 1996.
6. Otani S, Cheung CH. Behaviour of RC columns under biaxial lateral load reversals. *Publication 81-02*, University of Toronto, Canada, 1981.
7. Abrams DP. Influence of axial force variations on flexural behavior of reinforced concrete columns. *ACI Structural Journal*. 1987; **84**(3):246-54.
8. Aktan E, Pecknold DA, Sozen MA. R/C column earthquake response in two dimensions. *Journal of Structural Division, ASCE*. 1974; **100**(ST10).
9. Selna LG, Morill KB, Ersoy OK. Earthquake response analysis of the Olive View hospital psychiatric day clinic. *Earthquake Engineering and Structural Dynamics*. 1974; **3**(1):15-32.
10. Okada T, Seki M, Asai S. Response of reinforced concrete columns to bi-directional horizontal force and constant axial force. University of Tokyo1976.
11. Aoyama H, Sozen MA. Dynamic response of a reinforced concrete structure with tied and spiral columns. *Proceedings of 5th World Conference on Earthquake Engineering*, Rome, Italy, 1973.

12. Chopra AK, Bertero VV, Mahin SA. Response of the Olive View Medical Center main building during the San Fernando earthquake. *Proceedings of 5th World Conference on Earthquake Engineering*, Rome, Italy, 1973.
13. Nigam N. Inelastic interactions in the dynamic response of structures. *EERL 67-64*, Earthquake Engineering Research Laboratory, California Institute of Technology, Pasadena, Calif., 1967.
14. Shibata A. Inealstic response of 3-D structures and multi-dimensional seismic forces on structural components. *Proceedings of Ninth World Conference on Earthquake Engineering*, Tokyo-Kyoto, Japan, 1988.
15. NZS 3101:2006. *Concrete structures standard NZS 3101*. Standards association of New Zealand, Wellington, 2006.
16. Mahin SA. Inelastic behavior and modelling of reinforced concrete columns under multidirectional seismic excitations. *Proceedings of Ninth World Conference on Earthquake Engineering*, Tokyo-Kyoto, Japan, pp. 519-30, 1988.
17. Takizawa A, Aoyama H. Biaxial effects in modeling earthquake response of R/C structures. *Earthquake Engineering and Structural Dynamics*. 1976; **4**(6).
18. Takiguchi K, Kokusho S, Kobayashi A, Kimura M. Response of RC column to horizontal bi-directional deflection history. *Proceedings of 7th World Conference on Earthquake Engineering*, Istanbul, Turkey, 1980.
19. Kobayashi K, Kokusho S, Takiguchi K, Yang-Boo C. Study on the restoring force characteristics of RC solumn to bidirectional deflection history. *Proceedings of 8th World Conference on Earthquake Engineering*, San Francisco, Calif., 1984.
20. Li K, Aoyama H. Reinforced concrete columns under varyng axial load and bidirectional lateral load reversals. *Proceedings of Ninth World Conference on Earthquake Engineering*, Tokyo-Kyoto, Japan, 1988.
21. Saatcioglu M, Ozcebe G. Response of reinforced concrete columns to simulated seismic loading. *ACI Structural Journal*. 1989; **86**(6):3-12.
22. Bousias SN, Verzeletti G, Magonette G, Fardis MN. RC columns incyclic biaxial bending and axial load. *Proceedings of Tenth World Conference on Earthquake Engineering*, Madrid, Spain, 1992.
23. Boys A. Assessment of the seismic performance of inadequately detailed reinforced concrete columns. *M.E. Thesis*, University of Canterbury, Christchurch, 2009.
24. Zeris CA, Mahin SA. Behavior of reinforced concrete structures subjected to biaxial excitation. *Journal of Structural Engineering, ASCE*. 1991; **117**(9).
25. Suzuki N, Otani S, Kobayashi Y. Three dimensional beam-column subassemblages under bidirectional earthquake loadings. *Proceedings of 8th World Conference on Earthquake Engineering*, San Francisco, Calif., 1984.
26. Padilla-Mora R, Schnobrich W. Non-linear response of framed structures to two-dimensional earthquake motion. *Civil Engineering Studies, Research Series Report no. 408*, University of Ilinois, Urbana, 1974.
27. Lai S, Will G, Otani S. Model for inelastic biaxial bending of concrete members. *Journal of Structural Divison, ASCE*. 1984; **110**(11).
28. Pecknold D. Inelastic structural response to 2-D gorund motion *Journal of the Engineering Mechanics Division, ASCE*. 1974; **100**(5).
29. Saatcioglu M. Reinforced concrete columns subjected to uniaxial and biaxial load reversals. *Proceedings of 8th World Conference on Earthquake Engineering*, San Francisco, Calif., 1984.
30. Oliva MG, Clough RW. Biaxial seismic response of R/C frames. *Journal of Structural Engineering, ASCE*. 1987; **113**(6).
31. Wong Y-L, Paulay TP, J.N. Response of circular reinforced concrete columns to to multi-directional seismic attack. *ACI Structural Journal*. 1993; **90**(2):180-91.

32. Sezen H, Elwood KJ, Whittaker AS, Mosalam KM, Wallace JW, Stanton JF. Structural engineering reconnaissance of the August 17, 1999, Kocaeli (Izmit), Turkey Earthquake. *Report No. PEER 2000/09*, University of California, Berkeley, 1999.
33. Beckingsale CW. Post-elastic behaviour of reinforced concrete beam-column joints. *PhD Dissertation*, University of Canterbury, Christchurch, 1980.
34. Paulay T, Priestley MNJ. *Seismic design of reinforced concrete and masonry buildings*. Wiley: New York, 1992.
35. Cheung CH. Seismic Design of Reinforced Concrete Beam-Column Joints with Floor Slabs. Research Report 91-4, Department of Civil Engineering, University of Canterbury, Christchurch, New Zealand, 1991.
36. Bresler B. Design criteria for reinforced concrete columns under axial load and biaxial loading. *ACI Structural Journal*. 1960; **57**(5):481-90.
37. Furlong RW. Ultimate strength of square columns under biaxially eccentric loads. *ACI Structural Journal*. 1961; **57**(9):1129-40.
38. Trowland M. Modelling the Shear Hinge in Beam Column Joints. Third Professional Year Project, Department of Civil Engineering, University of Canterbury, Christchurch, New Zealand, 2003.
39. Leon R, Jirsa O. Bi-directional loading of RC beam-column joints. *Earthquake Spectra*. 1986; **2**(3):537-64.
40. Hertanto E. Seismic assessment of pre-1970s reinforced concrete beam-column joint subassemblies. *M.E. Thesis*, University of Canterbury, Christchurch, 2006.
41. Chen T. Retrofit strategy of non-seismically designed frame systems based on a metallic haunch system. *M.E. Thesis*, University of Canterbury, Christchurch, 2006.
42. Di Ludovico M, Prota A, Manfredi G, Cosenza E. Seismic strengthening of an under-designed RC structure with FRP. *Earthquake Engineering and Structural Dynamics*. 2008; **37**(1):141-62.
43. Balsamo A, Colombo A, Manfredi G, Negro P, Prota A. Seismic behavior of a full-scale RC frame repaired using CFRP laminates. *Engineering Structures*. 2005; **27**:769-80.

Chapter 8 EXPERIMENTAL PROGRAMME FOR 3D CORNER BEAM-COLUMN JOINTS

8.1 INTRODUCTION

In this chapter, the experimental programme performed on two 2/3 scale 3D corner nonseismically detailed RC beam-column joints is described. One as-built 3D corner joint was tested for benchmark purposes. After the successful test results of Specimen 2D4, it was decided to use the same retrofit solution for the corner joints and investigate the possible effects of multiaxial (bidirectional plus concurrent varying axial load) cyclic simulated earthquake loading on these specimens. Hence, the experimental study was pursued mainly to clarify the effect of multiaxial loading on the specimens, which were retrofitted based on the design methodology developed for the 2D exterior beam-column joints. Accordingly, most of the properties of the 2D specimens were replicated in 3D corner specimens for the additional y-direction. The test setup, reinforcing detail, global and local instrumentation used in the 2D plane frame joints were implemented in a similar fashion in the x- and y- direction of 3D corner specimens. The FRP application scheme was slightly modified in the corner joint applications, whilst the beam and column wrapping schemes were kept similar to that of the last tested 2D specimen, 2D4. Therefore, while some modifications implemented in 3D joints are explained in the following (i.e., test setup, fabrication, loading protocol, retrofit application etc.), the reader is generally referred to Chapter 5 in order to avoid repetition.

8.2 DESCRIPTION OF TEST UNITS

In the second part of the experimental campaign, a series of quasi-static cyclic tests was carried out on a total of two 2/3 scale comprising of one as-built, Unit 3D1, and one retrofitted, Unit 3D2, three-dimensional (3D) corner beam-column joint subassemblage. All tests were performed under bidirectional and varying axial loading. Test specimens represented the portion of first storey corner connections assuming that the points of contraflexure occur at mid-height and mid-span of the

prototype frame of a middle-rise (6-9 storeys) residential building designed for gravity loads. Dimensions of the prototype structure and tested corner joints are schematically drawn in Figure 8–1.

All specimens were detailed and built according to older construction practice (e.g., [1, 2]). The reader is referred to Section 5.2 of Chapter 5 for more detailed information regarding the considerations in selecting and designing the reinforcement details of the specimen.

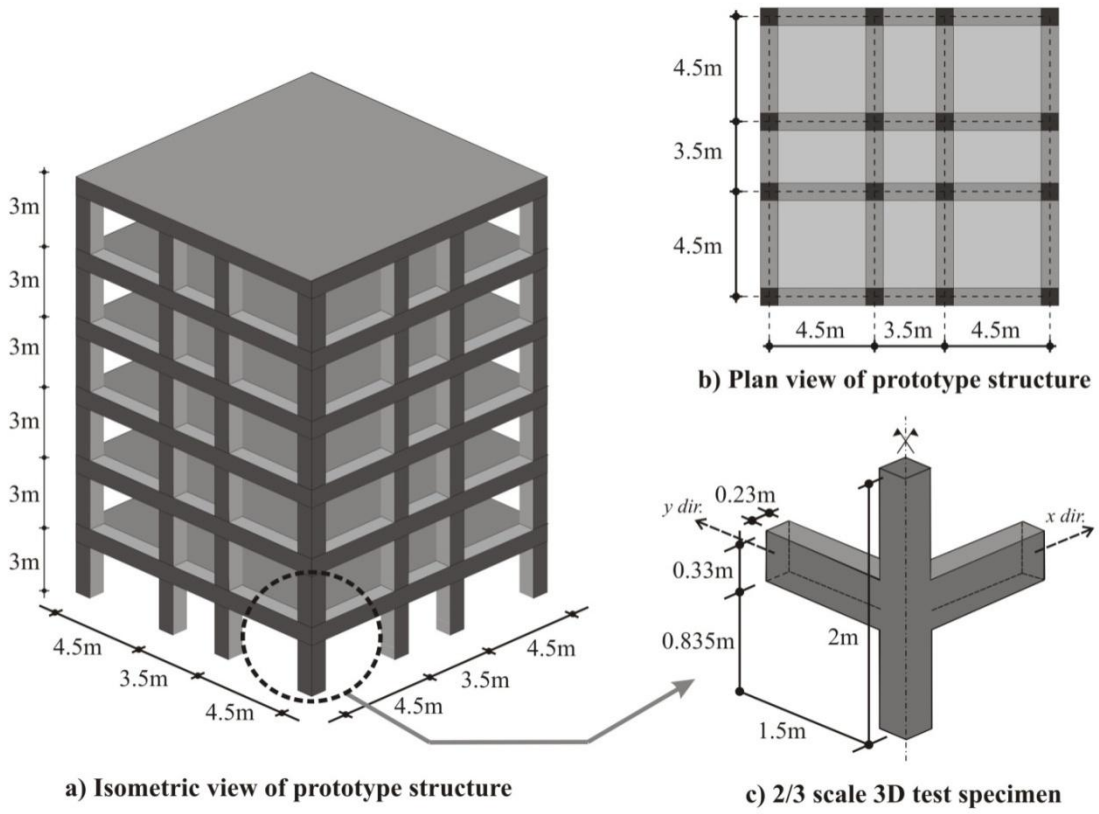

Figure 8–1 Schematic representation of prototype building

All units had identical beam detailing and dimensions in both x- and y-directions. Note that the reinforcement configuration for the 3D corner joints that are in the x- and y-direction are identical to the 2D plane frame joints. The beams were 330 mm in depth and 230 mm in width and the column was 230 mm square. The column was symmetrically reinforced in the y-direction, containing three 10 mm diameter Grade 300 plain round bars on both sides. The column transverse reinforcement was 6 mm diameter Grade 300 plain round bars placed at 100 mm centres, and the first tie was 50 mm from the beam face. The beams were symmetrically reinforced and contained four 10 mm diameter Grade 300 plain round bars in the top and four 10 mm diameter Grade 300 plain round bars in the bottom. The beam transverse reinforcement was 6 mm diameter Grade 300 plain round bars placed at 133 mm

centres, with the first stirrup being 50 mm from the column face. The beam-column joint core contained no transverse reinforcement. The overall dimensions and reinforcing details of the unit are shown in Figure 8–2.

The first specimen, Unit 3D1, was tested as a control specimen without any retrofit intervention. The aim was to (1) acquire information on the response of as-built corner beam-column joints under bidirectional loading for the assessment purposes for existing buildings; (2) to compare its performance with a 2D as-built specimen which was tested under uniaxial loading conditions; and (3) to provide data for the later investigation on the determination of the effectiveness of proposed retrofitting technique for 3D corner joints.

The second specimen, Unit 3D2, was retrofitted with the same R21 scheme to that of used in the last 2D specimen, 2D4. The main objective was to investigate the retrofit design assumptions based on the uniaxial retrofit design methodology which was covered in detail in Chapter 4. In this way, the drawbacks of the proposed methodology for corner joints subjected to multiaxial loading demands can be highlighted. Subsequently, possible solutions to improve the current assessment and retrofit design methodology are proposed in the following chapters. Specimen details are given in Figure 8–2. Table 8-1 provides a summary of test specimens` concrete compressive strength at day of testing, axial load levels and wrapping configurations.

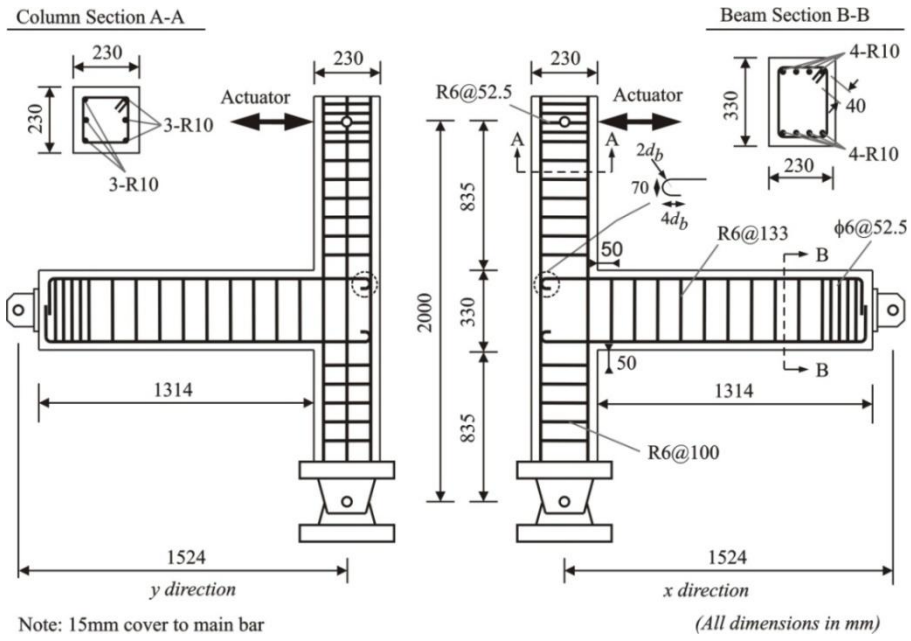

Figure 8–2 Details of 3D corner beam-column joint specimens

Table 8-1 Summary of specimen properties for bidirectional experimental programme

Specimen	f'_c [a] (MPa)	Axial load range		Retrofit scheme[d]			
		N_g [b] (kN)	$\alpha_x=\alpha_y$ [c]	Type	Beam horizontal layer #	Column vertical layer #	Joint U-shape horizontal sheet #
3D1	17.4	115	2.35	-	-	-	-
3D2	16.9	115	2.35	R21	2	1	2

Note:
[a] Compressive strength of 100mm dia. x 200mm concrete cylinder
[b] Constant axial load produced by the tributary gravity load for each prototype
[c] Proportionality coefficient for x and y direction
[d] Installed on each side

8.3 MATERIAL PROPERTIES

8.3.1 Reinforcing Steel

The longitudinal and transverse reinforcement used for all test specimens were plain round bars of mild steel Grade 300. The reinforcing steel properties were obtained with the similar method as explained in Section 5.3.1 of Chapter 5. The stress – strain curves for the reinforcing steel used in 3D corner joint specimens are shown in Figure 8–3. The measured tensile properties of the reinforcing steel are tabulated in Table 8-2.

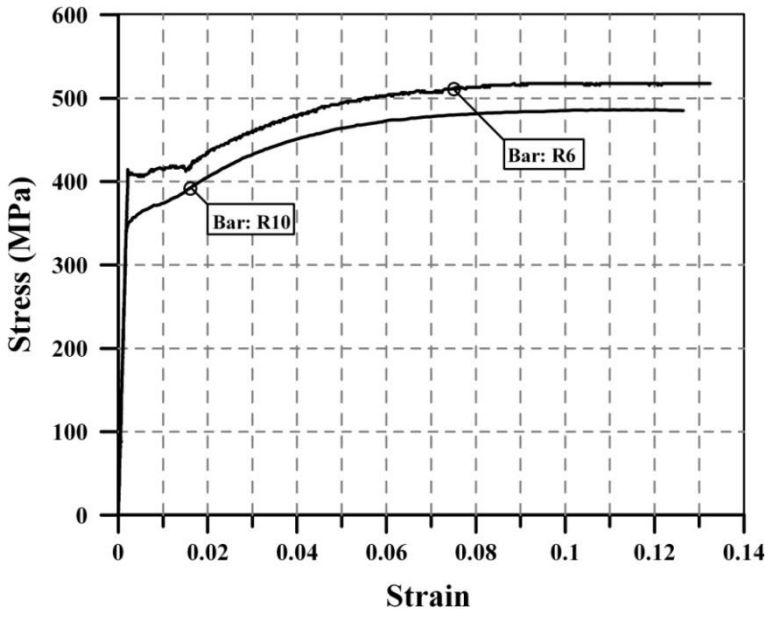

Figure 8–3 Stress – strain curves for the reinforcing steel used in 3D corner joint specimens

Table 8-2 Measured reinforcing steel properties for 3D corner joint

Specimen	3D1 and 3D2	
Bar Type	R6	R10
Yield Strength, f_y (MPa)	408	340
Yield Strain, ε_y	0.0024	0.0019
Strain at commencing strain hardening, ε_{sh}	0.016	0.079
Ultimate Stress, f_u (MPa)	515	440

Note: R6=6mm plain round bar of 6mm diameter
R10=10mm plain round bar of 10mm diameter
Each value was obtained from the average of three coupons

8.3.2 Concrete

The concrete for the test units was a standard mix type, and supplied by a local commercial ready-mix concrete company as in the 2D specimens. Specimen 3D1 was casted together with the 2D plane frame specimens. Specimen 3D2 was casted approximately five weeks later after removing the formworks of the Specimen 3D1. The concrete properties for 3D corner joints are given in Table 8-3.

Table 8-3 Measured concrete properties of 3D corner specimens

Specimen	At 28 days	At day of testing		
	f'_c *(MPa)*	*Slump (mm)*	f'_c *(MPa)*	f_t *(MPa)*
3D1	16.88	180	17.4	2.20
3D2	14.24	210	16.9	2.04

Note: f'_c = compressive strength of 100mm dia. x 200mm concrete cylinder
f_t = split cylinder tensile strength
Each value was obtained from the average of three cylinders

8.3.3 Composite Material

SikaWrap®-100G type high strength E-glass unidirectional fibre polymers were used for the retrofitting. A summary of the mechanical properties of fibres as provided by the manufacturer, Sika (NZ) Ltd., and are as follows: tensile E-modulus E_f = 76,000N/mm^2, failure strain ε_{fu}* = 2.8% (nominal) and fibre thickness, t_f= 0.36mm. Detailed information on the properties of glass fibre fabric and epoxy impregnation resin can be found in Appendix F.

8.4 SPECIMEN FABRICATION

A special modular formwork made of 6 mm thick plate steel was manufactured for casting of the 3D corner joints (Figure 8–4a). Before the casting, steel formwork units were assembled and the inside surfaces were cleaned and coated with oil. Specimens were fabricated in the upright position, with the first casting completing the lower column, the beams and the joint region (Figure 8–5a). A second casting completed the remainder of the upper column in the same day. In order to improve the quality and uniformity of the casted concrete, flex-shaft type internal vibration as well as external vibrators attached directly to the concrete form in the joint region was performed (Figure 8–5b). Note that, particular care was taken to prevent breaking the strain gauges during casting.

a) Steel plate formwork and reinforcement

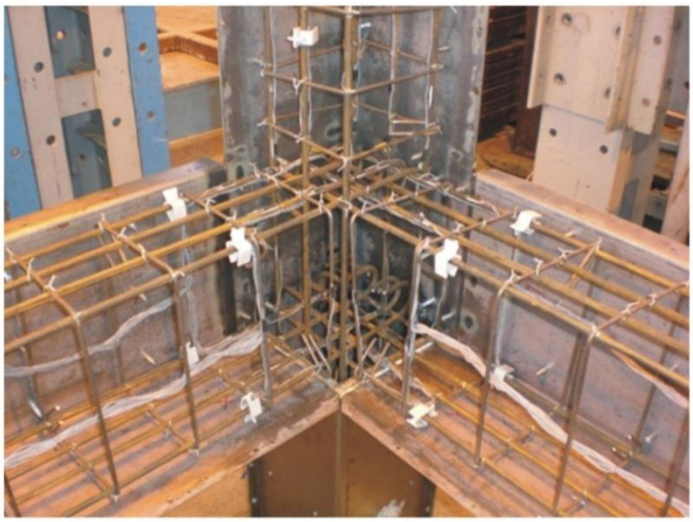

b) Close-up view of beam-column joint reinforcement

Figure 8–4 Formwork, reinforcing detail and casting of 3D corner beam-column joint specimens

a) Casting of concrete b) Internal and external vibration

Figure 8–5 Casting of concrete into steel formwork for 3D corner beam-column joint specimens

8.5 RETROFIT APPLICATION

8.5.1 Design of Retrofit Intervention

Chapter 4 contains information on the retrofit design and FRP application layout employed in Specimen 3D2. Figure 8–6 shows the GFRP application scheme and sequence.

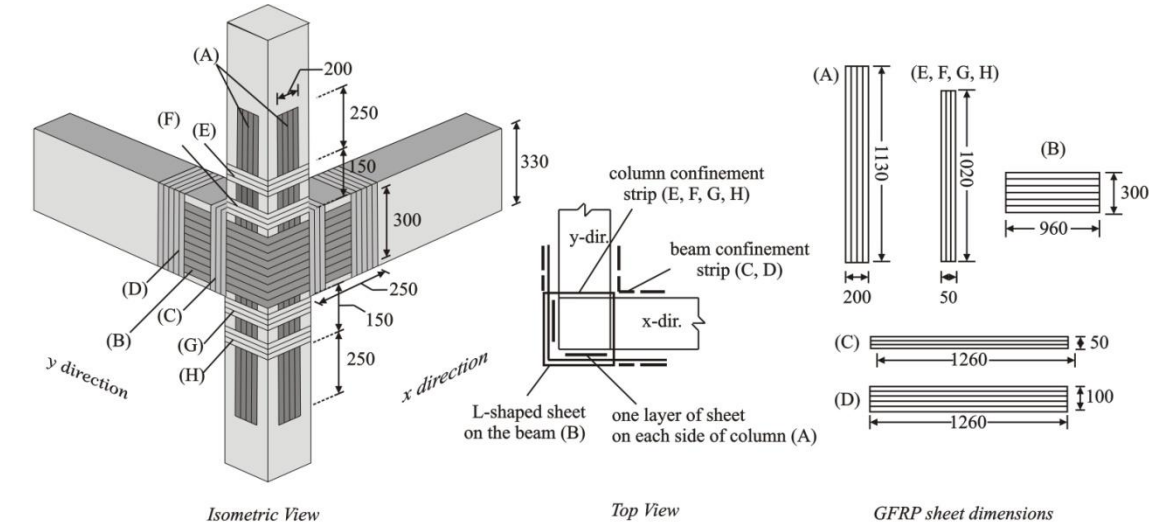

All dimensions in mm; not scaled

Notes:

FRP properties: Type=Uni-directional GFRP SikaWrap-100G; Elastic modulus=76,000 MPa; Failure strain=2.8%; Fiber thickness=0.36 mm

FRP application scheme: Specimen 3D2=R21

*Rij refers to a configuration with i number of GFRP layers in the beam and j number of GFRP layers in the column (on each side).

Figure 8–6 Schematic illustration of GFRP retrofit configuration for 3D specimens

8.5.2 GFRP Application

The same application steps were followed in Specimen 3D2 to those followed in 2D beam-column joint specimens. Section 5.5.2 of Chapter 5 contains more information regarding this procedure. Some close-up views of selected installation steps are presented in Figure 8–7 for the 3D corner specimen. It should be mentioned that there are two layers of L-shape horizontal laminate wrapped around the exterior face of the specimen at the joint level (Figure 8–7). In the retrofitted 3D specimen, 3D2, the intervention was intended to be carried out with minimum invasiveness from the outside of the building, thus allowing for limited disruption of the internal activities and/or relocation of people. To reduce invasiveness to the floor in the 3D configuration, in real practice, C-shape strips could be adopted and anchored on the top and bottom of the beam.

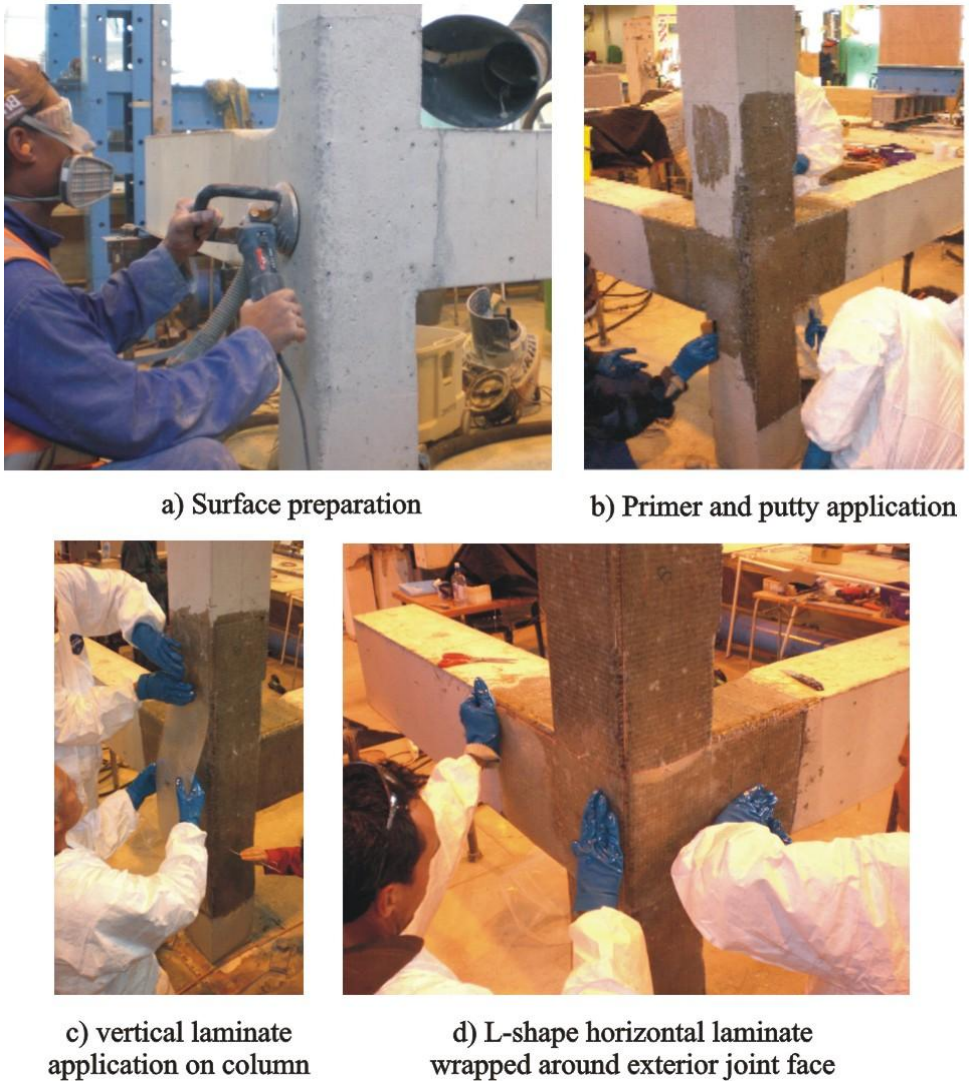

Figure 8–7 Selected close-up views for GFRP application of 3D corner joint specimen

8.6 TEST SETUP

The same test setup described in Chapter 5 was used in the testing of 3D corner beam-column joint specimens under bidirectional and varying axial loading. Section 5.6 of Chapter 5 contains more information regarding this procedure. However, it should be noted that no restraint was applied to the universal hinge in this case, allowing it to rotate in two directions freely. A similar approach was applied to prevent the lateral displacement and rotation along axial axes of the beams. This was deemed to (1) prevent the additional torsional rotation demand stemming from the lateral movement and rotation of the beam; and (2) to simulate the actual behaviour in the prototype RC frame structure. Figure 8–8 and Figure 10-9 show the front and dimetric view of the test rig used in 2D unidirectional tests.

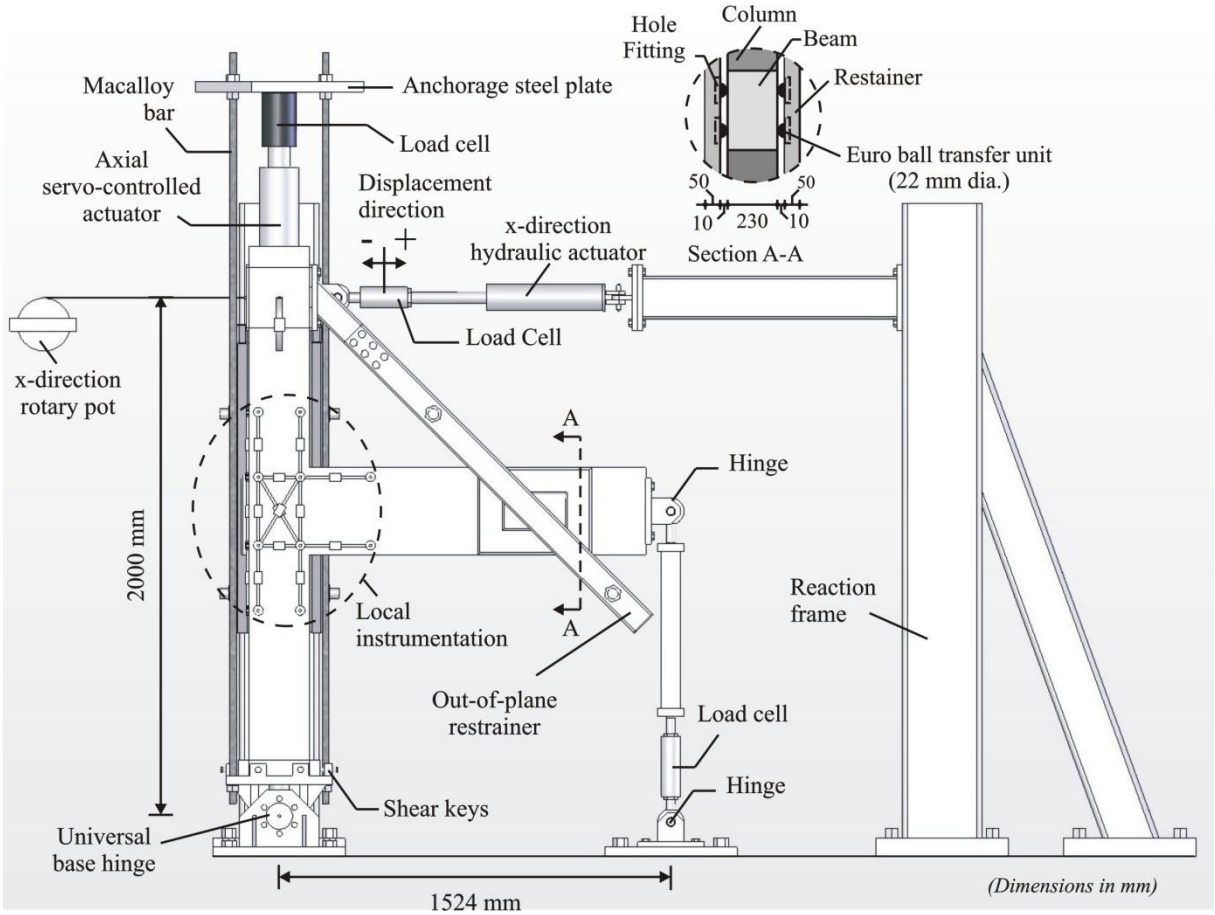

Figure 8–8 Test setup for 3D specimens: front view, x-direction

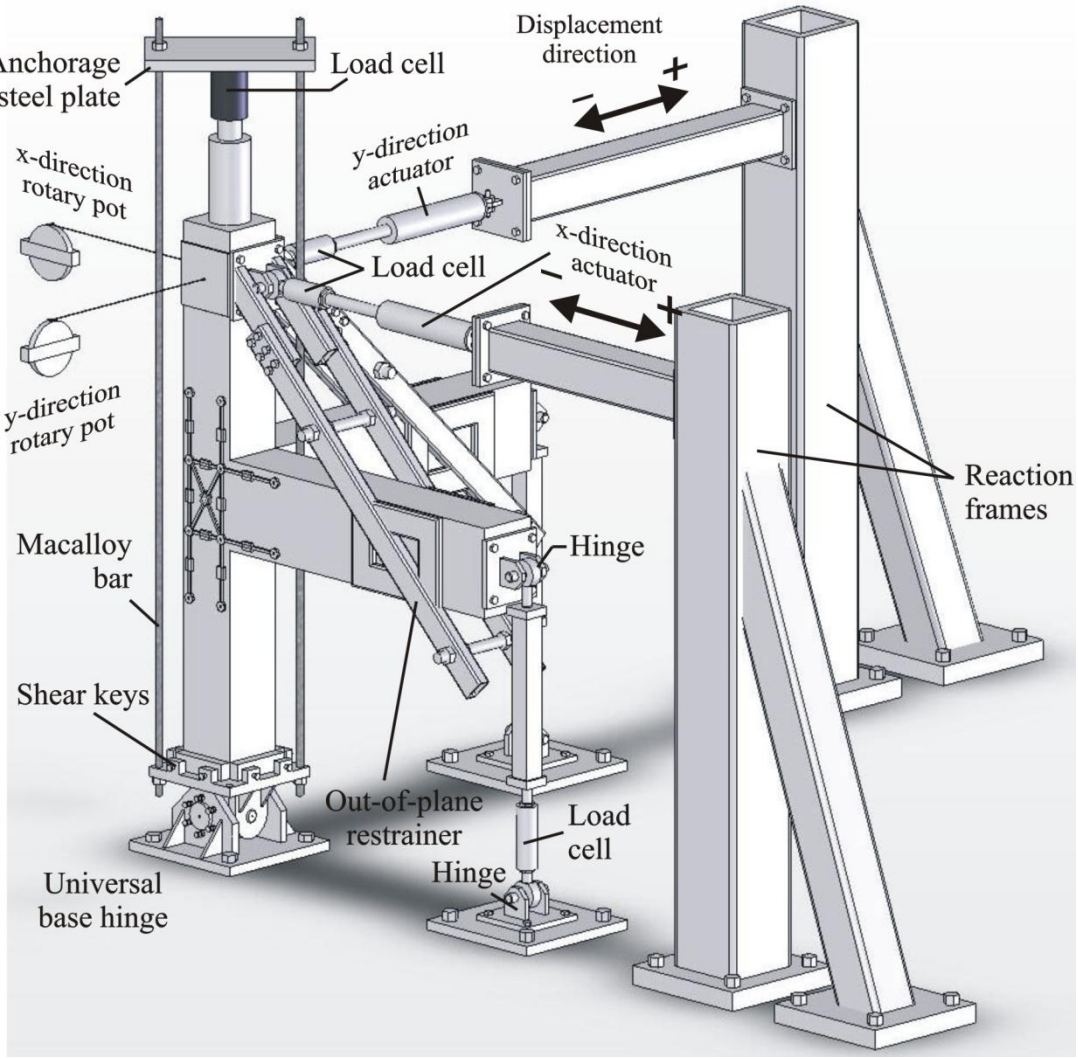

Figure 8–9 Test setup for 3D specimens: dimetric view

8.7 LOADING PROCEDURE

In 3D configuration testing, the 2D loading protocol (see Section 5.7, Chapter 5) was extended to 3D dimensions by adopting a cloverleaf loading path. The bidirectional lateral loading protocol along with its x- and y-direction components are given in Figure 8–10. In particular, one complete cycle of the clover-shape was performed at each specified drift level. In this way, 3D specimens were subjected to a total of two excursions into the positive and negative direction in the x-axis and y-axis during each complete cycle. Cloverleaf load pattern is constructed in polar coordinates employing a rose or rhodonea sinusoid curve expressed by $r(\theta) = R\sin(2\theta)$ where R represents the target displacement (i.e., magnitude of the maximum displacement vector at an angle of 45 degrees to the principal axis) of

the column top to the origin at the particular drift level (Figure 8–10c). θ is the measured angle of any point to the principal axes along the loading path.

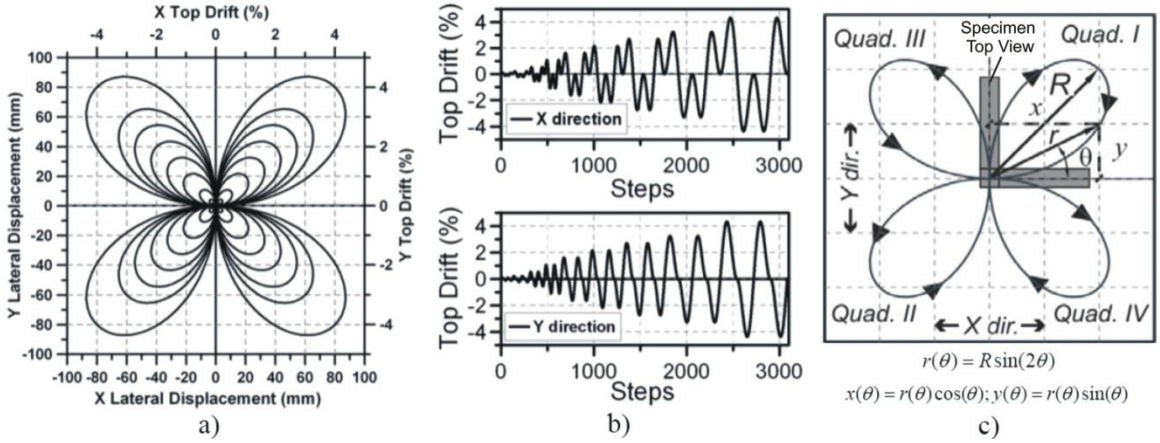

Figure 8–10 Bidirectional load pattern

3D corner joint specimens were subjected to the axial load that was varied around the gravity load value (i.e., based on tributary area) in proportion to the lateral force acting on the column as it would occur due to the frames' lateral sway in a similar fashion as employed in 2D unidirectional tests. The relationship between the lateral force in x-direction, V_{cx} and in y-direction V_{cy}, gravity load N_g and the proportionality coefficients for each direction, α_x and α_y, are given for the applied axial load during test, N in the following equation

$$N = N_g \pm \alpha_x V_{cx} \pm \alpha_y V_{cy} \tag{10-1}$$

It is important to note that the proportionality coefficient was used for both x- and y-directions of loading during testing. The identification of the proportionality coefficient along with the gravity load calculations for the selected prototype RC frame is presented in Appendix E. The applied gravity load on the column was 115 kN which was similar to that applied in the 2D unidirectional tests. However, it was anticipated that due to the high α coefficient used in the 2D unidirectional tests (4.63), axial tension could have occurred in the testing of 3D corner joint specimens. In order to prevent this effect, the α coefficient was reduced to about half (2.35) of that used in 2D specimens for these tests. According to the adopted sign convention, positive drift and positive lateral force correspond to a decrease in the axial load (pull direction that is also the direction of the starting cycle).

8.8 INSTRUMENTATION

8.8.1 Measurement of Loads

The load cell configuration in x-direction of 3D corner joints were similar to that used in the 2D unidirectional test campaign (i.e., two 150 kN to measure horizontal column force and beam reaction force along with 400 kN capacity load cell to measure axial load) as explained in Section 5.8.1 of Chapter 5. In addition, for the y-direction horizontal column load and beam measurements two 150 kN capacity load cells were used. These load cells were calibrated using the Avery Universal Testing Machine before installation into the test rig.

8.8.2 Measurement of Displacement and Deformations

The global directions for each direction were measured using loaded-spring rotary potentiometers which were attached to a rigid frame some distance from the column faces and connected to the column using a thin string Figure 8–9 Test setup for 3D specimens: dimetric view. The local deformations in the column, beams and joint panel were measured by installing linear potentiometers (Linear Variable Displacement Transducers, LVDTs) in each exterior face. The same local instrumentation positions used in 2D exterior plane joints were also adopted in each direction in the 3D corner joints. In Figure 8–11, the positions of the potentiometers on the exterior face of the Specimens 3D1 and 3D2 are given. More detailed information regarding the processing of the readings such as estimation of the section curvatures and shear deformations is presented in Section 5.8.2 of Chapter 5.

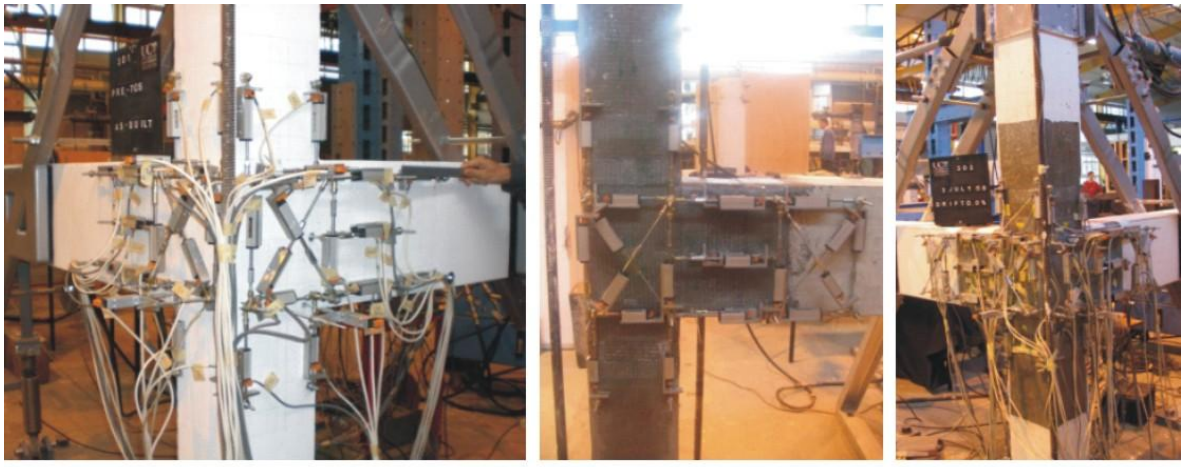

a) Unit 3D1 b) Unit 3D2: x-dir. c) Unit 3D2

Figure 8–11 Local deformation instrumentation for 3D corner joint specimens

8.8.3 Measurement of Strains

8.8.3.1 Measurement of Strains in Reinforcing Bars

The electrical resistance strain gauges (Type: FLA-3-11-3L) were attached to the sides of the bars, assumed to be their 'neutral axis' to carefully investigate the steel strains in the longitudinal bars. A similar strain gauge arrangement was used in the 3D corner joint specimens as that used in the 2D plane frame specimens as explained in Chapter 5. The y-direction strain gauge scheme was equivalent to that of the x-direction face of 3D specimens. In this way, the comparison of the steel strain demands under unidirectional and bidirectional loading conditions have been accomplished in the discussion of test results. The strain gauged bars in each direction is illustrated in Figure 8–12.

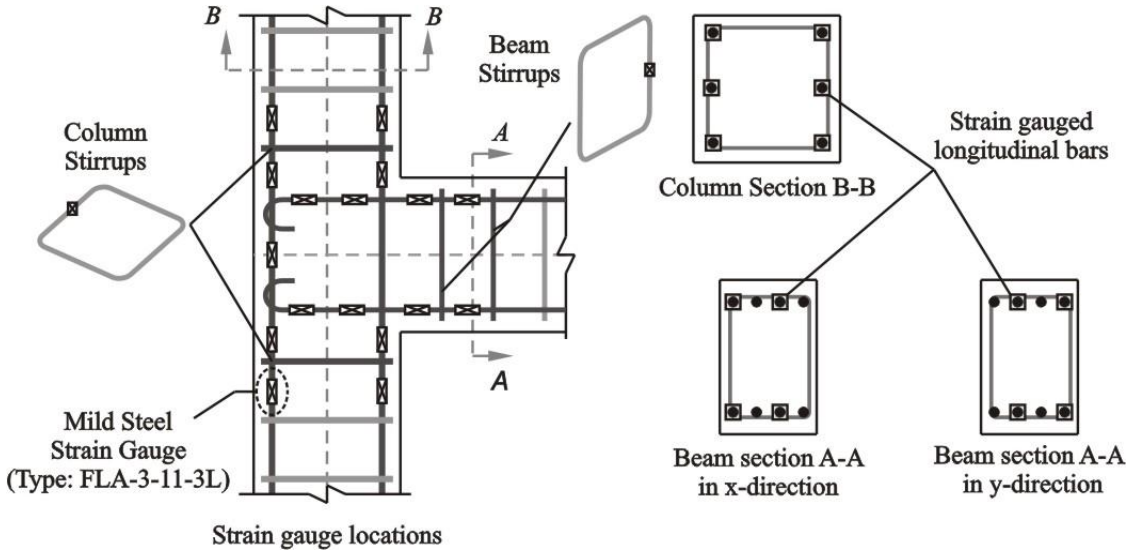

Figure 8–12 Layout of reinforcement strain gauges in 3D corner joint specimens

8.8.3.2 Measurement of Strains in FRP

The FRP sheets on each face of the 3D retrofitted specimen, 3D2, were extensively instrumented with Tokyo Sokki BFLA-5-8-3 type composite material stain gauges. They were mounted in both the longitudinal and transverse fibre direction of the beam, column and joint panel regions and applied in two directions (Figure 8–13). In this way, strain demand in the FRP sheets was able to be monitored in each loading sequence and compared to its counterparts in 2D retrofitted joints.

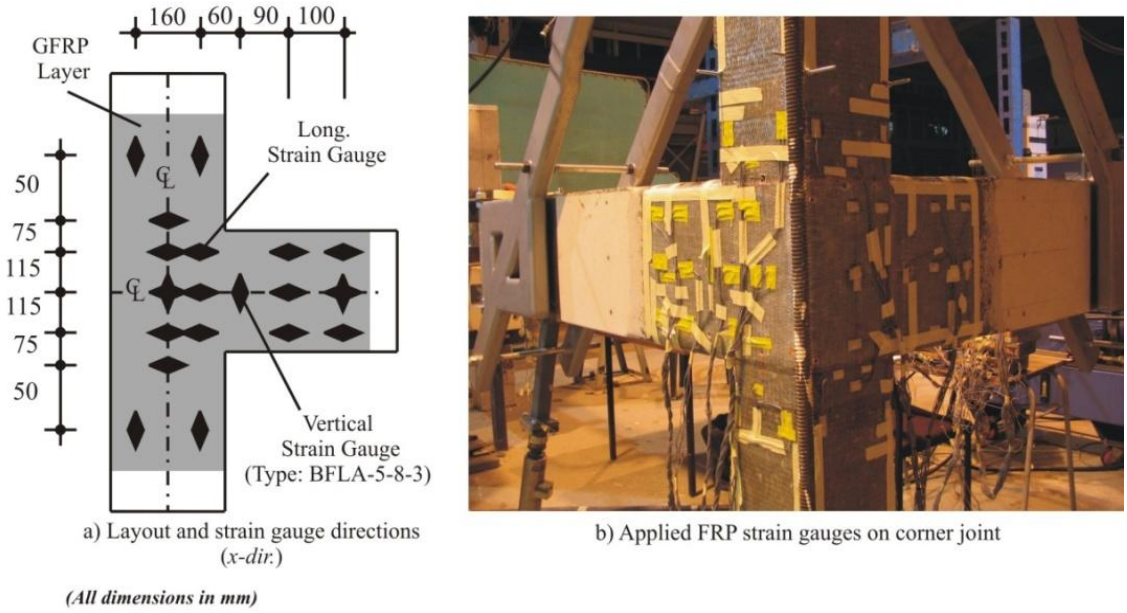

Figure 8–13 GFRP strain gauge application for 3D joint specimens

8.9 TEST CONTROL AND DATA COLLECTION

For test control and data collection similar methodology as used in 2D unidirectional specimens was followed. Section 5.9 of Chapter 5 contains more detailed information on methods used.

8.10 SUMMARY

In this chapter the information on the experimental programme pertaining to 3D corner beam-column joints in as-built and retrofitted configurations have been presented. In general, the same procedures and methodology were followed as in the experimental programme regarding test setup, instrumentation, data collection and analysis to that of 2D beam-column joint tests. The main differences consisted of the bidirectional loading protocol where a cloverleaf loading path was adopted to simulate bidirectional earthquake demand and the application of FRP in the joint area.

8.11 REFERENCES

1. *Regio Decreto.* November-XVIII(228) (in Italian), 1939.
2. NZS95:1955. *New Zealand Standard - Model Building By-Laws: Part IV and V.* New Zealand Standard Inst., Wellington, NZ, 1953.

Chapter 9 TEST RESULTS OF 3D CORNER JOINTS

9.1 INTRODUCTION

In the first part of this chapter the experimental findings of 3D space frame beam-column joints are presented. In order to provide useful information on the failure mechanisms, the behaviour and damage propagation of each specimen is examined in detail. In the second part, the test results are analysed to clarify the effects of bidirectional loading on the assessment criteria and retrofit design proposed and carried out based on unidirectional design assumptions. For this purpose, global as well as local failure modes, strength, stiffness and energy dissipation characteristics, strain demands in the steel reinforcement and FRP sheets are used to compare the performance of the 3D, as well as 2D beam-column joint specimens. In order to contribute to performance-based engineering assessment and retrofit design, damage limit states based on the experimental findings of this study are presented. A deformation-based retrofit design procedure is also introduced to evaluate the FRP retrofit scheme for beam-column joints for the selected target performance. Lastly, an upgraded retrofit scheme for corner beam-column joints is proposed to further improve seismic performance.

9.2 EXPERIMENTAL RESULTS

9.2.1 As-built Specimen 3D1

Specimen 3D1 is a 3D corner beam-column joint unit in its as-built configuration and tested under bidirectional quasi-static cyclic loading. During testing the axial load was varied simultaneously with the horizontal load around a load value of 114 kN. In order to prevent axial tension in the columns, the proportionality coefficient, α, was reduced to approximately half of that used in the 2D specimens (i.e., $\alpha_x=\alpha_y=2.35$ instead of $\alpha=4.67$). Further information on 3D loading protocol can be found in Chapter 8. Test results of this benchmark unit are crucially important (1) to identify the effect of bidirectional loading on the performance and development of assessment measures of corner beam-

column joints without slabs, and (2) to provide information on the seismic performance of the retrofitted 3D corner joint, Specimen 3D2.

As anticipated before the test and based on the findings of 2D as-built unit, Specimen 2D1, in the 3D as-built specimen, 3D1, a more complex three-dimensional concrete wedge mechanism, was developed due to the higher strength and deformation demands imposed by the bidirectional loading regime. As a result, a drastic drop in the strength capacity with decreased energy dissipation was noticed after the first cracking in the joint panel (at around 0.5% drift) in spite of the partial confinement effect provided by the orthogonal beam. Towards the end of the test, a sort of three-dimensional "shear hinge" mechanism was formed in the middle of the joint dominating the behaviour. The final damaged stage of Specimen 3D1 is also illustrated in Figure 9-1. The lateral force-displacement response in the x- and y- direction and bidirectional hysteresis loops are given in Figure 9–2, Figure 9–3, and Figure 9–4 respectively. In Table 9-1, a summary of the test results in terms of recorded values corresponding to 45 degrees of skew angle in the bidirectional loading is presented for each quadrant of the associated drift level. The observed damage and crack formation during the test are summarized in the following.

The hairline flexural cracks started to form at 0.1% drift in the beam and at the beam-column interface (Figure 9–5). At 0.2% drift existing flexural cracks surrounded the beam faces and joint boundaries. Also, some hairline cracks appeared in the bottom and top column (Figure 9–6). Diagonal shear cracks appeared at approximately 0.5% drift level in the first quadrant loading in the joint region (Figure 9–7). During the cycles of 0.5 and 1%, additional hairline cracks developed in the beam and column faces (Figure 9–8). The specimen reached its maximum load bearing capacity at the first quadrant of 1% drift level. The recorded values in the x-direction of loading were 15.3 and 18.8 kN with joint shear stress values of $0.39\sqrt{f`_c}$ and $0.48\sqrt{f`_c}$ for the pull and push directions, respectively. The recorded values in the y-direction of loading were 13.6 and 18.3 kN with joint shear stress values of $0.35\sqrt{f`_c}$ and $0.47\sqrt{f`_c}$ for the pull and push directions, respectively. After 1.5% drift, the crack formation in the beams stabilized (Figure 9–9). New diagonal cracks continued to form in the joint region developing a grid of inclined cracks. They also propagated into the column and the beams. At 2% drift, all cracks stabilized and flaking in the beam-joint interface and joint cover concrete was observed (Figure 9–10). The sudden increase in the width of diagonal shear cracks and the corner concrete wedge formation resulted in a drastic drop in the load capacity (Figure 9–11). The test was halted due to the loss of stability in the columns after complete failure of core concrete at the beginning of 3% drift (Figure 9–12).

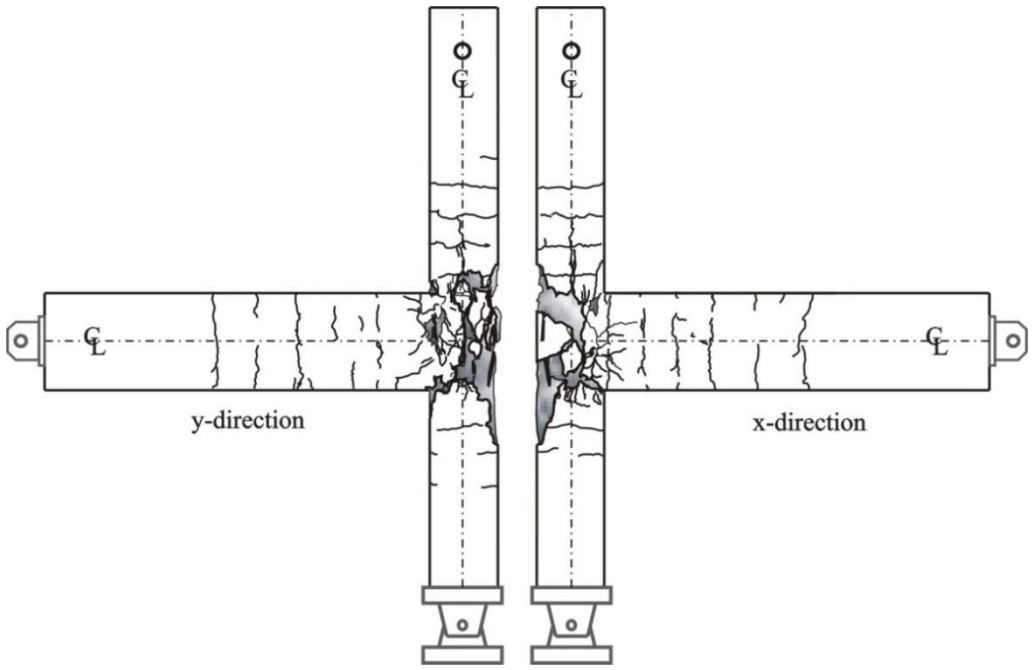

Figure 9–1 Crack patterns at final stage for Specimen 3D1

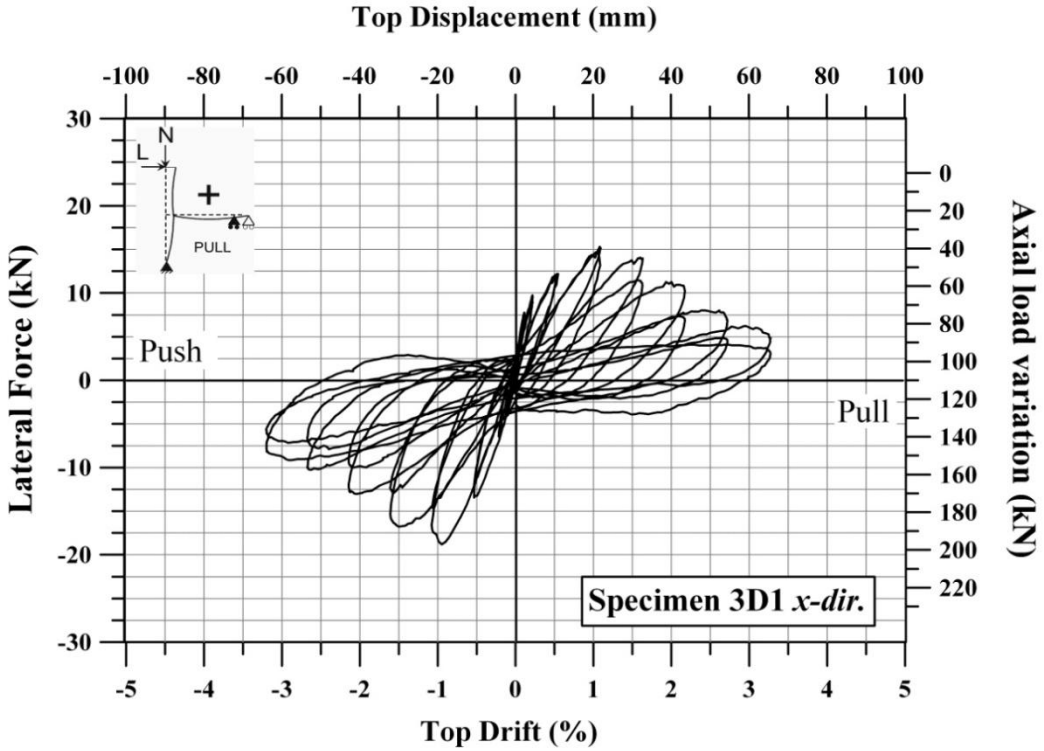

Figure 9–2 Lateral force paths for Specimen 3D1, x-direction

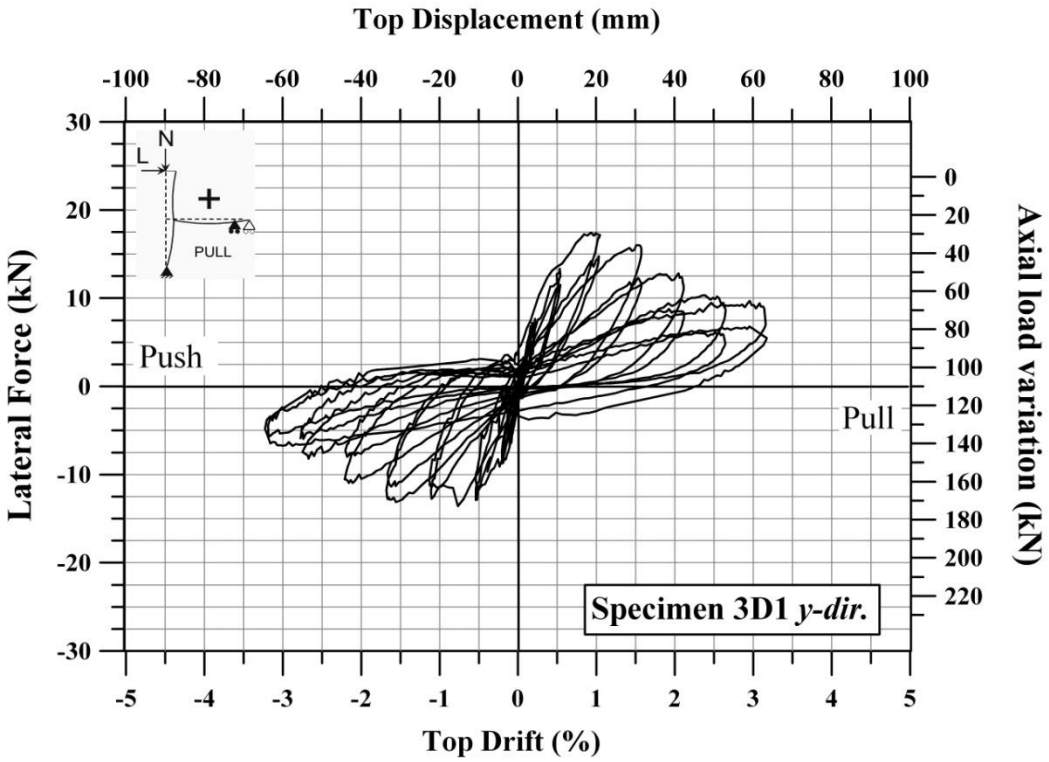

Figure 9–3 Lateral force paths for Specimen 3D1, y-direction

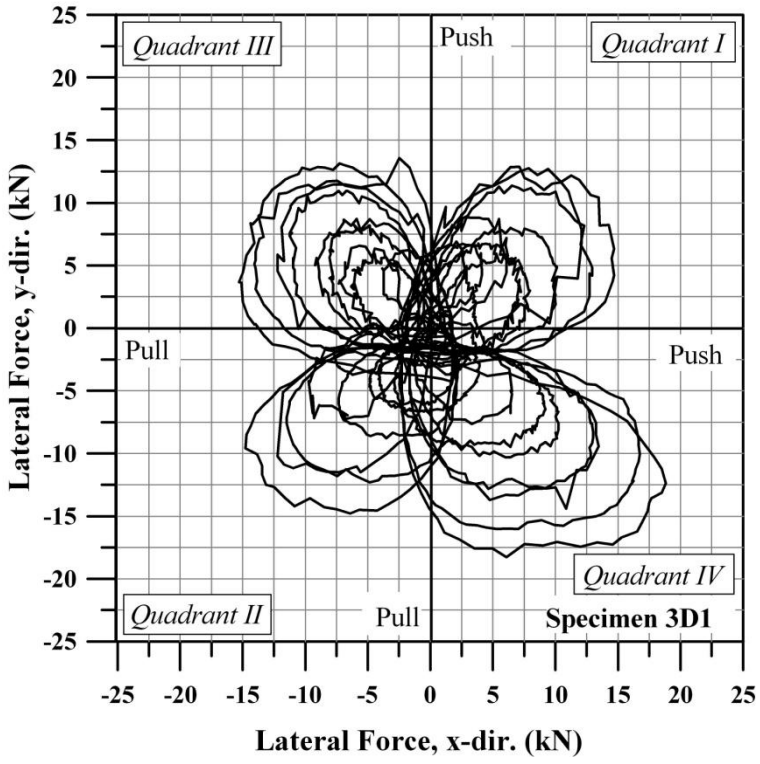

Figure 9–4 Bidirectional lateral force paths for Specimen 3D1

Table 9-1 Summary of test results for Specimen 3D1

Drift Level	Quadrant	Axial Load		Strength				Joint Panel Results					
		N^a	$N/(A_g f_c')^b$	$V_{cx}{}^c$	$V_{cy}{}^d$	$v_{jhx}{}^e$	$v_{jhy}{}^f$	$p_{cx}{}^g$	$p_{cy}{}^h$	$p_{tx}{}^i$	$p_{ty}{}^j$	$\gamma_x{}^k$	$\gamma_y{}^l$
		(kN)		(kN)	(kN)	(MPa)	(MPa)	(MPa)	(MPa)	(MPa)	(MPa)	(%)	(%)
0.1%	I	82.13	0.09	-6.31	6.39	-0.68	0.69	-1.81	-1.82	0.26	0.26	0.0046	-0.0090
	II	119.90	0.13	3.21	-2.56	0.35	-0.28	-2.32	-2.30	0.05	0.03	0.0169	0.0011
	III	98.41	0.11	2.59	6.16	0.28	0.67	-1.90	-2.08	0.04	0.21	0.0215	-0.0067
	IV	96.96	0.11	-7.34	-3.11	-0.80	-0.34	-2.13	-1.89	0.30	0.06	0.0001	0.0158
0.2%	I	71.09	0.08	-8.07	7.61	-0.87	0.82	-1.77	-1.74	0.43	0.39	0.0114	-0.0134
	II	135.90	0.15	6.41	-6.00	0.70	-0.65	-2.75	-2.72	0.18	0.16	0.0192	0.0181
	III	100.40	0.11	6.10	7.19	0.66	0.78	-2.11	-2.18	0.21	0.28	0.0249	-0.0225
	IV	98.41	0.11	-9.31	-7.19	-1.01	-0.78	-2.30	-2.14	0.44	0.28	0.0001	0.0124
0.5%	I	58.07	0.06	-11.17	9.75	-1.21	1.06	-1.88	-1.74	0.78	0.64	0.0161	-0.0528
	II	170.60	0.19	12.51	-11.33	1.36	-1.23	-3.72	-3.64	0.49	0.41	0.0696	0.0294
	III	111.60	0.12	11.27	10.17	1.22	1.10	-2.67	-2.58	0.56	0.47	0.0218	-0.1059
	IV	102.90	0.11	-12.20	-10.22	-1.32	-1.11	-2.61	-2.45	0.67	0.50	-0.0517	0.0068
1%	I	54.99	0.06	-12.10	10.71	-1.31	1.16	-1.93	-1.79	0.89	0.75	-0.0785	-0.1160
	II	194.50	0.21	16.55	-16.22	1.79	-1.76	-4.41	-4.38	0.73	0.71	0.2115	0.1203
	III	117.00	0.13	13.44	10.43	1.46	1.13	-2.94	-2.69	0.72	0.48	0.3249	-0.2630
	IV	104.60	0.11	-13.44	-11.69	-1.46	-1.27	-2.75	-2.60	0.77	0.62	-0.1708	0.4132
1.5%	I	52.28	0.06	-12.10	11.43	-1.31	1.24	-1.90	-1.83	0.91	0.84	-0.2207	-0.4401
	II	180.00	0.20	14.89	-14.13	1.61	-1.53	-4.05	-3.99	0.64	0.59	0.5177	0.3213
	III	104.70	0.11	10.34	9.88	1.12	1.07	-2.49	-2.45	0.51	0.47	0.5357	-0.6647
	IV	103.30	0.11	-10.55	-9.91	-1.14	-1.07	-2.48	-2.43	0.53	0.48	-0.3807	0.6831
2%	I	62.05	0.07	-10.55	9.60	-1.14	1.04	-1.87	-1.78	0.70	0.61	-0.6716	-1.0865
	II	165.30	0.18	11.17	-11.80	1.21	-1.28	-3.54	-3.58	0.41	0.46	1.4341	0.6019
	III	107.60	0.12	8.17	7.71	0.89	0.84	-2.37	-2.33	0.33	0.30	0.5186	-1.5402
	IV	107.50	0.12	-7.03	-7.12	-0.76	-0.77	-2.29	-2.29	0.25	0.26	-0.6123	0.9495
2.5%	I	73.63	0.08	-7.76	7.45	-0.84	0.81	-1.79	-1.76	0.40	0.37	-0.7047	-1.9294
	II	156.30	0.17	9.82	-8.93	1.07	-0.97	-3.30	-3.24	0.34	0.29	2.9864	1.5946
	III	113.40	0.12	7.03	5.43	0.76	0.59	-2.39	-2.29	0.24	0.15	2.0310	-2.4765
	IV	108.70	0.12	-4.65	-3.31	-0.50	-0.36	-2.17	-2.12	0.12	0.06	-1.0140	0.5982
3%	I	82.85	0.09	-5.79	4.86	-0.63	0.53	-1.79	-1.73	0.22	0.16	-1.5969	-2.3065
	II	145.60	0.16	8.38	-8.12	0.91	-0.88	-3.03	-3.01	0.27	0.26	0.1212	-0.0885
	III	109.30	0.12	6.52	5.56	0.71	0.60	-2.28	-2.23	0.22	0.16	0.1212	-0.0885
	IV	112.00	0.12	-3.72	-5.77	-0.40	-0.63	-2.19	-2.29	0.07	0.17	0.1212	-0.0885

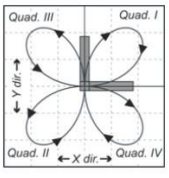

Quadrants in bidirectional loading pattern

[a] Axial load: $N=N_g \pm \alpha_x V_{cx} \pm \alpha_y V_{cy}$

[b] Axial load ratio; [c, d] Story column shear in x- and y-direction, respectively;

[e, f] Horizontal joint shear stress in the joint in x- and y-direction, respectively;

[g, h] Principal compression stress in the joint panel in x- and y-direction, respectively;

[i, j] Principal tension stress in the joint in x- and y-direction, respectively;

[k, l] Joint shear deformation in x- and y-direction, respectively;

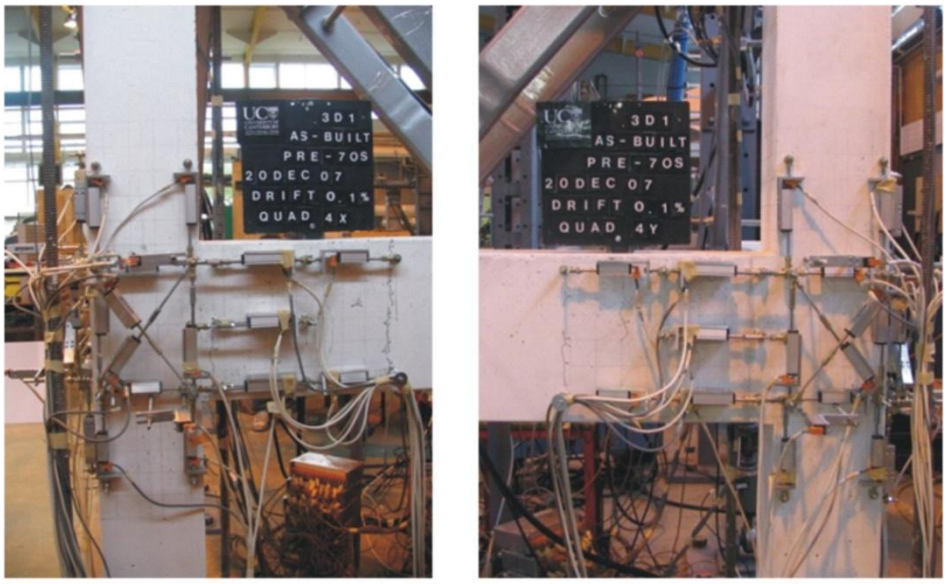

a) x-direction view - 4th quadrant

b) y-direction view - 4th quadrant

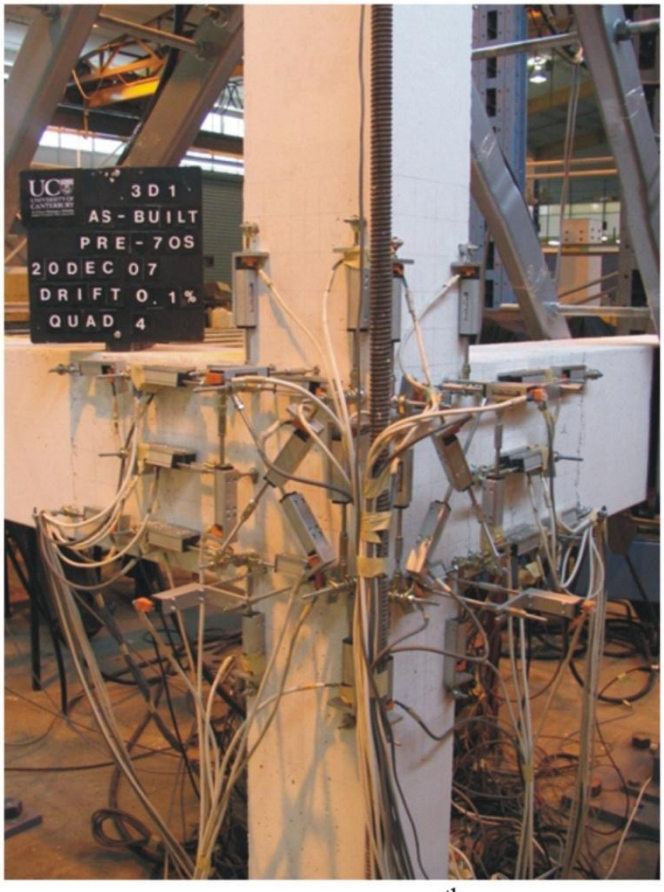

c) trimetric view of corner joint - 4th quadrant

Figure 9–5 Damage propagation - Specimen 3D1, 0.1% drift

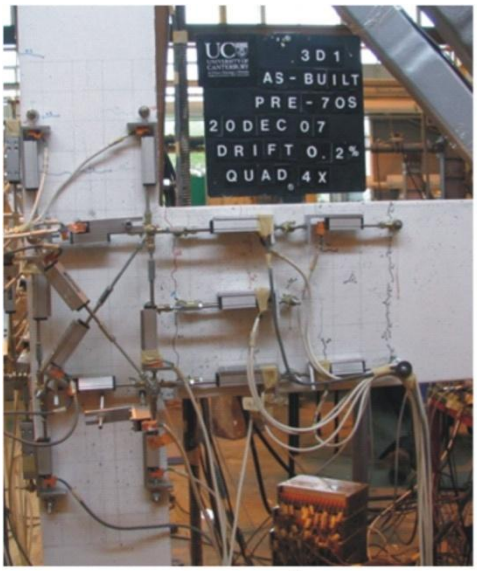

a) x-direction view - 4th quadrant

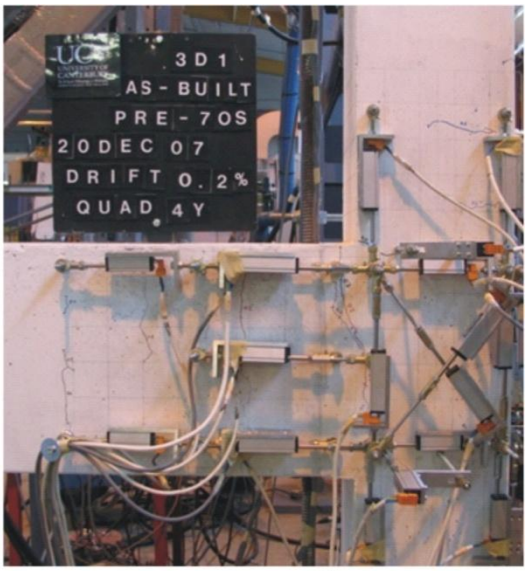

b) y-direction view - 4th quadrant

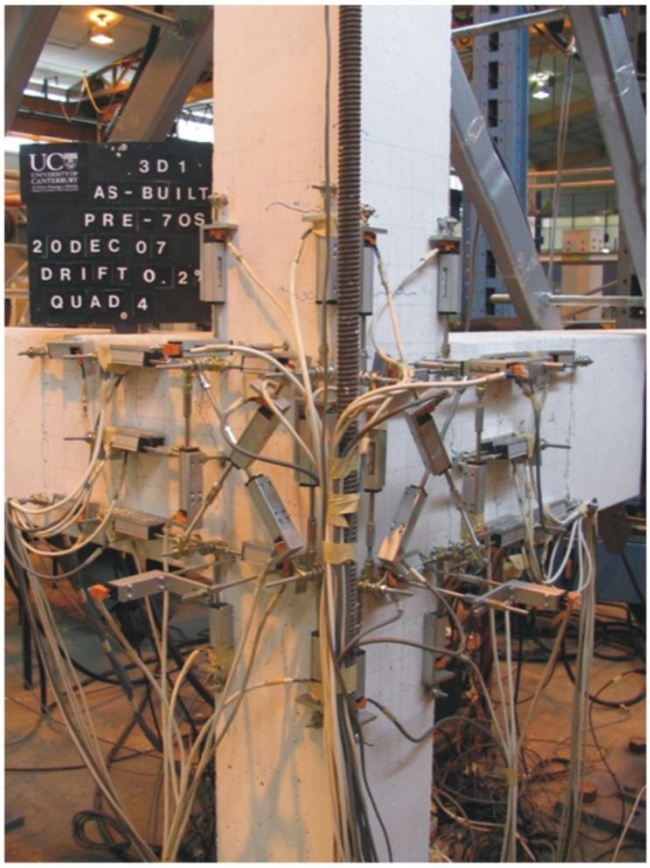

c) trimetric view of corner joint - 4th quadrant

Figure 9–6 Damage propagation - Specimen 3D1, 0.2% drift

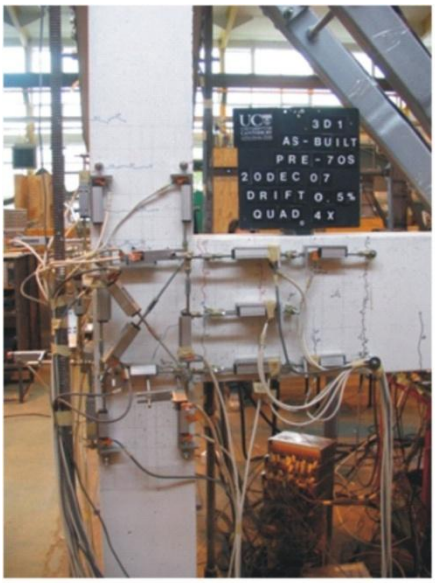

a) x-direction view - 4th quadrant

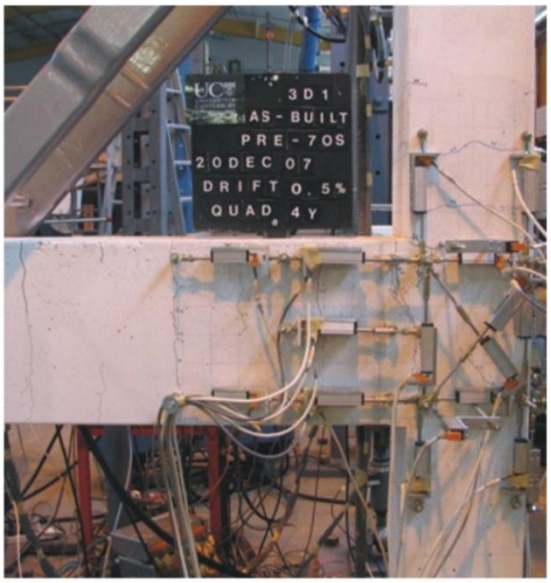

b) y-direction view - 4th quadrant

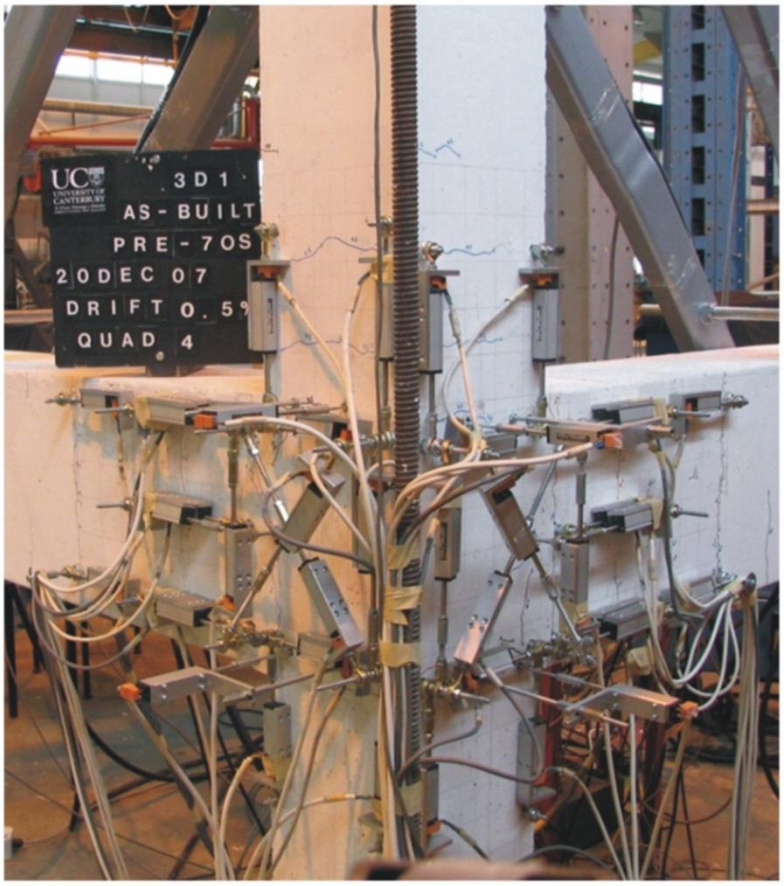

c) trimetric view of corner joint - 4th quadrant

Figure 9–7 Damage propagation - Specimen 3D1, 0.5% drift

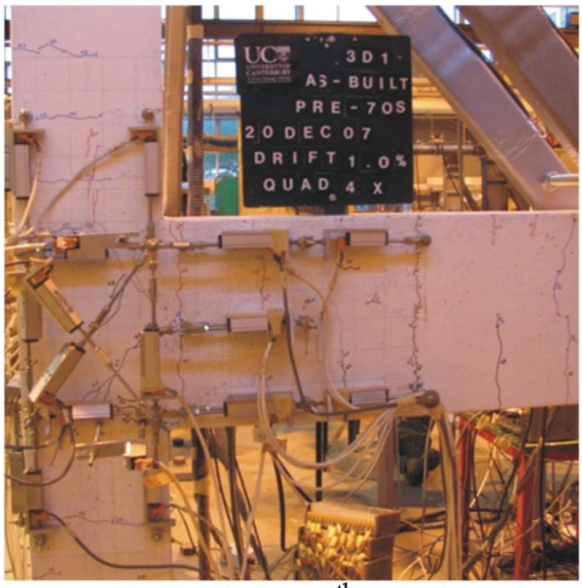

a) x-direction view - 4th quadrant

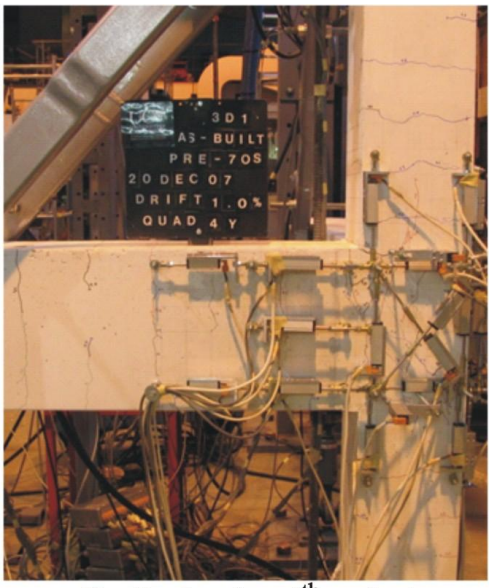

b) y-direction view - 4th quadrant

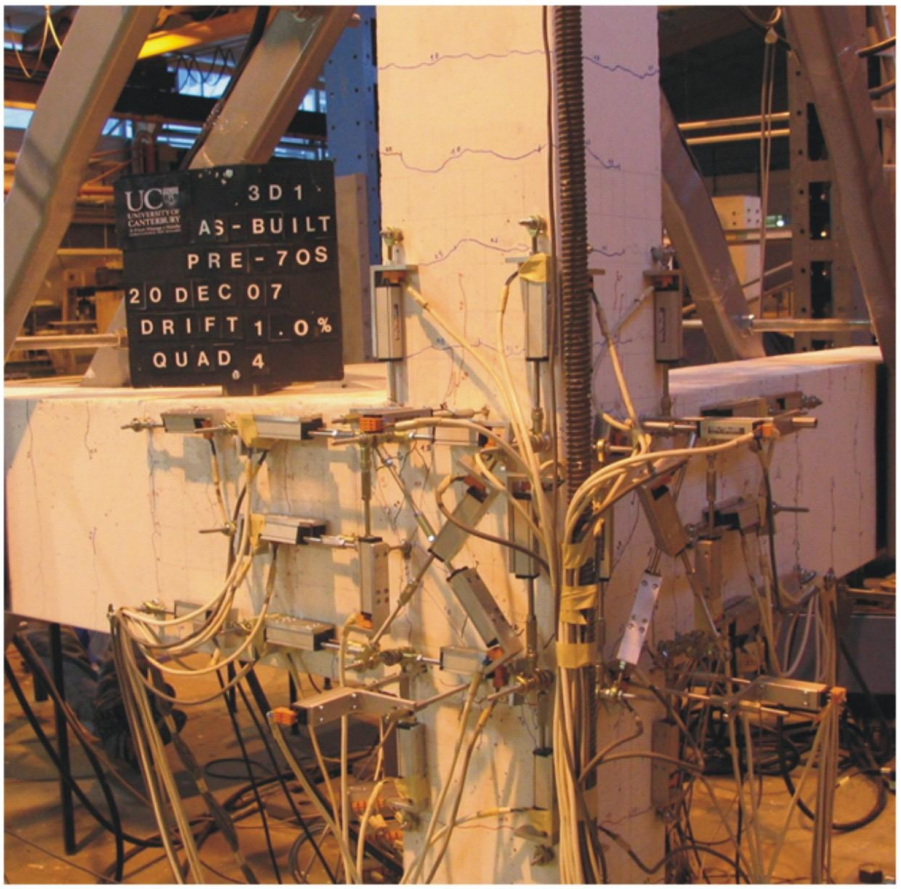

c) trimetric view of corner joint - 4th quadrant

Figure 9–8 Damage propagation - Specimen 3D1, 1% drift

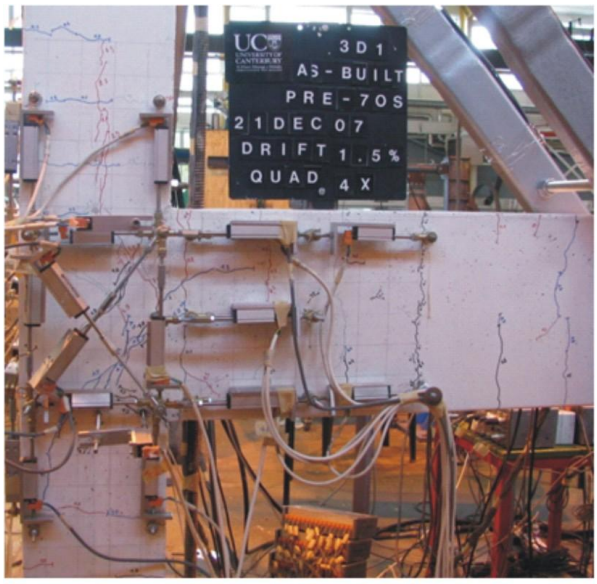

a) x-direction view - 4th quadrant

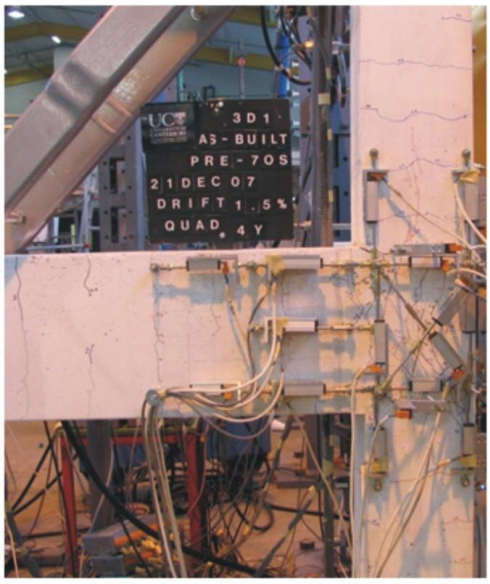

b) y-direction view - 4th quadrant

c) trimetric view of corner joint - 4th quadrant

Figure 9–9 Damage propagation - Specimen 3D1, 1.5% drift

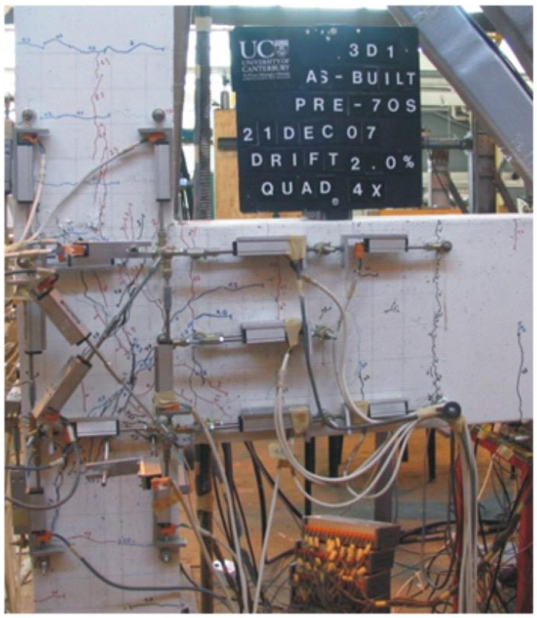

a) x-direction view - 4th quadrant

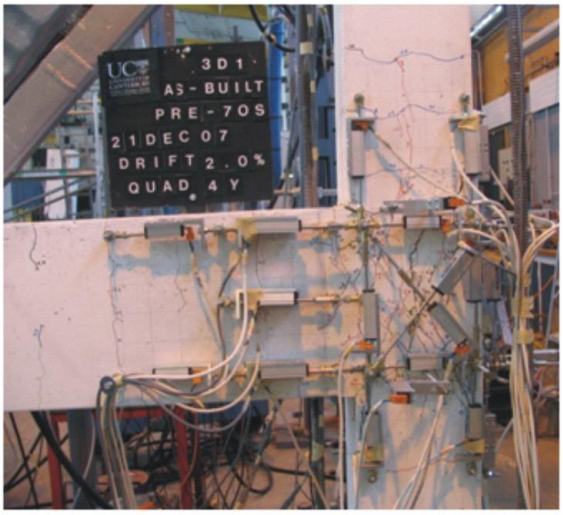

b) y-direction view - 4th quadrant

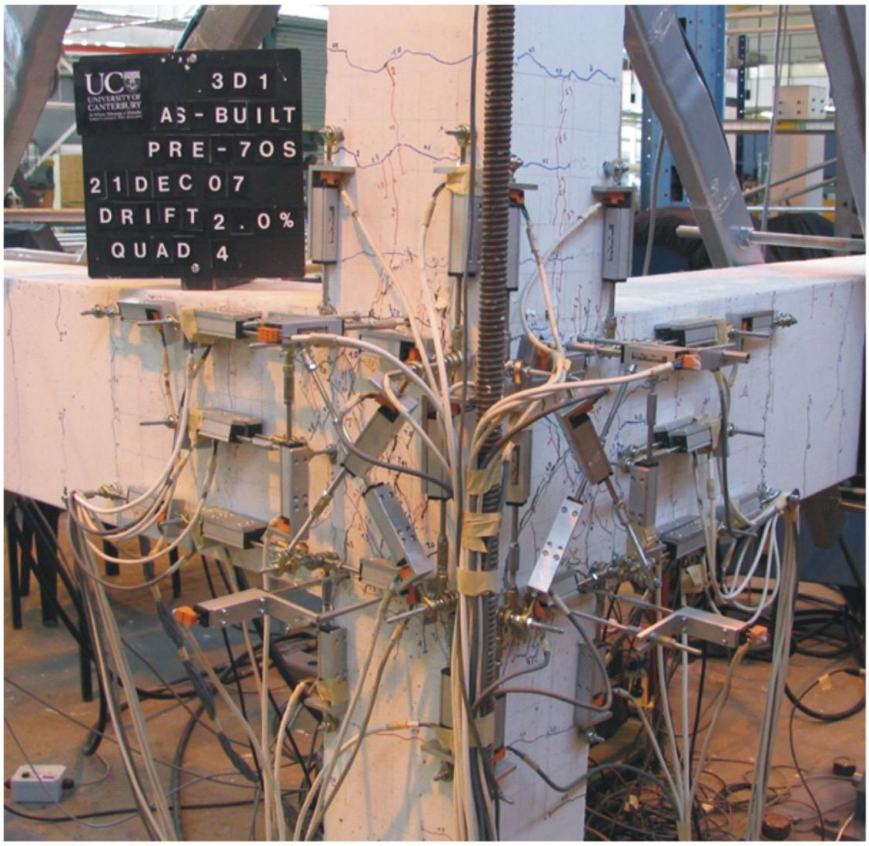

c) trimetric view of corner joint - 4th quadrant

Figure 9–10 Damage propagation - Specimen 3D1, 2% drift

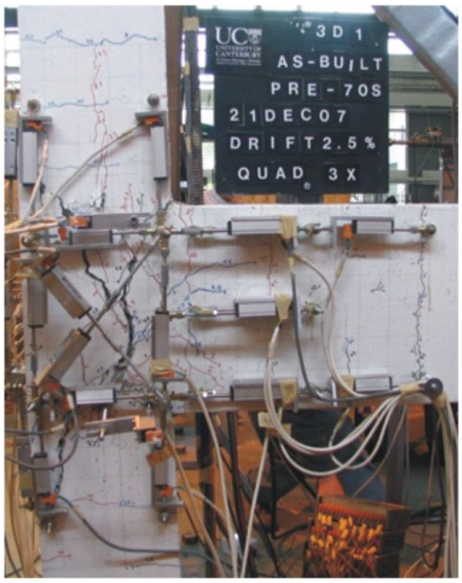

a) x-direction view - 4th quadrant

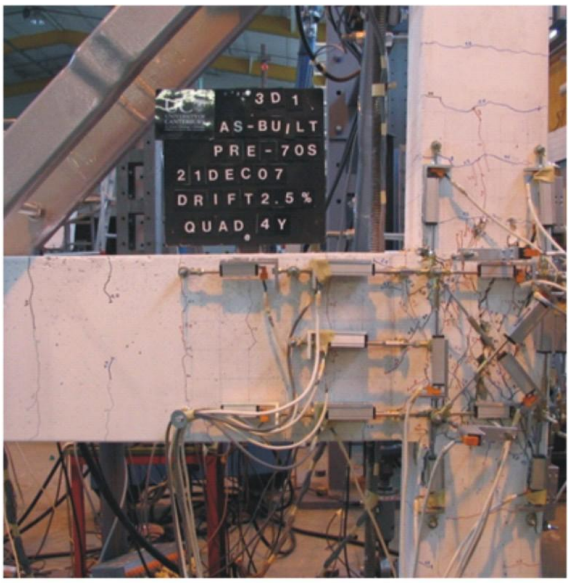

b) y-direction view - 4th quadrant

c) trimetric view of corner joint - 4th quadrant

Figure 9–11 Damage propagation - Specimen 3D1, 2.5% drift

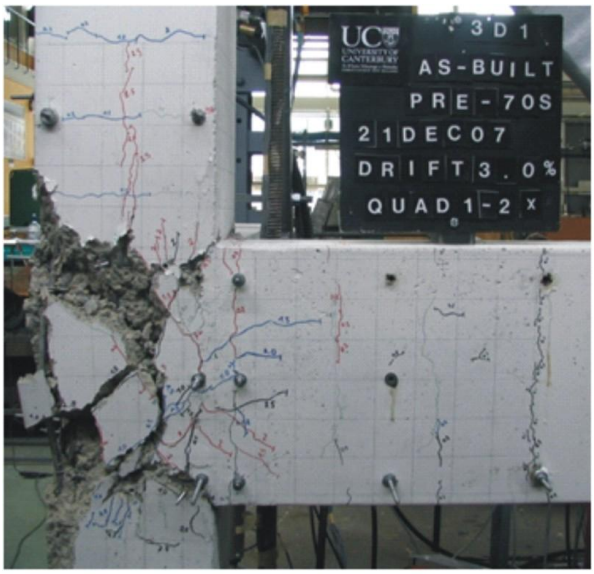

a) x-direction view - 4th quadrant

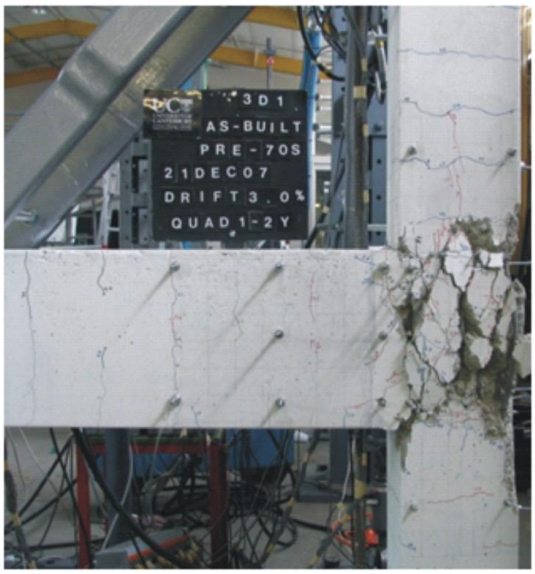

b) y-direction view - 4th quadrant

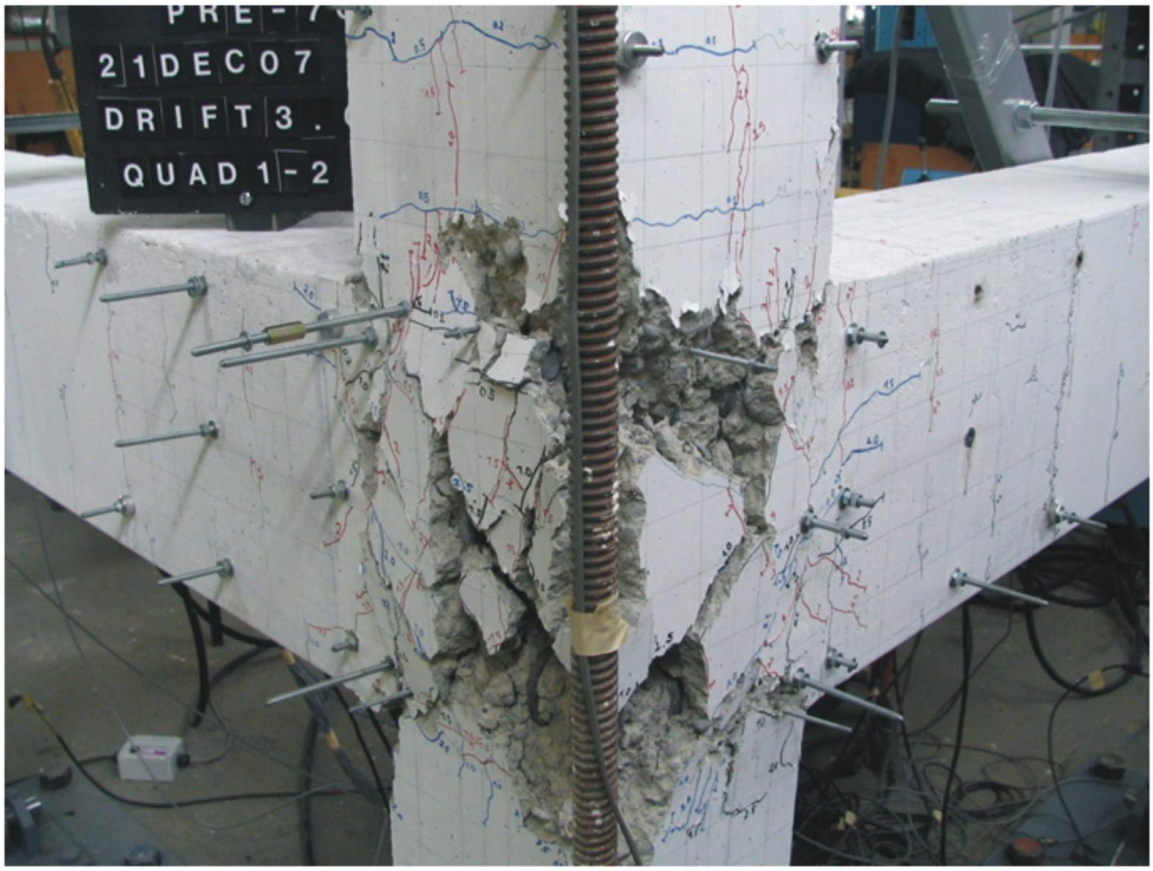

c) trimetric view of corner joint - 4th quadrant

Figure 9–12 Damage propagation - Specimen 3D1, 3% drift

9.2.2 Retrofitted Specimen 3D2

Specimen 3D2 is a 3D corner beam-column joint unit retrofitted with FRP and tested under bidirectional and concurrent axial load variation on the column. Using the same axial load and retrofit scheme which was successfully validated in the test of 2D4, also the same R21 FRP scheme was adopted in Specimen 3D2. The main aim was to investigate the possible negative effects of bidirectional loading on the performance of the retrofitted corner joints when designed according to unidirectional behaviour assumptions. Following the observations such as failure mechanisms and limit states, the retrofit design for corner beam-column joints was upgraded. A unified retrofit design scheme was then proposed for corner beam-column joints, as well as for those with floor slabs. The same loading protocol as described in the previous section for the Specimen 3D1 was employed. The test results highlighted the higher demands for the retrofitted 3D corner joint when compared to its counterpart 2D joint, Specimen 2D4. The Specimen 3D2 suffered more damage due to a different failure mechanisms and exhibited lower load bearing capacity. The observed damage and crack formation during the test are summarized in the following paragraph. The final damage stage of the Specimen 3D2 is also illustrated in Figure 9–13. The lateral force-displacement response in x- and y-direction and bidirectional hysteresis loops are given in Figure 9–14, Figure 9–15, and Figure 9–16 respectively. In Table 9-2, a summary of the test results in terms of recorded values corresponding to 45 degrees of skew angle in the bidirectional loading are tabulated for each quadrant of associated drift level.

Up to 1.5% drift level, no major damage occurred in the specimen. Uniformly distributed flexural cracks in the beams developed, starting from 0.2% drift with crack widths ranging from 0.20 to 0.75 mm (Figure 9–17 and Figure 9–18). The specimen reached its maximum load bearing capacity at the second quadrant of 1.5% drift level. The recorded values in the x-direction of loading were 17.79 and 20.48 kN with joint shear stress values of $0.51\sqrt{f`_c}$ and $0.59\sqrt{f`_c}$ for the pull and push directions, respectively. The recorded values in the y-direction of loading were 17.75 and 19.92 kN with joint shear stress values of $0.51\sqrt{f`_c}$ and $0.57\sqrt{f`_c}$ for the pull and push directions, respectively. Also, at this drift level detachment of the GFRP started in the beams (Figure 9–21). At the end of 1.5%, the beam-column interface FRP sheet started to detach on the top and bottom periphery of the column (Figure 9–22). In both directions of loading at 2.5% drift, an abrupt complete detachment of the beam GFRP sheets occurred (Figure 9–23). In the following cycles, due to the diagonal compression strut developing in the joint, bulging of the column sheet started to become evident. During the cycles of 3% and 4% drift, the load carrying capacity continued to drop drastically. As a result of the extension

of the GFRP debonding from the vicinity of the joint to the upper and lower column regions and crushed concrete under these regions, buckling and partial rupture of the column sheets continued (Figure 9–24 and Figure 9–25). Post-test observation revealed severe damage in the joint region.

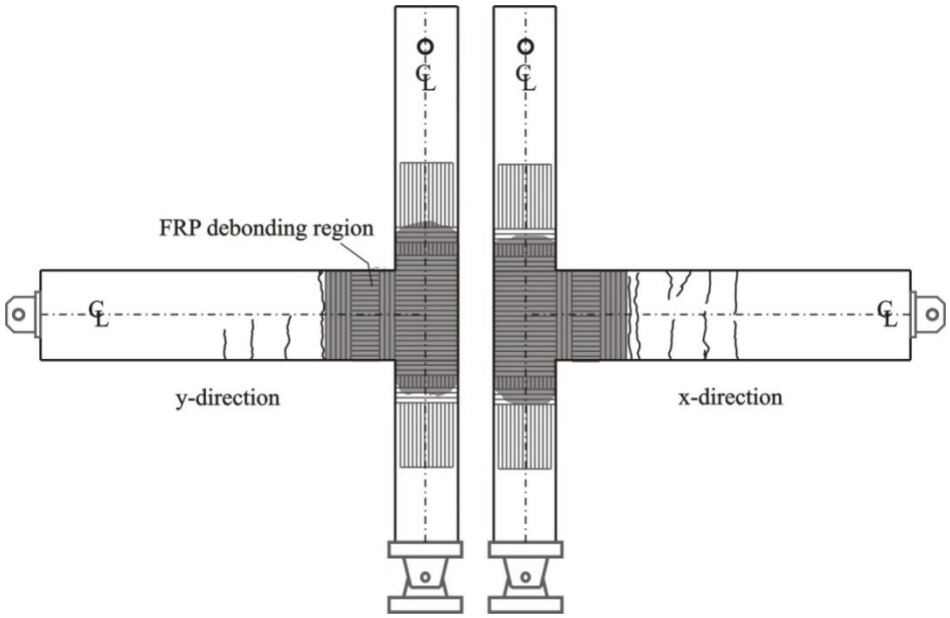

Figure 9–13 Crack patterns at final stage for Specimen 3D2

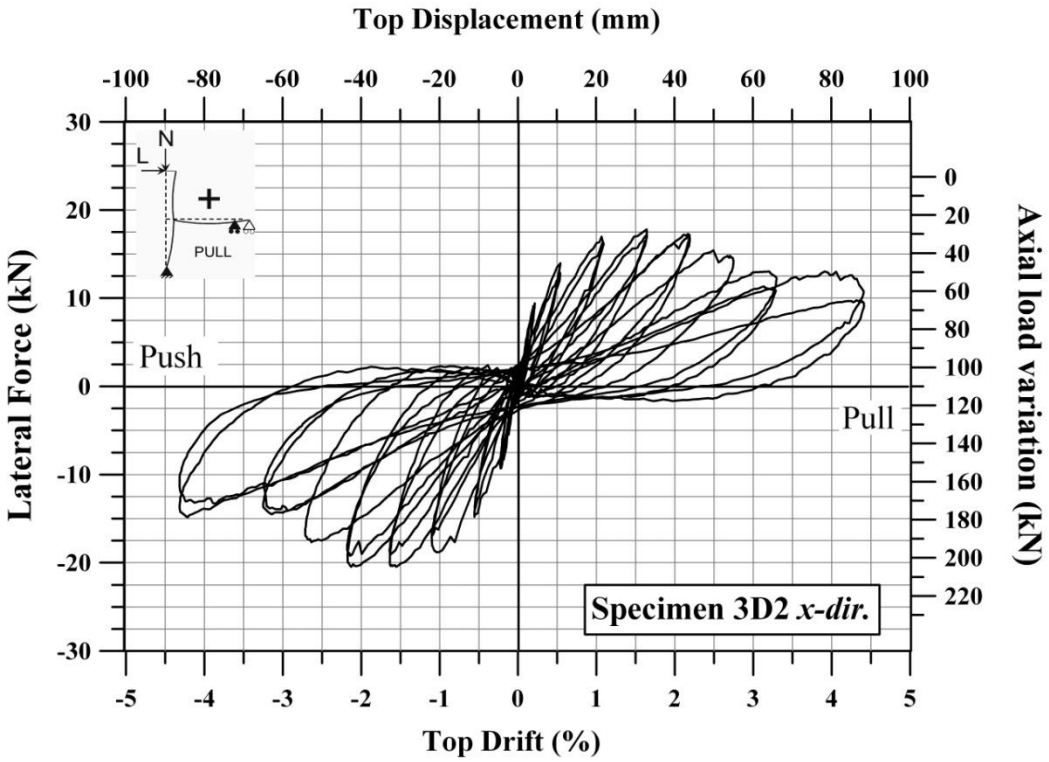

Figure 9–14 Lateral force paths for Specimen 3D2, x-direction

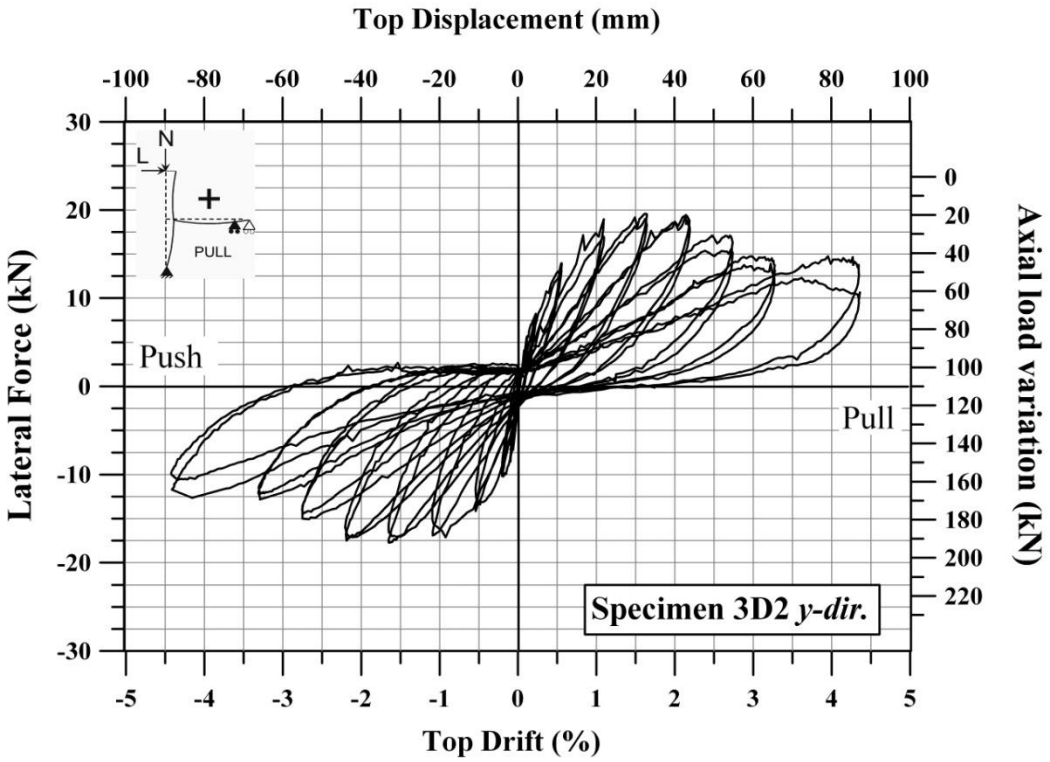

Figure 9–15 Lateral force paths for Specimen 3D2, y-direction

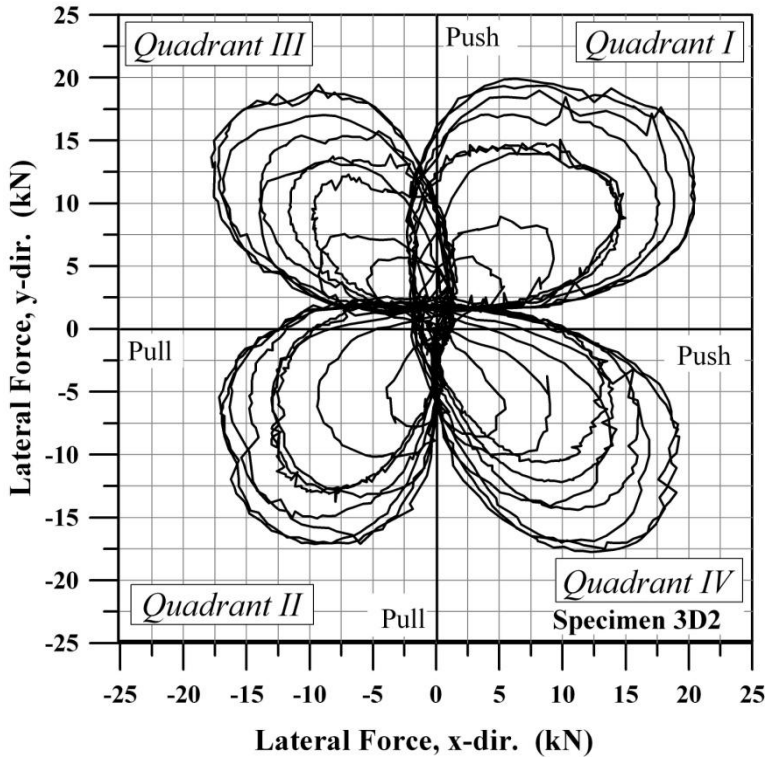

Figure 9–16 Bidirectional lateral force paths for Specimen 3D2

Table 9-2 Summary of test results for Specimen 3D2

Drift Level	Quadrant	Axial Load		Strength				Joint Panel Results					
		N [a] (kN)	$N/(A_g f_c')$ [b]	V_{cx} [c] (kN)	V_{cy} [d] (kN)	v_{jhx} [e] (MPa)	v_{jhy} [f] (MPa)	p_{cx} [g] (MPa)	p_{cy} [h] (MPa)	p_{tx} [i] (MPa)	p_{ty} [j] (MPa)	γ_x [k] (%)	γ_y [l] (%)
0.1%	I	85.24	0.10	-2.90	7.30	-0.31	-0.79	-1.67	-1.93	0.06	0.32	-0.0878	0.1085
	II	128.50	0.14	4.34	-4.71	0.47	0.51	-2.52	-2.53	0.09	0.10	-0.0885	0.1147
	III	98.31	0.11	4.34	8.25	0.47	-0.89	-1.97	-2.22	0.11	0.36	-0.0878	0.1092
	IV	108.10	0.12	-4.55	-5.51	-0.49	0.60	-2.16	-2.21	0.11	0.16	-0.0858	0.1154
0.2%	I	72.54	0.08	-8.07	8.59	-0.87	-0.93	-1.80	-1.84	0.43	0.47	-0.0851	0.1072
	II	145.60	0.16	8.79	-7.97	0.95	0.86	-3.05	-3.00	0.30	0.25	-0.0906	0.1201
	III	102.70	0.11	7.96	9.65	0.86	-1.05	-2.27	-2.40	0.33	0.46	-0.0892	0.1092
	IV	110.50	0.12	-8.38	-7.32	-0.91	0.79	-2.43	-2.36	0.34	0.27	-0.0796	0.1229
0.5%	I	59.65	0.07	-10.55	11.43	-1.14	-1.24	-1.84	-1.93	0.71	0.80	-0.0721	0.0635
	II	172.30	0.19	12.41	-12.75	1.35	1.38	-3.74	-3.76	0.48	0.51	-0.1098	0.1461
	III	109.00	0.12	12.20	12.81	1.32	-1.39	-2.71	-2.76	0.65	0.70	-0.1022	0.0335
	IV	111.20	0.12	-12.62	-11.98	-1.37	1.30	-2.78	-2.72	0.67	0.62	-0.0542	0.1420
1%	I	41.61	0.05	-13.24	13.87	-1.44	-1.50	-1.88	-1.95	1.10	1.16	-0.0234	-0.1257
	II	181.30	0.20	15.82	-16.20	1.72	1.76	-4.14	-4.17	0.71	0.74	-0.1616	0.0628
	III	106.60	0.12	14.17	15.96	1.54	-1.73	-2.84	-3.01	0.83	0.99	-0.2837	-0.2208
	IV	111.00	0.12	-15.61	-14.77	-1.69	1.60	-3.04	-2.96	0.94	0.87	0.1496	0.2072
1.5%	I	37.74	0.04	-14.06	14.62	-1.52	-1.59	-1.92	-1.98	1.21	1.27	0.0107	-0.2686
	II	191.30	0.21	18.20	-16.95	1.97	1.84	-4.48	-4.39	0.87	0.77	-0.2552	0.0332
	III	108.10	0.12	16.24	16.69	1.76	-1.81	-3.06	-3.10	1.01	1.06	-0.4265	-0.3528
	IV	110.10	0.12	-16.44	-16.30	-1.78	1.77	-3.10	-3.09	1.02	1.01	0.4298	0.3610
2%	I	42.90	0.05	-14.17	15.06	-1.54	-1.63	-1.99	-2.09	1.18	1.28	0.0878	-0.3445
	II	188.90	0.21	15.61	-17.64	1.69	1.91	-4.25	-4.40	0.67	0.83	-0.2183	0.0415
	III	111.00	0.12	16.75	16.20	1.82	-1.76	-3.15	-3.10	1.05	1.00	-0.4377	-0.5520
	IV	111.60	0.12	-16.24	-16.51	-1.76	1.79	-3.11	-3.13	1.00	1.02	0.6079	0.4957
2.5%	I	44.37	0.05	-13.55	13.25	-1.47	-1.44	-1.95	-1.92	1.11	1.08	0.2235	-0.2352
	II	179.90	0.20	14.48	-15.16	1.57	1.64	-4.01	-4.07	0.61	0.66	0.0163	4.2059
	III	111.00	0.12	13.75	13.25	1.49	-1.44	-2.87	-2.83	0.77	0.73	-0.1421	3.8492
	IV	110.10	0.12	-13.13	-13.32	-1.42	1.44	-2.80	-2.82	0.72	0.74	0.3812	4.1551
3%	I	53.21	0.06	-11.06	11.49	-1.20	-1.25	-1.80	-1.85	0.80	0.84	0.3304	3.9060
	II	166.80	0.19	13.13	-12.13	1.42	1.32	-3.70	-3.63	0.55	0.48	0.2162	3.8389
	III	106.60	0.12	11.79	11.33	1.28	-1.23	-2.64	-2.60	0.62	0.58	-0.1381	3.5742
	IV	111.00	0.12	-11.17	-11.62	-1.21	1.26	-2.65	-2.69	0.55	0.59	0.1544	3.7576
4%	I	53.21	0.06	-11.89	11.72	-1.29	-1.27	-1.89	-1.87	0.88	0.86	0.4125	3.6536
	II	165.50	0.19	12.41	-12.60	1.35	1.37	-3.63	-3.64	0.50	0.51	-0.0555	3.4464
	III	132.70	0.15	-1.24	-9.99	-0.13	1.08	-2.52	-2.91	0.01	0.40	-0.2391	3.4985
	IV	111.00	0.12	-9.62	-10.06	-1.04	1.09	-2.53	-2.56	0.43	0.46	-0.1039	3.1708

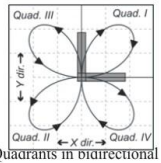

Quadrants in bidirectional loading pattern

[a] Axial load: $N=N_g \pm \alpha_x V_{cx} \pm \alpha_y V_{cy}$

[b] Axial load ratio; [c, d] Story column shear in x- and y-direction, respectively;

[e, f] Horizontal joint shear stress in the joint in x- and y-direction, respectively;

[g, h] Principal compression stress in the joint panel in x- and y-direction, respectively;

[i, j] Principal tension stress in the joint in x- and y-direction, respectively;

[k, l] Joint shear deformation in x- and y-direction, respectively;

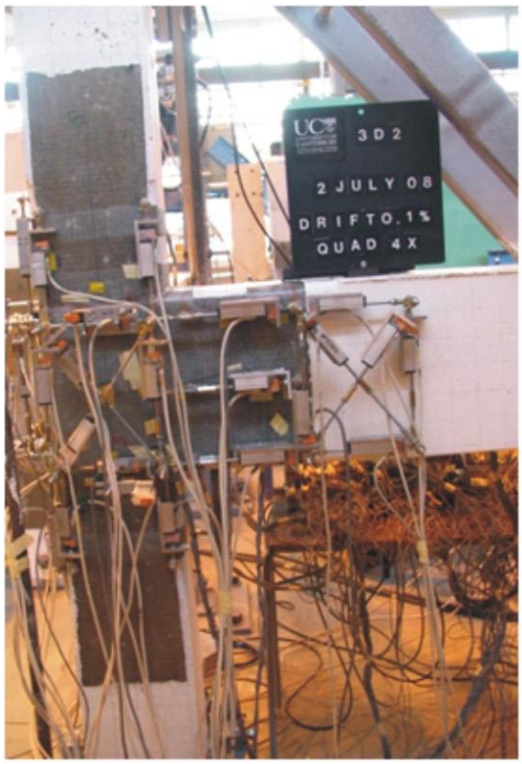

a) x-direction view - 4th quadrant

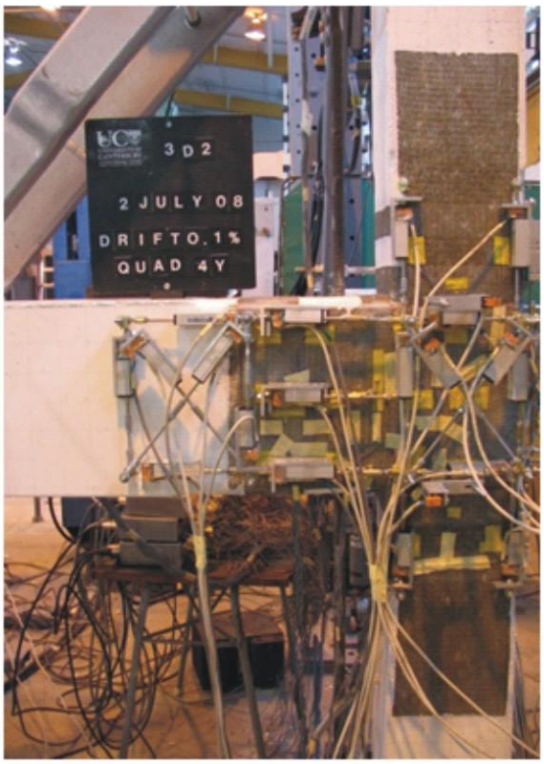

b) y-direction view - 4th quadrant

Figure 9–17 Damage propagation - Specimen 3D2, 0.1% drift

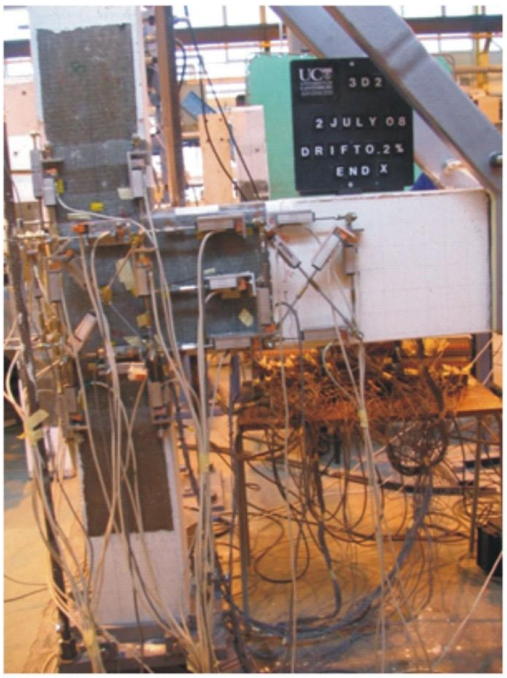

a) x-direction view - 4th quadrant

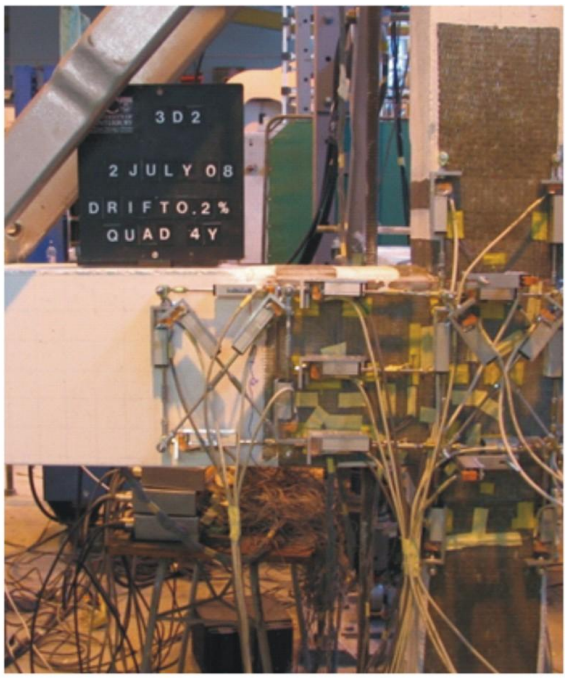

b) y-direction view - 4th quadrant

Figure 9–18 Damage propagation - Specimen 3D2, 0.2% drift

a) x-direction view - 4th quadrant b) y-direction view - 4th quadrant

Figure 9–19 Damage propagation - Specimen 3D2, 0.5% drift

a) x-direction view - 4th quadrant b) y-direction view - 4th quadrant

Figure 9–20 Damage propagation - Specimen 3D2, 1% drift

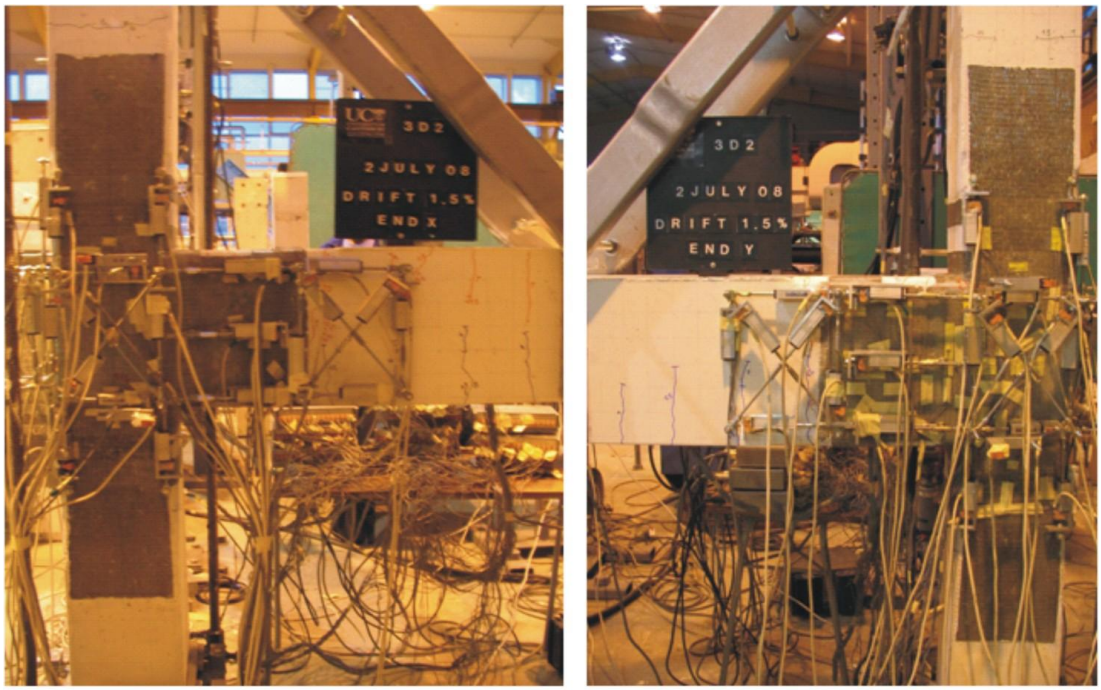

a) x-direction view - 4th quadrant b) y-direction view - 4th quadrant

Figure 9–21 Damage propagation - Specimen 3D2, 1.5% drift

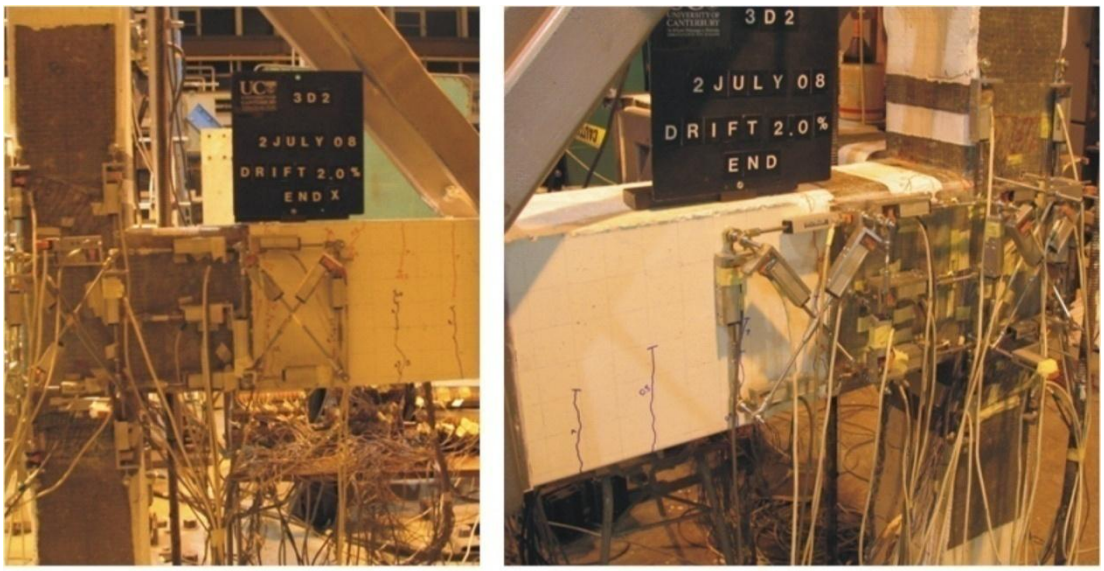

a) x-direction view - 4th quadrant b) y-direction view - 4th quadrant

Figure 9–22 Damage propagation - Specimen 3D2, 2% drift

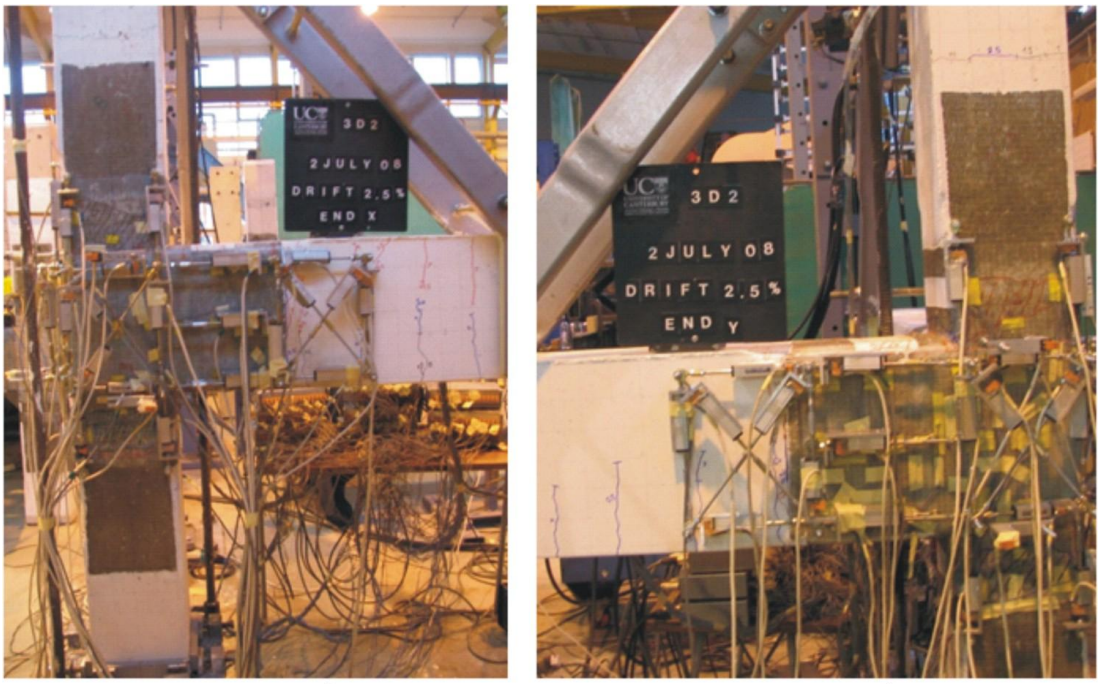

a) x-direction view - 4th quadrant b) y-direction view - 4th quadrant

Figure 9–23 Damage propagation - Specimen 3D2, 2.5% drift

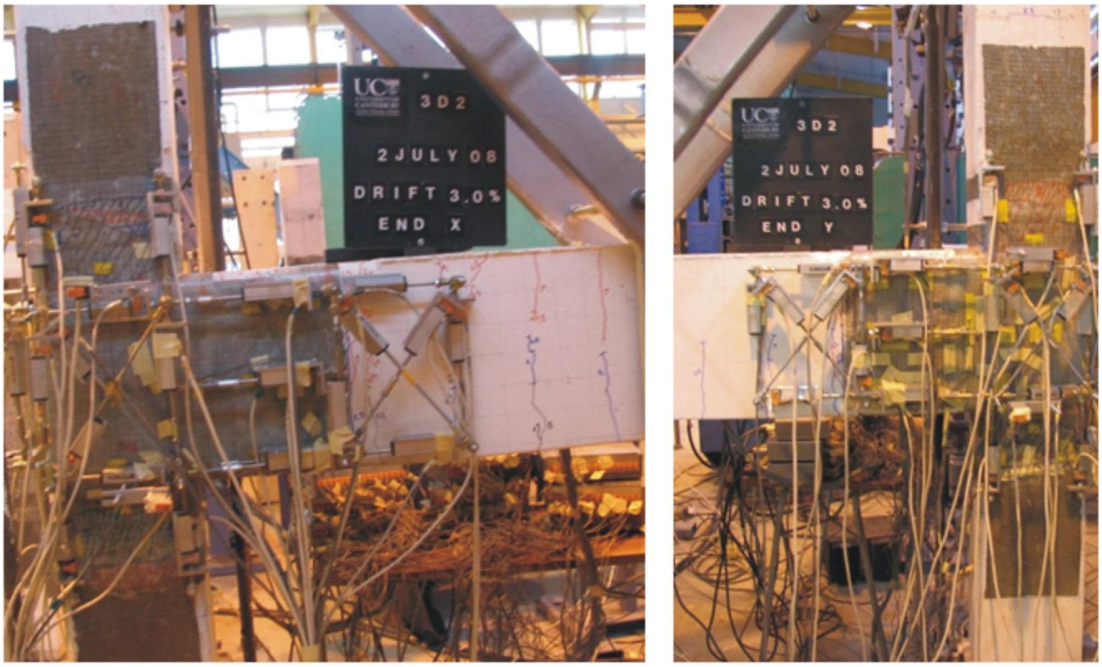

a) x-direction view - 4th quadrant b) y-direction view - 4th quadrant

Figure 9–24 Damage propagation - Specimen 3D2, 3% drift

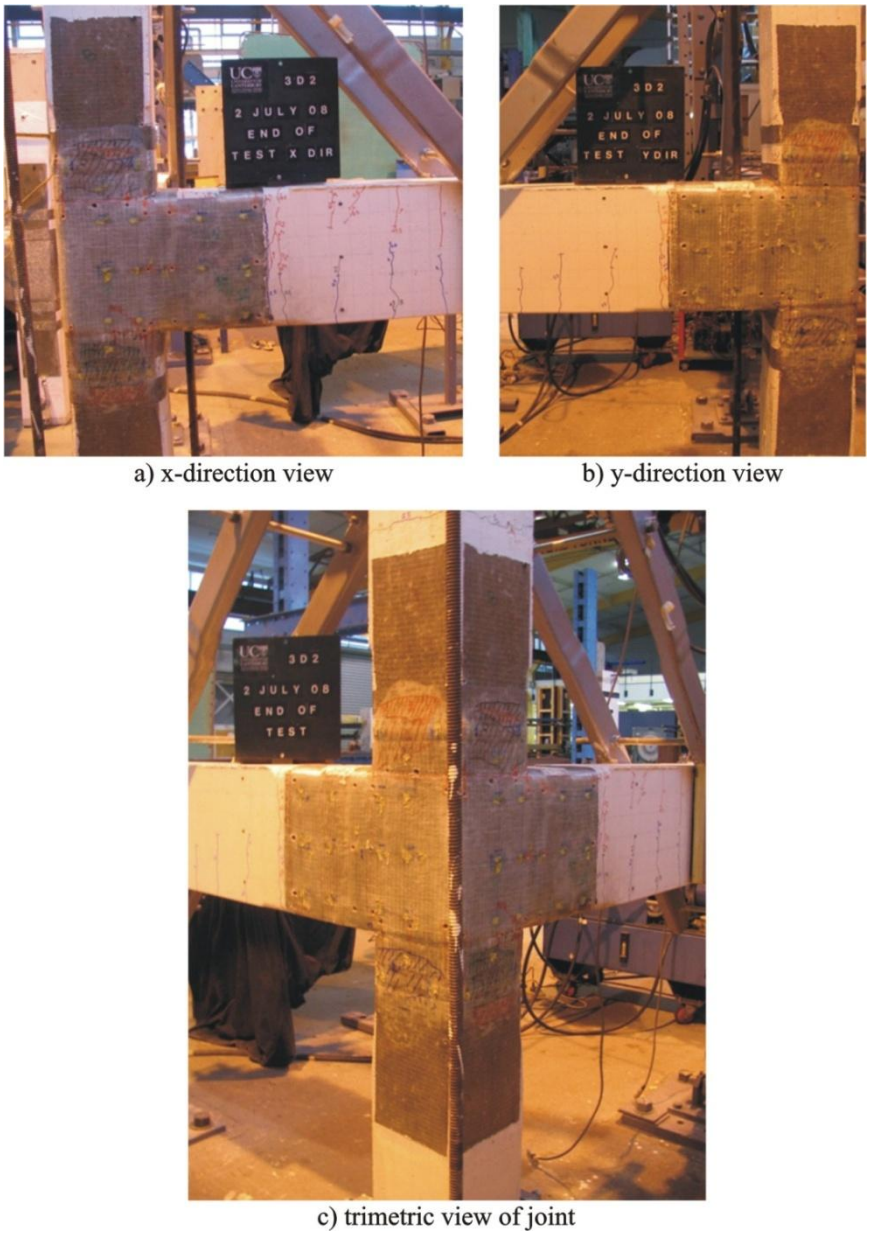

a) x-direction view b) y-direction view

c) trimetric view of joint

Figure 9–25 Damage propagation - Specimen 3D2, 4% drift

9.3 ANALYSIS OF TEST RESULTS

In this section the test results are analysed and discussed based on the observed damage and recorded instrumentation readings of all the specimens. In the comparison and discussion, particular focus is given to the effect of bidirectional loading with concurrent axial load variation to the performance of the as-built and retrofitted 3D beam-column joint units. Since one of the objectives pursued in this thesis is to investigate the possible effects of bidirectional loading on the corner joints retrofitted based on the unidirectional assumptions, it is of crucial importance to compare the seismic performance of

3D specimens with their 2D counterparts. For this purpose, the test results of unidirectional as-built and retrofitted 2D exterior joint units are included in this chapter. With this purpose in mind, results pertaining to both test series have been carefully selected in order to analyze the aforementioned points.

9.3.1 Strength and Failure Modes

In general, the cyclic biaxial bending moments and column shear forces in two axes worked in the direction of reducing the capacity of column, beam and joint elements of 3D corner beam-column joints in both the as-built and retrofitted configurations. A significant decrease in the strength and rapid stiffness degradation occurred when compared to their 2D counterpart units (i.e., Specimen 2D1 and Specimen 2D4). The test results showed that the inelastic biaxial interaction caused yielding of the reinforcement and/or crushing of the concrete, as well as debonding of FRP sheets at lower loads than the recorded values and at the comparable drift levels of unidirectional tests. The decay in resistance after reaching the maximum resistance was also faster. Hence, it is concluded that the additional demand stemming from biaxial effects should be taken into account in the assessment and/or retrofit design of older corner beam-column joints for more strength and deformation capacity of the structural members. In order to illustrate the bidirectional effects on the performance of the specimens, the force-drift response and the summary of test results are given in Figure 9-26 and Table 9-3, respectively.

Specimen 3D1 exhibited the worst seismic performance amongst the tested 2D and 3D joint units. Biaxial loading combined with significant variations in axial load imposed more deformation and strength demand on the specimen. The specimen 3D1 failed after heavy flexural and inclined cracking, spalling of concrete and disintegration of the core concrete (mainly due to propagation of inclined cracks and grinding along the concrete) followed by buckling of the column bars. A complex three-dimensional concrete wedge mechanism was observed to initiate during the early stages of the test (after 1% drift), following the shear cracking of joint panel zone at 0.5% drift.

Table 9-3 presents a summary of the test results at both global and local level (joint panel zone behaviour), as measured and/or calculated at peak drift values. The displacement ductility μ is defined, as Δ_u/Δ_y, where Δ_u is the horizontal displacement corresponding to the displacement, when the load carrying capacity undergoes a 20% reduction in load or significant failure of the specimen occurs. The yield displacement Δ_y is defined as the displacement of the equivalent elasto-plastic system with the same energy absorption as the real system [1].

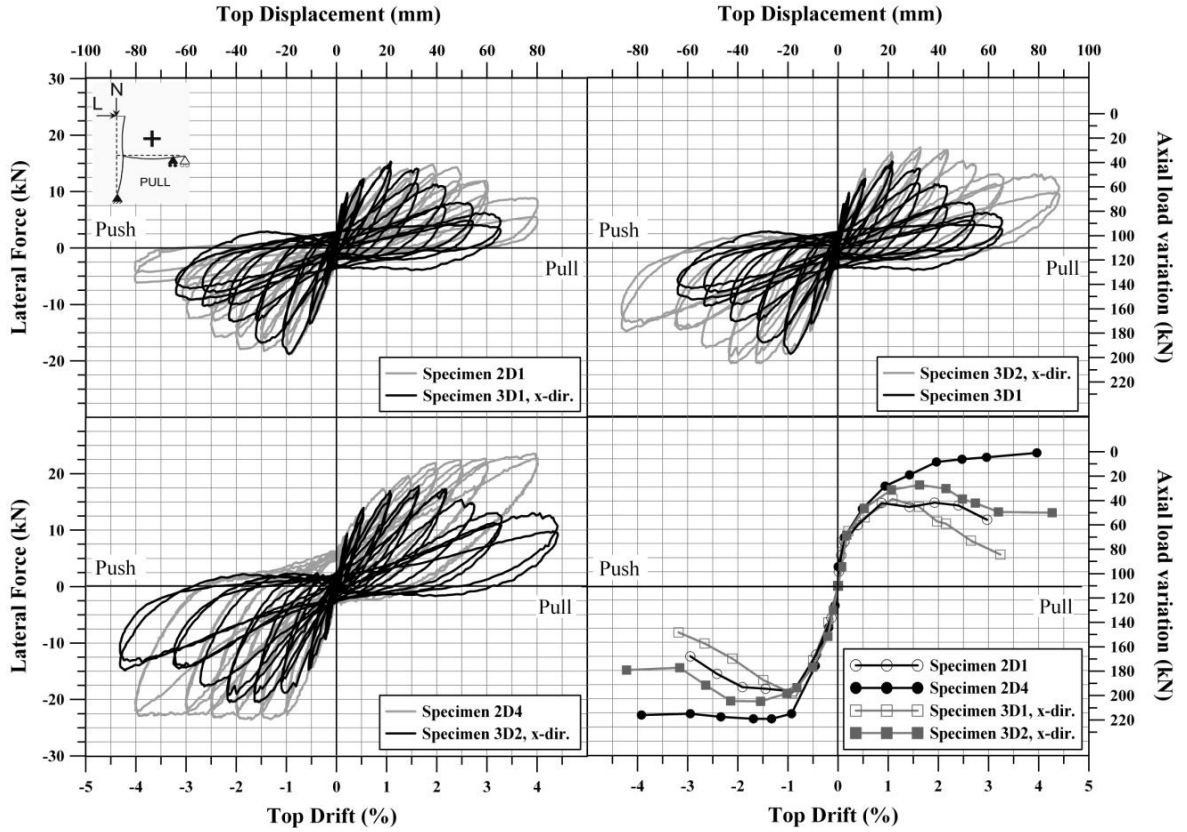

Figure 9–26 Force-drift response of 3D corner joints and comparison with 2D exterior joints

Table 9-3 Summary of test results of 3D corner joints and comparison with 2D exterior joints

Specimen	Direction	Strength		Axial Load		Ductility	Joint Panel Results					Dissipated Energy	Failure Mode
		V_c [a] (kN)	v_{jh} [b] (MPa)	f_v [c] (MPa)	Δ_y [d] (mm)	$\mu = \Delta u^e / \Delta y$	p_c [f] (MPa)	p_t [g] (MPa)	γ_1 [h] (%)	γ_2 [i] (%)	γ_3 [j] (%)	E_{df} [k] (kNmm)	
2D1	Pull	14.89	0.82	1.61	11.04	1	-2.08	1.25	0.260	0.942	1.739	3319	Joint shear
	Push	-18.92	2.05	3.67	-14.02	4	-4.59	0.91	0.014	0.342	1.200		
2D4	Pull	23.58	2.56	0.01	26.80	3	-2.60	2.51	0.374	0.390	0.410	9277	Ductile beam hinging
	Push	-23.89	-2.59	2.05	-16.48	5	-3.81	1.76	0.187	0.119	0.092		
3D1	Pull, x-dir.	15.30	1.66	1.16	10.70	3	-2.34	1.18	0.150	0.930	2.010	4848	Joint Shear
	Push, x-dir.	-18.82	-2.04	3.59	-14.97	1	-4.51	0.92	0.230	1.450	-		
	Pull, y-dir.	13.58	-1.47	1.33	7.91	4	-2.28	0.94	0.130	1.170	2.450	4431	
	Push, y-dir.	-18.26	1.98	3.33	-11.47	2	-4.25	0.92	0.220	1.130	-		
3D2	Pull, x-dir.	17.79	1.92	1.95	13.96	4	-3.13	1.18	0.020	0.250	0.370	7625	GFRP debonding and interface separation
	Push, x-dir.	-20.48	-2.22	3.49	-15.00	4	-4.57	1.08	0.160	0.270	0.180		
	Pull, y-dir.	17.75	-1.92	1.84	11.33	5	-3.06	1.21	0.120	0.340	-	7640	
	Push, y-dir.	-19.92	2.16	3.21	-15.98	4	-4.30	1.08	0.100	0.120	-		

[a] Story column shear; [b] Horizontal joint shear stress in the joint; [c] Nominal axial stress;
[d] Yield displacement defined as the displacement of the equivalent elasto-plastic system with the same energy absorption as the real system;
[e] Ultimate displacement corresponds to the displacement at a 20% reduction in load; [f] Principal compression stress in the joint; [g] Principal tension stress in the joint;
[h, i, j] Joint shear deformation at 1, 2 and 3 percent drift levels, respectively; [k] Cumulative dissipated energy for all cycles up to failure.

In the previous Chapters 3 and 7 the mechanism of exterior plane frame and space frame joints has been reviewed. It is noted that the shear resistance mechanism of a joint under unidirectional loading can be extended to a space frame joint. However, in the latter case, the orientation of the critical planes where the compression struts are forming in the joint panel zone is far more complex compared to that of the 2D joints tested under unidirectional loading. The stress concentrations at each end of the diagonal struts could develop at six faces of the joint core approximately across the diagonally opposite corners in 3D corner joints. The reinforcement pull-out, accompanied by the three-dimensional principal compression stresses generated in the joint of under-designed corner beam-column joint, eventually resulted in a brittle mode of failure with low dissipation of seismic energy. A close examination of the hysteresis loops (Figure 9-26) reveals that comparable peak strengths were attained in both 2D and 3D benchmark tests and also both specimens attained their highest loads in the push direction (increasing axial load). Nevertheless, due to the aforementioned reasons, Specimen 3D1 experienced a faster decay of bearing capacity.

The obvious detrimental effect of bidirectional loading revealed itself also in the early loading stages of Specimen 3D2. The debonding started at drift levels of 1.5% (last quadrant) and 2% (first quadrant) in each direction of the beam FRP sheets. In the following cycles, due to the imposed shear stress between the beam FRP sheet and the concrete, debonding continued to propagate through the joint panel. As a consequence, in each direction an abrupt detachment of the beam FRP sheet occurred at the end of the 2.5% drift level. It was observed that a compressive pressure was exerted on the external face of the column vertical GFRP sheets, causing them to bulge outward from the column face. In the following cycles vertical rupture of the GFRP sheets took place in the beam-column-joint interface region. In fact, in the case of the push direction, where the axial load level increase, it is observed that the amount of GFRP bulging on the column faces was drastically increased in biaxially tested specimens.

Yet, the retrofitted corner joint exhibited an improved seismic performance when compared to the 3D benchmark specimen and, thanks to the FRP sheets applied in the joint region the integrity of the joint concrete was maintained throughout the test. The bearing capacity of the retrofitted 3D corner joint increased around 15% compared to the 3D benchmark corner joint. In comparison, the test results showed the inadequacy of the R21 retrofit scheme for corner beam-column joints under bidirectional loading. Note that the R21 scheme was successfully implemented in the last 2D retrofitted specimen, 2D4, and a satisfactory seismic performance was obtained (see Chapter 6).

In addition to a 20% decrease in the strength capacity, a completely different mode of failure was observed in Specimen 3D2 (brittle debonding and excessive joint damage) compared to Specimen 2D4 (ductile beam hinging). The sustained damage under the joint panel and its vicinity is given in the close-up views of the post-test observations in Figure 9-27. In light of these observations, a modified and upgraded version of FRP retrofit scheme is proposed for the FRP retrofitting of corner beam-column joints in the last section of this chapter.

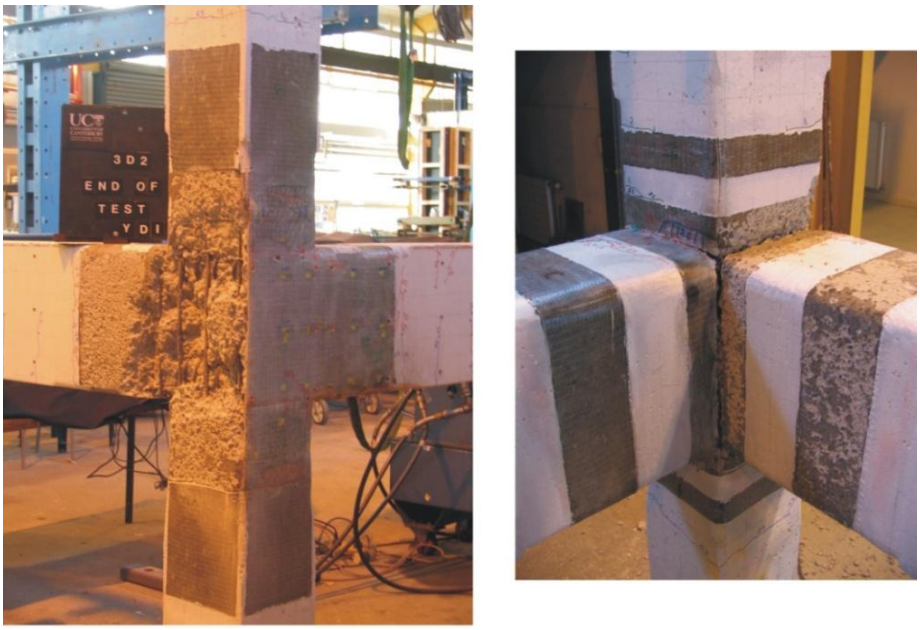

a) b)

Figure 9–27 Damage state of Specimen 3D2 joint region after test under FRP sheet after test: a) outside view; b) inside view

The local test findings and analysis of the recordings also support the global damage mechanisms mentioned above. The joint shear deformation readings showed that all retrofitted specimens sustained lesser shear deformation compared to benchmark specimens, which in turn indicates lesser joint distress. For instance, the joint region in Specimen 3D1 was subjected to five times greater shear distortion than that of Specimen 3D2. The stiffer joint panel behaviour of Specimen 3D2 can be seen in hysteresis loops of normalized shear stress vs shear deformation in Figure 9-28. However, due to the detachment and buckling of the FRP sheets in the joint region and columns, the maximum attained principal tensile stress in the joint of Specimen 3D2 was considerably decreased (around 50%) compared to Specimen 2D4. In Figure 10-28, a drastic decay of the joint shear stiffness of Specimen 3D1 can be seen due to the induced bidirectional deformation and strength demands. Particularly, after 0.5% drift and under the cycles of increasing axial load, this behaviour became more apparent. The

combined effect of high axial loads and biaxial moments and compression strut forces, accelerated the damage accumulation in the joint region.

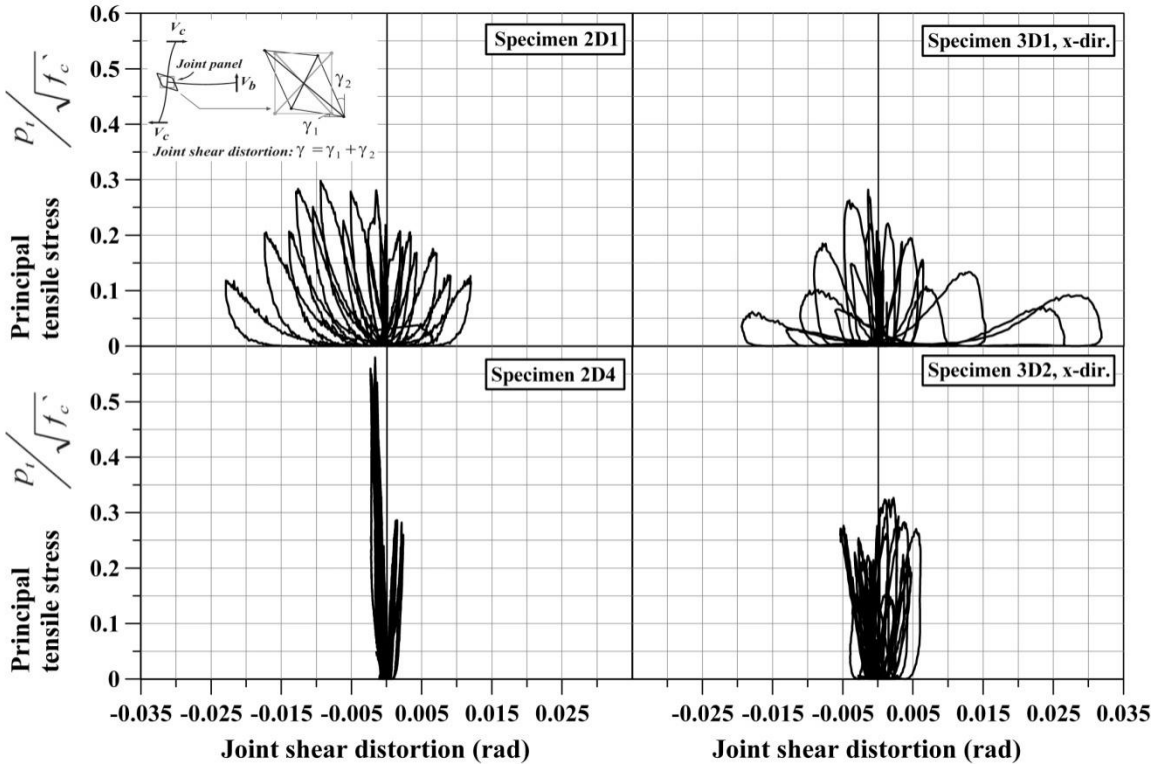

Figure 9–28 Comparison of principal tensile stress versus joint distortion of 3D corner and 2D exterior joints

9.3.2 Stiffness and Energy Dissipation Characteristics

The reduction in stiffness of the retrofitted corner beam-column joints may affect the overall response of a frame system, since the overall stiffness and period of vibration can be drastically changed. In addition, a torsional response may be generated in a symmetrically planned structure as a result of these effects. These asymmetric changes in lateral stiffness and resistance are accentuated by axial load fluctuations on the columns, associated with lateral response. Such fluctuations influence the bidirectional strength, stiffness, and cyclic hysteretic response of the members. In order to study the degree of the damage sustained based on the stiffness reduction in the 3D specimens, the degradation of peak-to-peak stiffness, along with the differences in terms of percentage with benchmark and retrofitted specimens are given in Figure 9–29 and Table 9-4, respectively. The peak-to-peak stiffness is defined as the slope of the line, joining the highest load points in the load-displacement curve attained at each displacement level.

Amongst all the specimens, Specimen 3D1 exhibited the highest stiffness degradation. Especially, after 1% drift level following the 3D concrete wedge formation in the joint region, a fast decay in peak-to-peak stiffness properties was observed. For instance, in comparison with the retrofitted specimen, 3D2, the initial peak-to-peak stiffness of the 3D benchmark specimen was 10% higher than the retrofitted specimen. However, after 1.5% drift the stiffness degradation accelerated around 50% in the Specimen 3D1. The 2D retrofitted specimen, 2D4, exhibited better stiffness properties compared to the similarly retrofitted 3D specimen, 3D2. The particular increase in the stiffness degradation in Specimen 3D2 can be attributed to the initiation of debonding in the beam FRP sheets in each direction at 1.5% drift and full detachment from the concrete surface after 2.5% drift. These findings clearly indicate the consequences of not taking into account the bidirectional loading and deformation demands in the retrofit design of corner beam-column joints.

The cumulative energy dissipation of the 3D specimens is evaluated by summarizing the area enclosed within the load versus displacement curves and is presented in Table 9-5 and Figure 9–30. In comparing the uniaxial and bidirectional response, it appears that while greater deformation demand is created in biaxial flexure, a reduction in hysteretic energy dissipation capacity is also observed. The 2D benchmark specimen dissipated almost 50% higher energy, compared to the 3D benchmark specimen. A similar trend was noted between the 3D retrofitted specimen, 3D2, and the 3D benchmark specimen, 3D1. In spite of the unfavourable failure mechanism of Specimen 3D2, due to early debonding of FRP sheets from the beam surfaces in each direction, the energy dissipation capacity increased approximately 60% in the retrofitted corner beam-column joint. On the other hand, it was observed that up to 2% drift level comparable energy dissipation values were obtained both in the Specimen 3D2 and Specimen 2D4. Nevertheless, the test results also showed that under bidirectional loading 20% less energy was dissipated by Specimen 3D2 compared to the counterpart 2D retrofitted specimen, 2D4 due to the lack of effective energy dissipation mechanisms. As a result, both 3D corner joint specimens experienced a drastic drop in the strength capacity with lesser energy dissipation compared to their 2D counterparts.

Table 9-4 Degradation of lateral stiffness of 3D corner joints and comparison with 2D joints

		Specimen 3D1, x-dir.	Specimen 3D2, x-dir.		Specimen 2D1		Specimen 2D4	
Drift	Cycle	K_p (kN/mm)	K_p (kN/mm)	difference with Spc. 3D1, x-dir (%)	K_p (kN/mm)	difference with Spc. 3D1, x-dir (%)	K_p (kN/mm)	difference with Spc. 3D2, x-dir (%)
0.1%	1st	2.40	2.14	-11.1	3.08	28.1	2.95	38.0
	2nd	2.44	2.47	1.2	3.08	26.0	2.97	20.0
0.2%	1st	1.91	2.19	14.7	2.46	28.6	2.19	0.0
	2nd	1.87	2.19	17.2	2.01	7.3	2.08	-4.9
0.5%	1st	1.20	1.27	6.2	1.43	19.7	1.40	10.3
	2nd	1.14	1.28	12.0	1.34	17.2	1.33	3.8
1%	1st	0.84	0.84	-0.2	0.96	13.9	1.04	24.1
	2nd	0.70	0.78	12.4	0.96	37.9	0.93	18.2
1.5%	1st	0.50	0.59	18.5	0.77	54.1	0.81	37.8
	2nd	0.39	0.56	44.5	0.71	83.0	0.70	24.6
2%	1st	0.31	0.44	42.9	0.63	105.4	0.62	41.1
	2nd	0.22	0.42	96.2	0.56	157.9	0.54	27.9
2.5%	1st	0.18	0.32	74.4	0.51	176.7	0.48	49.6
	2nd	0.13	0.28	119.0	0.45	250.9	0.44	54.6
3%	1st	0.13	0.22	63.7	0.40	206.5	0.41	88.1
	2nd	0.11	0.21	92.0	0.38	245.16	0.37	74.71
4%	1st		0.17		0.31		0.31	
	2nd		0.14		0.26		0.28	

Table 9-5 Cumulative energy dissipation of 3D joints and comparison with 2D joints

		Specimen 3D1, x-dir.		Specimen 3D2, x-dir.		Specimen 2D1		Specimen 2D4	
Drift	Cycle	$ED_{per\ cycle}$ (kNmm)	$ED_{cumulative}$ (kNmm)	$ED_{per\ cycle}$ (kNmm)	$ED_{cumulative}$ (kNmm)	$ED_{per\ cycle}$ (kNmm)	$ED_{cumulative}$ (kNmm)	$ED_{per\ cycle}$ (kNmm)	$ED_{cumulative}$ (kNmm)
0.1%	1st	5.2	5.2	3.0	3.0	3.7	3.7	3.1	3.1
	2nd	4.5	9.7	3.7	6.7	3.1	6.8	3.2	6.3
0.2%	1st	16.9	26.6	3.7	10.3	24.1	31.0	20.4	26.8
	2nd	14.3	40.8	16.4	26.8	12.9	43.8	12.4	39.2
0.5%	1st	83.5	124.3	74.9	101.7	88.0	131.8	86.3	125.4
	2nd	63.3	187.6	65.5	167.2	44.4	176.3	45.3	170.7
1%	1st	345.9	533.5	236.6	403.9	226.1	402.4	229.8	400.5
	2nd	217.3	750.8	201.3	605.2	131.4	533.8	124.8	525.3
1.5%	1st	462.4	1213.2	393.8	999.1	350.6	884.3	418.3	943.6
	2nd	358.7	1571.9	359.2	1358.2	221.4	1105.7	300.1	1243.7
2%	1st	534.4	2106.3	575.6	1933.8	509.5	1615.2	652.9	1896.6
	2nd	395.7	2502.0	537.6	2471.5	335.6	1950.8	487.5	2384.1
2.5%	1st	503.2	3005.2	795.0	3266.5	658.6	2609.4	874.3	3258.4
	2nd	386.7	3391.9	663.9	3930.4	508.7	3118.1	690.7	3949.1
3%	1st	749.6	4141.4	773.0	4703.4	773.1	3891.2	1067.1	5016.2
	2nd	706.7	4848.2	724.6	5428.0	689.3	4580.6	863.5	5879.8
4%	1st			1154.7	6582.7	1722.1	6302.7	1914.8	7794.6
	2nd			1042.6	7625.3	1224.2	7526.9	1482.4	9277.0

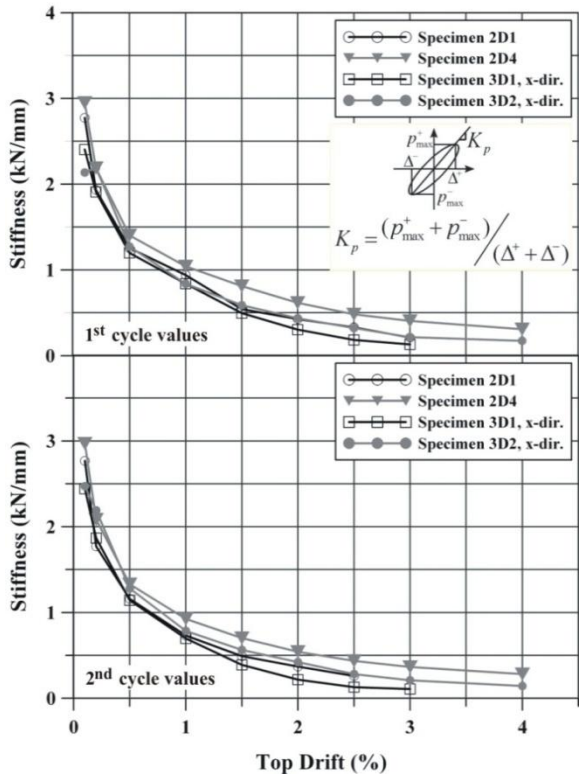

Figure 9–29 Degradation of lateral stiffness of 3D corner joints and comparison with 2D joints

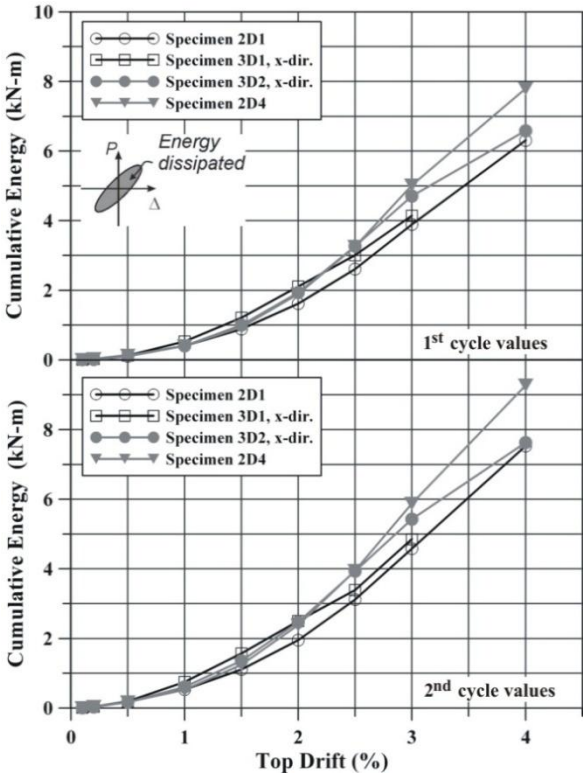

Figure 9–30 Cumulative energy dissipation of 3D joints and comparison with 2D joints

9.3.3 Strain Demand in the Steel Reinforcement

In this section the behaviours of the strain profiles of the beam, column and transverse reinforcing steels of the Specimens 3D1 and 3D2 are summarized. In Figure 9–31, the beam longitudinal bar strain profiles of Specimen 3D1 under the pull and push direction loadings are given at peak drift values for the x-direction. In the pull direction (decreasing axial load) top steel strain gauge readings at the end of the beam FRP sheet and beam-column interface, indicated that the strain readings remained elastic (-500 με $<\varepsilon_s<$ 500 με), which denotes that some bond still existed along the steel. The hook-ends in the beam bars experienced yielding after 2% drift. Also, in the bottom steel the strains in the longitudinal bars at the location of beam-column interface continued to increase. Nevertheless, they remained in the elastic region till the end of the test. In the push direction of loading, as well as in the push and pull loading of y-direction similar behaviour is noted. It is important to note that due to the excessive damage accumulation in the joint region most of the strain gauges broke. Therefore, after approximately 2% drift level the strain gauge readings can be considered erroneous.

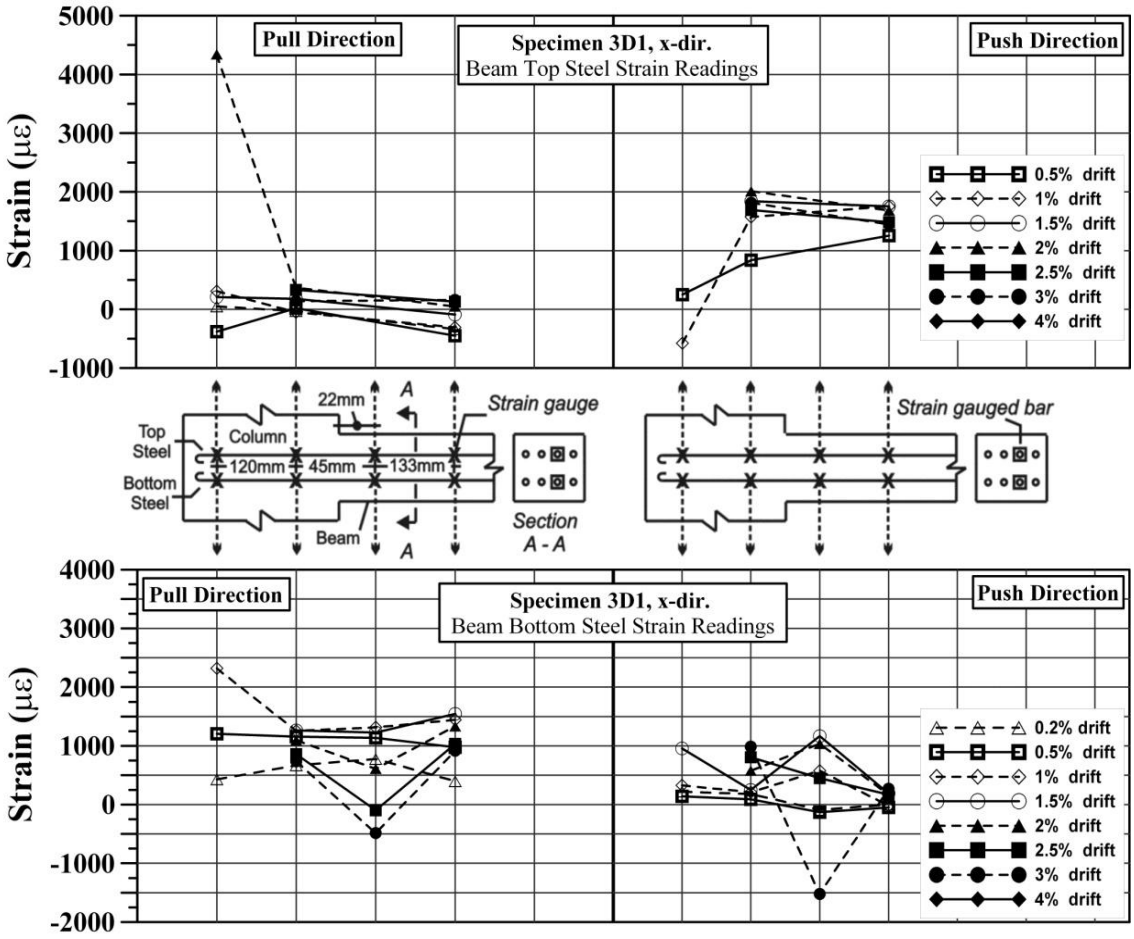

Figure 9–31 Beam longitudinal bars strain profiles of Specimen 3D1 – pull/push in x-direction

The examination of the strain gauge readings of the Specimen 3D2 along the beam longitudinal bars, under the pull direction loading (increasing axial load) in x- and y-direction, showed similar trends observed in Specimen 3D1: no particular steel yielding occurred along the beam bars. In Figure 9–32 the strain profiles of the beam longitudinal bars of Specimen 3D2 under pull and push directions of x-direction loading is given. Under the push direction loading (increasing axial load) the beam bottom steel bar at the beam FRP end-region exhibited yielding after 2% drift. Following the detachment of the FRP sheets after 2% drift level, the strain readings in the bottom steel bars yielded under compression loading. A significant yielding of the steel bars at the beam FRP end was recorded under pull direction of loading in y-direction. In addition, the localized yielding of beam hook-ends was also observed in y-direction.

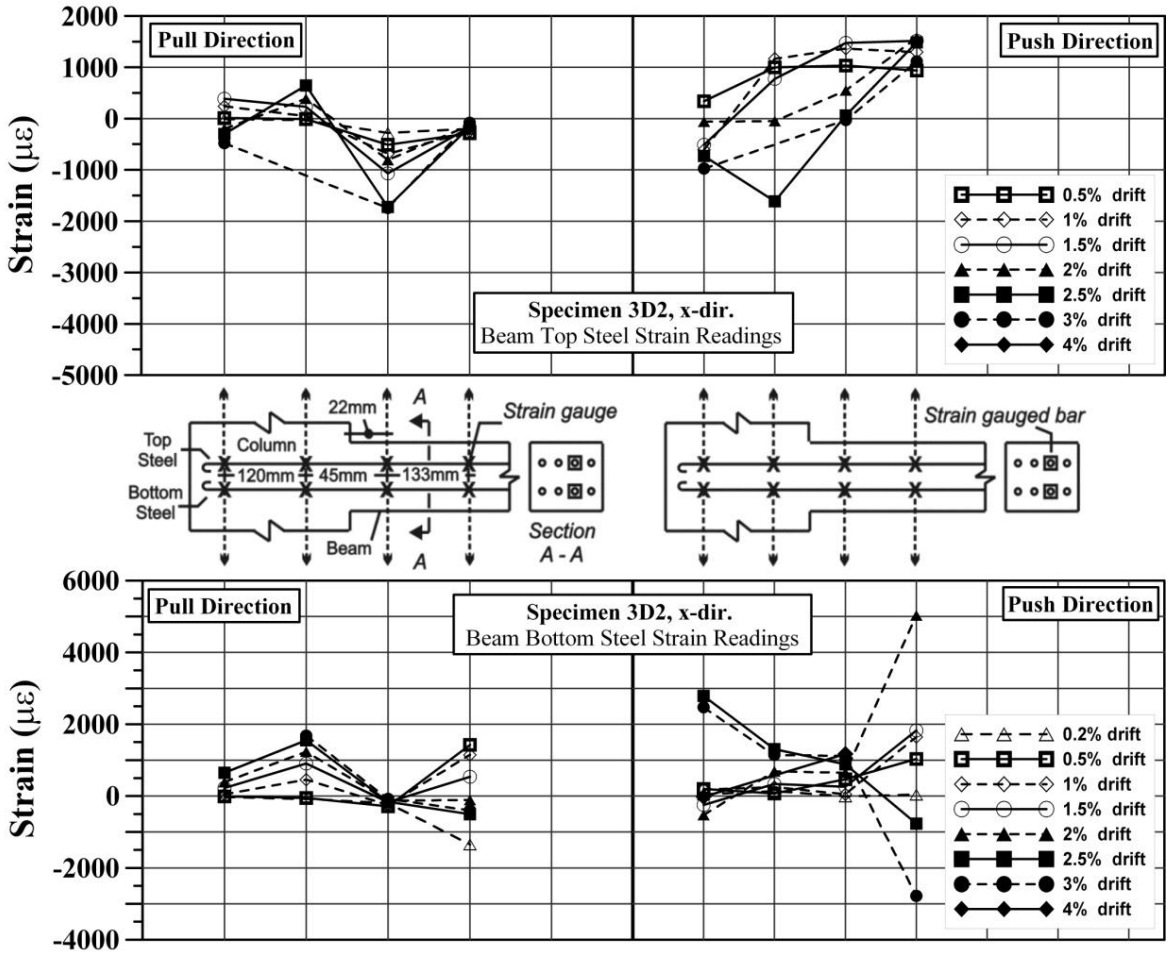

Figure 9–32 Beam longitudinal bars strain profiles of Specimen 3D2 – pull/push in x-direction

The column longitudinal bar strain profiles of Specimen 3D1 and Specimen 3D2 under pull and push loadings of x-direction are given from Figure 9–33 to Figure 9–36, respectively. Except for the steel

yielding observed after 2% drift in the bottom column longitudinal bar in Specimen 3D1, all the steel strain readings showed that the strain demand in the longitudinal bars remained in the elastic region.

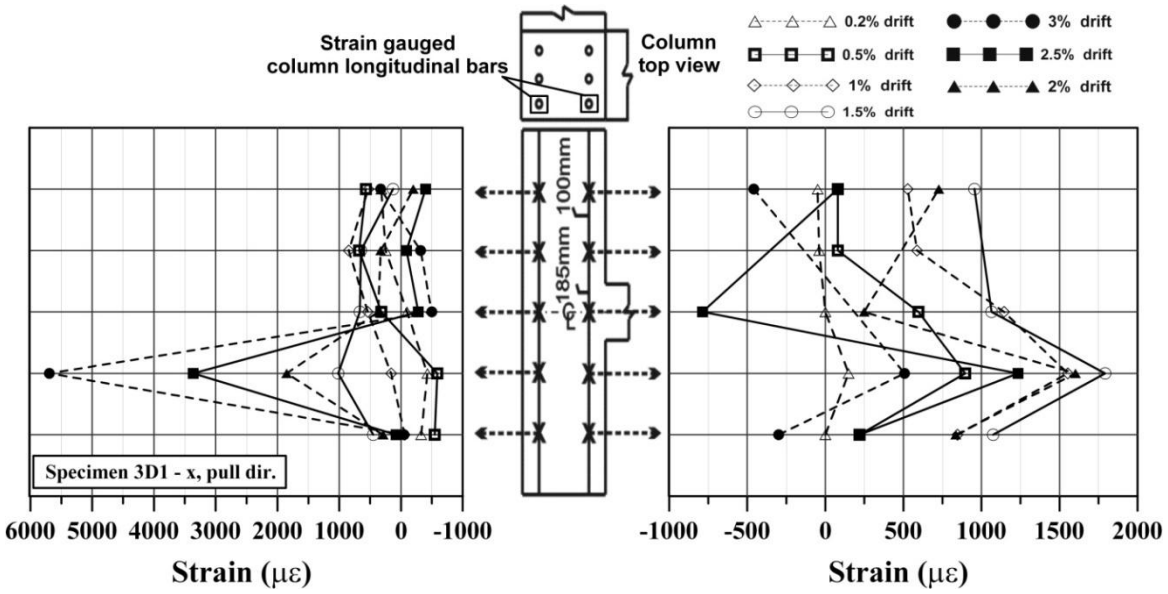

Figure 9–33 Column longitudinal bars strain profiles of Specimen 3D1x – pull direction

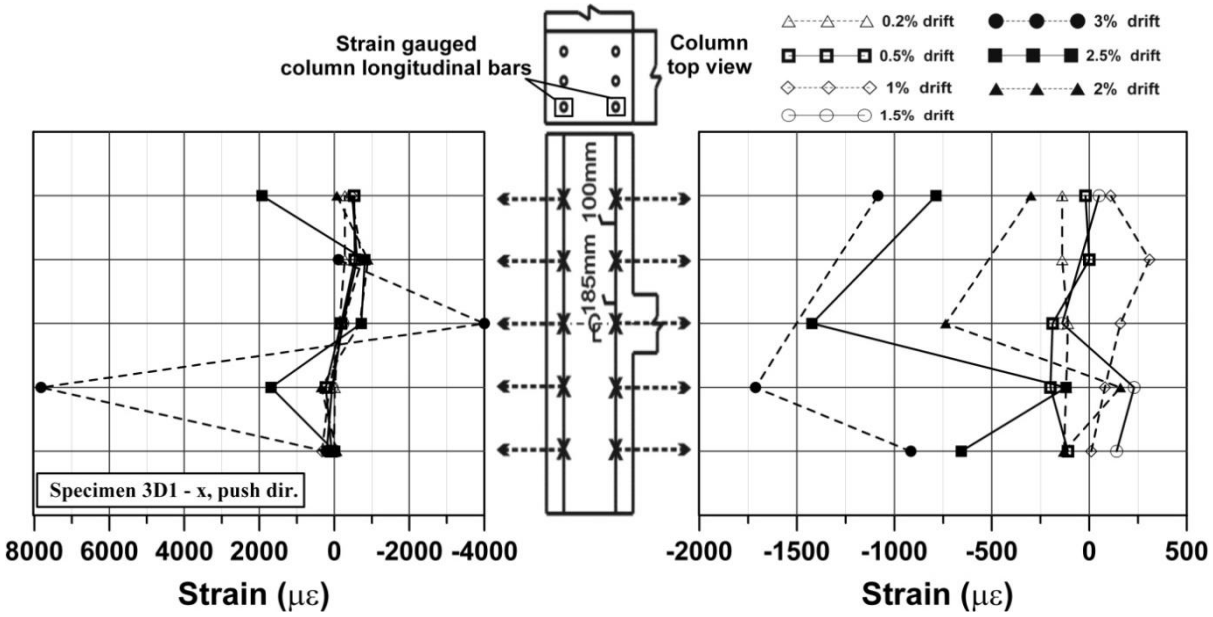

Figure 9–34 Column longitudinal bars strain profiles of Specimen 3D1x – push direction

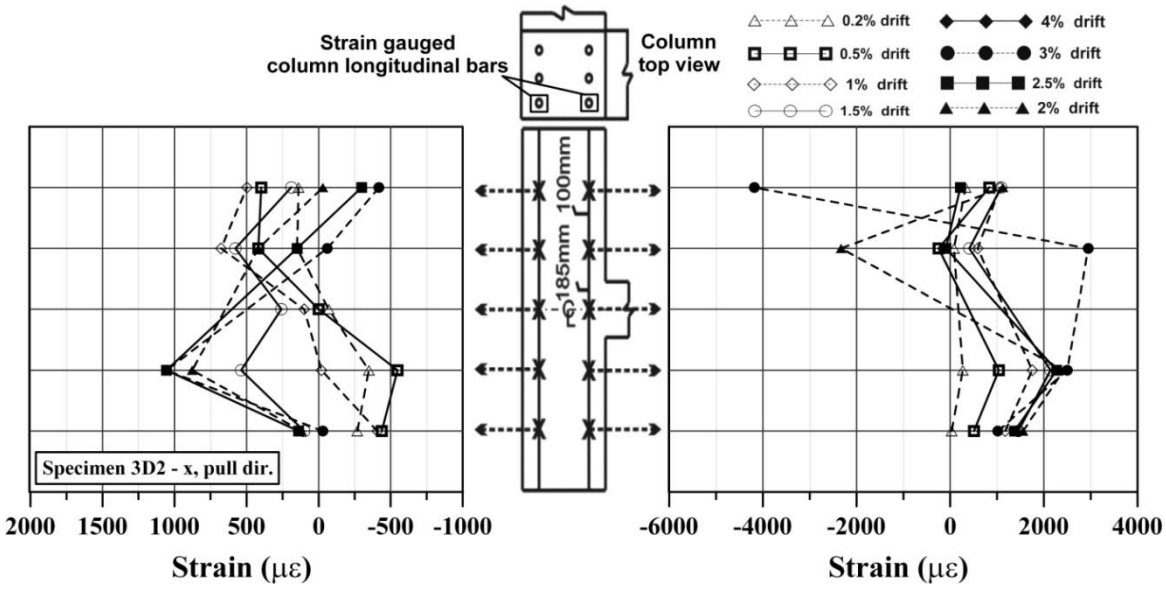

Figure 9–35 Column longitudinal bars strain profiles of Specimen 3D2x – pull direction

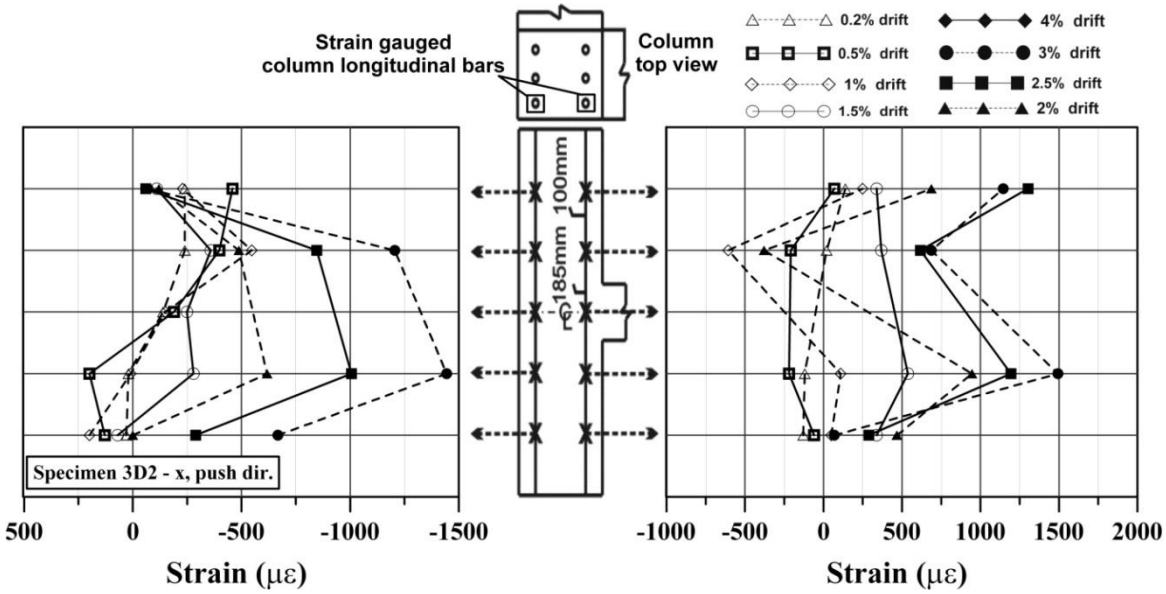

Figure 9–36 Column longitudinal bars strain profiles of Specimen 3D2x – push direction

9.3.4 Strain Demand in the FRP Sheets

In this section, the bidirectional loading effects on the behaviour of retrofitted 3D corner beam-column joints are studied based on the readings of strain gauges attached to the fibre sheets. The test results showed that the governing failure mechanism of the Specimen 3D2 was the debonding of the GFRP sheets from the beam and joint panel concrete surface. As discussed previously, this failure mode caused faster decay in the strength capacity and degradation of stiffness. Therefore, attention is given

to the analysis and discussion of the strain gauge values of FRP sheets applied on the beams. In addition, for comparison purposes the GFRP strain gauge readings obtained in the test of Specimen 2D4 are also provided. In Figure 9-37, the strain distribution in the horizontal GFRP sheets for pull direction at peak drift values of Specimen 3D2 and Specimen 2D4 is presented.

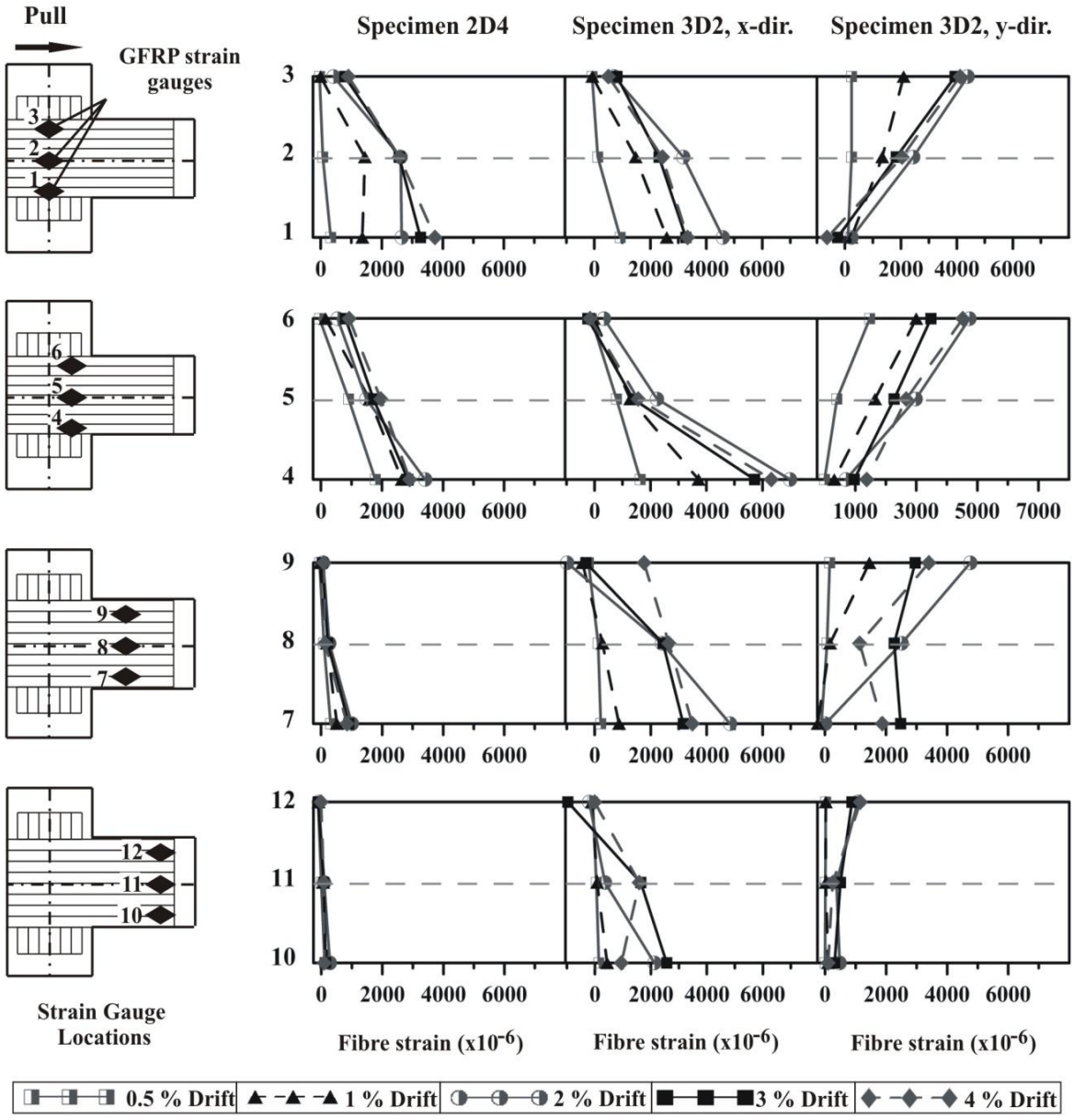

Figure 9–37 Comparison of strain distribution in the horizontal GFRP sheets of Specimen 2D4 and Specimen 3D2

The examination of Figure 9-37 reveals that, as a result of biaxial loading, higher strains were induced at the critical regions of 3D corner joint compared to Specimen 2D4 which was tested under

unidirectional loading. Particularly, in the regions of top and bottom of the beam-column interface and joint centre, such strains are greater than those obtained under strictly unidirectional loading, even though under similar imposed drifts at the ends. In general, test results indicated that the debonding initiated at the end of the 1.5% and the beginning of the 2% drift levels. It continued to propagate in the following cycles towards the joint panel centre and exterior face on one side, and to the end of the beam FRP sheet end on the other side. Note that, a similar propagation pattern was found in the failure mechanism of Specimen 2D3 (see Chapter 6). After the full detachment of beam GFRP sheets at approximately 2.5% drift, a decrease in the strain demand took place resulting in a strength and stiffness reduction in the global behaviour of the retrofitted 3D corner joint unit.

In order to study the strain gauges recording, the strain histories in the critical regions of the joint panel are given for the Specimen 3D2 in Figure 9–38 and Figure 9-39. The test results indicated that in addition to the retrofit scheme and the axial load variation, as discussed in Chapter 6, also the bidirectional loading has a strong influence on the debonding phenomena. A close examination of the local GFRP strain histories recorded in the critical regions, showed that the strain value and the locations in the corner joint subassembly at the instant of FRP debonding are more scattered compared to that of Specimen 2D3. For instance, at the top and bottom of the joint centre region (Figure 9-38, strain gauge # 4 and #7) the debonding strain values recorded were between 4000 to 5000 microstrains, which agrees very well with the predicted values based on the employed FRP debonding model (see Chapter 4). The strains measured at the instant of debonding from the top and bottom of the beam-column interface region strain gauges (Figure 9-39, strain gauge # 10 and #12) were between 5000 and 6000 microstrains. These values can be regarded as an underestimation according to the debonding model. On the other hand, the middle strain gauge reading in the beam-column interface (Figure 9-39, strain gauge # 11) fluctuated between the values of 500 and 2500 microstrains throughout the test. These lesser observed values indicate that the ineffectiveness of FRP in that region can be attributed to the excessive concrete damage accumulation underneath the FRP sheet (Figure 9-27). The extensive joint shear damage was evident due to the nonlinear shear deformation, and the visible expansion from the crushing of the concrete in the joint region. In light of these observations, the conclusion is made that local concentrations of damage in the FRP sheets of the corner beam-column joints at the critical regions will be generally higher in bidirectional excitations. Conventional measures of assessment and retrofit design of corner joints based on the tests performed under unidirectional cyclic loading are inadequate to quantify and trace this type of cumulative damage. Additional measures should be taken to prevent the brittle mode of failures and improve the existing

FRP design for corner beam-column joints, with taking into account the larger shear and deformation demands stemming from bidirectional loading.

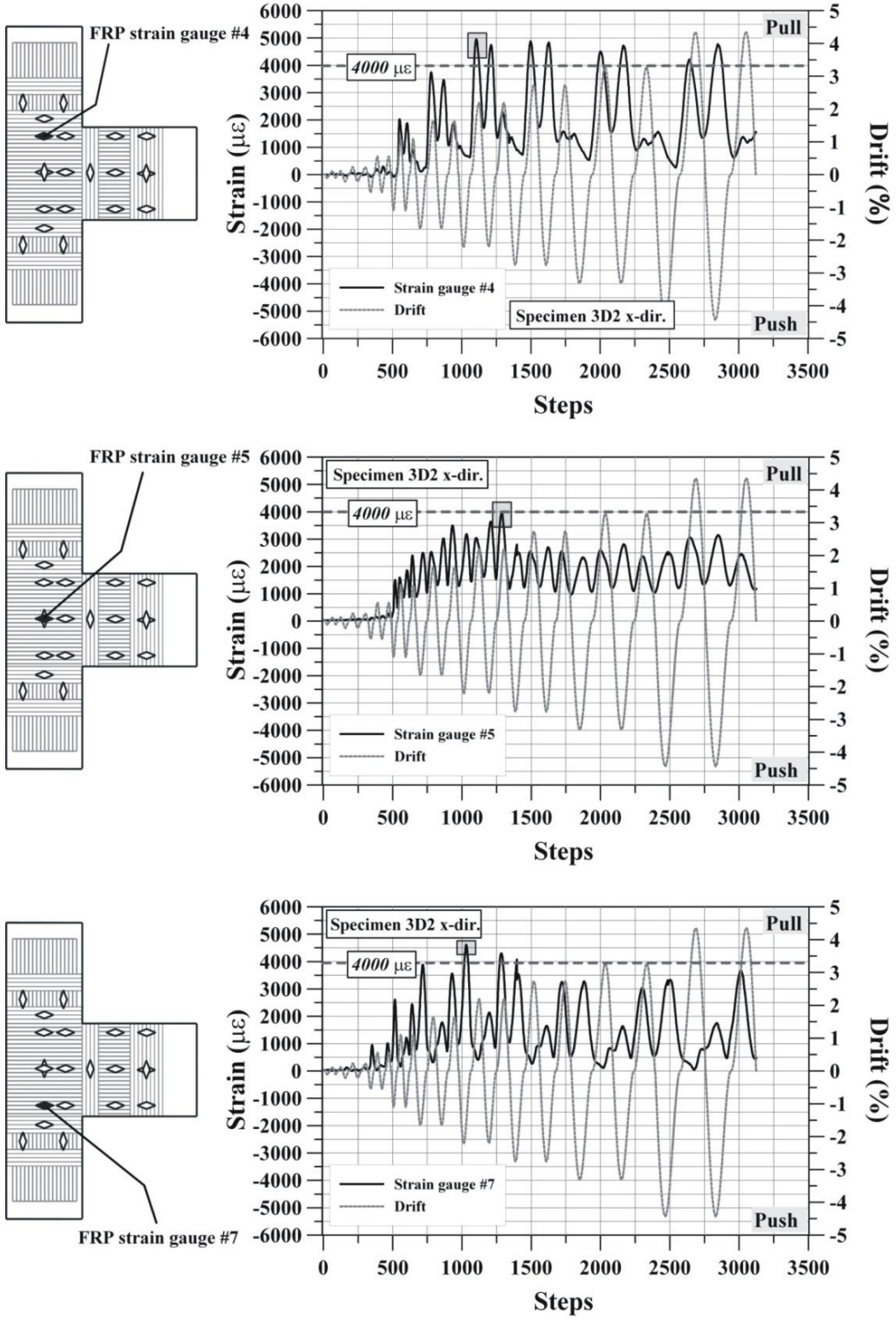

Figure 9–38 Horizontal GFRP strain profiles, Specimen 3D2, x-dir., strain gauges: #4, #5 and #7

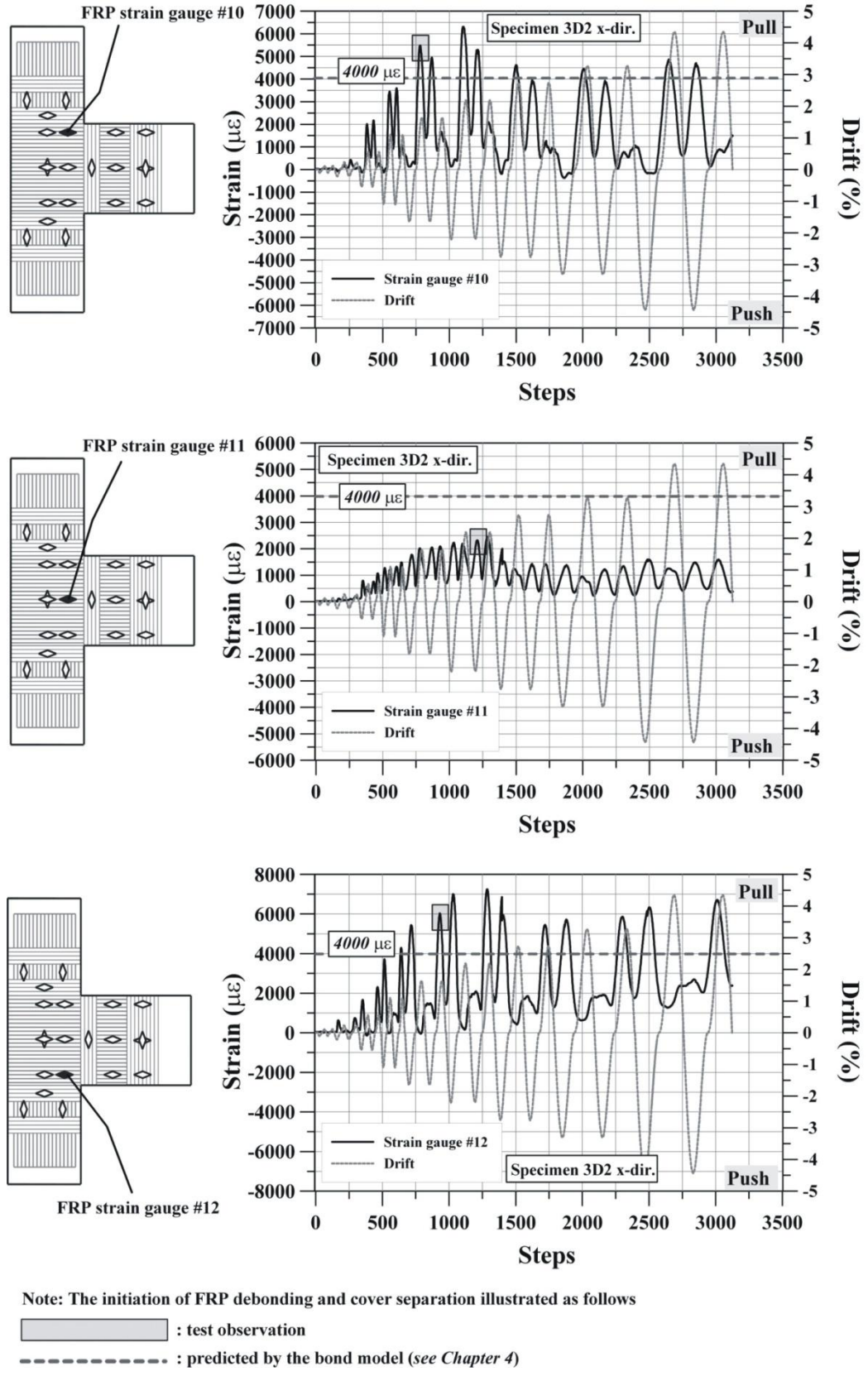

Figure 9–39 Horizontal GFRP strain profiles, Specimen 3D2, x-dir., strain gauges: #10, #11 and #12

9.4 REVIEW OF PERFORMANCE-BASED RETROFIT CRITERIA FOR PRE-1970S EXTERIOR BEAM-COLUMN JOINTS

A performance-based retrofit approach shall be defined and implemented, following the current design philosophy adopted for the design of new structures [2]. Different levels of performance (damage, cost of repairing and business downtime) are targeted or accepted, depending on the intensity of the earthquake event and its probability of occurrence during the life-time of the structure. The target level of performance (e.g., collapse prevention, minimum expectation, life safety, damage control or fully functionality) and the specific retrofit solution to achieve it, can be selected based on refined cost-benefit analyses implemented within a multi-criteria approach [3].

An ideal retrofit strategy for an existing frame would aim to protect the beam-to-column joint panel region, while upgrading the structure to exhibit the desired weak-beam strong-column behaviour, which is the basis of the design of new seismic resistant RC frames. However, due to the disproportionate flexural capacity of the beams, compared to that of the columns, a total inversion of the hierarchy of strength between beam and column can be difficult to achieve in all cases and for all beam-to-column connections (particularly for the interior beam-column joints) without major interventions.

According to a multi-level retrofit strategy approach [4], two levels of retrofit could be suggested:

- Total retrofit: consisting of a full upgrade, by protecting all joint panel zones and developing plastic hinges in the beams, while the columns are protected according to capacity design principles.

- Partial retrofit: consisting of protecting only the exterior joints and forming plastic hinges in the beams framing into exterior columns. It is in fact important to recognize that as long as flexural plastic hinges develop in the beams and sufficient deformation/rotation capacity (not necessarily ductility) is guaranteed within the critical elements and the overall system, the formation of a soft-storey mechanism can be critically prevented.

Within the context of this study, the seismic response of as-built and retrofitted exterior plane (2D) and space frame (3D) beam-column joints of reinforced concrete multi-storey frames is investigated using several performance-based criteria. As previously presented in Chapter 4, the retrofit application

methodology is performed under the umbrella of performance-based seismic retrofit criteria. While doing this, attention is also given to practical implementation of a partial retrofit approach, focusing on the exterior joints only in either a 2D or 3D configuration. Such a retrofit strategy would significantly reduce the invasiveness of a retrofit/strengthening intervention, as the targeted joints could be mainly accessed from the outside of the building with minimum inconvenience to the occupants and business interruption.

A major challenge to the performance-based seismic evaluation and retrofit design of existing beam-column joints is to develop simple methods to evaluate the expected level of damage limit states as a function of more traditional engineering demand parameters. In this contribution, to provide some aid to the engineering decisions in the assessment, methods of repair, retrofit design criteria and FRP scheme selection, the correspondence between limit states and critical engineering parameters based on the experimental findings of this study are given in Table 9-6.

An alternative to the traditional approach based on the evaluation of the nominal shear strength of the joint [5], the (normalized) principal tensile stresses associated with the joint shear distortion/strain and the inter-storey drift levels of the sub-assembly are selected as more reliable damage indicators. The influence of axial compression stresses on the joint, as well as the deformation demand at a structural system level, can be taken into account explicitly in both the as-built and retrofitted configurations.

In this context, along with the recommended damage limit states in Table 9-6, the retrofit design methodology and analytical tools, presented in Chapter 4 and validated by the experimental findings in Chapter 6, can be appropriately employed to develop a deformation-based FRP retrofit design procedure. In the first step, targeted performance objectives can be defined for the retrofit intervention based on the performance-based considerations. In the next step, the conceptually proposed deformation-based design procedure given in Figure 9-40, can be used to evaluate the selected retrofit configuration. Limit state (or envelope) curves can be generated for different retrofit applications in terms of principal tensile stresses due to the combined affect of as-built and selected retrofitted joint capacity, as a function of sub-assemblage drift level or joint shear deformation. Therefore, the effect of various retrofit schemes on the joint shear strength can be monitored under various performance goals (i.e., setting the joint deformation limits according to different limit states), which can be linked to the global lateral drift of the structure.

Table 9-6 Observed damage limit states for the assessment and retrofit design of exterior joints

Joint Type	Drift (%)	Degree of Damage (Appearance)	Damage State	Axial Load	$p_t/\sqrt{f_c'}$ [1]	Joint Deformation (%)
2D plane frame exterior joint (as-built)	0.2	Flexural cracking in the beam (w_c [2] = hairline - 0.2 mm)	Serviceable	$N\downarrow$ [3]	0.07	0.015
				$N\uparrow$ [4]	0.09	0.005
	1	Shear diagonal cracking in the joint (w_c = hairline - 0.1 mm)	Slight - Serviceable	N↓	0.28	0.150
				N↑	0.21	0.020
	2	Onset of joint panel concrete spalling	Critical damage - Repairability Issues	N↓	0.27	1.000
				N↑	0.19	0.400
	2.5	Significant concrete spalling in the joint region	Irrepairable	N↓	0.24	1.300
				N↑	0.17	0.770
3D space frame corner joint (as-built)	0.5	Shear diagonal cracking in the joint (w_c = hairline - 0.1 mm)	Slight - Serviceable	N↓	0.17	0.018
				N↑	0.11	0.049
	1	Significant cracking in the joint region (w_c = 0.5 - 1 mm) & Flexural cracking in the column (w_c =hairline - 0.25 mm)	Minor to moderate - Repairable	N↓	0.20	0.097
				N↑	0.17	0.166
	2	Onset of joint panel concrete spalling (w_c > 2 mm)	Critical damage - Repairability Issues	N↓	0.16	0.879
				N↑	0.10	1.018
	2.5	Joint core concrete crushing and buckled bars	Irrepairable	N↓	0.09	1.317
				N↑	0.08	2.290
2D plane frame exterior joint (retrofitted with R11)	0.5	Flexural cracking in the beam (w_c = 0.1 - 0.25 mm) & Onset of beam-FRP interface flexural cracking (w_c = 0.25 - 1 mm)	Slight - Serviceable	N↓	0.22	0.110
				N↑	0.14	0.062
	1	Distributed flexural cracking in the beam (w_c = 0.2 - 0.5 mm) Flexural cracking in the column (w_c = hairline)	Slight - Repairable	N↓	0.33	0.270
				N↑	0.29	0.200
	2	Onset of FRP debonding [5] in the beam and/or beam-column interface	Minor to moderate - Repairable	N↓	0.31	0.550
				N↑	0.31	0.650
	2.5	Onset of FRP debonding [5] in the joint panel	Critical damage - Repairability Issues	N↓	0.31	0.650
				N↑	0.48	0.750
2D plane frame exterior joint (retrofitted with R21)	0.5	Distributed flexural cracking in the beam (w_c = 0.1 - 0.25 mm)	Slight - Serviceable	N↓	0.24	0.210
				N↑	0.13	0.300
	1.5	Flexural cracking in the column (w_c = hairline - 2mm)	Slight - Repairable	N↓	0.46	0.120
				N↑	0.28	0.370
	2.5	Onset of plastic hinge formation in the beam [6]	Minor to moderate - Repairable	N↓	0.55	0.060
				N↑	0.40	0.000
3D space frame corner joint (retrofitted with R21)	0.2	Flexural cracking in the beam (w_c = hairline - 0.1 mm)	Serviceable	N↓	0.11	0.011
				N↑	0.07	0.015
	1	Flexural cracking in the beam (w_c = 0.1 - 0.25 mm) Flexural cracking in the column (w_c = 0.5 mm)	Slight - Serviceable	N↓	0.27	0.075
				N↑	0.18	0.049
	2	Onset of FRP debonding [7]	Minor to moderate - Repairable	N↓	0.30	0.128
				N↑	0.18	0.088
	2.5	Complete detachment of FRP beam and joint sheets	Critical damage - Repairability Issues	N↓	0.27	0.006
				N↑	0.16	2.111
	3	Buckling and tearing of FRP sheets in the joint and column face & Severe concrete crushing under the joint FRP sheet	Critical damage - Repairability Issues	N↓	0.20	2.118
				N↑	0.12	2.028

Notes : [1] Normalized principal tension stress in the joint panel; [2] Measured crack width; [3] N↓: decreasing in compression load to tension; [4] N↑: increasing in compression; [5] FRP debonding initiated at around 6000 με during testing; [6] No FRP debonding observed; The maximum attained FRP strain demand was 2500 με ; [7] FRP debonding initiated at around 4000 με during testing.

As shown in Figure 9-40, the total capacity of the joint can be expressed in terms of the sum of the principal tensile stresses due to the as-built solution p_{tc} and the fibre contribution p_{tf} (e.g., $p_{tt}= p_{tc} + p_{tf}$). The supplied lateral load capacity $V_{c,s}$ of the retrofitted beam-column joint can be evaluated using the total principal tensile stress p_{tt}, which is a function of the applied axial load and the specified joint shear deformation limit state.

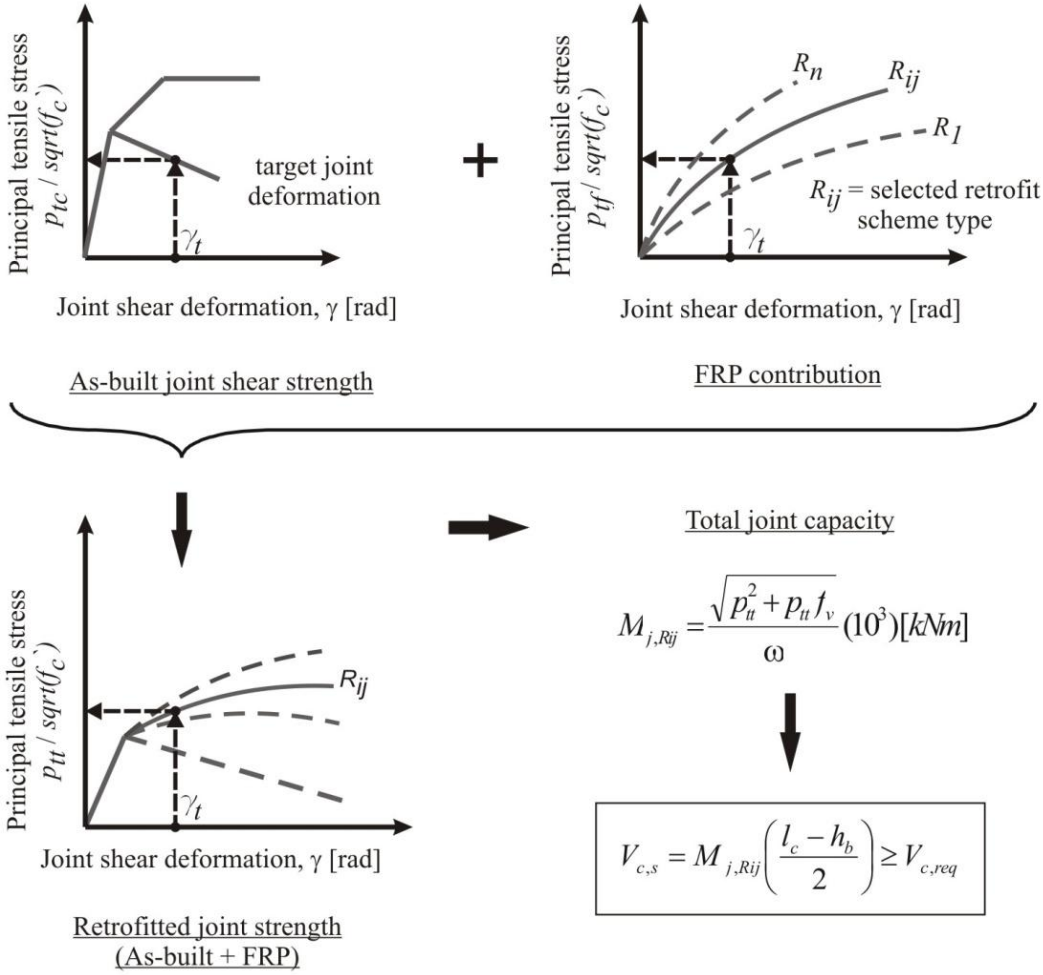

Figure 9–40 Proposed procedure for a deformation-based assessment and retrofit

The notations shown in Figure 9-40 are as follows

h_b : height of beam;

f_v : compressive stress on the column at the mid-depth of the joint core;

l_c : height of column;

$M_{j,Rij}$: moment capacity of joint with FRP retrofit scheme Rij;

p_{tc} : principal tension strength contribution due to plain concrete;

p_{tf} : principal tension strength contribution due to FRP;

p_{tt} : total principal tensile strength;

Rij : FRP retrofit scheme;

R_n : n*th* generic FRP retrofit scheme;

$V_{c,s}$: supplied column shear force due to FRP retrofitted joint;

$V_{c,req}$: required column shear force;

γ_t : target joint shear distortion;

ω : geometric coefficient.

For more detailed information regarding the retrofit design methodology and analytical tools for the evaluation of strengthened joint shear strength the reader is referred to Chapter 4.

9.5 REVISION OF THE FRP RETROFIT SCHEME FOR CORNER BEAM-COLUMN JOINTS

In the retrofit of Specimen 3D2, the same retrofit scheme was employed to that of Specimen 2D4. As presented in Chapter 6, Specimen 2D4 resulted in the development of a more appropriate hierarchy of strength with the formation of plastic hinges in the beam and protection of the weakest mechanism (shear failure in the joints and soft-storey mechanisms). On the other hand, the test results of Specimen 3D2 confirmed that multi-axial loading can in fact lead to a severe reduction in deformation and strength capacity and impair the efficiency of a retrofit solution designed under more traditional and simplified assumptions of 2D response and constant axial load.

In this context, based on the experimental findings of this study, possible revisions to the seismic retrofit of corner beam-column joints are presented. The recommendation for the new retrofit scheme is primarily aiming to (1) delay the initiation of FRP debonding in the critical regions (i.e., beam-column interface and centre of joint); (2) prevent the spread of FRP debonding; and (3) prevent the column and beam FRP sheets from buckling under compression forces. For this purpose, minor refinements of such implementation including the use of FRP dowel anchorages and wider anchorages wrapped around the beam and column sections are proposed to further improve the behaviour of 3D corner joints. The alternative layout is given along with the comparison of the original version of the retrofit scheme in Figure 9-41.

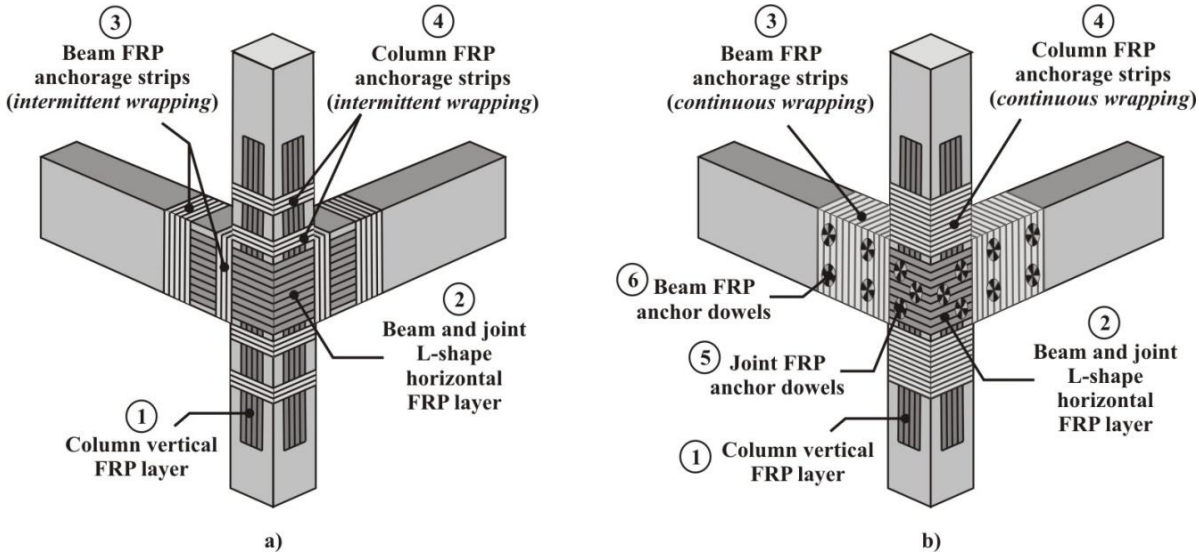

Figure 9–41 Revision in the application of FRP retrofit scheme for corner beam-column joints: a) original version applied in this study; b) proposed upgraded version
(Note: numbers in circles indicate the installation sequence)

Special FRP anchor dowels were successfully implemented in the previous studies on the investigation of the retrofit solutions using CFRP cross overlays to improve the interaction between the bare frame and masonry infills [6, 7]. They were basically used to reduce the delamination/debonding of the CFRP sheets from the surface of the wall (Figure 9–42).

Figure 9–42 Application of FRP anchor dowels: a) close-up view; b) epoxy saturation of anchor dowel; c) FRP anchor dowels placement in brick infills (after Akguzel [6])

Within the same line of thought, the FRP anchor dowels can be used appropriately in the FRP intervention of corner beam-column joints to prevent debonding/delaminations, as well as to strengthen the laminates against buckling under compression loads. They are prepared by twisting the strips of CFRP sheets, folding into two and epoxied into pre-drilled holes. Afterwards, epoxy saturated GFRP anchor dowels are plugged into the holes by means of tie-wires and are initially injected into the holes during the placement of the epoxy resin. The ends of the anchor dowels remaining outside

the holes, either in the beam or joint faces, are glued to the horizontal GFRP sheets already applied on the beam and joint faces for proper anchorage.

Lastly, it should be noted that although the proposed retrofit solution can be easily implemented with low-invasiveness and minimum disruption to building's functionality, workmanship in the design and application of FRP overlays and special anchors to the beam and joint faces is crucially important in retrofitting practice. Disregarding this fact may lead to unforeseen disastrous consequences in the performance of the retrofitted structure during seismic action.

9.6 SUMMARY

In this chapter, the test results of 3D space frame beam-column joints are presented in terms of global, as well as local failure mechanisms and damage propagation. Then the test results are analysed and compared with the findings of 2D plane frame beam-column joints to clarify the effects of bidirectional loading on the as-built, as well as retrofitted corner beam-column joints.

The test outcomes highlighted the potentially unconservative effects of neglecting the actual multi-axial load demand, when assessing the behaviour of existing beam-column joint and designing a proper retrofit intervention. Corner beam column joints within a frame building have been identified as being particularly vulnerable. As a result of bidirectional loading, the 3D corner joints exhibited significant strength and loss of stiffness at relatively low inter-storey drift levels compared to their 2D counterparts. The test results of the retrofitted corner beam-column joint, Specimen 3D2, also showed the inadequacy and drawbacks of the retrofit design performed without taken into account the effect of bidirectional loading demands. Note that, the retrofit scheme was implemented successfully in the Specimen 2D4, which yielded enhanced seismic performance during the test.

The performance-based retrofit strategy for older beam-column joints designed and constructed before 1970s was reviewed. Damage limit states based on the experimental findings of exterior beam-column joints tested under uni- and bidirectional loading conditions, either in as-built and retrofitted conditions, were provided to aid engineering decisions in the assessment and selection of retrofit schemes within the framework of performance-based engineering. Furthermore, a deformation-based retrofit design procedure was also presented conceptually to identify and evaluate the FRP retrofit scheme for shear strengthened beam-column joints based on a selected target performance.

In the last section, recommendations were made for the upgrade of the retrofit scheme of Specimen 3D2 to improve the seismic performance of the retrofitted corner joints. The main aim was to eliminate the brittle and low-energy dissipating failure modes such as the initiation and propagation of the FRP debonding/delamination and buckling of FRP sheets installed on the column and beam faces. For this purpose, the use of special FRP anchors along with wider FRP anchorage in the beam and columns was proposed and explained.

9.7 REFERENCES

1. Park R. Evaluation of ductility of structures and structural assemblages from laboratory testing. *Bulletin of the New Zealand National Society for Earthquake Engineering*. 1989; **22**(3):155-66.
2. SEAOC Vision 2000. *Performance-based seismic engineering structural engineers association of California.* Sacramento, California, 2000.
3. Giovinazzi S, Pampanin S. Multi-criteria approaches for regional earthquake retrofit strategies. *Pacific Conference on Earthquake Engineering*, Singapore, 2007.
4. Pampanin S, Bolognini D, Pavese A. Performance-based seismic retrofit strategy for existing reinforced concrete frame systems using fiber-reinforced polymer composites. *Journal of Composites for Construction*. 2007; **11**(2):211-26.
5. FEMA-273. *NEHRP guidelines for the seismic rehabilitation of buildings*. Federal Emergency Management Agency: Washington DC, 1997.
6. Akguzel U. Seismic retrofit of brick infilled R/C frames with lap splice problem in columns. *MSc Thesis*, Boğaziçi University, Istanbul, 2003.
7. Ozden S, Akguzel U, Ozturan T. Seismic retrofit of R/C frames with CFRP overlays. *Seismic Assessment and Rehabilitation of Existing Buildings*, Kluwer Academic Publishers, pp. 357-382, 2003.

PART III

NUMERICAL STUDIES AND CONCLUSIONS

Chapter 10 NUMERICAL STUDIES ON BEAM-COLUMN JOINTS

10.1 INTRODUCTION

Limited finite element analysis has been carried out on FRP-strengthened 2D exterior as well as on 3D corner beam-column joints subject to reversed cycling loading. As a contribution to fill this gap in knowledge and to provide a basis for future studies, in this chapter numerical studies have been carried out to develop three-dimensional finite element (FE) models to predict the response of 2D exterior retrofitted and 3D corner beam-column joints.

Firstly, an overview and a comprehensive literature review on the FE studies of retrofitted beam-column joints are presented. Next, the theoretical background of the fracture mechanics-based finite element code, MASA (MAcroscopic Space Analysis), which is used in the numerical analyses is given. The nonlinear finite element analysis programme MASA, was developed at the University of Stuttgart, specifically for three-dimensional non-linear analysis of quasi-brittle materials such as concrete. Afterwards, detailed information on the development of three-dimensional finite element numerical models for 2D exterior joints retrofitted using advanced composite materials and 3D as-built corner joints are presented. In the latter study, particular emphasis is given to the application of the bidirectional loading with concurrent varying axial load. The outcomes of the finite element analyses are compared with and validated against the experimental findings in terms of global load-displacement behaviour and damage propagation, as well as local behaviour such as FRP strains in the sheets and the cracking pattern.

10.2 OVERVIEW

Several techniques have been proposed in literature to simulate the nonlinear inelastic beam-column joint behaviour in RC frames subjected to earthquake loading. Depending on the levels of

discretisation and complexity these studies range from empirical approaches to refined finite element (FE) analyses [1-15]. At the preliminary stages of the analysis to assess the global response quantities, relatively simple macroscopic models can be used. In this case, to reduce the computational effort, phenomenological idealizations are often utilised, which mimic the observed behaviour of RC elements.

If more detailed information is required regarding the damage state in the individual elements, more complex analysis methods such as finite element methods (FEM) are generally utilised. The finite element method can be defined as a general method of structural analysis in which a continuous solid is replaced by a finite number of elements interconnected at a finite number of nodal points. With such an idealization, a problem in solid mechanics is transformed into a related problem of an articulated structure, which can be analysed by the standard methods of structural analysis [16].

In the past several years, this method gained attention in practice, as a powerful and reliable tool for modelling and evaluating as-built structures and designing new structures. One of the advantages of FEM is that it can be used to model structural members accurately. Many FEM modelling techniques have been proposed depending on the shape of element, number of nodes, linear or nonlinear approximations for deformation or displacement within the element, ranging from analyzing the behaviour of the total structure and the members to the bond relationship. The main concept, as stated previously, is dividing the member into elements small enough to yield the desired accuracy, with a specified node number, the proper displacement approximation, and finally, a suitable constitutive law [17].

The most robust method in terms of the highest level discretisation and complexity, amongst the existing finite element modelling techniques, is *the 3D continuum FE modelling*. This technique yields a more refined analysis, accurate results and information of the inner mechanics of the analysed structural member.

Early attempts to develop a finite element model for reinforced concrete were performed by Ngo and Scordelis [16] and Rashid [18]. The FE proposed by Ngo and Scordelis [16] was used to carry out an analysis of reinforced concrete beams with a predefined crack pattern. This model which included a cracking was called *the discrete crack model*. By using this model the stresses in the crack vicinity can be determined. The finite element idealization proposed by Ngo and Scordelis is presented in Figure 10–1. Following this approach, Rashid [18] introduced another method for the analysis of RC

members. In his approach, the cracked concrete was represented as an elastic orthotropic material with reduced elastic modulus in the direction normal to the crack plane. The cracked concrete behaviour was represented by the average stress strain relationship within the finite element. It located zones of cracking and how crack development affected the overall response of the structure. This model was called *the smeared crack model* [17]. In the next section more information is provided on these topics.

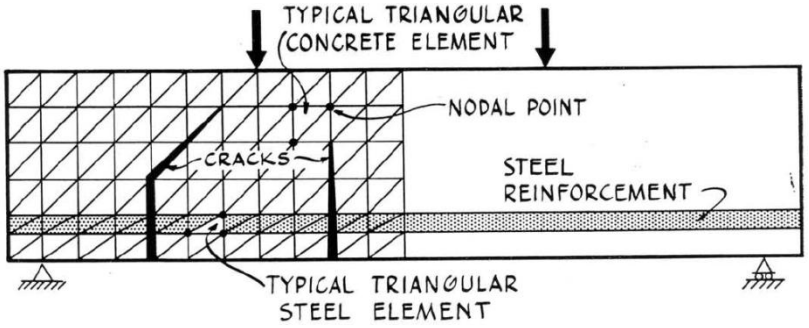

Figure 10–1 Finite element idealization by Ngo and Scordelis [16]

Since these early pioneering studies, the analysis of reinforced concrete using FEM has received great interest. However, due to its demanding computational requirements and existing uncertainties with regards to non-linear local failure mechanisms (i.e., bond and anchorage failures), few researchers attempted to utilise this technique in the modelling of beam-column joints (i.e., [19, 20]). Nevertheless, recent advances in FEM techniques led to more sophisticated and reliable analysis of beam-column joints. For instance, the implementation of cycling bond models [21] instead of linear steel reinforcing bond models, as well as the use of microscopic models instead of macroscopic models [22], which are covered in detail in the following sections, increased the efficiency and enabled more advanced and reliable FE analysis tools to be employed. For more information regarding these topics refer to [23-29].

As seen in the preceding chapters the behaviour of existing beam-column joints is influenced by a large number of variables interacting with each other. In order to reduce the amount of expensive and time-consuming laboratory testing, the behaviour of existing exterior as well as interior joints is studied using non-linear finite element methods. Providing that the FE model of the beam-column joint is developed to represent the behaviour and calibrated successfully using the results of the previous experimental study, the same model can be used to highlight the effect of different parameters on the behaviour. The research performed on the FE analysis of non-seismically designed as-built beam-column joints is reviewed in the following paragraphs.

Baglin and Scott [30] investigated the application of a nonlinear finite element analysis package to the modelling of external beam-column connections. The behaviour of the finite element model, which was developed using SBETA, was compared with the results of several experimental tests. The researchers modelled RC beam-column joints with various non-ductile beam longitudinal bar anchorages (e.g., U-bar lapped with straight bars; 90 hook top bar and discontinued bottom bar) and analysed under monotonic loading.

A parametric study was conducted by Hegger *et al.* [31] using the validated FE model to study the behaviour and critical parameters influencing the shear strength of non-seismically detailed beam-column exterior and interior joints. Tests used for validation and FE analyses were performed under monotonic loading. The researchers indicated that the most important factors affecting the shear capacity of exterior beam-column connections are the concrete compressive strength, the joint slenderness of the connection, the beam reinforcement ratio and the amount of stirrups inside the joint.

Representative beam-column joints were tested experimentally at the University of Pavia ([14]) and analysed by Eligehausen *et al.* [32] using the continuum finite element programme MASA. Particular focus was placed on modelling the behaviour of smooth reinforcement with hook-ends as well as the accurate representation of brittle shear failure modes in the joints. The parameter study showed that the bond resistance, the hook stiffness and local bending stiffness of reinforcement contributes to the resistance and prevents sudden failure typical of shear.

Recently, Genesio *et al.* [33] performed tests on five full scale exterior RC beam-column joints designed according to pre-1970s construction practice. Tests were carried out under reversed cyclic loading at BARC (Bhabha Atomic Research Centre) in Mumbai. Detailed information on this study can be found in Chapter 2 section 2.3. No axial load was applied to the columns. A numerical model was also developed and an extensive parametric study was carried out with monotonic analyses of the specimens in order to reduce the computational time. The analysis results indicated that the main influencing parameter on the shear capacity of a joint is the strength of the concrete. It also confirmed the significant effect of the column axial load on the joint shear strength, although it was generally ignored by the previous researchers. It was already shown that the influence of the column axial load on the first diagonal cracking of the joint core can be properly taken into account by considering the principle tensile stress, p_t, instead of the shear stress in the joint, v_{jh} [34].

In terms of numerical studies performed on the structural members strengthened with FRP materials, apart from a few studies on FRP strengthened columns and slabs [35-38], the majority of the research

effort has been focused on the numerical modelling of strengthened RC beams to address the bonding issue of FRP plates and sheets (i.e., [39-57]). The numerical modelling of FRP strengthened beam-column joints does not appear to have received adequate attention in the current literature. A few pertinent studies regarding the modelling of RC joints with FRP materials will be reviewed in the next paragraphs.

Parvin and Granata [58] performed an investigation involving parametric studies of the application of FRP overlays (i.e., overlays bonded to the tensile faces with and without wraps) to exterior beam-column connections. Different composite materials such as `E'-glass, Kevlar, and graphite and different overlay configurations were used. Researchers indicated that the choice of the composite materials affects the structural performance. Numerical analysis showed that the bond stress perpendicular to the overlay/concrete interface at the beam-column junction can easily exceed the tensile strength of the underlying concrete. Therefore, the configuration of the FRP overlay plays an important role in the prevention of peeling.

Mostof and Talaeitaba [59] proposed a finite element model for the non-linear analysis of RC joints covered FRP overlays. The model took into account the effects of anchorage slip and anchorage extension of the steel reinforcement in the connection zone. Some available experimental work (Parvin and Granata [58], see Chapter 2, Section 2.4) were modelled and non-linearly analysed using ANSYS. To eliminate the effects of debonding of FRP laminates in FE analysis, i.e., the effects of local failure due to shear or normal stress concentrations at the end of the laminates, the maximum strain in FRP laminates was limited to the quantities which are suggested in ACI 440.2R-08 [60]. Furthermore, a case study on a typical RC connection with some particular strengthening strategies using FRP laminates was performed. The results of this study can be summarised as follows (1) realistic non-linear analysis of RC connections with FRP overlays could be performed using available software; (2) the modelling of anchorage slip in the embedded reinforcement is possible using non-linear spring models; (3) ignoring the anchorage slip of the longitudinal reinforcement of the beam embedded in the column in FE analysis leads to underestimating the ultimate rotation of the joint up to 25%. Lastly, the researchers concluded that L shape overlays from FRP composites at the beam-column connection, plus column wrapping with FRP laminates and U shape overlays under the beam are very good strengthening strategies for the strength and ductility enhancement in the RC joints.

Parvin and Wu [61] investigated the effect of ply angle on the improvement of shear capacity and ductility of beam-column connections strengthened with carbon fibre-reinforced polymer (CFRP)

wraps under combined axial and cyclic loads. Three-dimensional nonlinear finite element models for the beam-column connections were developed and simulated with the Marc.Mentat™ 2001 finite element analysis (FEA) software under horizontal cyclic loading and constant axial load. Analysis results indicated that four layers of wrapping placed successively at ±45° ply angles, with respect to the horizontal axis, is the most suitable upgrade for improving shear capacity and ductility of beam-column joints under combined axial and cyclic loads. Particularly, the wrap ply angle stacking sequence of -45°/+45°/-45°/+45° appeared to offer prevention against the brittle shear failure of the joint, while exhibiting energy dissipating characteristics that are superior to the control model when subjected to combined axial and cyclic loads.

The effects of FRP reinforcement on the behaviour of beam-column joints was investigated by Ugo and Domenico [62] through a three-dimensional numerical analysis. For the calibration of the model the experimental work performed by Ghobarah and Said [63] (see Chapter 2, Section 2.4) was used. For the numerical simulation the Athena 3D software and for the mesh generation GiD software was implemented. In the numerical analysis, load was not applied monotonically but cyclically as in the experimental tests. The FRP reinforcement was represented with dimensional discrete elements distributed in the fibre direction. The bond-slip model of Monti and Spoelstra (2003) was used for the simulation of slip between the FRP and the concrete. The numerical and experimental comparisons demonstrated the reliability of numerical models to predict the response of joints with no reinforcement and retrofitted with FRP.

10.3 SCOPE AND OBJECTIVES

The literature survey shows that very limited finite element analyses have been carried out on FRP strengthened beam-column joints. All the previously mentioned studies are concentrated on the simulation of the FRP retrofitted 2D exterior joints, under monotonic loading and constant axial load. No numerical studies have been conducted for FRP retrofitted exterior beam-column joints under varying axial load and as-built or FRP retrofitted corner beam-column joints under biaxial loading.

As previously stated, finite element approaches can be utilised in order to obtain more detailed information regarding the damage state in individual elements and their effect on the global behaviour. Models should be able to reflect key events such as the softening of the material, spalling of the concrete and debonding or delamination of the fibre composite material from the concrete surface. It is obvious that additional work is needed to devise numerically efficient and stable methods for

predicting the behaviour of different types of joint (i.e., exterior and corner) under different loading conditions (i.e., uni- and bi-directional with varying axial load) and FRP retrofit configurations. As these models are verified, they should be implemented in general purpose computer programmes to enable researchers and designers to assess the behaviour of beam-column joints with different dimensions, and different reinforcing and FRP strengthening configurations under various loading combinations. In this way, the effects of these parameters on the overall performance of the structure can be clearly understood, while analytical models and proposed design procedures can be revised and modified according to the findings. In addition, experimental laboratory testing would be greatly reduced. It is well known that, in most cases, laboratory testing is very difficult to perform due to the limitations in laboratory facilities, such as the simulation of the realistic dimension of the specimens, cost and practical aspects.

In light of these observations and discussions, the present study in this chapter aims toward complementing the experimental programme presented in the previous chapters, with a benchmark numerical model for the simulation of FRP retrofitted 2D exterior, as well as 3D as-built corner beam-column joints. In addition, it is also aimed to overcome the limitations of the implemented FE code and suggest some possible solutions to enhance modelling capacities for future studies.

At the Institute of Construction Materials, University of Stuttgart, researchers recently developed a unique finite element modelling software, MASA, to be used for nonlinear smeared fracture finite element analysis of concrete and reinforced concrete structures [22]. The computer code MASA was used successfully to realistically predict structural behaviour for a number of rather complex practical cases [25]. It is important to mention that the present work herein was part of a collaborative research between the University of Canterbury (New Zealand) and the University of Stuttgart (Germany). The first phase of the FEM numerical studies was carried out by the researchers at the University of Stuttgart, particularly in the development of three-dimensional numerical models for poorly detailed as-built 2D exterior joints. In the previous section these studies were reviewed [32, 34, 33].

In the second phase, within the framework of this study, FEM numerical studies were carried out to calibrate and develop a versatile numerical model to predict the response of the 2D retrofitted exterior and 3D as-built corner beam-column joints. In the numerical studies MASA software was used. As anticipated, during the course of the investigation some limitations pertaining to modelling with MASA were encountered, identified and possible solutions are herein recommended to overcome them. The main challenges and new tasks for MASA-modelling confronted during the numerical

investigations can be summarised as (1) modelling the advanced composite materials attached to the concrete; (2) modelling of the FRP debonding; (3) implementation of the varying axial load in 2D and 3D beam-column joints and (4) simulating bidirectional loading pattern in the analysis of 3D corner joints.

To accurately predict the behaviour of as-built, as well as retrofitted exterior and corner beam-column joints the aforementioned issues should be resolved and explicitly included in the FE models. This is of crucial importance to develop a fully validated, robust model that could be utilised as an investigative tool in conjunction with the experimental findings. Due to the scope of this research, this study is concerned with the first, third and fourth issues above.

10.4 NONLINEAR FINITE ELEMENT CODE MASA

In this section, a summary of theoretical background of the finite element code MASA is given. It is important to note that the subject of nonlinear fracture mechanics and the implementation of this into the finite element analysis of concrete and reinforced concrete structures are beyond the scope of this study. Nevertheless, for the sake of completeness, an overview of the structure of the programme, the finite element analysis of quasi-brittle materials and the used constitutive law for concrete (microplane model) are described. For more detail refer to the above cited literature.

10.4.1 General

The programme MASA was mainly developed to be used for nonlinear analysis of concrete and reinforced concrete structures in the framework of local or nonlocal continuum theory, i.e., damaged and fracture phenomena are treated in a smeared way (smeared crack approach). In general, it can be employed in the nonlinear three-dimensional (3D) smeared fracture finite element analysis of structures made of quasi-brittle materials. For the standard analysis of concrete and RC structures the general *microplane model* is used for the concrete material model (constitutive law). The reinforcement is modeled by a uniaxial elasto-plastic stress-strain relationship with or without strain hardening. In addition to this, a special discrete bond element is available as well. Detailed information can be found in Ozbolt [64].

In order to discretize the concrete (quasi-brittle material) the eight node (hexa) or four node (tetra) solid finite elements can be used. The reinforced bars can be discretized by two-node truss or beam elements. One of the three solution strategies can be used (1) constant stiffness method (CSM); (2)

tangent stiffness method (TSM) and (3) secant stiffness method (SSM). The type of the analysis in the FE code of MASA is incremental. Therefore, for each load increment one has to specify the load multiplier, displacement multiplier and the tolerance. With these factors, both, the nodal displacements and loads are multiplied. The following set of load-displacement multipliers is related to all load groups.

A commercial pre- and post-processing package FEMAP™ is employed to prepare input data, as well as to analyze the results of the finite element analysis. An automatic mesh generation, definition of loads and boundary conditions, as well as the materials, loads and constraints were generated using FEMAP™. The link between FEMAP™ and MASA was established via an input interface programme which generates an input data of from FEMAP™ output data (neutral file). The post-processing output results are read and graphically interpreted by FEMAP™.

10.4.2 Modelling of Damage in Concrete

In the framework of continuum mechanics, significant efforts have been performed in the modelling of damage and failure phenomena of concrete and reinforced concrete structures. In order to simulate the behaviour of structural elements under various loading conditions realistic material models should be employed in the numerical simulations. It is an arduous task because concrete is a heterogeneous, cohesive-frictional material and exhibits complex non-linear inelastic behaviour under multi-axial stress states. Nevertheless, in recent decades, considerable effort has been undertaken to achieve this goal which has resulted in partial success.

In literature a large number of constitutive models are proposed for the description of the mechanical behaviour of concrete such as empirical models, linear elastic, nonlinear elastic, plasticity based models, models based on endochronic theory of inelasticity, fracturing models and continuum damage mechanics models, micromechanics models, etc. Detailed information on this subject can be found in Babu *et al.* [65]. These models can be divided into two distinct categories:

(1) macroscopic models, in which the material behaviour is considered to be an average response of a rather complex micro-structural stress transfer mechanism. The concrete constitutive laws relate to the macro-stress tensor $\boldsymbol{\sigma}$ to the macro-strain tensor $\boldsymbol{\varepsilon}$ [66, 67]. Depending on the type of this relation, these models can be further categorized into plasticity, damage, and endochronic models.

(2) microscopic models, were the micromechanics of deformation is described by stress-strain relations on the micro level. These types of models are based on the macroplane theory and they provide relations between stress and strain components on planes with prespecified orientations. The stress vectors acting on the different (micro) planes, are linked to the macroscopic stress tensor σ by the principal of virtual work. Although from a physical point of view microscopic models are more promising, due to the extremely demanding computational facilities, in practical applications macroscopic models have to be used [22].

At the macro scale level, the model has to correctly describe microstructural phenomena such as cohesion, friction, aggregate interlock and interaction of microcracks. However, an incompatibility of the cracking simulation problem and FE element technique, which is a continuum mechanics, arises. This apparently requires the development of special schemes which, while in keeping with the general notion of 'continuity' in the FE solution, exhibit drastic and sudden changes in the material at the location of cracks. Cracking and damage phenomena can principally be modeled in two different ways: (1) discrete (discrete crack model) or (2) smeared (smeared crack model).

The discrete-crack approach introduces an actual gap in the FE mesh at the location of crack. It achieves this by doubling and separating the nodal coordinates laying individual crack paths. This implies important changes in the numbering of nodes and element connectiveness, which in turn, affect the global stiffness matrix. The first discrete-crack model appears to have been used by [16] (Figure 10-1). On the other hand, the essence of smeared modelling is the setting up of cracked areas by modification of the stiffness and stresses (equilibrium conditions) at the relevant Gauss points, i.e., those points used for numerical integration of stiffness matrices and for the calculation of residual forces. Thus, while discrete models account for stiffness losses by doubling the nodes laying on individual cracks, smeared cracks simply replace constitutive matrices by cracked ones [68].

10.4.3 Localization Limiters

The classical local continuum smeared fracture analysis of materials which exhibit softening (quasi-brittle materials), leads in the finite element analysis to the results which are generally mesh dependent [69]. The reason for this is localization of damage and related energy consumption capacity, which depends on the element size, i.e., when the finite element mesh is coarse the energy consumption capacity will be larger than if the mesh was fine. Consequently, the model response depends on the mesh size. To assure mesh independent result, the total energy consumption capacity has to be

independent of the element size, i.e., one has to regularize the problem by introducing the so-called localization limiter [64].

Currently two different approaches are in use. The first one is relatively simple crack band method [70] and the second group of approaches are the so called higher order methods: Cosserat-continuum [71], nonlocal continuum of integral type [72, 73] or nonlocal gradient type of continuum [71].

The crack band method assumes that the damage (crack) is localised in a row of finite elements. To ensure the mesh independent energy consumption from cracking, the concrete constitutive law is modified such that the concrete fracture energy is constant. The same formulation is assumed for tensile fractures and compressive fractures, but the compressive fracture energy G_f is typically 100 times larger than the tensile fracture energy. Thus, the fracture propagation of concrete depends on three parameters – fracture energy of the material, G_f, material strength, f'_c, and width of crack band (recommended to be three times the aggregate size). Further details of the crack band method are available in references [74, 75, 25].

Compared to the crack band method the higher order procedures are rather complex, but more general. To obtain mesh independent results, one can alternatively use the discrete crack approach [76]. However, the main drawback of this approach is the need for continuous remeshing, which is rather complex and time consuming. Moreover, some stress-strain histories (for instance compression) are difficult to model in a discrete sense. Therefore, the smeared crack approach is a more general approach, especially for practical engineering applications [64].

10.4.4 Microplane Material Model for Concrete

With its complex physical behaviour which is closely interconnected with the grain size and shape, as well as the physical properties of its constituents, concrete is a heterogeneous material. In some aspects of the behaviour, concrete can be treated as a brittle material such as cast iron (i.e., under tensile stress) and also as a plastic material such as mild steel under compressive stresses. Yet, unlike brittle and plastic materials, concrete exhibits a considerable softening beyond the peak stress.

As mentioned previously, there are various possible approaches for the modelling of concrete, such as theory of plasticity, plastic-fracturing theory, continuum damage mechanics, endochronic theory and their combinations of various forms. However, due to the complexity of concrete these models cannot

always realistically represent the behaviour of concrete for general three-dimensional stress-strain histories. For example, since the deformation of the concrete under compressive stresses are induced by internal micro-cracking contrary to the flow of the material as in mild steel, the classical theory of plasticity cannot be employed to identify the observed behaviour of concrete [77].

In the traditional approach (i.e., using modified plastic and fracture theory or combination of both) to the problem of modelling the behaviour of concrete, macroscopic models are formulated by total or incremental formulation between the $\boldsymbol{\sigma_{ij}}$ and $\boldsymbol{\varepsilon_{ij}}$ components of the stress and strain tensor, using the theory of tensorial invariants [66, 67]. Nevertheless, these modelling approaches based on the analysis of simple homogenous materials becomes questionable, due to the fact that concrete is primarily a composite material with a failure mechanism controlled by micro-cracking, which is converted into inelastic and anisotropic behaviour.

The Microplane method is a totally different approach, which describes the complicated inelastic properties of concrete, not globally, but individually for planes at various orientations at a point within the material [74]. Accordingly, by constructing a microplane model [78], a fully three-dimensional material law that includes tensional and compressive softening, damage of the material, different combinations of loading, unloading and cyclic loading, along with the development of damage-induced anisotropy of the material can be simulated. As a result, it is fully capable of predicting the behaviour of real-world concrete structures [79] once provided with the correct input data.

In the microplane model the material is characterized by a relationship between the stress and strain components on planes of various orientations. These planes may be imagined to represent the damage planes or weak planes in the microstructure, such as contact layers between aggregates in concrete (Figure 10–2). This method originated from the work of [80] for the constitutive behaviour of polycrystalline metals. Due to the conceptual simplicity of the microplane approach, it was extended for more complicated materials, such as anisotropic rocks in the models formulated by [81], Bazant and co-workers [78]. These models were based on the static constraint, where the micro-stress on a typical plane was the projection of the macro-stress tensor on that plane. As the model was unsuitable for materials with noticeable softening, Bazant and Gambarova [74] replaced the static constraint with a kinematic constraint and extended the approach to geomaterials such as concrete [82]. Later to formulate a more general and relatively simple model, a significant effort was recently accomplished in the further development of the microplane model for concrete [83, 84, 73, 25, 64].

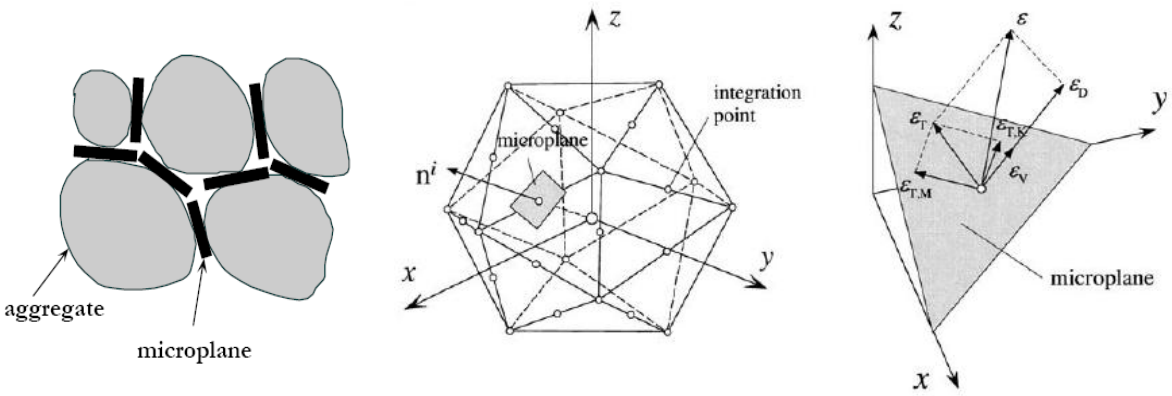

Figure 10–2 Microplane model: a) load transfer over a number of idealised contact planes; b) spatial discretization of unit-volume sphere by 21 microplanes; c) decomposition of the total macroscopic strain tensor on the microplane (after [22])

10.5 NUMERICAL STUDIES ON 2D RETROFITTED EXTERIOR BEAM-COLUMN JOINTS

In this section, detailed information on the numerical study performed to simulate the behaviour of the retrofitted 2D exterior beam-column joint, namely Specimen 2D2, is given. This specimen was designed according to the procedure described in Chapter 4, retrofitted with a minimum retrofit scheme and tested under constant axial load and quasi-static cyclic lateral loading. As anticipated, the specimen failed under the desired ductile failure mechanism with no FRP debonding during the test. More detailed information regarding the testing procedure and experimental results are provided in Chapter 5 and 6, respectively.

10.5.1 FE Model Development and Discretization

The FE code, MASA, was used in the study. In the code, the concrete was modelled using microplane model, which consists of a three dimensional microscopic model in which the material was characterized by a uniaxial relationship between the stress and strain components on planes of various orientations called "microplanes". The smeared-crack concept was used for the modelling of the cracking of the concrete. More information regarding the theoretical background can be found in the previous subsections. FE model data input such as material properties, definition of loads and boundary conditions, as well as an automatic mesh generation were performed using a commercial pre- and post-processing package FEMAP™.

The finite element mesh discretization with boundary conditions is shown in Figure 10–3. The same geometry and dimensions were employed in the model (see Chapter 5). The spatial discretization of

concrete and fibre sheets was performed by 4-node solid elements, whereas the reinforcement was modelled by 2-node truss elements (Figure 10–3 and Figure 10–4). Linear elastic material was used in the modelling of boundary elements to prevent a local failure of the concrete elements in the vicinity of the supports and at the axial lateral load application points. In order to capture the behaviour more accurately, the size length of the hexahedral elements of concrete and FRP sheets in the joint region was approximately 20 mm. The mesh size was increased in the elastic regions. Note that, due to the symmetry of loading and boundary conditions, only half of a joint was modelled.

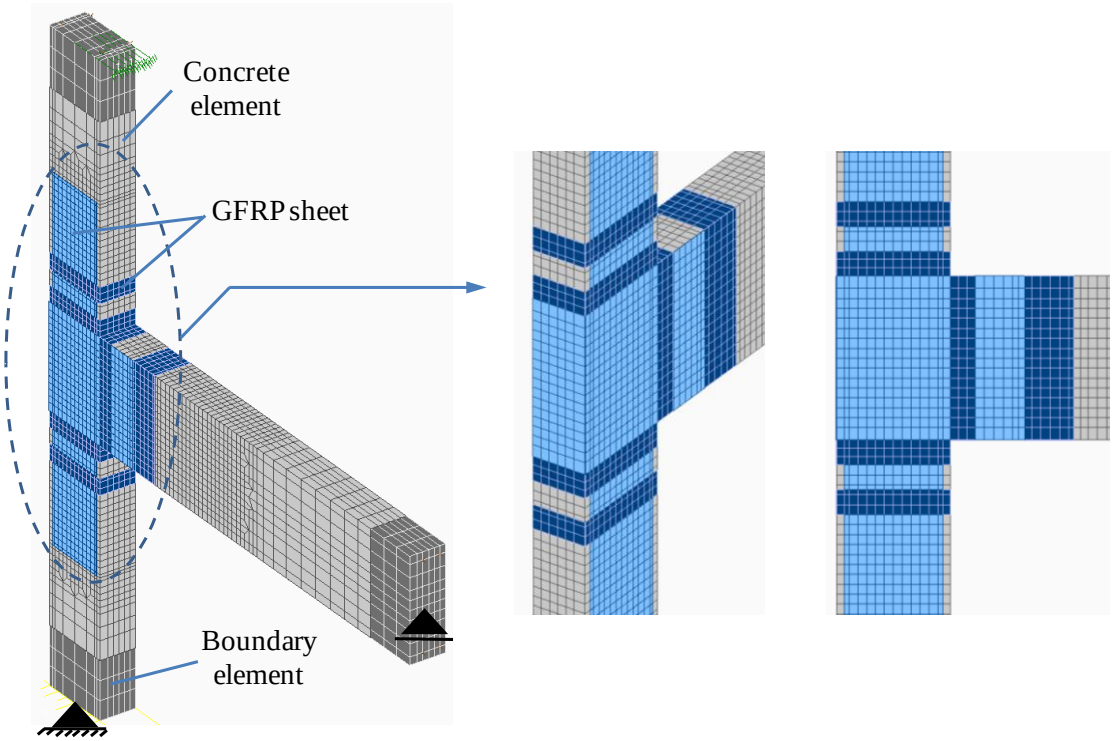

a) Dimetric view b) Dimetric back close-up c) Front close-up

Figure 10–3 FE model: discretization of concrete and composite material

For the finite element implementation, the values of compressive strength of concrete, f_c`, tensile strength, $f_t$, an elastic modulus were taken from the corresponding experimental set of data, or if not given, were calculated with the formulae given in Chapter 4. The strength of concrete is 18.9 MPa, with a modulus of elasticity of 20433 MPa, and a Poisson`s ratio of 0.18.

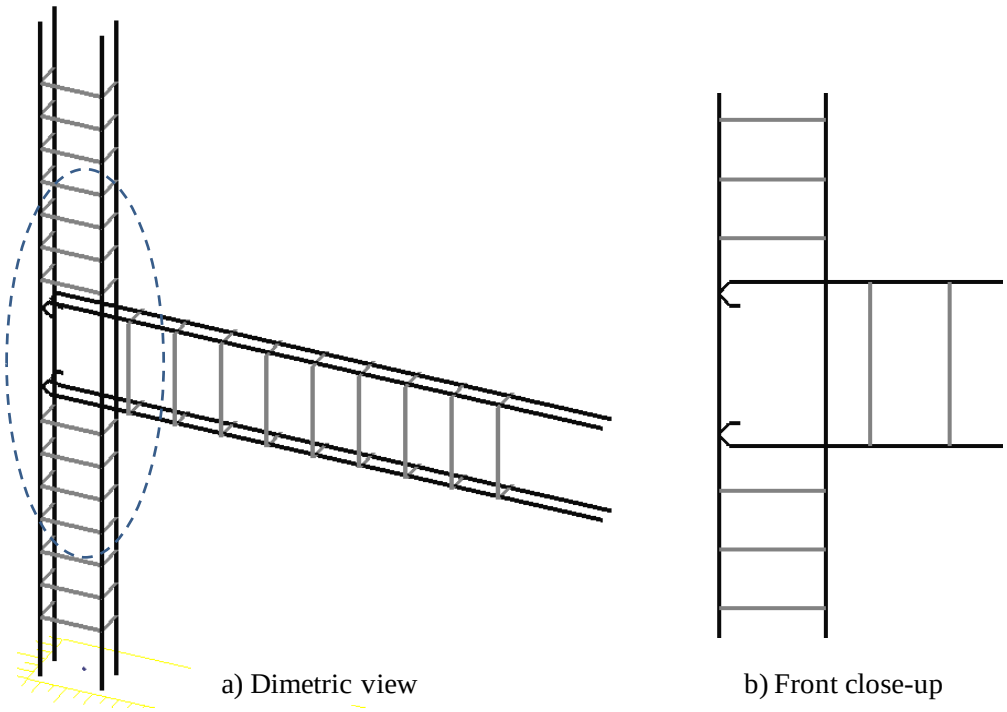

a) Dimetric view b) Front close-up

Figure 10–4 FE model: discretization of reinforcement

The reinforcing bars were represented with one-dimensional truss elements with uni-axial three-linear stress-strain constitutive law. The reinforcement steel bar had a yield strength value of 340 MPa, modulus of elasticity of 200000 MPa, Poisson`s ratio of 0.33, and ultimate strength of 440 MPa. The loading-unloading rules for the monotonic and cyclic version of the programme are plotted in Figure 10–5. For transverse reinforcement, a rigid connection between steel and concrete was assumed. This assumption neglects the influence of the relative displacement between stirrups and concrete ([85]).

As stated previously in this study, one of the major problems and typical deficiencies of pre-1970s RC structures is the use of plain round longitudinal bars with low bond capacity. Since plain reinforcement does not possess lugs or other surface deformations, the bond stresses cannot be transferred by mechanical interlock. Instead, bond is transferred by adhesion between the concrete and the reinforcing bar before slip occurs, and by wedging action of the small particles that break free from the concrete upon slip [86]. As a consequence, the selection of the bond model and parameters are of great importance in simulating the correct behaviour of deficient structural elements constructed with plain round bars.

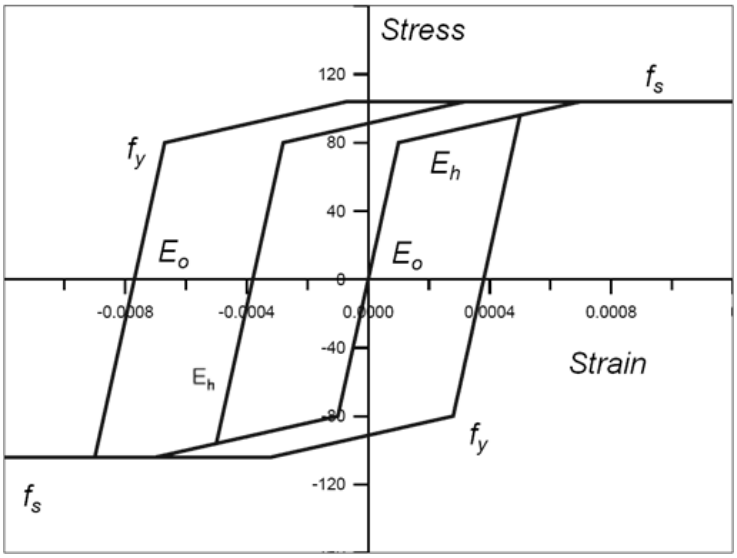

Figure 10–5 Uniaxial constitutive stress-strain relationship for reinforcement steel (after [64])

In this study, the modelling of the bond between the longitudinal reinforcement and concrete was performed by using discrete bond elements which consisted of 1D nonlinear springs. In order to simulate bond properties of plain round bars the existing bond-slip model was employed. This bond-slip model was originally developed for deformed bars and it has been demonstrated that the model is able to correctly predict the bond behaviour of deformed steel bars for monotonic and cyclic loading [21, 32]. In the calibration of the model for the simulating of bond elements, the results of the experimental study on beam tests with straight plain round bars conducted by Fabbrocino *et al.* [87] were used. Similar cyclic behaviour was assumed in the analysis (Genesio and Sharma, 2010).

The discrete bond model adopted in MASA is shown in Figure 10-6. The bond model is defined by three parameters which are the maximum bond strength, τ_{max}, and three characteristics slip limits, s_1, s_2 and s_3. The τ_{max} is comprised mechanical and adhesive (plain bar only) component, τ_m, and the frictional residual bond component, τ_f. The concrete confinement state and strength as well as the quality of the bond strength strongly influence these parameters. The calibrated bond parameters used in the numerical analysis are given as follows: mechanical bond = 0.75 MPa; friction and residual bond = 0.75 MPa; secant shear modul = 80 N/mm; k_1 modul = 100 N/mm; k_2 modul = 10 N/mm; s_2 = 0.1 mm and s_3 = 1.0 mm.

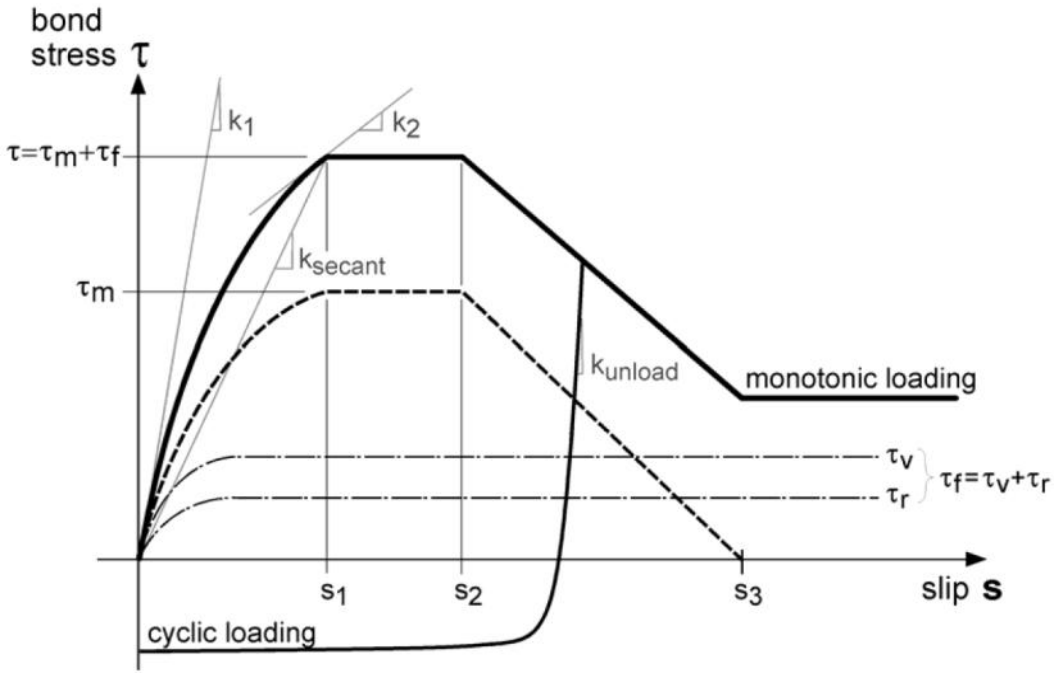

Figure 10–6 Discrete bond model as implemented in MASA

The GFRP sheets were modelled as an isotropic linearly elastic material with brittle fracture in tension. Taking the above consideration into account, hexahedral elements with the actual thickness of the FRP sheet (t_f=0.36 mm) in one dimension were adopted for the mesh of FRP sheets, so that an orthotropic layer in a plane stress condition can be achieved as in the real condition. It is important to note that, since no FRP debonding occurred in the test of Specimen 2D2, a perfect bond and no relative displacement were assumed between the concrete and the FRP sheet in the modelling. The modulus of elasticity along the fibre direction, Poisson`s ratio, and the ultimate strength of the CFRP material are 76000 MPa, 0.22 and 2300 MPa, respectively.

10.5.2 Results and Comparison with Experimental Data

In the first phase of the numerical studies the performance of the FE model was tested to reproduce the anticipated behaviour. For this purpose, the model was loaded monotonically in the pull direction up to 4% drift under constant axial load. The lateral top column displacement was applied at 0.25 mm steps up to 80 mm (4% drift). Particular focus was given to the global load-displacement behaviour and cracking pattern.

The monotonic lateral force-displacement response of the FE model, along with the experimental cyclic lateral force-displacement results are given in Figure 10–7. As seen in this figure, very

promising results were obtained: the monotonic FE load-displacement curve predicted the backbone curve of the experimental cyclic curve with very good accuracy. The cracking patterns under monotonic pull loading for various drift levels are given in sequence from Figure 10-8 to Figure 10-11. In these figures, the front view of the FE model, along with its close-up view, along with the middle section close-ups of the joint region are given. The examination of these figures reveals the development of two particular damage mechanisms in the course of the monotonic loading. These damage mechanisms are basically formed in the joint region as shear cracking (see the joint region middle section close-ups) and plastic hinge cracking in the beam-FRP sheet interface. However, the dominant failure mechanism was observed to be the latter one. Overall, it is concluded that the model developed within the FE programme MASA predicted the expected failure mode successfully and can be used as the basis model for the cyclic analyses.

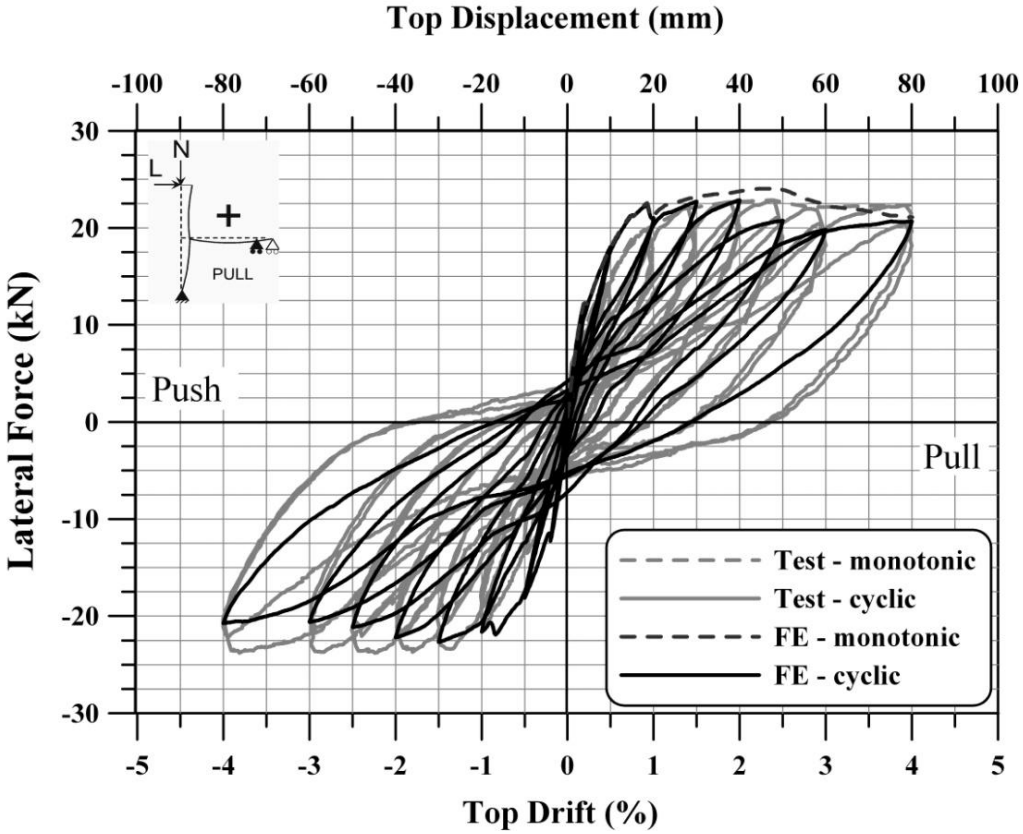

Figure 10–7 Comparison between numerical and experimental monotonic and cyclic behaviour - Specimen 2D2

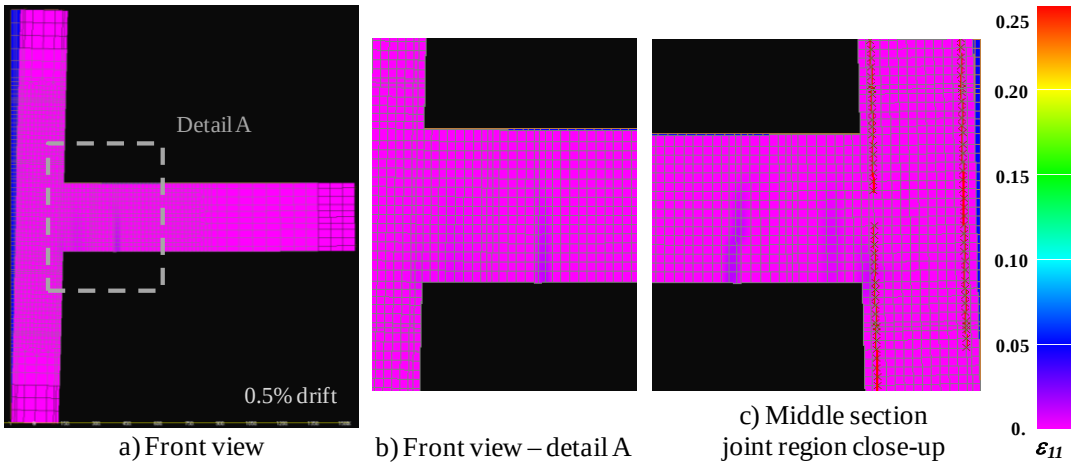

a) Front view b) Front view – detail A c) Middle section joint region close-up

Figure 10–8 Cracking pattern under monotonic pull loading at 0.5 % drift - Specimen 2D2

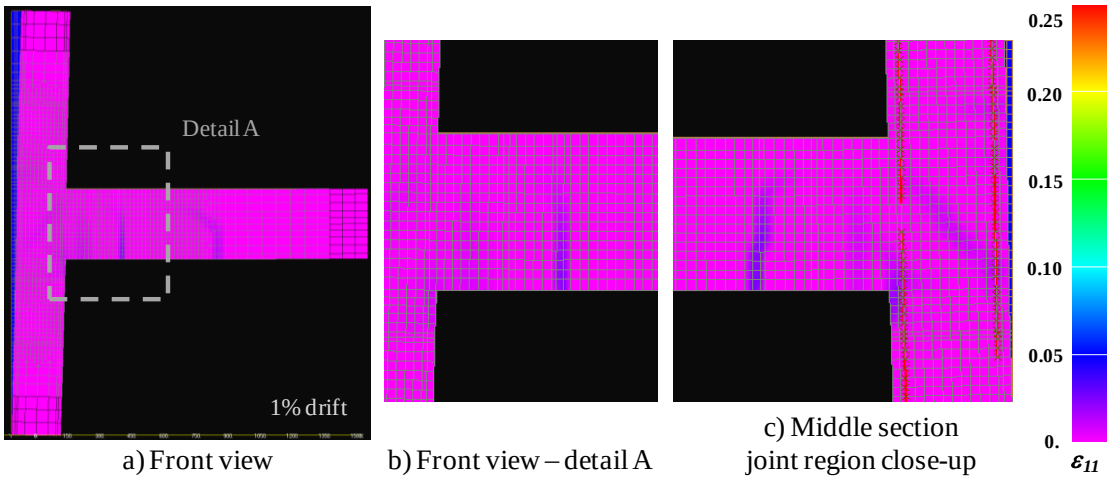

a) Front view b) Front view – detail A c) Middle section joint region close-up

Figure 10–9 Cracking pattern under monotonic pull loading at 1 % drift - Specimen 2D2

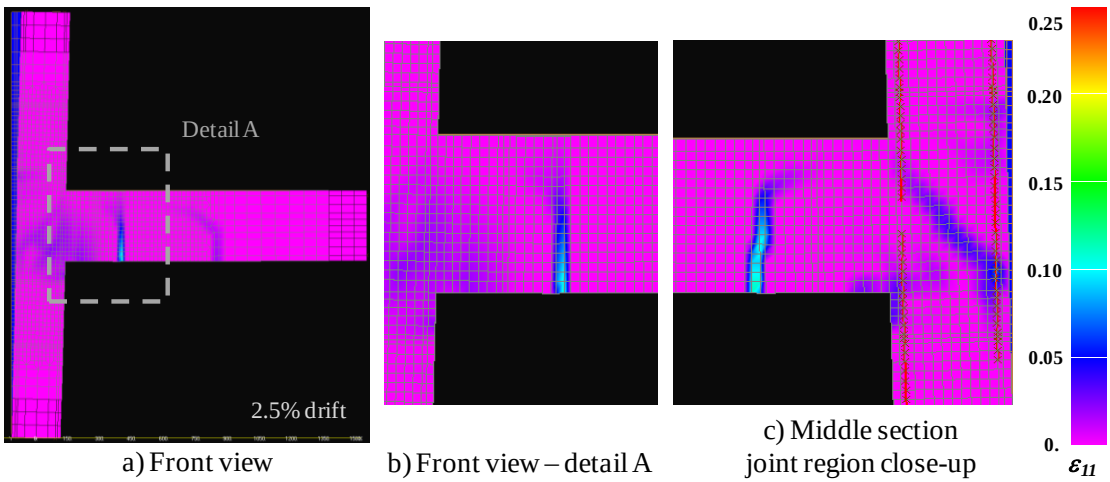

a) Front view b) Front view – detail A c) Middle section joint region close-up

Figure 10–10 Cracking pattern under monotonic pull loading at 2.5 % drift - Specimen 2D2

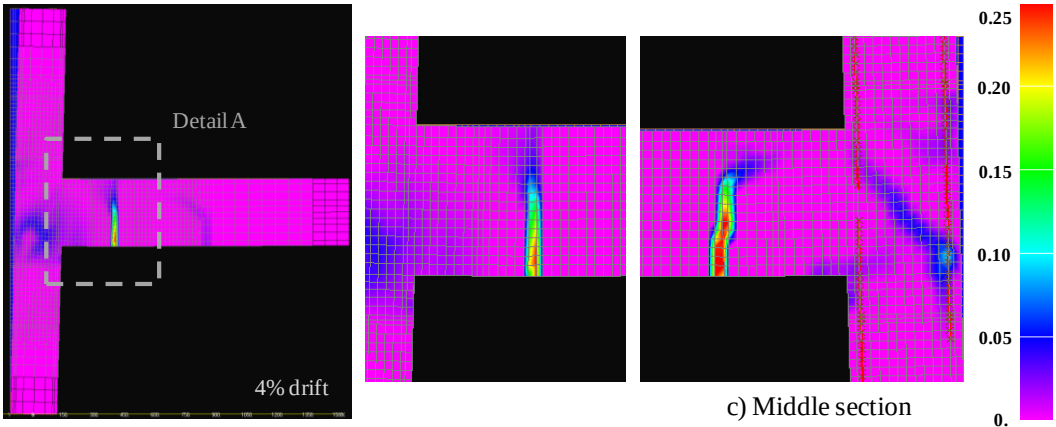

a) Front view b) Front view – detail A c) Middle section joint region close-up

Figure 10–11 Cracking pattern under monotonic pull loading at 4 % drift - Specimen 2D2

In the next stage, the model was analysed under reversed cyclic loading with constant axial load following the same load protocol employed during testing. Note that, due to limitation in computation memory and time, only one cycle per drift level was used. To validate the FE model against the experimental findings, several items from the experimental and numerical results are compared. They are the load-displacement hysteresis loops, crack patterns and damage propagation, strength and stiffness properties and lastly the strain development in GFRP sheets.

The comparison of the cyclic lateral force-displacement response of the FE model with the experimental cyclic lateral force-displacement results is given in Figure 10–7. As seen in this figure, apart from an underestimation of the load values in the push direction, which is within a 10% error margin, the predicted values by FE analysis agree well with the experimental measurements. This observation is also confirmed with the close examination of the peak values obtained from each loading direction in the numerical analysis. In Table 10-1 the maximum column shear forces obtained in the numerical analysis are compared with these values of experimental study. It is shown that apart from the first drift levels of loading (0.1, 0.2 and 0.5% drift), the average difference of the column shear forces between the observed test and numerical values is around 7%.

To further assist the validation of the FE model against the experimental results, the peak-to-peak stiffness K_p (see Chapter 6) of the numerical analysis are also compared with experimental findings in Table 10-1. Similar observations to the previous discussion on the column shear forces are made as well as the stiffness degradation characteristics. The difference between the numerical analysis results and experimental findings are reduced substantially after 1% drift level. Towards the end of the analysis, the difference became stable, which was around 15%.

The results of the numerical analysis in terms of the damage propagation and cracking patterns under quasi-static cyclic loading for various drift levels are given and compared with test observations between Figure 10–12 to Figure 10–15. In order to highlight the various damage states, the close-ups taken in the middle section of the joint region are also provided. The findings show that the cracking patterns and damage mechanism formation and propagation are realistically reproduced by the FE code MASA. The comparison of damage patterns, herein represented by the principal strain fields, revealed that, FRP composite effect in terms of reducing the damage and increasing the shear strength of the joint panel was simulated successfully in the FE analysis. The damage pattern in the joint region after removing the FRP layer at the end of the test is also corresponding to the observed damage in the model (Figure 10-15). It is interesting to note that, although an unavoidable damage in the joint region occurred due to an excessive compressive stress state, FRP was successful in preventing the dilation of the joint and excessive crack opening by the confinement effect. Hence, modification in the hierarchy of strength of the elements and sequence of the events led to a ductile mode of failure in the joint subassembly.

Table 10-1 Summary and comparison of numerical results with test results, Specimen 2D2

Drift Level	Direction	Strength			Stiffness		
		$V_{c,exp}$ [a] (kN)	$V_{c,num}$ [b] (kN)	difference with test (%)	$K_{p,exp}$ [c] (kN/mm)	$K_{p,num}$ [d] (kN/mm)	difference with test (%)
0.1%	Pull	6.23	7.90	26.9	3.02	3.78	25.1
	Push	-3.52	-7.20	104.8			
0.2%	Pull	8.38	12.13	44.9	2.08	3.05	46.8
	Push	-7.37	-12.27	66.5			
0.5%	Pull	14.27	18.03	26.4	1.48	1.81	22.3
	Push	-13.50	-18.12	34.2			
1%	Pull	19.70	21.02	6.7	1.05	1.07	1.9
	Push	-20.86	-21.63	3.7			
1.5%	Pull	22.00	22.71	3.2	0.82	0.76	-8.1
	Push	-23.89	-22.69	-5.0			
2%	Pull	22.65	22.87	1.0	0.63	0.56	-10.5
	Push	-20.86	-22.22	6.5			
2.5%	Pull	22.85	20.75	-9.2	0.50	0.42	-16.6
	Push	-23.76	-21.15	-11.0			
3%	Pull	21.98	19.81	-9.8	0.40	0.34	-16.0
	Push	-23.71	-20.62	-13.0			
4%	Pull	22.29	20.67	-7.2	0.30	0.26	-13.3
	Push	-23.63	-20.73	-12.2			

[a] Experimentalstory column shear; [b] Numerical story column shear

[c] Experimentalpeak-to-peak stiffness; [d] Numerical peak-to-peak stiffness

Lastly, the FE FRP strain demands in the joint region for top, middle and bottom regions are examined and compared with the experimental findings for all drift levels in Figure 10–16, 10-17 and 10-18, respectively. In general, three distinct trends are identified after the analysis and comparison of the FE FRP strain values. For all the regions, the FE results overestimate the FRP readings by up to around 1.5% drift and underestimated after 2.5% drift. At around 1, 1.5 and 2% drift levels relatively comparable FE results were obtained. Among the three different regions, the numerical analysis exhibited the best simulation for the middle joint FRP strains. The difference of the FRP strains in this region compared to test results was around 15%, while for the top and bottom FRP strains this value was around 58 and 40%, respectively.

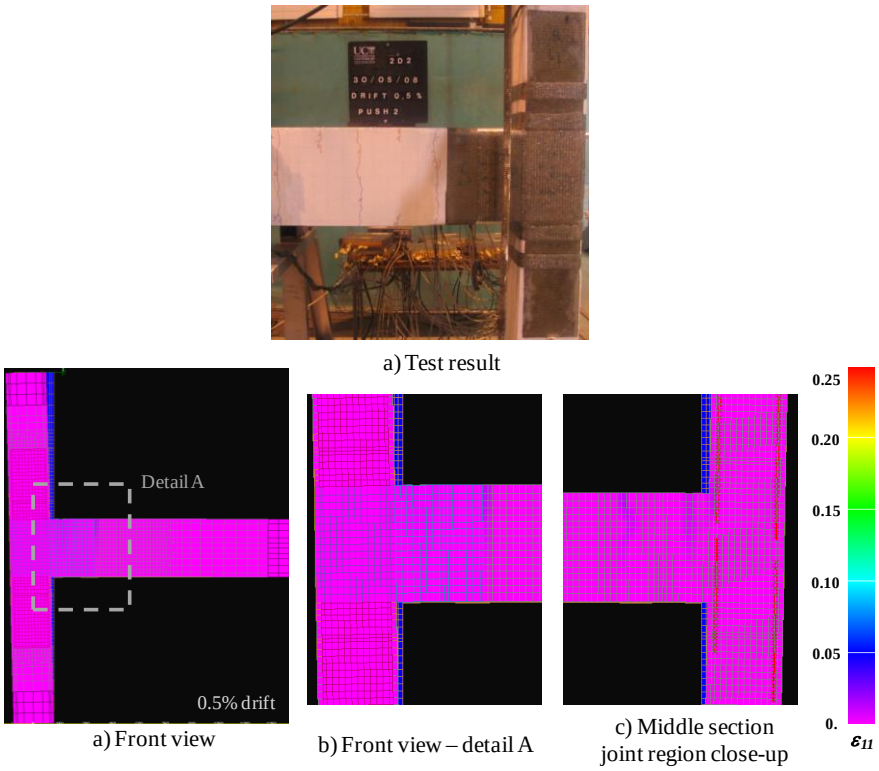

a) Test result

a) Front view b) Front view – detail A c) Middle section joint region close-up

Figure 10–12 Comparison of cracking pattern at 0.5% drift – push/pull direction - Specimen 2D2

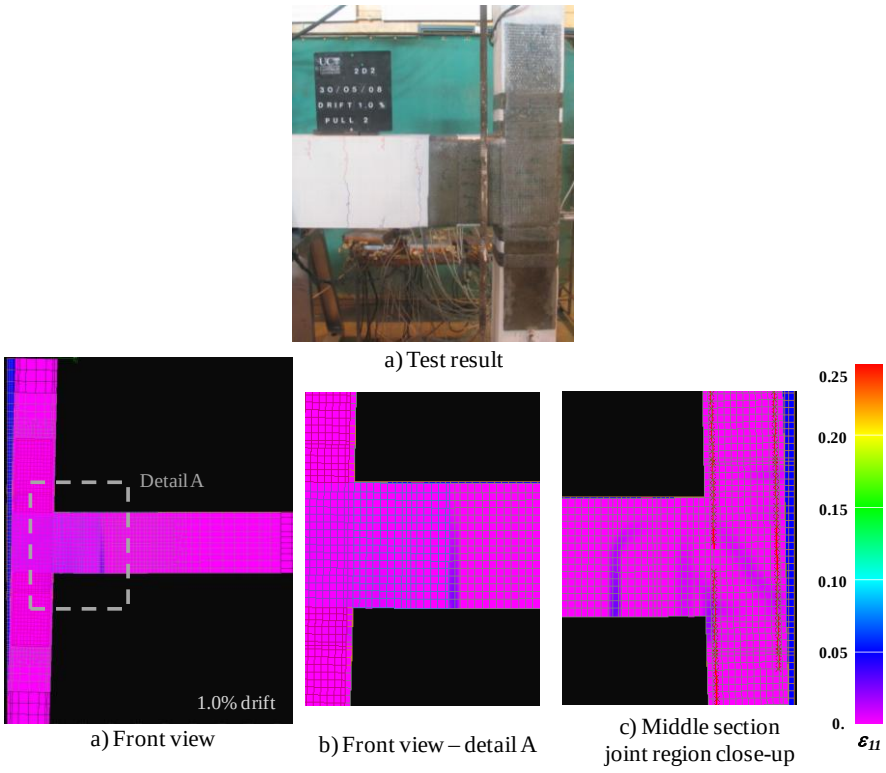

Figure 10–13 Comparison of cracking pattern at 1% drift – push/pull direction - Specimen 2D2

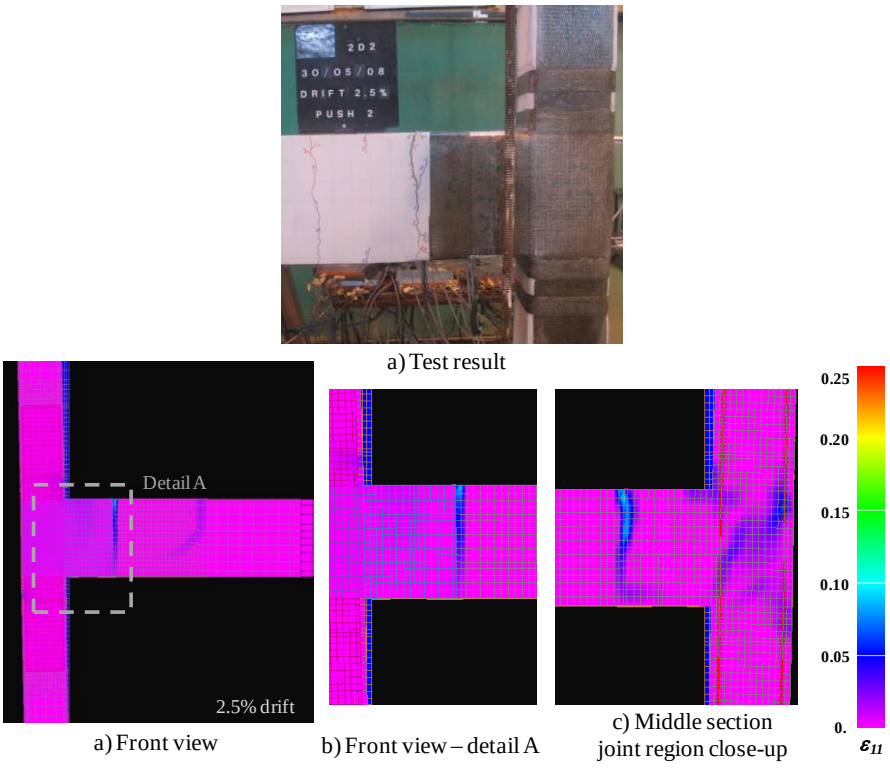

Figure 10–14 Comparison of cracking pattern at 2.5% drift – push/pull direction - Specimen 2D2

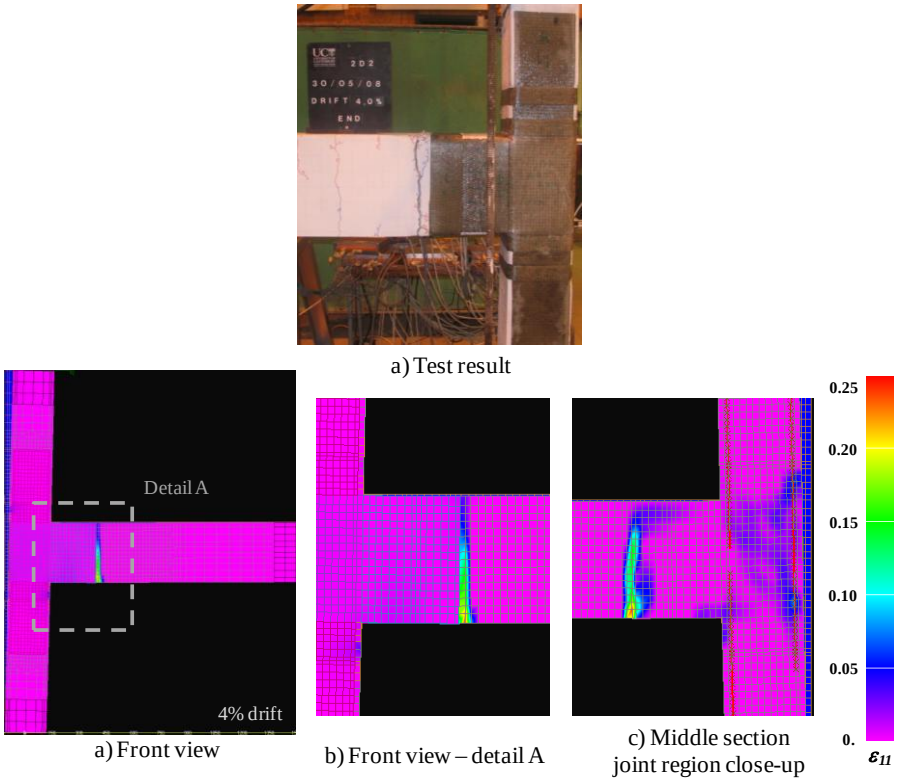

a) Test result

a) Front view

b) Front view – detail A

c) Middle section joint region close-up

Figure 10–15 Comparison of cracking pattern at 4% drift – push/pull direction- Specimen 2D2

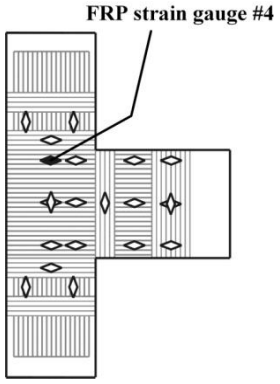

Drift	$\varepsilon_{f,exp}$ [a] ($\mu\varepsilon$)	$\varepsilon_{f,num}$ [b] ($\mu\varepsilon$)	difference with test (%)
0.1%	-10.0	0.0	-100.2
0.2%	-19.9	-18.7	-6.1
0.5%	-49.8	-75.1	50.8
1%	-119.5	-147.1	23.1
1.5%	-149.4	-191.5	28.2
2%	-209.1	-205.1	-1.9
2.5%	647.3	-228.4	-135.3
3%	1335.0	-128.8	-109.6
4%	2022.0	-574.1	-128.4

[a] Experimental FRP strain; [b] Numerical FRP strain

a) b)

Figure 10–16 Comparison of top joint FRP strains: a) gauge location; b) comparison table

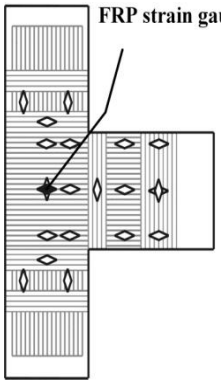

Drift	$\varepsilon_{f,exp}$ [a] ($\mu\varepsilon$)	$\varepsilon_{f,num}$ [b] ($\mu\varepsilon$)	difference with test (%)
0.1%	49.8	55.9	12.3
0.2%	69.7	95.0	36.3
0.5%	99.6	116.9	17.4
1%	1484.0	1630.7	9.9
1.5%	3376.0	3383.9	0.2
2%	4103.0	3862.0	-5.9
2.5%	4651.0	3862.0	-17.0
3%	4910.0	3535.3	-28.0

[a] Experimental FRP strain; [b] Numerical FRP strain

a) b)

Figure 10–17 Comparison of middle joint FRP strains: a) gauge location; b) comparison table.

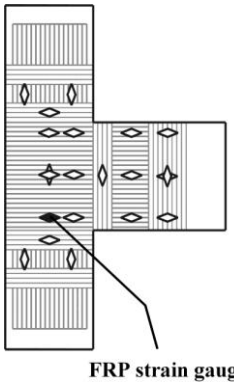

Drift	$\varepsilon_{f,exp}$ [a] ($\mu\varepsilon$)	$\varepsilon_{f,num}$ [b] ($\mu\varepsilon$)	difference with test (%)
0.1%	59.8	72.5	21.3
0.2%	79.7	112.4	41.1
0.5%	79.7	135.2	69.7
1%	806.7	909.3	12.7
1.5%	2042.0	1656.0	-18.9
2%	3486.0	2536.5	-27.2
2.5%	4641.0	2239.4	-51.7
3%	5527.0	1715.9	-69.0

[a] Experimental FRP strain; [b] Numerical FRP strain

a) b)

Figure 10–18 Comparison of bottom joint FRP strains: a) gauge location; b) comparison table.

10.6 NUMERICAL STUDIES ON 3D AS-BUILT CORNER BEAM-COLUMN JOINT

In this section, the capability of the FE Code MASA to numerically reproduce the behaviour of 3D as-built corner beam-column joint, Specimen 3D1, is investigated. Following the brief description of the FE model development and the implementation of the bidirectional load pattern in the analysis, the analysis results are compared and discussed along with the experimental findings in terms of the global load-displacement behaviour and cracking pattern. Special acknowledgements are given to a fellow postgraduate researcher, Giovacchino Genesio (University of Stuttgart, Germany), for his assistance in the development of the as-built 3D corner beam-column joint.

10.6.1 FE Model Development and Discretization

A similar type of approach to that of Specimen 2D2 was used in the finite model development of Specimen 3D1. The values of compressive strength of concrete, f_c`, tensile strength, $f_t$, an elastic modulus were taken from the corresponding experimental set of data, or if not given, were calculated with the formulae given in Chapter 4. The strength of concrete was 17.4 MPa, with a modulus of elasticity of 19605 MPa, and Poisson`s ratio of 0.18. The reinforcing bars were represented with one-dimensional (1D) truss elements with uniaxial tri-linear stress-strain constitutive law. The reinforcement steel bar had a yield strength value of 340 MPa, a modulus of elasticity of 200000 MPa, a Poisson`s ratio of 0.33, and an ultimate strength of 440 MPa. For transverse reinforcements, a rigid connection between reinforcement and concrete was assumed. The modelling of the bond between the longitudinal reinforcement and concrete was performed by using discrete bond elements consisting of 1D nonlinear springs with the same calibrated bond parameters as used in Specimen 2D2.

In Figure 10-19, the finite element mesh discretization of the Specimen 3D1 is presented. The same geometry and dimensions were employed in the FE model as the test specimen (see Chapter 10). The spatial discretization of concrete is performed by 4-node solid elements whereas the reinforcement was modelled by 2-node truss elements. Careful attention has been given to the description of the joint detailing. The 180° standard hook anchorage was modelled using stiff linear bar elements for each direction as shown in Figure 10-20. Linear elastic material was used in the modelling of boundary elements to prevent a local failure of the concrete elements in the vicinity of the supports and at the axial lateral load application points. In order to capture the behaviour more accurately, the size length of the hexahedral elements of concrete in the joint region was approximately 20 mm. The mesh size was increased in the elastic regions. It is important to note that, instead of using the vertical symmetry of the joint, the entire 3D1 specimen was modelled. The out-of-plan movement of the beams was restrained as performed during testing (Figure 10-21) to prevent the additional torsional rotation demand stemming from the lateral movement and rotation of the beam, and to simulate the actual behaviour in the prototype RC frame structure.

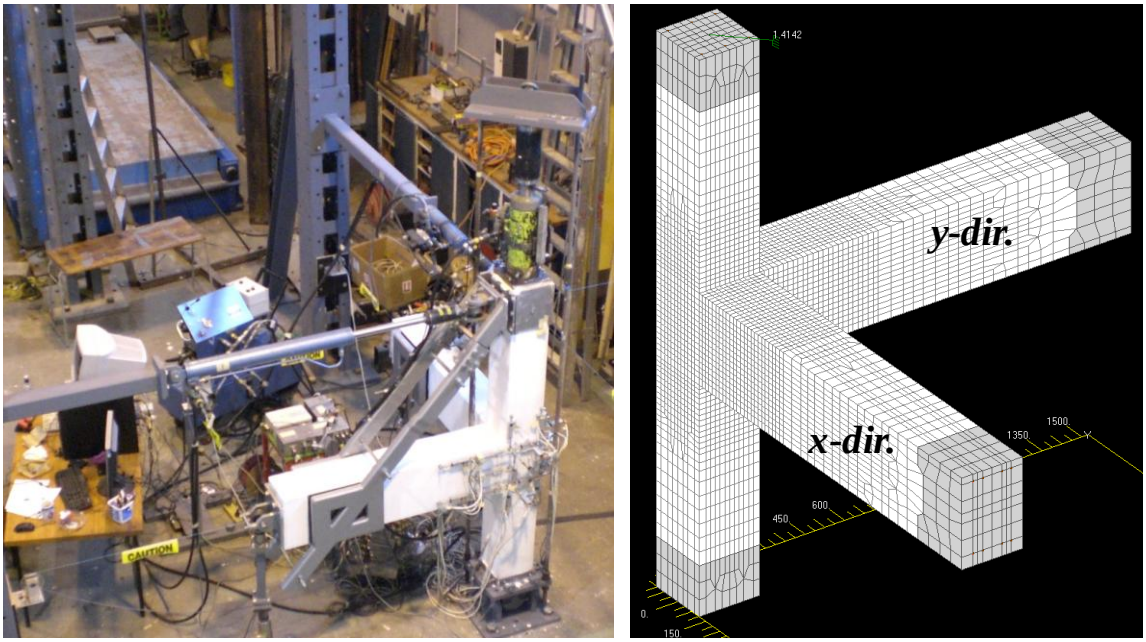

a) 3D as-built corner joint with test rig b) FE model

Figure 10–19 FE mesh of 3D benchmark corner joint unit, Specimen 3D1

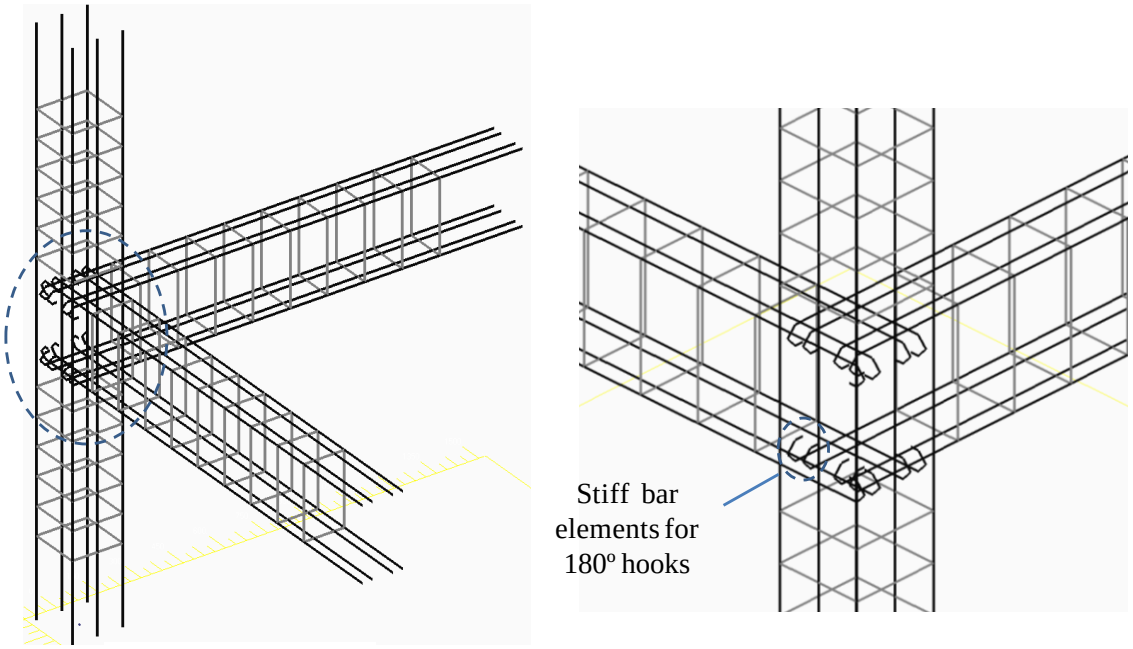

a) Dimetric view b) Joint reinforcement close-up

Figure 10–20 FE model: discretization of reinforcement of 3D specimen

As in the 3D configuration testing, the loading protocol applied in the numerical analysis of 2D specimen was extended to 3D dimensions by adopting a cloverleaf loading. The objective was to simulate the bidirectional loading pattern as close as possible to the experimental loading regime in the

numerical simulation of the 3D corner beam-column joint. Since this was a new task for the FE code MASA, the FE code was modified to run the analysis using the bidirectional loading pattern. A complex and realistic bi-directional lateral loading history, with interaction between the two orthogonal directions was generated to capture the behaviour of the Specimen 3D1 as seen in Figure 10-21. The displacement control cloverleaf load pattern consisted around 4700 loading steps. It is important to note that, each loading step was coupled with a varying axial load to simulate the triaxial loading as performed in the testing (see Chapter 10). The loading protocol for *N* used in the numerical analysis was back-calculated from the experimental data for the column axial load. Since the variation of axial load, *N*, was a function of the lateral load in each direction (i.e, V_{cx} and V_{cy}), from the experiment, it was not possible to determine the loading history of *N* prior to the analysis.

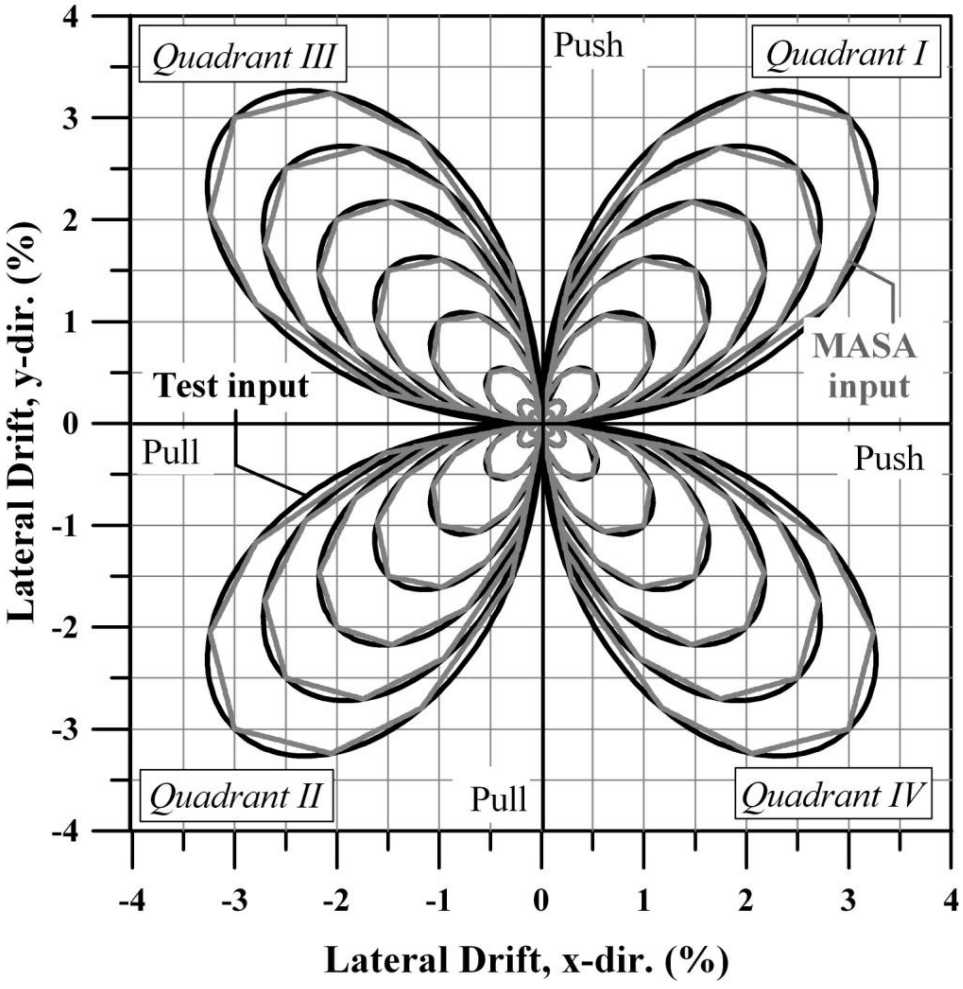

Figure 10–21 Bidirectional loading input for numerical study

10.6.2 Results of Analysis and Comparison with Experimental Data

In this section the results of the numerical analysis are examined in twofold: load-displacement response and failure mode in terms of correct simulation of the cracking pattern. It is important to note that due to stability problems, the FE analysis was halted between 2 and 3% drift levels. For this reason, the results up to 2% drift level are presented and discussed in the following. In Figure 10–22 and Figure 10–23 the comparisons of lateral force-displacement and bidirectional response of the FE model with test results are given, respectively.

The hysteresis loops in x-direction also show a similar trend of strength degradation for both directions of loading. The numerical initial stiffness values for x-direction loading were 3360 kN/m and 3118 kN/m for the pull and push loadings, respectively. These values were 5% lower and 48% higher than the experimental values. As seen in Figure 10–22, FE model matches quite well in the push direction of loading up to 2% drift and in pull direction up to 0.5% drift. However, in the following drift levels of the pull direction (decreasing axial load) the response of the specimen is under estimated.

Similar to the test observations, in the FE model the lateral stiffness began to soften after the first cracking in the joint panel after 0.5% drift. In the subsequent cycles the strength of the corner joint is greatly reduced due to the accumulation of the damage in the joint region (Figure 10–24). Towards the end of the FE analysis a type of three-dimensional “shear hinge” mechanism was formed in the middle of the joint dominating the behaviour the model. The excessive damage in the joint panel after 2% drift of bidirectional loading may be accounted for by the instability observed in the numerical analysis which led to the termination of the analysis between 2 and 3% drift. Recall that, in the test of Specimen 3D1, a wide concrete wedge developed, leading to the expulsion of the outer face of the column after the 3% drift level (see Chapter 10) which also led to the excessive instability and the test was also stopped. As a consequence, the hysteresis loops obtained in FE analysis are characterized by a substantial pinching. In spite of the good simulation of the dominating damage pattern by the FE model, the flexural cracking in the beams and columns that occurred in the test up to a 1% drift level could not be reproduced by the FE analysis. This is also confirmed by examining various cracking patterns in the course of the numerical analysis. For example, in Figure 10–25, the comparisons of the FE snapshots taken of the x-direction beam bottom and y-direction beam top at 1.5% drift are given as an example of the good prediction of cracking patterns.

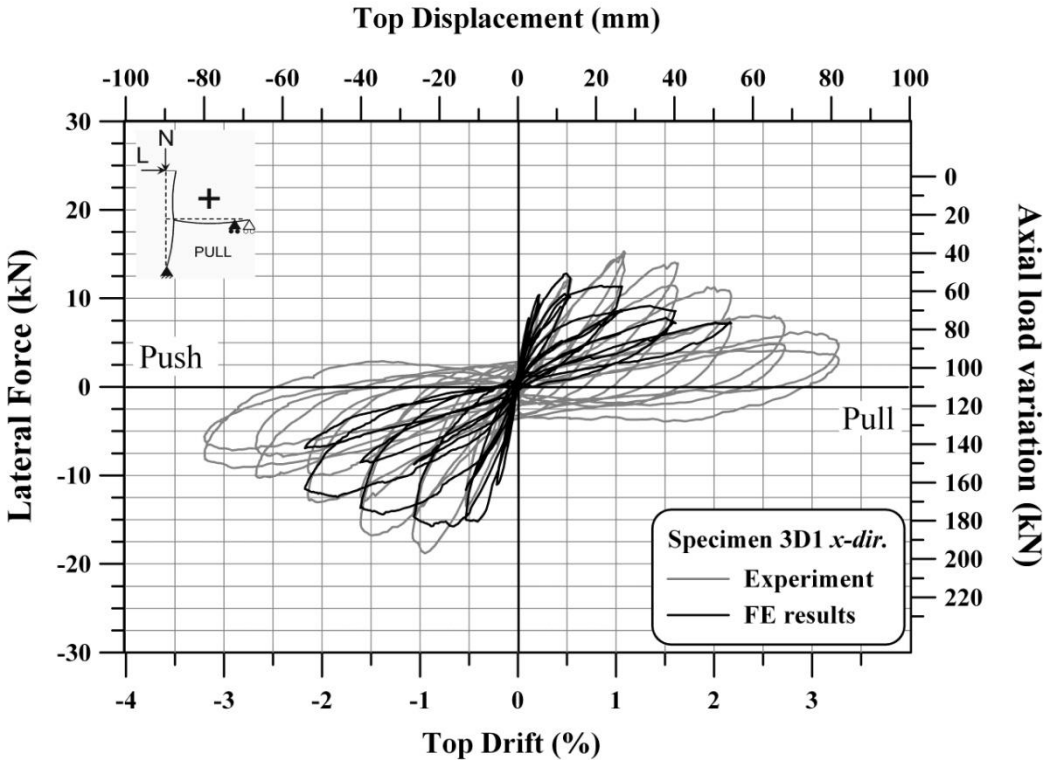

Figure 10–22 Comparison of x-direction load-displacement response – Specimen 3D1

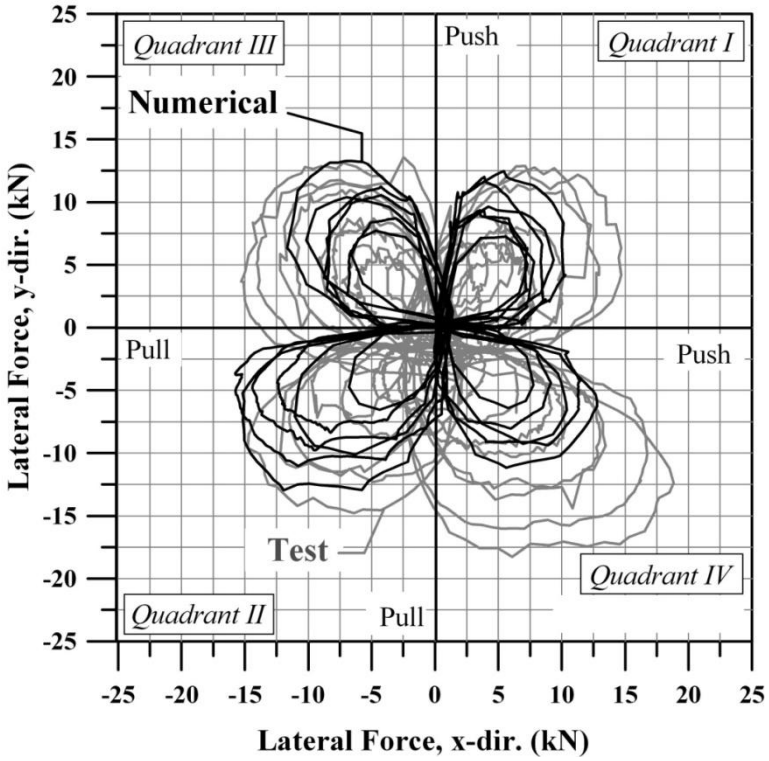

Figure 10–23 Comparison of bidirectional load-displacement response – Specimen 3D1

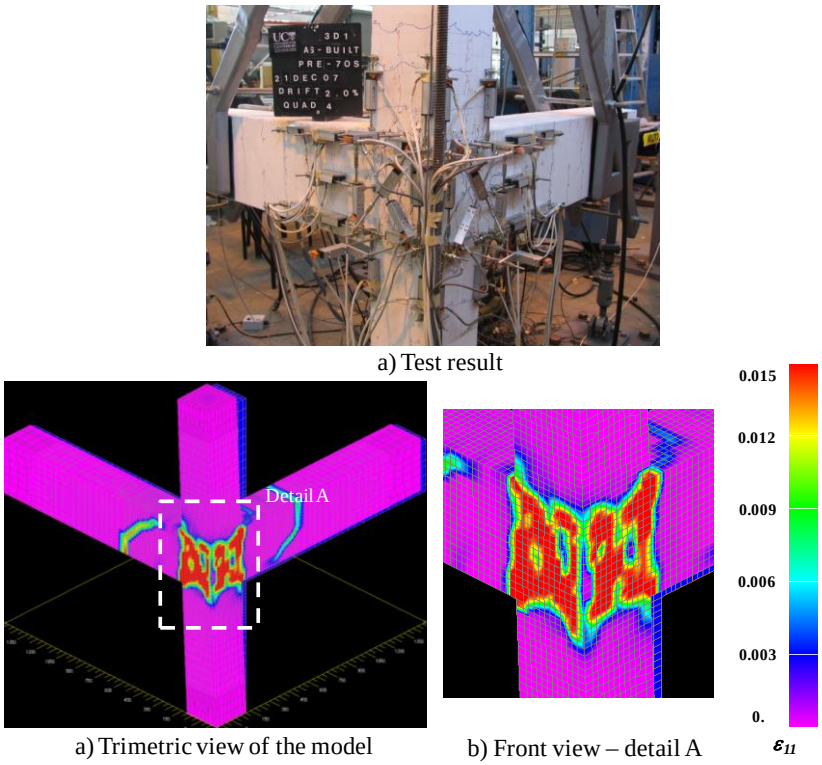

a) Test result

a) Trimetric view of the model b) Front view – detail A

Figure 10–24 Comparison of cracking pattern at 2% drift - Specimen 3D1

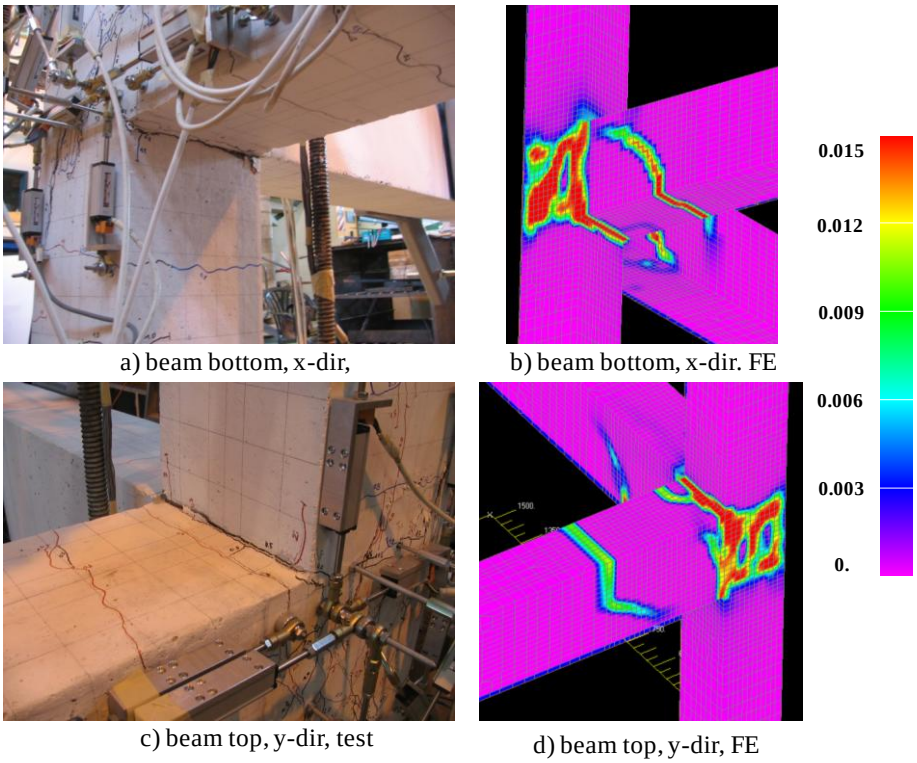

a) beam bottom, x-dir, b) beam bottom, x-dir. FE

c) beam top, y-dir, test d) beam top, y-dir, FE

Figure 10–25 Comparison of various cracking patterns at 1.5% drift, quadrant 4 - Specimen 3D1

In Table 10-2, a summary of the numerical analysis and comparison with test results in terms of recorded values corresponding to 45 degrees of skew angle in the bidirectional loading are also presented for each quadrant of the associated drift level. It is shown that the difference in the predicted values for both directions is quite similar to each other. The load-displacement curves were predicted with a margin of error of around 12% for the 0.5% drift ratio. On average, for the drift levels of 0.1 and 0.2%, the response was overestimated by 20%, and for the remaining drifts (1, 1.5 and 2%) it was underestimated by 25%.

Table 10-2 Comparison between experimental and FE analysis results, Specimen 3D1

Drift Level	Quadrant	Strength				difference with test	
		$V_{cx,exp}$ [a] (kN)	$V_{cy,exp}$ [b] (kN)	$V_{cx,num}$ [c] (kN)	$V_{cy,num}$ [d] (kN)	V_{cx} (%)	V_{cy} (%)
0.1%	I	-6.31	6.39	-6.72	6.45	6.5	0.9
	II	3.21	-2.56	6.52	-3.58	103.4	39.8
	III	2.59	6.16	2.34	7.02	-9.5	14.0
	IV	-7.34	-3.11	-7.25	-2.33	-1.3	-25.0
0.2%	I	-8.07	7.61	-8.18	8.24	1.4	8.3
	II	6.41	-6.00	9.48	-9.40	47.9	56.6
	III	6.10	7.19	9.39	9.37	53.9	30.3
	IV	-9.31	-7.19	-9.30	-8.50	-0.1	18.2
0.5%	I	-11.17	9.75	-8.34	10.87	-25.3	11.5
	II	12.51	-11.33	11.93	-12.97	-4.7	14.5
	III	11.27	10.17	9.78	12.04	-13.2	18.4
	IV	-12.20	-10.22	-10.19	-9.90	-16.5	-3.1
1%	I	-12.10	10.71	-6.91	8.86	-42.9	-17.3
	II	16.55	-16.22	11.11	-10.83	-32.9	-33.3
	III	13.44	10.43	8.16	8.72	-39.2	-16.4
	IV	-13.44	-11.69	-10.37	-7.80	-22.9	-33.3
1.5%	I	-12.10	11.43	-6.05	7.63	-50.0	-33.2
	II	14.89	-14.13	11.00	-8.78	-26.1	-37.9
	III	10.34	9.88	6.88	9.41	-33.5	-4.8
	IV	-10.55	-9.91	-8.41	-4.45	-20.2	-55.1
2%	I	-10.55	9.60	-8.76	5.43	-17.0	-43.4
	II	11.17	-11.80	10.88	-6.99	-2.6	-40.8
	III	8.17	7.71	4.35	8.48	-46.8	10.0
	IV	-7.03	-7.12	-6.69	-5.94	-4.9	-16.5

[a] Experiment story column shear in x-direction; [b] Numerical story column shear in x-direction;
[c] Experiment story column shear in y-direction; [d] Numerical story column shear in y-direction.

10.7 SUMMARY

In this chapter, following an overview and a comprehensive literature review on the FE studies of retrofitted beam-column joints, numerical studies have been carried out to develop three-dimensional finite element (FE) models to predict the response of 2D exterior beam-column joints retrofitted using advanced composite materials and 3D as-built corner beam-column joints. The development of the FE models for the selected test specimens, Specimen 2D2 and 3D1, are described in detail. The theoretical background of the implemented FE element code was also provided. The same test dimensions, boundary conditions and material properties were implemented in the numerical analysis. The 2D FE model was analysed under monotonic and cyclic quasi-static loading with constant axial load whereas the bidirectional loading pattern with varying axial load was applied in the analysis of 3D FE model.

The comparison of the FE models and the experimental results of the beam-column joints showed that the seismic performance of these specimens was simulated with a sufficient accuracy by the FE code MASA. In case of 2D retrofitted joint, the propagation of the damage was predicted in line with the experimental observations. Apart from an underestimation of the load values in the push direction which was within a 10% error margin, the predicted values in terms of load-displacement response and cracking patterns by the FE analysis agreed well with the experimental data. At the local level, the middle joint FRP strain demand was predicted by the FE model with acceptable confidence. The global behaviour in terms of cracking pattern and governing failure mechanism of the 3D corner beam-column joint was also realistically simulated by the FE code MASA. At the 0.5% drift level, the FE results matched well with the test observations. For other drift levels, the bidirectional load-displacement response was predicted by an error margin of 25% on average.

To evaluate the nonlinear behaviour of reinforced concrete structures effectively through FEM numerical simulation, four aspects must be adequately modelled (i) the behaviour of the concrete; (ii) the behaviour of the reinforcement; (iii) the bond-slip relation between the reinforcement and the concrete; and (iv) the interfacial behaviour between the externally bonded FRP reinforcement and the concrete. From this perspective, it can be said that the performance of the FEM numerical models were satisfactory and each proposed FE model can be used as the basis for future studies. It is important to note that, in order to obtain versatile FE models to be employed in the analysing of 2D exterior as well as 3D corner beam-column joints under various FRP retrofit configurations and loading patterns, the models are suggested to be calibrated with and validated against more experimental studies present in the literature.

10.8 REFERENCES

1. Giberson MF. Two nonlinear beams with definitions of ductility. *Journal of Structural Engineering, ASCE*. 1969; **95**(ST2):137-57.
2. Otani S. Inelastic analysis of RC frame structures. *Journal of Structural Engineering, ASCE*. 1974; **100**(ST7):1433-49.
3. Anderson DL, Townsend WH. Models for RC frames with degrading stiffness. *Journal of Structural Engineering, ASCE*. 1977; **103**(ST12):1433-49.
4. Krawinkler H, Mohasseb S. Effects of panel zone deformations on seismin response. *Journal of Construction Steel Research*. 1987; **8**:233-50.
5. El-Metwally SE, Chen WF. Moment-rotation modelling of reinforced concrete beam-column connections. *ACI Structural Journal*. 1988; **85**(4):384-94.
6. Raffaelle GS, Wight JK. R/C eccentric beam-column connections subjected to earthquake-type loading. *Report No. UMCEE 92-18*, University of Michigan, Ann Arbor, Michigan, 1992.
7. Pantazopoulou S, Bonacci J. On earthquake-resistant reinforced concrete frame connections. *Canadian Journal of Civil Engineering*. 1994; **21**:307-28.
8. Alath S, Kunnath SK. Modelling inelastic shear deformation in RC beam-column joints. *Proc of 10th Conf on Eng Mechanics*, Uni. of Colorado at Boulder, Boulder, CO, 822-5, 1995.
9. Ghobarah A, Biddah A. Dynamic analysis of reinforced concrete frames including joint shear deformation. *Engineering Structures*. 1999; **21**.
10. Elmorsi M, Kianoush MR, Tso WK. Modelling bond-slip deformations in reinforced concrete beam-column joints. *Canadian Journal of Civil Engineering*. 2000; **27**:490-505.
11. Fleury F, Reynouard JM, Merabet O. Multicomponent model of reinforced concrete joints for cyclic loading. *Journal of the Engineering Mechanics Division, ASCE*. 2000; **126**(8):804-11.
12. Youssef M, Ghobarah A. Modelling of RC beam-column joints and structural walls. 2001.
13. Lowes LN, Altoontash A. Modelling reinforced-concrete beam-column joints subjected to cyclic loading. *Journal of Structural Engineering, ASCE*. 2003; **129**(12):1686-97.
14. Pampanin S, Magenes G, Carr A. Modelling of shear hinge mechanism in poorly detailed RC beam-column joints. *Proc FIB Symp Concrete Structures in Seismic Regions, Federation International bu Beton*, Athens, Paper no. 171, 2003.
15. Ibarra LF, Krawinkler H. Global collapse of frame structures under seismic excitations. *Report No. TR 152*, John A. Blume Earthquake Engineering Center Dept. of Civil Eng., Stanford Uni., Stanford, CA., 2005.
16. Ngo D, Scordelis AC. Finite element analysis of reinforced concrete beams. *ACI Structural Journal*. 1967; **64**(3):152-63.
17. Esmaeily-Gh A, Xiao Y. Seismic behavior of bridge columns subjected to various loading patterns. *Report No. PEER 2002/15*, University of California, Berkeley, 2002.
18. Rashid YR. Ultimate strength analysis of prestressed concrete pressure vessels. *Nuclear Engineering & Design*. 1968; **267**:1-91.
19. Will GT, Uzumeri SM, Sinha SK. Application of finite element method to analysis of reinforced concrete beam-column joints. . *Proc of Specialty Conf on Finite Element Method in Civil Eng*, Canadian Soc. of Civil Engineers / Eng. Inst. of Canada, 745-66, 1972.
20. Noguchi H. Nonlinear finite element analysis of reinforced concrete beam-column joints. *Proc of IABSE Colloquium*, Delft, the Netherlands, 639-53, 1981.
21. Eligehausen R, Popov EP, Bertero V. Local bond-stress relationships of deformed bars under general excitation. *Report No. UCB/EERC:83-23*, University of California, Berkeley, 1983.
22. Ožbolt J, Yijun L, Kozar I. Microplane model for concrete with relaxed kinematic constraint. *International Journal of Solids and Structures*. 2001; **38**:2638-711.

23. Kashiwazaki T, Noguchi H. Blind analysis of RC beam-column joints subjected to multi-axial combined loadings using 3D nonlinear FEM. *Proceedings of the 14th European Conference on Earthquake Engineering*, Beijing, China, Paper No. 05-3-0131, 1998.
24. Nitereka C, Neale KW. Analysis of reinforced concrete beams strengthened in flexure with composite laminates. *Canadian Journal of Civil Engineering*. 1999; **26**:646-54.
25. Ožbolt J, Mayer U, Vocke H. Smeared fracture FE-analysis of reinforced concrete structures - theory and examples. *Proc of Seminar on Post-Peak Behaviour of RC Structures subjected to Seismic Loads - Recent Advances and Challenges on Analysis and Design*, Japan Concrete Inst. (JCI), Tokyo, Japan, 23-41, 1999.
26. Maekawa K, Pimanmas A, Okamura H. *Nonlinear mechanics of reinforced concrete*. Digital Print 2009 ed. Spon Press, New York City, NY.: New York, 2003.
27. H. N. Three-Dimensional FEM analysis of RC beam-column joints subjected to two-directional loads. *ACI Special Publication, SP-237*. 2006:149-64.
28. N. S. Evaluation of cyclic deterioration and post-peak behaviour of RC beamcolumn joints assemblages by 3-D FE analysis. *ACI Special Publication, SP-237*. 2006:129-48.
29. Mitra N. An analytical study of reinforced concrete beam-column joint behavior under seismic loading *PhD Dissertation*, Uni. of Washington, Seattle, WA., 2007.
30. Baglin PS, Scott RH. Finite element modelling of reinforced concrete beam-column connections. *ACI Structural Journal*. 2000; **97**(6):886-94.
31. Hegger J, Sherif A, Roeser W. Nonlinear finite element analysis of reinforced concrete beam-column joints. *ACI Structural Journal*. 2004; **101**(5):604-14.
32. Eligehausen R, Ozbolt J, Genesio G, Hoehler M, Pampanin S. Three-dimensional modelling of poorly detailed RC frame joints. *NZSEE Conference*, paper no. 23, 2006.
33. Genesio G, Eligehausen R, Pampanin S. Seismic assessment of pre-1970s RC beam column-joints. *Proc of 14th European Conf on Earthquake Eng,*, Ohrid, Macedonia, 639-53, 2010.
34. Eligehausen R, Genesio G, Ožbolt J, Pampanin S. 3D analysis of seismic response of RC beam-column exterior joints before and after retrofit. *2nd ICCRRR*, Vol. I:407-8, 2008.
35. Hörmann M, Menrath H, Ramm E. Numerical investigation of fiber reinforced polymers poststrengthened concrete slabs. *Journal of Engineering Mechanics, ASCE*. 2002; **128**(5):552-61.
36. Li G, Kidane S, Pang S-S, Helms JE, Stubblefield MA. Investigation into FRP repaired RC columns. *Composite Structures*. 2003; **62**(1):83-9.
37. Limam O, Nguyen VT, Foret G. Numerical and experimental analysis of two-way slabs strengthened with CFRP strips. *Engineering Structures*. 2005; **27**(6):841-5.
38. Zhang D-c, Wu Z-s. Finite Element Simulation Analysis on Strengthening of Reinforced Concrete Columns with Different Kinds of Frp Sheets. 2006.
39. Malek AM, Saadatmanesh H, Ehsani MR. Prediction of failure load of RC beams strengthened with FRP plate due to stress concentration at the plate end. *ACI Structural Journal*. 1989; **95**(1):142-52.
40. Arduini M, Nanni A. Parametric study of beams externally bonded FRP reinforcements. *ACI Structural Journal*. 1997; **94**(5):493-501.
41. Ravinovich O, Frostig Y. Closed-form high-order analysis of RC beams strengthened with FRP strips. *Journal of Composites for Construction, ASCE*. 2000; **4**(2):65-74.
42. Ravinovich O, Frostig Y. Nonlinear high-order analysis of cracked RC bemas strengthened with FRP strips. *Journal of Composites for Construction, ASCE*. 2001; **127**(4):381-9.
43. Teng JG, Chen JF, Smith ST, Lam L. *FRP Strengthened RC Structures*. John Wiley & Sons: New York, 2001.
44. Teng JG, Zhang JW, Smith ST. Interfacial stresses in reinforced concrete beams bonded with a soffit plate: A finite element study. *Construction and Building Materials*. 2002; **16**(1):1-14.
45. Chansawat K. Nonlinear finite element analysis of reinforced concrete structures strengthened with FRP laminates. *Ph.D.*, Oregon State University, United States -- Oregon, 2003.

46. Pesic N, Pilakoutas K. Concrete beams with externally bonded flexural FRP-reinforcement: analytical investigation of debonding failure. *Composites Part B: Engineering*. 2003; **34**(4):327-38.
47. Yang ZJ, Chen JF, Proverbs D. Finite element modelling of concrete cover separation failure in FRP plated RC beams. *Construction and Building Materials*. 2003; **17**(1):3-13.
48. Lu X-Z, Tan Z, Ye L-P, Jiang J-J. Finite element analysis of debonding at the interface between FRP sheet and concrete. *Gongcheng Lixue/Engineering Mechanics*. 2004; **21**(6):45-50.
49. Yang QS, Peng XR, Kwan AKH. Finite element analysis of interfacial stresses in FRP-RC hybrid beams. *Mechanics Research Communications*. 2004; **31**(3):331-40.
50. Lu XZ, Ye LP, Teng JG, Jiang JJ. Meso-scale finite element model for FRP sheets/plates bonded to concrete. *Engineering Structures*. 2005; **27**(4):564-75.
51. Pham HB, Al-Mahaidi R. Finite Element Modelling of RC Beams Retrofitted with CFRP Fabrics. SP-230: 7th International Symposium on Fibre-Reinforced (FRP) Polymer Reinforcement for Concrete Structures: American Concrete Institute; 2005.
52. Ali N, Bruno M, Emre Y, Viacheslav K. Finite element modelling of concrete structures reinforced with internal and external fibre-reinforced polymers. *Canadian Journal of Civil Engineering*. 2007; **34**(3):340.
53. Lu XZ, Teng JG, Ye LP, Jiang JJ. Intermediate crack debonding in FRP-strengthened RC beams: FE analysis and strength model. *Journal of Composites for Construction*. 2007; **11**(2):161-74.
54. Tan Y, Xue W-C. FEM analysis on innovative FRP/concrete composite beams. *Harbin Gongye Daxue Xuebao/Journal of Harbin Institute of Technology*. 2007; **39**(SUPPL. 2):296-9.
55. Hedong N, Karbhari VM. FE investigation of material and preload parameters on FRP strengthening performance of RC beams, I: model development. *Journal of Reinforced Plastics and Composites*. 2008; **27**(5):507-22.
56. Karbhari VM, Niu H. FE investigation of material and preload parameters on FRP strengthening performance of RC beams II: Results. *Journal of Reinforced Plastics and Composites*. 2008; **27**(12):1245-67.
57. Barbato M. Efficient finite element modelling of reinforced concrete beams retrofitted with fibre reinforced polymers. *Computers & Structures*. 2009; **87**(3-4):167-76.
58. Parvin A, Granata P. Numerical study of structural joints reinforced with composite fabrics. *Proceedings of the 1998 6th International Conference on Computer Methods in Composite Materials, CADCOMP'98*, Montreal, Can, 411-22, 1998.
59. Mostofinejad D, Talaeitaba SB. Finite Element Modelling of RC Connections Strengthened with FRP Laminates. *Iranian Journal of Science and Technology*. 2006; **30**(B1):21-30.
60. ACI-440.2R-08. Guide for Design and Construction of Externally Bonded FRP Systems for Strengthening Concrete Structures. 2008.
61. Parvin A, Wu S. Ply angle effect on fiber composite wrapped reinforced concrete beam-column connections under combined axial and cyclis loads. *Composite Structures*. 2007; **82**:532-8.
62. Ianniruberto U, Pennucci D. Analisi numerica del comportamento di nodi in c.a. rinforzati con FRP. 2009.
63. Ghobarah A, Said A. Shear strengthening of beam-column joints. *Engineering Structures*. 2002; **24**:881-8.
64. Ožbolt J. *Finite element program for 3D nonlinear analysis of concrete and reinforced concrete structures*. Institut fur Werkstoffe im Bauwesen, Stuttgart, Germany: 2008.
65. Babu RR, Benipala GS, Singh AK. Constitutive modelling of concrete: An overview. *Asian Journal of Civil Engineering (Building and Housing)*. 2005; **6**(4):211-46.
66. Willam KJ, Warnke EP. Constitutive model for triaxial behaviour of concrete. *Seminar on Concrete Structures Subjected to Triaxial Stresses, International Association of Bridge and Structural Engineering Conference*, Bergamo, Italy, 1974.
67. Ortiz MA. A constitutive theory for the inelastic behaviour of concrete. *Mechanics of Materials*. 1985; **4**:67-93.

68. Kotsovos MD, Pavlovic M. *Structural Concrete: Finite Element Analysis for Limit-State Design*. Thomas Telford Publications: London, 1995.
69. Bažant ZP, Cedolin L. Blunt crack propagation in finite element analysis. *Journal of Engineering Mechanics Div ASCE*. 1979; **105**:297-315.
70. Bažant ZP, Oh B-H. Crack band theory for fracture of concrete. *Materials and Structures*. 1983; **93**(16):155-77.
71. de Borst, R. Continuum models for discontinuous media. *Proceedings of the International RILEM/ESIS Conference on "Fracture processes in concrete, rock and ceramics"*, Noordwijk, The Netherlands, 601-18, 1991.
72. Pijaudier-Cabot G, Bažant ZP. Nonlocal damage theory. *Journal of Engineering Mechanics, ASCE*. 1987; **113**(10):1512-33.
73. Ožbolt J, Bažant ZP. Numerical smeared fracture analysis: Nonlocal microcrack interaction approach. *International Journal for Numerical Methods in Engineering*. 1996; **39**(4):635-61.
74. Bažant ZP, Gambarova P. Crack shear in concrete: crack band microplane model. *Journal of Structural Engineering, ASCE*. 1984; **110**(9):2015–35.
75. Bažant Z, Planas J. *Fracture and size effect in concrete and other quasibrittle materials*. CRC Press, Boca Raton and London: 1998.
76. Hillerborg A, Moder M, Petersson PE. Analysis of crack formation and crack growth in concrete by means of fracture mechanics and finite elements. *Cement and Concrete Research*. 1976; **6**:773-82.
77. Chen WF. *Plasticity in Reinforced Concrete*. McGraw-Hill: New York, 1982.
78. Bažant ZP, Caner FC, Carol I, Adley MD, Akers SA. Microplane model M4 for concrete. Part I: Formulation with work-conjugate deviatoric stress, Part II: Algorithm and calibration. *Journal of Engineering Mechanics, ASCE*. 2000; **126**:944-61.
79. Nemecek J, Patzak B, Rypl D, Bittnar Z. Microplane models: Computational aspects and proposed parallel algorithm. *Computers and Structures*. 2002; **80**(4):2099–108.
80. Taylor GI. Plastic strain in metals. *Journal of the Institute of Metals*. 1938; **62**:307-24.
81. Zienkiewicz OC, Pande GN. Time-dependent multi-laminate model of rocks—A numerical study of deformation and failure of rock masses. *Int J Numer Anal Meth Geomech*. 1977; **1**:219-47.
82. Ghazi M, Attard MM, Foster SJ. Modelling triaxial compression using the Microplane formulation for low confinement. *Composite Structures*. 2002; **80**:919-34.
83. Bažant ZP, Prat PC. Microplane model for brittle-plastic material - parts I and II. *Journal of Engineering Mechanics, ASCE*. 1984; **114**(10):1672-702.
84. Carol I, Prat P, Bažant ZP. New explicit microplane model for concrete: Theoretical aspects and numerical implementation. *International Journal of Solids and Structures*. 1992; **29**(9):1173-91.
85. Genesio G, Eligehausen R, Sharma A, Pampanin S. Experimental and numerical study towards a deformation-based seismic assessment of substandard exterior RC beam-column joints. *FraMCoS-7*, Jeju, Korea, 639-53, 2010.
86. Abrams DA. Test of bond between concrete and steel. *University of Illinois Bulletin, No. 71*, University of Illinois,1913.
87. Fabbrocino G, Verderame GM, Manfredi G. Experimental behaviour of anchored smooth rebars in old type reinforced concrete buildings. *Engineering Structures*. 2005; **27**(10):1575-85.

Chapter 11 CONCLUSIONS AND RECOMMENDATIONS FOR FUTURE RESEARCH

11.1 INTRODUCTION

Extensive experimental and analytical investigations have been carried out in the past with the intent to enhance the seismic performance of existing deficient exterior beam-column joints using FRP composite materials. Nevertheless, it is recognized that there is still a significant need to further investigate and address this issue. Most of previous experimental studies available in literature have been performed under unidirectional cyclic loading with a constant axial load regime, ignoring the effects of more realistic and complex bidirectional loading demands. In addition, the lack of consideration of a variation of axial load due to seismic effects has to be considered a major limit and drawback of current assessment procedures for existing beam-column joints.

In light of these considerations, in this thesis, the effects of the variation of axial load and bidirectional loading on the assessment and design of retrofit interventions using FRP composite materials were investigated based on experimental, analytical and FEM numerical studies. The main conclusions and contributions of this study are described in this chapter together with recommendations for future research.

11.2 CONCLUSIONS AND CONTRIBUTIONS

The seismic performance of RC frame structures is strongly dependent on the `hierarchy of strength ` within the lateral-load carrying system. In order to achieve a satisfactory seismic performance, a proper retrofit strategy should aim to convert the (often inadequate) hierarchy of strength in existing beam-column joint subassemblies (consisting of beam, column and joint panel zone elements). The likely brittle modes of failure (e.g., joint shear failure, column hinging and soft storey mechanism,

shear failure in beams and columns) can be converted into more ductile and energy-dissipating modes of failure, i.e., protection of the joint region with development of plastic hinge mechanisms in the beam and a beam-sway global mechanism.

Another important aspect in the process of retrofit design is to take into account the appropriate demand curves for beam-column joints for the variation of axial load due to the effects of lateral loads on a frame system. An incorrect assessment of the sequence of events can otherwise result, possibly leading to an inadequate, and not necessarily conservative, design and retrofit intervention.

The main aim of the retrofit strategy adopted in this study was to provide adequate protection to the joint region in such a way that the 'hierarchy of strength' in the as-built subassembly could be converted into a more favourable ductile failure mechanism. For practical reasons, the intervention was intended to be carried out with minimum invasiveness from the outside of the building, thus allowing for limited disruption of the internal activities and/or relocation of people.

To achieve the target performance of the retrofit strategy, a simplified step-by-step design procedure was proposed. Accordingly, a detailed assessment of each joint component in the as-built and retrofitted configuration was performed and explicitly shown within moment-axial force (*M*-*N*) performance domains. For this purpose, an existing procedure in the literature was refined and elaborated upon based on the experimental evidence gathered and analytical considerations. The demand curves accounting for the variation of the axial load as a function of the lateral load were also plotted in the same domains in order to determine the sequence of events within the beam-column joint subassembly. Hence, the aim was to develop a useful tool for the designer to evaluate the feasibility of different retrofit techniques and modify them by rearranging the sequence of events based on considerations of the local material limit states (e.g., concrete crushing, steel yielding and FRP debonding) first and then on the associated global mechanisms and expected seismic performance levels (e.g., damage control, collapse prevention, life safety etc.). The proposed assessment methodology was successfully verified by the experimental study performed on retrofitted exterior beam-column joints in this study.

In order to assist the retrofit design and assessment procedure, an analytical model was developed to evaluate the joint shear resistance after FRP retrofit. A semi-empirical approach was followed to evaluate the behaviour of the strengthened joint panel zone, based on the experimental and proposed

physical models on joint mechanics. The subsequent analytical procedure was validated by the results of a set of experimental tests available in the literature.

The seismic vulnerability of existing beam-column joints designed according to the non-seismic pre-1970s codes was confirmed by the benchmark tests conducted on the 2D exterior and 3D corner joints. A particular brittle mixed failure mechanism was observed in the test of 2D as-built joint. This mechanism was characterized by the combination of two separate mechanisms in the joint region (1) shear damage in the form of cross diagonal cracking due to the inadequate confinement; (2) slippage of the beam longitudinal plain round bars leading to a concentrated compressive force at the end-hook anchorages.

The tests also revealed a significantly lower performance of corner joints subjected to a bidirectional loading protocol when compared to their counterparts subjected to more typically adopted unidirectional testing loading protocol. A remarkable reduction in the joint shear strength capacity occurred due to the simultaneous loading in the two orthogonal directions, as well as due to the reduction of axial load in a corner joint during the frame sway mechanism. In both 2D and 3D as-built specimens a shear hinge mechanism developed in the joint region, providing the main source of inelastic deformation and behaviour. The as-built 3D corner specimen exhibited a more complex three-dimensional concrete wedge mechanism.

As demonstrated by the experimental studies, a minimum retrofit scheme designed under constant load assumptions can provide satisfactory results in terms of seismic performance (Specimen 2D2). However, the same scheme was proved to be an inadequate retrofit solution in the case of exterior joints subjected to a high fluctuation of the axial load, due to the high shear demand accompanied by reduced joint strength as the axial load decreased in one loading direction (Specimen 2D3). As a consequence, a hybrid failure mechanism occurred consisting of gradual debonding of the GFRP sheet in the vicinity of the joint, bond deterioration and damage to the joint concrete core.

The improved retrofit scheme provided satisfactory confirmation of the efficiency of the proposed retrofit solutions for existing poorly detailed frame buildings. Overall and most importantly, the targeted performance after retrofit, consisting of preventing the joint from excessive damage while relying on the flexural inelastic deformation capability of the beam, was achieved (Specimen 2D4).

Experimental and analytical studies performed within the framework of the 2D exterior as-built and retrofitted joints confirmed the inherent limitations and drawbacks of the majority of research previously undertaken. It is concluded that, because of the varying axial load, some retrofit solutions may be insufficient, although they are found to be adequate under constant axial load assumptions. As a result, a strengthening intervention could lead to the formation of a column hinge before any beam hinging, possibly resulting into the development of a soft storey mechanism, in spite of the (possibly quite expensive and invasive) retrofit intervention already implemented. A correct retrofit strategy would strengthen the column and the joint so that the sequence of events would be beam hinge – column hinge – joint hinge. This would meet capacity design principles and prevent a soft storey mechanism forming. An incorrect and non-conservative assessment of the sequence of events can result in the inadequate design of the retrofit intervention.

The negative effects of a more realistic multiaxial load demand on the performance of the retrofitted corner beam-column joints designed according to unidirectional behaviour assumptions were shown by the experimental study. The test results highlighted the higher demands for the retrofitted 3D corner joint, Specimen 3D2, when compared to its counterpart 2D joint, Specimen 2D4. The Specimen 3D2 suffered more damage due to different failure mechanisms and exhibited a lower load bearing capacity.

Following the experimental findings of the retrofitted corner beam-column joint, the adopted FRP retrofit scheme was upgraded. The main aim was to eliminate the brittle and low-energy dissipating failure modes, such as the initiation and propagation of the FRP debonding/delamination and buckling of FRP sheets installed on the column and beam faces. For this purpose, the use of special FRP anchors along with wider FRP anchorage in the beam and columns was proposed.

Similar to the current design process for modern structures, a performance-based approach can be conveniently adopted for assessing the vulnerability and defining the retrofit strategy for existing buildings. A major challenge to performance-based seismic evaluation and retrofit design of existing beam-column joints is to develop simple methods to evaluate the expected level of damage limit states as a function of more traditional engineering demand parameters. In order to provide some aid to the engineering decisions in the assessment, retrofit design criteria and FRP scheme selection, the correspondence between damage limit states and critical engineer parameters obtained from the experimental studies was provided. For this purpose, alternatives to the traditional approach based on the evaluation of the nominal shear strength of the joint, the (normalized) principal tensile stresses

associated with the joint shear distortion/strain and the interstorey drift levels of the subassembly were selected as a more reliable damage indicator. The influence of axial compression stresses on the joint as well as the deformation demand at a structural system level can be taken into account explicitly in both the as-built and retrofitted configurations.

In addition, a deformation-based retrofit design procedure was presented conceptually to identify and evaluate the FRP retrofit scheme for shear strengthened beam-column joints based on a selected target performance. Following the targeted performance objectives defined for the retrofit intervention based on performance-based considerations, a deformation-based retrofit approach can be conveniently applied in the design process.

Numerical studies have been carried out to develop three-dimensional finite element (FE) models of the test specimens. Detailed information on the development of finite element models for 2D exterior joints retrofitted using advanced composite materials was provided. The 3D as-built corner joint was also modelled and analysed with a particular emphasis given to the application of the bidirectional loading with concurrent varying axial load.

The comparison of the propagation of the damage and load-displacement response of exhibited that the 2D retrofitted exterior joint behaviour under constant axial load regime was predicted with sufficient accuracy. The analysis of the 3D corner beam-column joint showed that the FE model reproduced the hysteretic behaviour and cracking pattern of the test unit with sufficient accuracy. It is concluded that these modellings can be used in conjunction with experimental testing in a research environment, as well as in practice, as a predictive tool for the expected performance of existing structure before and after retrofitting.

11.3 RECOMMENDATIONS FOR FUTURE RESEARCH

Further experimental investigations are suggested to be undertaken focusing mainly on the multi-axial behaviour of the corner beam-column joints which contain: (1) typically inadequate column lap-splices; (2) different anchorage solutions in the joint region based on the pre-1970s construction practice; (3) bidirectional fabrics for retrofit and (4) floor slabs. In this way, the applicability range of the FRP materials can be expanded for their adoption in practice. It is worth noting that, a study regarding the design of beam-column joints with slabs using FRP materials has been recently

presented in literature by the author [1]. This study was conducted during the revision period of this thesis.

In addition, based on the experimental findings, phenomenological models can be developed to predict the subassemblage behaviour. Consequently, more research with time-history analyses are required in order to quantify the effect of differing parameters (i.e., different type of building configurations with various structural element dimensions) on the cyclic response of frames. In addition, in order to obtain versatile FE models for the analyses of 2D exterior and 3D corner beam-column joints under various FRP retrofit configurations and loading patterns, the models should be calibrated and validated using more experimental studies. The proper modelling of the interface behaviour between the externally bonded FRP reinforcement and the concrete is of crucial importance. At a later stage parametrical studies can be carried out to evaluate the influence of several parameters such as concrete strength, amount of beam and column reinforcement, joint aspect ratio, different FRP scheme and materials on the joint shear capacity.

User friendly programmes should be developed for engineering practitioners for their daily practice based on the information gathered from the experimental, analytical and numerical studies. Depending on the case in question, within the framework of the performance-based seismic retrofit, target limit states or performance levels can be more realistically adjusted to account for the difficulties encountered in the assessment phase, as well as for the several issues associated to costs, feasibility and invasiveness of the proposed strengthening/retrofit solution.

11.4 REFERENCES

1. Akguzel U, Quintana-Gallo P, Pampanin S. Seismic strengthening of a seismically deficient RC structure using GFRP sheets. *Pacific Conference on Earthquake Engineering*, Auckland, paper no197, 2011.

APPENDICES

APPENDIX A EXPERIMENTAL STUDIES ON RC COLUMNS UNDER AXIAL LOAD VARIATION

A.1 EXPERIMENTAL STUDIES ON RC COLUMNS TESTED UNDER VARYING AXIAL LOAD

Abrams [1] carried out an experimental study on ten RC column specimens to investigate the influence of variations in axial load on the hysteretic flexural behaviour. The axial column load applied to the specimens was varied directly with either the moment or lateral deflection. The range of the variation in axial force was small and the tests were carried out with relatively low magnitudes of axial load. The results of this study indicated that variations in axial compression can influence strength, stiffness, and deformation capacity of RC columns. The relationship measured between moment and rotation or strain were asymmetrical even though cross sections were symmetrical about the axis of bending and deflections were equal for each direction of sway (Figure A-1). The shape of hysteretic loop was influenced by the range of axial-force variation and the rate of change of axial force with lateral deflection. In terms of structural analysis, on the basis of test results, the researcher concluded that design shear forces should be based on an analysis that considers the effects of axial-force variations of stiffness in case of asymmetrical layout of columns in the structure.

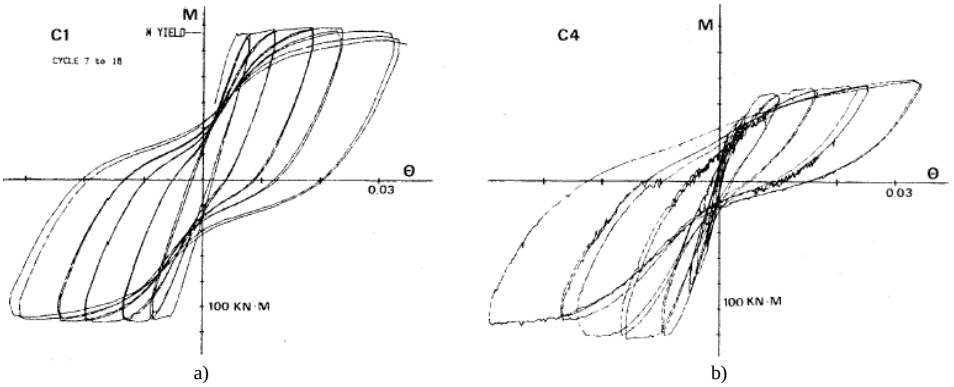

a) b)

Figure A-1 Experimental study by Abrams [1]: moment-rotation relation for a) constant load; b) axial-force moment variation

In most of the studies axial load was proportional to the moment or lateral load. Furthermore, the level of axial force was small compared to the balance load for the section. The literature is very limited with regard to the effects of nonproportionally varying axial load on postelastic behaviour of RC columns. It should be noted that uncoupled variation in axial and lateral loads prevails when structures are under the combined effects of vertical and horizontal earthquake motion.

One of the few studies where uncoupled variations of axial and lateral forces has been considered is an experimental test on a single column by Kreger and Linbeck [2]. The relationship between the lateral load and the axial column load applied was coupled and in direct proportion to each other in two specimens. The results showed that the response of reinforced concrete columns under varying axial and lateral loads is significantly different from those of columns subjected to reversals of lateral loads under constant axial load.

Saadeghvaziri and Foutch [3] also performed an analytical investigation into the effect of nonproportionally fluctuating axial load on the inelastic cyclic behaviour of RC columns. Several types of variation of axial loading history were investigated. It was found that nonproportional variations in axial and lateral load, caused considerable pinching in the lateral load-displacement hysteresis loops which affected the energy dissipation capacity of structural element significantly.

Li *et al.* [4] presented the results of an analytical investigation on the cyclic moment-curvature response of RC columns under the axial load variations. The results showed that variation in axial load level can significantly influence the strength, stiffness and deformation capacity of column sections. As an example, the variation in yield curvature is given in Figure A-2a. For low axial load levels, the yielding of steel closest to the tension face of the section occurs before the extreme concrete section fibre compressive strain reaches 0.002 and the yield curvature increases as the axial load level increases. For high axial load levels, however, the tension steel will not yield before the extreme concrete fibre compressive strain reaches 0.002 and the yield curvature decreases with the increase in axial load level.

The moment-curvature response was also studied under two types of axial loading path. In the first type of axial loading path, type A, the axial load applied was considered to vary in proportion to the bending moment. This case could occur in the external columns of a moment resisting frame subjected to earthquake attack responding mainly in the first mode of vibration. On the other hand, in the second axial loading path, type B, the RC section was assumed to be subjected to uncoupled variations and

cyclic curvature increment. This situation might arise in the columns of a structure under the combined effects of vertical and horizontal earthquake motions.

The computed moment curvature hysteresis curve for type A is given in Figure A-2a. A regular hysteresis behaviour with decreasing stiffness as the curvature magnitude which increased in successive cycles can be seen in this figure. The hysteresis loops exhibit an asymmetric shape. As the magnitude of axial load was very low or even in tension in the negative curvature direction, the section produced much lower flexural strength in the negative curvature direction than in the positive curvature direction. The progressive loss of section stiffness may be attributed to degradation of concrete strength under cyclic loading. The degradation in stiffness and strength for the section with larger magnitude of axial load appeared more pronounced than the section with a lower magnitude of axial load.

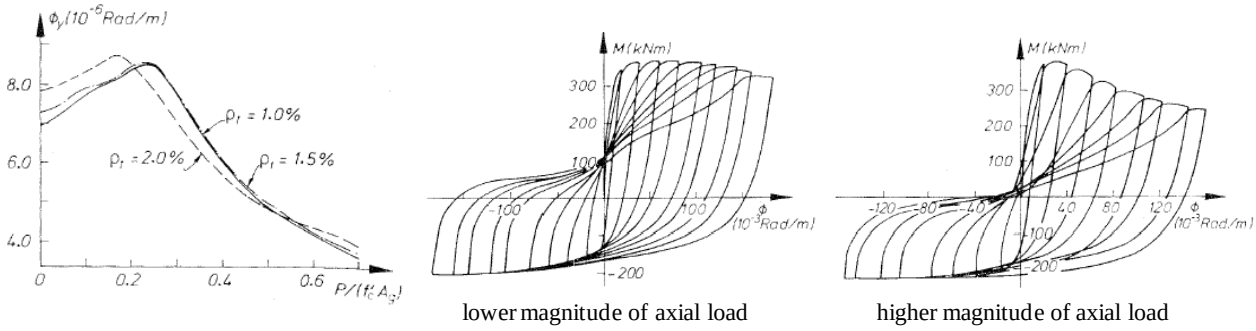

Figure A-2 Analytical study by Li *et al.* [4] a) variation of yield curvature with the axial load level; b) moment-curvature hysteresis loops for type A loading

Figure A-3 shows the analytical moment-curvature hysteresis loops for the column section under an uncoupled axial loading history. The results indicated that variations in axial load level induced the irregular asymmetry of the moment-curvature hysteresis loops. It was found that the flexural strength of the section, which can be developed at the peak of each loading reversal, was not dependant on the axial loading sequence, but mainly on the axial load that was present in that loading sequence. It was also noted that with a small range of variation in axial load, the column section displays quite stable hysteresis behaviour (Figure A-3b) similar to that observed from the constant axial load test. The stiffness of the column section was strongly dependent on the axial load level. As the axial load decreases, the location of the neutral axis shifts towards the extreme compression fibre. Consequently, the effective area of cracked section reduces and the column softens.

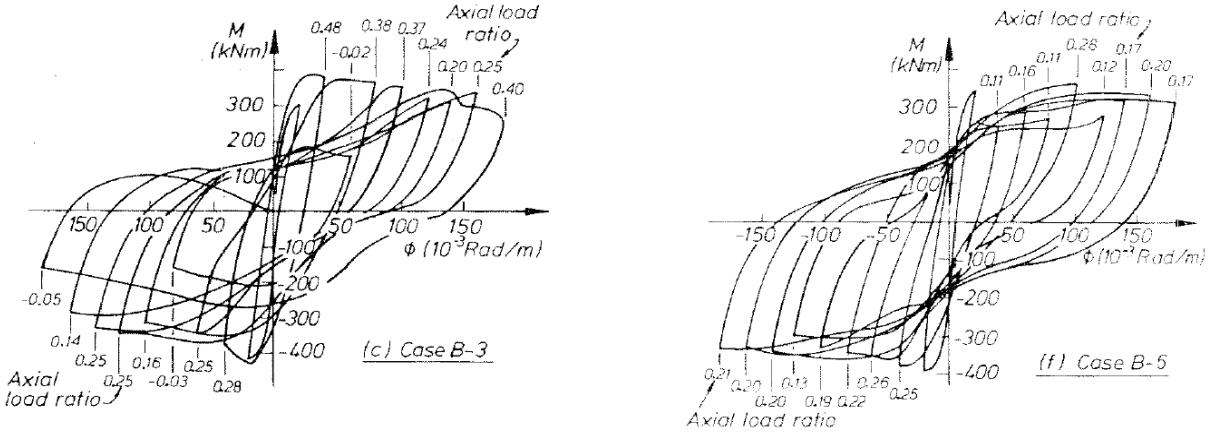

Figure A-3 Analytical study by Li *et al.* [4]: moment-curvature hysteresis loops for type B loading

Li [5] carried out an experimental study to investigate the flexural behaviour of RC columns designed according to the 1982 New Zealand concrete design code [6] under simulated seismic lateral loading and varying axial load. The first series of six RC column units were tested to obtain the variations in flexural hysteretic behaviour with fluctuation in axial load level. In the second phase, three specimens were tested to study the shear strength of an RC column subjected to cyclic lateral loading with emphasis placed on the study of degrading concrete shear resisting mechanisms. Specimen details and testing setup are given in Figure A-4.

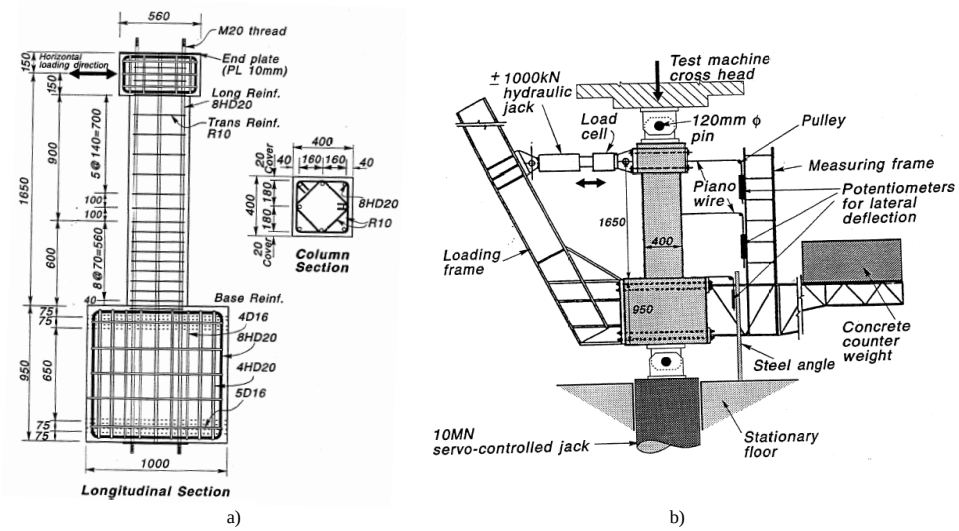

Figure A-4 Experimental study by Li [5]: a) specimen details (units 1,2 and 3); b) test setup

The test results indicated that by alternating compression and tension, the axial load has significant effect on the behaviour of RC columns subjected to cyclic lateral loading (Figure A-5). The load carrying capacity of the columns subjected to varying axial load levels was about 10 to 15% lower

than those subjected to constant axial load at moderate displacement ductility levels. This increased to 15 to 20% at higher displacement ductility levels. The varying axial load pattern resulted in serious pinching of the hysteresis loops. Considerable change in the column was observed. The flexural rigidity of the column subjected to varying axial loading was about 20% less than that subjected to constant compression axial load at nominal displacement level two. It was also revealed that alternating tension and compression axial loading patterns resulted in a more severe degradation in the shear strength and stiffness in the compression axial loading cycles. It was observed that tension axial load encouraged the opening and delayed the closure of diagonal cracks. The formation of major diagonal crack and deterioration of the concrete shear carrying capacity were observed during compression axial loading cycles. The presence of tension axial load degraded the shear strength of the column in the compression axial load direction, but little degradation in shear strength was observed in the tension axial load direction. It was also found that a fairly large portion of total shear was able to be transferred by the concrete mechanism even under a small tension axial force.

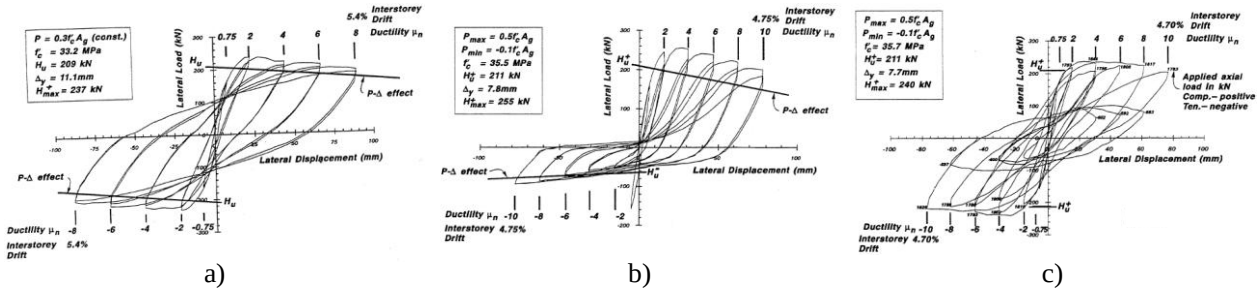

a) b) c)

Figure A-5 Experimental study by Li [5]: test results of specimens under a) constant compression axial load; b) coupled axial load patterns; c) uncoupled axial load patterns

Esmaeily and Xiao [7] studied the effects of variable axial load on the seismic behaviour of bridge piers. For this purpose six large-scale reinforced concrete circular columns were tested under different axial loading patterns such as constant and variable loading, either proportional or nonproportional to the lateral forces. Experimental results showed that under a constant axial force, the peak flexural strength and displacement capacity of the column under reversed lateral forces were similar to those for a monotonic push-over loading case. For the same peak maximum or minimum values of axial force, however, the flexural strength and displacement capacities were different under different variable axial loading paths. A relatively high axial load, either constant or variable, causes concrete to crush excessively, and, thus, more confinement was required to achieve sufficient ductility. The investigators also indicated that the peak moments of a column under variable axial forces may be less than the predicted values using conventional methods for ultimate strength analysis, assuming the same level of axial load. For a variable axial load, the variation pattern of the axial loading had a significant effect on the response of the column, which, thus needs to be taken into consideration for

assessment of the load-carrying capacity and deformability of the column. The loading path also significantly affected the failure pattern of a column, such as the length of plastic hinge. It was also highlighted that the existing plastic hinge models with a fixed length were insufficient to give a realistic estimation for the plastic hinge formation in the case of a variable axial load. The effect of axial load on the flexural strength and ductility of the columns can be clearly seen in Figure A-6.

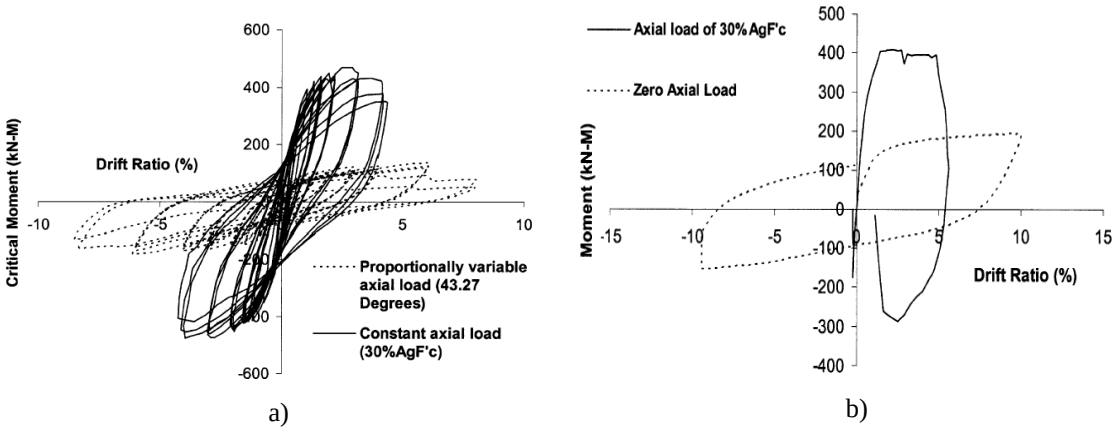

a) b)

Figure A-6 Experimental study by Esmaeily and Xiao [7]

Han and Lee [8] investigated the seismic behaviour of columns which were designed according to the minimum design and reinforcement detailing requirements specified in ACI 318-02. Among the test variables were the type of axial force (constant and varying, and low and high), the existence of lap splices (with or without lap splice) and type of moment resisting concrete frame: Ordinary Moment Resisting Concrete Frames (OMRCF) and Intermediate Moment Resisting Concrete Frames (IMRCF). Quasi-static reversed cyclic loading was applied to the eight 2/3 scale column specimens with either constant or varying axial forces. Interior column specimens were tested with a constant axial load of $0.28A_gf_c$. For exterior column specimens, proportional varying axial load in the range of $0.07\sim0.28A_gf_c$ was applied. The relationship between the lateral load and vertical load was obtained using SAP 2000 commercial software under first mode lateral force profile.

Test results showed that in the interior column specimens of OMRCF, the existence of lap splices in the column specimen prominently influences the drift capacity. In contrast, the existence of lap splices did not affect drift capacities of IMRCF column specimens. In the exterior column specimens, no discernible differences in the hysteretic behaviours were found between OMRCF and IMRCF column specimens. The specimens having lap splices showed inferior hysteretic behaviour to the corresponding specimens without lap splices. Since smaller axial force was applied to the exterior column specimens, the effect of transverse reinforcement spacing seems to be less influential than for interior columns. However, it was noted that this study considered a three-storey building, in which

axial forces in columns are small compared with those in high-rise buildings. When axial forces in columns become large, the spacing of transverse reinforcement may be influential even on the behaviour of exterior columns. The effect of axial load variation on the hysteretic curves for the OMRCF columns with no lap splice are presented in Figure A-7.

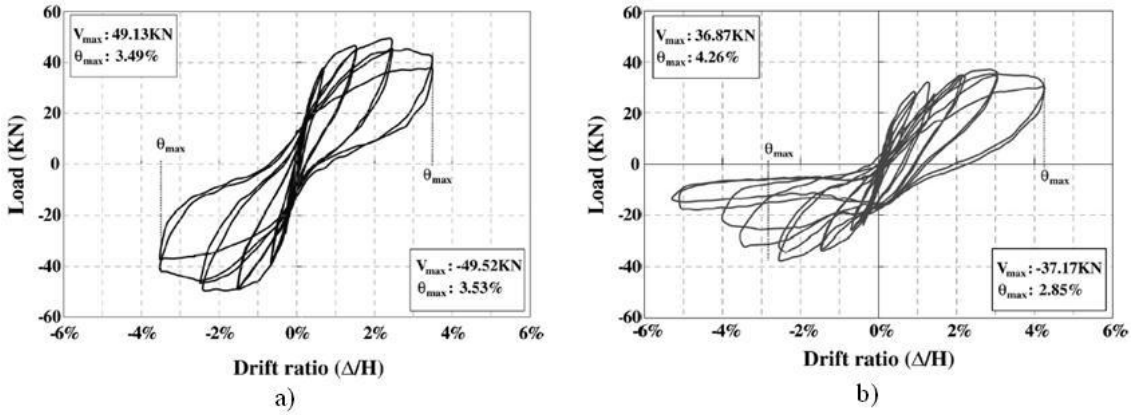

Figure A-7 Experimental study by Han and Lee [8]: hysteresis loops for OMRCF columns with no lap splice: a) interior specimen – constant axial load; b) exterior specimen – varying axial load

A.2 REFERENCES

1. Abrams DP. Influence of axial force variations on flexural behavior of reinforced concrete columns. *ACI Structural Journal*. 1987; **84**(3):246-54.
2. Kreger ME, Linbeck L. Behavior of reinforced concrete columns subjected to lateral and axial load reversals. *Proceedings of the Third US National Conference on Earthquake Engineering*, Charleston, S.C., pp. 1475-86, 1986.
3. Saadeghvaziri MA, Foutch DA. Seismic response of reinforced concrete buildings designed for gravity loads. Part2: Experimental test on a three storey frame. *ASCE Journal of Structural Engineering*. 1990; **116**(7):1835-56.
4. Li X, Park R, Tanaka H. Effects of variations in axial load level on the strength and ductility of reinforced concrete columns. *Pacific Conference on Earthquake Engineering*, New Zealand, pp. 147-58, 1991.
5. Li X. Reinforced concerte columns under seismic lateral force and varying axial load. *Ph.D. Dissertation*, University of Canterbury, Christchurch, 1994.
6. NZS 3101:1982. *Concrete structures standard, NZS 3101*. Standards association of New Zealand, Wellington, 1982.
7. Esmaeily A, Xiao Y. Behavior of reinforced concrete columns under variable axial loads *ACI Structural Journal*. 2004; **101**(1):124-32.
8. Han SW, Jee NY. Seismic behaviors of columns in ordinary and intermediate moment resisting concrete frames. *Engineering Structures*. 2005; **27**:951-62.

APPENDIX B SHEAR STRENGTH OF AS-BUILT AND RETROFITTED BEAMS AND COLUMNS

The expected shear strength of the beam and column members of the tested 2D plane frame specimens, either in as-is or retrofitted configurations, are calculated in this section. Detailed information on the dimensions and material properties are provided in Chapter 5. The shear strength assessment of as-built and retrofitted configurations are performed based on the recommendations in NZSEE assessment guideline [1] and ACI guide for design and construction of externally bonded FRP systems for strengthening concrete structures [2].

B.1 SHEAR STRENGTH OF AS-BUILT BEAM SECTION

The probable shear strength of beams without plastic hinging with rectangular stirrups is given by:

$$V_p = 0.85(v_c b_w d + A_v f_{yt} d / s) = 0.85(k\sqrt{f_c`} b_w d + A_v f_{yt} d / s) \quad \text{(A-1)}$$

where v_c = nominal shear stress carried by the concrete mechanisms
$f_c`$ = expected concrete compressive strength
b_w = width of beam web
d = effective depth of beam
A_v = area of transverse shear reinforcement at spacing s
f_{yt} = expected yield strength of the shear reinforcement
k = 0.2

This equation assumes that the critical diagonal tension crack is inclined at 45° to the longitudinal axis of the beam. The calculated shear strength for a 2D joint beam section is

$$V_p = 0.85((0.2)\sqrt{16.8}(200)(305) + (28.26)(400)(305)/(130)) = 65\,kN$$

B.2 SHEAR STRENGTH OF AS-BUILT COLUMN SECTION

Following the recommendations given in [1] the probable shear strength of columns without plastic hinging can be taken as

$$V_p = 0.723\,(V_c + V_s + V_n) \tag{A-2}$$

where V_c is the shear resisted by the concrete mechanisms and given by:

$$V_c = v_c\,0.8\,A_g = k\sqrt{f_c`}\,0.8\,A_g \tag{A-3}$$

where $k = 0.29\alpha\beta$, v_c = nominal shear stress carried by the concrete mechanisms; A_g = gross area of the column, and $1 \le \alpha = 3\text{-}M/VD \le 1.5$; and $\beta = 0.5 + 20p_l$ is the area of the longitudinal column reinforcement divided by the column cross-sectional area.

In Eq. (A-2) V_s is the shear resisted by the shear reinforcement assuming that the critical diagonal tension crack is inclined at 30° to the longitudinal axis of the column. For rectangular hoops:

$$V_s = \frac{A_v f_{yt} d''}{s} \cot 30^\circ \tag{A-4}$$

where A_v = total effective area of hoops and cross ties in the direction of the shear force at a spacing s

A_{sp} = area of spiral of or circular hoop bar

f_{yt} = expected yield strength of the transverse reinforcement

d'' = depth of the concrete core of the column measured in the direction of the shear force for rectangular hoops

In Eq. (A-2) V_n is the shear resisted as a result of the axial compressive load N^* on the column and is given by:

$$V_n = N^* \tan \alpha \tag{A-5}$$

where for a cantilever column α is the angle between the longitudinal axis of the column and the straight line between the centroid of the column section at the top and the centroid of the concrete compression force of the column section at the base, and for a column in double curvature α is the angle between the longitudinal axis of the column and the straight line between the centroids of the concrete compressive forces of the column section at the top and the bottom of the column.

The shear strength of a test specimen column based on the geometry, material and loading properties are given as follows:

The shear resisted by the concrete mechanisms:

$$V_c = v_c 0.8 A_g = k\sqrt{f_c`}0.8 A_g = [(0.29)(1)((0.5 + 20 * 0.0089)]\sqrt{16.8}(0.8)(230)(230) = 34\,kN$$

The shear resisted by the shear reinforcement:

$$V_s = \frac{A_v f_{yt} d''}{s}\cot 30^\circ = \frac{(56.52)(400)(196)}{(100)}\cot 30^\circ = 76.75\,kN$$

The shear resisted as a result of the axial compressive load N_v on the column:
For the constant axial load level of 110 kN $V_n = N_v * \tan\alpha = (115)(0.046) = 5.06\,kN$

The total shear strength of column is calculated as:
$V_p = 0.723\,(V_c + V_s + V_n) = 0.723\,(34 + 76.75 + 5.06) = 83.73\,kN$

B.3 SHEAR STRENGTH OF RETROFITTED SECTIONS

The FRP system is provided in the beam and column locations of expected plastic hinges or stress reversals (1) for shear strengthening; (2) for enhancing the post-yield flexural behaviour of the members and (3) to prevent debonding of the FRP flexural strengthening system. This has been achieved by wrapping discrete narrow FRP sheets completely around the beam and column sections (*four-sided wrap*), as shown schematically in Figure B-1. It is important to note that non-fully wrapped FRP systems are susceptible to detachment failures at their ends.

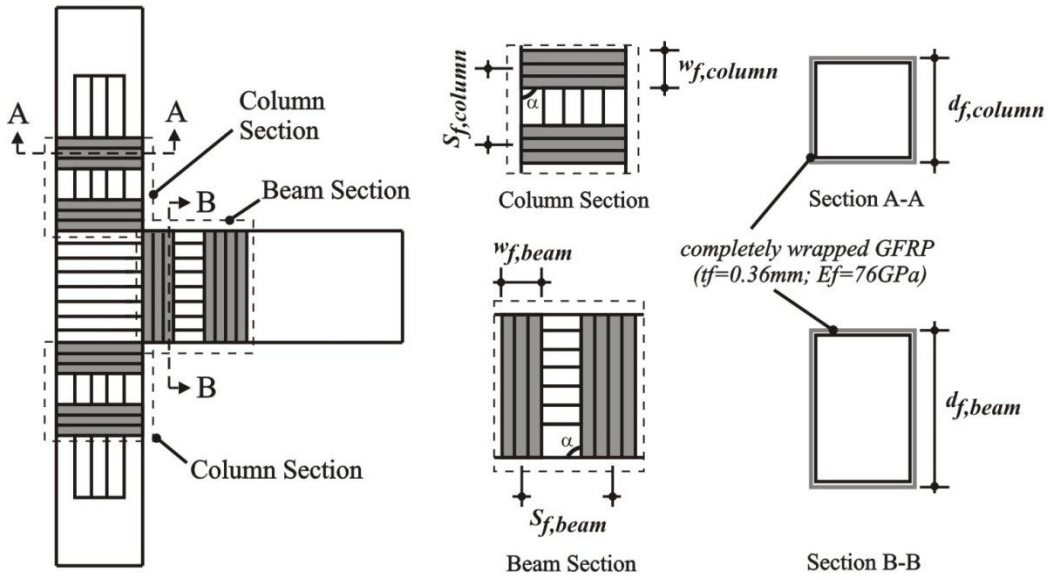

Figure B-1 Illustration of dimensional variables used in shear-strengthening calculations

The nominal shear strength of an FRP-strengthened concrete member can be determined by adding the contribution of the FRP strenghening system to the existing shear capacity from the reinforcing steel and the concrete. As recommended in [2], an additional reduction factor ψ_f is applied to the contribution of the FRP system which is taken as 0.95 for a completely wrapped section (called *contact critical*) and as 0.85 for two- or three-sided wrapped sections (called *bond critical*). The existing shear capacity is given as

$$V_n = V_c + V_s + \psi_f V_f \tag{A-6}$$

where V_c is the existing shear capacity of the concrete (e.g., due to aggregate interlock, dowel action of the main bars, and resistance of the uncracked compression zone above the shear crack), V_s the shear capacity of the existing steel shear reinforcement, and V_f the shear capacity of the FRP strenthening system. Since V_c and V_s have already been calculated in the previous section, the FRP contribution to shear strength, V_f, for intermittent wrapping type strengthening is herein presented.

For intermittent strips having a width (measured perpendicular to the major fibre orientation of the strengthening system) of w_f and spaced at a spacing s_f (measured parallel to the member axis) the equation given below can be used for the shear contribution of the FRP shear reinforcement

$$V_f = \frac{A_{fv} f_{fe} (\sin \alpha + \cos \alpha) df}{s_f} \tag{A-7}$$

where A_{fv} is the area of the FRP shear reinforcement and computed as

$$A_{fv} = 2nt_f w_f \tag{A-8}$$

where n is number of plies applied on one surface and t_f is the FRP thickness per ply.

Substituting Eq. (A-8) into Eq. (A-7) gives

$$V_f = \frac{2nt_f w_f f_{fe} d_f (\sin\alpha + \cos\alpha)}{s_f} \tag{A-9}$$

with the geometric condition that

$$s_f = \frac{w_f}{\sin\alpha} \tag{A-10}$$

In case of α=90°, the shear contribution of the FRP strengthening system can be computed as follows

$$V_f = \frac{A_{fv} f_{fe} d_f}{s_f} \tag{A-11}$$

where f_{fe} is the tensile stress in the FRP shear reinforcement system at nominal strength and given as

$$f_{fe} = \varepsilon_{fe} E_f \tag{A-12}$$

where ε_{fe} is the effective strain in the FRP shear strengthening system. It is the maximum strain that can be attained in the FRP system at the nominal strength and is governed by the failure mode of the FRP system and of the strengthened reinforced concrete member. ACI guide for FRP systems [2] recommended that all possible failure modes should be considered and the design professional should use an effective strain representative of the critical failure mode. In case of completely wrapped members, it is suggested that the maximum strain used for design should be limited to 0.4%

$$\varepsilon_{fe} = 0.004 \le 0.75\varepsilon_{fu} \tag{A-13}$$

The strain limitation is based on testing and experience [3]. The calculated values for the beam and column sections are given as follows:

The shear capacity of the FRP retrofitted beam section:

$$V_{f,beam} = \frac{A_{fv} f_{fe} d_{f,beam}}{s_f} = \frac{2nt_f w_{f,beam} f_{fe} d_{f,beam}}{s_{f,beam}} = \frac{2(1)(0.36)(50)[(0.004)(76000)](330)}{(125)} = 36\,kN$$

The shear capacity of the FRP retrofitted column section:

$$V_{f,column} = \frac{A_{fv} f_{fe} d_{f,column}}{s_f} = \frac{2nt_f w_{f,column} f_{fe} d_{f,column}}{s_{f,column}} = \frac{2(1)(0.36)(50)[(0.004)(76000)](230)}{(100)} = 25\,kN$$

Total shear capacity of the sections:

$$V_{n,beam} = V_c + V_s + \psi_f V_f = (65) + (0.95)(36) = 99.2\,kN$$

$$V_{n,column} = V_c + V_s + \psi_f V_f = (83.73) + (0.95)(25) = 107.4\,kN$$

The results of shear strength assessment in as-built and retrofitted configurations indicated that the total shear capacity of this sections are far more exceeding the demand observed in the experiments. For instance, in Specimen 2D4, the maximum observed shear demand in the column and beam elements were around 24 kN and 31 kN, respectively. Therefore no shear damage was expected and also observed before or during the tests.

B.4 REFERENCES

1. NZSEE. Recommendations of a NZSEE Study Group on Earthquake Buildings. Engineers New Zealand, Department of Building and Housing, 2006, (study group draft).
2. ACI-440.2R-08. Guide for Design and Construction of Externally Bonded FRP Systems for Strengthening Concrete Structures. 2008.
3. Priestley MJN, Seible F, Calvi GM. *Seismic Design and Retrofit of Bridges*. Wiley: New York, 1996.

APPENDIX C DERIVATION OF THE QUADRATIC POLYNOMIAL EQUATION

Mohr`s circle is employed along with the kinematics of the retrofitted 2D joint in the derivation of the closed form of quadratic polynomial equation of $tan^2\theta$. For this purpose, the equilibrium and compatibility conditions of the average compressive transverse and longitudinal stresses, σ_t and σ_l, in the retrofitted joint panel concrete are used as discussed in Chapter 4.

Using Mohr`s circle given in Figure 4-11 of Chapter 4, the definition of the average direction of the principal stresses, $tan\theta$ can be evaluated as

$$\tan^2\theta = \frac{\sigma_1 - \sigma_t}{\sigma_1 - \sigma_l} = \frac{\sigma_2 - \sigma_l}{\sigma_2 - \sigma_t} \tag{C-1}$$

hence $tan^2\theta$ is written as

$$\tan^2\theta = \left(\frac{\sigma_2}{E_c} - \varepsilon_l\right)\left(\frac{\sigma_2}{E_c} - \varepsilon_t\right)^{-1}$$

$$= \frac{\sigma_2 - \varepsilon_l E_c}{\sigma_2 - \varepsilon_t E_c} \tag{C-2}$$

The minimum principal stress in the concrete, σ_2,is a function of nominal shear stress contribution due to FRP, v_f, and $tan^2\theta$ as follows

$$\sigma_2 = -\nu_f\left(\tan\theta + \frac{1}{\tan\theta}\right) = \frac{-\nu_f\left(\tan^2\theta + 1\right)}{\tan\theta} \tag{C-3}$$

The subsitution of Eq. (C-3) in Eq. (C-2) gives

$$\tan^2\theta = \frac{\dfrac{-\nu_f(\tan^2\theta+1)}{\tan\theta} - \varepsilon_l E_c}{\dfrac{-\nu_f(\tan^2\theta+1)}{\tan\theta} - \varepsilon_t E_c} \tag{C-4}$$

Rearranging the above equation gives

$$\left(-\nu_f\right)\tan^3\theta + \left(-\varepsilon_t E_c\right)\tan^2\theta + \frac{\nu_f}{\tan\theta} + \varepsilon_l E_c = 0 \tag{C-5}$$

multiplication of the both sides of the Eq. (C-5) with $tan\theta$ yields

$$\left(-\nu_f\right)\tan^4\theta + \left(-\varepsilon_t E_c\right)\tan^3\theta + \varepsilon_l E_c \tan\theta + \nu_f = 0 \tag{C-6}$$

Definition of the average normal strains along normal directions *l* and *t* can be obtained as a function of v_f and $tan\theta$ by rearranging previously established relationships which are given below (see section 4.7 of Chapter 4)

$$\sigma_t = -\rho_{ft} E_f \varepsilon_t \tag{C-7}$$

$$\sigma_t = -\nu_f \cdot \tan\theta \tag{C-8}$$

$$\sigma_l = -\rho_{fl} E_f \varepsilon_l - \frac{N_v}{h_c b_c} \tag{C-9}$$

$$\sigma_l = -\frac{\nu_f}{\tan\theta} \tag{C-10}$$

Hence, the average normal strains ε_t and ε_l are

$$\varepsilon_t = \frac{\nu_f \tan\theta}{\rho_{ft} E_f} \tag{C-11}$$

$$\varepsilon_l = \frac{\frac{v_f}{\tan\theta} - \frac{N_v}{h_c b_c}}{\rho_{fl} E_f} \tag{C-12}$$

Substituting Eq. (C-11) and (C-12) into the Eq. (C-6) yields

$$\left(-v_f\right)\tan^4\theta + \left(-\frac{v_f \tan\theta}{\rho_{ft} E_f} E_c\right)\tan^3\theta + \left(\frac{\frac{v_f}{\tan\theta} - \frac{N_v}{h_c b_c}}{\rho_{fl} E_f}\right) E_c \tan\theta + v_f = 0 \tag{C-13}$$

which can be written in a more condensed form after rearranging as follows

$$\left(-v_f\right)\left(1 + \frac{E_c}{\rho_{ft} E_f}\right)\tan^4\theta + \left(-\frac{N_v}{h_c b_c}\frac{E_c}{\rho_{fl} E_f}\right)\tan\theta + \left(1 + \frac{E_c}{\rho_{fl} E_f}\right)v_f = 0 \tag{C-14}$$

In the next step, the nominal shear stress contribution due to the FRP given in Eq. (C-15) is inserted into the Eq. (C-14) to obtain Eq. (C-16)

$$v_f = \frac{\rho_{ft} E_f \varepsilon_t}{\tan\theta} \tag{C-15}$$

hence,

$$\left(-\frac{\rho_{ft} E_f \varepsilon_t}{\tan\theta}\right)\left(1 + \frac{E_c}{\rho_{ft} E_f}\right)\tan^4\theta + \left(-\frac{N_v}{h_c b_c}\frac{E_c}{\rho_{fl} E_f}\right)\tan\theta + \left(1 + \frac{E_c}{\rho_{fl} E_f}\right)\frac{\rho_{ft} E_f \varepsilon_t}{\tan\theta} = 0 \tag{C-16}$$

Rearranging Eq. (C-16) gives

$$\left(-\rho_{ft} E_f \varepsilon_t - E_c \varepsilon_t\right)\tan^3\theta + \left(-\frac{N_v}{h_c b_c}\frac{E_c}{\rho_{fl} E_f}\right)\tan\theta + \left(\rho_{ft} E_f \varepsilon_t + \frac{E_c \rho_{ft} \varepsilon_t}{\rho_{fl}}\right)\frac{1}{\tan\theta} = 0 \tag{C-17}$$

Lastly, multiplication of the both sides of the Eq. (C-17) with $\left(-\frac{\tan\theta}{\rho_{ft} E_f \varepsilon_t E_c} \right)$ yields the quadratic polynomial equation of $\tan\theta$

$$\left(\frac{1}{E_c} + \frac{1}{\rho_{ft} E_f} \right) \tan^4\theta + \left(\frac{N_v}{h_c b_c \rho_{fl} \rho_{ft} E_f^2 \varepsilon_t} \right) \tan^2\theta - \left(\frac{1}{E_c} + \frac{1}{\rho_{fl} E_f} \right) = 0 \qquad \text{(C-18)}$$

APPENDIX D MATLAB CODE FOR FRP RETROFITTED 2D RC EXTERIOR JOINTS

This Appendix includes the template code written in Matlab® which is a high-performance language for technical computing. The code, which follows the basic principals and theoretical background provided in Chapter 4, is used to determine the shear strength assessment of 2D beam-column joints retrofitted with FRP materials.

```
%%%%  Shear Strength Assessment of 2D Beam-Column Joint Strengthened with FRP %%%%
%%%%  by Umut Akguzel
%%%%  Last modified: September 29, 2010

clear all; close all; clc;
%_____________________________________________________
%%% General Info
%         Specimen ID: 2D2
%         Section Dimensions:
%         Beam=230x330 mm, Column=230x230 mm
%         FRP Application Properties:
%         Scheme Type = R11 : 1 layer of GFRP sheet in the beam and 1 layer of GFRP in the column
%_____________________________________________________
%%% Material Properties
fc = 18;                    % Compressive Strength of Concrete [N/mm2]
Ec = 5700*sqrt(fc);         % Elastic Modulus of Concrete   [N/mm2]
f_ctm = 0.5*sqrt(fc);       % Tensile Strength of Concrete [N/mm2]
E_fibre = 76000;            % Tensile E-modulus of fibres   [N/mm2]
tf = 0.36;                  % FRP thickness [m] (tf=0.36 mm for SikaWrap-100G)
CE_factor=0.65;             % Environmental reduction factor for exterior exposure from ACI440.2R-08
eps_fu = 0.018;             % Ultimate strain of GFRP
%_____________________________________________________
%%% Details of Specimen (dimensions in mm)
beam_height = 330; hb = beam_height/1000;
beam_width  = 230; bw = beam_width/1000;
column_depth = 230; hc =  column_depth/1000; % Overall depth of column in the direction of the horizontal shear to be considered
column_width = 230;
```

```
lc = 2000; lc =lc / 1000;          % Height of column
lb = 1524; lb = lb / 1000;         % Column center to contraflexure point
d = 305; d = d / 1000;             % Effective depth
lbb = lb-hc/2;                     % Half clear span length
Ae = hc * bw;                      % Effective joint area
omega = (2*lbb*lc - 1.8*d*lb) / (0.9 * d * lb * Ae * (lc - hb)); % Geometric coefficient for Mcol calculation in the joint
%_____________________________________________________________
%%% FRP Application Properties
FRP_depth_beam = 300;              % Depth of CFRP sheet on the beam surface
FRP_depth_column = 200;            % Depth of CFRP sheet on the column surface
nFRP_beam = 1;                     % Number of sheet on beam
nFRP_column = 1;                   % Number of sheet on column
nsidesFRP_beam = 2;                % Number of beam sides covered by the FRP: 1 for one-sided patching when a transverse % beam exists (ie like 3D specimens) or 2 for two-sided patching, when both sides of the joint are accessible (ie like in
% 2D specimens)
nsidesFRP_column = 2;              % Number of column sides covered by the FRP (1 or 2)
%_____________________________________________________________
%%% FRP Reinforcement Ratio in Each Direction:
% rho_ft: in transverse (horizontal direction)
rho_ft = (nFRP_beam*nsidesFRP_beam*tf*FRP_depth_beam)/(beam_height*beam_width);
% rho_fl: in longitudinal (vertical direction)
rho_fl = (nFRP_column*nsidesFRP_column*tf*FRP_depth_column)/(column_depth*column_width);
%_____________________________________________________________
%%% Debonding Characteristics of FRP (according to model of Holzenkampfer (1997))
% Maximum bond length: lb_max [mm]
c1 = 0.64; c2 = 2; % (Neubauer and Rostasy (1997))
lb_max_t = sqrt((E_fibre*tf*nFRP_beam)/(c2*f_ctm));
lb_max_l = sqrt((E_fibre*tf*nFRP_column)/(c2*f_ctm));
% If bond length (lb, which is from midwidth or midheight of the joint) is chosen greater than lb_max
% then stresses in FRP when debonding (MPa) occurs in both directions are calculated as
f_ft_deb = c1*sqrt(E_fibre*f_ctm/(tf*nFRP_beam));
%_____________________________________________________________
%%% Iteration Control
eps_t_deb = f_ft_deb / E_fibre;                 % strain level in CFRP when debonding occurs - transverse direction % (beam) A and C coefficients for quadratic equation
A = (1/Ec+1/(rho_ft*E_fibre));
C = (1/Ec+1/(rho_fl*E_fibre));
C = -1*C;
% Selection of the iteration boundary for eps_t..
eps_t = linspace(0.00005,eps_t_deb,300);        % Strain value in the transverse direction - 1st step of iteration – (ie, start from small value such as eps_t=0.005% to eps_t_deb)
Nv = 0:50000:300000;               % Axial load level [Newton]
% n=length(Nv);                    % Iteration counter for axial load increments (ie, for i=1:n)
% m=length(eps_t);                 % Iteration counter for epsilon_t increments (ie, for j=1:m)
for i=1:length(Nv)
        fv(i) = (Nv(i)/(column_depth*column_width));

  for  j=1:length(eps_t)
```

```
    B(j,i)=(Nv(i)/(column_depth*column_width*rho_ft*rho_fl*E_fibre^2*eps_t(j)));    % Solution of quadratic polynomial %
of tan2teta (compression is positive)
    D(j,i) =((-B(j,i)+sqrt(B(j,i)^2-4*A*C))/(2*A));
    tan_theta(j,i) = sqrt(D(j,i));
    vf(j,i) = (rho_ft*E_fibre*eps_t(j)) / tan_theta(j,i);          %Average joint shear stress with fibre [MPa]
    sigma_t(j,i) = -1*vf(j,i) * tan_theta(j,i);                    %Average stress in the concrete along direction
% transverse direction [MPa]
    sigma_l(j,i) = -1*vf(j,i) / tan_theta(j,i);                    % Average stress in the concrete along direction
% longitudinal direction [MPa]
    sigma_2(j,i) = sigma_t(j,i) + sigma_l(j,i);                    % Minimum principle stress in concrete [MPa]
    f_ft(j,i) = - sigma_t(j,i)/rho_ft;                             % Average normal stress in FRP along
% transverse direction (at midwidth of the joint) [MPa]
    f_fl(j,i) = - (sigma_l(j,i)+Nv(i)/(column_depth*column_width))/rho_fl;  % Average normal stress in FRP along
% lateral direction (at midheight of the joint) [MPa]
    eps_l(j,i) = f_fl(j,i) / E_fibre;
    eps_1(j,i) = (eps_t(j)-tan_theta(j,i)^2*eps_l(j,i)) / (1- tan_theta(j,i)^2);  % Maximum principle strain

    % CHECK # 1: FRP debonding check
    if f_ft(j,i) > f_ft_deb
      vf(j,i) = 0;
    end

    pt_f(j,i) = -1*fv(i)/2 + sqrt((fv(i)/2)^2 + vf(j,i)^2);        % Principal tension stress due to FRP contribution
    pt_f_(j,i) = pt_f(j,i) / sqrt(fc);                             % For grapher plotting purposes...
    gamma(j,i) = 2*(eps_1(j,i) - eps_t(j)) / (tan_theta(j,i));     % Shear distortion in joint panel

    % CHECK # 2: Diagonal compression failure check
    pt_c_x = [0;0.000098275;0.02];       % emprical gamma values (plain concrete (pre70s) shear deformation versus
 % pt_gamma value according to as-built 2D test results corresponding to y coordinate of envelope function)
    pt_c_y = [0;0.19;0];                 % emprical principal tension values (principal tension stress
% corresponding to x coordinate of envelope function)
    pt_c_(j,i) = (interp1(pt_c_x, pt_c_y, gamma(j,i))); % this value found by interpolation equals to pt/sqrt(fc`)
    % ! Note: underscore `_` means that actual value is normalized by sqrt(fc) !
    pt_c(j,i) = pt_c_(j,i) * sqrt(fc);  % Attention to ... sqrt(fc`) ...

   % Check 1: (vjh<0.2fc`, Hakuto et al. (2000))
   vjh_concrete(j,i) = sqrt(pt_c(j,i)^2 + pt_c(j,i)*fv(i));  % ! Note: Compression is negative!! for positive pt !
   % if   vjh_concrete( j,i) > 0.2*fc break, end

   % Check 2: according to Priestley: if sigma2> 0.3fc --> Stop!
    if   sigma_2(j,i) > 0.3*fc; break, end
    pt_sum = pt_c + pt_f;
    pt_sum_ =  pt_sum/sqrt(fc);

  end
end
%_____________________________________________________________
% Mcol_f=max(vf)*1000/alfa; % Moment capacity contribution due to fibre...
```

```
%_____________________________________________________

%%% Output Plotting
for z=1:length(Nv);
  subplot(2,2,1);
  plot(gamma(:,z),vf(:,z),'-ro'),xlabel('\fontsize{24} \it{\gamma}'),ylabel(' \fontsize{16} v_f');axis on;hold on;grid on; title(' \fontsize{12} \bf{Strengthened Joint Shear vs Joint Shear Deformation [R11]}');
  subplot(2,2,2);
  plot(gamma(:,z),pt_c_(:,z),'ro'),('-ro'),xlabel(' \fontsize{18} \fontsize{24} \it{\gamma}'),ylabel(' \fontsize{16} pt_{c}/sqrt(f_c`)');axis on;hold on;grid on; title(' \fontsize{12} \bf{Normalized Principal Joint Stress (Concrete) vs Joint Shear Deformation [R11]} ');
  subplot(2,2,3);
  plot(gamma(:,z),pt_f_(:,z),'ro'),('-ro'),xlabel(' \fontsize{18} \fontsize{24} \it{\gamma}'),ylabel(' \fontsize{16} pt_{f}/sqrt(f_c`)');axis on;hold on;grid on; title(' \fontsize{12} \bf{Normalized Principal Joint Stress (FRP) vs Joint Shear Deformation [R11]} ');
  subplot(2,2,4);
  plot(gamma(:,z),pt_sum_(:,z),'ro'),('-ro'),xlabel(' \fontsize{18} \fontsize{24} \it{\gamma}'),ylabel(' \fontsize{16} pt_{sum}/sqrt(f_c`)');axis on;hold on;grid on; title(' \fontsize{12} \bf{Normalized Principal Joint Stress (FRP+Concrete) vs Joint Shear Deformation [R11]} ');
% subplot(2,2,3)
%   plot(Nv/1000,max(vf),'-ro'),xlabel(' \fontsize{22} N_v'),ylabel(' \fontsize{22} v_{f,max}');axis on; grid on; title('
 % \fontsize{16} \bf{Maximum Strengthened Joint Shear vs Axial Load [R11]} ');
%   subplot(2,2,4)
%   plot(Nv/1000,max(vf)*1000/alfa,'-ro'),xlabel(' \fontsize{22} N_v'),ylabel(' \fontsize{22} M_{col}');axis on; grid on;
% title(' \fontsize{18} \bf{Equivalent Column Moment vs Axial Load [R11]} ');
end
%_____________________________________________________
```

Typical output plots are given in Figure D-1.

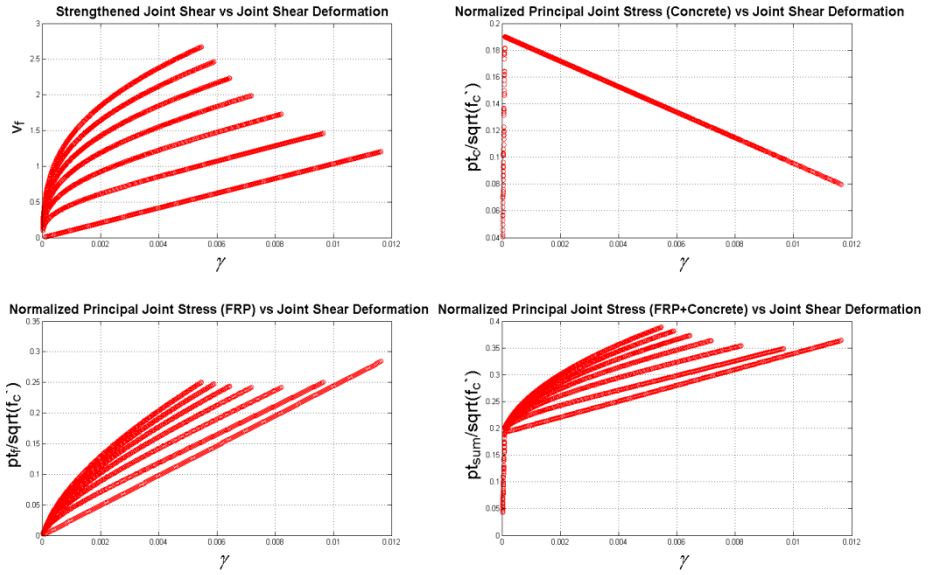

Figure D-1 Typical output plots at the end of analysis

APPENDIX E IDENTIFICATION OF VARYING AXIAL LOAD COEFFICIENT

E.1 BUILDING TYPOLOGY AND SELECTION OF THE SPECIMENS

The building configuration chosen for the study was a typical residential building with symmetric floor plan and floor levels of equal height. The selected prototype building for the experimental investigation is given in Figure E-1.

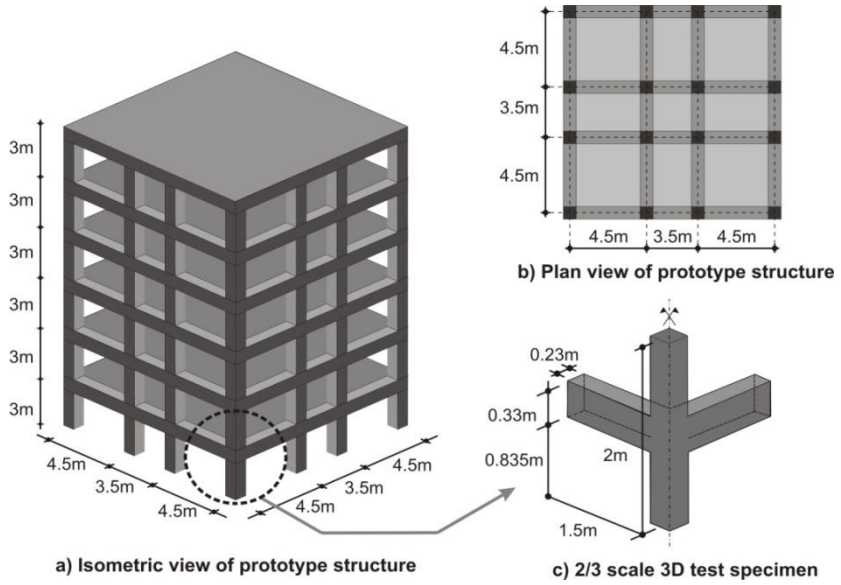

Figure E-1 Schematic representation of prototype building and test specimen

Test specimens represented the exterior and corner joint subassemblies at the first storey of the prototype residential building (Figure E-1). In the selection process, following considerations have been taken into account:

- To be consistent with the scope of this thesis, the configuration of the building was selected in order to employ the maximum varying axial load forces that can be applied within the limitations of the structures laboratory facility. Therefore, axial force was limited only in compression range without going under tension axial force in the columns. The axial load

variation coefficient used in 3D tests was reduced to approximately half of that used in the 2D specimens (i.e., 2.35 instead of 4.67).

- To provide a common comparison ground with the previous experimental and analytical findings of an ongoing extensive research on seismic retrofit solutions for existing reinforced concrete buildings being performed at the University of Canterbury and also with existing literature.
- To represent a typical mid-rise–6 to 9 storey– reinforced concrete (RC) frame designed and constructed according to typical older design code provisions and construction practice.

E.2 CONSTANT AXIAL LOAD EVALUATION

For the prototype building shown in Figure E-1, the gravity loading of each floor was evaluated using NZS95:1955 model building by-law Part I-V published in 1955. Calculation steps are given in the following Table E-1.

Table E-1 Gravity load evaluation for experiment

Gravity Load Calculation		
Prototype structure geometry		
Number of floors	6	
Structure width	12.5	m
Structure height	18	m
Beam height	0.500	m
Beam width	0.350	m
Column height	3.000	m
Column depth	0.350	m
Half of the clear bay length	2.075	m
Slab thickness[1]	0.130	m
Unit weight of concrete	0.130	m
Prototype structure components load		
SDL[2]	0.500	kPa
Live load[3]	1.430	kPa
Reduction of live loads[4]	0.500	
Beam dead load	15.960	kN
Column dead load	8.820	kN
Roof column dead load	4.410	kN
Tributary slab area	4.306	m^2
Tributary slab area load[5]	13.434	kN
Prototype building load		
Total load per floor	42.8	kN
Roof load	41.2	kN
Total load	255.3	kN
Model (test specimen) gravity load		
Scale factor	0.67	
Total load	**114.6**	kN

[1]minimum thickness = 5 inch= 0.127m (NZSS 95, July 1965)
[2]Superimposed dead load
[3]30 lb/ft2 for residentials (NZSS 95 part IV March 1955)
[4]NZSS 95 part IV March 1955
[5]Tributary slab area of corner joint

E.3 PROPORTIONALITY COEFFICIENT FOR VARYING AXIAL LOAD

The axial load, N, was varied around the gravity load value (i.e., based on the tributary area) in proportion to the lateral force acting on the column, V_c, as it would occur due to the frame lateral sway. The value of axial load during testing can be calculated as

$$N = N_{gravity} + \alpha V_c \tag{E-1}$$

where α is the proportionality coefficient and V_c is the applied shear force in the column. The derivation of this coefficient relies on the basis that the solution of the problem relies on the recognition that any structural analysis is approximate, and that the fundamental requirement is that equilibrium is maintained between internal and external forces [1].

Once the governing failure mechanism is assured, the designer can easily identify the total base shear capacity based on the flexural hinge capacity of the beam sections. The retrofit design, which follows the capacity based design philosophy, requires that plastic hinges are permitted to form at the ground floor level to complete the desired beam-sway mechanism (Figure E-2c), while ensuring that columns remain elastic to prevent the formation of any soft storey mechanism (Figure E-2a).

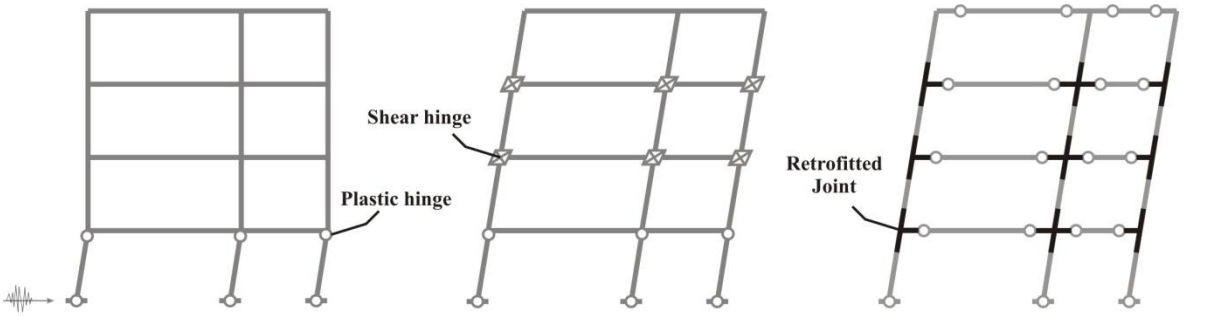

Figure E-2 Possible failure mechanisms for existing moment resisting frames before and after retrofit under seismic loading

The moment capacities of the column-base and retrofitted beam sections in the existing structure can be determined by moment-curvature. Upon converting the beam moment capacity to the equivalent beam moment in the first level column, the column shear is determined. Note that, ground columns may need to be retrofitted to increase the total axial load bearing capacity and ductility. In this situation, enhanced plastic moment capacity of the column on the ground floor should be taken into account. However, in this study a P-M interaction diagram for unstrengthened column is used under the assumption that a constant axial load level of 115kN is acting on the column.

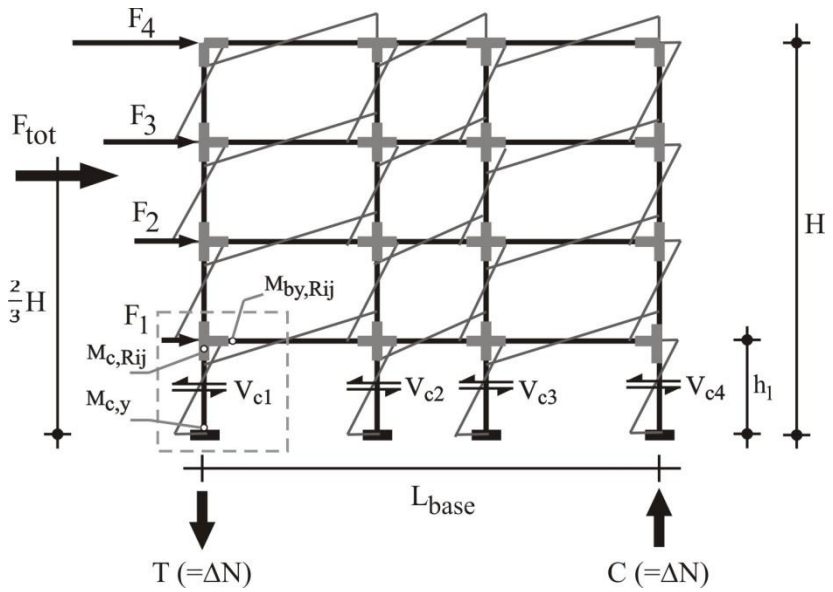

Figure E-3 Schematic view of the actions on plane frame structure

In order to determine the proportionality coefficient of varying axial load, firstly a generic example of a retrofitted RC frame is analysed under lateral forces using simplified assumptions of structural statics. Later on, capacity analysis results of the as-is and retrofitted joint sections are used in the calculations.

Considering equilibrium at the foundation level of the building in Figure E-3, the total overturning moment induced by lateral seismic forces can be written as follows

$$F_{tot}\left(\frac{2}{3}H\right) = TL_{base} \tag{E-2}$$

where F_{tot} is the total lateral force that equals to the summation of base column shear forces (Eq. (E-2)); H is the total height of the frame which equals to 12m; L_{base} (i.e., 8.33m for the model structure) is the distance between the exterior columns L_{base} which is equal to 8.33 m for the model structure; T is the seismic axial force in the exterior columns, which causes the axial load fluctuations during the lateral sway of the building. For the interior columns of a regular building it is assumed that beam shear at the opposite sides of the interior columns will cancel each other out. As a consequence, there is no seismic axial force contribution in these columns.

$$F_{tot} = V_{c1} + V_{c2} + V_{c3} + ... + V_{cn} \tag{E-3}$$

Rearranging Eq. (E-2) gives the induced axial force in the exterior columns as

$$T = \Delta N = F_{tot}\left(\frac{2}{3}\frac{H}{L_{base}}\right) \tag{E-4}$$

Using the relationships derived from the simple statics of the frame given in Figure E-3, a link can be established for the varying axial load coefficient α. During the test varying axial load was induced in the columns as an additional axial load to the constant gravity load, N_g, which is proportion to the column horizontal shear force of the exterior joint V_{c1} as given below

$$N = N_{gravity} + \alpha V_{c1} \tag{E-5}$$

where αV_{c1} can be regarded as the ΔN induced by the lateral force. Therefore, the α coefficient can be determined by substituing αV_{c1} in Eq. (E-3) as follows

$$\alpha = F_{tot}\left(\frac{2}{3}\frac{H}{L_{base}}\right)\frac{1}{V_{c1}} \tag{E-6}$$

where the column base shear, V_{c1} is evaluated by dividing the summation of the upper and the lower column moment value by the height of the storey, h_1. The upper column moment $M_{c,Rij}$ is the equivalent beam yielding moment at the FRP-ending section in the column, whereas the lower column moment $M_{c,y}$ is the capacity of the as-built column under the axial gravity load.

As a summary, step-by-step calculations to obtain the α coefficient are given as follows:

- From the M-N interaction diagram, column moment capacity for the gravity axial load of 115kN is $M_{c,y}=25kNm$
- Base column shears of the exterior columns of ground floor:

  $$V_{c1} = V_{c4} = \frac{17.52 + 25}{2} = 21.26\ kN$$

- Base column shears of the interior columns of ground floor:

  $$V_{c2} = V_{c3} = \frac{(2)(17.52) + 25}{2} = 30\ kN$$

- Total base shear:

  $\sum V_{c2} = 2 * 21.26 + 2 * 30 = 102.5kN$ which equals to the total lateral force F_{tot}

- Hence, varying axial load coefficient α for test specimen

$$\alpha = (102.5)\left[\left(\frac{2}{3}\right)\left(\frac{12}{8.33}\right)\right]\frac{1}{21.26} = 4.63$$

E.4 REFERENCES

1. Priestley MNJ, Calvi GM, Kowalsky MJ. *Displacement–Based Seismic Design of Structures*. IUSS Press Pavia, 2007.

APPENDIX F COMPOSITE MATERIAL PROPERTIES

The mechanical properties of fibres and epoxy impregnation resin provided by the manufacturer Sika (NZ) Ltd. are given in Tables F-1 and F-2.

Table F-1 Properties of glass fibre fabric

SikaWrap®-100G

Glass fibre fabric for structural strengthening

Positioning	
Description	Unidirectional, woven glass fibre fabric for the wet application process. Equipped with weft fibres that keep the fabric stable (heat-set process)
Uses	Flexural, shear or confinement strengthening of reinforced concrete, brickwork and timber structures: • Increased loading • Changes of building utilization • Repair of defects (damage to structural parts; design or construction defects) • Seismic strengthening (column wrapping, masonry walls) • Changes to standards or specifications
Advantages	• Can be used on a wide range of structural members (Beams, columns, chimneys, piles, walls) • Excellent cost performance
Product Data	
Fibre type:	High strength E-glass fibres
Fibre orientation:	0° (unidirectional)
Construction:	Warp: Glass fibres (98% of total areal weight) Weft: Thermoplastic heat-set fibres (2% of total areal weight)
Areal weight:	935 g/m² ± 47 g/m²
Fibre Density:	2.56 g/cm³
Fabric design thickness:	0.36mm (based on total glass content)
Tensile strength of fibres:	2,300 N/mm² (nominal)
Tensile E-modulus of fibres:	76,000 N/mm² (nominal)
Strain at break of fibres:	2.8% (nominal)

Source: http://buildsite.com/query/detail/product/sikawrap_hex_100g

Table F-2 Properties of epoxy impregnation resin

Sikadur®-300

Impregnation resin for fabric reinforcement

Positioning	
Description	Solvent free, two-component epoxy impregnation resin.
Uses	Impregnation resin for the wet application of SikaWrap fabric reinforcement.
Advantages	• Easy application by roller • High mechanical strengths • Solvent free
Approvals	• ICBO Evaluation Report ER 5558 (USA) • SOCOTEC (France)
Product Data	
Colour:	Comp. A: light-yellow to amber Comp. B: pale yellow to clear liquid
Mix ratio:	A:B = 100:34.5 by weight. Exact mixing ratio to be ensured by using scales.
Density:	1.16 kg/l (A+B mixed)
Pot Life:	15°C 23°C 40°C 6 hours 4 hours 90 minutes
Open time:	At 40°C: 60 minutes
Viscosity:	At 23°C: 750 mPas
Tensile strength:	45 N/mm^2 (After seven days curing at +23°C)
Flexural Modulus:	3,000 N/mm^2 (After seven days curing at +23°C)
Tensile Modulus:	3,500 N/mm^2 (After seven days curing at +23°C)
Application Temperature:	Substrate and ambient temperature: Min. +15°C; Max. +40°C
Service temperature:	Min. -40°C; Max. +60°C
Elongation at break:	1.5% (After seven days curing at +23°C)
Heat distortion Temperature:	Curing HDT 7 days, +15°C +43°C 7 days, +23°C +49°C 7 days, +40°C +60°C 7 days, +40°C +66°C
Packaging and Sizes	• Component A: 22.305 kg, Component B: 7.695 kg

Source: http://buildsite.com/query/detail/product/sikawrap_hex_100g

APPENDIX G EXPERIMENTAL STUDIES ON RC MEMBERS UNDER BIDIRECTIONAL LOADING

G.1 TESTS ON RC COLUMNS

The first tests employing various biaxial loading patterns carried out by Takizawa and Aoyama [1] and measuring biaxial transverse force paths are shown in Figure G-1. Test No. 2 was essentially uniaxial, but bending was within a plane through the diagonal of the square cross-section of the specimen at a 45° angle. In test No. 3 the transverse displacement path, applied after initial monotonic uniaxial post-yield loading, parallel to one side of the specimens cross section, had the form of three nested expanding squares rotated by 45° with respect to the sides of the cross-section. Test No. 4 aimed again at three nested square transverse displacement paths, this time parallel to the sides of the cross-section. Two interesting features can be recognized by examining the biaxial resultant paths of test No. 3 and No. 4. The first is the cluster of all square-like force paths into a single square, although the side of the outermost applied displacement path was almost twice that of the innermost. This shows that the specimen behaved in an elastoplastic fashion during the subsequent biaxial displacement cycles following the yielding during the uniaxial virgin loading. Secondly, as seen in Figure G-1b, c the resultant displacement vector trailed the resultant force vector by a phase lag equal about 15-20° with respect to the corresponding applied displacement paths. The main reason for this phenomenon was noted as a drop in the force, which is required to keep the corresponding orthogonal displacement constant, when the displacement in one direction was changed. Similar observations have also been made by other researchers (e.g., [2]).

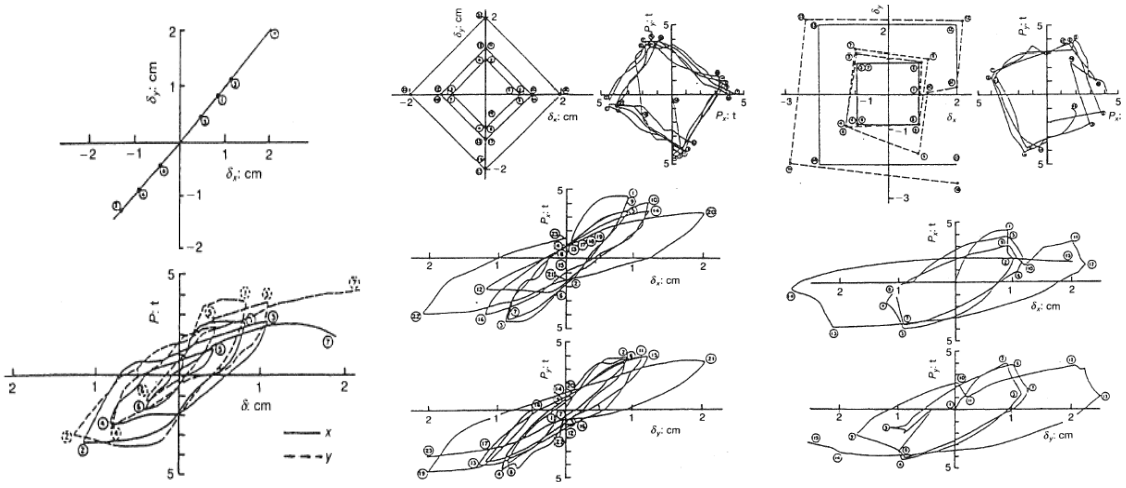

a) Test no. 2 b) Test no. 3 c) Test no. 4

Figure G-1 Experimental study by Takizawa and Aoyama [1]: Load patterns and test results

Other types of biaxial displacement patterns were employed by Takiguchi *et al.* [3] and Kobayashi *et al.* [4] within the framework of the experimental programme. Six companion specimens of those subjected to uniaxial cyclic flexure, were subjected to lateral displacement histories, which followed four expanding nested circular or elliptical orbits on planes transverse to the specimen axis (Figure G-2a, b). The radius of the imposed displacement cycles was equal to the amplitude of the uniaxial displacement cycles to which the companion specimens were subjected; approximately 0.5, 1.5, 2.5, and 3.5 times the yield deformation. The researchers reported that the hysteresis loops in the individual transverse directions were found to be similar to (only narrower) the corresponding loops in uniaxial loading. Due to this, it can be said that all these findings cannot be generalized, as they are mainly due to the peculiar imposed inelastic displacement histories, in conjunction with the symmetry of the square or circular cross-sectional shapes [5].

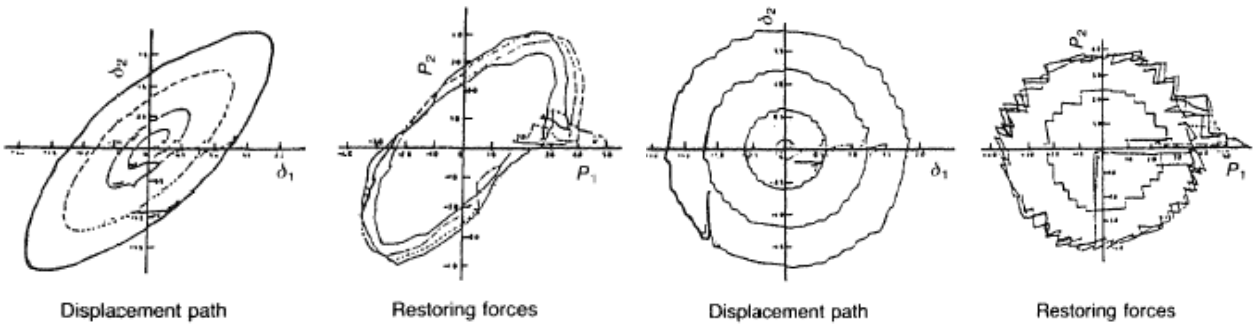

a) b)

Figure G-2 Experimental study by Takiguchi *et al.* [3] and Kobayashi *et al.*[4]: Test results in cyclic biaxial flexure with constant axial force

Saatcioglu [6] and Saatcioglu and Ozcebe [7] also used similar biaxial load patterns to that of the previously mentioned elliptical types. The test specimens were subjected to transverse displacement paths with the shape of the nested and concentric ellipses (Figure G-3). The major semi-axis was twice the minor. The test setup is given in Figure 7-2 in Chapter 7. Its length was chosen be equal to a fraction of multiple of the uniaxial yield displacement with values of: 0.5, 1.0, 2.0, 3.0 and 4.0. Each ellipse was traced three times in a clockwise direction. The test results indicated that columns subjected to simultaneously varying bidirectional load reversals, have a different response than those subjected to unidirectional load reversals. The level of damage in one direction adversely affected the column in the other direction. If the deformation in one direction was less than the yield deformation, the bidirectional effects on the response in the orthogonal direction were small. However, if post-yield deformations were experienced in each direction, severe strength and stiffness degradation might have been observed.

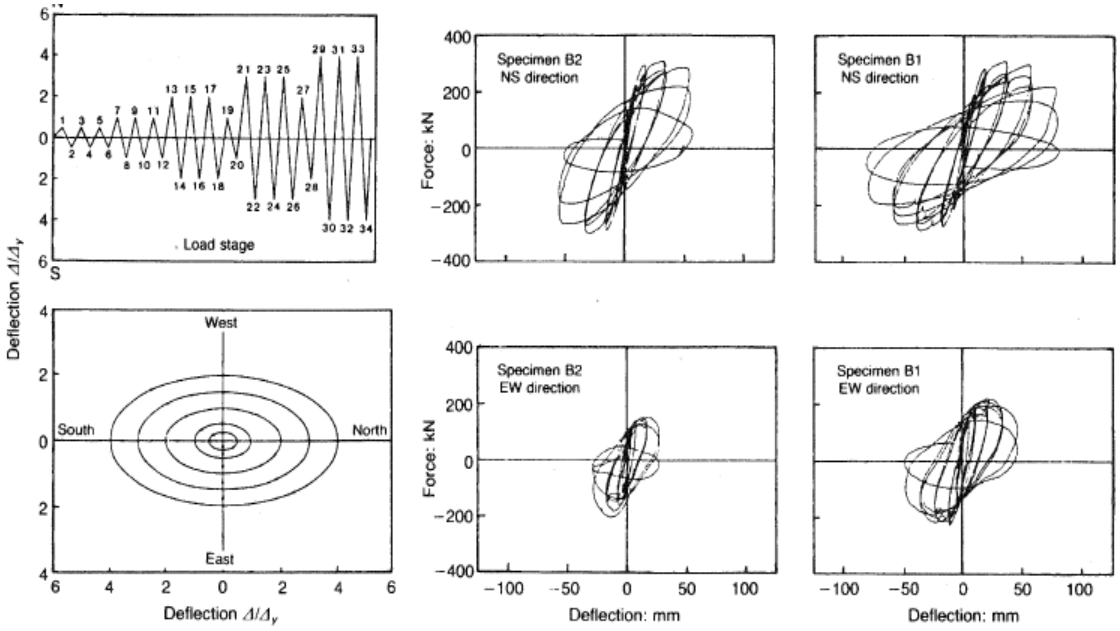

Figure G-3 Experimental study by Saatcioglu and Ozcebe [7]: Elliptic biaxial displacement pattern and corresponding force-deflection results

Another type of biaxial loading sequence was employed in the experimental programme performed by Li and Aoyama [8]. The same displacement pattern was used in a single test under constant axial load and three more tests under varying axial load in order to investigate the effect of the axial load variations on biaxial behaviour. The biaxial displacement paths as shown in Figure G-4 consisted of two squares connected in the form of an 8. At each peak displacement magnitude four 8s were applied, with the long axis of the 8 along one diagonal of the cross-section in the first and the third, and along the other in the second and the fourth. The two squares of the 8 were traced in the counterclockwise

sense in the first and the third quadrant of the sequence, but in different order, while in the second and the fourth quadrant, the two squares were traced in the clockwise direction. The resultant hysteresis loops in the two orthogonal transverse directions obtained from the study are given in Figure G-4. As seen in this figure, the force-displacement curves of the tests in which the axial load varied linearly with the transverse forces, exhibited the familiar unsymmetric strengthening, stiffening and strength deterioration effect of the axial load. At the peaks of the hysteresis loops (shown within the circles in Figure G-4c, d) the values of axial forces were very different in the two opposite directions of loading and therefore the effect was rather pronounced. It is interesting to note that when the axial load varied with both components of the transverse force, the loops were strongly asymmetric in both directions for the low mean value of the axial force (Figure G-4c), but showed no systematic effect of the axial force variation for the high mean value.

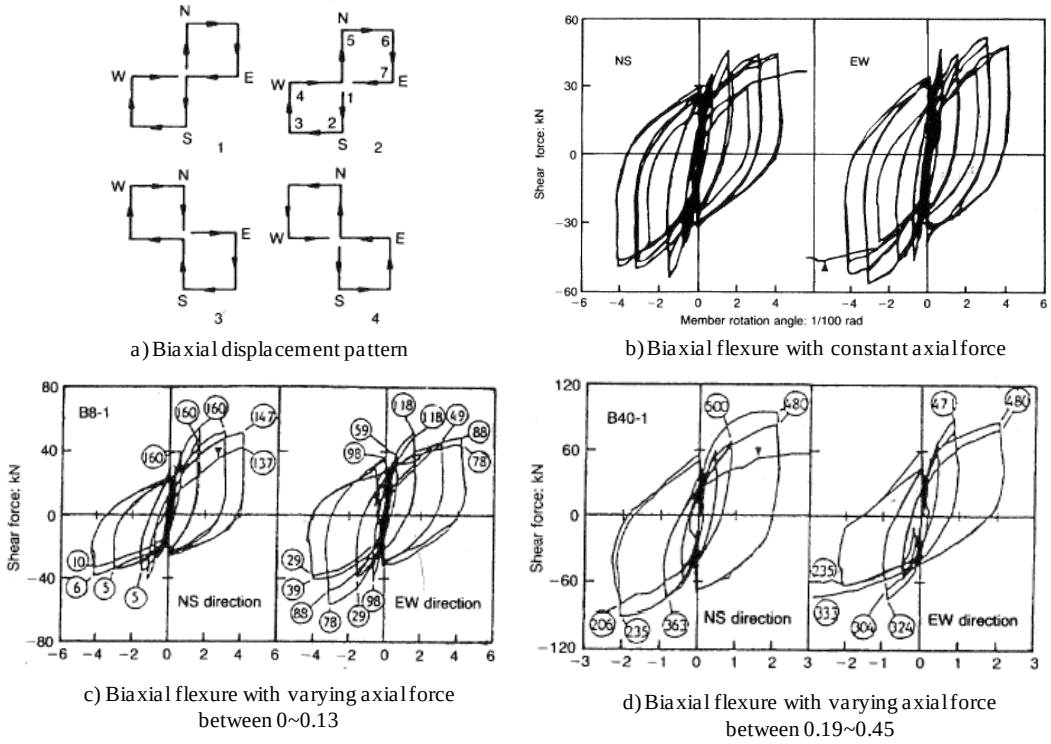

a) Biaxial displacement pattern

b) Biaxial flexure with constant axial force

c) Biaxial flexure with varying axial force between 0~0.13

d) Biaxial flexure with varying axial force between 0.19~0.45

Figure G-4 Experimental study by Li and Aoyama [8]: Imposed biaxial load pattern and test results

Low and Moehle [9] also considered variation of the axial load ratio from 0 to 0.13 with the displacement in the weak direction of bending in tests No. 4 and 5, which were companion tests to No. 2 and 3. In all specimens unequal strength and stiffness characteristics in the two principal directions of bending were implemented. Tests No. 2 was actually tested uniaxially, as biaxial displacements were controlled to be nearly equal, so that bending was effectively constrained within a plane at 45° to the weak direction of bending (Figure G-5). Due to the difference in the strength and stiffness between the two principal directions, the force resultant was not at 45° with these two directions but closer to

the strong axis of the cross-section. Test No. 3 was truly biaxial with concentric nested imposed biaxial displacement paths in the form of a cloverleaf at four different displacement levels. Test results indicated that hysteresis loops in the strong direction of bending are similar to those obtained in square displacement paths, such as those tested by Takizawa and Aoyama [1] and Otani and Cheung [2], (i.e., they were characterised by an abrupt drop of force at the beginning of unloading, due to the increase of the displacement in the orthogonal direction, and by their large width and energy dissipation). In the weak direction, since a cloverleaf cycle consists of two pairs of repeated displacement cycles in the opposite direction, hysteresis loops consisted of two interconnected half-loops in each direction of loading.

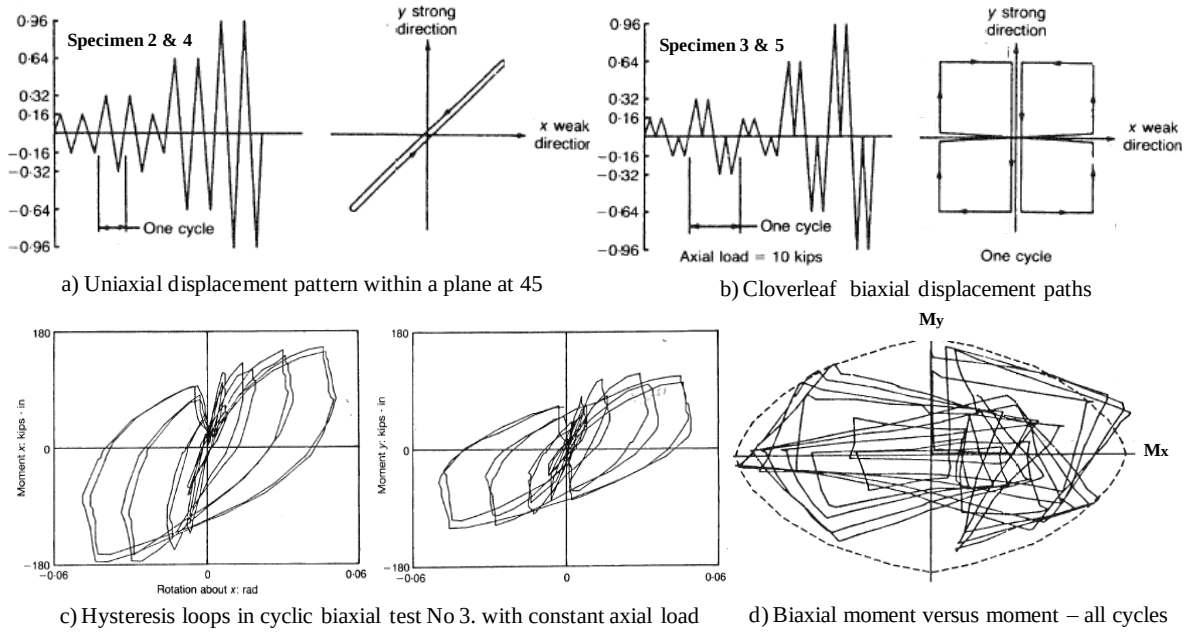

a) Uniaxial displacement pattern within a plane at 45

b) Cloverleaf biaxial displacement paths

c) Hysteresis loops in cyclic biaxial test No 3. with constant axial load

d) Biaxial moment versus moment – all cycles

Figure G-5 Experimental study by Low and Moehle [9]: Imposed load patterns and test results under constant axial load

The test results of the specimen No. 4 tested under uniaxial loading within a plane at 45° and varying axial load were reported as inconclusive with regards to the effect of axial load variation. For bending at the weak axis the hysteresis loops showed a reduction of strength and stiffness in the direction of increasing axial compression, and no effect in the direction of decreasing axial compression. On the contrary, for bending about the strong axis, the hysteresis loops exhibited the familiar softening in the direction of decreasing compression and stiffening in the direction of increasing. In test No.5, the hysteresis loops in the weak direction of bending showed a significant reduction of strength and stiffness in the direction of decreasing axial compression (Figure G-6b), but no noticeable effect on the side of increasing axial load.

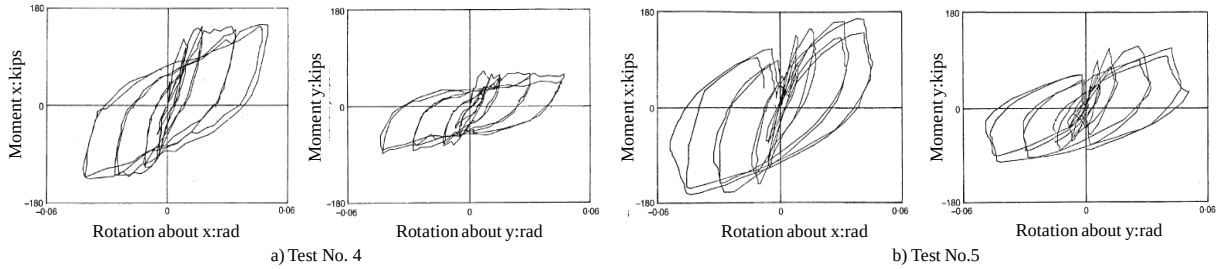

a) Test No. 4 b) Test No.5

Figure G-6 Experimental study by Low and Moehle [9]: Test results under varying axial load

Wong *et al.* [10] presented the test results of a total of sixteen short circular columns subjected to biaxial lateral displacements. The main intent was to investigate the sensitivity of the strength and stiffness of shear-resisting mechanisms to various displacement patterns and axial compression load intensities. Test results showed that both the hysteretic performance and displacement ductility capacity of the columns were improved by increased spiral steel content or by increased axial compression. In comparison with uniaxial displacement paths, biaxial displacement patterns (Figure G-7b) led to more severe degradation of strength and stiffness. However, it is interesting to note that, it was observed that the difference in the responses of columns with identical properties subjected to simple biaxial b-type displacement patterns or to more sophisticated s-type patterns was small enough to be disregarded in design. Furthermore, the performance of the unit tested with a random biaxial displacement pattern was found to be better than its companion unit under the b-type displacement history. Researchers suggested that if biaxial seismic effects are to be studied further, tests using biaxial b-type (orthogonal) displacement paths should be sufficient. It was also revealed by the test results that the displacement ductility capacity was not sensitive to the type of biaxial displacement pattern. In other words, although it was shown that biaxial, rather than uniaxial testing is important for columns suffering shear failures, the form of the biaxial displacement patterns is not significant, provided that the same peak displacements were achieved.

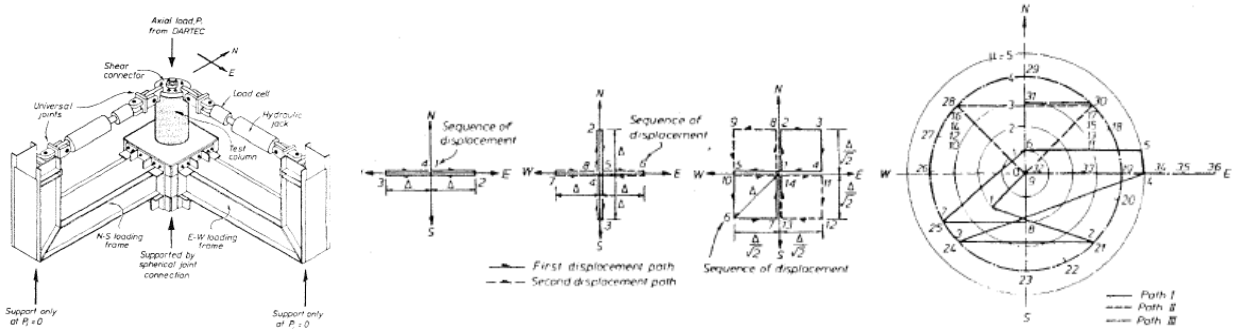

uniaxial 'u' type biaxial 'b' type biaxial 's' type multidirectional 'r' type

a) Test setup b) Different displacement patterns

Figure G-7 Experimental study by Wong *et al.* [10]: Displacement patterns used in testing

All these experimental studies have focused on the investigations of well designed columns under biaxial loading with or without varying axial loads. Recently, an experimental study was performed by Boys [11] to investigate the performance of columns designed to carry only gravity loads under bidirectional loading. The test specimens are representative of columns, constructed during the period from the introduction of deformed bars in the mid 1960's through to the early 1990's. For this purpose, two unidirectional and four bidirectional tests were conducted on full scale column elements. The bidirectional loading imposed was a development of the increasingly familiar 'cloverleaf' protocol (Figure G-8a). In this version the 'leaves' were scaled such that the peak displacement in each of the principal component directions was equivalent to the drift for the associated level of drift for the uni-directional protocol. Each of the 'leaves' was traversed once only at each level of drift, and an additional uni-directional excursion was undertaken for each of the four principal axis. The global performance of columns with inadequate detailing was shown to be poor, with loss of axial capacity occurring at drift ratios as low as 1.5% for the bidirectional tests (Figure G-8b). The inadequate detailing investigated included, minimal transverse reinforcement, lap-splices in the potential plastic hinge zone, and cranked bars at the top of the lap splice. Of these parameters the transverse reinforcement ratio was critical (in combination with the axial load ratio). Both shear and axial load failure were proportional to the transverse reinforcement ratio and inversely proportional to the imposed axial load ratio.

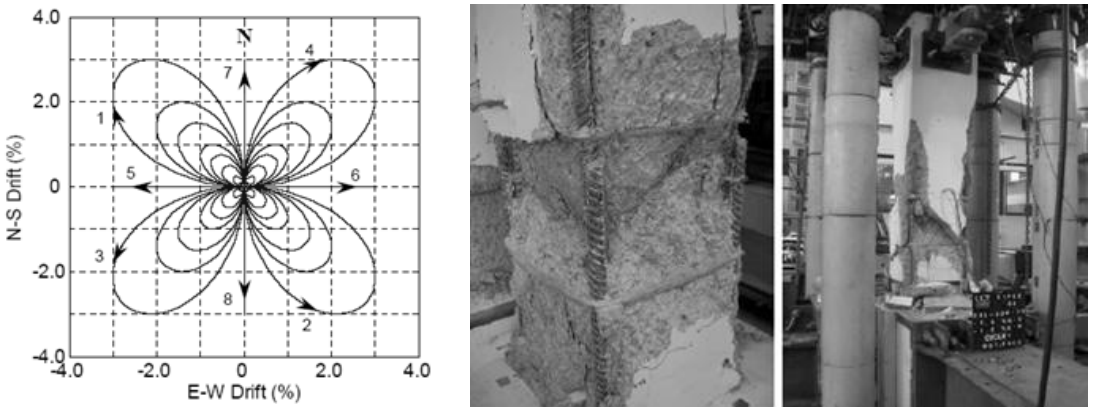

a) Bidirectional loading protocol b) Typical damage pattern of column under biaxial loading

Figure G-8 Experimental study by Boys [11]: Test results under varying axial load

G.2 RESEARCH CONDUCTED BY OLIVA AND CLOUGH

The existing results cannot completely simulate the earthquake loading in real columns, where lateral deformations vary depending on the state of resistance in the columns and axial load changes due to overturning moments. Under these considerations, Oliva and Clough [12] performed a research programme that included shaking table tests of RC frames to expand existing information on the

biaxial behaviour of individual RC column elements gained from the previous studies. Due to the significance in understanding of the behaviour of RC frame systems designed according to 1970s code provisions under bidirectional loading, results from this study are presented, including a description of the interaction effects in members, the manner in which uniaxial and biaxial response varies and how and where they cause inelasticity to develop in a structure. A large-scale model of an RC frame was tested under earthquake motion on the shaking table. The ground motion occurred at a skew angle to the frame`s principal axes. Another identical frame was also shaken with uniaxial motion to compare the effects of uniaxial and multiaxial loading. Frame and rectangular column dimensions are shown in Figure G-9. The design of the frame was intended to meet the Uniform Building Code [13] and ACI 318-71 [14], but was purposely proportioned to develop and study yielding in columns. The table motion during the tests followed the displacement record derived from an accelerogram of the 1952 Taft N69W earthquake record.

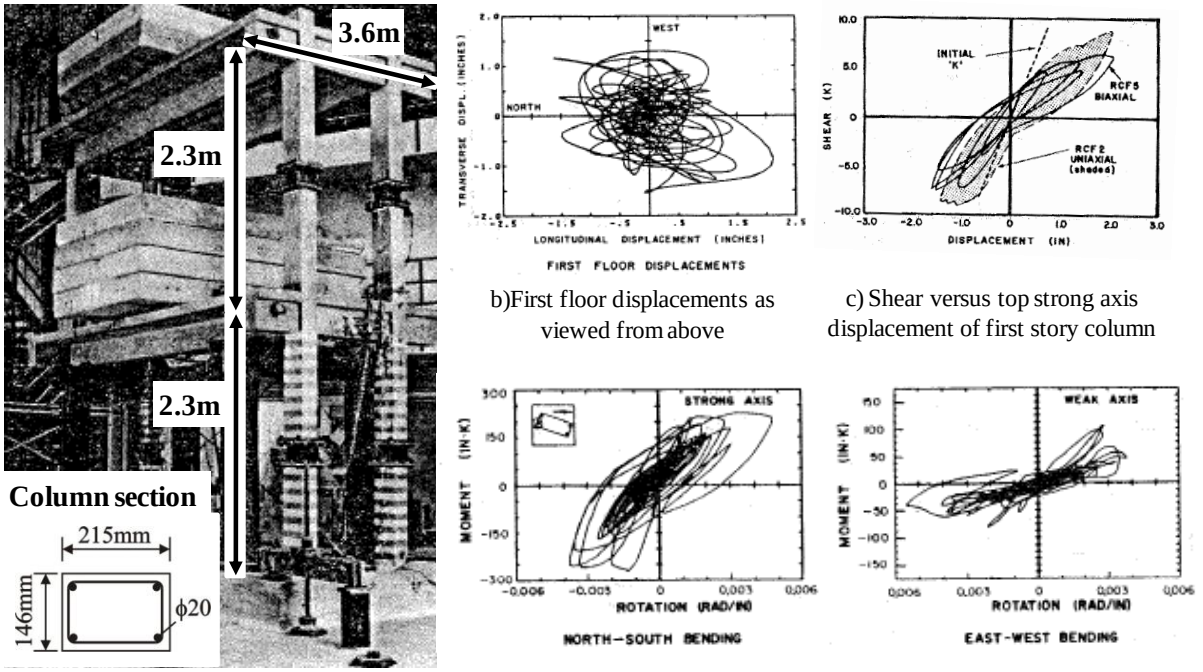

a) Test frame dimensions

b)First floor displacements as viewed from above

c) Shear versus top strong axis displacement of first story column

d) Moment versus base rotation from inelastic frame test

Figure G-9 Experimental study by Oliva and Clough [12]: Test frame dimensions and measured displacements

Test results highlighted the significant effects of biaxial loading, which can be seen in the comparison of stiffness and strength of a column from the biaxial frame and one from the uniaxial frame as shown in Figure G-9. Important points noticed from that figure can be summarized as (1) both columns had identified initial stiffness; (2) the biaxial column yielded at a lower level; (3) the biaxial column had greater stiffness degradation and a lower strength envelope and (4) energy dissipation in the biaxial

test was lower. Observations made on the behaviour of columns indicated that the flexural response of the column in the weak or transverse direction was significantly different from the cyclic flexural response normally seen in reinforced concrete members. No obvious yield point was observed, even though the deformations were greater than that of along the column`s strong axis. It was noted that the stiffness decreased drastically from the initial amount to a low and variable level. This peculiar response along the weak axis was a result of interaction between simultaneous loads and the damage induced. The yielding and damage caused by the strong axis motion resulted in a considerable decrease in weak axis stiffness with large deformation and little energy dissipation.

Considerable differences were also recorded in terms of the overall response, as well as in the dynamic response of the frame system under biaxial loading when compared to uniaxial loading. For instance, although cracking in the longitudinal beams over the full depths of the webs and cracking in the flanges of the transverse beams occurred in the uniaxial frame; there was no beam cracking or slab cracking in the biaxial frame. The failure mode in the latter case was the formation of considerable cracking with yielding in the columns. No damage occurred in the beams. These observations lead to the fact that under biaxial loading there is a markedly increased tendency for inelastic deformation to develop in columns before developing in beams.

It was also observed that the corner columns of a multibay structure can yield first, even though the moment along either of its principal axes is less than the uniaxial yield level, through interaction of the simultaneous biaxial moments and a changing axial load caused by overturning. Once yielding develops in a column, stiffness degradation ensues and the deformation demand in the member escalated. The researchers noted that the lack of yielding in the beams of the frame test was significant, because it proves that early column yield and hinging due to biaxial bending may act as a force limiting mechanism for the remainder of the frame. Obviously this mechanism may result in inhibiting yield level forces from developing in other elements (no spreading of inelasticity over an increased portion of the structural system). As a consequence, energy dissipation and deformation demands become concentrated in the columns, contrary to the design philosophy and intentions.

Another significant affect of initial yielding and damage concentration in corner columns at any instant, may be an unsymmetric stiffness in the lateral load resisting system and inducement of torsional motion. This phenomenon may emerge even though a three-dimensional frame is designed with symmetrical lateral stiffness, or its centre of lateral resistance is at the centre of mass, if inelasticity develops in the columns. Since columns near the corner of a framed structure will always have the most critical combination of biaxial moments and axial load, due to lateral vibration,

overturning moment, and accidental torsion, these are liable to yield and soften. The centre of the lateral stiffness of the system changes, additional torsion follows, and increased deformation demand is placed upon the already yielding corner columns.

G.3 FAILURE SURFACE FOR RC COLUMN SECTIONS SUBJECT TO FLEXURE AND AXIAL LOAD

Serious interaction effects have been observed in circular and square columns as a result of the ellipsoidal shape of the moment versus axial load yield interaction surface. The effects of biaxial loading in increasing deformations are particularly evident in rectangular columns where strengths and stiffnesses are considerably different along the principal axes. When yielding is initiated in a rectangular member by an increase in strong axis moment, the plastic deformation will generally have a large component in the weak axis direction, because of the ellipsoidal shape of the yield surface. This large weak axis component produces what appears to be lowered stiffness, i.e., large deformation with a small reversed sign moment, in the weak axis direction. Thus, yielding rectangular columns may maintain flexural resistance along their strong axis, but may lose a major portion of their resistance capacity in the weak axis direction. Moreover, similar to uniaxial bending, spalling of the compression concrete includes deformation softening under biaxial demands, which may result in a permanent modification of the biaxial yield surface.

In order to illustrate these effects, the results of an analytical study performed by Zeris and Mahin [15] on a rectangular column, which was analysed under a hypothetical excitation consisting of a monotonically increasing lateral tip displacement and constant axial load, are briefly reviewed. The axial load considered in the study was one ninth of the ultimate axial load. The tip displacement was monotonically increased along a line of constant inclination. This can be referred to as skew angle and denoted by Θ, with respect to the strong axis (referred to here as the x-axis). The inclinations considered were 0°, 30°, 45°, 60°, and 90°. The same displacement magnitude is used for all values of Θ.

The predicted base moment paths and projected base moment-chord rotation characteristics are given in Figure G-10. Some observations can be summarized as (1) biaxial loading resulted in considerable reductions in the projected resistances compared to the uniaxial capacities about either axis; (2) the postcracking flexural stiffnesses in each direction exhibited a reduction in each direction, particularly in the y-direction. In the x direction, such a significant change in stiffness occurs only for Θ equal to 60° (Figure G-10c); (3) a drop in resistance due to the disintegration of the concrete at the

compression corner can be seen for all cases (Figure G-10c, d); (4) lastly, as seen in Figure G-10c, and d, although considerable reduction in the base moment about the x-axis occurs for θ equal to 60°, this is not followed by an equally significant drop in the y bending resistance due to the tendency of the neutral axis to align itself with the y-axis for higher Θ values (Figure G-10, point a). For the lower Θ values (Figure G-10, point b), although softening occurs in both directions, the resistance about the y-axis drops by 40-50% of the maximum value, while the corresponding resistance about the x-axis only drops by 10-15%.

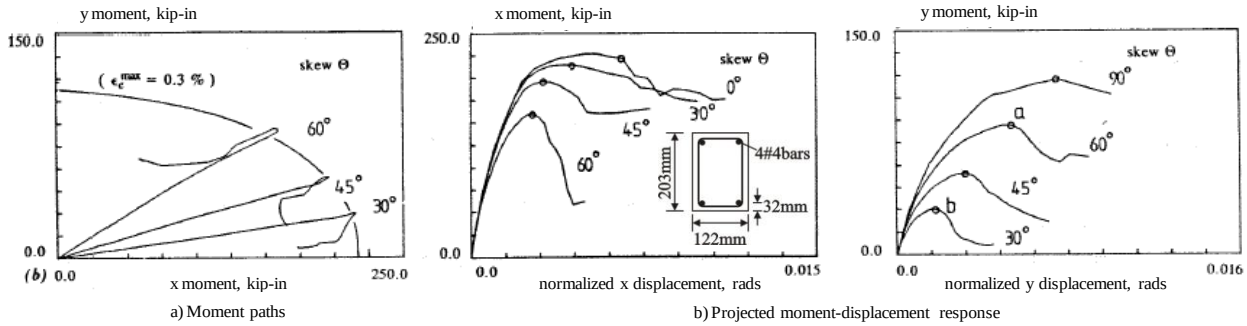

Figure G-10 Analytical study by Zeris and Mahin [15]: Biaxial response of rectangular column under static displacement control

The previous discussion suggests that a very convenient way to design or analyze RC columns, subjected to biaxial bending can be performed by constructing *interaction surfaces,* which make up the column`s complete failure surface. An interaction surface can be defined as the complete set of *interaction diagrams,* which describe column capacity for bending in one particular plane. An interaction diagram for a typical column section under eccentric loading can easily be found using conventional section analysis. A maximum extreme fibre strain of concrete in compression (i.e., the strain at crushing of concrete, ε_{cu}) can be taken as a limit state for the strength of eccentrically loaded columns. Using this criteria, along with the assumption that plane sections remain plane after bending, strains at all points of a cross section can be determined for any assumed neutral axis. In the next stage, resultant force and moment that created the assumed strain distribution can be evaluated with the established strains at all points and knowledge of the stress-strain characteristics for the reinforcement used. The resultant force and moment causing the assumed strain distribution are obtained by the summation of forces and moments about the centre of column. If this evaluation procedure is repeated for a series of neutral axes that are assumed perpendicular to an axis of symmetry, eventually an interaction diagram that represents a graph of the ultimate forces against the corresponding ultimate moments can be produced. As an example, a schematic illustration of external forces and resultant strain distribution in a reinforced concrete column member subjected to axial force and biaxial bending is given in Figure G-11.

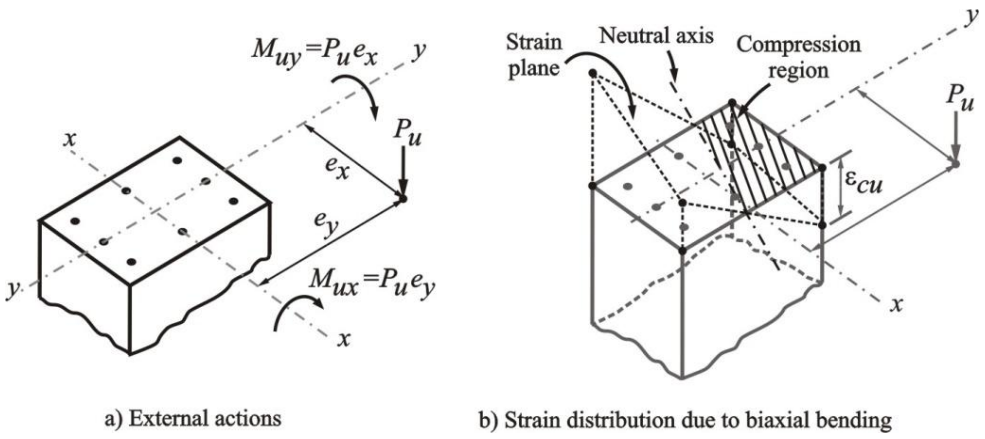

Figure G-11 Reinforced concrete column member subjected to axial force and biaxial bending

By varying the angles and locations of the assumed neutral axes, the complete failure surface can effectively be created from these particular interaction diagrams at many angles between the axes of symmetry of a cross section. A complete set of interaction diagrams at all angles will illustrate and describe *an interaction surface* (Figure G-12). Each point on the generated failure surface, where abscissas and ordinates are depicted by moment capacity in directions of principal axes, represents the capacity of the section, i.e., the maximum compressive strain in the concrete and corresponds to a specific orientation and location of the neutral axis. For cross sections with two axes of symmetry, each quadrant of the interaction surface will be identical and therefore one quadrant is sufficient to describe the surface. Columns in which the bending capacity is the same about the each principal axis will have identical interaction diagrams for bending in the plane of each axis, and an interaction surface should approach a surface of revolution generated as the interaction diagram rotates about the *P* axis as suggested by the grid lines of (Figure G-12) [16].

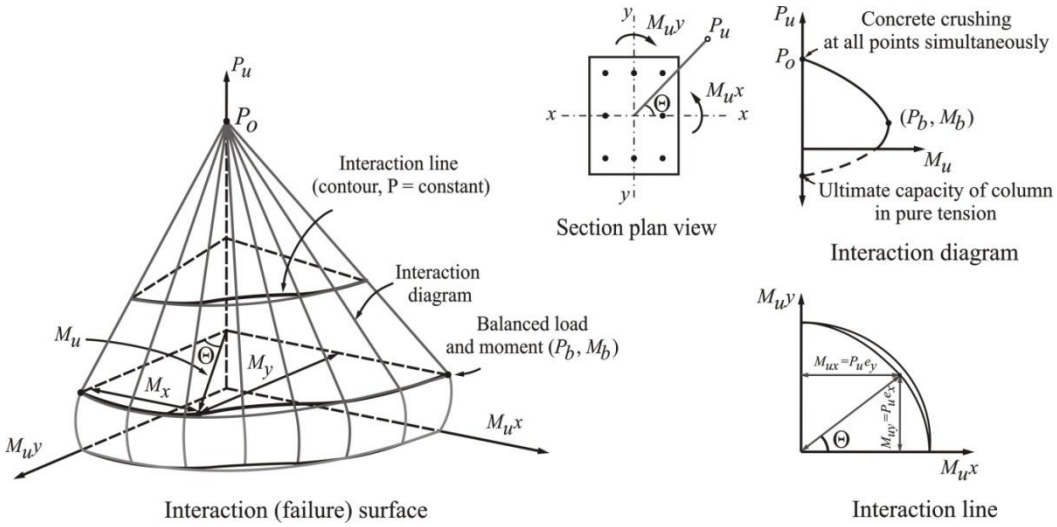

Figure G-12 Interaction surface for a RC column with biaxial loading after Furlong [16]

Since the shape of the contour lines are influenced by many factors (i.e., section geometry, the strength of materials, the arrangement of reinforcement and content of steel, and the axial load level) the evaluation of them in general is difficult. Application of the basic principles of equilibrium and stress-strain compatibility offers the most direct approach for analyzing and designing RC members, subjected to a combination of axial force and biaxial bending moments using strength theory. However, this approach is not generally used because it is computationally impractical without the benefit of a computer. These numerical difficulties can be attributed to the well-known behaviour of concrete, which has an assumed negligible strength in tension and a nonlinear stress-strain relationship in compression, in addition to the aforementioned factors. Hence, instead of using conventional elastic theory to determine the stress distribution due to a set of P, M_x, and $M_{y,}$ computers can be used for trial-and-error techniques, although they become too lengthy for hand computation.

In the past many investigators considered the problem of the calculation of flexure strength of rectangular RC columns subjected to biaxial bending (i.e., [17, 16, 18-26]). Generally, these investigators attempted to simplify the problem of biaxial design and analysis by generalizing the failure surface with some mathematical formulation based on the knowledge of both uniaxial interaction relationships and in some cases a particular skew interaction relationship. The well known expression originating from the Russian code and which was published by Bresler in 1960 for the strength of a biaxially loaded column is

$$\frac{1}{P_u} = \frac{1}{P_{ux}} + \frac{1}{P_{uy}} - \frac{1}{P_o} \tag{G-1}$$

where P_u = ultimate load under biaxial loading, P_{ux} = ultimate load when only eccentricity e_x is present (i.e., load applied at point 1 of Figrue G-12a), P_{uy} = ultimate load when only eccentricity e_y is present (i.e., load applied at point 2 of Figure G-12a), and P_o = ultimate load when there is no eccentricity. [17] has also shown that the family of interaction lines corresponding to the various levels of constant P_u for a rectangular RC column subjected to axial load and bending about both major and minor axes, the relationship between the moment capacities at the given axial load is closely approximated by the interaction contour as

$$\left(\frac{M_{ux}}{M_{uxo}}\right)^m + \left(\frac{M_{uy}}{M_{uyo}}\right)^n = 1 \tag{G-2}$$

in which $M_ux = P_ue_y$, $M_uy = P_ue_x$, e_x and e_y are the eccentricities of P_u and M_ux and M_uy are the corresponding uniaxial bending capacities about the x and y axes for the constant load under consideration. The constants m and n are interaction exponents, which is a function of the axial load, section, and material properties of the column and determined experimentally. Knowing m and n, for a given moment capacity about one axis, the moment capacity about the other axis can be determined from Eq. (G-2).

One of the first significant contributions to the design and analysis for biaxial actions was reported from work done by Weber [19]. Charts were produced for square columns reinforced symmetrically by 4, 8, 12 and 16 bars with a yield strength of 60 ksi (420MPa) and loaded along a diagonal. These charts have been reproduced in a handbook issued by the American Concrete Institute [27]. These interaction charts for diagonal loading, combined with the existing uniaxial interaction charts, provided a useful basis for the design or analysis of square columns when Weber`s simple interpolation method was utilised [21].

Many researchers extended the applicability and scope of the interaction charts proposed by Weber [19], by adopting various design techniques for the ultimate strength analysis of various concrete sections such as rectangular, L-shape and polygonal, under biaxial bending moments and axial load. Several analysis methods with simplifying assumptions have evolved in an attempt to overcome the numerical difficulties: method of superposition and method of equivalent uniaxial eccentricity [22] approximated shape of strength envelopes [28, 22], utilizing of the Newton-Raphson method in solving the roots of non-linear equations [29], load-fraction method [30] modified secant-modulus method [31] and a recently proposed method based on an analytical approximation of the moment contours [26]. For more detailed information on the approximate methods of analysis and design for biaxial bending and axial load of square and rectangular columns, the reader is referred to the literature and the texts by Fergusan *et al.* [32] and Hassoun and Al-Manaseer [33].

G.4 TESTS ON RC BEAM-COLUMN JOINTS

In his PhD study, Beckingsale [34] performed experimental investigation on the behaviour of well-designed beam-column joints under uniaxial and bidirectional loading. One interior space frame beam-column joint unit was tested under a heavy axial load level ($0.50f`_cA_g$) to compare it's performance with the performance of similar plane frame specimen tested previously under uniaxial loading conditions. The test was conducted in several parts. Initially the East-West beams, and then the North-South beams, were loaded separately up to displacement ductility factors of four in a similar cyclic loading pattern to that used in the plane frames. At load run 31 two-directional (or skew loading) of

the test unit commenced. Even though larger joint deformations and more yielding of joint reinforcing occurred under bidirectional loading than unidirectional loading, test results were found to be very satisfactory even though only unidirectional loading was considered in the design. Some stiffness degradation was apparent as a result of the greater joint flexibility under skew loading, but the beam strengths attained at a constant level of displacement, did not diminish greatly. Reduction of the test data also showed that joint shear caused by skew loading was carried by similar mechanisms to those mobilized under unidirectional loading. The researcher reported that no enhancement of the strength of space frame joints can be assumed to the confining action of the beams on all faces of the joint. The prior cyclic loading of the transverse beam diminished the effectiveness of the confinement, which was initially available, while skew loading imposed more severe demands on the joint than it did in unidirectional loading.

Leon and Jirsa [35] carried out an experimental investigation into the behaviour of space frame joints to investigate the effects of load history, beam reinforcement size, beam geometry and floor slabs on joint behaviour under cyclic bidirectional load reversals. A total of fourteen full scale specimens comprising of twelve interior (eleven without slab and one with slab) and two exterior (with and without slab) were tested. All specimens were designed to simulate a multi-storey ductile moment-resisting frame. The specimens were loaded by subjecting the beam ends to a severe bidirectional monotonic history. Axial load was applied in most tests, but axial load was not varied. Details of the specimens and test results from this research are shown in Figure G-13. Although there was a minimal amount of transverse joint reinforcement in the joints, the reinforcing bars were deformed and the detailing was based on modern practice. Test results showed that joint behaviour was significantly affected by biaxial loading, due to the deterioration of column strength, the beam and slab geometry and bond conditions. Large stiffness losses were recorded due to shear cracking of the joint, section losses in the column, and bar slip due to inadequate anchorage lengths. The experimental results confirmed the validity of utilizing a uniaxial approach in design if proper precautions are taken. The overall shear capacity of the joints was about 28 to $30\sqrt{f_c`}$ regardless of the direction of loading. It was concluded that axial load had relatively little importance on joint behaviour. However, the researchers noted two observations: 1) the column without axial load cracked very early in tension; 2), the column corners did not crush in compression at an early stage. The joint was identified as the “weakest link” because stiffness and strength deterioration in this region can lead to substantial drifts and the possibility of collapse, due to P-Delta effects and thus contributed significantly to the inelastic deformation. It was noted that a large number of transverse reinforcement ties should be provided in order to control the cracking and properly confine the joint. Exterior joints are confirmed to be inherently more vulnerable than interior joints under seismic loading. In addition to a less efficient

compression strut mechanism, the bond deterioration in the anchorage of beam bars in the joint can cause damage to the concrete cover with subsequent spalling. This phenomena obviously leads to partial loss of anti-buckling protection of the column longitudinal bars.

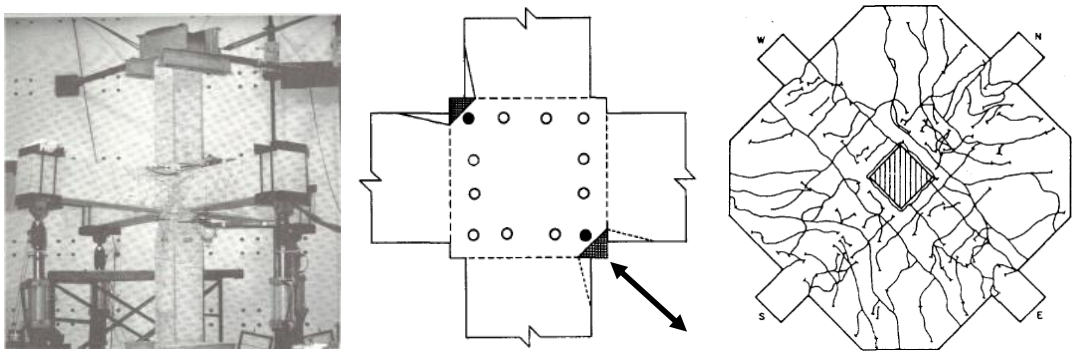

a) b) c)

Figure G-13 Experimental study by Leon and Jirsa [35]: a) specimen view; b) monotonic bidirectional loading direction; c) typical distribution of crack patterns

Suzuki *et al.* [36] tested a half-scale three dimensional RC interior beam-column subassembly with slab, under unidirectional and bidirectional simulated earthquake loadings, to study the effect of the slab on the flexural behaviour of the beams and the influence of bidirectional lateral loadings on the behaviour of the column (Figure G-14). Regarding the effects of bidirectional loading, it was observed that although beams were subjected to biaxial bending in the vertical and horizontal planes, biaxial interaction was negligible. In addition, the deflections of the column became greater than the deflection in the column subjected to a uniaxial lateral load of the corresponding amplitudes.

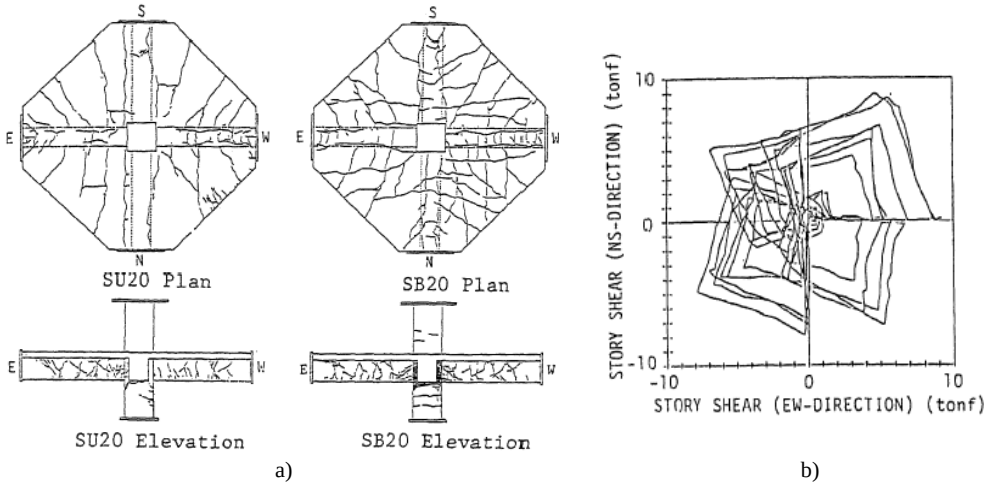

a) b)

Figure G-14 Experimental study by Suzuki *et al.* [36]: a) crack patterns of tested specimens; b) trace of storey shear (SB20)

Kurose *et al.* [37] and Guimaraes *et al.* [38] conducted a study to evaluate the behaviour of slab-beam-column connections constructed with normal and high strength materials. For this purpose a series of six full-scale specimens were tested under unidirectional and bidirectional loadings under the U.S.–Japan–New Zealand–China cooperative research programme on design of beam-column connections. The main objective of the above mentioned quadri-lateral project was to study the behaviour of beam-column joints, designed in accordance with the building code of the respective countries. The test setup and loading protocol used are given in Figure G-15. The specimens were designed using recommendations of the ACI 352 Building Code [39]. Columns were reinforced to have greater flexural strength than beams for both unidirectional and bidirectional loading. Joint transverse reinforcement was the same as column transverse reinforcement with at least three stirrups located in the joint between beam bars.

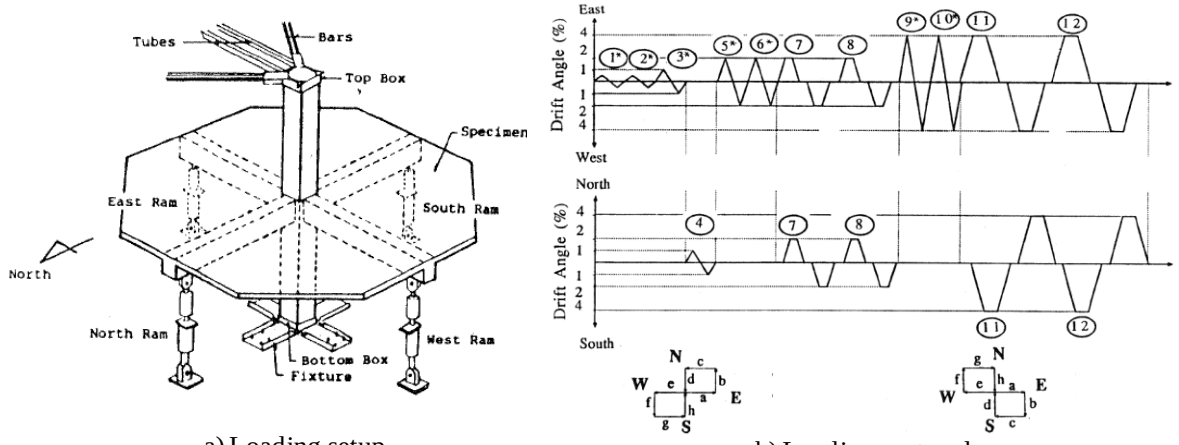

a) Loading setup b) Loading protocol

Figure G-15 Experimental study by Kurose *et al.* [37] and Guimaraes *et al.* [38]: Setup and loading protocol

All specimens experienced flexural cracks that occurred in the slab, beams and column. Test results of Specimen J2 are shown in Figure G-16 in order to illustrate typical crack patterns and drift angle – storey shear response behaviour. Normal-strength specimens failed in joint shear at 4% drift after formation of beam hinges adjacent to the column. High-strength specimens were stiffer and showed minor joint distress at 2% drift levels. All specimens exhibited higher strength than calculated for a beam hinging mechanism. Bidirectional strength exceeded measured unidirectional strength. Considerable pinching occurred in the storey shear-drift angle curves, especially for the high-strength concrete specimens. Regarding the effectiveness of slab, it was observed that the portion of slab participating with the beam resisting negative bending moments generally increased with increased drift. Beam moment capacities, assuming the effective slab width to be 60% of the total slab width, showed very good agreement with test results.

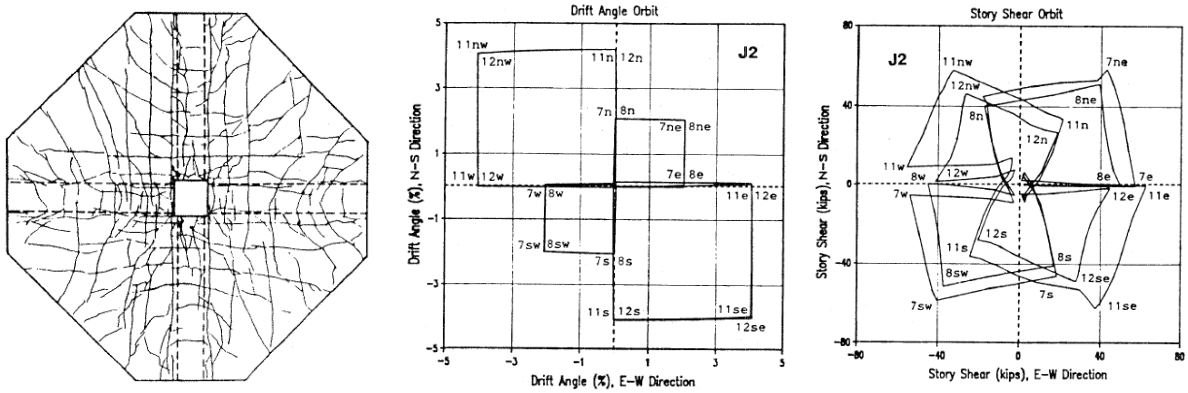

a) Final crack patterns b) Drift angle and story shear orbits

Figure G-16 Experimental study by Kurose *et al.* [37] and Guimaraes *et al.* [38]: Typical test results (Specimen J2)

The effects of bidirectional load reversals on the behaviour of eight one-third scale exterior beam-column joints of a two-way RC concrete ductile frame, were investigated by Fuiji and Morita [40] as a supplemental test to the previously described four country co-operative tests. Simultaneous bidirectional load reversals or unidirectional load reversals were applied to five beam-column-slab specimens. In addition to these, three beam-column specimens without slab, but having identical beam and column sections were tested to clarify the effects of slab and/or transverse beams. Details of test specimens and test setup are given in Figure G-17.

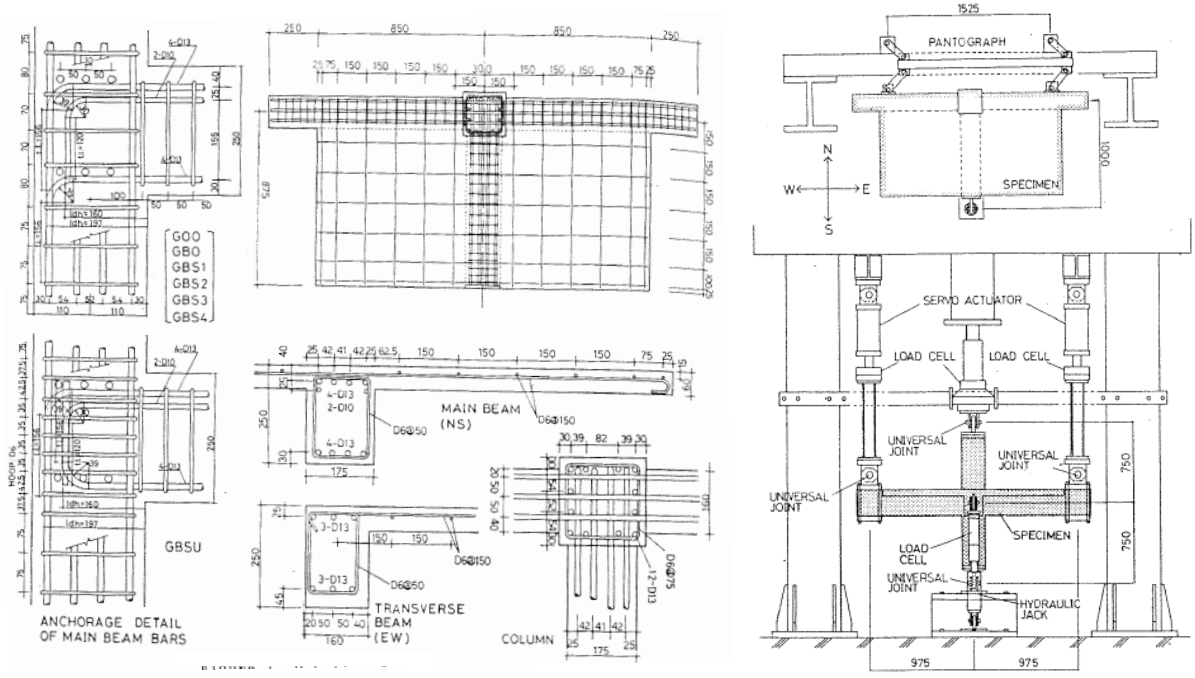

Figure G-17 Experimental study by Fuiji and Morita [40]: Specimen details and loading protocol

The space frame joint specimens exhibited considerable loss of shear resistance and stiffness, due to bidirectional load reversals. The spalling of the concrete cover at the corners of the column and the joint were observed. In order to illustrate the effect of bidirectional loading on the response, the joint shear force versus joint shear strain relationships of two selected specimens are shown in Figure G-18. As seen in the figure, simultaneous orthogonal loading damaged the joint shear resistance and caused the increase of the displacement component due to joint shear distortion in the principal direction. The maximum joint shear stress along either direction was about $1.0\sqrt{f_c}$` in MPa. It was noted that the increase of column deformation under the bidirectional load reversals resulted from the reduced bi-axial capacity of columns, due to crushing of the concrete cover at the corner in compression and also from the accompanying poor bond condition of column bars. Researchers indicated that the slab significantly influenced the overall behaviour of the subassemblage. Owing to the collaboration of slab bars of flexural resistance of beams, joint shear input increased and column to beam flexural strength ratio decreased. This might have resulted in the early degradation of joints and columns.

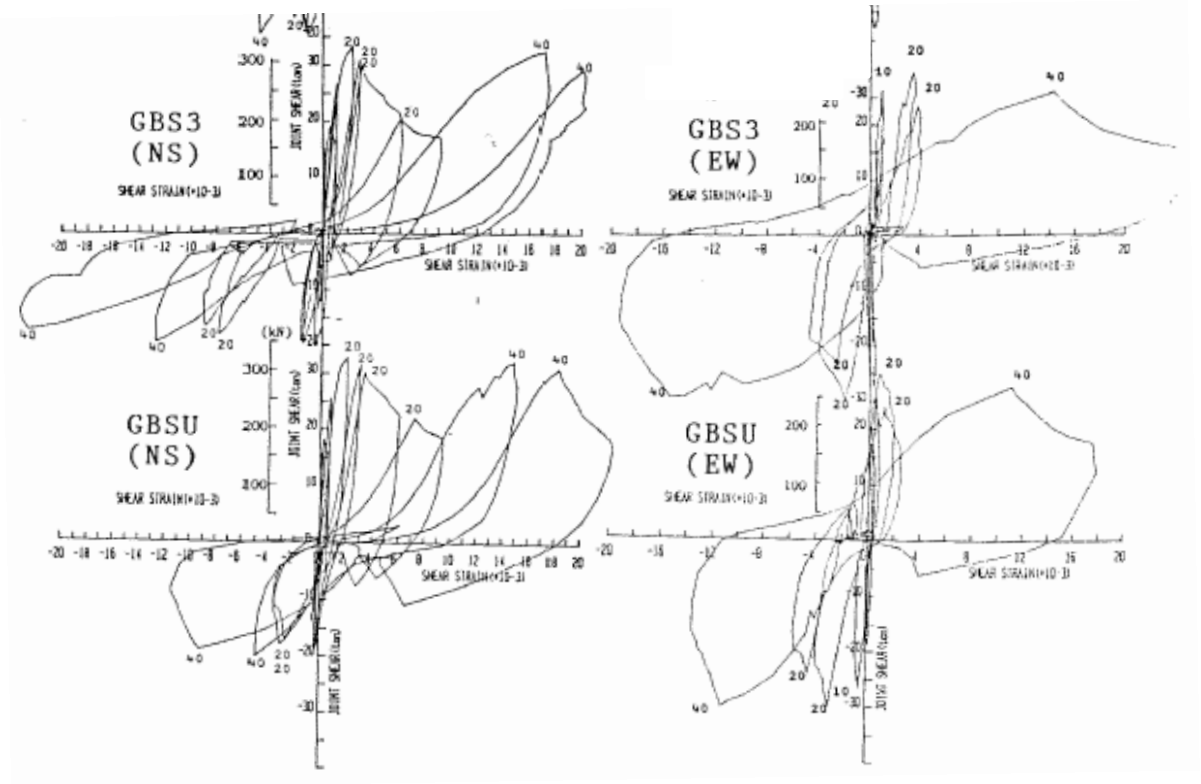

Figure G-18 Experimental study by Fuiji and Morita [40]: Effect of bidirectional loading on joint shear versus joint shear strain curves

Joh *et al.* [41] carried out an experimental study to clarify the shear resistance behaviour of interior beam-column joints in two-way RC frames in comparison with the strength equations proposed in Japan and the requirements of both the ACI code and New Zealand Standard. Four three-dimensional

subassemblages with slab were used as specimens to whom lateral cyclic forces were applied in two directions perpendicular to each other. Specimen details and loading protocol are given in Figure G-19.

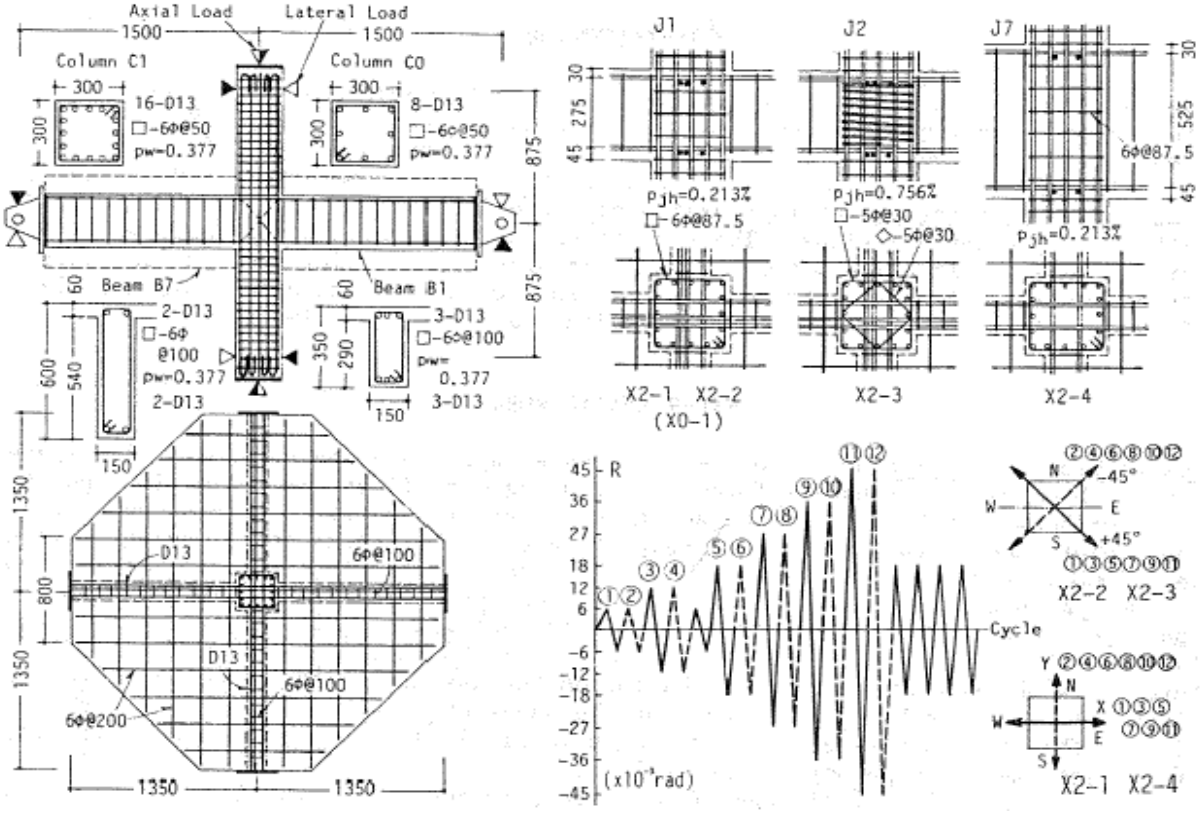

Figure G-19 Experimental study by Joh *et al.* [41]: Specimen details and loading protocol

Crack patterns of the joints after testing are shown in Figure G-20. It was noted that although occurrence of shear cracks on the faces of the joints could not be observed, an abrupt increase of strains in the joint reinforcement was recorded. Researchers indicated that shear cracking in the beam-column joint could be assessed with the principal stress concept by assuming the normalized interaction curve of an arc of circle for the bidirectional shear; however they also noted that some modifications are necessary for the shear cracking stress decline in oblong joints. It was recommended that the effective width of slab to participate the bending resistance of a beam shall be taken as about one-fifth of span length at the yielding of beams. In addition, for the estimation of design shear forces in the joint, the effective width should be taken as the entire width of slab. It was also found that calculated values of shear strength of joint panels using the previous equations or according to the requirements of the codes, did not show good agreement with the observed values. In the frames subjected to bidirectional loading, the slippage of beam bars was a little greater compared with that in the frames subjected to beam directional loading.

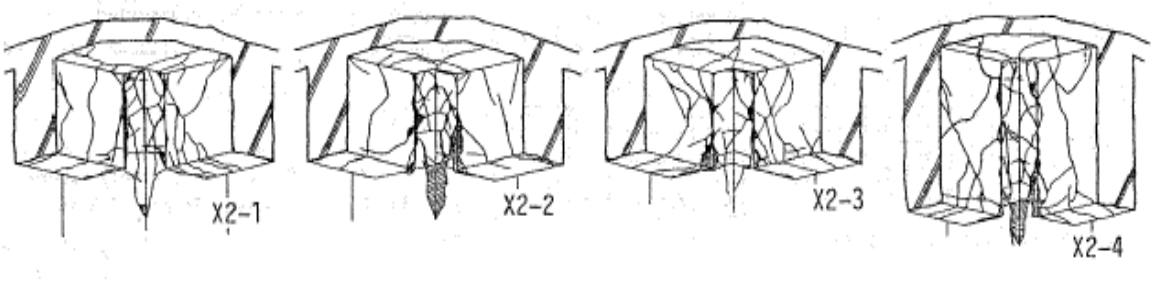

Figure G-20 Experimental study by Joh *et al.* [41]: Crack patterns of joints after tests

Kitayama *et al.* [42] reported the test results of three half-scale (two interior: specimen K1 and K2 and one exterior: specimen K3) three-dimensional RC beam-column joints tested under bidirectional cyclic reversed loading. Reinforcement details of the specimens, along with loading apparatus and crack patterns after test are given in Figure G-21.

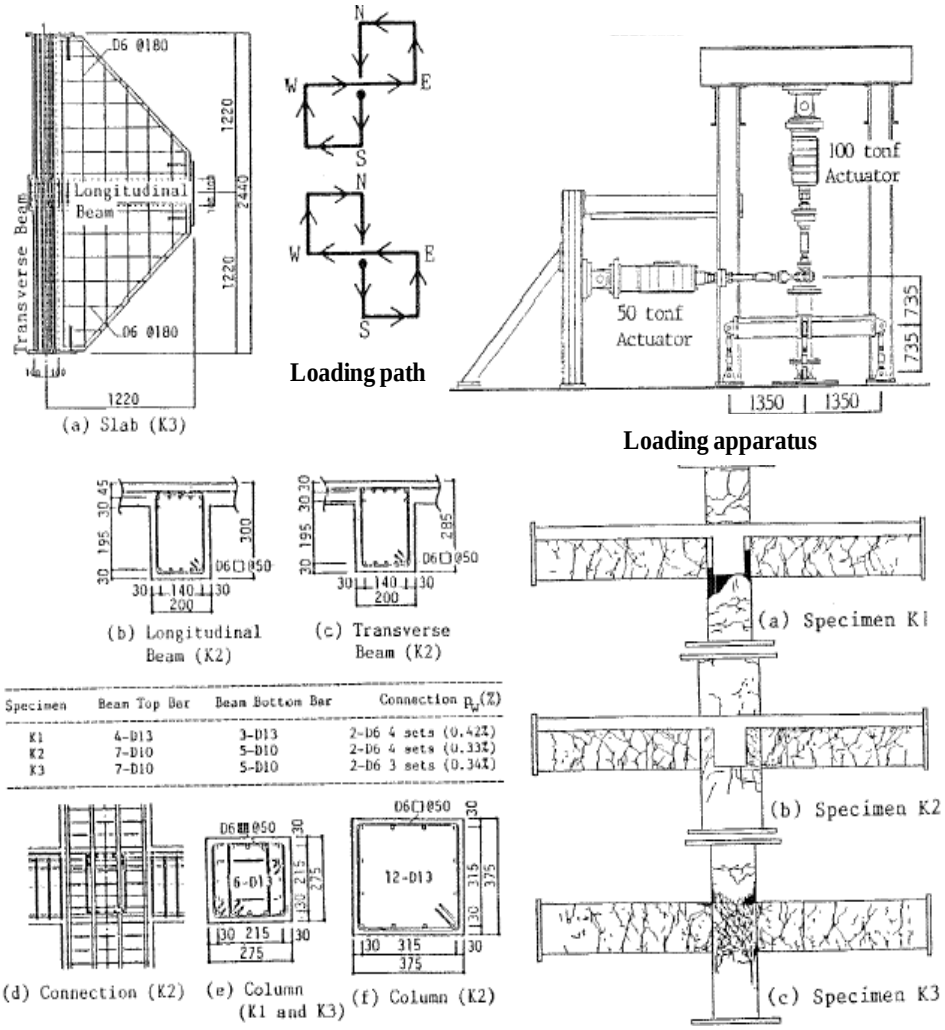

Figure G-21 Experimental study by Kitayama *et al.* [42]: Crack patterns of joints after tests

From the tests the following observations were drawn (1) three-dimensional specimens did not fail in joint shear despite a high shear stress level in the connection, probably because the orthogonal beams and slabs enhanced the joint shear capacity; (2) the interior beam-column subassembly with slab, provided with good bond characteristics along beam bars within the joint, showed a pinching behaviour, which may be caused by the delay in crack closing attributable to a shift in the locations of the neutral axis above the beam top bars under positive loading and (3) the slab width contributing to the beam flexural resistance spreads with beam deformation. The entire slab width needs to be regarded effectively as a large deformation.

As a part of the aforementioned quadri-lateral research project between four countries, Bolong and Yuzhou [43] carried out experimental work on three full-scale RC beam-column joint specimens to analyze the influences of the aseismic behaviour of beam-column joints, due to different loading systems and a monolithic slab. Three full-scale RC beam-column joint specimens were subjected to one and to directional reversed loading. The relevant provisions for joints in the Chinese design code for RC structures were also checked. The units were full-scale taken from the design of Beijing Hospital of Traditional Chinese Medicine. Deformed longitudinal bars were used in the specimens. Specimen details are given in Figure G-22.

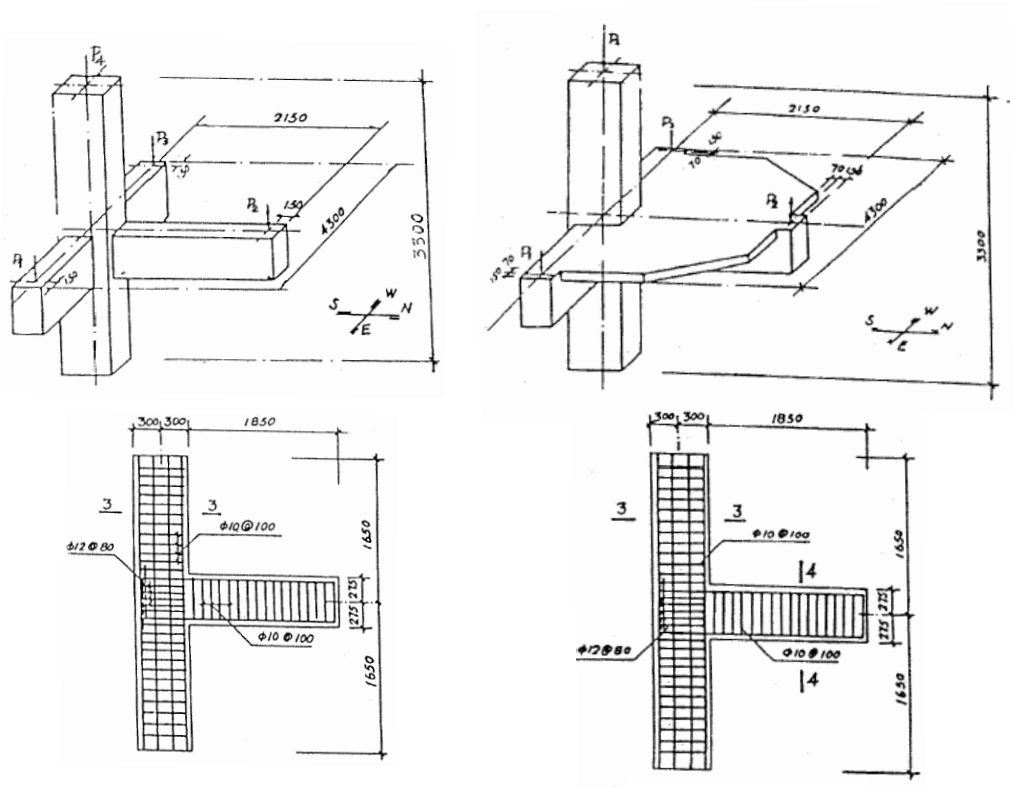

Specimen J4 and J5 Specimen J6

Figure G-22 Experimental study by Bolong and Yuzhou [43]: Specimen details

The performance of all units was satisfactory when compared with the design requirements. Cracks occurred mostly in the beam region, followed by the joint and then the slab (only for Unit J6 with slab) (Figure G-23). The failure mechanisms of all specimens were quite similar. From the test results, these conclusions were drawn: (1) for the exterior joint, the transverse beams were also subjected to the torque action and not only subjected to the bidirectional bending moment and shear. Therefore the longitudinal reinforcement area in the joint and transverse beam should be increased; (2) the presence of the slab had a significant influence of the stiffness and strength of the beam. The researchers indicated that when similar cast-in-situ floor configurations were adopted, the effect of the slab should be appropriately taken into account in the capacity design process.

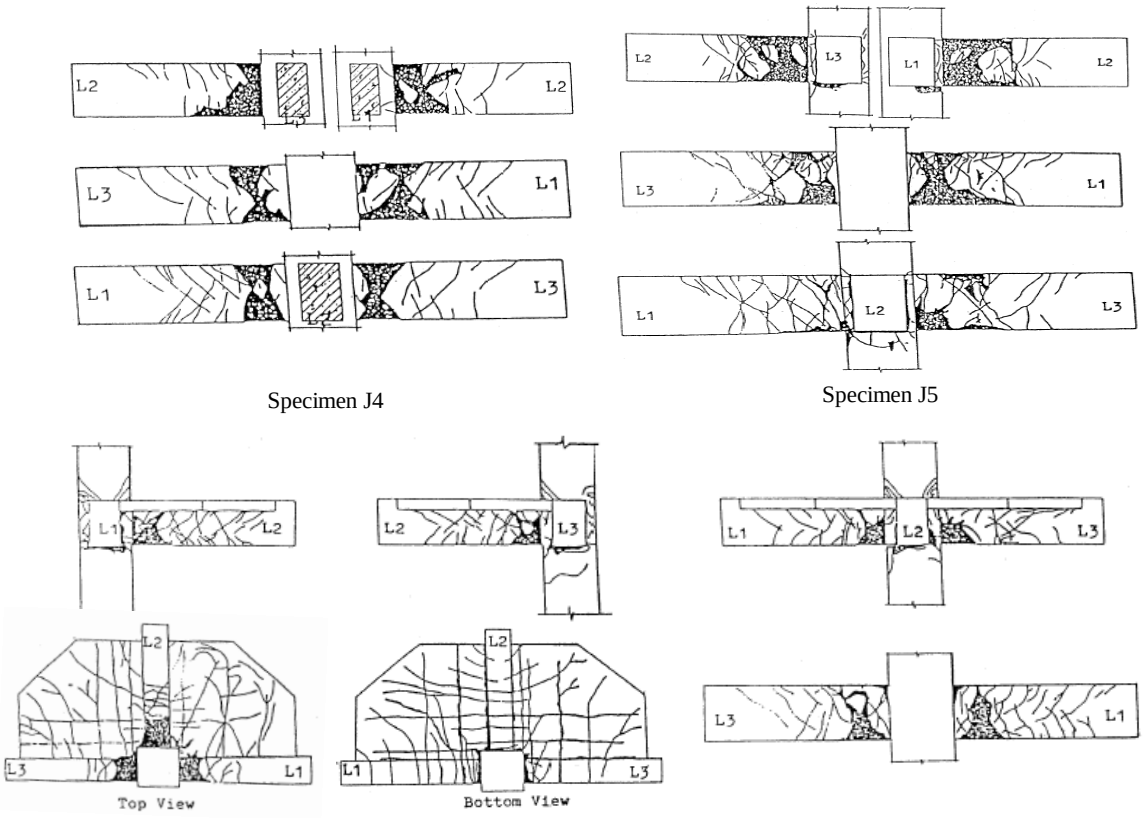

Figure G-23 Experimental study by Bolong and Yuzhou [43]: Crack patterns of joints after tests

Cheung [44] performed a series of tests on full scale plane and space frame behaviour beam-column joint units with slab, designed according to the New Zealand design code [45]. Deformed longitudinal bars were used. One plane frame interior beam-column-slab joint, one space frame interior beam-column-slab joint and one space frame exterior beam-column-slab joint unit were tested under simulated bidirectional seismic loading. The tests were carried out at the University of Canterbury, Christchurch, New Zealand. Figure G-24 show the specimen details and damage observed of the specimens tested under biaxial loading.

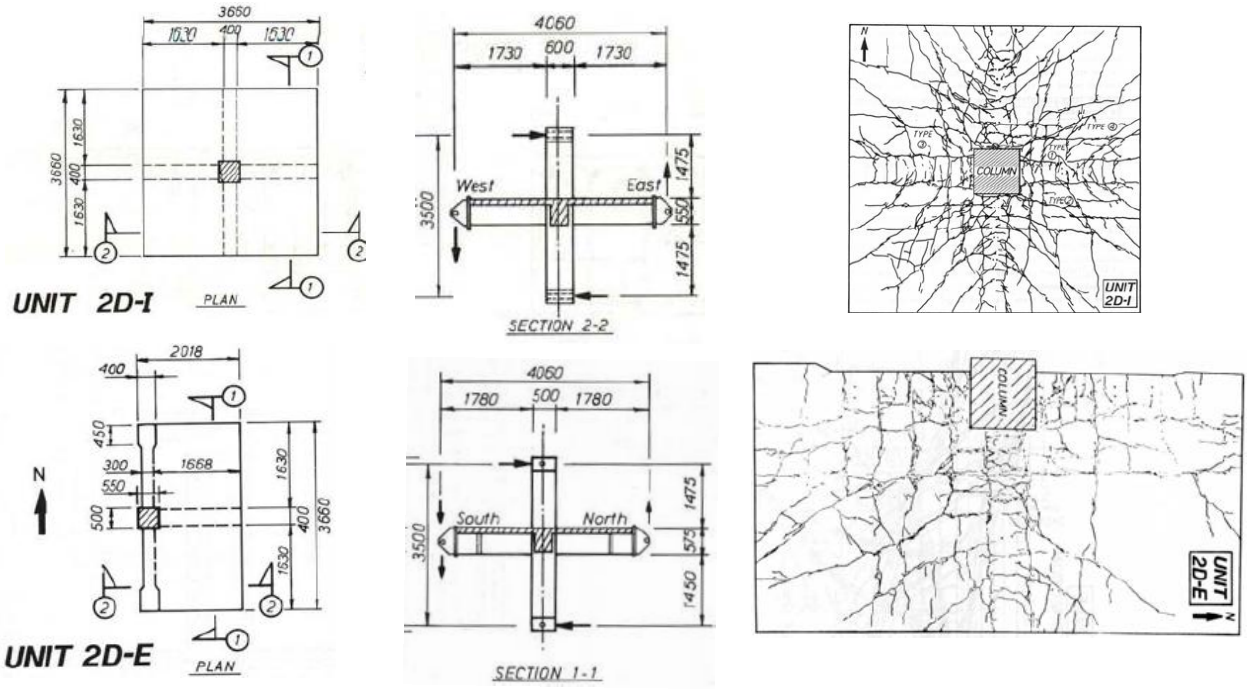

Figure G-24 Experimental study by Cheung [44]: Specimen dimensions and crack patterns

The behaviour of all units was satisfactory and complied with the performance criteria in the New Zealand loading code [45]. Plastic hinges occurred in the beams and columns during the loading in the inelastic range. Few diagonal cracks occurred in the joint core regions without causing strength loss. The test results showed that no additional confinement was provided by the transverse beams or the floor slab during biaxial seismic loading whereby the performance would have been improved. The joint regions were sufficiently reinforced with stirrups to prevent an extensive level of damage and inelastic shear deformation occurring. However, the contribution of joint deformation was up to 26% of the total interstorey drift. The strength and stiffness of the units reduced if loaded biaxially, mainly due to the change of slab reinforcement contribution to the beam flexural strength.

G.5 REFERENCES

1. Takizawa A, Aoyama H. Biaxial effects in modeling earthquake response of R/C structures. *Earthquake Engineering and Structural Dynamics*. 1976; **4**(6).
2. Otani S, Cheung CH. Behaviour of RC columns under biaxial lateral load reversals. *Publication 81-02*, University of Toronto, Canada, 1981.
3. Takiguchi K, Kokusho S, Kobayashi A, Kimura M. Response of RC column to horizontal bi-directional deflection history. *Proceedings of 7th World Conference on Earthquake Engineering*, Istanbul, Turkey, 1980.
4. Kobayashi K, Kokusho S, Takiguchi K, Yang-Boo C. Study on the restoring force characteristics of RC solumn to bidirectional deflection history. *Proceedings of 8th World Conference on Earthquake Engineering*, San Francisco, Calif., 1984.
5. CEB. *RC frames under earthquake loading*. Comite Euro-International du Beton, Bulletin d`Information: Paris, 1996.
6. Saatcioglu M. Reinforced concrete columns subjected to uniaxial and biaxial load reversals. *Proceedings of 8th World Conference on Earthquake Engineering*, San Francisco, Calif., 1984.
7. Saatcioglu M, Ozcebe G. Response of reinforced concrete columns to simulated seismic loading. *ACI Structural Journal*. 1989; **86**(1):3-12.
8. Li K, Aoyama H. Reinforced concrete columns under varyng axial load and bidirectional lateral load reversals. *Proceedings of Ninth World Conference on Earthquake Engineering*, Tokyo-Kyoto, Japan, 1988.
9. Low S, Moehle J. Experimental study of reinforced concrete columns subjected to multiaxial cyclic loading. *Report No. UCB/EERC - 87/14*, University of California, Berkeley, 1987.
10. Wong Y-L, Paulay TP, J.N. Response of circular reinforced concrete columns to to multi-directional seismic attack. *ACI Structural Journal*. 1993; **90**(2):180-91.
11. Boys A. Assessment of the seismic performance of inadequately detailed reinforced concrete columns. *M.E. Thesis*, University of Canterbury, Christchurch, 2009.
12. Oliva MG, Clough RW. Biaxial seismic response of R/C frames. *Journal of Structural Engineering, ASCE*. 1987; **113**(6).
13. *Uniform Building Code.* International Conference of Building Officials, 1970.
14. American Concrete Institute (ACI). *Building code requirements for reinforced concrete. ACI 318-71*. American Concrete Institute, Detroit, Mich., 1971.
15. Zeris CA, Mahin SA. Behavior of reinforced concrete structures subjected to biaxial excitation. *Journal of Structural Engineering, ASCE*. 1991; **117**(9).
16. Furlong RW. Ultimate strength of square columns under biaxially eccentric loads. *ACI Structural Journal*. 1961; **57**(9):1129-40.
17. Bresler B. Design criteria for reinforced concrete columns under axial load and biaxial loading. *ACI Structural Journal*. 1960; **57**(5):481-90.
18. Parme AL, Nieves JM, Gouwens A. Capacity of reinforced rectangular columns subjeect to biaxial bending. *ACI Structural Journal*. 1966; **63**(9):911-23.
19. Weber DC. Ultimate strength design charts for columns with biaxial bending. *ACI Structural Journal*. 1966; **63**(11):1205-30.
20. Hsu CT, Mirza MS. Structural concrete-biaxial bending and compression. *Journal of Structural Engineering, ASCE*. 1973; **99**(2).
21. Row DG, Paulay T. Biaxial flexure and axial load interaction in short rectangular reinforced concrete columns. *Bulletin of the New Zealand National Society for Earthquake Engineering*. 1973; **6**(3):217-50.
22. Park R, Paulay T. *Reinforced Concrete Structures*. John Wiley & Sons: New York, 1975.
23. Brondum-Nielsen T. Ultimate flexural capacity of cracked polygonal concrete sections under biaxial bending. *ACI Structural Journal*. 1985; **82**(6):863-9.

24. Hsu CT. Biaxially loaded L-shaped reinforced concrete columns. *Journal of Structural Engineering, ASCE*. 1985; **3**(12).
25. Zahn FA, Park R, Priestley MJN. Strength and ductility of square reinforced concrete column sections subjected to biaxial bending. *ACI Structural Journal*. 1989; **56**(2):123-31.
26. Cedolin L, Cusatis G, Eccheli S, Roveda M. Capacity of rectangular cross sections under biaxially eccentric loads. *ACI Structural Journal*. 2008; **105**(2):215-24.
27. ACI Committe 340, Ultimate strength design handbook. *ACI special Publication, SP 17A, Columns*. 1972; **2**.
28. CP 110. *Code of practice for the structural use of concrete: Part 1: Design, materials and workmanship; Part 3: Design charts for circular columns and prestressed beams.* British Standards Institution, London, 1972.
29. Dundar C. Concrete box sections under biaxial bending and axial load. *Journal of Structural Engineering, ASCE*. 1990; **116**(3).
30. Kwan KH, Liauw TC. Computerized ultimate strength analysis of reinforced concrete sections subjected to axial compression. *Computers & Structures*. 1985; **21**(6):1119-27.
31. Zak ML. Computer analysis of reinforced concrete sections under biaxial bending and longitudinal load. *ACI Structural Journal*. 1993; **90**(2):163-9.
32. Ferguson PM, Breen JE, Jirsa JO. *Reinforced Concrete Fundamentals*. John Wiley & Sons: New Jersey, 1988.
33. Hassoun MN, Al-Manaseer A. *Structural Concrete*. John Wiley & Sons: New Jersey, 2008.
34. Beckingsale CW. Post-elastic behaviour of reinforced concrete beam-column joints. *PhD Dissertation*, University of Canterbury, Christchurch, 1980.
35. Leon R, Jirsa O. Bi-directional loading of RC beam-column joints. *Earthquake Spectra*. 1986; **2**(3):537-64.
36. Suzuki N, Otani S, Kobayashi Y. Three dimensional beam-column subassemblages under bidirectional earthquake loadings. *Proceedings of 8th World Conference on Earthquake Engineering*, San Francisco, Calif., 1984.
37. Kurose Y, Guimaraes GN, Zuhua L, Kreger ME, Jirsa JO. Evaluation of slab-beam-column connections subjected to bidirectional loading. *ACI Special Publication, SP-123-3*. 1991:39-67.
38. Guimaraes GN, Kurose Y, Kreger EM, Jirsa JO. Bi-directional response of slab-beam-column connections using high strength materials. *Proceedings of Ninth World Conference on Earthquake Engineering*, Tokyo-Kyoto, Japan, pp. 575-80, 1988.
39. American Concrete Institute (ACI). *Recommendations for design for beam-column-joint in monolithic reinforced concrete structures. ACI 352-85.* American Concrete Institute, Detroit, Mich., 1985.
40. Fuiji S, Morita S. Behaviour of exterior reinforced concrete beam-column-slab subassemblages under bi-directional loading. *Pacific Conference on Earthquake Engineering*, New Zealand, 1987.
41. Joh O, Goto Y, Shibata T. Behaviour of three-dimensional reinforced concrete beam-column subassemblages with slabs. *Proceedings of Ninth World Conference on Earthquake Engineering*, Tokyo-Kyoto, Japan, pp. 587-92, 1988.
42. Kitayama K, Otani S, Aoyama H. Behaviour of reinforced concrete beam-column-slab subassemblages subjected to bi-directional load reversals. *Proceedings of Ninth World Conference on Earthquake Engineering*, Tokyo-Kyoto, Japan, pp. 581-6, 1988.
43. Bolong Z, Yuzhou C. Behaviour of exterior reinforced concrete beam-column joints subjected to bi-directional cyclic loading. *ACI Special Publication, SP-123-3*. 1991:pp. 69-96.
44. Cheung CH. Seismic Design of Reinforced Concrete Beam-Column Joints with Floor Slabs. Research Report 91-4, Department of Civil Engineering, University of Canterbury, Christchurch, New Zealand, 1991.
45. NZS 3101:1982. *Concrete structures standard, NZS 3101*. Standards association of New Zealand, Wellington, 1982.